Università degli Studi di Padova

Dipartimento di Matematica"Tullio Levi-Civita"
Corso di Dottorato di Ricerca in Scienze Matematiche
Curriculum Matematica
Ciclo XXXV

Hamiltonian secular theory and KAM stability in exoplanetary systems with 3D orbital architecture

Coordinatore
Ch.mo Prof. Giovanni Colombo

Supervisore
Ch.mo Prof. Christos Efthymiopoulos

Co-Supervisore
Ch.mo Prof. Ugo Locatelli

Dottoranda
Rita Mastroianni

A Piero

Abstract

In the present thesis, we first revisit the secular 3D planetary three-body problem aiming to provide a unified formalism for studying the structure of the phase space for progressively higher values of the mutual inclination i_{mut} between the two planets' orbits. We propose a "book-keeping" technique yielding (after Jacobi reduction) a clear decomposition of the secular Hamiltonian as $\mathcal{H}_{sec} = \mathcal{H}_{planar} + \mathcal{H}_{space}$, where $\mathcal{H}_{space}$ contains all terms depending on i_{mut}. We explore the transition from a "planar-like" to the Lidov-Kozai regime. We show how the structure of the phase portraits of the integrable secular dynamics of the planar case is reproduced to a large extent also in the 3D case. We estimate semi-analytically the level of i_{mut} up to which the dynamics remains nearly-integrable, and propose a normal form method to compute the basic periodic orbits (apsidal corotation resonances) and quasi-periodic orbits in this regime. We explore the families of periodic orbits dominant in the other limit, of the Lidov-Kozai regime, as well as the connection between all the above families of periodic orbits. We study numerically the form of the phase portraits for different mass and semi-major axis ratios of the two planets, for systems' parameters close to one or more hierarchical limits (in the planets' mass or distance ratio).
Secondly, we introduce a quasi-periodic restricted Hamiltonian to describe the secular motion of a small-mass planet in a multi-planetary system. As an example, we refer to the motion of υ-And **b** (the innermost planet in the extrasolar υ-Andromedæ system). We reconstruct the orbits of υ-And **c** and υ-And **d** in a stable configuration through Frequency Analysis of their secular motions. These orbits are then injected in the equations describing the orbital dynamics of υ-And **b**, ending up with a Hamiltonian model having 2+3/2 degrees of freedom validated through a comparison of numerical integrations with the complete 4-body problem. We also add relativistic corrections to the above model. We study the stability of υ-And **b** as a function of the initial values of the inclination and of the longitude of the node, which are subject to observational uncertainties. Studying the evolution of the eccentricity, we show how to exclude orbital configurations with long-time high probability of (quasi)collision with the central star. We introduce a normal form approach, based on averaging of the angles associated with the secular motions of the major exoplanets, leading to a further reduced model with 2 dof. This allows to quickly preselect, by a numerical criterion, the domains of stability for υ-And **b**.
After the above steps, we implement the Kolmogorov normalization algorithm in order to provide a computer-assisted proof of existence of KAM (Kolmogorov-Arnold-Moser) tori in the framework of the above secular models for planet υ-And **b**. We compute the Kolmogorov normal form and provide a computer-assisted proof of existence of KAM tori for the inner planet's secular motion for pre-selected initial conditions in i) the secular Hamiltonian model found after the elimination of all the fast angles of the problem (SQPR 2+2/2 model), and ii) in the reduced model after normalizing the secular motions of the outer planets (SQPR 2 model). We show how the KAM tori persist when general-relativistic corrections are added to the models.
Finally, we present a Kolmogorov-like normal form algorithm in the neighborhood of an invariant torus in Hamiltonian systems $\mathcal{H} = \mathcal{H}_0 + \varepsilon\mathcal{H}_1$, where $\mathcal{H}_0$ is the Hamiltonian of N linear oscillators, and $\mathcal{H}_1$ is a polynomial series. This yields a normal form analogue of a corresponding Lindstedt method for coupled oscillators. We comment on the possible use of the Lindstedt method itself under two distinct schemes, i.e., one analogous to the Birkhoff and another analogous to the Kolmogorov (torus fixing) normal form.

Contents

1. Introduction

The general *problem of dynamics*, as defined by Poincaré in *Les méthodes nouvelles de la mécanique céleste* ([94]), is described by the following Hamiltonian

$$\mathcal{H}(\boldsymbol{\varphi}, \boldsymbol{I}) = h(\boldsymbol{I}) + \varepsilon\, f(\boldsymbol{\varphi}, \boldsymbol{I})\,, \tag{1.1}$$

with action variables $\boldsymbol{I} \in \mathcal{G} \subset \mathbb{R}^n$ ($\mathcal{G}$ an open set), angle variables $\boldsymbol{\varphi} \in \mathbb{T}^n$ and ε a "small" parameter. The Hamiltonian (1.1) is called "nearly-integrable": it is composed by two terms, $h(\boldsymbol{I})$ and $\varepsilon\, f(\boldsymbol{\varphi}, \boldsymbol{I})$. The term $h(\boldsymbol{I})$ is integrable and it yields a trivial to recover dynamics. However, the complete Hamiltonian $\mathcal{H}(\boldsymbol{\varphi}, \boldsymbol{I})$ is "perturbed" by the presence of the term $\varepsilon\, f(\boldsymbol{\varphi}, \boldsymbol{I})$. At first, one can (wrongly) conjecture that since the complete Hamiltonian $\mathcal{H}(\boldsymbol{\varphi}, \boldsymbol{I})$ is close to the integrable one $h(\boldsymbol{I})$, the same holds true for its dynamics. However, the integrable problem is only *a first approximation* and a wide range of new phenomena appear in general as a result of the perturbation. In nearly-integrable systems, the solutions cannot in general be found in an explicit form. For this reason, a *qualitative study* plays an important role in the treatment of such systems. Moreover, it is possible to find approximate solutions of the pertubed systems through *perturbative methods*, i.e., normal forms.

The present thesis is devoted to the qualitative study, as well as the application of a number of methods of canonical perturbation theory, in a class of nearly-integrable problems arising within the framework of the modelling of *3D planetary systems*. With the discovery of many extrasolar planetary systems in the last 30 years, the study of nearly-integrable systems, referring either to the, short term, *nearly-Keplerian*, or to the, long-term, *secular* motions of exoplanets around their hosting star, has provided a wide new arena for the application of known methods of study of nearly-integrable systems, or the discovery of new ones. In the present thesis, our focus is on methods stemming from the use of canonical perturbation theory in exo-planetary dynamics. In particular, we emphasize how the methods of perturbation theory allow to normalitation procedures, i.e. procedures involving a suitably defined sequence of canonical change of coordinates, which are specially adapted to the particular phisical problem under study. Thus, these procedures lead to a control of the dynamics of the complete system, as well as a quantification of the difference between the perturbed and the integrable dynamics. In particular, we will see how these methods help to address a question of key interest, both mathematical and astronomical, namely the question of the *secular stability* of an exo-planetary system.

Section 1.1 to 1.4 below serve to introduce some basic notions and definitions pertinent to the content of all subsequent Chapters of the thesis. This is followed by a statement of the thesis' scope and structure, given in the last section (1.5) of the present introduction.

1.1 Definitions and basic notions of Hamiltonian systems

Given the Hamiltonian function $\mathcal{H} : \mathcal{F} \to \mathbb{R}$, with $(\boldsymbol{q}, \boldsymbol{p}) \in \mathcal{F} \subseteq \mathbb{R}^n \times \mathbb{R}^n$, we call *Hamilton's equations* the following system of $2n$ differential equations of the first order:

$$\begin{cases} \dot{q}_j = \partial \mathcal{H}(\boldsymbol{q}, \boldsymbol{p})/\partial p_j \\ \dot{p}_j = -\partial \mathcal{H}(\boldsymbol{q}, \boldsymbol{p})/\partial q_j \end{cases} \qquad j = 1, \dots, n \,, \tag{1.2}$$

where the dot $\dot{}$ means the time derivative d/dt. The variables $(\boldsymbol{q}, \boldsymbol{p})$ are called *canonical positions* and *momenta* respectively and the space $\mathcal{F}$ spanned by them is called the *phase space*. The system (1.2) is said to define a *n-degree of freedom* (DOF) Hamiltonian dynamical system.[1] The solutions of Hamilton's equations (1.2) define a *flow* which maps the inizial values $(\boldsymbol{q}(0), \boldsymbol{p}(0))$ to the solution at time t, i.e. $\phi^t_{\mathcal{H}}(\boldsymbol{q}(0), \boldsymbol{p}(0)) = (\boldsymbol{q}(t), \boldsymbol{p}(t))$. An *orbit* is defined as $\cup_{t \in I} \phi^t_{\mathcal{H}}$, where I is the maximal set of definition of the solution.
Whenever the Hamiltonian does not depend explicitely on time (i.e. $\partial \mathcal{H}/\partial t = 0$) it is said *autonomous*. For an autonomous Hamiltonian the value $\mathcal{E} = \mathcal{H}(\boldsymbol{q}(t), \boldsymbol{p}(t))$ is preserved along any orbit, since (using Hamilton's equations (1.2))

$$\frac{d\mathcal{H}}{dt} = \sum_{i=1}^{n} \left(\frac{\partial \mathcal{H}}{\partial q_i} \dot{q}_i + \frac{\partial \mathcal{H}}{\partial p_i} \dot{p}_i \right) + \frac{\partial \mathcal{H}}{\partial t} = \frac{\partial \mathcal{H}}{\partial t} \,.$$

$\mathcal{E}$ is called the energy of the orbit. In the case when the Hamiltonian depends explicitly on the time, it is called *non autonomous* with $n + 1/2$ degrees of freedom. Through an 'extension of the phase space', i.e., by including an additional variable conjugate to the time, it is possible to formally remove the explicit dependence on time, producing an equivalent autonomous Hamiltonian with $n + 1$ degrees of freedom (see, for istance, [31]).

A classical method to visualize the global behaviour of a system is to pass from the continuous flow $\phi^t_{\mathcal{H}}$ to a discrete map $\Pi : \Sigma \to \Sigma$, with $\Sigma \subset \mathbb{R}^{2n}$ a surface of dimension $2n-1$; this is called the Poincaré section method. In particular, taken a surface Σ transversal to the flow, an orbit is followed until crossing, in a given direction, the surface Σ. Denoting by P_0 the first point of intersection between the flow and Σ, $P_1 := \Pi(P_0)$ the successive point of intersection, etc., an orbit can be represented by the discrete sequence of the successive intersections $P_0, P_1 = \Pi(P_0), P_2 = \Pi(P_1), \dots$, instead of the continuous curve $(\boldsymbol{q}(t), \boldsymbol{p}(t))$.
Now we give a series of definitions useful in the sequel.

1.1.1 Poisson brackets and Lie derivative

Definition 1.1.1. *The Poisson bracket between two functions f and g is the bilinear map $\{\cdot, \cdot\} : \mathcal{C}^\infty(\mathcal{F}) \times \mathcal{C}^\infty(\mathcal{F}) \to \mathcal{C}^\infty(\mathcal{F})$ defined by*

$$\{f, g\} = \{f, g\}_{(\boldsymbol{q}, \boldsymbol{p})} = \sum_{j=1}^{n} \left(\frac{\partial f}{\partial q_j} \frac{\partial g}{\partial p_j} - \frac{\partial f}{\partial p_j} \frac{\partial g}{\partial q_j} \right) = \nabla f \cdot \mathbb{J} \nabla g \,,$$

where $\mathbb{J} = \begin{pmatrix} \mathbb{O}_n & \mathbb{I}_n \\ -\mathbb{I}_n & \mathbb{O}_n \end{pmatrix}$ is the symplectic matrix, with $\mathbb{O}_n$ and $\mathbb{I}_n$ respectively the $n \times n$ zero and unit matrices.

By the Poisson bracket of a function f with the Hamiltonian $\mathcal{H}$, we find

$$\{f, \mathcal{H}\} = \sum_{j=1}^{n} \left(\frac{\partial f}{\partial q_j} \frac{\partial \mathcal{H}}{\partial p_j} - \frac{\partial f}{\partial p_j} \frac{\partial \mathcal{H}}{\partial q_j} \right) = \dot{f} \,,$$

[1] In general, denoting by M the n-dimensional manifold in which the trajectories of the system $\boldsymbol{q}(t)$ lie, the phase space is the cotangent bundle of M, i.e. $\mathcal{F} = T^*M$ being $(\boldsymbol{q}, \boldsymbol{p}) \in T^*M$. In the present thesis we deal with the simple case of Hamiltonian systems in which the phase space $\mathcal{F}$ is an open set of $\mathbb{R}^{2n}$.

that gives the time derivative of the dynamical variable f along the Hamiltonian flow induced by $\mathcal{H}$.

Definition 1.1.2. *The Lie derivative along the Hamiltonian vector field induced by $\mathcal{H}$ is defined as the operator*

$$L_{\mathcal{H}}\cdot = \{\cdot, \mathcal{H}\} = \sum_{j=1}^{n} \left(\frac{\partial \mathcal{H}}{\partial p_j} \frac{\partial \cdot}{\partial q_j} - \frac{\partial \mathcal{H}}{\partial q_j} \frac{\partial \cdot}{\partial p_j} \right) . \tag{1.3}$$

It is possible to rewrite now Hamilton's equations as

$$\begin{cases} \dot{q_j} = \{q_j, \mathcal{H}\} = L_{\mathcal{H}} q_j \\ \dot{p_j} = \{p_j, \mathcal{H}\} = L_{\mathcal{H}} p_j \end{cases} \qquad j = 1, \dots, n \ .$$

1.1.2 Canonical transformations

Given the Hamiltonian $\mathcal{H}(\boldsymbol{q}, \boldsymbol{p})$, with $(\boldsymbol{q}, \boldsymbol{p}) \in \mathcal{F}$, we can introduce a change of coordinates $(\boldsymbol{q}, \boldsymbol{p}) \mapsto (\boldsymbol{Q}, \boldsymbol{P})$ such that the new variables $(\boldsymbol{Q}, \boldsymbol{P})$ satisfy Hamilton's equations (1.2) for a new Hamiltonian $H(\boldsymbol{Q}, \boldsymbol{P}) = \mathcal{H}(\boldsymbol{q}(\boldsymbol{Q}, \boldsymbol{P}), \boldsymbol{p}(\boldsymbol{Q}, \boldsymbol{P}))$. More precisely, we have the following definition:

Definition 1.1.3. *Consider the change of coordinates $(\boldsymbol{q}, \boldsymbol{p}) \mapsto (\boldsymbol{Q}, \boldsymbol{P})$, given by $\boldsymbol{z} = \boldsymbol{z}(\boldsymbol{y})$, with $\boldsymbol{y} := \begin{pmatrix} \boldsymbol{q} \\ \boldsymbol{p} \end{pmatrix}$ and $\boldsymbol{z} := \begin{pmatrix} \boldsymbol{Q} \\ \boldsymbol{P} \end{pmatrix}$. Let $M = \partial \boldsymbol{z} / \partial \boldsymbol{y}$ be the Jacobian matrix of the tranformation. The transformation is called canonical if the matrix M satisfies the symplectic property*

$$M \mathbb{J} M^T = M^T \mathbb{J} M = \mathbb{J}.$$

It is straightforward to demonstrate that, if the trasformation $\boldsymbol{z} = \boldsymbol{z}(\boldsymbol{y})$ is canonical, the new variables $(\boldsymbol{Q}, \boldsymbol{P})$ satisfy Hamilton's equations for $H(\boldsymbol{z}) = \mathcal{H}(\boldsymbol{y}(\boldsymbol{z}))$.
It is easy to observe that the *Hamiltonian flow* defines a canonical mapping. Namely, given $(\boldsymbol{q}, \boldsymbol{p}) \in \mathcal{F}$ the evolution of the orbit with initial condition $(\boldsymbol{q}, \boldsymbol{p})$ along the Hamiltonian flow leads, after a time t, to the mapping $(\boldsymbol{q}_t, \boldsymbol{p}_t) = \phi^t_{\mathcal{H}}(\boldsymbol{q}, \boldsymbol{p})$ which is canonical.

The condition $M \mathbb{J} M^T = \mathbb{J}$ can be reformulated as follows: a transformation $(\boldsymbol{q}, \boldsymbol{p}) = \mathscr{C}(\boldsymbol{Q}, \boldsymbol{P})$ is canonical if and only if it preserves the fundamental Poisson brackets, i.e. if the following are satisfyied

$$\{\boldsymbol{q}_i, \boldsymbol{q}_j\}_{(\boldsymbol{Q}, \boldsymbol{P})} = \{\boldsymbol{p}_i, \boldsymbol{p}_j\}_{(\boldsymbol{Q}, \boldsymbol{P})} = 0, \qquad \{\boldsymbol{q}_i, \boldsymbol{p}_j\}_{(\boldsymbol{Q}, \boldsymbol{P})} = \delta_{ij},$$

with $1 \leq i, j \leq n$ and δ_{ij} the Kronecker symbol.

In order to explicitly construct a canonical transformation, it is useful to construct a *generating function* S according to:

Proposition 1.1.4. *If we have a function $\mathcal{S}(\boldsymbol{p}, \boldsymbol{Q})$ such that* $\det \left(\dfrac{\partial^2 \mathcal{S}}{\partial p_j \partial Q_k} \right)_{1 \leq j, k \leq n} \neq 0$, *then the transformation*

$$\boldsymbol{P} = \frac{\partial \mathcal{S}}{\partial \boldsymbol{Q}}, \qquad \boldsymbol{q} = \frac{\partial \mathcal{S}}{\partial \boldsymbol{p}}$$

is canonical.

Analogous formulas yielding canonical transformations can be derived also in the case in which the generating function $\mathcal{S}$ has a different dependence on the variables. In particular, we say that $\mathcal{S}$ is of

- 1 *class*, if it depends on the old and new coordinates, i.e. $\mathcal{S}(\boldsymbol{q}, \boldsymbol{Q})$;
- 2 *class*, if it depends on the old coordinates and new momenta, i.e. $\mathcal{S}(\boldsymbol{q}, \boldsymbol{P})$;
- 3 *class*, if it depends on the old momenta and new coordinates, i.e. $\mathcal{S}(\boldsymbol{p}, \boldsymbol{Q})$;
- 4 *class*, if it depends on the old and new momenta, i.e. $\mathcal{S}(\boldsymbol{p}, \boldsymbol{P})$.

1.1.3 Lie series

In canonical perturbation theory a crucial role is played by canonical transformations *near to the identity*. A convenient method to obtain such a tranformations is the method of Lie series.

Definition 1.1.5. *Given $\chi \in \mathcal{C}^\infty(\mathcal{F})$ and ε real, we call Lie series operator the exponential operator of εL_χ , i.e.*

$$\exp\left(\varepsilon L_\chi\right) \cdot = \sum_{j\geq 0} \frac{\varepsilon^j}{j!} L_\chi^j \cdot .$$

Remembering that $\dot{f} = \{f, \mathcal{H}\}$, and performing a Taylor series expansion, it is easy to prove that, for any function $f \in \mathcal{C}^\infty(\mathcal{F})$ we have $f(\boldsymbol{q}(t), \boldsymbol{p}(t)) = \exp\left(tL_\mathcal{H}\right) f(\boldsymbol{q}(0), \boldsymbol{p}(0))$; this means that the Lie series map the function from its initial value in $t = 0$ to its value at time t, along the Hamiltonian flow. Then, taking as function f the canonical coordinates, we have that

$$(\boldsymbol{q}(\varepsilon), \boldsymbol{p}(\varepsilon)) = \phi_\mathcal{H}^\varepsilon(\boldsymbol{q}(0), \boldsymbol{p}(0)) = \left(\exp\left(\varepsilon L_\mathcal{H}\right) \boldsymbol{q}, \exp\left(\varepsilon L_\mathcal{H}\right) \boldsymbol{q}\right)\Big|_{\substack{\boldsymbol{q}=\boldsymbol{q}(0)\\ \boldsymbol{p}=\boldsymbol{p}(0)}}.$$

For ε small, the transformation

$$(\boldsymbol{q}, \boldsymbol{p}) \longmapsto \Big(\exp\left(\varepsilon L_\mathcal{H}\right) \boldsymbol{q}, \exp\left(\varepsilon L_\mathcal{H}\right) \boldsymbol{p}\Big)$$

is a canonical transformation near to the identity, i.e.

$$\left(\exp\left(\varepsilon L_\mathcal{H}\right) \boldsymbol{q}\,, \exp\left(\varepsilon L_\mathcal{H}\right) \boldsymbol{p}\right) - (\boldsymbol{q}, \boldsymbol{p}) = \mathcal{O}(\varepsilon)\,.$$

In practice, in Hamiltonian perturbation theory, we use the method of the Lie series to generate changes of coordinates of this form, i.e., given an appropriate generating function χ, we will consider $\exp(\varepsilon L_\chi)$. To this end, the following theorem will be useful:

Theorem 1.1.6. ***(Exchange)*** *Given $\chi, f \in \mathcal{C}^\infty(\mathcal{F})$, then*

$$f(\boldsymbol{q}, \boldsymbol{p})|_{\substack{\boldsymbol{q}=\exp(\varepsilon L_\chi)\widehat{\boldsymbol{q}}\\ \boldsymbol{p}=\exp(\varepsilon L_\chi)\widehat{\boldsymbol{p}}}} = \exp(\varepsilon L_\chi) f|_{\substack{\boldsymbol{q}=\widehat{\boldsymbol{q}}\\ \boldsymbol{p}=\widehat{\boldsymbol{p}}}}.$$

Theorem 1.1.6 establishes that, given a function f, the act of replacing 'old' variables with 'new' ones (obtained through the Lie series canonical transformation) is equivalent to acting directly on the function with the Lie series, and renaming, at the end, the 'old' variables as the 'new' ones.

1.2 Integrability

In the present Subsection we briefly recall the concept of integrability for Hamiltonian systems and we characterize the solutions of an integrable Hamiltonian. First, we need the following defintions:

Definition 1.2.1. *The function $f(\boldsymbol{q}, \boldsymbol{p})$ is called first integral of $\mathcal{H}$ if it is constant under the Hamiltonian flow, i.e.*

$$\dot{f} = \sum_{j=1}^{n} \left(\frac{\partial f}{\partial q_j}\frac{\partial \mathcal{H}}{\partial p_j} - \frac{\partial f}{\partial p_j}\frac{\partial \mathcal{H}}{\partial q_j}\right) = \{f, \mathcal{H}\} := L_\mathcal{H} f = 0\,.$$

An autonomous Hamiltonian is a first integral of its own flow, since $L_\mathcal{H}\mathcal{H} = 0$. Moreover, if f and g are first integrals of $\mathcal{H}$, then, by the Jacobi identity, $\{f, g\}$ is also a first integral for $\mathcal{H}$.

Definition 1.2.2. *The functions $f_1, \ldots, f_r \in \mathcal{C}^\infty(\mathcal{F})$ are called*

- *independent, if* $rank\left(\dfrac{\partial(f_1,\dots,f_r)}{\partial(q_1,\dots,q_n,p_1,\dots,p_n)}\right)=r$;
- *in involution, if* $\{f_i,f_j\}=0\ \ \forall\, i,\, j=1,\dots,r$.

In order to define the concept of integrability we need the following theorem:

Theorem 1.2.3. (Liouville) *Let* $\mathcal{H}:\mathcal{F}\to\mathbb{R}$ *be a* n*-degrees of freedom Hamiltonian with* n *first integrals* $f_1,\dots,f_n$ *independent and in involution. Then the system is integrable by quadrature.*

From now on by *integrability* we mean *Liouville integrability*. In order to characterize the solutions of an integrable system, the following theorem is essential:

Theorem 1.2.4. (Liouville-Arnold-Jost) *Let* $\mathcal{H}:\mathcal{F}\to\mathbb{R}$ *be a* n*-degrees of freedom Hamiltonian admiting* n *first integrals independent and in involution* $f_i:\mathcal{F}\to\mathbb{R}\ \ i=1,\dots,n$. *Assume there exists a compact and connected component* $M_{\boldsymbol{c}}$ *of the level set* $\{(\boldsymbol{q},\boldsymbol{p})\in\mathcal{F}\ :\ f_i(\boldsymbol{q},\boldsymbol{p})=c_i,\ i=1,\dots,n\}$, $\boldsymbol{c}=(c_1,\dots,c_n)\in\mathbb{R}^n$. *Then:*

- $M_{\boldsymbol{c}}$ *is diffeomorphic to the* n*-dim torus* $\mathbb{T}^n$*;*
- *in a neighbourhood* U *of* $M_{\boldsymbol{c}}$ *there exists a canonical transformation*

$$\begin{array}{rcl}\mathscr{C}:\mathcal{G}\times\mathbb{T}^n & \to & U\\ (\boldsymbol{I},\boldsymbol{\varphi}) & \mapsto & (\boldsymbol{p},\boldsymbol{q})\end{array}$$

with $\mathcal{G}\subseteq\mathbb{R}^n$ *an open set, such that the Hamiltonian takes the form* $\mathcal{H}\left(\mathscr{C}(\boldsymbol{I},\boldsymbol{\varphi})\right)=h(\boldsymbol{I})$.

The canonical variables $(\boldsymbol{I},\boldsymbol{\varphi})$ are called action-angle variables. The equations of motion in these variables are

$$\begin{cases}\dot{\varphi}_j=\dfrac{\partial h(\boldsymbol{I})}{\partial I_j}:=\omega_{0_j}(\boldsymbol{I})\\ \dot{I}_j=-\dfrac{\partial h(\boldsymbol{I})}{\partial\varphi_j}=0\end{cases}\qquad j=1,\dots,n. \tag{1.4}$$

Thus the orbits lie on n-dimensional tori, parametrized by the actions, with linear motions on $\mathbb{T}^n$, i.e. $t\mapsto\{(\boldsymbol{I},\boldsymbol{\varphi})\ :\ \boldsymbol{I}(t)=\boldsymbol{I}_0,\,\boldsymbol{\varphi}(t)=\boldsymbol{\varphi}_0+\boldsymbol{\omega}_0(\boldsymbol{I}_0)t\}$ are the solutions of (1.4). The motions are non-periodic, and are instead dense in $\mathbb{T}^n$, if the frequency vector $\boldsymbol{\omega}_0$ is *non-resonant*, i.e. $\boldsymbol{k}\cdot\boldsymbol{\omega}_0\neq 0\,\forall\,\boldsymbol{k}\in\mathbb{Z}^n\setminus\{\boldsymbol{0}\}$. In this case the motion is called quasi-periodic. In particular, if $n=2$, setting $\boldsymbol{\omega}_0=(\omega_1,\omega_2)$, the orbit is *periodic* if and only if $\omega_1/\omega_2\in\mathbb{Q}$; otherwise, the orbit is dense on $\mathbb{T}^2$. Also, it is useful to observe that, in a Poincaré section Σ , the linear flow on a torus yields a finite number of points, if the orbit is periodic, or a closed curve, if the orbit is quasi-periodic.

1.3 Near-integrability

In the previous section we have characterized the solutions of an integrable system. However most dynamical systems in nature are non integrable. The general *problem of dynamics*, described in (1.1), is defined by

$$\mathcal{H}(\boldsymbol{\varphi},\boldsymbol{I})=h(\boldsymbol{I})+\varepsilon\, f(\boldsymbol{\varphi},\boldsymbol{I})$$

whith action variables $\boldsymbol{I}\in\mathcal{G}\subset\mathbb{R}^n$ ($\mathcal{G}$ an open set), angle variables $\boldsymbol{\varphi}\in\mathbb{T}^n$ and ε a "small" parameter. The Hamiltonian (1.1) is called "nearly-integrable": it is composed by two terms, $h(\boldsymbol{I})$ and $\varepsilon\, f(\boldsymbol{\varphi},\boldsymbol{I})$. By the *Liouville-Arnold-Jost Theorem* 1.2.4 the first term $h(\boldsymbol{I})$ is integrable; thus for $\varepsilon=0$, the Hamiltonian is integrable and the motions are conjugated to linear flows on $\mathbb{T}^n$. However, the complete Hamiltonian $\mathcal{H}(\boldsymbol{\varphi},\boldsymbol{I})$ is "perturbed" by the presence of the term $\varepsilon\, f(\boldsymbol{\varphi},\boldsymbol{I})$. Thus, the question now is: if $\varepsilon\neq 0$, do there exist quasi-periodic solutions lying on invariant tori?

1.3.1 Kolmogorov-Arnold-Moser (KAM) theorem

An answer to the above question is given by the celebrated Kolmogorov-Arnold-Moser (KAM) Theorem, which states that, under suitable assumptions and if the size of the perturbation ε is 'small enough', the existence of invariant tori is ensured. Furthermore, these tori are deformations of those of the integrable case.

Theorem 1.3.1. (KAM (according to Kolmogorov)) *Consider a Hamiltonian function* $\mathcal{H} : \mathbb{T}^n \times \mathcal{G} \to \mathbb{R}$ *(where* $\mathcal{G} \subseteq \mathbb{R}^n$ *open) of the form* $\mathcal{H}(\boldsymbol{\varphi}, \boldsymbol{I}) = \boldsymbol{\omega}_0 \cdot \boldsymbol{I} + h(\boldsymbol{I}) + \varepsilon\, f(\boldsymbol{\varphi}, \boldsymbol{I})$ *where* $h(\boldsymbol{I}) = \mathcal{O}(||\boldsymbol{I}||^2)$ *for* $\boldsymbol{I} \to 0$ *.*
Assume the following hypotheses:

i. $\boldsymbol{\omega}_0$ *is Diophantine, i.e.* $\exists$ *two constants* $\gamma > 0$ *and* $\tau \geq n-1$ *s.t.* $|\boldsymbol{k} \cdot \boldsymbol{\omega}_0| \geq \gamma |\boldsymbol{k}|^{-\tau} \quad \forall\, \boldsymbol{k} \in \mathbb{Z}^n \setminus \{\boldsymbol{0}\}$;

ii. $\mathcal{H}$ *is analytic on* $\mathcal{G} \times \mathbb{T}^n$ *;*

iii. $h(\boldsymbol{I})$ *is non-degenerate, i.e.* $\det\left(\partial^2 h(\boldsymbol{I})/(\partial I_i \partial I_j)\right)_{i,j} \neq 0 \ \forall\, \boldsymbol{I} \in \mathcal{G}$ *;*

iv. ε *is a small parameter, i.e.* $\exists\, \varepsilon_\star > 0$ *s.t.* $|\varepsilon| \leq \varepsilon_\star$ *.*[2]

Then, there exists a canonical transformation $(\boldsymbol{\varphi}, \boldsymbol{I}) = \mathcal{C}_\varepsilon(\tilde{\boldsymbol{\varphi}}, \tilde{\boldsymbol{I}})$ *leading* $\mathcal{H}$ *in the so called Kolmogorov normal form, i.e.* $\mathcal{K}(\tilde{\boldsymbol{\varphi}}, \tilde{\boldsymbol{I}}) = \mathcal{H}\left(\mathcal{C}_\varepsilon(\tilde{\boldsymbol{\varphi}}, \tilde{\boldsymbol{I}})\right)$*, where* $\mathcal{K}(\tilde{\boldsymbol{\varphi}}, \tilde{\boldsymbol{I}}) = \boldsymbol{\omega}_0 \cdot \tilde{\boldsymbol{I}} + \mathcal{O}(||\tilde{\boldsymbol{I}}||^2)$ *.*

We can easily verify that if the Hamiltonian is in Kolmogorov normal form $\mathcal{K}(\tilde{\boldsymbol{\varphi}}, \tilde{\boldsymbol{I}}) = \boldsymbol{\omega}_0 \cdot \tilde{\boldsymbol{I}} + \mathcal{O}(||\tilde{\boldsymbol{I}}||^2)$, a solution for Hamilton's equations

$$\begin{cases} \dot{\tilde{\boldsymbol{\varphi}}} = \dfrac{\partial \mathcal{K}}{\partial \tilde{\boldsymbol{I}}} = \boldsymbol{\omega}_0 + \mathcal{O}(||\tilde{\boldsymbol{I}}||) \\ \dot{\tilde{\boldsymbol{I}}} = -\dfrac{\partial \mathcal{K}}{\partial \tilde{\boldsymbol{\varphi}}} = \mathcal{O}(||\tilde{\boldsymbol{I}}||^2) \end{cases}$$

is given by $t \to (\tilde{\boldsymbol{I}}(t) = \boldsymbol{0},\ \tilde{\boldsymbol{\varphi}}(t) = \tilde{\boldsymbol{\varphi}}(0) + \boldsymbol{\omega}_0 t)$.

Despite the fact that this formulation of KAM theorem gives the existence of a single invariant torus, it can be extended, ensuring the existence, for the perturbed Hamiltonian, of a set of invariant tori of large measure. In particular, remembering that if $\tau > n-1$ almost all the n-dimentional vectors $\boldsymbol{\omega}_0 \in \mathbb{R}^n$ belong to the set $\mathcal{D}_\gamma = \cup_{\gamma>0}\{\boldsymbol{\omega}_0 \in \mathbb{R}^n : |\boldsymbol{k} \cdot \boldsymbol{\omega}_0| \geq \gamma |\boldsymbol{k}|^{-\tau}\ \forall \boldsymbol{k} \neq \boldsymbol{0}\}$, i.e., they are diophantine, and that the so-called action-frequency map $\tilde{\boldsymbol{I}} \mapsto \boldsymbol{\omega}_0(\tilde{\boldsymbol{I}})$ is a local bijection (from the non-degeneracy of h), it is possible to prove the following:

Corollary 1.3.2. (KAM (according to Arnold)) *Consider a Hamiltonian* $\mathcal{H} : \mathbb{T}^n \times \mathcal{G} \longrightarrow \mathbb{R}$ *(where* $\mathcal{G} \subseteq \mathbb{R}^n$ *open) of the form* $\mathcal{H}(\boldsymbol{\varphi}, \boldsymbol{I}) = h(\boldsymbol{I}) + \varepsilon\, f(\boldsymbol{\varphi}, \boldsymbol{I})$*. Assume the hypotheses ii-iv of the previous Theorem 1.3.1. Then there is a set* $\mathcal{S}_\varepsilon$ *that is made by invariant tori and s.t. its Lebesque measure* $\mu(\mathcal{S}_\varepsilon) > 0$*. Moreover,* $\lim_{\varepsilon \to 0} \mu\left((\mathcal{G} \times \mathbb{T}^n) \setminus \mathcal{S}_\varepsilon\right) = 0$*.*

This means that a set of large measure in the phase space $\mathcal{G} \times \mathbb{T}^n$ is filled by invariant tori hosting quasi-periodic motions. In fact, the measure of the set increases as ε decreases. For further details see [47], [71] (and the references theirein) and [4].

[2] The definition of this ε is quite complicated and it depends on different parameters. It's definition is explicitly given during the proof of the theorem.

1.3.1.1 Normalization procedure

The KAM theorem is an example of *convergent normalization procedure*; in particular, we pass from a pertubed Hamiltonian, of which we do not control the dynamics, to a 'normal form' (the Kolmogorov one), of which we can characterize a particular solution. In general, the goal of canonical perturbation theory can be stated as follows: consider a Hamiltonian of the form

$$\mathcal{H}(\boldsymbol{\varphi}, \boldsymbol{I}) = Z_0(\boldsymbol{\varphi}, \boldsymbol{I}) + \varepsilon f(\boldsymbol{\varphi}, \boldsymbol{I}),$$

where Z_0, called the *normal form* term, is a term of which we have a control of the dynamics (for example, it can be integrable $Z_0(\boldsymbol{\varphi}, \boldsymbol{I}) = Z_0(\boldsymbol{I})$ (and we know that the solutions are linear on invariant tori), or it can be in Kolmogorov normal form (and we know a particular solution that is the torus $\{(\boldsymbol{\varphi}, \boldsymbol{I}) : \boldsymbol{I}(t) = \boldsymbol{0}, \boldsymbol{\varphi}(t) = \boldsymbol{\varphi}(0) + \boldsymbol{\omega} t)\}$), and so on). Now, applying a normalization procedure means to apply a sequence of r canonical transformations

$$\tilde{\mathscr{C}}^{(r)} : (\boldsymbol{\varphi}, \boldsymbol{I}) := (\boldsymbol{\varphi}^{(0)}, \boldsymbol{I}^{(0)}) \overset{\mathscr{C}^{(1)}}{\to} (\boldsymbol{\varphi}^{(1)}, \boldsymbol{I}^{(1)}) \overset{\mathscr{C}^{(2)}}{\to} \ldots\ldots \overset{\mathscr{C}^{(r)}}{\to} (\boldsymbol{\varphi}^{(r)}, \boldsymbol{I}^{(r)}),$$

such that, after r steps we arrive at new coordinates $(\boldsymbol{\varphi}^{(r)}, \boldsymbol{I}^{(r)})$ and at a 'new' Hamiltonian $\mathcal{H}^{(r)}$

$$\mathcal{H}^{(r)}(\boldsymbol{\varphi}^{(r)}, \boldsymbol{I}^{(r)}) = \mathcal{H}\left(\boldsymbol{\varphi}(\boldsymbol{\varphi}^{(r)}, \boldsymbol{I}^{(r)}), \boldsymbol{I}(\boldsymbol{\varphi}^{(r)}, \boldsymbol{I}^{(r)})\right) = \mathcal{H}\left(\tilde{\mathscr{C}}^{(r)^{-1}}(\boldsymbol{\varphi}^{(r)}, \boldsymbol{I}^{(r)})\right)$$

of the form

$$\mathcal{H}^{(r)}(\boldsymbol{\varphi}^{(r)}, \boldsymbol{I}^{(r)}) = \underbrace{Z^{(r)}(\boldsymbol{\varphi}^{(r)}, \boldsymbol{I}^{(r)})}_{Normal\ form\ term} + \underbrace{R^{(r)}(\boldsymbol{\varphi}^{(r)}, \boldsymbol{I}^{(r)})}_{Remainder}.$$

As before, $Z^{(r)}(\boldsymbol{\varphi}^{(r)}, \boldsymbol{I}^{(r)})$, called the *normal form*, is a term of which we control the dynamics, while $R^{(r)}(\boldsymbol{\varphi}^{(r)}, \boldsymbol{I}^{(r)})$, called the *remainder*, is a term describing how the real dynamics differs from the one of $Z^{(r)}$.
The normalization procedure can be of different types:[3]

- If $\lim_{r\to\infty} ||R^{(r)}|| = 0$ we have a **convergent** normalization procedure (e.g. KAM);
- If $\lim_{r\to\infty} ||R^{(r)}|| = \infty$ and $\exists\, r_{opt}$, called the optimal normalization order, such that $||R^{(r)}||$ as a function of r has a global minimum at $r = r_{opt}$, we have an **asymptotic** normalization procedure (e.g. Birkhoff normal form).

By these two types of methods we can establish various results concerning the stability of the orbits. For example, in the case of KAM theorem, we can take the initial conditions (for the actions) in a Cantor set and establish 'perpetual' stability, in the sense that orbits with initial conditions on the torus remain always on that torus. Instead, in the case of the *Birkhoff normal form* (see [31]), the initial values for the initial actions are taken in an open set and we can state only an asymptotic result of stability, such as:

Theorem 1.3.3. (Nekhoroshev) *Let $\mathcal{H}(\boldsymbol{\varphi}, \boldsymbol{I}) = h(\boldsymbol{I}) + \varepsilon f(\boldsymbol{\varphi}, \boldsymbol{I})$ analytic on the domain $\mathcal{G} \times \mathbb{R}^n$ where $\mathcal{G} \subset \mathbb{R}^n$ open and s.t. the imperturbed part $h(\boldsymbol{I})$ is convex[4], i.e.*

$$|\langle C(\boldsymbol{I})\, \boldsymbol{v}, \boldsymbol{v}\rangle| \geq m||\boldsymbol{v}||^2 \quad \forall\, \boldsymbol{v} \in \mathbb{R}^n, \quad C_{jk} = \frac{\partial^2 h}{\partial \varphi_j \partial \varphi_k}\,.$$

Then, for ε sufficiently small, it holds the following: for every orbit with initial value $(\boldsymbol{I}_0, \boldsymbol{\varphi}_0) \in \mathcal{G} \times \mathbb{T}^n$, one has

$$|\boldsymbol{I}(t) - \boldsymbol{I}_0| \leq \varepsilon^b \quad \forall\, t \quad \text{s.t.} \quad |t| \leq T(\varepsilon) \sim \exp(1/\varepsilon^a)\,,$$

for suitable positive values of $a < 1$ and $b < 1$.

[3] $||R^{(r)}||$ is a norm whose definition depends on the domain in which we define the normalization method. For example, in the KAM Theorem, the domains are a complexification of $\mathcal{G} \times \mathbb{T}^n$ and the used norms are the so called *weighted Fourier norms*. (See, for example, [31]).

[4] It is possible to substitute the convexity condition with other conditions, such as the quasi-convexity, or the 'steepness' condition. (See [95]).

The Nekhoroshev theorem guarantees stability of the actions in timescales which, albeit finite, are exponentially long in the inverse of the small parameter ε.

1.4 The secular Hamiltonian of the planetary 3-body problem

1.4.1 The Hamiltonian of the 3-body problem

In a barycentric inertial reference frame the planetary 3-body problem (i.e. two planets (point masses P_1 and P_2) orbiting around a star (point mass P_0) under the effect of the gravitational force) is governed by the following Hamiltonian

$$\mathcal{H} = \frac{\tilde{\boldsymbol{u}}_0^2}{2m_0} + \frac{\tilde{\boldsymbol{u}}_1^2}{2m_1} + \frac{\tilde{\boldsymbol{u}}_2^2}{2m_2} - \frac{\mathcal{G}\, m_0\, m_1}{\Delta_{01}} - \frac{\mathcal{G}\, m_0\, m_2}{\Delta_{02}} - \frac{\mathcal{G}\, m_1\, m_2}{\Delta_{12}}\,, \tag{1.5}$$

with m_i the mass of the i-th body, $\Delta_{ij} = |\boldsymbol{u}_i - \boldsymbol{u}_j|$ $(0 \le i < j \le 2)$ with $\boldsymbol{u}_i$ the position of the i-th body with respect to the system's barycenter B and $\tilde{\boldsymbol{u}}_i$ the conjugate momentum vector (see Figure 1.1).

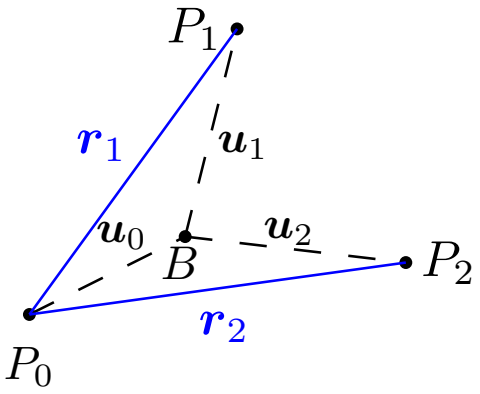

Figure 1.1: Representation of the baricentric reference frame, with the system's barycenter B at the origin (in black): $\boldsymbol{u}_i$ represents the position vector of the i-th body with respect to B $(i = 0,\, 1,\, 2\,)$. The heliocentric reference frame, with the star P_0 at the origin (in blue): $\boldsymbol{r}_i$ represents the position of the i-th body with respect to the star P_0 $(i = 1,\, 2\,)$.

It is possible to pass from the barycentric reference frame $(\boldsymbol{u}, \tilde{\boldsymbol{u}})$ to a heliocentric reference frame (i.e., with the star placed in the origin) $(\boldsymbol{r}, \boldsymbol{p})$ through the generating function

$$\mathcal{S}(\boldsymbol{u}_0, \boldsymbol{u}_1, \boldsymbol{u}_2, \boldsymbol{p}_0, \boldsymbol{p}_1, \boldsymbol{p}_2) = \boldsymbol{u}_0 \cdot \boldsymbol{p}_0 + \sum_{i=1}^{2} (\boldsymbol{u}_i - \boldsymbol{u}_0) \cdot \boldsymbol{p}_i\,,$$

yielding (from Lemma 1.1.4) the following canonical change of coordinates:

$$\boldsymbol{r}_0 = \boldsymbol{u}_0\,, \quad \boldsymbol{r}_i = \boldsymbol{u}_i - \boldsymbol{u}_0\,, \quad \boldsymbol{p}_0 = \tilde{\boldsymbol{u}}_0 + \tilde{\boldsymbol{u}}_1 + \tilde{\boldsymbol{u}}_2\,, \quad \boldsymbol{p}_i = \tilde{\boldsymbol{u}}_i \qquad i = 1, 2\,. \tag{1.6}$$

From the above change of coordinates, some properties arise:

i) The canonical coordinates $\boldsymbol{r}_0 = \boldsymbol{u}_0$ are ignorable, thus the corresponding momentum $\boldsymbol{p}_0$ is conserved. Physically, the momentum vector $\boldsymbol{p}_0$ is the sum of all the barycentric momenta vectors. As well known, the center of mass remains stationary or in constant rectilinear motion. Thus, without loss of generality, we can put $\boldsymbol{p}_0 = \boldsymbol{0}$. Then, the Hamiltonian is reduced to six degrees of freedom $(\boldsymbol{r}_1,\, \boldsymbol{p}_1)\,,\, (\boldsymbol{r}_2,\, \boldsymbol{p}_2)$; while it is possible to recover the motion of the star by the relation $\sum_{i=0}^{2} m_i \boldsymbol{u}_i = 0$, i.e. $\boldsymbol{r}_0 = -(m_1\boldsymbol{r}_1 + m_2\boldsymbol{r}_2)/(m_0 + m_1 + m_2)$.

ii) The angular momentum vector $\boldsymbol{L} = \boldsymbol{r}_1 \times \boldsymbol{p}_1 + \boldsymbol{r}_2 \times \boldsymbol{p}_2$ is an exact first integral also in the heliocentric reference frame. Indeed, starting from the preservation of the angular momentum

vector $\boldsymbol{L} = \boldsymbol{u}_0 \times \tilde{\boldsymbol{u}}_0 + \boldsymbol{u}_1 \times \tilde{\boldsymbol{u}}_1 + \boldsymbol{u}_2 \times \tilde{\boldsymbol{u}}_2$ in the barycentric reference frame, we find (by Eq. (1.6) and setting $\boldsymbol{p}_0 = \boldsymbol{0}$)

$$\begin{aligned}\boldsymbol{L} = \boldsymbol{u}_0 \times \tilde{\boldsymbol{u}}_0 + \boldsymbol{u}_1 \times \tilde{\boldsymbol{u}}_1 + \boldsymbol{u}_2 \times \tilde{\boldsymbol{u}}_2 &= \boldsymbol{r}_0 \times (\boldsymbol{p}_0 - \boldsymbol{p}_1 - \boldsymbol{p}_2) + (\boldsymbol{r}_1 + \boldsymbol{r}_0) \times \boldsymbol{p}_1 + (\boldsymbol{r}_2 + \boldsymbol{r}_0) \times \boldsymbol{p}_2 \\ &= \boldsymbol{r}_0 \times \boldsymbol{p}_0 + \boldsymbol{r}_1 \times \boldsymbol{p}_1 + \boldsymbol{r}_2 \times \boldsymbol{p}_2 = \boldsymbol{r}_1 \times \boldsymbol{p}_1 + \boldsymbol{r}_2 \times \boldsymbol{p}_2 \,.\end{aligned}$$

Setting $\boldsymbol{p}_0 = \boldsymbol{0}$, the Hamiltonian of the 3-body problem (1.5) in Poincaré heliocentric canonical variables is reduced to

$$\mathcal{H} = \underbrace{\frac{{\boldsymbol{p}_1}^2}{2\,m_1} - \frac{\mathcal{G}\,m_0\,m_1}{r_1} + \frac{{\boldsymbol{p}_2}^2}{2\,m_2} - \frac{\mathcal{G}\,m_0\,m_2}{r_2}}_{\textit{Keplerian part}} + \underbrace{\frac{(\boldsymbol{p}_1 + \boldsymbol{p}_2)^2}{2\,m_0}}_{\textit{"Indirect" part}} - \underbrace{\frac{\mathcal{G}\,m_1\,m_2}{|\boldsymbol{r}_1 - \boldsymbol{r}_2|}}_{\textit{"Direct" part}} \,. \tag{1.7}$$

The above formulation can be extended to the $(N+1)$-body problem (i.e. N bodies orbiting around a star under the effect of the gravitational force), giving rise to the Hamiltonian

$$\mathcal{H} = \sum_{j=1}^{N} \left(\frac{\boldsymbol{p}_j^2}{2m_j} - \frac{\mathcal{G}\,m_0\,m_j}{r_j} \right) + \sum_{1 \le i < j \le N} \frac{(\boldsymbol{p}_i + \boldsymbol{p}_j)^2}{2m_0} - \sum_{1 \le i < j \le N} \frac{\mathcal{G}\,m_i\,m_j}{\Delta_{ij}} \,, \tag{1.8}$$

where $\boldsymbol{r}_i$ is the heliocentric position vector of the i-th planet orbiting the star, $\boldsymbol{p}_i$ the conjugate momenta (relative to the barycentre of the $(N+1)$-body system), and $\Delta_{ij} = ||\boldsymbol{r}_i - \boldsymbol{r}_j||$. Another useful way to write the same Hamiltonian is

$$\mathcal{H} = \sum_{j=1}^{N} \left(\frac{\boldsymbol{p}_j^2}{2\beta_j} - \frac{\mathcal{G}\,m_0\,m_j}{r_j} \right) + \sum_{1 \le i < j \le N} \frac{\boldsymbol{p}_i \cdot \boldsymbol{p}_j}{m_0} - \sum_{1 \le i < j \le N} \frac{\mathcal{G}\,m_i\,m_j}{\Delta_{ij}} \,, \tag{1.9}$$

where $\beta_j = m_0 m_j/(m_0 + m_j)$ $j = 1, \ldots, N$ is called the *reduced mass* of the j-th body. For the purpose of the present thesis, use is made of both the two formulations above of the Hamiltonian (i.e. Eq. (1.8) and (1.9)). This is motivated by the need to adopt the formulation to past literature on each treated subject. However, all formulations are essentially equivalent. Indeed, they affect only the definition of the action variables $\boldsymbol{L}$ (see Eq. (1.19)) where $L_j = \beta_j \sqrt{\mu_j a_j}$ $j = 1, \ldots N$; in the first case (Eq. (1.8)) the constants β_j and μ_j are defined as $\beta_j = m_j$ and $\mu_j = \mathcal{G}m_0$. Instead, in the second one (Eq. (1.9)) $\beta_j = m_0 m_j/(m_0 + m_j)$ and $\mu_j = \mathcal{G}(m_0 + m_j)$. Since we are interested in expansions of the Hamiltonian at order one in the masses, both choices are possible, producing only a difference in the Keplerian constant term.

In order to simplify the notation, in the rest of the thesis we adopt the following convention for the indices i, j: the representative example chosen for concrete applications of the various perturbative methods discussed in the thesis is the υ-Andromedae system. This is a double star system with four planets (υ-And **b**, υ-And **c**, υ-And **d** and υ-And **e**) orbiting one of the stars. Since the masses of m_b and m_e are much smaller than m_c, m_d, the motion of the innermost planet υ-And **b** can be modeled to a good approximation via a restricted four-body problem (with planets υ-And **c**, υ-And **d** providing the main perturbations), or more detailed models including planet υ-And **e** and the second star.[5] Such models, however, require providing first a good analytical model for the orbits of the giant planets of the system, say, for example, the planets υ-And **c** and υ-And **d**, whose masses are available larger than $10 M_J$ (see Table 1.1).

In the rest of the thesis, the indices $i = 1, 2, 3$ refer, respectively, to the planets υ-And **b**, υ-And **c** and υ-And **d**; thus, for simplicity, the 3-body problem Hamiltonian describing the motion of υ-And **c** and υ-And **d** around the star is written in the sequel as:

$$\mathcal{H} = \underbrace{\frac{{\boldsymbol{p}_2}^2}{2\,m_2} - \frac{\mathcal{G}\,m_0\,m_2}{r_2} + \frac{{\boldsymbol{p}_3}^2}{2\,m_3} - \frac{\mathcal{G}\,m_0\,m_3}{r_3}}_{\textit{Keplerian part}} + \underbrace{\frac{(\boldsymbol{p}_2 + \boldsymbol{p}_3)^2}{2\,m_0}}_{\textit{"Indirect" part}} - \underbrace{\frac{\mathcal{G}\,m_2\,m_3}{|\boldsymbol{r}_2 - \boldsymbol{r}_3|}}_{\textit{"Direct" part}} \,, \tag{1.10}$$

[5] The second star, called υ-And B, is a low-mass stellar companion of υ-And A. The companion shares common proper motion with the primary star, lies at a projected separation of ~ 750 AU, and has a spectral type of $M4.5$ V (see [74]).

	Mass and elliptic elements	References		
		McArthur et al 2010 ([78])	Deitrick et al 2015 ([18])	Locatelli et al 2022 ([71])
υ-And **c**	$m\,[M_J]$	$13.98^{+2.3}_{-5.3}$	–	15.9792
	$a(0)\,[AU]$	0.829 ± 0.043	–	0.829
	e(0)	0.245 ± 0.006	0.2445	0.239
	i(0) [°]	7.868 ± 1.003	11.347	6.865
	$M(0)$ [°]	–	–	355
	$\omega(0)$ [°]	247.659 ± 1.76	247.629	245.809
	$\Omega(0)$ [°]	236.853 ± 7.528	248.181	229.325
υ-And **d**	$m\,[M_J]$	$10.25^{+0.7}_{-3.3}$	–	9.9578
	$a(0)\,[AU]$	2.53 ± 0.014	–	2.53
	e(0)	0.316 ± 0.006	0.316	0.31
	i(0) [°]	23.758 ± 1.316	25.609	25.074
	$M(0)$ [°]	–	–	335
	$\omega(0)$ [°]	252.991 ± 1.311	252.991	254.302
	$\Omega(0)$ [°]	4.073 ± 3.301	11.425	7.374

Table 1.1: Possible values of the masses and of the initial orbital parameters for υ-And **c** and υ-And **d**, according to (from left to right): Table 13 of [78], Table 1 of [18] and Figure 5 of [71]. As reported in section 2.2.3.2, in Chapters 2 and 3 we adopt m_j and a_j according to [78] and e_j , i_j , ω_j , Ω_j according to [18] ($j = 2, 3$). Instead, in Chapter 4, where a particular 'robust' quasi-periodic orbit is required, we adopt m_j , a_j , e_j , i_j , ω_j , Ω_j as in [71] ($j = 2, 3$) (see section 4.2, Table 4.1).

i.e., as in Eq. (1.7) with indices $i, j = 2, 3$ instead of $i, j = 1, 2$.

1.4.2 Orbital elements

The Keplerian osculating *orbital elements* are quantities used to describe i) the geometrical properties of the instantaneous orbital ellipse corresponding to the motion of a point mass with canonical coordinates and momenta $(\boldsymbol{r}, \boldsymbol{p})$ in absence of any perturbation besides the gravity of the central mass, ii) the ellipse's orientation in space, and iii) the instantaneous position of the point mass on the ellipse.
The shape of the ellipse is completely determined by the *semimajor axes* a and by the *eccentricity* e . In order to locate the position of the celestial body m on the ellipse, we determine an orthogonal reference frame (X, Y) (called *orbital plane*) with origin at the position of the central body m_0 (located at one focus of the ellipse) and the X axis oriented towards the pericenter of the orbit. We then introduce the polar coordinates (r, f) , where r is the distance between m_0 and m and the polar angle f is called *true anomaly*. It is convenient to define also the new angle, E , called the *eccentric anomaly*, subtended at the center of the ellipse by the projection of the position of the body on the circle with radius a and tangent to the ellipse at pericenter and apocenter (Figure 1.2). We then have the relations

$$\cos f = \frac{\cos E - \mathrm{e}}{1 - \mathrm{e}\,\cos E}\,, \qquad \sin f = \frac{\sqrt{1-\mathrm{e}^2}\,\sin E}{1 - \mathrm{e}\,\cos E}\,, \qquad r = a\,(1 - \mathrm{e}\,\cos E)\,. \tag{1.11}$$

The position in the (X, Y) orbital plane is given by

$$\mathrm{X} = r\,\cos f\,, \qquad\qquad \mathrm{Y} = r\,\sin f \quad , \tag{1.12}$$

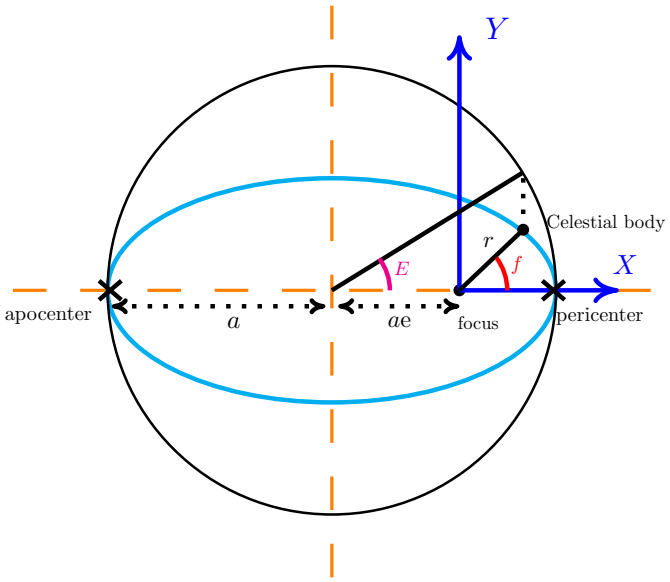

Figure 1.2: Representation of the Keplerian motion. The ellipse is defined through the semimajor axis a and the eccentricity e. The angles E and f are the eccentric and true anomalies.

or

$$\mathrm{X} = a\,(\cos E - \mathrm{e})\;, \qquad\qquad \mathrm{Y} = a\sqrt{1-\mathrm{e}^2}\,\sin E\quad .$$

The eccentric anomaly E is connected to the *mean anomaly*

$$M = n(t - t_0)\,, \tag{1.13}$$

t_0 = time of passage from the pericenter, where

$$n = \frac{\sqrt{\mathcal{G}(m_0 + m)}}{a^{3/2}} \tag{1.14}$$

is the orbital frequency or *mean motion*, by *Kepler's equation*

$$E - \mathrm{e}\sin E = M\,.$$

The solution of Kepler's equation, giving the one-to-one corrispondence between E and M, takes the form

$$E = M + 2\sum_{s=1}^{+\infty} \frac{1}{s}\, J_s(s\,\mathrm{e})\,\sin(sM)\,, \tag{1.15}$$

where J_s are Bessel functions.

In order to characterize the position and orientation of the ellipse in space with respect to an arbitrary orthogonal reference frame (x, y, z) centered on the position of the central body, let i be the angle of inclination of the orbital plane with respect to the reference plane (x, y). If $\mathrm{i} \neq 0$, the orbital plane (X, Y) intersects the reference plane (x, y) at the *line of the nodes* and the orbit intersects the plane (x, y) at the *ascening node*, where the celestial body passes from negative to positive values of z, and the *descending node*, from positive to negative values of z. The *longitude of node* Ω represents the angular position of the ascending node measured from the x axis. Finally the *argument of pericenter* ω gives the angular position of the pericenter with respect to the line of nodes, measured from the ascending node.

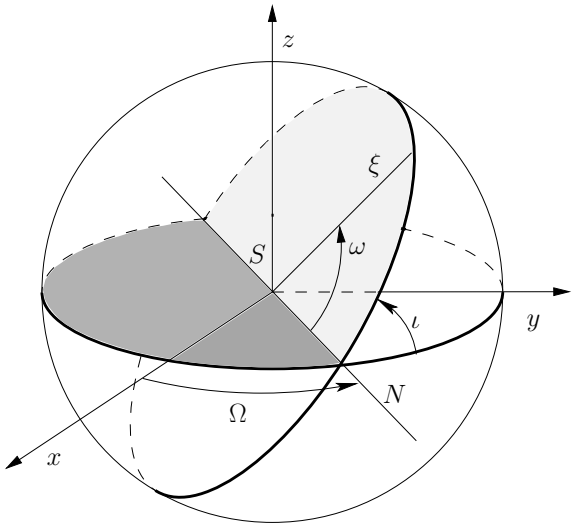

Figure 1.3: Orbital motion with respect to the reference plane (x, y) in three-dimensional space. The ascending node is denoted by the label N. The direction of the pericenter is denoted with the symbol ξ. This figure can be found in [31].

The set $(a\,, \mathrm{e},\, \mathrm{i},\, \omega,\, \Omega,\, M)$ is known as *orbital elements* (Figure 1.3). The correspondence between positions and velocities $(x, y, z, \dot{x}, \dot{y}, \dot{z})$ and orbital elements is given by the relations

$$\begin{pmatrix} x \\ y \\ z \end{pmatrix} = P_3 P_2 P_1 \begin{pmatrix} r\cos f \\ r\sin f \\ 0 \end{pmatrix}, \qquad \begin{pmatrix} \dot{x} \\ \dot{y} \\ \dot{z} \end{pmatrix} = P_3 P_2 P_1 \begin{pmatrix} \dot{r}\cos f - r\sin f\,\dot{f} \\ \dot{r}\sin f + r\cos f\,\dot{f} \\ 0 \end{pmatrix},$$

where

$$P_1 = \begin{pmatrix} \cos\omega & -\sin\omega & 0 \\ \sin\omega & \cos\omega & 0 \\ 0 & 0 & 1 \end{pmatrix}, \quad P_2 = \begin{pmatrix} 1 & 0 & 0 \\ 0 & \cos\mathrm{i} & -\sin\mathrm{i} \\ 0 & \sin\mathrm{i} & \cos\mathrm{i} \end{pmatrix}, \quad P_3 = \begin{pmatrix} \cos\Omega & -\sin\Omega & 0 \\ \sin\Omega & \cos\Omega & 0 \\ 0 & 0 & 1 \end{pmatrix}. \tag{1.16}$$

The derivatives $\dot{r}\,,\ \dot{f}$ can be computed through the chain rule $d/dt = n\, d/dM$ (see [87], [86], [31] for details).

However, in the cases $\mathrm{i} = 0$ or/and $\mathrm{e} = 0$ the set of the orbital parameters $(a\,, \mathrm{e},\, \mathrm{i},\, \omega,\, \Omega,\, M)$ is not completely well defined; in order to avoid this inconsistency, it is convenient to introduce an alternative set of orbital elements (completely defining the position and velocity of the body). More precisely, if $\mathrm{i} = 0$ the angles $\omega\,,\ \Omega$ are not well defined, since the position of the ascending node is not determined. If $\mathrm{e} = 0\,,\ M$ is not well defined (the position of the pericenter is not determined). Thus, it is convenient to introduce two new angles: the *longitude of the pericenter*

$$\varpi = \omega + \Omega\,, \tag{1.17}$$

is well defined in the case $\mathrm{i} = 0\,,\ \mathrm{e} \neq 0\,.$ The *mean longitude*

$$\lambda = M + \varpi \tag{1.18}$$

is well defined in the case $\mathrm{e} = 0$ for all values of $\mathrm{i}\,.$

1.4.3 Delaunay and Poincaré variables

A convenient set of action-angle variables, stemming from the application of the Arnold-Liouville theorem to the integrable Hamiltonian of the 2-body problem are the *Delaunay variables*, defined as

$$\begin{aligned} L &= \beta\sqrt{\mu\, a}\,, & l &= M\,, \\ G &= L\sqrt{1-\mathrm{e}^2}\,, & g &= \omega\,, \\ H &= G\cos\mathrm{i}\,, & h &= \Omega\,, \end{aligned} \tag{1.19}$$

where the constants β, μ can be defined either as $\beta = m_0 m/(m_0+m)$ (reduced mass), $\mu = \mathcal{G}(m_0+m)$, or as $\beta = m$, $\mu = \mathcal{G}m_0$. In order to deal with cases in which the angles l, g and h are not well defined, it is convenient to introduce also the *modified Delaunay variables*, given by

$$\begin{aligned} &\Lambda = L = \beta\sqrt{\mu\, a}\,, && \lambda = l+g+h = M+\varpi\,,\\ &\Gamma = L-G = \Lambda\left(1-\sqrt{1-\mathrm{e}^2}\right), && \gamma = -g-h = -\varpi\,,\\ &\Theta = G-H = \Lambda\sqrt{1-\mathrm{e}^2}\,(1-\cos\mathrm{i})\,, && \theta = -h = -\Omega\,. \end{aligned} \tag{1.20}$$

The variables $(\Lambda, \Gamma, \Theta)$ gives information, respectively, on the semimajor axes, the eccentricity and the inclination. In particular, for small eccentricities and inclinations we have $\Gamma = \mathcal{O}(\mathrm{e}^2)$ and $\Theta = \mathcal{O}(\mathrm{i}^2)$. The angles γ and θ are not well defined when Γ or Θ are equal to zero (i.e. in the cases $\mathrm{e}=0$ or $\mathrm{i}=0$). To address this problem, it is convenient to define a canonical set of variables, called *Poincaré variables*, described by

$$\begin{aligned} &\eta = \sqrt{2\Gamma}\sin\gamma\,, && \xi = \sqrt{2\Gamma}\cos\gamma\,,\\ &Q = \sqrt{2\Theta}\sin\theta\,, && P = \sqrt{2\Theta}\cos\theta\,, \end{aligned} \tag{1.21}$$

with η and Q the new coordinates, and ξ and P their conjugate momenta. Alternatively, we can use the following set of *Poincaré variables*

$$\begin{aligned} &\mathcal{X} = -\sqrt{2\Gamma}\cos\gamma\,, && \mathcal{Y} = \sqrt{2\Gamma}\sin\gamma\,,\\ &\mathcal{Q} = -\sqrt{2\Theta}\cos\theta\,, && \mathcal{P} = \sqrt{2\Theta}\sin\theta\,, \end{aligned} \tag{1.22}$$

with $\mathcal{X}$ and $\mathcal{Q}$ the new coordinates, and $\mathcal{Y}$ and $\mathcal{P}$ their conjugate momenta.

1.4.4 The Laplace reference frame

The Laplace reference frame is an invariant reference frame (x,y,z) defined so that the plane (x,y) ('Laplace plane') is orthogonal to the total angular momentum vector $\boldsymbol{L} = \boldsymbol{r}_2\times\boldsymbol{p}_2 + \boldsymbol{r}_3\times\boldsymbol{p}_3$. In this new frame the invariance $\Omega_3 - \Omega_2 = \pi$ holds, i.e. the ascending nodes of the two planets are opposite one to the other; this is a consequence of the fact that the projection of the angular momentum vectors of the two planets (in the Laplace plane) are equal in modulo and opposite. In summary, setting (x,y,z) to be the Laplace reference plane, we have the following relations:

$$\begin{cases} \Omega_3 - \Omega_2 = \pi\,,\\ L_z = const := C\,,\\ L_x = L_y = 0\,. \end{cases} \tag{1.23}$$

Observing that the Delaunay coordinate G (introduced in (1.19)) coincides with the modulus of the angular momentum vector of the Keplerian orbit, Eqs. (1.23) lead to the following relation in *Delaunay variables*

$$\begin{cases} \Omega_3 - \Omega_2 = \pi\,,\\ G_2\cos\mathrm{i}_2 + G_3\cos\mathrm{i}_3 = H_2 + H_3 = C\,,\\ G_2\sin\mathrm{i}_2 - G_3\sin\mathrm{i}_3 = 0\,. \end{cases} \tag{1.24}$$

It is convenient to express the previous relations also in *modified Delaunay variables* (introduced in (1.20)):

$$\begin{cases} \Omega_3 - \Omega_2 = \pi\,,\\ \Lambda_2 - \Gamma_2 - \Theta_2 + \Lambda_3 - \Gamma_3 - \Theta_3 = C\,,\\ 2\,(\Lambda_2-\Gamma_2)\,\Theta_2 - \Theta_2^2 = 2\,(\Lambda_3-\Gamma_3)\,\Theta_3 - \Theta_3^2\,, \end{cases} \tag{1.25}$$

where the last relation is found by setting $L_{2_x}^2 + L_{2_y}^2 = L_{3_x}^2 + L_{3_y}^2$.
In order to move from a randomly chosen inertial reference frame (x, y, z) to the Laplace reference frame, denoted with $(\widehat{x}, \widehat{y}, \widehat{z})$, it is sufficient to perform two rotations, by the angles Ω_R and i_R , defined as in Figure 1.4.

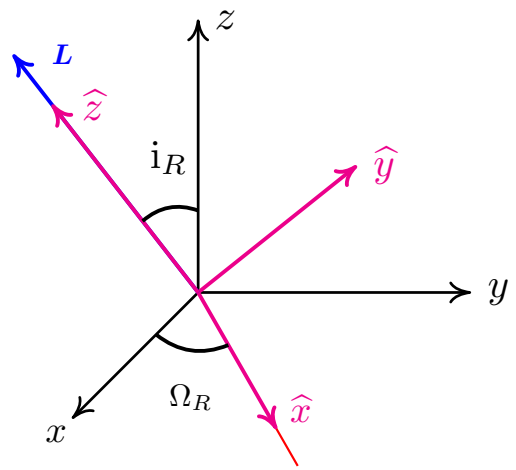

Figure 1.4: Representation of the Laplace reference frame $(\widehat{x}, \widehat{y}, \widehat{z})$. The $\widehat{z}$ and $\widehat{x}$ axes have the same direction, respectively, of the total angular momentum $\boldsymbol{L}$ (outlined in blue in the picture) and of the line of nodes, pointing toward the ascending node N (outlined in red).

More precisely

$$\begin{pmatrix} \widehat{x} \\ \widehat{y} \\ \widehat{z} \end{pmatrix} = P_{2,R}^{-1} P_{3,R}^{-1} \begin{pmatrix} x \\ y \\ z \end{pmatrix} ,$$

where, according to (1.16),

$$P_{2,R}^{-1} = \begin{pmatrix} 1 & 0 & 0 \\ 0 & \cos \mathrm{i}_R & \sin \mathrm{i}_R \\ 0 & -\sin \mathrm{i}_R & \cos \mathrm{i}_R \end{pmatrix} , \qquad P_{3,R}^{-1} = \begin{pmatrix} \cos \Omega_R & \sin \Omega_R & 0 \\ -\sin \Omega_R & \cos \Omega_R & 0 \\ 0 & 0 & 1 \end{pmatrix} .$$

The angles Ω_R and i_R can be found through the following relations:[6]

$$\Omega_R = sign(L_x) \arccos \left(\frac{-L_y}{\sqrt{L_x^2 + L_y^2}} \right) , \qquad \mathrm{i}_R = \arccos \left(\frac{L_z}{||\boldsymbol{L}||} \right) ,$$

where $(L_x, L_y, L_z) = \boldsymbol{L} = \boldsymbol{r}_2 \times \boldsymbol{p}_2 + \boldsymbol{r}_3 \times \boldsymbol{p}_3$ is the total angular momentum.[7] Thus, having determined the angles Ω_R and i_R it is possible to determine the positions and momenta $(\widehat{x}, \widehat{y}, \widehat{z}, p_{\widehat{x}}, p_{\widehat{y}}, p_{\widehat{z}})$ of the celestial body in the Laplace reference frame. Moreover, known the orbital parameters $(a\,, \mathrm{e},\, \mathrm{i},\, \omega,\, \Omega,\, M)$ with respect to an inertial reference frame (x, y, z) (introduced in

[6] In order to decide the direction of the rotations, we have to pay attention to the position of the total angular momentum vector in the space; if the y-component of the "rotated" total angular momentum $P_3^{-1}\boldsymbol{L}$ became positive, it is necessary to apply the rotation of P_2^{-1} evaluated in $-\mathrm{i}_R$ (instead of i_R) so to invert the sense of the rotation.

[7] In order to compute the angular momentum, we need $\boldsymbol{r} = (x, y, z)$ and $\boldsymbol{p} = (p_x, p_y, p_z)$. It is easy to compute $\boldsymbol{r}$ remembering the equations (1.11) and (1.12) and performing three rotations with respect to the angles ω , i and Ω . Consequently we know $r = ||\boldsymbol{r}||$. Instead, a possible way to compute $\boldsymbol{p}$ is the following: first, defined $\boldsymbol{l} = \boldsymbol{r} \times \boldsymbol{p}$, we can compute $||\boldsymbol{l}||$ and $\mathcal{H}_{kepl}$ as $||\boldsymbol{l}|| = G = m\sqrt{\mathcal{G}m_0\, a(1 - \mathrm{e}^2)}$ and $\mathcal{H}_{kepl} = -\frac{\mathcal{G}m_0 m}{2a}$ (where a is known). Then, we can determine $(p_r, p_\varphi, 0)$ through the relations $p_\varphi = \frac{||\boldsymbol{l}||}{r}$, $p_r = \pm\sqrt{2m\left(\mathcal{H}_{kepl} - \frac{||\boldsymbol{l}||^2}{2r^2 m} + \frac{\mathcal{G}m_0 m}{r}\right)}$, where we choice $+$ if we are moving from the pericenter to the apocenter (i.e. $0 \le f < \pi$) and $-$ otherwise. Thus, performing three rotations with respect to the angles $\omega + f$, i and Ω we obtain (p_x, p_y, p_z) .

Subsection 1.4.2), it is possible to express them in the Laplace reference frame using the following formulas:

$$a_L = -\frac{\mathcal{G}m_0 m}{2\,\mathcal{H}_{kepl}}, \qquad \mathrm{e}_L = \sqrt{1 - \frac{||\boldsymbol{l}||^2}{\mathcal{G}\,m_0\,a\,m^2}},$$

$$\Omega_L = sign(l_x)\arccos\left(\frac{-l_y}{\sqrt{l_x^2 + l_y^2}}\right), \qquad \mathrm{i}_L = \arccos\left(\frac{l_z}{||\boldsymbol{l}||}\right),$$

where $\mathcal{H}_{kepl} = -\dfrac{\mathcal{G}m_0 m}{2a} = \dfrac{\boldsymbol{p}^2}{2m} - \dfrac{\mathcal{G}m_0 m}{r}$, $(l_x, l_y, l_z) = \boldsymbol{l} = \boldsymbol{r} \times \boldsymbol{p}$ is the angular momentum vector of a single celestial body and where we denote with the subindexes L the orbital elements with respect to the Laplace reference frame. We have that $a_L = a$, $\mathrm{e}_L = \mathrm{e}$ and $f_L = f$, implying also $E_L = E$, $M_L = M$. In order to obtain ω_L we have first to determine the angle $f_L + \omega_L$, given by

$$f_L + \omega_L = sign(y')\arccos\left(\frac{x'}{\sqrt{x'^2 + y'^2}}\right)$$

where

$$\begin{pmatrix} x' \\ y' \\ 0 \end{pmatrix} = P_{2,L}^{-1} P_{3,L}^{-1} \begin{pmatrix} \widehat{x} \\ \widehat{y} \\ \widehat{z} \end{pmatrix},$$

with

$$P_{2,L}^{-1} = \begin{pmatrix} 1 & 0 & 0 \\ 0 & \cos\mathrm{i}_L & \sin\mathrm{i}_L \\ 0 & -\sin\mathrm{i}_L & \cos\mathrm{i}_L \end{pmatrix}, \qquad P_{3,L}^{-1} = \begin{pmatrix} \cos\Omega_L & \sin\Omega_L & 0 \\ -\sin\Omega_L & \cos\Omega_L & 0 \\ 0 & 0 & 1 \end{pmatrix}$$

and $(\widehat{x}, \widehat{y}, \widehat{z})$ are the coordinates of the celestial body in the Laplace reference frame.

1.4.5 The secular Hamiltonian of the planetary 3-body problem

1.4.5.1 Averaging by scissors

Let us start from the Hamiltonian of the 3-body problem, reported in Eq. (1.10):

$$\mathcal{H} = \underbrace{\frac{\boldsymbol{p}_2{}^2}{2\,m_2} - \frac{\mathcal{G}\,m_0\,m_2}{r_2} + \frac{\boldsymbol{p}_3{}^2}{2\,m_3} - \frac{\mathcal{G}\,m_0\,m_3}{r_3}}_{\textit{Keplerian part}} + \underbrace{\frac{(\boldsymbol{p}_2 + \boldsymbol{p}_3)^2}{2\,m_0}}_{\textit{"Indirect" part}} - \underbrace{\frac{\mathcal{G}\,m_2\,m_3}{|\boldsymbol{r}_2 - \boldsymbol{r}_3|}}_{\textit{"Direct" part}},$$

where we assume $m_0 \gg m_2, m_3$. Thus, m_0 represents the mass of the star, and m_i, $\boldsymbol{p}_i$, $\boldsymbol{r}_i$, $i = 2, 3$ are the masses, barycentric momenta and heliocentric position vectors of of two planets orbiting the star, at distances $r_i = |\boldsymbol{r}_i|$. According to Eqs. (1.11), (1.12) and (1.15), it is possible to provide series expansions in powers of the eccentricity for the Cartesian position coordinates (X, Y) on the orbital plane. Through (1.16) we then obtain series expansions of the Cartesian coordinates of a body in any fixed heliocentric reference frame (x, y, z). As regards the momenta, we obtain their expansion via the relations

$$\boldsymbol{p} = m\,\frac{d\boldsymbol{r}}{dM}\,\sqrt{\frac{\mu}{a^3}}, \tag{1.26}$$

being $\boldsymbol{p} = m\,d\boldsymbol{r}/dt$ and $dM/dt = n$ (by Eq. (1.13)), with n defined in Eq. (1.14).

These relations can now be used in order to expand the direct term in (1.10) in powers of the eccentricities and inclinations (see [87]). This leads to a sum of terms of the form

$$\frac{C(a_2,a_3,\mathrm{e}_2,\mathrm{e}_3,\mathrm{i}_2,\mathrm{i}_3)}{\left(a_2^2+a_3^2-2\,a_2\,a_3\,\cos(\lambda_2-\lambda_3)\right)^{\frac{2\,s+1}{2}}}\cos(\alpha_2\lambda_2+\alpha_3\lambda_3+\beta_2\Omega_2+\beta_3\Omega_3+\gamma_2\varpi_2+\gamma_3\varpi_3)\,, \tag{1.27}$$

where $\varpi_i=\omega_i+\Omega_i$ and $\lambda_i=M_i+\varpi_i$ have been introduced in Eqs. (1.17), (1.18). The integers α_2, α_3, β_2, β_3, γ_2, γ_3 satisfy the *D'Alembert rule* $\alpha_2+\alpha_3+\beta_2+\beta_3+\gamma_2+\gamma_3=0$, expressing the invariance of the Hamiltonian with respect to rotations around the z axis.

The denominator of (1.27) can be Fourier expanded leading to

$$\frac{1}{\left(a_2^2+a_3^2-2\,a_2\,a_3\,\cos(\lambda_2-\lambda_3)\right)^{\frac{2\,s+1}{2}}}=a_3^{-(2\,s+1)}\sum_{j\geq 0}b^{(j)}_{s+\frac{1}{2}}\left(\frac{a_2}{a_3}\right)\cos(j(\lambda_2-\lambda_3))\,, \tag{1.28}$$

where $b^{(j)}_{s+\frac{1}{2}}$ are the Laplace coefficients:

$$\begin{aligned} b^{(0)}_{s+\frac{1}{2}}(\alpha)&=\frac{1}{2\pi}\int_0^{2\pi}\left(1+\alpha^2-2\,\alpha\,\cos(\vartheta)\right)^{-(s+\frac{1}{2})}\,d\vartheta\,,\\ b^{(j)}_{s+\frac{1}{2}}(\alpha)&=\frac{1}{\pi}\int_0^{2\pi}\left(1+\alpha^2-2\,\alpha\,\cos(\vartheta)\right)^{-(s+\frac{1}{2})}\cos(j\vartheta)\,d\vartheta\qquad j\geq 1\,, \end{aligned} \tag{1.29}$$

with $\alpha=a_2/a_3$. In practical computations, the integrals (1.29) can be computed numerically, for a fixed numerical value of α, or via a multipolar expansion (see the Appendix A).

After having performed the above expansions of the Hamiltonian in orbital parameters, a key remark stems from the observation that there exist two different time scales for the evolutions of the orbital parameters; the angle λ (related to the revolution of the planet around the star) is 'fast' with respect to the angles ω, Ω. In particular, the frequency ratios $\dot\omega_j/\lambda_j$ and $\dot\Omega_j/\lambda_j$ are of order $\mathcal{O}(m_j/m_0)$, with typical values $10^{-4}-10^{-2}$ for most observed exoplanetary systems[8]. Being interested in the *secular evolution* of the system, we want to derive a *secular* model of the Hamiltonian, in which the *short period terms* depending on the angles λ_2, λ_3 are no longer considered. A simple way to obtain the *secular Hamiltonian* is through the so-called "scissor" process; it consists of dropping from the original Hamiltonian all terms depending on the 'fast' angles λ_i:

$$\mathcal{H}_{sec}=\frac{1}{4\pi^2}\int_0^{2\pi}\int_0^{2\pi}\mathcal{H}(\boldsymbol{r}_2,\boldsymbol{r}_3,\boldsymbol{p}_2,\boldsymbol{p}_3)\,d\lambda_2\,d\lambda_3\,. \tag{1.30}$$

A theoretical justification for the averaging (1.30) is through the 'averaging principle' (see [87]). Other possibilities to obtain useful secular models are the *closed-form averaging* (requiring the expansion of the Hamiltonian in 'multipolar series'), that will be discussed in Chapter 2, and the second order (in the mass ratios) averaging (requiring canonical transformations in order to remove the dependence of the Hamiltonian on the fast angles), described in Appendix C.

After the 'scissor' averaging process, we end up with a Hamiltonian of the form:

$$\mathcal{H}_{sec}=\underbrace{-\frac{\mathcal{G}m_0m_2}{2a_2}-\frac{\mathcal{G}m_0m_3}{2a_3}}_{\textbf{\textit{Keplerian part}}}+\underbrace{\frac{\mathcal{G}m_2^2}{2a_2}+\frac{\mathcal{G}m_3^2}{2a_3}}_{\textbf{\textit{"Indirect" part}}}-\underbrace{\mathcal{R}_{sec}(a_2,a_3,\mathrm{e}_2,\mathrm{e}_3,\mathrm{i}_2,\mathrm{i}_3,\varpi_2,\varpi_3,\Omega_2,\Omega_3)}_{\textbf{\textit{"Direct" part}}}\,. \tag{1.31}$$

We observe the following:

i) In the Hamiltonian (1.31) the angles λ_2, λ_3 are ignorable, a fact implying the constancy of the semi-major axes under the secular model. In terms of *modified Delaunay variables* (Eq. (1.20)), we have that

$$\dot\Lambda_j=\frac{\partial\mathcal{H}_{sec}}{\partial\lambda_j}=0\,,$$

[8] A detailed explanation of the different time scales involved in the evolution of the *fast* and *secular* variables is given in Section C.1 of Appendix C.

thus Λ_j (hence a_j) are constant.

ii) The total angular momentum $\mathbf{L} = \mathbf{r}_2 \times \mathbf{p}_2 + \mathbf{r}_3 \times \mathbf{p}_3$, which is an exact first integral of the Hamiltonian (1.10) (subsection 1.4.1), is conserved in the averaged model (1.30) as well. Indeed, we recall that in the Laplace reference frame we have $\boldsymbol{L} = (0, 0, L_z)$. From the constancy of $L_z = H_2 + H_3$ it follows that $\{L_z, \mathcal{H}\} = 0$. Then

$$\frac{1}{4\pi^2}\int_0^{2\pi}\int_0^{2\pi} dM_2 dM_3 \, \{L_z, \mathcal{H}\} = 0 \implies \frac{1}{4\pi^2}\int_0^{2\pi}\int_0^{2\pi} dM_2 dM_3 \left(-\frac{\partial L_z}{\partial H_2}\frac{\partial \mathcal{H}}{\partial \Omega_2} - \frac{\partial L_z}{\partial H_3}\frac{\partial \mathcal{H}}{\partial \Omega_3}\right) = 0 \implies$$

$$-\frac{1}{4\pi^2}\left[\frac{\partial L_z}{\partial H_2}\frac{\partial}{\partial \Omega_2}\int_0^{2\pi}\int_0^{2\pi} dM_2 dM_3 \, \mathcal{H} + \frac{\partial L_z}{\partial H_3}\frac{\partial}{\partial \Omega_3}\int_0^{2\pi}\int_0^{2\pi} dM_2 dM_3 \, \mathcal{H}\right] = 0 \implies \{L_z, \mathcal{H}_{sec}\} = 0\,.$$

iii) The constancy of L_z under the secular Hamiltonian $\mathcal{H}_{sec}$ implies that the dependence of $\mathcal{H}_{sec}$ on the angles Ω_2, Ω_3 can only be through the difference $\Omega_2 - \Omega_3$. In fact, from $\{L_z, \mathcal{H}_{sec}\} = 0$ it follows that $\dot{H}_2 + \dot{H}_3 = 0$, i.e. (by Hamilton equations)

$$\frac{\partial \mathcal{H}_{sec}}{\partial \Omega_2} + \frac{\partial \mathcal{H}_{sec}}{\partial \Omega_3} = 0\,.$$

Now, setting $\Omega_+ = \Omega_2 + \Omega_3$ and $\Omega_- = \Omega_2 - \Omega_3$, it is easy to see that

$$\frac{\partial \mathcal{H}_{sec}}{\partial \Omega_+} = \frac{\partial \mathcal{H}_{sec}}{\partial \Omega_2}\frac{\partial \Omega_2}{\partial \Omega_+} + \frac{\partial \mathcal{H}_{sec}}{\partial \Omega_3}\frac{\partial \Omega_3}{\partial \Omega_+} = \frac{1}{2}\left(\frac{\partial \mathcal{H}_{sec}}{\partial \Omega_2} + \frac{\partial \mathcal{H}_{sec}}{\partial \Omega_3}\right) = 0\,.$$

1.4.5.2 Jacobi's reduction of the nodes

Treating the (constant) semi-major axes a_2, a_3 as parameters, the secular Hamiltonian $\mathcal{H}_{sec}$ is a system with 4 degrees of freedom depending on the canonical variables $(\gamma_j, \theta_j, \Gamma_j, \Theta_j)$, $j = 2, 3$. However, the existence of two independent integrals in involution (i.e. the components L_z and $L_{plane} = (L_x^2 + L_y^2)^{1/2} = 0$ of the total angular momentum $\mathbf{L}$) allows to reduce the number of degrees of freedom by two. This process is known as 'Jacobi's reduction (or elimination) of the nodes' (see [45]). Different strategies are, a priori, allowed in order to perform this reduction. However, different methods can lead to a different control of the small parameters appearing in the problem. Here we present a classical procedure, used, for example, by Libert & Henrard in [59]. In Chapter 2, instead, we present a novel method based on the use of a 'book-keeping parameter'.

The 'Jacobi's reduction of the nodes' exploits the features of the Laplace reference frame, already introduced in Subsection 1.4.4.

From the second equation of (1.25), the z-th component of the angular momentum can be expressed in modified Delaunay variables as

$$L_z = \Lambda_2 - \Gamma_2 - \Theta_2 + \Lambda_3 - \Gamma_3 - \Theta_3 = C\,.$$

This implies the constancy of the so-called *angular momentum deficit* $\mathrm{AMD} = \Lambda_2 + \Lambda_3 - C$, defined as

$$\mathrm{AMD} := \Lambda_2 + \Lambda_3 - L_z = \Gamma_2 + \Gamma_3 + \Theta_2 + \Theta_3 = \sum_{j=2}^{3} \Lambda_j \left(1 - \sqrt{1 - \mathrm{e}_j^2}\cos \mathrm{i}_j\right)\,. \tag{1.32}$$

The AMD yields the difference between the norm of the angular momentum of a coplanar and circular system and the norm of the angular momentum $\boldsymbol{L}$,[9] for equal semi-major axes a_2, a_3 (see,

[9] In the Laplace reference frame the angular momentum is directed along the z-axis, thus $||\boldsymbol{L}|| = L_z = \sum_{j=2}^{3} \Lambda_j \sqrt{1 - \mathrm{e}_j^2}\cos \mathrm{i}_j$.

for istance, [50], [53]). Then, Eqs. (1.25) take the form

$$\begin{cases} \Omega_3 - \Omega_2 = \pi\,, \\ \mathrm{AMD} = \Gamma_2 + \Theta_2 + \Gamma_3 + \Theta_3 = \Lambda_2 + \Lambda_3 - C\,, \\ 2\,(\Lambda_2 - \Gamma_2)\,\Theta_2 - \Theta_2^2 = 2\,(\Lambda_3 - \Gamma_3)\,\Theta_3 - \Theta_3^2\,. \end{cases} \tag{1.33}$$

Starting from $\mathcal{H}_{sec}(\Gamma_2, \Gamma_3, \Theta_2, \Theta_3, \gamma_2, \gamma_3, \theta_2, \theta_3)$, consider the canonical transformation

$$\begin{aligned} J_2 &= \Gamma_2\,, & \varphi_2 &= \gamma_2 - \theta_2\,, \\ J_3 &= \Gamma_3\,, & \varphi_3 &= \gamma_3 - \theta_3\,, \\ J_4 &= \Gamma_2 + \Theta_2\,, & \varphi_4 &= \theta_2 - \theta_3\,, \\ J &= \Gamma_2 + \Gamma_3 + \Theta_2 + \Theta_3\,, & \varphi &= \theta_3\,, \end{aligned} \tag{1.34}$$

given by the generating function of the third kind

$$\mathcal{S}(\Gamma_2, \Gamma_3, \Theta_2, \Theta_3, \varphi_2, \varphi_3, \varphi_4, \varphi) = (\Gamma_2 + \Gamma_3 + \Theta_2 + \Theta_3)\varphi + \Gamma_2\varphi_2 + \Gamma_3\varphi_3 + (\Gamma_2 + \Theta_2)\varphi_4$$

(Section 1.1.2, Proposition 1.1.4).

The angles φ_2, φ_3 correspond, in this definition, to the opposites of the arguments of the pericenter ω_2, ω_3, so that Γ_2 and Γ_3 are conjugated, respectively, to $-\omega_2$, $-\omega_3$. Furthermore, by the definition (1.32), the action J represents the AMD. We have seen (subsection 1.4.5.1) that the constancy of the total angular momentum vector $\boldsymbol{L}$ leads to the dependence of the Hamiltonian on the angles Ω_2, Ω_3 *only* through the difference $\Omega_2 - \Omega_3$. Hence, in the new variables $(J_2, J_3, J_4, J, \varphi_2, \varphi_3, \varphi_4, \varphi)$, the secular Hamiltonian (1.31) does not depend on the angle φ, implying the constancy of J, i.e. of the AMD. Thus, the choice of the Laplace plane fixes the values of $J = \mathrm{AMD} = \Lambda_2 + \Lambda_3 - C$, and (following the first of Eq. (1.25)), the value of the angle φ_4 to π. Consequently, we have that $\dot{\varphi}_4 = (\partial\mathcal{H}_{sec}/\partial J_4)_{\varphi_4=\pi,\, J=\mathrm{AMD}} = 0$, implying that, setting $\varphi_4 = \pi$ within $\mathcal{H}_{sec}$, the associated moment J_4 should no longer appear in the expansion of the Hamiltonian. This effectively reduces the problem to two degrees of freedom $(J_2, J_3, \varphi_2, \varphi_3)$, while J_4 can be found, as function of (J_2, J_3), by the third relation of Eq. (1.25)[10]. This allows, in turn, to express the values of the inclinations as functions of the eccentricities.

Note that, by the above analysis, it follows that, in order to compute the equations of motion in the Laplace reference frame, the following two strategies are equivalent:

i) first perform the elimination of nodes, substituting $\varphi_4 = \pi$ into the Hamiltonian, and then compute the equations of motion for the variables $(J_2, J_3, \varphi_2, \varphi_3)$, while the evolution of the inclinations is derived from the total angular momentum conservation,

ii) first compute the equations of motion of the full Hamiltonian, before Jacobi's reduction, and then evaluate them in $\varphi_4 = \pi$.

This is a crucial fact, because the application of i) considerably simplifies the evolution equations. However, it is possible to use the Hamiltonian with the nodes eliminated (i.e. the method called i)) as long as the evolution equations for the inclinations are derived from the total angular momentum conservation, instead of using the canonical relations. As remarked by Naoz et al. in [89], if, instead, the relation $\varphi_4 = \Omega_3 - \Omega_2$ is substituted into the Hamiltonian before deriving the equations of motion, after the substitution, the Hamiltonian appears as independent of the longitudes of ascending nodes (Ω_2 and Ω_3), and this can lead to the incorrect conclusion that $\dot{H}_2 = \dot{H}_3 = 0$ (or, equivalently, $\dot{J}_4 = 0$) by the canonical equations of motion. However, in strategy i), it is correct to

[10] Recalling that $\Gamma_3 + \Theta_3 = J - J_4$, from the third relation of Eq. (1.25) we get, $J_4 = J_4(J_2, J_3; J) = \dfrac{J_3^2 - J^2 - J_2^2 + 2\Lambda_2 J_2 + 2\Lambda_3 J - 2\Lambda_3 J_3}{2(\Lambda_2 + \Lambda_3 - J)}$, where $J = \Lambda_2 + \Lambda_3 - C$ is a constant of motion.

derive equations of motion from the node-eliminated Hamiltonian only for the canonical variables $(\varphi_2,\, \varphi_3,\, J_2,\, J_3\,)$, i.e. $(-\omega_2,\, -\omega_3,\, \Gamma_2,\, \Gamma_3\,)$. Expressions for $\dot{H}_2$ and $\dot{H}_3$ can then be derived from the conservation of the angular momentum. More precisely, we know that $J = \mathrm{AMD} = \Lambda + \Lambda_3 - C$ and $\varphi_4 = \pi$. Moreover, the equation $\dot{\varphi} = \partial \mathcal{H}_{sec}/\partial J$ (as well as $J_4 = J_4(J_2, J_3; J)$, explicitely given in footnote (10)) can be solved when the rest of the equations of motion have been integrated.

The equivalence between the methods i) and ii) as regards the equations of motion for the variables $(J_2, J_3, \varphi_2, \varphi_3)$ correspond to the following equalities: denote by $\mathcal{H}^{'}_{sec}$ the secular Hamiltonian after the elimination of nodes, i.e.

$$\mathcal{H}^{'}_{sec} = \mathcal{H}_{sec}(J_2, J_3, J_4, J, \varphi_2, \varphi_3, \varphi_4)\Big|_{\substack{\varphi_4=\pi \\ J=\mathrm{AMD} \\ J_4=J_4(J_2,J_3;J)}} . \tag{1.35}$$

Then[11]

$$\begin{aligned}
\frac{\partial \mathcal{H}^{'}_{sec}}{\partial \varphi_2} &= \frac{\partial}{\partial \varphi_2}\left(\mathcal{H}_{sec}(J_2, J_3, J_4, J, \varphi_2, \varphi_3, \varphi_4)\Big|_{\substack{\varphi_4=\pi \\ J=\mathrm{AMD} \\ J_4=J_4(J_2,J_3;J)}} \right) \\
&= \left(\frac{\partial \mathcal{H}_{sec}(J_2, J_3, J_4, J, \varphi_2, \varphi_3, \varphi_4)}{\partial \varphi_2} \right)\Big|_{\substack{\varphi_4=\pi \\ J=\mathrm{AMD} \\ J_4=J_4(J_2,J_3;J)}} ,
\end{aligned}$$

$$\begin{aligned}
\frac{\partial \mathcal{H}^{'}_{sec}}{\partial J_2} &= \frac{\partial}{\partial J_2}\left(\mathcal{H}_{sec}(J_2, J_3, J_4, J, \varphi_2, \varphi_3, \varphi_4)\Big|_{\substack{\varphi_4=\pi \\ J=\mathrm{AMD} \\ J_4=J_4(J_2,J_3;J)}} \right) \\
&= \left(\frac{\partial \mathcal{H}_{sec}}{\partial J_2} \right)\Big|_{\substack{\varphi_4=\pi \\ J=\mathrm{AMD} \\ J_4=J_4(J_2,J_3;J)}} + \left(\frac{\partial \mathcal{H}_{sec}}{\partial J_4} \right)\Big|_{\substack{\varphi_4=\pi \\ J=\mathrm{AMD} \\ J_4=J_4(J_2,J_3;J)}} \frac{\partial J_4(J_2, J_3; \mathrm{AMD})}{\partial J_2} = \left(\frac{\partial \mathcal{H}_{sec}}{\partial J_2} \right)\Big|_{\substack{\varphi_4=\pi \\ J=\mathrm{AMD} \\ J_4=J_4(J_2,J_3;J)}} ,
\end{aligned}$$

being $\dot{\varphi}_4 = (\partial \mathcal{H}_{sec}/\partial J_4)_{\varphi_4=\pi,\, J=\mathrm{AMD}} = 0$. Analogous expressions hold for the derivatives $\partial \mathcal{H}^{'}_{sec}/\partial \varphi_3$, $\partial \mathcal{H}^{'}_{sec}/\partial J_3$. This means that i) and ii) are equivalent and that the following equations hold in the Laplace reference frame:

$$\begin{aligned}
\dot{\varphi}_2 &= \partial \mathcal{H}^{'}_{sec}/\partial J_2 \,, \\
\dot{\varphi}_2 &= \partial \mathcal{H}^{'}_{sec}/\partial J_3 \,, \\
\dot{J}_2 &= -\partial \mathcal{H}^{'}_{sec}/\partial \varphi_2 \,, \\
\dot{J}_3 &= -\partial \mathcal{H}^{'}_{sec}/\partial \varphi_3,
\end{aligned}$$

where $\mathcal{H}^{'}_{sec}$ has only two degrees of freedom (for furthermore details see Chapter XIII of [102].)

[11] Recalling that the Hamiltonian is of the form $\mathcal{H}_{sec} = \sum c(J_2, J_3, J_4, J)\cos(k_2\varphi_2 + k_3\varphi_3 + k_4\varphi_4)$, then $\partial \mathcal{H}^{'}_{sec}/\partial \varphi_2 = -\sum c(J_2, J_3, J_4(J_2, J_3; \mathrm{AMD}); \mathrm{AMD})\sin(k_2\varphi_2 + k_3\varphi_3 + k_4\pi)k_2 = (\partial \mathcal{H}_{sec}/\partial \varphi_2)\Big|_{\substack{\varphi_4=\pi \\ J=\mathrm{AMD} \\ J_4=J_4(J_2,J_3;J)}}$.

Any canonical transformation of the variables $(\varphi_2,\ \varphi_3,\ J_2,\ J_3\,)$ can be applied to the Hamiltonian $\mathcal{H}'_{sec}$. For example, following Libert & Henrard [59], we introduce the Poincaré variables

$$\begin{aligned}\mathcal{X}_2 &= -\sqrt{2\,J_2}\cos(\varphi_2)\,, &\qquad \mathcal{Y}_2 &= \sqrt{2\,J_2}\sin(\varphi_2)\,,\\ \mathcal{X}_3 &= -\sqrt{2\,J_3}\cos(\varphi_3)\,, &\qquad \mathcal{Y}_3 &= \sqrt{2\,J_3}\sin(\varphi_3)\,,\end{aligned}$$

i.e.

$$\mathcal{X}_i = -\sqrt{2\Gamma_i}\cos(\omega_i)\,, \qquad \mathcal{Y}_i = -\sqrt{2\Gamma_i}\sin(\omega_i)\,, \tag{1.36}$$

where $(\mathcal{X}_i, \mathcal{Y}_i)\,,\ i = 2, 3$ are positions-momenta coordinates (as in Subsection 1.4.3, Eq. (1.22)). The Hamiltonian $\mathcal{H}'_{sec}$ takes of the form

$$\mathcal{H}'_{sec} = \sum_{k_l, l\in\mathbf{6}} D_{k_l}\mathcal{X}_2^{k_1}\mathcal{X}_3^{k_2}\mathcal{Y}_2^{k_3}\mathcal{Y}_3^{k_4}\sqrt{\Theta_2}^{\,k_5}\sqrt{\Theta_3}^{\,k_6}\,, \tag{1.37}$$

where $k_5 + k_6$ is even. From (1.33) it is possible to determine the expressions for Θ_2 and Θ_3 as function of $(\mathcal{X}_2, \mathcal{X}_3, \mathcal{Y}_2, \mathcal{Y}_3)$; in fact, defined

$$\chi = \Theta_2 + \Theta_3 = \mathrm{AMD} - \Gamma_2 - \Gamma_3 = \mathrm{AMD} - (\mathcal{X}_2^2 + \mathcal{Y}_2^2 + \mathcal{X}_3^2 + \mathcal{Y}_3^2)/2\,, \tag{1.38}$$

(i.e. the part of the AMD due to the mutual inclination of the orbits), we have

$$\begin{aligned}2\Theta_2 &= \chi\left(2\Lambda_3 - \chi - \mathcal{X}_3^2 - \mathcal{Y}_3^2\right)/(\Lambda_2 + \Lambda_3 - \mathrm{AMD})\,,\\ 2\Theta_3 &= \chi\left(2\Lambda_2 - \chi - \mathcal{X}_2^2 - \mathcal{Y}_2^2\right)/(\Lambda_2 + \Lambda_3 - \mathrm{AMD})\,.\end{aligned} \tag{1.39}$$

Finally, we substitute the previous expressions in (1.37) and develop in power series of $\mathcal{X}_i\,,\ \mathcal{Y}_i$, $(i = 2, 3)$ and $\sqrt{\chi}$, leading to[12]

$$\mathcal{H}'_{sec} = \sum_{n_l, l\in\mathbf{6}} E_{n_l}\mathcal{X}_2^{n_1}\mathcal{X}_3^{n_2}\mathcal{Y}_2^{n_3}\mathcal{Y}_3^{n_4}\chi^{n_5}D^{n_6}\,, \tag{1.40}$$

with $D = (\Lambda_2 + \Lambda_3 - \mathrm{AMD})^{-1/2}$ and the exponent n_5 is an integer as $k_5 + k_6$.

We conclude with some remarks about the symmetries of the reduced problem. It can be proved that in Eq. (1.40) the sums $n_1 + n_2$ and $n_3 + n_4$ are always even (since the initial Hamiltonian (1.31) is an even function of the angular variables). Then, the following relations hold:

$$\begin{aligned}\dot{\mathcal{X}}_j &= (\partial\mathcal{H}'_{sec}/\partial\mathcal{Y}_j) = \mathcal{F}_j(\mathcal{X}_2, \mathcal{X}_3, \mathcal{Y}_2, \mathcal{Y}_3)\\ &= \mathcal{F}_j(-\mathcal{X}_2, -\mathcal{X}_3, \mathcal{Y}_2, \mathcal{Y}_3) = -\mathcal{F}_j(\mathcal{X}_2, \mathcal{X}_3, -\mathcal{Y}_2, -\mathcal{Y}_3) = -\mathcal{F}_j(-\mathcal{X}_2, -\mathcal{X}_3, -\mathcal{Y}_2, -\mathcal{Y}_3)\,,\\ \dot{\mathcal{Y}}_j &= -(\partial\mathcal{H}'_{sec}/\partial\mathcal{X}_j) = \tilde{\mathcal{F}}_j(\mathcal{X}_2, \mathcal{X}_3, \mathcal{Y}_2, \mathcal{Y}_3)\\ &= -\tilde{\mathcal{F}}_j(-\mathcal{X}_2, -\mathcal{X}_3, \mathcal{Y}_2, \mathcal{Y}_3) = \tilde{\mathcal{F}}_j(\mathcal{X}_2, \mathcal{X}_3, -\mathcal{Y}_2, -\mathcal{Y}_3) = -\tilde{\mathcal{F}}_j(-\mathcal{X}_2, -\mathcal{X}_3, -\mathcal{Y}_2, -\mathcal{Y}_3)\,,\end{aligned} \tag{1.41}$$

with $j = 2, 3$; thus, for each solution $(\mathcal{X}_2(t), \mathcal{X}_3(t), \mathcal{Y}_2(t), \mathcal{Y}_3(t))$, also $(-\mathcal{X}_2(-t), -\mathcal{X}_3(-t), \mathcal{Y}_2(-t), \mathcal{Y}_3(-t))$, $(\mathcal{X}_2(-t), \mathcal{X}_3(-t), -\mathcal{Y}_2(-t), -\mathcal{Y}_3(-t))$ and $(-\mathcal{X}_2(t), -\mathcal{X}_3(t), -\mathcal{Y}_2(t), -\mathcal{Y}_3(t))$ are solutions. Finally, again by the evenness of $n_1 + n_2$ and $n_3 + n_4$, we derive the following:

$$\begin{aligned}\dot{\mathcal{X}}_j &= \frac{\partial\mathcal{H}'_{sec}}{\partial\mathcal{Y}_j} = \mathcal{Y}_2 G_{j_2}(\mathcal{X}_2, \mathcal{X}_3, \mathcal{Y}_2, \mathcal{Y}_3) + \mathcal{Y}_3 G_{j_3}(\mathcal{X}_2, \mathcal{X}_3, \mathcal{Y}_2, \mathcal{Y}_3)\,,\\ \dot{\mathcal{Y}}_j &= -\frac{\partial\mathcal{H}'_{sec}}{\partial\mathcal{X}_j} = \mathcal{X}_2 F_{j_2}(\mathcal{X}_2, \mathcal{X}_3, \mathcal{Y}_2, \mathcal{Y}_3) + \mathcal{X}_3 F_{j_3}(\mathcal{X}_2, \mathcal{X}_3, \mathcal{Y}_2, \mathcal{Y}_3)\,,\end{aligned} \tag{1.42}$$

[12] We have already observed (in Subsection 1.4.3) that $\Gamma_j = \mathcal{O}(\mathrm{e}_j^2)$, and $\Theta_j = \mathcal{O}(\mathrm{i}_j^2)$; thus, the Poincaré variables $\mathcal{X}_j$ and $\mathcal{Y}_j$ are $\mathcal{O}(\mathrm{e}_j)\,,\ j = 2, 3$. Instead, $\chi = \mathcal{O}(\mathrm{i}_2^2 + \mathrm{i}_3^2)$. Let us observe that, concerning the expansion leading to the Hamiltonian described in Eq. (1.40), two possible choices are possible; if we think to AMD as a constant and we do not take it into account as a parameter to be expanded, then we end up with Eq. (1.40), where the coefficient D appears. Instead, if we think to $\mathrm{AMD} = \mathcal{O}(\mathrm{e}_2^2 + \mathrm{e}_3^2 + \mathrm{i}_2^2 + \mathrm{i}_3^2)$ (so that $\chi = \mathcal{O}(\mathrm{i}_2^2 + \mathrm{i}_3^2)$), developing also in power series of $\sqrt{\mathrm{AMD}}$, the coefficient D disappears in Eq. (1.40). Both choices are, at priori, possible, leading, nevertheless, to Hamiltonians with some (small) differences.

with $G_{j_2}, G_{j_3}, F_{j_2}, F_{j_3}$ functions of $(\mathcal{X}_2, \mathcal{X}_3, \mathcal{Y}_2, \mathcal{Y}_3)$ and $j = 2, 3$. A consequence is that the origin is always an equilibrium, because the velocities $\dot{\mathcal{X}}_j$ and $\dot{\mathcal{Y}}_j$ vanish, respectively, whenever $\mathcal{Y}_2 = \mathcal{Y}_3 = 0$ and $\mathcal{X}_2 = \mathcal{X}_3 = 0$. For furthermore details and remarks see [59].

1.5 Goal and structure of the thesis

After having introduced some basic notions and definitions, we now state the main goal of the present thesis, which is: *to study the basic features of the secular dynamics as well as the long-term stability* in 3D multiplanetary systems, using, as mathematical tools, the *Hamiltonian normal form methods of canonical perturbation theory.*

The inspiring case for this thesis, to which we refer for concrete applications, is the υ-Andromedæ system. We aim to: i) provide the main elements leading to a systematic study of the most important phenomena in the phase space of secular motions of a spatial planetary 3-body problem, analyzing the phase space structures observed in such systems, ii) introduce a secular quasi-periodic restricted Hamiltonian model for the description of the secular dynamics of a small-mass planet in a mutiplanetary system, providing semi-analytical solutions through the applications of different normal forms, iii) enrich the model with corrections given by the general relativity.

The thesis is organized as follows:

Chapter 2 describes all the steps followed in order to arrive at the finally adopted secular Hamiltonian model. This includes the introduction of an appropriate 'book-keeping', the way this is used in the Jacobi reduction of the Hamiltonian, the chain of canonical transformations leading the Hamiltonian to its final form in Poincaré canonical variables, as well as a number of precision tests about the order of the multipole truncation, comparison with the Laplace-Lagrange series, etc. Moreover we show the natural split of the Hamiltonian in integrable and pertubed part. Then, we provide an analysis of the phase space structures for the full (non-integrable) 3D Hamiltonian, starting from the *planar-like* regime, characterized by the presence of the apsidal-corotations, arriving (through a sequence of bifurcations) to the Kozai instability. Moreover we show some results related to the 'Kozai mechanism', i.e., the transition from linear stability to instability for the inclined circular orbit of one of the two planets. These results are compared to an analytical approximation obtained in the framework of the quadrupolar approximation. Finally we include the investigation of how the phase portraits change in cases with different distance or mass ratios of the planets, covering various hierachical models ($r_2/r_3 = 1/7,\ 1/3,\ m_2/m_3 = 1/10,\ 1/3,\ 1,\ 3,\ 10$).

Chapter 3 deals with semi-analytical computations of the periodic and quasi-periodic orbits surrounding the 3D apsidal-corotations of the full Hamiltonian, based on a suitably defined local normal form construction around each fixed point of the secular Hamiltonian.

In ***Chapter 4***, first, the motion of the two outermost planets of the υ-Andromedæ systems is preassigned, through the so called *Frequency Analysis method* ([51]). Then, we derive the secular quasi-periodic restricted Hamiltonian model allowing to describe the dynamics of the small-mass innermost planet of the υ-Andromedæ system. We validate the above approximation by the comparison with long-term integrations of the complete 4 body problem. Moreover, through a double normalization procedure, the Hamiltonian model is further simplified, passing to a 2 degrees of freedom problem, which serves to obtain the stability domain for the innermost planet υ-And **b**; this allows to provide possible information on the unknown orbital parameters (such as the inclination and longitude of nodes) of υ-And **b**. Finally, the model is enriched with the general relativistic correction on the motion of υ-And **b**.

Chapter 5 is devoted to the application of the algorithm constructing the Kolmogorov normal form of the doubly normalized 2 degrees of freedom secular quasi-periodic restricted Hamiltonian, producing semi-analytical results for the description of the secular dynamics of υ-And **b**. Moreover, through a *Computer-Assisted Proof* (for $n = 2$ DOF), we specify the stability region where secular motions are KAM stable.

In ***Chapter 6*** we apply an algorithm of construction of the Kolmogorov normal form, without

frequency fixing, to the $2 + 3/2$ DOF Hamiltonian, normalized through an algorithm leading to the explicit construction of solutions lying on elliptic tori. The resulting model is reduced by one DOF, thus it is less simplified than the 2 DOF model of Chapter 5. We succeed, however, to provide semi-analytical results for selected orbits, performing in that case too the corrisponding *Computer-Assisted Proof* (for $n > 2$ DOF).

In ***Chapter 7*** we revisit the Kolmogorov algorithm, proposing a novel method by which a Kolmogorov normal form can be derived in generic systems with a isochronous integrable part. This algorithm allows to compute quasi-periodic orbits with a frequency vector fixed in advance, that differs from the initial frequency vector for the *counterterms*. Moreover, through basic examples, we analyze the solutions produced by different types of normal form, i.e. i) the *no-torus fixing methods*, based on Lindstedt series (direct method) and the Birkhoff normal form (indirect method) and ii) the *torus fixing metods* (in which the frequency of the torus is fixed in advance), based on Lindstedt series (direct method) and the Kolmogorov algorithm (indirect method).

2. The phase-space architecture in the 3D planetary three body problem

2.1 Introductory remarks

Starting from the planetary three body problem in Poincaré heliocentric canonical variables given by Eq. (1.10)

$$\mathcal{H}(\boldsymbol{r}_2, \boldsymbol{r}_3, \boldsymbol{p}_2, \boldsymbol{p}_3) = \frac{{\boldsymbol{p}_2}^2}{2\,m_2} - \frac{\mathcal{G}\,m_0\,m_2}{r_2} + \frac{{\boldsymbol{p}_3}^2}{2\,m_3} - \frac{\mathcal{G}\,m_0\,m_3}{r_3} + \frac{(\boldsymbol{p}_2+\boldsymbol{p}_3)^2}{2\,m_0} - \frac{\mathcal{G}\,m_2\,m_3}{|\boldsymbol{r}_2-\boldsymbol{r}_3|}\,,$$

(where m_0 represents the mass of a star, $m_i\,,\ \boldsymbol{p}_i\,,\ \boldsymbol{r}_i\,,\ i=2,3$ the masses, barycentric momenta and heliocentric position vectors of two planets orbiting the star, at distances $r_i = |\boldsymbol{r}_i|$ and $m_0 \gg m_2,\ m_3$), the focus of the present Chapter is on a systematic study of how the structure of the phase space of the above Hamiltonian system is altered as the planetary masses and distances and, most importantly, the *mutual inclination* between the two planets' trajectories is varied. Answering this question in the framework of the three-body problem is a key step towards understanding the phase-space architecture in planetary systems with two or more planets in orbits with high mutual inclination. A well-studied case of the latter is the υ-Andromedae system. As already remarked in subsection 1.4.1, this is a double star system with four planets (**b**, **c**, **d** and **e**) orbiting one of the stars. Since the masses m_b and m_e are much smaller than $m_c\,, m_d\,$, the motion of the innermost planet **b** can be modelel to a good approximation via a restricted four-body problem, with planets **c**, **d** providing the main perturbations. The long-term motion of the innermost planet $(m_1, \boldsymbol{r}_1, \boldsymbol{p}_1)$ is considered in Chapters 4, 5, 6. At any rate, the above model requires providing first a good analytical model for the orbits of the giant planets of the system, say, for example, the planets **c** and **d**, whose masses, as estimated by observations, are larger than $10\,M_J$ (see e.g [18] and [78]).

Now, the available data for the orbital parameters of an extrasolar system are typically affected by wide observational error bars. As will be discussed in detail below, one important problem with the uncertainties in the observations stems from the fact that even small changes in a system's estimated parameters, consistent with the observations, may imply a drastic change in the type of orbital state in which the observed system is assumed to have been settled. We will argue below that this sensitive dependence on available parameter estimates affects mostly those predictions referring to the secular evolution of the orbital state, i.e., the variations of the planets' eccentricity and inclination vectors which take place in timescales of the order of $\sim 10^2 - 10^4$ orbital periods. Notwithstanding these long timescales, characterizing the whole variety of possible stable secular orbital states of exoplanetary systems can be relevant also in the interpretation of short-in-time observations: most importantly, it can serve the purpose of constraining observational uncertainties

on the basis of stability considerations, i.e., indicating which subdomains in parameter space favor the long-term stability of the planetary orbits [92].

Our study in the present Chapter focuses on one phenomenon, whose role appears central to the aim of classifying and characterizing the variety of possible secular orbital states in 3D planetary systems: this is the chain of bifurcations of periodic orbits which mark the transition, as the planets' mutual inclination increases, from the *apsidal corotation* to the *Lidov-Kozai* regime.

As is well known, the apsidal corotation (AC) states (see, for example, [56], [2], [57]) provide the backbone of the phase space of secular motions for two planets in coplanar orbits. Formally, the apsidal corotations are the continuation, in the nonlinear regime, of the linear (Laplace-Lagrange) normal mode solutions of the planar two-planet secular Hamiltonian. Physically, they represent periodic orbits along which the pericenters of the two planets constantly precess by remaining either always anti-aligned (state A) or always aligned (state B). Periodic orbits having the same property in the exact (non-averaged with respect to fast angles) Hamiltonian can also be found [38], [39] once the dynamics is regarded in a frame rotating with angular velocity equal to the (common) precession rate of the apsides.

Given their importance in the planar case, a natural question regards how the family of apsidal corotation orbits is continued, as well as what is the dynamical role played by the AC periodic, and nearby quasi-periodic, orbits, when we pass from the coplanar to the 3D planetary orbital configuration. Both the above questions have been addressed in the literature using diverse formalisms (see [3] and references therein, as well as the discussion below). Owing to reasons explained in detail in section 2.2 below, in our present study we employ our own-proposed formalism, in which, by applying a so-called *book-keeping* technique already at the level of Jacobi's reduction of the nodes [45]), we arrive at a natural decomposition of the 3D secular Hamiltonian of a system with fixed AMD as

$$\mathcal{H}_{sec} = \mathcal{H}_{planar}(\boldsymbol{\mathcal{X}}, \boldsymbol{\mathcal{Y}}) + \mathcal{H}_{space}(\boldsymbol{\mathcal{X}}, \boldsymbol{\mathcal{Y}}; \mathrm{AMD}) \quad . \tag{2.1}$$

In Eq.(2.1), $(\boldsymbol{\mathcal{X}}, \boldsymbol{\mathcal{Y}})$ are Poincaré canonical variables for the two planets ($(\mathcal{X}_2, \mathcal{Y}_2)$, $(\mathcal{X}_3, \mathcal{Y}_3)$ are approximately proportional to the planets' eccentricity vectors). The Angular Momentum Deficit is defined by

$$\mathrm{AMD} = L_2 + L_3 - L_z$$

where L_2, L_3 are the angular momenta of the circular orbits at semi-major axes a_2, a_3 equal to those of the two planets, and L_z the modulus of the total angular momentum normal to the system's Laplace plane.

The methodological benefits from working with a decomposition of the secular Hamiltonian as in Eq. (2.1) stem from the following properties (see sections 2.2 and 2.3 for details):

i) $\mathcal{H}_{planar}(\boldsymbol{\mathcal{X}}, \boldsymbol{\mathcal{Y}})$ is an integrable Hamiltonian, the quantity $J = (\mathcal{X}_2^2 + \mathcal{Y}_2^2 + \mathcal{X}_3^2 + \mathcal{Y}_3^2)/4$ being a second integral independent of the energy.

ii) For every permissible value of the energy $\mathcal{E}$, all the orbits $(\boldsymbol{\mathcal{X}}(t), \boldsymbol{\mathcal{Y}}(t))$ under Hamilton's equations with the Hamiltonian $\mathcal{H}_{planar}$ are confined to the Laplace plane, i.e., they have zero mutual inclination at the given (and fixed in advance) level of AMD.

iii) The Hamiltonian $\mathcal{H}_{planar}$ can be explicitly shown to admit two periodic orbits (called below the 'modes' A and B) which correspond to the anti-aligned and aligned apsidal corotation states for the two planets in the planar case.

iv) The Hamiltonian $\mathcal{H}_{space}$ can be further decomposed as $\mathcal{H}_{space} = \mathcal{H}_{0,space} + \mathcal{H}_{1,space}$, where $\mathcal{H}_{0,space}$ also admits $J = (\mathcal{X}_2^2 + \mathcal{Y}_2^2 + \mathcal{X}_3^2 + \mathcal{Y}_3^2)/4$ as a second integral. Then, the Hamiltonian

$$\mathcal{H}_{int} = \mathcal{H}_{planar} + \mathcal{H}_{0,space} \tag{2.2}$$

is integrable, and it has a similar formal structure as the Hamiltonian $\mathcal{H}_{planar}$. In particular, the existence of periodic orbits of the type A and B can be explicitly demonstrated for the Hamiltonian $\mathcal{H}_{int}$ using the integrability property, in the same way as for the Hamiltonian $\mathcal{H}_{planar}$.

v) Focusing, now, on the full secular Hamiltonian

$$\mathcal{H}_{sec} = \mathcal{H}_{int} + \mathcal{H}_{1,space} \tag{2.3}$$

a Birkhoff-like normal form construction (presented in the next Chapter 3) allows to demonstrate (up to an exponentially small error) that the periodic orbits A, B (accompanied by neighboring quasi-periodic orbits) continue to exist in the full 3D regime. Hence, we call these orbits the *3D apsidal corotation states*.

vi) We parameterize the level of non-coplanarity (mutual inclination $\mathrm{i}_2 + \mathrm{i}_3$) of the system in terms of the (constant) energy level of the full Hamiltonian $\mathcal{E} = \mathcal{H}_{sec}$. One way to regard the connection between the value of the energy $\mathcal{H}_{sec}$ and the level of non-coplanarity of the orbits is by noting that the energy grows in absolute value nearly as a quadratic function of the planetary eccentricities, i.e., nearly proportionally to a linear combination of e_2^2 and e_3^2. Thus, restricted to the chosen Poincaré surface of section (see below), the constant energy condition $\mathcal{E} = \mathcal{H}_{sec}$ yields an ellipsoid-like surface. Also (see section 2.3), for fixed AMD, the condition of constant mutual inclination yields the contour of a function also quadratic in the orbital eccentricities. Then, as shown in detail in section 2.3, for any fixed value of the energy $\mathcal{E}$, there are two values of the mutual inclination $\mathrm{i}_{mut} = \mathrm{i}_2 + \mathrm{i}_3$, namely $\mathrm{i}_{mut}^{min}(\mathcal{E})$, $i_{mut}^{max}(\mathcal{E})$ such that, the corresponding contours of constant mutual inclination come tangent to the ellipsoidal surface of constant energy $\mathcal{E} = \mathcal{H}_{sec}$. As a consequence, for any value of the mutual inclination in the interval $\mathrm{i}_{mut}^{min}(\mathcal{E}) \leq \mathrm{i}_{mut} \leq \mathrm{i}_{mut}^{max}(\mathcal{E})$ there is an energetically permissible domain of motions. By the geometric properties of the above considerations, we find that both $\mathrm{i}_{mut}^{min}(\mathcal{E})$ and $\mathrm{i}_{mut}^{max}(\mathcal{E})$ are monotonically increasing functions of the energy. Thus, selecting a particular level value of the energy $\mathcal{E}$ fixes the overall level of mutual inclinations allowed at the energy $\mathcal{E}$. The minimum possible energy $\mathcal{E}_{min}$ is defined by the condition that the level surface $\mathcal{H}_{sec} = \mathcal{E}_{min}$ is tangent to the level surface of minimum possible mutual inclination $\mathrm{i}_{mut} = 0$ (planar case), while all other points of the surface $\mathrm{i}_{mut} = 0$, except for the points of tangency, are in the interior of the surface $\mathcal{H} = \mathcal{E}_{min}$. Solving for these conditions allows to specify the value of $\mathcal{E}_{min}$.

In conclusion, the level of mutual inclination for all orbits increases in general with the quantity $\delta\mathcal{E} = \mathcal{E} - \mathcal{E}_{min}$, where $\mathcal{E}_{min} \leq \mathcal{E} \leq 0$. Thus, the lowermost value of $\delta\mathcal{E}$ is $\delta\mathcal{E}_{min} = 0$, while the highermost limit is $\delta\mathcal{E}_{max} = -\mathcal{E}_{min}$, i.e., $\mathcal{E} = 0$. At this latter limit, the available phase space shrinks to a point with $\mathrm{e}_2(t) = \mathrm{e}_3(t) = 0$. This means a unique possible orbital configuration of two mutually-inclined circular planetary orbits. We call this the *limiting trajectory of the Lidov-Kozai regime*. Actually, we will see in section 2.3 that, for negative energies $\mathcal{E}$ close to zero, the phase space acquires a structure reminiscent to the one of the non-integrable Lidov-Kozai case of the restricted three-body problem (i.e. non intersecting trajectories examined in a higher than quadrupolar development of the disturbing function, see [60]). The typical behavior of the trajectories in the Lidov-Kozai regime is to (quasi-)periodically exchange eccentricity for mutual inclination. However, we will see that such a coarse illustration of the dynamics is rather simplistic in the case of non-hierarchical (in distance ratios or masses) two-planet systems; in reality, the dynamics around the central Lidov-Kozai periodic orbit is highly unstable and the corresponding phase space turns to exhibit strong chaos.

In summary, our focus in the present Chapter will be on describing, with sufficient detail, the observed transition in the structure of the phase space, as the parameter $\delta\mathcal{E}$ increases from its lowermost limit, corresponding to a nearly planar orbital configuration, to the highermost limit, corresponding to nearly circular orbits with a high degree of mutual inclination.

As expected in the study of any dynamical system, structural changes in the phase space are associated with the birth, bifurcations and stability evolution of the most important periodic orbits of the system. We already mentioned that these are the ACs, in the nearly planar limit, and the Lidov-Kozai orbits, in the maximum mutual inclination limit. We follow the evolution and the connections between these periodic orbits, as well as other ones emerging in half the way between the two limiting regimes. In our study we work with analytical estimates, as well as with a numerical example inspired by the υ-Andromedae system. This is an example of system being reasonably far from any hierarchical limit: the estimated mass ratio of the two planets is $m_2/m_3 \simeq 1.3$, while the estimated semi-major axis ratio is $a_2/a_3 \simeq 0.3$. On the other hand, section 2.4 contains results from a numerical investigation referring to different choices for the mass and semi-major axis ratios,

representing every one of all possible cases of hierarchical models that could arise in the problem under consideration. As a rough guide, the phenomena discussed below should cover most cases of interest in the range of mass ratios $1/10 \leq m_2/m_3 \leq 10$, distance ratios $1/7 \leq r_2/r_3 \leq 1/3$ and mutual inclination $0 \leq \mathrm{i}_{mut} \leq 45^\circ$.

Few more words about our hereby proposed formalism and method of study: the spectrum of methods and formalisms proposed for the study of the secular planetary three body problem is nearly as wide as the literature itself on the subject. Different proposals distinguish between cases in which the three body problem dealt with is considered hierarchical (e.g. in the distances $r_2/r_3 \ll 1$; see [5], [26], [83]), or non-hierarchical (see [42], [89]). The choice of variables and/or proposed representation of the phase space of the system has often been motivated by whether the focus of a particular study is on phenomena related to apsidal-corotations (see [2], [56], [57]), or the Kozai instability (see [48], [58], [61], [67]). In addition, different formalisms stem from choices related to:

i) the type of *Hamiltonian expansion*: this can be performed as the usual (Laplace-Lagrange) series expansion in powers of the planets' eccentricities and inclinations (see for example [87] and [59]) or as a Legendre multipolar expansion (see [88], [58] and references therein). One can note that, although the two types of expansions are equivalent *in the limit* of infinite order of the expansion, different truncations (even with the same type of series) can lead to quantitatively, and even qualitatively, different results. Libert & Henrard in [59] have discussed the question of the correct order of truncation in the framework of the Laplace-Lagrange expansion. Mogaszewki & Goździewki and Naoz (see [83], [89] and [88]) discuss various truncated multipolar models for spatial hierarchical systems. To our knowledge, there is no literature on a comparison between the results obtained by truncated models with the two types of expansion for non-hierarchial spatial systems.

ii) *Method of averaging*: different secular models are obtained by a different choice of method for averaging the Hamiltonian with respect to the fast angles. Such methods include: a) averaging "by scissors", i.e., by just dropping-off the Hamiltonian all fast periodic terms (see, for example, [59], [42]). b) "Closed-form" averaging (e.g. [83]). This method has the benefit of avoiding expansions in the orbital eccentricities (whose convergence becomes limited due to the limit in the series inversion of Kepler's equation, see, for example [99]). However, closed-form averaging can only be performed after a multipolar expansion of the Hamiltonian. Thus the method is particularly suited for systems hierachical with respect to the planetary distances, while its precision in the case of non-hierarchical systems is an open issue (see some results in section 2.4). c) Numerical computation (e.g. by Gauss' method) of the quadratures involved in the averaging (see [100], [81]). This method is particularly suited for systems with intersecting trajectories, owing to theorems (see, for example, [37]) establishing the continuity of the secular equations of motion at the points of intersection, which are singularities of the integrand functions appearing in the quadratures. d) Elimination of the mean anomalies from the Hamiltonian via a canonical transformation (see [5] or [89]). From the theoretical point of view, the use of a canonical transformation is imperative when precision of second order in the planetary masses is sought for in the secular model. It should be stressed that while $\mathcal{O}(m^2)$ expansions are straightforward to obtain in the framework of the Laplace-Lagrange series (see [73]), their counterpart in the form of closed-form series is an open question. In fact, closed-form averaging in the framework of the three-body problem requires the use of some 'relegation' technique (see [90]), or alternatives as those recently proposed in [9]).

iii) *Choice of coordinates*. Several sets of variables have been proposed as convenient for the visualization and study of the phase space of secular motions. Examples are: $(\mathrm{e}_2 \sin(\omega_2), \mathrm{e}_3 \sin(\omega_3))$ (see for istance [59], [83], [61]); $(\mathrm{e}_j \cos(\Delta\varpi), \mathrm{e}_j \sin(\Delta\varpi))\,, j = 2, 3$ (see [80]); $(\mathrm{e}_2 \cos(2\omega_2), \mathrm{e}_3 \cos(\Delta\omega))$ (see [58]); $(\mathrm{e}_2 \cos(\Delta\varpi), \mathrm{e}_3 \cos(2\,\omega_2)\,)$ (see [83], [79]); $(\mathrm{e}_j \cos(\omega_j), \mathrm{e}_j \sin(\omega_j))$ (see [100]). Among the motivations behind the choice of a particular set of variables are: a) the treatment of singular cases (e.g. $\mathrm{e}_2 = 0$, $\mathrm{e}_3 = 0$, in which the longitude of the perihelium is no longer defined), b) the possibility to include all the main families of possible orbital states in one plot. As a characteristic

example of the latter, see figure 3 of [79]; one can remark, however, the complexity involved in properly deciphering the information given in that figure, which is evident from the accompanying caption.

Our own choice regarding the points (i) to (iii) above is: (i) and (ii) we base most of our results on a closed-form averaging of a multipolar expansion (in powers of the distance ratio $r_2/r_3 < 1$) of the Hamiltonian (1.10). Besides its compact form, convenient for analytic studies (as, for example, in subsection 2.3.4), such a model, truncated at a sufficiently high multipole order, circumvents the problem of slow convergence of the Laplace-Lagrange series for highly eccentric orbits, without compromising precision even far from the hierarchical limit (e.g. for $r_2/r_3 \sim 0.3$). Indeed, the closed-form averaging is based on a multipolar expansion, which produces a smaller number of terms in the Hamiltonian with respect to the Laplace-Lagrange expansion, rendering the procedure faster. Moreover, the closed-form averaging allows to avoid the singularity of Kepler equation. The rational dependence of the Hamiltonian on the quantity $\sqrt{1-\mathrm{e}_3^2}$ implies that any expansion in the eccentricities performed after the closed-form averaging is convergent in the entire domain $|\mathrm{e}_2| < 1$, $|\mathrm{e}_3| < 1$. However, we have to recall that multipolar expansions have singularities for values of the eccentricities e_2 and e_3 for which the distance of the apocenter of the inner planet is equal to the distance of the pericenter of the outer planet, i.e. such that $a_2(1+\mathrm{e}_2) = a_3(1-\mathrm{e}_3)$. In order to specify the suitable order of multipole truncation, in section 2.2 we make a comparison of the phase portraits obtained via the secular Hamiltonian arrived at by the above method versus those obtained by a scissors' averaging of the Laplace-Lagrange series truncated at order 10 in the eccentricities. Also, in obtaining the final Hamiltonian we introduce a book-keeping procedure for the Jacobi reduction of the nodes, which, as mentioned already, leads to a convenient decomposition of the Hamiltonian as in Eq. (2.1). (iii) We illustrate all phase portraits using the usual Poincaré surface of section $(\mathrm{e}_2\cos\omega_2, \mathrm{e}_2\sin\omega_2)$ every time when $\omega_3 = \pi$, $\dot{\omega}_3 \geq 0$. The sequence of canonical transformations leading to such a representation of phase portraits is described in section 2.2. Owing to the conservation of angular momentum, one can easily see ([17]) that the phase space of the integrable models $\mathcal{H}_{planar}$ and $\mathcal{H}_{int}$ is the sphere S^2 (instead of $\mathbb{R}^4$, as generically true for Hamiltonian systems with two degrees of freedom). Furthermore, as analyzed in section 2.2, some points of the sphere 'inflate' to curves in the Poincaré surface of section defined as above. Finally, using an appropriate set of good variables whose Poisson algebra admits the angular momentum as a Casimir, the two modes A and B are seen to be separated by a meridian circle in the sphere S^2, which however does not correspond to a dynamical separatrix (since the integrable model contains no unstable periodic orbits). We devote some effort to carefully describe these phenomena, which are often found to generate some confusion in the literature when use is made of some of the components of the planets' eccentricity vectors to describe the structure of the problem's phase space.

The content of the following sections (jointly with section 3.1) is largely based on the article [75].

2.2 Hamiltonian model

2.2.1 Averaged Hamiltonian

We will focus below mostly on the properties of a secular model $\mathcal{H}_{sec}$ for the Hamiltonian (1.10) obtained by performing averaging with respect to the fast angles just 'by scissors':

$$\begin{aligned}
\mathcal{H}_{sec} &= \frac{1}{4\pi^2}\int_0^{2\pi}\int_0^{2\pi} H(\boldsymbol{r}_2,\boldsymbol{r}_3,\boldsymbol{p}_2,\boldsymbol{p}_3)\,dM_2\,dM_3 \\
&= \frac{1}{4\pi^2}\int_0^{2\pi}\int_0^{2\pi}\left(\left(\frac{1}{m_0}+\frac{1}{m_2}\right)\frac{{\boldsymbol{p}_2}^2}{2} - \frac{\mathcal{G}\,m_0\,m_2}{r_2} + \left(\frac{1}{m_0}+\frac{1}{m_3}\right)\frac{{\boldsymbol{p}_3}^2}{2} - \frac{\mathcal{G}\,m_0\,m_3}{r_3}\right) dM_2\,dM_3 \\
&+ \frac{1}{4\pi^2}\int_0^{2\pi}\int_0^{2\pi}\frac{\boldsymbol{p}_2\cdot\boldsymbol{p}_3}{m_0}dM_2\,dM_3 - \frac{1}{4\pi^2}\int_0^{2\pi}\int_0^{2\pi}\frac{\mathcal{G}\,m_2\,m_3}{|\boldsymbol{r}_2-\boldsymbol{r}_3|}\,dM_2\,dM_3 \quad . \qquad (2.4)
\end{aligned}$$

We have

$$\frac{1}{4\pi^2}\int_0^{2\pi}\int_0^{2\pi}\left(\left(\frac{1}{m_0}+\frac{1}{m_2}\right)\frac{\boldsymbol{p}_2{}^2}{2}-\frac{\mathcal{G}\,m_0\,m_2}{r_2}+\left(\frac{1}{m_0}+\frac{1}{m_3}\right)\frac{\boldsymbol{p}_3{}^2}{2}-\frac{\mathcal{G}\,m_0\,m_3}{r_3}\right)dM_2\,dM_3$$
$$= \quad -\frac{\mathcal{G}m_0m_2}{2a_2}-\frac{\mathcal{G}m_0m_3}{2a_3}+\frac{\mathcal{G}m_2^2}{2a_2}+\frac{\mathcal{G}m_3^2}{2a_3}\quad . \tag{2.5}$$

The indirect part of the disturbing function, depending on the product $\boldsymbol{p}_2\cdot\boldsymbol{p}_3$, yields zero average

$$\frac{1}{4\pi^2}\int_0^{2\pi}\int_0^{2\pi}\frac{\boldsymbol{p}_2\cdot\boldsymbol{p}_3}{m_0}\,dM_2\,dM_3=\frac{1}{4\pi^2}\frac{\mathcal{G}\,m_2m_3}{\sqrt{a_2^3\,a_3^3}}\left(\int_0^{2\pi}\frac{d\boldsymbol{r}_2}{dM_2}\,dM_2\int_0^{2\pi}\frac{d\boldsymbol{r}_3}{dM_3}\,dM_3\right)=0\quad . \tag{2.6}$$

To compute the average of the direct part $\mathcal{G}m_2m_3/|\boldsymbol{r}_2-\boldsymbol{r}_3|$, we assume a dynamical regime of the planetary system in which the distance ratio r_2/r_3 (where $r_i=|\boldsymbol{r}_i|\,,\ i=2,3$) remains always smaller than unity. Then, the quantity $\mathcal{G}m_2m_3/|\boldsymbol{r}_2-\boldsymbol{r}_3|$ admits a convergent Legendre multipolar expansion in powers of the quantity $r_2/r_3<1$:

$$-\frac{1}{4\pi^2}\int_0^{2\pi}\int_0^{2\pi}\frac{\mathcal{G}\,m_2\,m_3}{|\boldsymbol{r}_2-\boldsymbol{r}_3|}\,dM_2\,dM_3\;=$$
$$-\frac{\mathcal{G}\,m_2\,m_3}{4\pi^2}\int_0^{2\pi}\int_0^{2\pi}\left(\frac{1}{r_3}+\frac{\boldsymbol{r}_2\cdot\boldsymbol{r}_3}{r_3^3}-\frac{1}{2}\frac{r_2^2}{r_3^3}+\frac{3}{2}\frac{(\boldsymbol{r}_2\cdot\boldsymbol{r}_3)^2}{r_3^5}+\dots\right)dM_2\,dM_3\,.$$

We have:

$$-\frac{\mathcal{G}\,m_2\,m_3}{4\pi^2}\int_0^{2\pi}\int_0^{2\pi}\frac{1}{r_3}dM_1dM_2=-\frac{\mathcal{G}m_2m_3}{a_3}\,,\qquad\int_0^{2\pi}\int_0^{2\pi}\frac{\boldsymbol{r}_2\cdot\boldsymbol{r}_3}{r_3^3}\,dM_2\,dM_3=0\quad .$$

We then need to compute

$$\mathcal{R}_{sec}=\frac{1}{4\pi^2}\int_0^{2\pi}\int_0^{2\pi}-\frac{\mathcal{G}\,m_2\,m_3}{r_3}\left(-\frac{1}{2}\frac{r_2^2}{r_3^2}+\frac{3}{2}\frac{(\boldsymbol{r}_2\cdot\boldsymbol{r}_3)^2}{r_3^4}+\dots\right)dM_2\,dM_3\,. \tag{2.7}$$

Keeping only the lowest order term in the integrand of (2.7), proportional to $(r_2/r_3)^2$, leads to the so-called *quadrupole* approximation; the next truncation (up to terms proportional to $(r_2/r_3)^3$) is the *octupole* approximation, etc. The integrals of any multipole approximation can be computed in so-called *closed form* (i.e. without expansions in the eccentricities), by avoiding completely the series reversion of Kepler's equation, using, instead, the change of variables $M_2\to u_2$ (eccentric anomaly), $M_3\to f_3$ (true anomaly). We have

$$dM_2=(1-\mathrm{e}_2\cos u_2)\,du_2,\ dM_3=\frac{r_3^2}{a_3^2\sqrt{1-\mathrm{e}_3^2}}\,df_3,\ r_2=a_2(1-\mathrm{e}_2\cos(u_2)),\ \frac{1}{r_3}=\frac{1+\mathrm{e}_3\cos(f_3)}{a_3\,(1-\mathrm{e}_3^2)}\,. \tag{2.8}$$

Replacing the above expressions in (2.7) and performing all trigonometric reductions, we find a trigonometric polynomial series containing only terms of the form $\cos(K_2u_2+K_3f_3+...)$, with K_2,K_3 integers. This implies that the average can be computed by just scissor-cutting all the terms in the integrand of (2.7) for which $|K_2|+|K_3|\neq 0$. This leads to a closed-form expression for the secular Hamiltonian

$$\mathcal{H}_{sec}=-\frac{\mathcal{G}m_0m_2}{2a_2}-\frac{\mathcal{G}m_0m_3}{2a_3}+\frac{\mathcal{G}m_2^2}{2a_2}+\frac{\mathcal{G}m_3^2}{2a_3}-\frac{\mathcal{G}m_2m_3}{a_3}+\mathcal{R}_{sec}(a_2,a_3,\mathrm{e}_2,\mathrm{e}_3,\mathrm{i}_2,\mathrm{i}_3,\omega_2,\omega_3,\Omega_2-\Omega_3)\quad . \tag{2.9}$$

The following are some relevant remarks regarding the Hamiltonian (2.9):

Remark 1: the averaging (2.7) yields a valid secular model only when the system is assumed

to be *far from any low-order mean-motion resonance*. By 'low' it is implied that no resonance condition of the form

$$|K_2 n_2 + K_3 n_3| < \mathcal{O}\left((\mathcal{G}m_0\mu)^{1/2}/a_2^{3/2}\right) \quad ,$$

should be satisfied, with K_2, K_3 integers, $\mu = \max(m_2/m_0, m_3/m_0)$, $n_2 = \left(\mathcal{G}(m_0+m_2)/a_2^3\right)^{1/2}$, $n_3 = \left(\mathcal{G}(m_0+m_3)/a_3^3\right)^{1/2}$, for an order $|K_2|+|K_3|$ inferior or equal to the order N_P of the multipole expansion in Eq.(2.7). Formally, such a requirement reflects the fact that the averaging by scissors serves to substitute the complete procedure of first-order averaging, which involves a canonical transformation to properly eliminate from the Hamiltonian the fast angles M_2, M_3. Such a transformation can be defined in closed form (see, for example, [9]), but it involves divisors of the form $K_2 n_2 + K_3 n_3$ which become very small near any mean motion resonance of order smaller or equal to N_P.

Remark 2: the function $\mathcal{R}_{sec}$ is trigonometric polynomial in the angles ω_2, ω_3, as well as $\Omega_2 - \Omega_3$. The dependence on Ω_2, Ω_3 only by the difference $\Omega_2 - \Omega_3$ is a consequence of the fact that the sum of the angular momenta $H_2 + H_3$ perpendicularly to the system's Laplace plane is an invariant of the motion of the complete Hamiltonian (1.10), which is preserved also in the secular Hamiltonian (2.9).

Remark 3: the function $\mathcal{R}_{sec}$ is polynomial in the quantities $a_2, \mathrm{e}_2, \mathrm{e}_3, \sin\mathrm{i}_2, \sin\mathrm{i}_3, \cos\mathrm{i}_2, \cos\mathrm{i}_3$, while it is rational in the quantities $a_3, \eta_3 = \sqrt{1-\mathrm{e}_3^2}$. As regards the dependence on $\sin\mathrm{i}_2, \sin\mathrm{i}_3, \cos\mathrm{i}_2, \cos\mathrm{i}_3$, this follows the symmetry that $\mathcal{R}_{sec}$ can only depend on the quantity $\cos(\mathrm{i}_2+\mathrm{i}_3)$, where $\mathrm{i}_2+\mathrm{i}_3 = \mathrm{i}_{mut}$ is the *mutual inclination* of the planetary trajectories. This symmetry is exploited when performing Jacobi reduction of the nodes in the Hamiltonian $\mathcal{H}_{sec}$ (see next subsection). On the other hand, the rational dependence on the quantity $\sqrt{1-\mathrm{e}_3^2}$ implies that any expansion in the eccentricities performed *after* the closed-form averaging is convergent in the entire domain $|\mathrm{e}_2| < 1, |\mathrm{e}_3| < 1$. This allowance to perform an a posteriori expansion of the Hamiltonian $\mathcal{H}_{sec}$ in the planetary eccentricities proves useful in the theoretical analysis of the dynamical properties of such a Hamiltonian (see section 2.3).

2.2.2 Book-keeping and Jacobi reduction of the nodes

Consider the set of Delaunay canonical variables, introduced in Eq. (1.19):

$$\begin{aligned} L_j &= m_j\sqrt{\mathcal{G}\, m_0\, a_j}\,, & l_j &= M_j\,, \\ G_j &= L_j\sqrt{1-\mathrm{e}_j^2}\,, & g_j &= \omega_j\,, \\ H_j &= G_j\cos(\mathrm{i}_j)\,, & h_j &= \Omega_j \end{aligned} \tag{2.10}$$

with $j = 2, 3$. Since $a_j = a_j(L_j)$, $\mathrm{e}_j = \mathrm{e}_j(L_j, G_j)$, $\mathrm{i}_j = \mathrm{i}_j(L_j, G_j, H_j)$, substituting the corresponding expressions in the Hamiltonian $\mathcal{H}_{sec}$ (Eq. (2.9)) leads to a Hamiltonian model with six degrees of freedom

$$\mathcal{H}_{sec} \equiv \mathcal{H}_{sec}(L_2, L_3, G_2, G_3, H_2, H_3, \omega_2, \omega_3, \Omega_2 - \Omega_3) \quad . \tag{2.11}$$

Since the angles M_2, M_3 are ignorable, the Delaunay momenta L_2, L_3 are integrals of motion under the Hamiltonian flow of $\mathcal{H}_{sec}$. There are two more integrals of motion in involution with L_2, L_3, corresponding to the two components of the total angular momentum, normal and parallel to the Laplace plane. For the normal component we have $L_z = H_2 + H_3 = C = const$, while for the parallel component we have $L_\parallel = G_2\sin(\mathrm{i}_2(L_2, G_2, H_2)) - G_3\sin(\mathrm{i}_3(L_3, G_3, H_3)) = 0$.

In our analytical treatment of the Hamiltonian $\mathcal{H}_{sec}$ it turns convenient to perform the Jacobi reduction of the nodes (subsection 1.4.5.2) by simultaneously introducing two 'book-keeping symbols', ε, η [19], both with numerical values $\varepsilon = 1$, $\eta = 1$, whose role is the following: i) ε keeps track of the order of a certain term in the planetary eccentricities and inclinations, ii) η separates

Hamiltonian terms which depend on powers of the quantity $\cos(\mathrm{i}_2 + \mathrm{i}_3)$ from those terms which do not depend on the mutual inclination $\mathrm{i}_{mut} = \mathrm{i}_2 + \mathrm{i}_3$.

More specifically, we Jacobi-reduce the Hamiltonian $\mathcal{H}_{sec}$ by the following steps:

Step 1: Canonical transformation. Similarly as in [59] (see also subsection 1.4.5.2), we introduce the canonical transformation

$$\begin{aligned}
\Lambda_2 &= L_2\,, & \lambda_2 &= M_2 + \omega_2 + \Omega_2\,,\\
\Lambda_3 &= L_3\,, & \lambda_3 &= M_3 + \omega_3 + \Omega_3\,,\\
W_2 &= L_2 - G_2\,, & w_2 &= -\omega_2\,,\\
W_3 &= L_3 - G_3\,, & w_3 &= -\omega_3\,,\\
R_2 &= L_2 - H_2\,, & \theta_{r2} &= \Omega_3 - \Omega_2\,,\\
R_3 &= L_2 + L_3 - H_2 - H_3 = \mathrm{AMD}\,, & \theta_{r3} &= -\Omega_3\,.
\end{aligned} \tag{2.12}$$

Inverting the transformation (2.12) and substituting the result into the Hamiltonian (2.11), the secular Hamiltonian obtains the form:

$$\mathcal{H}_{sec} \equiv \mathcal{H}_{sec}(\Lambda_2, \Lambda_3, W_2, W_3, R_2, R_3, w_2, w_3, \theta_{r2}) \quad . \tag{2.13}$$

Step 2: Jacobi reduction with book-keeping. Hamilton's equations for the Hamiltonian (2.13) yield $\dot{\Lambda}_2 = \dot{\Lambda}_3 = 0$ (constancy of the semi-major axes a_2, a_3), as well as $\dot{R}_3 = 0$ (constancy of L_z, implying the constancy of the AMD). The crucial point stems from the following invariance property of the Hamiltonian (2.13):

$$\dot{\theta}_{r2} = \frac{\partial \mathcal{H}_{sec}(\Lambda_2, \Lambda_3, W_2, W_3, R_2, R_3 = \mathrm{AMD}, w_2, w_3, \theta_{r2} = \pi)}{\partial R_2} = 0 \tag{2.14}$$

corresponding to the invariance in time of the relation $\theta_{r2} = \Omega_3 - \Omega_2 = \pi$ for all trajectories. Equation (2.14), however, implies that when the substitution $\Omega_3 = \Omega_2 + \pi$ is made in the Hamiltonian (2.13), the resulting expression becomes independent of R_2, and the reduced set of Hamilton's equations

$$\begin{aligned}
\dot{w_2} &= \frac{\partial \mathcal{H}_{sec}(\Lambda_2, \Lambda_3, W_2, W_3, R_3 = \mathrm{AMD}, w_2, w_3, \theta_{r2} = \pi)}{\partial W_2}\,,\\
\dot{w_3} &= \frac{\partial \mathcal{H}_{sec}(\Lambda_2, \Lambda_3, W_2, W_3, R_3 = \mathrm{AMD}, w_2, w_3, \theta_{r2} = \pi)}{\partial W_3}\,,\\
\dot{W}_2 &= -\frac{\partial \mathcal{H}_{sec}(\Lambda_2, \Lambda_3, W_2, W_3, R_3 = \mathrm{AMD}, w_2, w_3, \theta_{r2} = \pi)}{\partial w_2}\,,\\
\dot{W}_3 &= -\frac{\partial \mathcal{H}_{sec}(\Lambda_2, \Lambda_3, W_2, W_3, R_3 = \mathrm{AMD}, w_2, w_3, \theta_{r2} = \pi)}{\partial w_3}\,,
\end{aligned} \tag{2.15}$$

remains valid. Note that Λ_2, Λ_3 in the above *secular equations of motion* are constant, and can be effectively treated as parameters, depending on the (also constant) parameters a_2, a_3. Also, the terms

$$-\frac{\mathcal{G}m_0m_2}{2a_2} - \frac{\mathcal{G}m_0m_3}{2a_3} + \frac{\mathcal{G}m_2^2}{2a_2} + \frac{\mathcal{G}m_3^2}{2a_3} - \frac{\mathcal{G}m_2m_3}{a_3}$$

appearing in Eq. (2.9), do not contribute to the secular equations of motion, and can be omitted from further analysis, by just renaming $\mathcal{R}_{sec} \to \mathcal{H}_{sec}$. Finally, Eqs. (2.15) allow to compute the secular evolution of only the eccentricity vectors of the two planets. To obtain the evolution in inclination, instead, we use the following relations, obtained directly from the conservation of the angular momentum:

$$\cos(\mathrm{i}_2) = \frac{\Lambda_2^2(1-\mathrm{e}_2^2) - \Lambda_3^2(1-\mathrm{e}_3^2) + L_z^2}{2L_z\Lambda_2\sqrt{1-\mathrm{e}_2^2}}, \qquad \cos(\mathrm{i}_3) = \frac{\Lambda_3^2(1-\mathrm{e}_3^2) - \Lambda_2^2(1-\mathrm{e}_2^2) + L_z^2}{2L_z\Lambda_3\sqrt{1-\mathrm{e}_3^2}}, \tag{2.16}$$

where the last relation follows from

$$\cos(\mathrm{i}_3) = \frac{L_z - \Lambda_2\sqrt{1-\mathrm{e}_2^2}\cos(\mathrm{i}_2)}{\Lambda_3\sqrt{1-\mathrm{e}_3^2}}\,.$$

In the practical implementation of *step 2*, we perform the substitutions of the angle variables $\Omega_3 = \Omega_2 + \pi$, as well as $\omega_2 = -w_2$, $\omega_3 = -w_3$ in the Hamiltonian, but leave implicit the latter's dependence on the action variables $(\Lambda_2, \Lambda_3, W_2, W_2, R_2, R_3)$ through the elements $(a_2, a_3, \mathrm{e}_2, \mathrm{e}_3, \mathrm{i}_2, \mathrm{i}_3)$. Owing, however, to the non-dependence of the Hamiltonian on R_2 *after* the substitution $\Omega_3 = \Omega_2 + \pi$, we have that the Hamiltonian depends on the inclinations only through the trigonometric combination $\cos(\mathrm{i}_2 + \mathrm{i}_3) = \cos(\mathrm{i}_2)\cos(\mathrm{i}_3) - \sin(\mathrm{i}_2)\sin(\mathrm{i}_3)$. Taking into account that

$$(1 - \cos(\mathrm{i}_2)\cos(\mathrm{i}_3)) = \mathcal{O}(\varepsilon^2)\,, \qquad \sin(\mathrm{i}_2)\sin(\mathrm{i}_3) = \mathcal{O}(\varepsilon^2) \quad ,$$

where the attribution of $\mathcal{O}(\varepsilon^2)$ to an expression stands for 'second order in the eccentricities and inclinations', we then introduce the following *book-keeping control identities*:

$$\cos(\mathrm{i}_2)\cos(\mathrm{i}_3) = \varepsilon^2\eta\,(\cos(\mathrm{i}_2)\cos(\mathrm{i}_3) - 1) + 1\,, \qquad \sin(\mathrm{i}_2)\sin(\mathrm{i}_3) = \varepsilon^2\eta\sin(\mathrm{i}_2)\sin(\mathrm{i}_3)\,. \tag{2.17}$$

We also use the substitution rule

$$\sin(\mathrm{i}_2)\sin(\mathrm{i}_3) = \cos(\mathrm{i}_2)\cos(\mathrm{i}_3) + \frac{\Lambda_2\sqrt{1-\mathrm{e}_2^2}}{2\,\Lambda_3\sqrt{1-\mathrm{e}_3^2}} + \frac{\Lambda_3\sqrt{1-\mathrm{e}_3^2}}{2\,\Lambda_2\sqrt{1-\mathrm{e}_2^2}} - \frac{L_z^2}{2\,\Lambda_2\sqrt{1-\mathrm{e}_2^2}\,\Lambda_3\sqrt{1-\mathrm{e}_3^2}}\,. \tag{2.18}$$

Substituting the above expressions into the Hamiltonian, and truncating the resulting expression up to a pre-selected *maximum order in book-keeping* N_{bk}, by symmetry the terms in equal powers of the products $\sin(\mathrm{i}_2)\sin(\mathrm{i}_3)$ and $\cos(\mathrm{i}_2)\cos(\mathrm{i}_3)$ are opposite, and thus they are canceled. Hence, the Hamiltonian resumes the form:

$$\mathcal{H}_{sec} = \sum_{s_1=0}^{N_{bk}/2} \eta^{s_1}\varepsilon^{2s_1}\mathcal{H}_{sec,s1}(\mathrm{e}_2, \mathrm{e}_3, w_2, w_3; a_2, a_3, L_z) \quad . \tag{2.19}$$

We finally restore the values $\varepsilon = 1$ and $\eta = 1$ of the book-keeping parameters, and write the truncated (up to book-keeping order N_{bk}) Hamiltonian as:

$$\mathcal{H}_{sec} = \mathcal{H}_{planar} + \mathcal{H}_{space} \tag{2.20}$$

where

$$\mathcal{H}_{planar} = \mathcal{H}_{sec,0}(\mathrm{e}_2, \mathrm{e}_3, w_2 - w_3; a_2, a_3), \quad \mathcal{H}_{space} = \sum_{s_1=1}^{N_{bk}/2} \mathcal{H}_{sec,s1}(\mathrm{e}_2, \mathrm{e}_3, w_2, w_3; a_2, a_3, L_z)\,. \tag{2.21}$$

Note that the term $\mathcal{H}_{planar}$ depends only on the difference $w_2 - w_3$, since, in the planar case, the sum $W_2 + W_3$, which represents the total angular momentum deficit for planar orbits, is a conserved quantity.

Step 3: Expansion in the orbital eccentricities. We re-introduce the book-keeping:

$$\mathrm{e}_2 \to \varepsilon\mathrm{e}_2, \quad \mathrm{e}_3 \to \varepsilon\mathrm{e}_3, \quad L_z \to \Lambda_2 + \Lambda_3 - \varepsilon^2\mathrm{AMD}\,. \tag{2.22}$$

Substituting the above expressions in the Hamiltonian (2.21), and expanding the resulting expressions in powers of the book-keeping parameter ε, apart from a term depending only on the constants a_1, a_2 and AMD, we arrive at the truncated Hamiltonian:

$$\begin{aligned} \mathcal{H}_{sec} &= \mathcal{H}_{planar} + \mathcal{H}_{space} \qquad (2.23)\\ &= \sum_{s_2=1}^{N_{bk}/2} \varepsilon^{2s_2} h_{s_2}(\mathrm{e}_2, \mathrm{e}_3, w_2 - w_3; a_2, a_3) + \sum_{s_2=1}^{N_{bk}/2} \varepsilon^{2s_2}\tilde{h}_{s_2}(\mathrm{e}_2, \mathrm{e}_3, w_2, w_3; a_2, a_3, \mathrm{AMD}) \quad . \end{aligned}$$

Step 4: introduction of Poincaré variables: The Hamiltonian (2.23) is polynomial in the eccentricities e_2, e_3. It was already stressed that the series expansion with respect to the quantities $\eta_2 = \sqrt{1-\mathrm{e}_2^2}$ and $\eta_3 = \sqrt{1-\mathrm{e}_3^2}$ introduces no divergence in the polydisc $|\mathrm{e}_2| < 1$, $|\mathrm{e}_3| < 1$. Besides, the Hamiltonian satisfies the D'Alembert rules in the eccentricities: every trigonometric term in it is of the form $h_{\ell_2,\ell_3,k_2,k_3}(a_2,a_3)(\mathrm{AMD})^{\ell_1}\mathrm{e}_2^{\ell_2}\mathrm{e}_3^{\ell_3}\cos(k_2w_2+k_3w_3)$, with ℓ_1 positive integer, and the integers ℓ_2,ℓ_3,k_2,k_3 satisfying i) $\ell_2,\ell_3>0$, ii) $\ell_2+\ell_3 \geq |k_2|+|k_3|$, and iii) $mod(\ell_2,2) = mod(k_2,2)$, $mod(\ell_3,2) = mod(k_3,2)$. Rules (i) to (iii) imply, now, that the Hamiltonian is polynomial in the Poincaré canonical variables stemming from the variables (w_j, W_j), $j = 2,3$ through the canonical transformation

$$\mathcal{X}_j = -\sqrt{2\,W_j}\cos(w_j)\,, \qquad \mathcal{Y}_j = \sqrt{2\,W_j}\sin(w_j)\,, \qquad j=2,3\ . \tag{2.24}$$

To obtain a truncated polynomial series of the Hamiltonian in the variables $(\mathcal{X}_j, \mathcal{Y}_j)$, we substitute into the Hamiltonian (2.23) the expressions

$$\sin(w_j) = \frac{\mathcal{Y}_j}{\sqrt{2W_j}}, \quad \cos(w_j) = -\frac{\mathcal{X}_j}{\sqrt{2W_j}}, \quad \mathrm{e}_j = \sqrt{\frac{2W_j}{\Lambda_j} - \varepsilon^2\left(\frac{W_j}{\Lambda_j}\right)^2}, \quad j=2,3$$

and expand the result in powers of the book-keeping parameter ε, up to the truncation order N_{bk}. This leads to an expression which no longer contains trigonometric functions of the angles w_j, while it still contains integer powers of the actions W_j. We then substitute $W_j \to (\mathcal{X}_j^2+\mathcal{Y}_j^2)/2$, and, finally, set back $\varepsilon = 1$. In this way we arrive at the final secular model:

$$\begin{aligned}
\mathcal{H}_{sec}(\mathcal{X}_2,\mathcal{X}_3,\mathcal{Y}_2,\mathcal{Y}_3;\mathrm{AMD}) &= \mathcal{H}_{planar}(\mathcal{X}_2,\mathcal{X}_3,\mathcal{Y}_2,\mathcal{Y}_3) + \mathcal{H}_{space}(\mathcal{X}_2,\mathcal{X}_3,\mathcal{Y}_2,\mathcal{Y}_3;\mathrm{AMD}) \\
&= \sum_{\ell\in\mathbb{N}^4,|\ell|=2}^{N_{bk}} \mathcal{K}_{plane,\ell}\,\mathcal{X}_2^{\ell_1}\,\mathcal{X}_3^{\ell_2}\,\mathcal{Y}_2^{\ell_3}\,\mathcal{Y}_3^{\ell_4} \\
&+ \sum_{\ell\in\mathbb{N}^4,|\ell|=2}^{N_{bk}} \mathcal{K}_{space,\ell}(\mathrm{AMD})\,\mathcal{X}_2^{\ell_1}\,\mathcal{X}_3^{\ell_2}\,\mathcal{Y}_2^{\ell_3}\,\mathcal{Y}_3^{\ell_4}\ .
\end{aligned} \tag{2.25}$$

Note that, by symmetry, the value of the disturbing function (and hence of the secular Hamiltonian) remains invariant by the rotation of both planets' argument of the pericenter by π, hence the secular Hamiltonian is necessarily even in the planetary eccentricities. This implies that the Hamiltonian (2.25) contains only even powers of the Poincaré variables $(\mathcal{X}_j, \mathcal{Y}_j)$, i.e. $\ell_1+\ell_2$ and $\ell_3+\ell_4$ are even. In particular, Hamilton's equations take the form:

$$\begin{aligned}
\dot{\mathcal{X}}_i &= \frac{\partial\mathcal{H}_{sec}}{\partial\mathcal{Y}_i} = \mathcal{Y}_2\,F_{\mathcal{X}_i,2}(\mathcal{X}_2,\mathcal{X}_3,\mathcal{Y}_2,\mathcal{Y}_3) + \mathcal{Y}_3\,F_{\mathcal{X}_i,3}(\mathcal{X}_2,\ X_3,\mathcal{Y}_2,\mathcal{Y}_3)\,, \\
\dot{\mathcal{Y}}_i &= -\frac{\partial\mathcal{H}_{sec}}{\partial\mathcal{X}_i} = \mathcal{X}_2\,F_{\mathcal{Y}_i,2}(\mathcal{X}_2,\mathcal{X}_3,\mathcal{Y}_2,\mathcal{Y}_3) + \mathcal{X}_3\,F_{\mathcal{Y}_i,3}(\mathcal{X}_2,\mathcal{X}_3,\mathcal{Y}_2,\mathcal{Y}_3)\,,
\end{aligned} \tag{2.26}$$

where the polynomials $F_{\mathcal{X}_i,2}$, $F_{\mathcal{X}_i,3}$, $F_{\mathcal{Y}_i,2}$, $F_{\mathcal{Y}_i,2}$, $i = 2,\,3$, are even, starting with constant terms.

Note that, in the practical implementation of the above algorithm, *steps 3* and *4* can be resumed in a single step, simply substituting into the Hamiltonian. (2.21) the expressions

$$L_z = \Lambda_2 + \Lambda_3 - \varepsilon^2\mathrm{AMD}\,, \qquad \mathrm{e}_j = \sqrt{\frac{2W_j\,\varepsilon^2}{\Lambda_j} - \left(\frac{W_j\,\varepsilon^2}{\Lambda_j}\right)^2}$$

and expanding the resulting expressions in powers of the book-keeping parameter ε. Finally, through the substitutions

$$\sin(w_j) = \frac{\mathcal{Y}_j}{\sqrt{2W_j}}, \qquad \cos(w_j) = -\frac{\mathcal{X}_j}{\sqrt{2W_j}}, \qquad W_j = \frac{\mathcal{X}_j^2+\mathcal{Y}_j^2}{2}\,,$$

and restoring the numerical value $\varepsilon = 1$, the Hamiltonian is lead to the final (in Poincaré variables) form described by Eq. (2.25).

2.2.3 Poincaré surface of section. Precision tests

We now discuss several precision tests, based on the method of comparison of phase portraits, which aim to establish which is the minimum multipole order, as well as minimum order in the eccentricities of the Hamiltonian $\mathcal{H}_{sec}$, such that the Hamiltonian, truncated at the above orders, represents with sufficient precision the dynamics at the timescales of the secular system produced by averaging of the original Hamiltonian (1.10).

2.2.3.1 Poincaré surface of section: definitions

To visualize phase portraits, use is made below of a Poincaré surface of section $\mathcal{P}(\mathcal{E};\mathrm{AMD})$ defined by the relations:

$$\mathcal{P}(\mathcal{E};\mathrm{AMD}) =\Bigg\{ (\mathcal{X}_2,\mathcal{Y}_2,\mathcal{X}_3,\mathcal{Y}_3)\in\mathbb{R}^4:\ \mathcal{Y}_3=0,\ \dot{\mathcal{Y}}_3=-\frac{\partial\mathcal{H}_{sec}(\mathcal{X}_2,\mathcal{Y}_2,\mathcal{X}_3,\mathcal{Y}_3=0;\mathrm{AMD})}{\partial\mathcal{X}_3}\geq 0,\\ \cos(\mathrm{i}_{max})\leq\cos(\mathrm{i}_{mut})(\mathcal{X}_2,\mathcal{Y}_2,\mathcal{X}_3,\mathcal{Y}_3=0;\mathrm{AMD})\leq 1\Bigg\}\ , \tag{2.27}$$

where the mutual inclination $\mathrm{i}_{mut}=\mathrm{i}_2+\mathrm{i}_3$ for fixed AMD, or angular momentum $L_z=\Lambda_2+\Lambda_3-\mathrm{AMD}$, is given (consistently with Eq. (12) of [97]) by

$$\cos(\mathrm{i}_{mut})=\frac{L_z^2-\Lambda_2^2-\Lambda_3^2+\Lambda_2^2\,\mathrm{e}_2^2+\Lambda_3^2\,\mathrm{e}_3^2}{2\Lambda_2\Lambda_3\sqrt{1-\mathrm{e}_2^2}\sqrt{1-\mathrm{e}_3^2}}=\frac{L_z^2-\Lambda_2^2\left(1-\frac{\mathcal{X}_2^2+\mathcal{Y}_2^2}{2L_2}\right)^2-\Lambda_3^2\left(1-\frac{\mathcal{X}_3^2+\mathcal{Y}_3^2}{2L_3}\right)^2}{2\Lambda_2\Lambda_3\left(1-\frac{\mathcal{X}_2^2+\mathcal{Y}_2^2}{2L_2}\right)\left(1-\frac{\mathcal{X}_3^2+\mathcal{Y}_3^2}{2L_3}\right)} \tag{2.28}$$

and the maximum possible mutual inclination consistent with the given AMD is

$$\mathrm{i}_{max}=\cos^{-1}\left(\frac{L_z^2-\Lambda_2^2-\Lambda_3^2}{2\Lambda_2\Lambda_3}\right)\ . \tag{2.29}$$

The phase portrait corresponding to the Poincaré surface of section at a fixed level of energy $\mathcal{E}$ is obtained numerically, by choosing several initial conditions $(\mathcal{X}_2,\mathcal{Y}_2)\in\mathcal{D}(\mathcal{E})\subset\mathbb{R}^2$, where $\mathcal{D}(\mathcal{E})$ is the domain of permissible initial conditions consistent with the definition of the surface of section as in Eq.(2.27). For each initial condition, we then iterate the corresponding orbit under the Hamiltonian $\mathcal{H}_{sec}$, and plot the consequent points $(\mathcal{X}_2,\mathcal{Y}_2)$, or, equivalently $(\mathrm{e}_2\cos\omega_2,\mathrm{e}_2\sin\omega_2)$, with

$$\mathrm{e}_2=\left(1-(1-(\mathcal{X}_2^2+\mathcal{Y}_2^2)/(2\Lambda_2))^2\right)^{1/2},\quad \omega_2=\mathrm{sgn}\left(\frac{-\mathcal{Y}_2}{\sqrt{\mathcal{X}_2^2+\mathcal{Y}_2^2}}\right)\arccos\left(\frac{-\mathcal{X}_2}{\sqrt{\mathcal{X}_2^2+\mathcal{Y}_2^2}}\right) \tag{2.30}$$

every time when the orbit intersects the surface of section. Note that the conditions $\mathcal{Y}_3=0,\dot{\mathcal{Y}}_3\geq 0$ imply i) that the Poincaré mapping defined by the successive iterates is symplectic, and ii) that the section definition corresponds physically to instants when the orbit of the outer planet crosses the pericenter $\omega_3=\pi$. The symplecticity of the Poincaré mapping, along with the straightforward physical interpretation, are the main motives for the choice of variables and for the visualization of phase portraits via the definition of the Poincaré section as above.

The domain $\mathcal{D}(\mathcal{E})$ is non-null in a range of energies $\mathcal{E}_{min}\leq\mathcal{E}<0$. The energy $\mathcal{E}_{min}$ is computed as follows: consider the surface $\mathcal{I}_0$ of all possible points satisfying the section condition $\mathcal{Y}_3=0$ as well as the lowermost limit of possible mutual inclination $\mathrm{i}_{mut}=0$. The surface $\mathcal{I}_0$ is the sphere given by

$$\mathcal{I}_0=\left\{\mathcal{X}_3^2+\mathcal{X}_2^2+\mathcal{Y}_2^2=2\mathrm{AMD}\right\}\ . \tag{2.31}$$

We then find the point $(\mathcal{X}_{2,0}, \mathcal{Y}_{2,0})$ on the surface $\mathcal{I}_0$ where the energy is minimum by looking to the solutions of the system of equations

$$\begin{aligned} \frac{\partial \mathcal{H}_{sec}(\mathcal{X}_2, \mathcal{Y}_2, \mathcal{X}_3^2 = 2\mathrm{AMD} - \mathcal{X}_2^2 - \mathcal{Y}_2^2, \mathcal{Y}_3 = 0; \mathrm{AMD})}{\partial \mathcal{X}_2} &= 0 \\ \frac{\partial \mathcal{H}_{sec}(\mathcal{X}_2, \mathcal{Y}_2, \mathcal{X}_3^2 = 2\mathrm{AMD} - \mathcal{X}_2^2 - \mathcal{Y}_2^2, \mathcal{Y}_3 = 0; \mathrm{AMD})}{\partial \mathcal{Y}_2} &= 0 \ , \end{aligned} \tag{2.32}$$

satisfying also the section condition

$$\dot{\mathcal{Y}}_3 = \left(\frac{\partial \mathcal{H}_{sec}(\mathcal{X}_2, \mathcal{Y}_2, \mathcal{X}_3, \mathcal{Y}_3 = 0; \mathrm{AMD})}{\partial \mathcal{X}_3} \right)_{\mathcal{X}_3^2 = 2\mathrm{AMD} - \mathcal{X}_2^2 - \mathcal{Y}_2^2} \geq 0 \ . \tag{2.33}$$

We find two solutions $(\mathcal{X}_{2,0}, \mathcal{Y}_{2,0} = 0)$ and $(\mathcal{X}_{2,1}, \mathcal{Y}_{2,1} = 0)$ of the system of equations (2.32) and (2.33); however, only $(\mathcal{X}_{2,0}, \mathcal{Y}_{2,0} = 0)$ corresponds to the minimum value of the energy, i.e. $\mathcal{H}(\mathcal{X}_2 = \mathcal{X}_{2,0}, \mathcal{Y}_2 = \mathcal{Y}_{2,0} = 0, \mathcal{X}_3 = \mathcal{X}_{3,0} = \sqrt{2\mathrm{AMD} - \mathcal{X}_{2,0}^2}, \mathcal{Y}_3 = 0) = \mathcal{E}_{min}$, as verified by the Hessian matrix

$$\left(\begin{array}{cc} \frac{\partial^2 \mathcal{H}_{sec}(\mathcal{X}_3 = \sqrt{2\mathrm{AMD} - \mathcal{X}_2^2}, \mathcal{Y}_3 = 0)}{\partial \mathcal{X}_2^2} & \frac{\partial^2 \mathcal{H}_{sec}(\mathcal{X}_3 = \sqrt{2\mathrm{AMD} - \mathcal{X}_2^2}, \mathcal{Y}_3 = 0)}{\partial \mathcal{Y}_2 \partial \mathcal{X}_2} \\ \frac{\partial^2 \mathcal{H}_{sec}(\mathcal{X}_3 = \sqrt{2\mathrm{AMD} - \mathcal{X}_2^2}, \mathcal{Y}_3 = 0)}{\partial \mathcal{X}_2 \partial \mathcal{Y}_2} & \frac{\partial^2 \mathcal{H}_{sec}(\mathcal{X}_3 = \sqrt{2\mathrm{AMD} - \mathcal{X}_2^2}, \mathcal{Y}_3 = 0)}{\partial \mathcal{Y}_2^2} \end{array} \right)_{(\mathcal{X}_2 = \mathcal{X}_{2,0}, \mathcal{Y}_2 = \mathcal{Y}_{2,0})}$$

which is positive definite. On the other hand, the solution $(\mathcal{X}_{2,1},\ \mathcal{Y}_{2,1} = 0,\ \mathcal{X}_{3,1} = \sqrt{2\mathrm{AMD} - \mathcal{X}_{2,1}^2})$ corresponds to the energy $\mathcal{E}_{2,3}$, and yield a negative definite Hessian matrix. Thus, $\mathcal{E}_{2,3}$ corresponds to the maximum energy for which we can have co-planar orbits (see discussion below).

The uniqueness of the solution realizing the minimal value of the energy can be understood by the following argument: for every fixed value of the energy $\mathcal{E}$, sufficiently close to the origin the restriction of the manifold of constant energy to the section $\mathcal{Y}_3 = 0$

$$\mathcal{M}(\mathcal{E}) = \left\{ (\mathcal{X}_2, \mathcal{Y}_2, \mathcal{X}_3) \in \mathbb{R}^3 : \mathcal{H}_{sec}(\mathcal{X}_2, \mathcal{X}_3, \mathcal{Y}_2, \mathcal{Y}_3 = 0; \mathrm{AMD}) = \mathcal{E} \right\} \tag{2.34}$$

yields a surface. We will show in the next section that, for energies smaller than a suitably defined threshold, the surface $\mathcal{M}(\mathcal{E})$ is close to the surface of an integrable model

$$\mathcal{M}_{int}(\mathcal{E}) = \left\{ (\mathcal{X}_2, \mathcal{Y}_2, \mathcal{X}_3) \in \mathbb{R}^3 : \mathcal{H}_{int}(\mathcal{X}_2, \mathcal{X}_3, \mathcal{Y}_2, \mathcal{Y}_3 = 0; \mathrm{AMD}) = \mathcal{E} \right\} \tag{2.35}$$

where $\mathcal{H}_{int}$ contains $\mathcal{H}_{planar}$ as well as a part of $\mathcal{H}_{space}$. The manifolds $\mathcal{M}_{int}(\mathcal{E})$, in turn, are ellipsoidal-like closed convex surfaces. The ellipsoidal form follows from the fact that the leading order terms of the restriction of $\mathcal{H}_{int}$ to the section $\mathcal{Y}_3 = 0$ yield a negative-definite quadratic form

$$\mathcal{H}_{int}(\mathcal{X}_2, \mathcal{X}_3, \mathcal{Y}_2, \mathcal{Y}_3 = 0) = -\nu_2 \left(\frac{\mathcal{X}_2^2 + \mathcal{Y}_2^2}{2} \right) - \nu_3 \frac{\mathcal{X}_3^2}{2} + c_{23} \mathcal{X}_2 \mathcal{X}_3 + \dots$$

with $\nu_2, \nu_3 > 0$, $|c_{2,3}| < \min(\nu_2, \nu_3)$.

Owing to their proximity to the manifolds $\mathcal{M}_{int}(\mathcal{E})$, for energies low enough, the manifolds $\mathcal{M}(\mathcal{E})$ are also ellipsoidal-like (the exact evolution of the form of $\mathcal{M}(\mathcal{E})$ as the energy increases will be discussed in the next section). As a consequence, there is a negative value of the energy $\mathcal{E} = \mathcal{E}_{min}$ such that for $\mathcal{E} < \mathcal{E}_{min}$ the ellipsoidal manifold $\mathcal{M}(\mathcal{E})$ surrounds the sphere $\mathcal{I}_0$, thus leading to the unphysical condition $\cos(\mathrm{i}_{mut}) > 1$. At the energy $\mathcal{E} = \mathcal{E}_{min}$ the ellipsoidal manifold $\mathcal{M}(\mathcal{E}_{min})$ has two points of tangency with the sphere $\mathcal{I}_0$ (see Fig.2.1). Both tangencies occur at

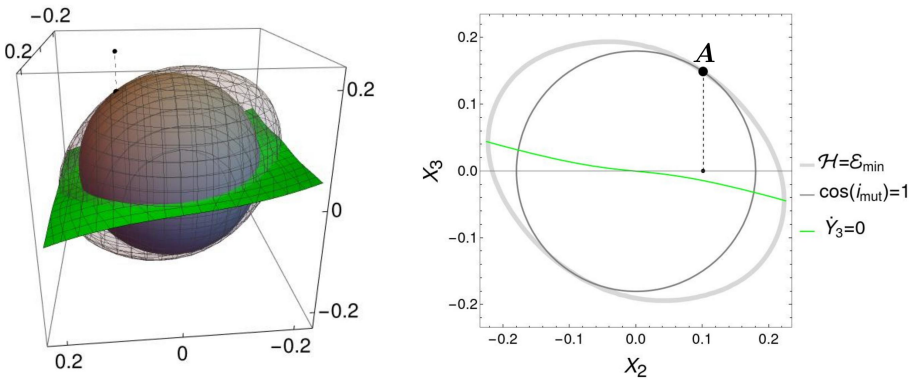

Figure 2.1: Left: tangency between the ellipsoidal surfaces of minimum possible energy $\mathcal{M}(\mathcal{E}_{min})$, with $\mathcal{E}_{min} = -1.18237 \cdot 10^{-4}$ (light gray) and the sphere $\mathcal{I}_0$ (gray). The only permissible initial condition on the surface of section corresponds to the point of tangency (black dot). The green slightly inclined surface represents the condition $\dot{\mathcal{Y}}_3 = 0$. Right: the tangency between the surfaces $\mathcal{M}(\mathcal{E}_{min})$ (thick light gray closed curves) and the sphere $\mathcal{I}_0$ (thin gray curve) as seen in the plane $(\mathcal{X}_2, \mathcal{X}_3)$ for $\mathcal{Y}_2 = 0$. The green slightly inclined curve represents the condition $\dot{\mathcal{Y}}_3 = 0$ and separates the plane $(\mathcal{X}_2, \mathcal{X}_3)$ in an upper domain, where $\dot{\mathcal{Y}}_3 > 0$, and a lower domain ($\dot{\mathcal{Y}}_3 < 0$). The point of tangency (thick dot) marks a fixed point corresponding to a planar periodic orbit of the apsidal corotation type called 'mode A' (anti-aligned) in section 2.3, yielding $(\mathcal{X}_2 = \mathcal{X}_{2,0} = 0.101237,\ \mathcal{X}_3 = \mathcal{X}_{3,0} = \sqrt{2\text{AMD} - \mathcal{X}_{2,0}^2} = 0.148862,\ \mathcal{Y}_2 = \mathcal{Y}_{2,0} = 0,\ \mathcal{Y}_3 = 0\,)$, that correspond to $\mathrm{e}_2 = 0.337415$, $\mathrm{e}_3 = 0.433811$.

the plane $\mathcal{Y}_2 = 0$, but only one of them satisfies the condition $\dot{\mathcal{Y}}_3 \geq 0$. Then, we set $(\mathcal{X}_{2,0}, \mathcal{Y}_{2,0} = 0, \mathcal{X}_{3,0}^2 = 2\text{AMD} - \mathcal{X}_{2,0}^2\,)$ equal to the coordinates of the corresponding point of tangency, and $\mathcal{E}_{min} = \mathcal{H}_{sec}(\mathcal{X}_2 = \mathcal{X}_{2,0}, \mathcal{X}_3 = \mathcal{X}_{3,0}, \mathcal{Y}_2 = 0, \mathcal{Y}_3 = 0; \text{AMD})$.

In order to numerically specify, now, the limits of the domain $\mathcal{D}(\mathcal{E})$ on the Poincaré section for any value of the energy in the range $\mathcal{E}_{min} < \mathcal{E} < 0$ we work as follows: fixing any value of the angle $w_2 = -\omega_2$ in the interval $0 \leq w_2 \leq \pi$, the line defined parametrically by the relations:

$$\mathcal{L}(w_2) : \{\mathcal{X}_2 = s_2 \cos(w_2),\ \mathcal{Y}_2 = s_2 \sin(w_2), s_2 \in \mathbb{R}\} \tag{2.36}$$

defines a plane $\mathcal{PL}(w_2) : \{(\mathcal{X}_2, \mathcal{Y}_2) \in \mathcal{L}(w_2), \mathcal{X}_3 \in \mathbb{R}\}$. The plane $\mathcal{PL}(w_2)$ intersects the ellipsoidal manifold $\mathcal{M}(\mathcal{E})$ at a nearly-elliptic closed curve $\mathcal{C}_{PLM}(\mathcal{E}, w_2)$, while it intersects the sphere $\mathcal{I}_0$ at the circle $\mathcal{C}_{PLI_0} : s^2 + \mathcal{X}_3^2 = 2\text{AMD}$. The curve $\mathcal{C}_{PLM}(\mathcal{E}, w_2)$ has central symmetry, and, owing to the fact that its quadratic-form approximation is negative definite, its overall size decreases as $\mathcal{E}$ increases from the most negative possible value $\mathcal{E} = \mathcal{E}_{min}$ towards the value $\mathcal{E} = 0$, at which $\mathcal{C}_{PLM}(\mathcal{E}, w_2)$ reduces to a point at the origin of the plane $\mathcal{PL}(w_2)$. Finally, the surface $\dot{\mathcal{Y}}_3 = 0$ also intersects the plane $\mathcal{PL}(w_2)$ at a curve $\mathcal{C}_{PL\dot{\mathcal{Y}}_3=0}(w_2)$. As a result, fixing the value of w_2, there are three possibilities as regards the intersections of the curve $\mathcal{C}_{PLM}(\mathcal{E}, w_2)$, which varies with the energy, and the curves $\mathcal{C}_{PL\dot{\mathcal{Y}}_3=0}(w_2)$ and $\mathcal{C}_{PLI_0}$:

Regime 1: the curve $\mathcal{C}_{PLM}(\mathcal{E}, w_2)$ intersects the circle $\mathcal{C}_{PLI_0}$ at four points, two of which (P_1, P_2) are above the curve $\mathcal{C}_{PL\dot{\mathcal{Y}}_3=0}(w_2)$, hence corresponding to $\dot{\mathcal{Y}}_3 > 0$, while it intersects the curve $\mathcal{C}_{PL\dot{\mathcal{Y}}_3=0}(w_2)$ itself at two points which are *exterior* to the circle $\mathcal{C}_{PLI_0}$ (Fig.2.2). In this case, the permissible initial conditions in the Poincaré surface of section are given by $\mathcal{X}_2 = s_2 \cos(w_2)$, $\mathcal{Y}_2 = s_2 \sin(w_2)$ with s_2 in the interval $s_{P_1} \leq s_2 \leq s_{P_2}$, where s_{P_1}, s_{P_2} are the values of s_2 to which project the points of intersection P_1, P_2. At both these points we have $\dot{\mathcal{Y}}_3 > 0$.

Regime 2: for larger energies, the curve $\mathcal{C}_{PLM}(\mathcal{E}, w_2)$ still intersects the circle $\mathcal{C}_{PLI_0}$ at four points, two of which (P_1, P_2) are above the curve $\mathcal{C}_{PL\dot{\mathcal{Y}}_3=0}(w_2)$, while now intersecting the curve $\mathcal{C}_{PL\dot{\mathcal{Y}}_3=0}(w_2)$ itself at two points (P_3, P_4), which are *interior* to the circle $\mathcal{C}_{PLI_0}$ (Fig.2.3). In this case, the permissible initial conditions in the Poincaré surface of section are given by $\mathcal{X}_2 =$

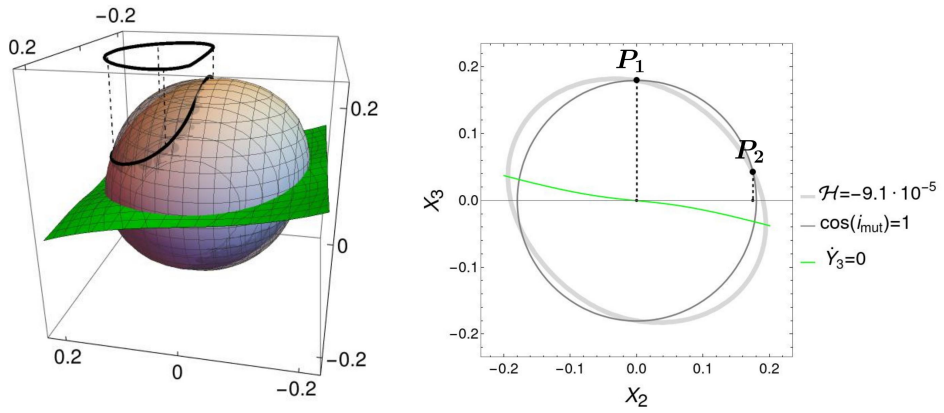

Figure 2.2: Left: intersections between the surfaces $\mathcal{M}(\mathcal{E})$ at the energy $\mathcal{E} = -9.16 \cdot 10^{-5}$ (light gray), the sphere $\mathcal{I}_0$ (thin gray), and the surface $\dot{\mathcal{Y}}_3 = 0$ (green slightly inclined). The thick black curve projected on the plane $(\mathcal{X}_2, \mathcal{Y}_2)$ defines the permissible domain of initial conditions (see text). Right: the intersections between the surface $\mathcal{M}(\mathcal{E})$ (thick light gray closed curve), the sphere $\mathcal{I}_0$ (thin gray curve and the condition $\dot{\mathcal{Y}}_3 = 0$) (green slightly inclined curve) as viewed in the plane $(\mathcal{X}_2, \mathcal{X}_3)$ for $\mathcal{Y}_2 = 0$. The points of intersection mark the limits of possible initial conditions along $\mathcal{X}_2$ for $\mathcal{X}_3 = \mathcal{Y}_2 = 0$.

$s_2 \cos(w_2)$, $\mathcal{Y}_2 = s_2 \sin(w_2)$ with s_2 in one of the intervals $s_{P_3} \leq s_2 \leq s_{P_1}$, or $s_{P_2} \leq s_2 \leq s_{P_4}$, where s_{P_1}, s_{P_2}, s_{P_3}, s_{P_4} are the values of s_2 to which project the points of intersection P_1,P_2,P_3,P_4. In this case we have $\dot{\mathcal{Y}}_3 > 0$ at the inner limits P_1, P_2, while we have $\dot{\mathcal{Y}}_3 = 0$ (i.e. the orbit arrives tangently to the surface of section) at the outer limits P_3, P_4.

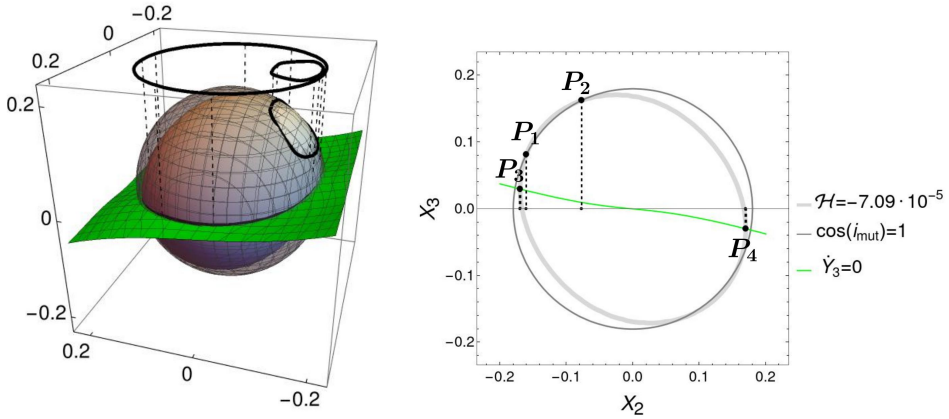

Figure 2.3: Same as in Fig.2.2 but for the surface $\mathcal{M}(\mathcal{E})$ calculated at $\mathcal{E} = -7.09 \cdot 10^{-5}$. The limits of possible initial conditions along $\mathcal{X}_2$ for $\mathcal{X}_3 = \mathcal{Y}_2 = 0$ are marked by the intersections $\mathcal{M}(\mathcal{E})$ both with $\mathcal{I}_0$ and the curve $\mathcal{C}_{PL\dot{\mathcal{Y}}_3=0}(w_2)$, for $w_2 = 0$ (see text).

Regime 3: for still larger energies, the curve $\mathcal{C}_{PLM}(\mathcal{E}, w_2)$ decreases in size in such a way that it no longer intersects the circle $\mathcal{C}_{PLI_0}$. Then the only limits are posed by its intersections with the curve $\mathcal{C}_{PL\dot{\mathcal{Y}}_3=0}(w_2)$ at the points (P_3, P_4), which remain interior to the circle $\mathcal{C}_{PLI_0}$ (Fig.2.4). Then, the permissible initial conditions in the Poincaré surface of section are given by $\mathcal{X}_2 = s_2 \cos(w_2)$, $\mathcal{Y}_2 = s_2 \sin(w_2)$ with s_2 in the interval $s_{P_3} \leq s_2 \leq s_{P_4}$, and both limits correspond to $\dot{\mathcal{Y}}_3 = 0$, i.e. to orbits tangent to the surface of section.

Having fixed the value of the energy $\mathcal{E}$, and repeating the computation of the above intersection

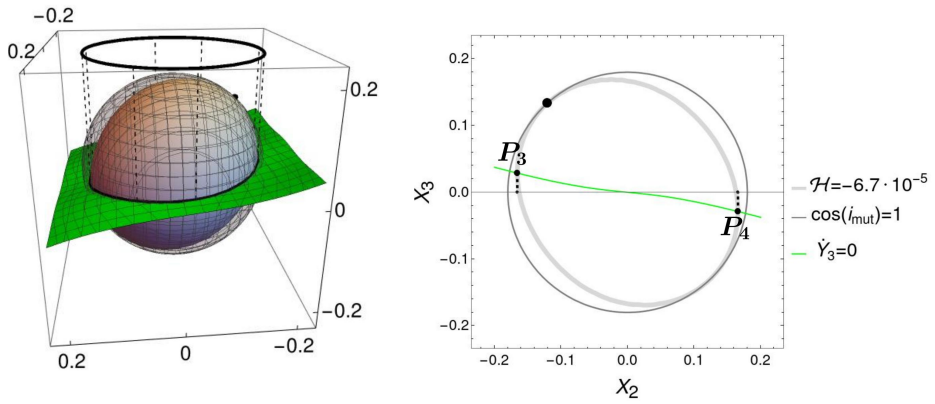

Figure 2.4: Inner tangency between the surface $\mathcal{M}(\mathcal{E}_{2,3})$ at the energy $\mathcal{E}_{2,3} = -6.77 \times 10^{-5}$ and the sphere $\mathcal{I}_0$. The point of tangency marks a fixed point which corresponds to a planar periodic orbit of the type 'mode B' (aligned apsidal corotation).

points for various lines $\mathcal{L}(w_2)$ (i.e. various choices of the argument of the perihelion ω_2), we can explicitly compute the limits of the whole domain $\mathcal{D}(\mathcal{E})$ and proceed in the computation of the phase portraits, obtaining several initial conditions within the domain $\mathcal{D}(\mathcal{E})$.

In practice, owing to the symmetries of the Hamiltonian, it is sufficient to consider only a scanning of initial conditions along the line $\mathcal{L}(w_2 = 0)$, i.e., $\mathcal{X}_2 = s_2$, $\mathcal{Y}_2 = 0$. A practical way to find the limiting values of $\mathcal{X}_2 = s_2$ is through the *Lagrange multiplier method*. More precisely, setting

$$\widetilde{\mathcal{L}}(\mathcal{X}_2, \mathcal{X}_3, \mu) = \mathcal{X}_2 + \mu \left(\mathcal{H}_{sec}(\mathcal{X}_2, \mathcal{X}_3, \mathcal{Y}_2 = 0, \mathcal{Y}_3 = 0) - \mathcal{E}\right) ,$$

the minimum and maximal allowed values of $\mathcal{X}_2$ for which the constrain $\mathcal{H}(\mathcal{X}_2, \mathcal{X}_3, \mathcal{Y}_2 = 0, \mathcal{Y}_3 = 0) = \mathcal{E}$ is fulfilled can be found computing the stationary points of $\widetilde{\mathcal{L}}$, i.e. solving $\nabla_{(\mathcal{X}_2, \mathcal{X}_3, \mu)} \widetilde{\mathcal{L}} = 0$. Between the different possible mathematical solutions, it is necessary to choose the ones compatible with the pre-selected fixed value of AMD (i.e., for which Eq. (2.28) is well defined); in this way we find $\mathcal{X}_{2_{min}}$ and $\mathcal{X}_{2_{max}}$ (and the corresponding $\mathcal{X}_3$) allowed for a fixed level of energy. Note that, at both solutions $\mathcal{X}_{2_{min}}$ and $\mathcal{X}_{2_{max}}$, we have $\dot{\mathcal{Y}}_3 = 0$. In fact, having determined $\mathcal{X}_{2_{min}}$ and $\mathcal{X}_{2_{max}}$ by the condition $\nabla \widetilde{\mathcal{L}} = 0$, it follows that $\dot{\mathcal{Y}}_3(\mathcal{X}_{2_{min}}, \mathcal{X}_3, \mathcal{Y}_2 = 0, \mathcal{Y}_3 = 0) = -\left(\partial \mathcal{H}_{sec}(\mathcal{X}_{2_{min}}, \mathcal{X}_3, \mathcal{Y}_2 = 0, \mathcal{Y}_3 = 0)/\partial \mathcal{X}_3\right) = 0$ and, analogously, $\dot{\mathcal{Y}}_3(\mathcal{X}_{2_{max}}, \mathcal{X}_3, \mathcal{Y}_2 = 0, \mathcal{Y}_3 = 0) = 0$.

The regimes 1 and 2, as well as 2 and 3, are separated at the energies $\mathcal{E}_{1,2}$ and $\mathcal{E}_{2,3}$ respectively. The topological differences in the phase portraits between the various regimes are discussed in the next section. We only note here that the generic regime is regime 3, which emerges beyond the energy $\mathcal{E}_{2,3}$, at which the manifold of constant energy $\mathcal{M}(\mathcal{E}_{2,3})$ has an inner tangency with the sphere $\mathcal{I}_0$. Finally, we note that both critical tangencies occuring at the energies $\mathcal{E}_{min}$ and $\mathcal{E}_{2,3}$ correspond to basic periodic orbits of the system (the apsidal corotation resonances), while the final limit $\mathcal{E} = 0$ corresponds to the Kozai-Lidov fixed point of the system, at which $\mathrm{i}_{mut} = \mathrm{i}_{max}$ and $\mathrm{e}_2 = \mathrm{e}_3 = 0$.

2.2.3.2 Poincaré surface of section: precision tests

Figure 2.5 shows a summary of our basic example of computation of phase portraits, in the form of Poincaré surfaces of section computed as explained in the previous subsection, referring to a 3D planetary system with mass, periods and AMD parameters as those estimated for the υ-Andromedae system. We adopt the value $\mathcal{G} = 4\pi^2\ AU^3/(yr^2 M_\odot)$ for Newton's gravity constant, as well as the mass parameters $m_0 = 1.31 M_\odot$, $m_2 = 13.98 M_J$, $m_3 = 10.25 M_J$ ($M_\odot$ = mass of the Sun,

$M_J = 0.0009546 M_\odot$ = mass of Jupiter), and the semi-major axes $a_2 = 0.829$ AU, $a_3 = 2.53$ AU (according to Table 13 of [78]). For what concerns the constants L_z or AMD, we estimate their values adopting for the two planets' eccentricities, inclinations and arguments of periastron and of the nodes the values proposed in Table 1 of [18], namely, $e_2 = 0.2445$, $e_3 = 0.316$, $i_2 = 11.347°$, $i_3 = 25.609°$, $\omega_2 = 247.629°$, $\omega_3 = 252.991°$, $\Omega_2 = 248.181°$, $\Omega_3 = 11.425°$. As emphasized in section 2.1, there are great uncertainties in the observation as regards, in particular, the estimates on the planetary eccentricity and inclination vectors. However, starting with parameters as above, we can have a representative value for the system's AMD, which then serves to analyze the secular orbital dynamics under different assumptions for the planets' initial conditions. The value of the AMD is estimated from the above data, by first computing the angular momentum vector with respect to a heliocentric frame of reference whose x-axis points to the observer, then computing the rotation matrix connecting the observer's frame with Laplace's reference frame, and finally rotating the positions and velocities of both planets to the Laplace frame of reference and re-calculating their inclinations and arguments of periastron and of the nodes. This yields the values $i_2 = 18.4748°$, $i_3 = 14.6462°$, $\omega_2 = 289.049°$, $\omega_3 = 235.464°$, $\Omega_2 = 217.318°$, $\Omega_3 = 37.3176°$. Then, we obtain $Lz = 0.183101\ AU^2 M_\odot/yr$, which, together with $\Lambda_2 = 0.0873819$, $\Lambda_3 = 0.111923$, leads to AMD $= L_2 + L_3 - L_z = 0.0162044\ AU^2 M_\odot/yr$.

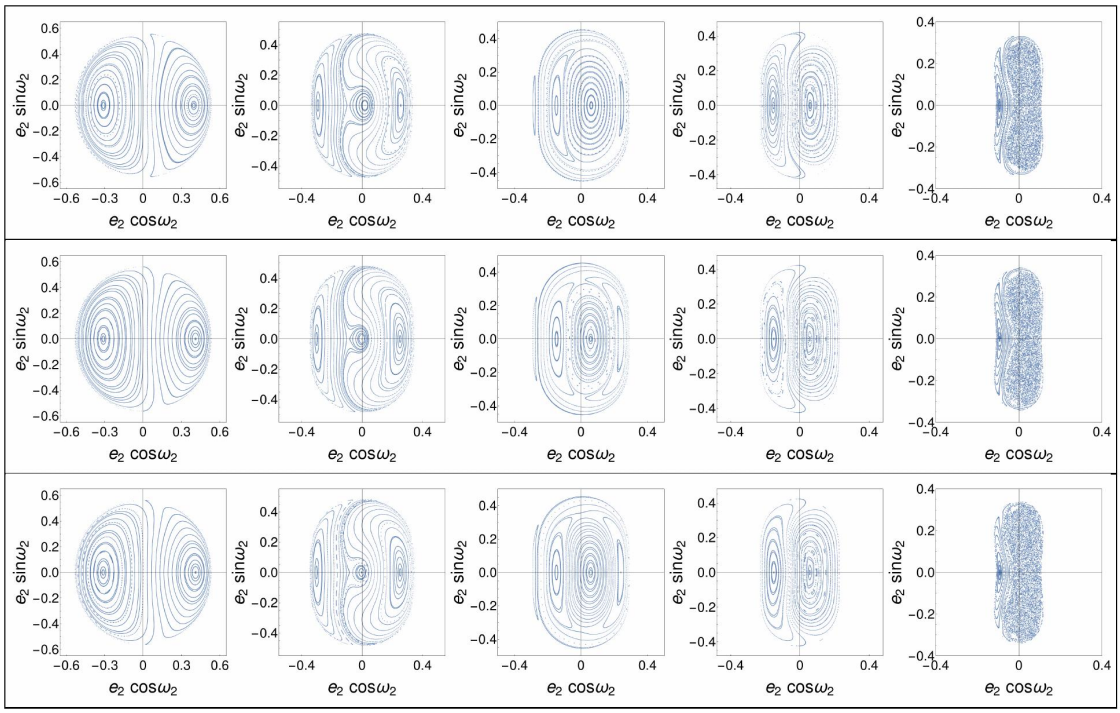

Figure 2.5: Poincaré surfaces of section in the plane $(e_2\cos(\omega_2), e_2\sin(\omega_2))$ with L_z fixed and different values of energy. The surfaces of section are computed by a numerical integration of trajectories in the Hamiltonian truncated at: *Top* multipolar degree $N_P = 5$, order $N_{bk} = 10$ in the eccentricities, and energies (from left to right) $\mathcal{E} = -6.67 \cdot 10^{-5}, -2.53 \cdot 10^{-5}, -1.9 \cdot 10^{-5}, -1.17 \cdot 10^{-5}, -2.61 \cdot 10^{-6}$. *(Middle)* $N_P = 6$, $N_{bk} = 10$, and energies top $\mathcal{E} = -6.75 \cdot 10^{-5}, -2.69 \cdot 10^{-5}, -1.9 \cdot 10^{-5}, -1.16 \cdot 10^{-5}, -2.61 \cdot 10^{-6}$. *(Bottom)* $N_P = 6$, $N_{bk} = 12$, and energies $\mathcal{E} = -6.75 \cdot 10^{-5}, -2.69 \cdot 10^{-5}, -1.9 \cdot 10^{-5}, -1.16 \cdot 10^{-5}, -2.59 \cdot 10^{-6}$.

Fig.2.5 already illustrates some of the significant changes in the phase portraits when the energy is varied from a value close to $\mathcal{E}_{min} \simeq -1.2 \cdot 10^{-4}$ (slightly different in each of the models considered in the figure), to another close to $\mathcal{E}_{max} = 0$. These are discussed in detail in the next section. Here we only discuss how these figures probe the robustness of the phase portraits with respect to

the model chosen, which can differ in the maximum multipole degree N_P up to which the original Hamiltonian $\mathcal{H}$ is expanded, before the averaging, as well as in the maximum order in book-keeping N_{bk} of the Hamiltonian $\mathcal{H}_{sec}$ (equal to the maximum order at which the eccentricities appear in $\mathcal{H}_{sec}$). Checking with increasing values of N_P and N_{bk}, we find that the phase portraits stabilize at $N_P = 5$, $N_{bk} = 10$. Beyond these values, the sequence of bifurcations of new fixed points and the corresponding changes in the topological features of the phase portraits become marginal, with only changes in the second significant figure observed as regards both the value of the energy $\mathcal{E}$ where a bifurcation occurs, and the position of the corresponding fixed points, separatrices, etc.

Since we are interested only in a qualitative description of the structure and evolution of the phase portraits, for reducing computational time we choose as our basic model the one with $N_P = 5$, $N_{bk} = 10$. As an independent test, we perform a comparison between the phase portraits obtained with this model and those obtained by a completely independent Laplace-Lagrange expansion of the Hamiltonian $\mathcal{H}$ averaged over the fast angles. In the latter case, the book-keeping process described in subsection 2.2.2 must be altered for the decomposition $\mathcal{H} = \mathcal{H}_{planar} + \mathcal{H}_{space}$ to naturally emerge while the Jacobi reduction is performed. Namely, we first introduce the book-keeping $\mathrm{e}_j \to \varepsilon \mathrm{e}_j$, $j = 2, 3$ and expand the direct term $-\mathcal{G}m_2m_3/|\mathbf{r}_2 - \mathbf{r}_3|$ in powers of the orbital eccentricities up to the book-keeping order $N_{bk} = 10$. The so-computed expression has the form:

$$-\frac{\mathcal{G}m_2m_3}{|\mathbf{r}_2 - \mathbf{r}_3|} = \sum_{s=0}^{N_{bk}} \sum_{\alpha,\beta,\gamma} \frac{D_{\alpha,\beta,\gamma}(a_2, a_3, \mathrm{e}_2, \mathrm{e}_3, \mathrm{i}_2, \mathrm{i}_3; \varepsilon)}{(\Delta_{2,3})^{\frac{2\,s+1}{2}}} \cos(\alpha_2\lambda_2 + \alpha_3\lambda_3 + \beta_2\Omega_2 + \beta_3\Omega_3 + \gamma_2\varpi_2 + \gamma_3\varpi_3)\,, \tag{2.37}$$

where the denominator $\Delta_{2,3}$, after the substitution $\Omega_3 = \Omega_2 + \pi$, takes the form:

$$\begin{aligned}\Delta_{2,3} =& a_2^2 + a_3^2 - a_2a_3\cos(\lambda_2 - \lambda_3) - a_2a_3\cos(\lambda_2 - \lambda_3)\cos(\mathrm{i}_2 + \mathrm{i}_3) \\ &+ a_2a_3\cos(\lambda_2 + \lambda_3 - 2\Omega_2)\cos(\mathrm{i}_2 + \mathrm{i}_3) - a_2a_3\cos(\lambda_2 + \lambda_3 - 2\Omega_2)\,,\end{aligned} \tag{2.38}$$

with $\varpi_j = \omega_j + \Omega_j$ and $\lambda_j = M_j + \varpi_j$ denoting the longitudes of the pericenter and the mean longitudes of the bodies $j = 2, 3$ respectively. The integer vectors $\alpha \equiv (\alpha_2, \alpha_3)$, $\beta \equiv (\beta_2, \beta_3)$, $\gamma \equiv (\gamma_2, \gamma_3)$ satisfy the D'Alembert rule $\alpha_2 + \alpha_3 + \beta_2 + \beta_3 + \gamma_2 + \gamma_3 = 0$. The coefficients $D_{\alpha,\beta,\gamma}$ are polynomial in the book-keeping parameter ε. At this point, we introduce the book-keeping identities:

$$\cos(i_2 + i_3) = \eta\varepsilon^2(\cos(i_2 + i_3) - 1) + 1\,,$$

i.e. (see Eq (2.17))

$$\cos(\mathrm{i}_2)\cos(\mathrm{i}_3) = \varepsilon^2\eta\,(\cos(\mathrm{i}_2)\cos(\mathrm{i}_3) - 1) + 1\,, \qquad \sin(\mathrm{i}_2)\sin(\mathrm{i}_3) = \varepsilon^2\eta\sin(\mathrm{i}_2)\sin(\mathrm{i}_3)\,,$$

and expand again the expression (2.37) with respect to the book-keeping parameter ε up to the truncation order $N_{bk} = 10$. This leads to an expression of the same form as Eq. (1.27)

$$-\frac{\mathcal{G}m_2m_3}{|\mathbf{r}_2 - \mathbf{r}_3|} = \sum_{s=0}^{N_{bk}} \sum_{\alpha,\beta,\gamma} \frac{C_{\alpha,\beta,\gamma}(a_2, a_3, \mathrm{e}_2, \mathrm{e}_3, \mathrm{i}_2, \mathrm{i}_3; \varepsilon, \eta)}{(a_2^2 + a_3^2 - 2\,a_2\,a_3\,\cos(\lambda_2 - \lambda_3))^{\frac{2\,s+1}{2}}} \cos(\alpha_2\lambda_2 + \alpha_3\lambda_3 + (\beta_2 + \beta_3)\Omega_2 + \gamma_2\varpi_2 + \gamma_3\varpi_3)\,,$$

where the coefficients $C(a_2, a_3, \mathrm{e}_2, \mathrm{e}_3, \mathrm{i}_2, \mathrm{i}_3; \varepsilon, \eta)$ are polynomial in the book-keeping parameters ε, η. Finally, we perform the classical Laplace-Lagrange averaging 'by scissors', introduced in section 1.4.5.1: the denominator of (1.27) is Fourier-expanded (Eq. (1.28))

$$\frac{1}{(a_2^2 + a_3^2 - 2\,a_2\,a_3\,\cos(\lambda_2 - \lambda_3))^{\frac{2\,s+1}{2}}} = a_3^{-(2\,s+1)} \sum_{j\geq 0} b^{(j)}_{s+\frac{1}{2}}\left(\frac{a_2}{a_3}\right)\cos(j(\lambda_2 - \lambda_3))\,,$$

where $b^{(j)}_{s+\frac{1}{2}}$ are Laplace coefficients, which can be computed numerically by Eq. (1.29), as

$$b^{(0)}_{s+\frac{1}{2}}(\alpha) = \frac{1}{2\pi}\int_0^{2\pi}\left(1+\alpha^2-2\,\alpha\,\cos(\vartheta)\right)^{-(s+\frac{1}{2})}\,d\vartheta\,,$$
$$b^{(j)}_{s+\frac{1}{2}}(\alpha) = \frac{1}{\pi}\int_0^{2\pi}\left(1+\alpha^2-2\,\alpha\,\cos(\vartheta)\right)^{-(s+\frac{1}{2})}\cos(j\vartheta)\,d\vartheta \qquad j\geq 1\,,$$

where $\alpha = a_2/a_3$, or via a multipolar expansion (see the Appendix A). After performing the above expansions, the secular Hamiltonian is obtained by dropping from the original Hamiltonian all terms depending on the 'fast' angles λ_i. This leads to a model in which the inclinations appear only through the combination $\cos(i_2+i_3)$. Switching, now, back to the angles ω_j, Ω_j, performing the Jacobi reduction as in subsection 2.2.2 (i.e., using Eq. (2.18), collecting together all terms independent or depending on η, and restoring the numerical values of the book-keeping coefficients $\varepsilon = \eta = 1$), we arrive at a 'Laplace-Lagrange' model $\mathcal{H}_{LL} = \mathcal{H}_{LL,planar} + \mathcal{H}_{LL,space}$ which has the same form as the model of Eq. (2.23). This is further processed with the introduction of Poincaré variables as in *step 4* of subsection 2.2.2.

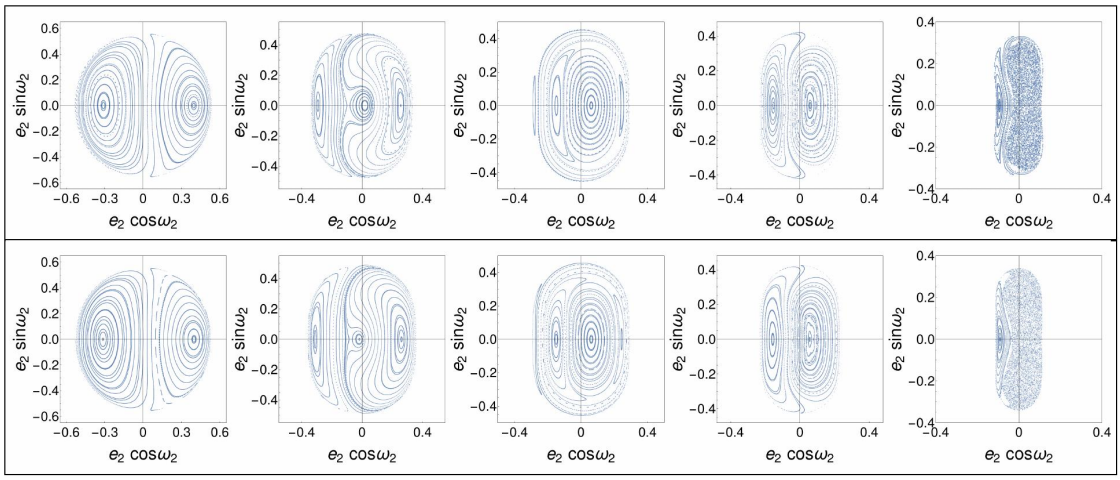

Figure 2.6: Comparison of the Poincaré surfaces of section in the plane $(\mathrm{e}_2\cos(\omega_2), \mathrm{e}_2\sin(\omega_2))$ with L_z fixed and different values of the energy, in two models: *Top:* our basic model $N_P = 5$, $N_{bk} = 10$ (same as in the top row of Fig.2.5). *Bottom:* the Laplace-Lagrange secular Hamiltonian model $\mathcal{H}_{LL}$ (see text) truncated at order 10 in the eccentricities, with energies (from left to right) $\mathcal{E} = -6.62\cdot 10^{-5}, -2.94\cdot 10^{-5}, -1.92\cdot 10^{-5}, -1.18\cdot 10^{-5}, -2.73\cdot 10^{-6}$.

From Fig.2.6 we conclude that similar remarks as those of Fig.2.5 can be made as regards the comparison of the secular model $\mathcal{H}_{sec}$ adopted in the present work, based on a multipolar expansion, and the model $\mathcal{H}_{LL}$ obtained by the classical Laplace-Lagrange expansion in the eccentricities. We note, however, that the latter is much harder to compute, while it is obtained by using a series reversion of Kepler's equation which has a limited convergence. On the other hand, the model based on closed-form averaging of the multipole Hamiltonian expansion requires a special treatment as regards the computation of the underlying canonical transformation which eliminates (instead of 'scissor cutting') the fast angles (see [9]). Since we presently do not consider this transformation, we will hereafter deal with results derived only by use of the simple multipole and closed-form averaged model $\mathcal{H}_{sec}$, with the truncation orders $N_P = 5$, $N_{bk} = 10$.

2.3 Dynamics

2.3.1 General

In this section we are interested in analyzing the most important phenomena observed in the phase portraits of the Hamiltonian $\mathcal{H}_{sec}(\mathcal{X}_2, \mathcal{X}_3, \mathcal{Y}_2, \mathcal{Y}_3; \text{AMD})$ computed with the basic reference model corresponding to the truncation orders $N_P = 5$, $N_{bk} = 10$. In the following subsections we first present the general picture of the transitions taking place in the structure of the phase space as the energy increases in the range $\mathcal{E}_{min} \leq \mathcal{E} \leq 0$. Such transitions are caused, for example, by changes in the nature (e.g. stability) of the main equilibria of the system, giving birth to new families of periodic orbits which connect the families dominant in the planar-like regime (high eccentricities, low mutual inclination) with those of the highly inclined regime (low eccentricities, high mutual inclination).

In the analysis of phase portraits as in the sequel, we parametrize all transitions due to bifurcations of new periodic orbits using the fixed (in the Poincaré section) energy $\mathcal{E}$ as the parameter. All energies referred to below are given in units of $M_\odot AU^2/yr^2$. It is easy to see that a certain value of the energy $\mathcal{E}$ establishes a range of allowed mutual inclinations

$$\mathrm{i}_{mut}^{min}(\mathcal{E}) \leq \mathrm{i}_{mut} \leq \mathrm{i}_{mut}^{max}(\mathcal{E}) \tag{2.39}$$

where both $\mathrm{i}_{mut}^{min}(\mathcal{E})$ and $\mathrm{i}_{mut}^{max}(\mathcal{E})$ are increasing functions of $\mathcal{E}$, as shown in Fig.2.7.

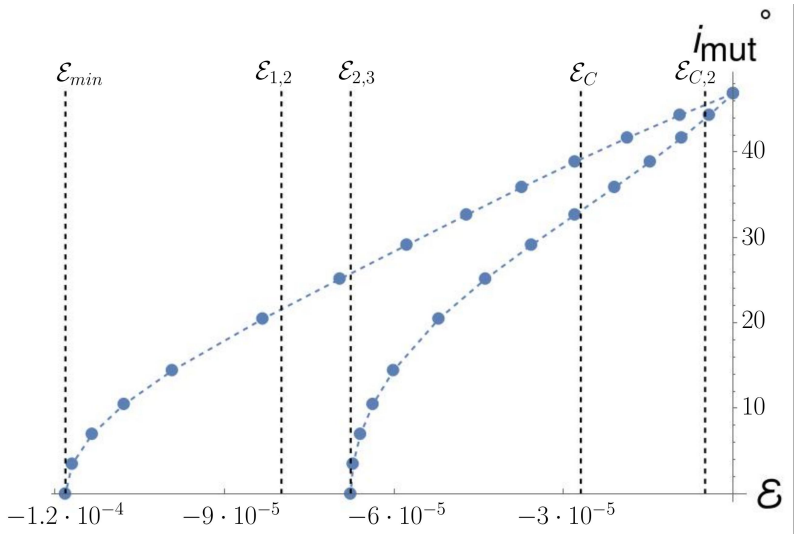

Figure 2.7: The minimum and maximum possible values of the mutual inclination i_{mut}^{min}, i_{mut}^{max}, as a function of the energy $\mathcal{E}$. The vertical lines correspond to the energies $\mathcal{E}_{min} = -1.18237 \cdot 10^{-4}$ (birth of the mode A - anti-aligned apsidal corotation), $\mathcal{E}_{1,2} = -8 \cdot 10^{-5}$ (completion of the libration domain around the mode A), $\mathcal{E}_{2,3} = -6.77 \cdot 10^{-5}$ (birth of the mode B - aligned apsidal corotation), $\mathcal{E}_C = -2.7 \times 10^{-5}$ (bifurcation of the inclined Kozai-Lidov periodic orbits C_1, C_2), and $\mathcal{E}_{C,2} = -5.0 \cdot 10^{-6}$ (inclined orbit C_2 becomes unstable, see text).

The minimum and maximum possible values of the mutual inclination i_{mut}^{min}, i_{mut}^{max}, as a function of the energy $\mathcal{E}$ are computed as follows: consider the ellipsoidal surface $\mathcal{I}_{\mathrm{i}_{mut}}$ defined by setting $\mathcal{Y}_3 = 0$ in Eq.(2.28) for a certain value of i_{mut}. Consider the critical energy $\mathcal{E} = \mathcal{E}_{2,3}$, equal to $\mathcal{E}_{2,3} = -6.77 \times 10^{-5}$ in our example. For energies $\mathcal{E} \geq \mathcal{E}_{2,3}$, we compute the values $\mathrm{i}_{mut} = \mathrm{i}_{mut}^{min}(\mathcal{E})$ and $\mathrm{i}_{mut} = \mathrm{i}_{mut}^{max}(\mathcal{E})$ for which the ellipsoid $\mathcal{I}_{\mathrm{i}_{mut}}$ comes tangent to the ellipsoidal manifold of constant energy $\mathcal{M}(\mathcal{E})$, with $\mathcal{I}_{\mathrm{i}_{mut}}$ being at the interior of $\mathcal{M}(\mathcal{E})$ (for $\mathrm{i}_{mut} = \mathrm{i}_{mut}^{max}$) or at the exterior of $\mathcal{M}(\mathcal{E})$

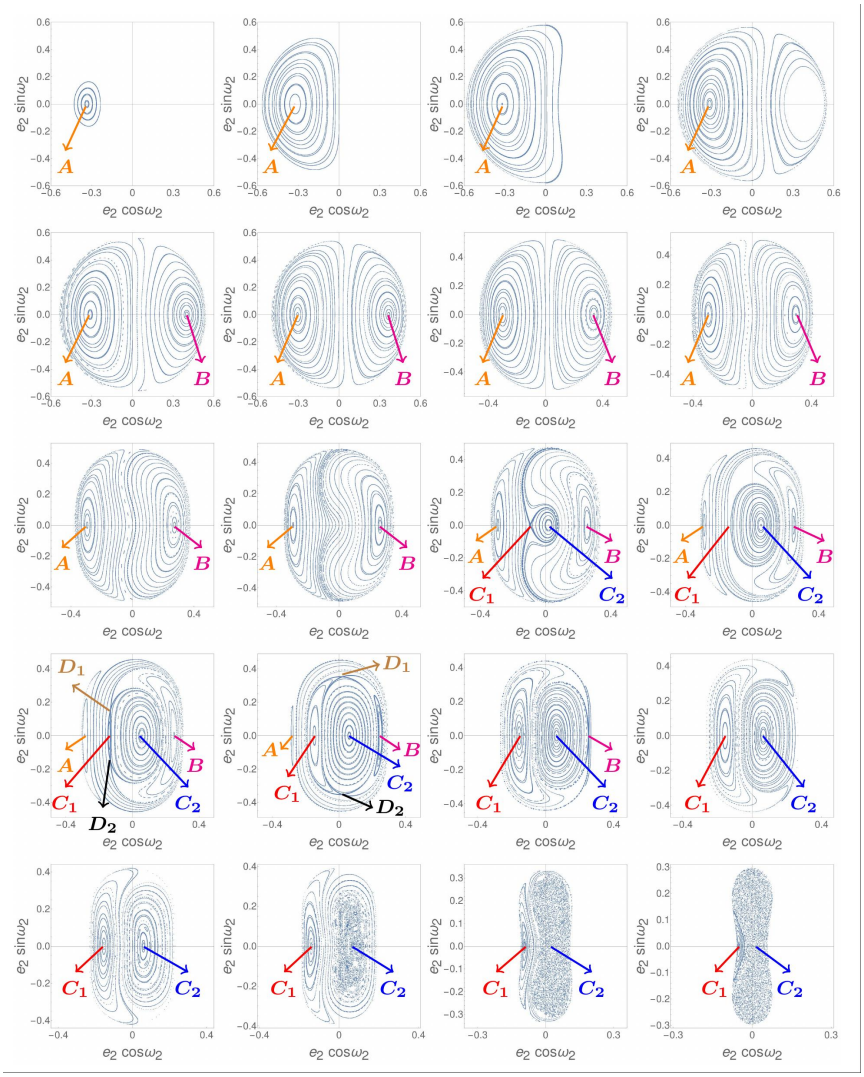

Figure 2.8: Phase portraits (Poincaré surfaces of section in the plane $(e_2\cos(\omega_2), e_2\sin(\omega_2))$) in the basic model $N_P = 5$, $N_{bk} = 10$, and for the energies (from from top left to bottom right) $\mathcal{E} = -1.145 \cdot 10^{-4}$, $-9.16{\cdot}10^{-5}$, $-8.23{\cdot}10^{-5}$, $-7.09{\cdot}10^{-5}$, $-6.77{\cdot}10^{-5}$, $-5.72{\cdot}10^{-5}$, $-4.93{\cdot}10^{-5}$, $-3.81{\cdot}10^{-5}$, $-3.19{\cdot}10^{-5}$, $-2.76{\cdot}10^{-5}$, $-2.53 \cdot 10^{-5}$, $-2.16 \cdot 10^{-5}$, $-2.08 \cdot 10^{-5}$, $-1.9 \cdot 10^{-5}$, $-1.58 \cdot 10^{-5}$, $-1.53 \cdot 10^{-5}$, $-1.17 \cdot 10^{-5}$, $-7.69 \cdot 10^{-6}$, $-2.61 \cdot 10^{-6}$, $-7.39 \cdot 10^{-7}$. The positions of the fixed points corresponding to the periodic orbits of the modes A, B, C_1, C_2, D_1, D_2 (see text) are marked by arrows.

(for $\mathrm{i}_{mut} = \mathrm{i}_{mut}^{min}$). For energies $\mathcal{E}_{min} \leq \mathcal{E} < \mathcal{E}_{2,3}$ (with $\mathcal{E}_{min} = -1.182 \times 10^{-4}$ in our example), the condition of tangency of $\mathcal{I}_{\mathrm{i}_{mut}}$ at the exterior of $\mathcal{M}(\mathcal{E})$ leads to unphysical values $\cos(\mathrm{i}_{mut}) > 1$. Thus, in this interval of energies we have $\mathrm{i}_{mut}^{min} = 0$, while i_{mut}^{max} keeps being represented by an increasing function of $\mathcal{E}$ (Fig.2.7).

The vertical lines in Fig. 2.7 indicate values of the energy where important changes take place in the structure of the phase portraits due to the birth, or change of stability character, of some of the most important families of periodic orbits of the system. The most important transitions taking place in the structure of the phase portraits are shown in Fig.2.8, whose details will be presented in subsequent subsections. Increasing the energy $\mathcal{E}$, these transitions appear in summary by the following sequence:

i) At the energy $\mathcal{E} = \mathcal{E}_{min}$, the available domain $\mathcal{D}(\mathcal{E})$ reduces to a point, corresponding to the point of tangency of Fig.2.1. This is a fixed point of the Poincaré map, whose associated orbit yields two coplanar ellipses with anti-aligned pericenters precessing by the same frequency, known as the *apsidal corotation orbit* (see [56], [57], [2]). For energies $\mathcal{E} > \mathcal{E}_{min}$, the above fixed point is continued by a family of periodic orbits, called below the *mode A*. These correspond physically to inclined planetary orbits whose eccentricities undergo small periodic oscillations around some non-zero constant values $\mathrm{e}_{2,A}$, $\mathrm{e}_{3,A}$ (functions of the energy), while the arguments of perihelia undergo small periodic oscillations around the fixed relation $\omega_2 - \omega_3 = 0$ (see subsections 2.3.3). For energies $\mathcal{E}_{min} < \mathcal{E} \leq \mathcal{E}_{2,3}$ (equal to $-6.77 \cdot 10^{-5}$ in our numerical example), the mode A, which generalizes the anti-aligned apsidal corotation family to the non-planar case, is the unique important stable family in the surface of section (see first three panels of top row of Fig.2.8). The corresponding fixed point is surrounded by closed invariant curves, which represent orbits performing quasi-periodic oscillations around the configuration of anti-aligned perihelia. Up to the energy $\mathcal{E}_{1,2}$ (equal to about $-8 \cdot 10^{-5}$ in our example), which marks the transition from two to four limits of permissible motion as in Figures 2.2 and 2.3, only quasi-periodic orbits around the A mode exist. On the other hand for energies $\mathcal{E}_{1,2} < \mathcal{E} < \mathcal{E}_{2,3}$, we can also have trajectories with argument $\omega_3 - \omega_2$ either circulating or librating around the value $\omega_3 - \omega_2 = \pi$ (alignment). As explained in detail in subsection 2.3.2, the separation between the various librating or circulating regimes is not due to the presence of a dynamical separatrix, but can be explained by an integrable Hamiltonian model approximating $\mathcal{H}_{sec}$ in the corresponding energy regime, whose phase space has the topology of a 3-sphere rather than the plane $\mathbb{R}^2$.

ii) For energies $\mathcal{E}_{1,2} < \mathcal{E} < \mathcal{E}_{2,3}$ there is a prohibited domain surrounding the center of the librating motions around $\omega_3 - \omega_2 = \pi$ (see fourth panel, top row of Fig.2.8). At the energy $\mathcal{E} = \mathcal{E}_{2,3}$ this domain shrinks to zero, and at the center of the librations appears a second fixed point of the Poincaré map, which is a periodic orbit physically corresponding to the planar aligned apsidal corotation orbit (see the first panel in the second row of Fig. 2.8). This also marks the inner point of tangency of the sphere $\mathcal{I}_0$ with the energy manifold $\mathcal{M}(\mathcal{E}_{2,3})$ (Fig.2.4). As indicated in Fig.2.7, for energies $\mathcal{E} > \mathcal{E}_{2,3}$ there can no longer be any planar orbit intersecting the surface of section. However, similarly as for the mode A, the fixed point corresponding to the aligned apsidal corotation is continued as a family of off-plane periodic orbits, hereafter called the *mode B*. Physically, such orbits undergo small periodic oscillations around some non-zero constant values $\mathrm{e}_{2,B}$, $\mathrm{e}_{3,B}$ (also being both functions of the energy), while the arguments of perihelia undergo small periodic oscillations around the fixed relation $\omega_2 - \omega_3 = \pi$ (see also subsection 2.3.3). The mode B also is surrounded by quasi-periodic orbits with arguments of the perihelia librating around the relation $\omega_3 - \omega_2 = \pi$.

iii) The topology of the phase space induced by the alternation between the domains of libration and circulation around the modes A and B dominates the picture obtained for the phase portraits in a large subinterval within the permissible range of values of the energy (up to about $\mathcal{E} = -3 \cdot 10^{-5}$ in our example). As seen in Fig.2.7, this covers most cases of highly-inclined orbits, with mutual inclinations being in our example as high as $\sim 40^\circ$. However, at a critical energy $\mathcal{E}_C$ (equal to about $-2.7 \cdot 10^{-5}$ in our example), a saddle-node bifurcation takes place, giving rise to two new fixed points of the Poincaré map, corresponding to periodic orbits hereafter called the *Kozai-Lidov* orbits C_1 and C_2. Physically, these are highly inclined orbits with planetary eccentricities e_2 and e_3 smaller than those of the modes A and B, tending actually to zero as $\mathcal{E} \to 0$. The detailed sequence of bifurcations related to these orbits is discussed in detail in subsection 2.3.4 (see panels 11 to 20 of Fig.2.8). The most important transitions regard the orbit C_1, which becomes stable nearly immediately after its birth, while the orbit C_2 undergoes the classical Lidov-Kozai transition from stability to instability, accompanied by the appearance of chaotic motions around it. Such phenomena appear in a small range of energies near the limit $\mathcal{E} = 0$, where the whole phase space

shrinks again to a unique point at the origin of the surface of section, corresponding to two circular orbits having the maximum possible mutual inclination ($\mathrm{i}_{mut}^{max}(\mathcal{E}=0) \simeq 46^\circ$ in our example). In fact, Fig.2.7 indicates that in this Lidov-Kozai regime, the range in possible inclinations for all orbits becomes narrow, being limited to values around the critical $\mathcal{E}_{C,2}$ where the periodic orbit C_2 underhgoes the Lidov-Kozai instability.

In the following subsections we examine these phenomena in more detail, following the sequence of their appearance as the value of the energy $\mathcal{E}$ increases.

2.3.2 Planar-like regime

In the present section we will discuss in detail the structure of the phase portraits in the range of energies $\mathcal{E}_{2,3} \leq \mathcal{E} < \mathcal{E}_C$, were the dominant periodic orbits are the Modes A and B, which generalize the apsidal corotations (anti-aligned and aligned, respectively) of the planar case. It was already mentioned that the phase portait in this case contains two domains where the argument $\omega_2 - \omega_3$ librates (around the values 0 and π respectively), separated by a domain where $\omega_2 - \omega_3$ circulates, as in panels 5 to 10 of Fig.2.8. Owing to its similarity with the phase portrait of the planar problem, this will be called the *planar-like* regime. It was emphasized, however, that the maximum mutual inclination can be quite high in this regime (see Fig.2.7), thus the analogy with the planar case stems from the dynamics, and not necessarily from the degree of coplanarity of the orbits in this regime. Excluding the energetically prohibited domains (as specified in subsection 2.2.3.1), this can be extended to cover the cases where the librational domains are only partly covered by quasi-periodic orbits, as in panels 1-4 of Fig.2.8.

2.3.2.1 Integrable approximation of the Hamiltonian

The main qualitative features of the planar-like regime, as well as precise computations regarding its periodic and surrounding quasi-periodic orbits, can be obtained in the context of an integrable approximation for the Hamiltonian $\mathcal{H}_{sec}$, stemming from the splitting $\mathcal{H}_{sec} = \mathcal{H}_{planar} + \mathcal{H}_{space}$ as in Eq. (2.20). Starting from

$$\mathcal{H}_{sec}(a_2, a_3, \mathrm{e}_2, \mathrm{e}_3, w_2, w_3; L_z) = \mathcal{H}_{planar}(w_2 - w_3, W_2, W_3) + \mathcal{H}_{space}(w_2, w_3, W_2, W_3; L_z)\,. \quad (2.40)$$

and splitting $\mathcal{H}_{space}$ into those terms which depend only on the difference $w_2 - w_3 = \omega_3 - \omega_2$, denoted by $\mathcal{H}_{0,space}$, and those which do not, denoted by $\mathcal{H}_{1,space}$, we arrive at the following decomposition of the Hamiltonian

$$\mathcal{H}_{sec} = \underbrace{\mathcal{H}_{planar}(w_2 - w_3, W_2, W_3) + \mathcal{H}_{0,space}(w_2 - w_3, W_2, W_3; L_z)}_{\textbf{\textit{Integrable part}}:=\mathcal{H}_{int}} + \mathcal{H}_{1,space}(w_2, w_3, W_2, W_3; L_z)\,. \quad (2.41)$$

The first two terms in the above expression give rise to a 2 degrees of freedom integrable Hamiltonian

$$\mathcal{H}_{int}(w_2 - w_3, W_2, W_3; \mathrm{AMD}) = \mathcal{H}_{planar}(w_2 - w_3, W_2, W_3) + \mathcal{H}_{0,space}(w_2 - w_3, W_2, W_3; \mathrm{AMD}) \quad (2.42)$$

whose second integral is $W_2 + W_3$.

A fact hidden in the process of Jacobi reduction is that a decomposition of the Hamiltonian as in Eq.(2.41) yields a relative importance of the terms $\mathcal{H}_{int}$ and $\mathcal{H}_{1,space}$ *varying with the energy level* $\mathcal{E}$ at which the orbits are computed. This is due to the fact that, after throwing apart constants, all the terms in $\mathcal{H}_{space}$ stem from substitutions of the inclinations i_2 and i_3 depending only on the small quantity $1 - \cos(\mathrm{i}_2 + \mathrm{i}_3)$ and being of order second or higher in the eccentricities, according to Eq. (2.17) and (2.18). Thus, both $\mathcal{H}_{0,space}$ and $\mathcal{H}_{1,space}$ contain terms weighted by factors $(1 - \cos(\mathrm{i}_2 + \mathrm{i}_3))^s(\mathrm{e}_j^2 + \ldots)$ (with $s \geq 1$, $j = 2, 3$). On the other hand, the terms $\mathcal{H}_{planar}$ contain no factors $(1 - \cos(\mathrm{i}_2 + \mathrm{i}_3))^s$ and are of degree quadratic or higher in the eccentricities. Thus, due to the bound between increasing energy $\mathcal{E}$ and increasing mutual inclination (Fig.2.7),

the relative importance of the terms $\mathcal{H}_{1,space}$ with respect to the terms $\mathcal{H}_{int}$ in the Hamiltonian rises as the energy (and hence the level of mutual inclination) increases. This is demonstrated graphically in Fig.2.9, which shows a comparison between the form of the manifolds of constant energy $\mathcal{M}(\mathcal{E})$ and $\mathcal{M}_{int}(\mathcal{E})$ (Eqs.(2.34) and (2.35)) computed at four different energy levels chosen as $\mathcal{E}_{min} < \mathcal{E}_1 < \mathcal{E}_{2,3}$, $\mathcal{E}_{2,3} < \mathcal{E}_2 < \mathcal{E}_{C,2}$, $\mathcal{E}_3 = \mathcal{E}_{C,2}$, $\mathcal{E}_{C,2} < \mathcal{E}_4 < 0$. While the manifolds of $\mathcal{H}_{int}$ remain always ellipsoidal-like, we note the progressive change of the form of the manifolds of constant energy in the complete model from an ellipsoidal to a peanut-shaped form, as the energy increases. This is caused by the growing importance of some terms in $\mathcal{H}_{1,space}$, in particular the terms $\cos(2\omega_2)$ quadratic in e_2, which are the same terms causing the transition to the Lidov-Kozai regime (see subsection 2.3.4). In fact, near the energy $\mathcal{E}_{C,2}$, where the orbit C_2 turns from stable to unstable, the manifold $\mathcal{M}(\mathcal{E})$ under the complete model becomes nearly cylindrical, marking the change of its section with the plane $(\mathcal{X}_2, \mathcal{Y}_2)$ from elliptic-like to hyperbolic-like, as implied by the Lidov-Kozai mechanism.

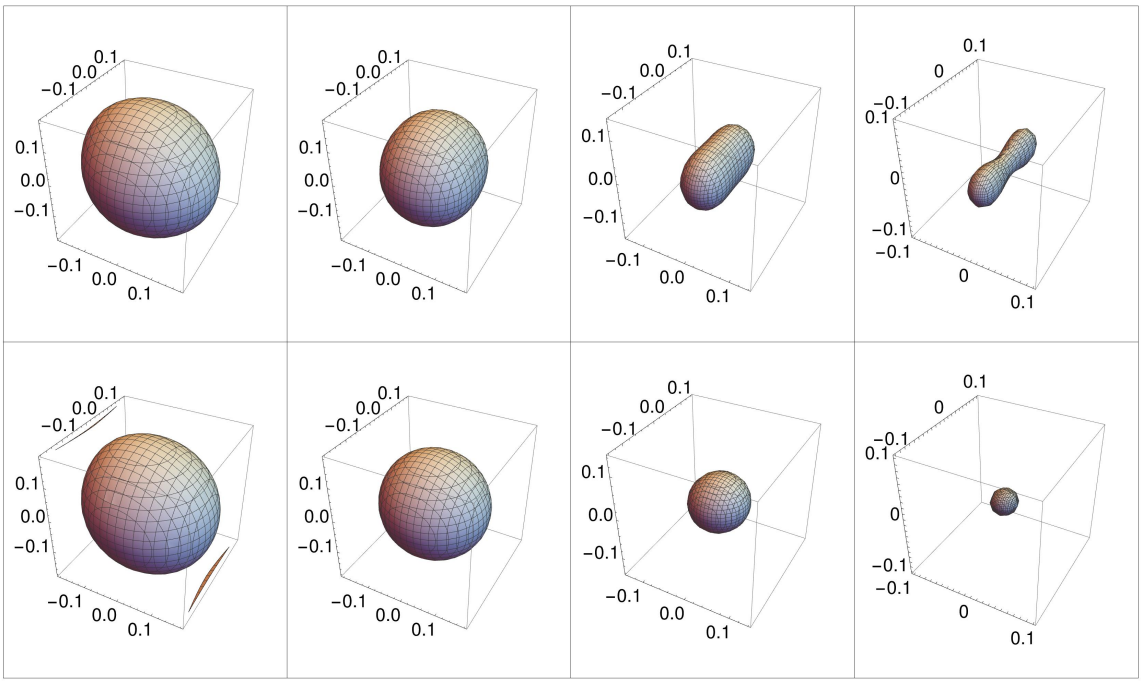

Figure 2.9: The top row shows the manifolds of constant energy $\mathcal{M}(\mathcal{E})$ compared to the manifolds of constant energy $\mathcal{M}_{int}(\mathcal{E})$ of the integrable model $\mathcal{H}_{int}$ (bottom row), for the energies (from left to right) $\mathcal{E}_1 = -8 \cdot 10^{-5}$ $(\mathcal{E}_1 < \mathcal{E}_{2,3})$, $\mathcal{E}_2 = -4 \cdot 10^{-5}$ $(\mathcal{E}_{2,3} < \mathcal{E}_2 < \mathcal{E}_{C,2})$, $\mathcal{E}_3 = -5 \cdot 10^{-6}$ $(\mathcal{E}_3 = \mathcal{E}_{C,2})$, $\mathcal{E}_4 = -5 \cdot 10^{-7}$ $(\mathcal{E}_4 > \mathcal{E}_{C,2})$.

Given the above, we will now focus on a description of the phase portraits in the energy regime (roughly identified as $\mathcal{E} < \mathcal{E}_C$) where the dynamics induced by $\mathcal{H}_{sec}$ can be well approximated by the dynamics of $\mathcal{H}_{int}$. In this regime, the following canonical transformation proves useful in semi-analytical (normal form) calculations related to the periodic orbits A and B and their surrounding quasi-periodic orbits:

$$\psi = w_2 - w_3\,, \qquad \Gamma = \frac{W_2 - W_3}{2}\,,$$
$$\varphi = w_2 + w_3\,, \qquad J = \frac{W_2 + W_3}{2}\quad . \tag{2.43}$$

The Hamiltonian in the new variables reads (apart from a constant)

$$\mathcal{H}_{sec}(\psi,\varphi,\Gamma,J)=\mathcal{H}_{int}(\psi,\Gamma;J)+\eta\,\mathcal{H}_{1,space}(\psi,\varphi,\Gamma,J)\,. \tag{2.44}$$

Figure 2.10 shows the phase portrait (in the representative planes $(\mathrm{e}_2\cos(\omega_2),\mathrm{e}_2\sin(\omega_2)$ and (ω_2,e_2)) corresponding to the Hamiltonian $\mathcal{H}_{int}$ at the energy $\mathcal{E}=-6.6\cdot10^{-5}$. The phase portrait, computed as a Poincaré surface of section $\mathcal{P}(\mathcal{E}=-6.6\cdot10^{-5}$, AMD $=0.0162044)$ (see Eq. (2.27)), yields invariant curves equivalent to those obtained by the continuous flow after treating $\mathcal{H}_{int}$ as a one degree of freedom Hamiltonian in the variables (ψ,Γ), with J serving as parameter.

We observe that with the integrable model $\mathcal{H}_{int}$ we obtain a phase portrait with features qualitatively very similar to those of the phase portraits in the 'planar-like' regime under the complete Hamiltonian (e.g. the panels 5-10 in Fig.2.8). In particular, the modes A and B of the integrable model are found as fixed points of $\mathcal{H}_{int}$, given by the solutions of the equations

$$\begin{cases}\dot{\psi}=\dfrac{\partial\mathcal{H}_{int}}{\partial\Gamma}=0\\ \dot{\Gamma}=-\dfrac{\partial\mathcal{H}_{int}}{\partial\psi}=0\end{cases}\,. \tag{2.45}$$

Since J is an integral of motion of $\mathcal{H}_{int}$, setting $J=K=$ constant implies that any solution $(\psi_*,\,\Gamma_*)$ satisfying (2.45) is a periodic orbit with period given by $T_\varphi=2\pi/\omega_\varphi$, where $\dot{\varphi}=\omega_\varphi=\dfrac{\partial\mathcal{H}_{int}}{\partial J}|_{(\psi=\psi_*,\,\Gamma=\Gamma_*\,,J=K)}$. In particular, the modes A and B are given, respectively, by $(\psi^{(A)}=0,\,\Gamma^{(A)}\,,K^{(A)})$ and $(\psi^{(B)}=\pi,\,\Gamma^{(B)},\,K^{(B)})$, where $(\psi^{(A)},\,\Gamma^{(A)})$, $(\psi^{(B)},\,\Gamma^{(B)})$ are solutions of (2.45). In fact, since the Hamiltonian $\mathcal{H}_{int}$ depends only on the harmonics $\cos(k\psi)$, with $k\in\mathbb{N}$, the partial derivative in the second of Eqs. (2.45) yields only $\sin(k\psi)$ terms, hence, it admits the solution $\psi=\psi^{(A)}=0$ and $\psi=\psi^{(B)}=\pi$. Given now that $\Omega_3=\Omega_2+\pi$, the condition $\omega_3=\omega_2$, i.e. $\psi=0=\psi^{(A)}$, implies $\varpi_3=\varpi_2+\pi$ (perihelia anti-aligned), while the condition $\omega_3=\omega_2+\pi$, i.e. $\psi=\pi=\psi^{(B)}$, implies (modulo 2π) $\varpi_3=\varpi_2$ (perihelia aligned). On the other hand, substituting one of the angles, $\psi^{(A)}$ or $\psi^{(B)}$, in the first of the Eqs. (2.45), we obtain an algebraic equation of the form $\dot{\psi}(\psi=\psi^{(A)},\Gamma,J)=0$ or $\dot{\psi}(\psi=\psi^{(B)},\Gamma,J)=0$. This, together with the constant energy condition $\mathcal{H}_{int}(\psi=\psi^{(A)},\Gamma,J)=\mathcal{E}$, or $\mathcal{H}_{int}(\psi=\psi^{(B)},\Gamma,J)=\mathcal{E}$, can be solved to yield the pairs of values $\Gamma^{(A)},J=K^{(A)}$, or $\Gamma^{(B)},J=K^{(B)}$. Finally, the frequency of the apsidal precession for anyone of the periodic orbits A, B is given by $\nu_{apsidal}=-\omega_\varphi/2=-\dot{\varphi}/2=-(1/2)(\partial\mathcal{H}_{int}(\psi,\,\Gamma,\,J)/\partial J)$, with $(\psi,\,\Gamma,\,J)$ substituted with one of the solutions A or B. Note that, in order to find the modes A and B , it is possible to fix one of the two parameters, that are J and $\mathcal{E}$; more precisely, we can determine A and B corresponding to *the same fixed value of* $J=K^{(A)}=K^{(B)}=K$ (having $(\psi^{(A)}=0,\,\Gamma^{(A)}\,,K)$ and $(\psi^{(B)}=\pi,\,\Gamma^{(B)}\,,K)$) but to *different levels of energy* $\mathcal{E}^{(A)}$ and $\mathcal{E}^{(B)}$, or at *the same fixed value of the energy* $\mathcal{E}$ but with *different values of* J (having $(\psi^{(A)}=0,\,\Gamma^{(A)}\,,J=K^{(A)})$ and $(\psi^{(B)}=\pi,\,\Gamma^{(B)}\,,J=K^{(B)})$).

2.3.2.2 The phase space of $\mathcal{H}_{int}$: Hopf variables

An alternative method to compute the equilibria A and B stems from the use of a particular set of variables, called the *Hopf variables* [17], which, besides the computation of the equilibria, provides a global mapping of the phase space of the integrable Hamiltonian $\mathcal{H}_{int}$ to the 3-sphere, thus allowing for a clear identification of all possible orbital dynamical regimes. We introduce the variables $(\sigma_1,\,\sigma_2,\,\sigma_3\,)$ defined by:

$$\sigma_1=\mathcal{X}_2\mathcal{X}_3+\mathcal{Y}_2\mathcal{Y}_3\,,\qquad \sigma_2=\mathcal{Y}_2\mathcal{X}_3-\mathcal{Y}_3\mathcal{X}_2\,,\qquad \sigma_3=\frac{1}{2}\left(\mathcal{X}_2^2+\mathcal{Y}_2^2-\mathcal{X}_3^2-\mathcal{Y}_3^2\right)\,, \tag{2.46}$$

satisfying the Poisson algebra $\{\sigma_i,\sigma_j\}=-2\,\epsilon_{ijk}\sigma_k$, where ϵ_{ijk} is the Levi-Civita symbol and $i,j,k=1,2,3$. Furthermore, we introduce the variable

$$\sigma_0=\frac{1}{2}\left(\mathcal{X}_2^2+\mathcal{Y}_2^2+\mathcal{X}_3^2+\mathcal{Y}_3^2\right) \tag{2.47}$$

which is a Casimir invariant of the previous algebra, since all Poisson brackets $\{\sigma_i, \sigma_0\}$, $i = 1, 2, 3$, vanish. From the definition (2.46) it follows that

$$\sigma_1 = 2\sqrt{J+\Gamma}\sqrt{J-\Gamma}\cos(\psi)\,, \qquad \sigma_2 = -2\sqrt{J+\Gamma}\sqrt{J-\Gamma}\sin(\psi)\,, \qquad \sigma_3 = W_2 - W_3 = 2\Gamma\,. \tag{2.48}$$

We also have the relation $\sigma_0 = W_2 + W_3 = 2J$, as well as

$$\sigma_1^2 + \sigma_2^2 + \sigma_3^2 = \sigma_0^2 = 4J^2\,. \tag{2.49}$$

Then, given the values of $(\sigma_1, \sigma_2, \sigma_3)$, the values of Γ, J and ψ can be computed unequivocally using the relations (2.48) and (2.49). Furthermore, since $J = \sigma_0/2$, and since the only trigonometric terms in the Hamiltonian $\mathcal{H}_{int}$ are terms $\cos(k(w_3 - w_2)) = \cos(k\psi)$, $k = \mathbb{N}^*$, it follows that $\mathcal{H}_{int} = \mathcal{H}_{int}(\sigma_1, \sigma_3; \sigma_0)$, i.e. the Hamiltonian $\mathcal{H}_{int}$ does not depend on σ_2. This implies that, fixing a value of σ_0 (i.e. of the integral J), the continuous in time phase flow obtained by solving the equations

$$\dot{\sigma}_1 = \{\sigma_1, \sigma_3\}\frac{\partial \mathcal{H}_{int}}{\partial \sigma_3}, \quad \dot{\sigma}_2 = \{\sigma_2, \sigma_1\}\frac{\partial \mathcal{H}_{int}}{\partial \sigma_1} + \{\sigma_2, \sigma_3\}\frac{\partial \mathcal{H}_{int}}{\partial \sigma_3}, \quad \dot{\sigma}_3 = -\{\sigma_1, \sigma_3\}\frac{\partial \mathcal{H}_{int}}{\partial \sigma_1}, \tag{2.50}$$

yields a flow equivalent to the one obtained under the Hamiltonian $\mathcal{H}_{int}(\psi, \Gamma; J)$, i.e., treating J as a parameter. Due to the constrain on the sphere (Eq.(2.49)), the curves of the flow (2.50) are given by the intersection of the constant energy surface $\mathcal{H}_{int}(\sigma_1, \sigma_3; \sigma_0) = \mathcal{E}$ with the sphere, i.e., they are closed curves which can be mapped to invariant curves in the plane (Γ, ψ). These are geometrically equivalent to the invariant curves of the Poincaré surface of section of $\mathcal{H}_{int}$ treated as a 2DOF system, mapping $(\mathcal{X}_2, \mathcal{Y}_2)$ as $\mathcal{X}_2 = -\sqrt{2(\Gamma + J)}\cos(\psi - \pi)$, $\mathcal{Y}_2 = \sqrt{2(\Gamma + J)}\sin(\psi - \pi)$. It should be stressed, however, that the above Hamiltonian reduction only yields a geometric equivalence of the two curves, since in the 1DOF reduced system the flow is continuous, while in the 2DOF full system the curves are traced stroboscopically, and they correspond to the intersection of the 2D invariant tori involving both the angles (ψ, φ) with the selected surface of section.

The above information can now be used to the purpose of analyzing the structure of the phase portraits using the mapping of each invariant curve in the sphere (2.49) to the corresponding curve in the usual Poincaré surface of section. To this end, let

$$\mathcal{S}_{\sigma_0} = \{(\sigma_1, \sigma_2, \sigma_3) \in \mathbb{R}^3 \,:\, \sigma_1^2 + \sigma_2^2 + \sigma_3^2 = \sigma_0^2\} \tag{2.51}$$

denote the sphere corresponding to the value $\sigma_0 = 2J$ of the integral J, and

$$\mathcal{C}_{\sigma_0, \mathcal{E}} = \{(\sigma_1, \sigma_2, \sigma_3) \in \mathbb{R}^3 \,:\, \mathcal{H}_{int}(\sigma_0, \sigma_1, \sigma_3) = \mathcal{E}\}\,, \tag{2.52}$$

denote the energy surface in the space $(\sigma_1, \sigma_2, \sigma_3) \in \mathbb{R}^3$ corresponding to a fixed energy value $\mathcal{E}$. We can have a physical trajectory for all values of σ_0 (i.e., of J) for which the surfaces $\mathcal{S}_{\sigma_0}$ and $\mathcal{C}_{\sigma_0, \mathcal{E}}$ intersect, limited by two values of σ_0, that are $\sigma_0^{(A)}$ and $\sigma_0^{(B)}$ (corresponding to $J^{(A)} = \sigma_0^{(A)}/2$ and $J^{(B)} = \sigma_0^{(B)}/2$), where the two surfaces become tangent (Fig. 2.10). By the non-dependence of $\mathcal{H}_{int}$ on σ_2, the constant energy surface $\mathcal{C}_{\sigma_0, \mathcal{E}}$ is normal to any plane (σ_1, σ_3) with $\sigma_2 = const.$ Hence, at a tangency point of $\mathcal{S}_{\sigma_0}$ with $\mathcal{C}_{\sigma_0, \mathcal{E}}$ we necessarily have that $\sigma_2 = 0$, as well as the tangency condition

$$\text{rank}\begin{pmatrix} 2\sigma_1 & 2\sigma_2 & 2\sigma_3 \\ \dfrac{\partial \mathcal{H}_{int}}{\partial \sigma_1} & 0 & \dfrac{\partial \mathcal{H}_{int}}{\partial \sigma_3} \end{pmatrix} = 1 \quad .$$

The latter condition implies that

$$\dot{\sigma}_2 = \sigma_3\frac{\partial \mathcal{H}_{int}}{\partial \sigma_1} - \sigma_1\frac{\partial \mathcal{H}_{int}}{\partial \sigma_3} = 0$$

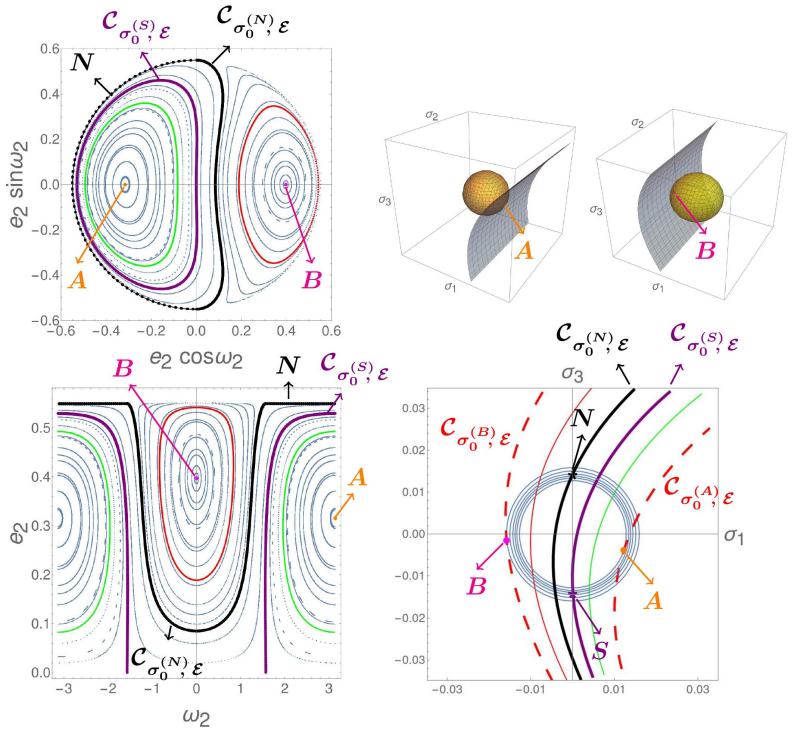

Figure 2.10: Left column: The phase portrait of the integrable Hamiltonian $\mathcal{H}_{int}$ at the energy $\mathcal{E} = -6.6\cdot10^{-5}$, projected in the variables $(\mathrm{e}_2\cos\omega_2, \mathrm{e}_2\sin\omega_2)$ (top), or simply (ω_2, e_2) (bottom). Right column, top: At the values $\sigma_0 = \sigma_0^{(A)}$ and $\sigma_0 = \sigma_0^{(B)}$, the corresponding spheres $\mathcal{S}_{\sigma_0^{(A)}}$, $\mathcal{S}_{\sigma_0^{(B)}}$ become tangent to the energy surfaces $\mathcal{C}_{\sigma_0^{(A)},\mathcal{E}}$, $\mathcal{C}_{\sigma_0^{(B)},\mathcal{E}}$. The points of tangency yield the position of the fixed points A and B in the surface of section (see text). Right column, bottom: the intersection of the spheres $\mathcal{S}_{\sigma_0}$ and of the energy surfaces $\mathcal{C}_{\sigma_0,\mathcal{E}}$ with the plane (σ_1, σ_3) for $\sigma_2 = 0$, for various values of σ_0. The intersection of one sphere with one energy surface yields a curve on the sphere which is projected to a curve in the above plane. For a particular value of $\sigma_0 = \sigma_0^{(S)}$, the curve (thick purple) passes through the south pole S of the corresponding sphere $\mathcal{S}_{\sigma_0}$. This corresponds to a trajectory forming a closed curve in the Poincaré section, which surrounds mode A and passes through the origin. This curve delimits the domain of orbits whose angle $\psi = \omega_3 - \omega_2$ librates around the value $\psi = 0$. At a different value of $\sigma_0 = \sigma_0^{(N)}$ the curve of constant energy (thick black in the right column, bottom) passes through the corresponding sphere's north pole N. This corresponds to a curve in the surface of section which surrounds the previous curve as well as the origin. In particular, the whole black curve, except for the point N, yields the part of the corresponding curve in the Poincaré section (left, top figure) contained in the positive semi-plane, while the point N itself inflates to the part of the corresponding closed curve in contained in the negative semi-plane. The domain in the surface of section between the thick purple and the thick black curves corresponds to orbits whose argument $\psi = \omega_3 - \omega_2$ circulates. All trajectories beyond the outer delimiting curve exhibit librations of the argument $\omega_3 - \omega_2$ around the value π, characteristic of the B-mode.

that is, the point of tangency is a fixed point of the flow. Up to terms of second order in the variables σ_i (i.e. of fourth order in the eccentricities), we find

$$\mathcal{H}_{int} = A\sigma_1^2 + B\sigma_3^2 + C\sigma_1\sigma_3 + D(\sigma_0)\sigma_1 + E(\sigma_0)\sigma_3 + F(\sigma_0) + ...$$

where A, B, C are constants, while the functions $D(\sigma_0)$ and $E(\sigma_0)$ are linear in σ_0 and $F(\sigma_0)$ contains terms linear and quadratic in σ_0. The quadratic form $A\sigma_1^2 + B\sigma_3^2 + C\sigma_1\sigma_3$ yields hyperbolas, being A, B, C such that $C^2 > AB$. Thus, for any permissible value σ_0 (or, equivalently, of the integral J), the surface $\mathcal{C}_{\sigma_0,\mathcal{E}}$ intersects the plane $\sigma_2 = 0$ along hyperbola-like curves (Fig.2.10). The two

points of tangency occur at the values $\sigma_0^{(A)} = 2J^{(A)}$ and $\sigma_0^{(B)} = 2J^{(B)}$. We find that $\sigma_0^{(A)} < \sigma_0^{(B)}$, while, checking the sign of $\cos(w_3 - w_2)$ for the corresponding fixed points, we identify the left tangency (see Fig.2.10) as the B-mode and the right tangency as the A-mode at the given level of energy.

With the help of the bottom-right panel of Fig.2.10 it is possible, now, to interpret the form of the phase portraits as in the left column of the same figure. To this end, we specify the correspondence between the various curves of the phase flow on the sphere, obtained by the intersections between the surfaces $\mathcal{S}_{\sigma_0}$ and $\mathcal{C}_{\sigma_0,\mathcal{E}}$ as σ_0 is altered in the interval $\sigma_0^{(A)} \leq \sigma_0 \leq \sigma_0^{(B)}$, and the mapping of these curves to the surface of section $(\mathrm{e}_2 \cos\omega_2, \mathrm{e}_2 \sin\omega_2)$. Since $\mathcal{H}_{int}$ does not depend on σ_2, all the curves produced by intersections of the surfaces $\mathcal{S}_{\sigma_0}$ and $\mathcal{C}_{\sigma_0,\mathcal{E}}$ contain points which lie in the meridian circle produced by the intersection of $\mathcal{S}_{\sigma_0}$ with the plane $\sigma_2 = 0$. In particular, the points of tangency A and B belong to this meridian. Besides these points, there are two critical curves which separate domains of libration of the angle $\omega_2 - \omega_3$ around the value 0 (mode A), or π (mode B), from domains where the angle $\omega_2 - \omega_3$ circulates.

By varying, now, the value of σ_0 in the interval $\sigma_0^{(A)} \leq \sigma_0 \leq \sigma_0^{(B)}$ we progressively obtain curves on the sphere which pass from a librating domain around the fixed point A to a circulating domain, and then to a librating domain around the fixed point B. The first such transition occurs at a value $\sigma_0^{(S)}$ where the curve corresponding to the intersection between $\mathcal{S}_{\sigma_0^{(S)}}$ and $\mathcal{C}_{\sigma_0^{(S)},\mathcal{E}}$ passes from the south pole S of the sphere $\mathcal{S}_{\sigma_0^{(S)}}$. The coordinates of the south pole are $\sigma_1^{(S)} = \sigma_2^{(S)} = 0$, $\sigma_3^{(S)} = -\sigma_0^{(S)}$, implying $J = -\Gamma$ or $W_2 + W_3 = -(W_2 - W_3)$, hence $W_2 = 0$. This means a curve in the Poincaré section (thick purple) which crosses the origin $\mathrm{e}_2 = 0$. As clear from Fig.2.10, we stress the well known fact that this curve means no real separatrix in the surface of section, generated by any kind of unstable periodic orbit, but it merely reflects the singularity induced by projecting an (all continuous) transition taking place in the phase space of the integrable Hamiltonian $\mathcal{H}_{int}$, which is the 3-sphere, to the usual Poincaré section applicable to the full problem, i.e., the plane $(\mathrm{e}_2 \cos\omega_2, \mathrm{e}_2 \sin\omega_2)$.

Passing, now, the value $\sigma_0 = \sigma_0^{(S)}$, we have curves of the sphere which are projected to invariant curves still surrounding the fixed point A, but for which the argument $\omega_2 - \omega_3$ (or $\omega_2 - \pi$, in the surface of section) circulates. A second limit of the circulation domain occurs at a value $\sigma_0^{(N)}$ where the curve corresponding to the intersection between $\mathcal{S}_{\sigma_0^{(N)}}$ and $\mathcal{C}_{\sigma_0(N),\mathcal{E}}$ passes from the north pole N of the sphere $\mathcal{S}_{\sigma_0^{(N)}}$. We readily find that the whole curve in the sphere $\mathcal{S}_{\sigma_0^{(N)}}$, except for the pole N itself, yields the open black curve in the surface of section corresponding to the positive semi-plane $\mathrm{e}_2 \cos(\omega_2) \geq 0$ (or $-\pi/2 \leq \omega_2 \leq \pi/2$), while the north pole itself inflates to the dotted semicircle obtained in the negative semi-plane $\mathrm{e}_2 \cos(\omega_2) < 0$ (or $\pi/2 < \omega_2 < 3\pi/2$). Here again the singularity is not real but only due to the choice of the variables representing the surface of section (see e.g. [91], [42], [79]). In fact, N has coordinates $\left(\sigma_0^{(N)}, \sigma_1^{(N)} = 0, \sigma_2^{(N)} = 0, \sigma_3^{(N)} = \sigma_0^{(N)}\right)$, implying $W_3 = 0$, i.e. $\mathrm{e}_3 = 0$. However, the equality $\sigma_3^{(N)} = \sigma_0^{(N)}$ implies also $\mathcal{X}_2^2 + \mathcal{Y}_2^2 = 2\sigma_0$, i.e. a circle on the section $\mathcal{Y}_3 = 0$. Together with the condition $\dot{\mathcal{Y}}_3 \geq 0$ of the Poincaré section, this implies the semi-circle $\mathcal{X}_2 \geq 0$, i.e. the dotted part of the black curve in the top-left panel of Fig.2.10. It can be shown that the two parts or the curve join each other smoothly at two limiting values $\mathcal{X}_2 = 0, \mathcal{Y}_2 = \pm\mathcal{Y}_{2,max} = \pm\sqrt{2\sigma_0^{(N)}}$. In fact, the semi-circle $\mathcal{Y}_2 = \pm\sqrt{2\sigma_0^{(N)} - \mathcal{X}_2^2}$, $\mathcal{X}_2 > 0$, corresponding to the inflation of the north pole, yields $\lim_{\mathcal{X}_2 \to 0^+}(d\mathcal{Y}_2/d\mathcal{X}_2) = 0$, while the open curve $\mathcal{Y}_2 = \mathcal{Y}_2(\mathcal{X}_2)$, corresponding to all other points of the intersection of $\mathcal{S}_{\sigma_0^{(N)}}$ and $\mathcal{C}_{\sigma_0(N),\mathcal{E}}$ except for the pole, yields the limit

$$\lim_{\mathcal{X}_2 \to 0^-} \frac{d\mathcal{Y}_2}{d\mathcal{X}_2} = \lim_{\mathcal{X}_2 \to 0^-} \left(-\frac{\frac{\partial \mathcal{H}_{int}}{\partial \mathcal{X}_2}}{\frac{\partial \mathcal{H}_{int}}{\partial \mathcal{Y}_2}} \right) \quad . \tag{2.53}$$

From the form of H_{int}, recalling Eq. (2.26), we readily find $\partial\mathcal{H}_{int}/\partial\mathcal{X}_2 = 0$, $\partial\mathcal{H}_{int}/\partial\mathcal{Y}_2 \neq 0$ at the

north pole limit $\mathcal{X}_2 = \mathcal{X}_3 = \mathcal{Y}_3 = 0$, $\mathcal{Y}_2 = \pm\mathcal{Y}_{2,max}$.

Finally, for σ_0 in the interval $\sigma_0^{(N)} < \sigma_0 \leq \sigma_0^{(B)}$ we find invariant curves in the sphere $\mathcal{S}_{\sigma_0}$ mapped to closed invariant curves around the tangency corresponding to the B-mode fixed point, which yield also closed curves in the Poincaré section for which the argument $\omega_2 - \omega_3$ (or $\omega_2 - \pi$ in the section) librates around the value π, i.e., ω_2 librates around the value $\omega_2 = 0$ of the B-mode.

A similar analysis as above can be repeated fixing, as parameter, the value of the integral J instead of the level of energy $\mathcal{E}$. The details are reported in Appendix B.

2.3.3 Transition regime between planar-like and Lidov-Kozai: sequences of bifurcations

The planar-like regime discussed in the previous subsection characterizes the structure of the phase portraits of the full system up to the energy $\mathcal{E}_C$, where the orbits C_1, C_2 are generated by a saddle node bifurcation in the taking place in the neighborhood of the mode B, as in the transition seen in the third row of Fig.2.8. We call *transition regime* the one holding at energies in the interval $\mathcal{E}_C \leq \mathcal{E}_{C,2}$.

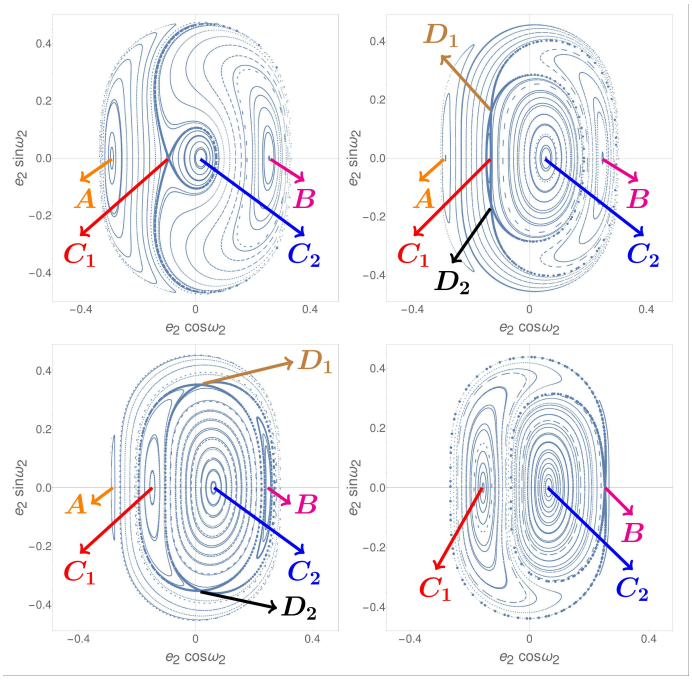

Figure 2.11: Poincaré surfaces of section for some values of the energy illustrating the sequence of bifurcations taking place in the 'transition regime' (see text): $\mathcal{E} = -2.53 \cdot 10^{-5}$ (top left), $\mathcal{E} = -2.08 \cdot 10^{-5}$ (top right), $\mathcal{E} = -1.9 \cdot 10^{-5}$ (bottom left), $\mathcal{E} = -1.58 \cdot 10^{-5}$ (bottom right), corresponding, respectively, to panels 11 , 13 , 14 and 15 of Figure 2.8.

Figure 2.11 presents in detail the sequence of bifurcations taking place across the transition regime, which eventually lead to turning unstable the periodic orbit of mode B. At the beginning of the transition, for energies slightly larger than $\mathcal{E}_C$, the orbit C_1 turns from unstable to stable by a pitchfork bifurcation, which gives rise to an unstable periodic orbit yielding two fixed points, D_1, D_2, in the Poincaré surface of section. As the energy increases, these fixed points move initially away from the fixed point of the orbit C_1, while later (for still larger energy) they approach the fixed point of the mode B. Finally, at a second critical value of the energy the fixed points D_1, D_2

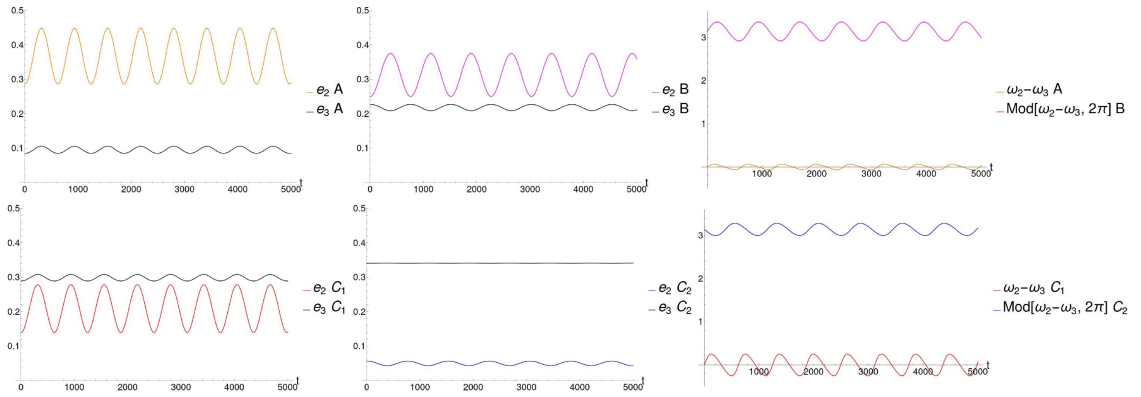

Figure 2.12: Top row: the evolution of the orbital eccentricities e_2, e_3 for the periodic orbits corresponding to the modes A (top left panel: top curve e_2, bottom curve e_3), and B (top middle panel: top curve e_2, bottom curve e_3). The top right panel shows the librations of the argument $\omega_2 - \omega_3$ for the B-mode (top curve) or the A-mode (bottom curve). Bottom row: the evolution of the orbital eccentricities e_2, e_3 for the periodic orbits corresponding to the fixed points C_1 (bottom left panel: top curve e_3, bottom curve e_2), and C_2 (bottom middle panel: top curve e_2, bottom curve e_3).The bottom right panel shows the librations of the argument $\omega_2 - \omega_3$ for the orbit C_2 (top curve) or C_1 (bottom curve). The above time series are computed at the value of the energy $\mathcal{E} = -2.08 \cdot 10^{-5}$, corresponding to the 13-th panel of Figure 2.8.

collide with the B-mode. This terminates the D-family of periodic orbits, by an inverse pitchfork bifurcation which renders the B-mode unstable.

Figure 2.12 illustrates the evolution of the eccentricity vectors for all four periodic orbits A, B, C_1, C_2. In all four cases the eccentricities of both planets oscillate periodically, while the argument $\omega_2 - \omega_3$ undergoes small librations around one of the values 0 or π.

2.3.4 Lidov-Kozai regime

We finally discuss the transition seen in the last row of Figure 2.8, in which the periodic orbit C_2 turns from stable to unstable via the *Lidov-Kozai mechanism*. This is accompanied by a large volume of trajectories around C_2 becoming chaotic. In the case of a test inner particle ($m_2 = 0$) at circular orbit $e_2 = 0$, the mutual inclination is a preserved quantity, equal to the inclination of the test particle $i_{mut} = i_2$ (since $m_2 = 0$ the Laplace plane coincides with the constant orbital plane of the outer particle). Furthermore, the stability character of the so-called Lidov-Kozai state ([62], [48], [63], [44]) depends only on the value of the inclination. In particular, in the quadrupolar approximation, the transition from stability to instability occurs at a critical inclination equal to $\cos^{-1}\sqrt{\frac{3}{5}} \sim 39^\circ.2$ (see [88] for a review).

Here, instead, we use a criterion analogous to the one of the classical Lidov-Kozai mechanism in order to obtain an estimate of the critical energy $\mathcal{E}_{C,2}$ at which the orbit C_2 turns from stable to unstable in the framework of the quadrupolar approximation to the secular Hamiltonian $\mathcal{H}_{sec}$ in the full three body problem, i.e., for $m_2 \neq 0$. The quadrupolar Hamiltonian, apart from constants, reads

$$\mathcal{H}_{quad} = -\frac{3\,\mathcal{G}\,m_2\,m_3}{8\,a_3}\left(\frac{a_2}{a_3}\right)^2 \frac{1}{(1-e_3^2)^{3/2}}\mathcal{F}_{quad}\,, \tag{2.54}$$

where

$$\mathcal{F}_{quad} = -\frac{1}{3} - \frac{e_2^2}{2} + \frac{3}{2}\,e_2^2\,\theta^2 + \theta^2 + \frac{5}{2}\,e_2^2\left(1-\theta^2\right)\cos(2\,\omega_2)\,, \tag{2.55}$$

with $\theta = \cos(\mathrm{i}_2 + \mathrm{i}_3)$. Following the process of Jacobi reduction, without any book-keeping control, amounts to expanding the cosine of the mutual inclinations as $\cos(\mathrm{i}_2 + \mathrm{i}_3) = \cos(\mathrm{i}_2)\cos(\mathrm{i}_3) - \sin(\mathrm{i}_2)\sin(\mathrm{i}_3)$, we can use expression (2.18), that automatically cancel the dependence of the Hamiltonian on the mutual inclination. The Hamiltonian takes now the form (apart from constants):

$$\begin{aligned}
\mathcal{H}_{quad} = &- \frac{3\,a_2\mathcal{G}\left(3\,\mathrm{e}_2^2+2\right)\,m_3^3}{64\,a_3^2\left(1-\mathrm{e}_2^2\right)\sqrt{1-\mathrm{e}_3^2}\,m_2} - \frac{a_2^2\mathcal{G}\left(3\,\mathrm{e}_2^2+2\right)\,m_2\,m_3}{32\,a_3^3\left(1-\mathrm{e}_3^2\right)^{3/2}} + \frac{3\,a_2^3\mathcal{G}\left(3\,\mathrm{e}_2^4-\mathrm{e}_2^2-2\right)\,m_2^3}{64\,a_3^4\left(1-\mathrm{e}_3^2\right)^{5/2}\,m_3} \\
&+ L_z^2\left(\frac{3\,a_2\left(3\,\mathrm{e}_2^2+2\right)\,m_3}{32\,a_3^3\left(1-\mathrm{e}_2^2\right)\left(1-\mathrm{e}_3^2\right)^{3/2}\,m_0\,m_2} + \frac{3\,a_2^2\left(3\,\mathrm{e}_2^2+2\right)\,m_2}{32\,a_3^4\left(1-\mathrm{e}_3^2\right)^{5/2}\,m_0\,m_3}\right) \\
&- \frac{3\,a_2\left(3\,\mathrm{e}_2^2+2\right)\,L_z^4}{64\,a_3^4\mathcal{G}\left(1-\mathrm{e}_2^2\right)\left(1-\mathrm{e}_3^2\right)^{5/2}\,m_0^2\,m_2\,m_3} \\
&+ \cos(2\,\omega_2)\left[\frac{15\,a_2\mathcal{G}\,\mathrm{e}_2^2\,m_3^3}{64\,a_3^2\left(1-\mathrm{e}_2^2\right)\sqrt{1-\mathrm{e}_3^2}\,m_2} - \frac{15\,a_2^2\mathcal{G}\,\mathrm{e}_2^2\,m_2\,m_3}{32\,a_3^3\left(1-\mathrm{e}_3^2\right)^{3/2}} + \frac{15\,a_2^3\mathcal{G}\,\mathrm{e}_2^2\left(1-\mathrm{e}_2^2\right)\,m_2^3}{64\,a_3^4\left(1-\mathrm{e}_3^2\right)^{5/2}\,m_3}\right. \\
&\qquad + L_z^2\left(-\frac{15\,a_2\,\mathrm{e}_2^2\,m_3}{32\,a_3^3\left(1-\mathrm{e}_2^2\right)\left(1-\mathrm{e}_3^2\right)^{3/2}\,m_0\,m_2} - \frac{15\,a_2^2\,\mathrm{e}_2^2\,m_2}{32\,a_3^4\left(1-\mathrm{e}_3^2\right)^{5/2}\,m_0\,m_3}\right) \\
&\qquad \left. + \frac{15\,a_2\,\mathrm{e}_2^2\,L_z^4}{64\,a_3^4\mathcal{G}\left(1-\mathrm{e}_2^2\right)\left(1-\mathrm{e}_3^2\right)^{5/2}\,m_0^2\,m_2\,m_3}\right].
\end{aligned} \tag{2.56}$$

It can be observed that the secular Hamiltonian at the quadrupolar level does not depend on the argument of the pericenter of the outer planet ω_3, therefore the system is integrable (a fact known as the "happy coincidence", see [63] or [88] for a review). In particular, the non-dependence of the Hamiltonian on ω_3 implies that the eccentricity of the outer planet e_3 is a conserved quantity.

Using e_3 as a parameter, the Hamiltonian $\mathcal{H}_{quad}$ can now be regarded as a one degree of freedom system. This can obtain a polynomial form by passing to the Poincaré variables $(\mathcal{X}_2, \mathcal{Y}_2)$ described by (2.24). After such a substitution, the quadratic part of the above Hamiltonian is given by

$$\mathcal{H}_{2,quad}(\mathcal{X}_2, \mathcal{Y}_2; G_3, L_z) = \frac{\mathfrak{a}(G_3, L_z)}{2}\,\mathcal{Y}_2^2 - \frac{\mathfrak{b}(G_3, L_z)}{2}\,\mathcal{X}_2^2\,, \tag{2.57}$$

where the coefficients $\mathfrak{b}$ and $\mathfrak{a}$ are functions of $G_3 = L_3\sqrt{1-\mathrm{e}_3^2}$ =const and of L_z; in particular

$$\begin{aligned}
\mathfrak{b} &= \frac{3\,\mathcal{G}^2\,L_2^3\,\left(3\,G_3^2 - L_2^2 + L_z^2\right)\,m_0\,m_3^7}{8\,G_3^5\,L_3^3\,m_2^3} \\
\mathfrak{a} &= -\frac{3\,\mathcal{G}^2\,L_2\left(5\,G_3^4 - 4\,G_3^2\,L_2^2 + 3\,L_2^4 - 10\,G_3^2\,L_z^2 - 8\,L_2^2\,L_z^2 + 5\,L_z^4\right)m_0\,m_3^7}{16\,G_3^5\,L_3^3\,m_2^3}\,.
\end{aligned} \tag{2.58}$$

Now, in order to find the critical value of the energy $\mathcal{E}_{C,2}$, for fixed L_z, at which the periodic orbit $\mathrm{e}_3 = const$, $\mathrm{e}_2 = 0$ becomes unstable, it is sufficient to compute the eigenvalues of the Jacobian matrix of the Hamiltonian vector field:

$$M = \begin{pmatrix} \dfrac{\partial\dot{\mathcal{X}}_2}{\partial\mathcal{X}_2} & \dfrac{\partial\dot{\mathcal{X}}_2}{\partial\mathcal{Y}_2} \\ \dfrac{\partial\dot{\mathcal{Y}}_2}{\partial\mathcal{X}_2} & \dfrac{\partial\dot{\mathcal{Y}}_2}{\partial\mathcal{Y}_2} \end{pmatrix} = \begin{pmatrix} \dfrac{\partial^2\mathcal{H}_{quad}}{\partial\mathcal{X}_2\,\partial\mathcal{Y}_2} & \dfrac{\partial^2\mathcal{H}_{quad}}{\partial^2\mathcal{Y}_2} \\ -\dfrac{\partial^2\mathcal{H}_{quad}}{\partial^2\mathcal{X}_2} & -\dfrac{\partial^2\mathcal{H}_{quad}}{\partial\mathcal{Y}_2\,\partial\mathcal{X}_2} \end{pmatrix} = \begin{pmatrix} 0 & \mathfrak{a} \\ \mathfrak{b} & 0 \end{pmatrix}. \tag{2.59}$$

The transition occurs at a critical value of $\mathrm{e}_3 = \mathrm{e}_{3,C_2}$ at which the eigenvalues of M pass from imaginary to real. The critical energy is then given by $\mathcal{E}_{C,2} = \mathcal{H}_{quad}(\mathrm{e}_2 = 0, \mathrm{e}_{3,C_2}; L_z)$. The critical value e_{3,C_2} can be computed by the following

Proposition 2.3.1. *Consider the secular Hamiltonian developed up to a quadrupolar expansion. Define the quantities*

$$\begin{aligned} A &= \frac{1}{5}\left(4L_2^2 + 5L_3^2(1-\mathrm{e}_3^2) - L_2\sqrt{L_2^2 + 60L_3^2(1-\mathrm{e}_3^2)}\right), \\ B &= \frac{1}{5}\left(4L_2^2 + 5L_3^2(1-\mathrm{e}_3^2) + L_2\sqrt{L_2^2 + 60L_3^2(1-\mathrm{e}_3^2)}\right), \\ C &= L_2^2 - 3L_3^2(1-\mathrm{e}_3^2), \end{aligned} \tag{2.60}$$

with $L_2 = m_2\sqrt{\mathcal{G}m_0 a_2} > 0$, $L_3 = m_3\sqrt{\mathcal{G}m_0 a_3} > 0$. *Then, the following cases hold:*

Case i) *:* $0 < L_2 < \sqrt{3}L_3 \wedge 0 \leq \mathrm{e}_3 \leq \sqrt{1 - \frac{L_2^2}{3L_3^2}}$, *the periodic orbit* C_2 *is Floquet-stable if* $0 < L_z^2 < A$ *or* $L_z^2 > B$ *and Floquet-unstable if* $A < L_z^2 < B$.

Case ii) *:* $0 < L_2 < \sqrt{3}L_3 \wedge \sqrt{1 - \frac{L_2^2}{3L_3^2}} < \mathrm{e}_3 < \sqrt{1 - \frac{L_2^2}{4L_3^2}}$ ***or*** $\sqrt{3}L_3 \leq L_2 < 2L_3 \wedge 0 \leq \mathrm{e}_3 < \sqrt{1 - \frac{L_2^2}{4L_3^2}}$, *the periodic orbit* C_2 *is Floquet-stable if* $C < L_z^2 < A$ *or* $L_z^2 > B$ *and Floquet-unstable if* $0 < L_z^2 < C$ *or* $A < L_z^2 < B$.

Case iii) *:* $0 < L_2 \leq 2L_3 \wedge \mathrm{e}_3 = \sqrt{1 - \frac{L_2^2}{4L_3^2}}$, *the periodic orbit* C_2 *is Floquet-stable if* $L_z^2 > B$ *and Floquet-unstable if* $0 < L_z^2 < B$.

Case iv) *:* $0 < L_2 \leq 2L_3 \wedge \mathrm{e}_3 > \sqrt{1 - \frac{L_2^2}{4L_3^2}}$ ***or*** *if* $L_2 > 2L_3$, *the periodic orbit* C_2 *is Floquet-stable if* $A < L_z^2 < C$ *or* $L_z^2 > B$ *and Floquet-unstable if* $0 < L_z^2 < A$ *or* $C < L_z^2 < B$.

Moreover, having the critical points of L_z^2, it is easy to compute the critical values for the mutual inclination, being (by Eq. (2.28))

$$\cos(\mathrm{i}_2 + \mathrm{i}_3) = \frac{L_z^2 - \Lambda_2^2 - \Lambda_3^2 + \Lambda_2^2\,\mathrm{e}_2^2 + \Lambda_3^2\,\mathrm{e}_3^2}{2\Lambda_2\Lambda_3\sqrt{1-\mathrm{e}_2^2}\sqrt{1-\mathrm{e}_3^2}}, \qquad \max \mathrm{i}_{mut} = \arccos\left(\frac{L_z^2 - L_2^2 - L_3^2}{2\,L_2\,L_3}\right). \tag{2.61}$$

Proof. The eigenvalues of the matrix M (2.59) are $\lambda_{1,2} = \pm\sqrt{\mathfrak{a}\mathfrak{b}}$; then if $\mathfrak{a}\mathfrak{b} > 0$, then the eigenvalues are real and opposite, instead if $\mathfrak{a}\mathfrak{b} < 0$, then the eigenvalues are complex and conjugate. We have to analyze all the possible cases. We can have

$$\begin{cases} \mathfrak{a} > 0 \\ \mathfrak{b} > 0 \end{cases}, \qquad \begin{cases} \mathfrak{a} < 0 \\ \mathfrak{b} < 0 \end{cases} \quad \Longrightarrow \quad \lambda_{1,2} \quad \textit{real} \tag{2.62a}$$

$$\begin{cases} \mathfrak{a} > 0 \\ \mathfrak{b} < 0 \end{cases}, \qquad \begin{cases} \mathfrak{a} < 0 \\ \mathfrak{b} > 0 \end{cases} \quad \Longrightarrow \quad \lambda_{1,2} \quad \textit{immaginary}\,. \tag{2.62b}$$

Let us start to understand the change of sign of $\mathfrak{b}$; remembering the definition (2.58)

$$\mathfrak{b} = \frac{3\mathcal{G}^2 L_2^3\,(3G_3^2 - L_2^2 + L_z^2)\,m_0\,m_3^7}{8\,G_3^5\,L_3^3\,m_2^3} > 0 \quad \Longleftrightarrow \quad \tilde{\mathfrak{b}} := L_z^2 + 3L_3^2(1-\mathrm{e}_3^2) - L_2^2 > 0\,,$$

being $(3\mathcal{G}^2 L_2^3 m_0 m_3^7)/(8(1-\mathrm{e}_3^2)^{5/2} L_3^8 m_2^3) > 0$. Now, let us observe that if

$$C := L_2^2 - 3L_3^2(1-\mathrm{e}_3^2) < 0 \quad \Longrightarrow \quad \mathrm{e}_3^2 < 1 - \frac{L_2^2}{3L_3^2}\,, \tag{2.63}$$

then $\tilde{\mathfrak{b}} > 0$ automatically; in order to have that, it is necessary that $1 - \frac{L_2^2}{3L_3^2} > 0$, i.e. to have $0 < L_2 < \sqrt{3}L_3$. Thus, we can conclude that $\mathfrak{b} > 0$ (or equivalently $\tilde{\mathfrak{b}} > 0$) if one of the two is fullfilled

i) $0 < L_2 < \sqrt{3}L_3 \ \wedge \ 0 \le \mathrm{e}_3 \le \sqrt{1 - \frac{L_2^2}{3L_3^2}}$, with $L_z^2 > 0$ **or**

ii) $\left(0 < L_2 < \sqrt{3}L_3 \ \wedge \ \mathrm{e}_3 > \sqrt{1 - \frac{L_2^2}{3L_3^2}}\right) \ \vee \ L_2 \ge \sqrt{3}L_3$, with $L_z^2 > C$.

Now, let us study the sign of $\mathfrak{a}$; as before, from definition (2.58)

$$\begin{aligned} \mathfrak{a} &= -\frac{3\mathcal{G}^2 L_2(5G_3^4 - 4G_3^2L_2^2 + 3L_2^4 - 10G_3^2L_z^2 - 8L_2^2L_z^2 + 5L_z^4)m_0m_3^7}{16G_3^5L_3^3m_2^3} > 0 \quad \Longleftrightarrow \\ \tilde{\mathfrak{a}} &:= L_3^4(1-\mathrm{e}_3^2)^2 - \frac{4}{5}L_3^2L_2^2(1-\mathrm{e}_3^2) + \frac{3}{5}L_2^4 - 2L_3^2(1-\mathrm{e}_3^2)L_z^2 - \frac{8}{5}L_2^2L_z^2 + L_z^4 < 0\,, \end{aligned} \tag{2.64}$$

being $-(3\mathcal{G}^2L_2\, m_0\, m_3^7)/(16\, L_3^8(1-\mathrm{e}_3)^{5/2}m_2^3) < 0$. Then $\mathfrak{a} > 0$ (or equivalently $\tilde{\mathfrak{a}} < 0$) iff $A < L_z^2 < B$, where A and B are defined as in (2.60), i.e.

$$\begin{aligned} A &= \frac{1}{5}\left(4L_2^2 + 5L_3^2(1-\mathrm{e}_3^2) - L_2\sqrt{L_2^2 + 60L_3^2(1-\mathrm{e}_3^2)}\right), \\ B &= \frac{1}{5}\left(4L_2^2 + 5L_3^2(1-\mathrm{e}_3^2) + L_2\sqrt{L_2^2 + 60L_3^2(1-\mathrm{e}_3^2)}\right). \end{aligned}$$

Let us observe that A and B are both greater than zero. Infact, being $0 \le \mathrm{e}_3 < 1$, it is obvious that $B > 0$; on the other hand $A > 0$ iff

$$\begin{aligned} &\sqrt{L_2^2 + 60L_3^2(1-\mathrm{e}_3^2)} < 4L_2 + \frac{5L_3^2}{L_2}(1-\mathrm{e}_3^2) && \Longleftrightarrow \\ &L_2^2 + 60L_3^2(1-\mathrm{e}_3^2) < 16L_2^2 + 25\frac{L_3^4}{L_2^2}(1-\mathrm{e}_3^2)^2 + 40L_3^2(1-\mathrm{e}_3^2) && \Longleftrightarrow \\ &3L_2^4 - 4L_3^2(1-\mathrm{e}_3^2)L_2^2 + 5(1-\mathrm{e}_3^2)^2L_3^4 > 0 \end{aligned}$$

that holds $\forall\ L_2, L_3, 0 \le \mathrm{e}_3 < 1$, being $\Delta = -44L_3^4(1-\mathrm{e}_3^2)^2 < 0$. Then, we can conclude that if we are in the case i), (i.e. $0 < L_2 < \sqrt{3}L_3 \ \wedge \ 0 \le \mathrm{e}_3 \le \sqrt{1 - \frac{L_2^2}{3L_3^2}}$) and $A < L_z^2 < B$, then $\mathfrak{b} > 0$ and $\mathfrak{a} > 0$, then we have real eigenvalues; instead if, in the same case i), $0 < L_z^2 < A$ or $L_z^2 > B$, then $\mathfrak{b} > 0$, $\mathfrak{a} < 0$, having complex immaginary eigenvalues. This proves the **Case i)** of the Proposition.

In the case ii), i.e. $\left(0 < L_2 < \sqrt{3}L_3 \ \wedge \ \mathrm{e}_3 > \sqrt{1 - \frac{L_2^2}{3L_3^2}}\right) \ \vee \ L_2 \ge \sqrt{3}L_3$, we have to solve (2.62b) and (2.62b), that become, respectively

$$\begin{cases} \mathfrak{a} > 0 \\ \mathfrak{b} > 0 \end{cases} = \begin{cases} A < L_z^2 < B \\ L_z^2 > C \end{cases}, \qquad \begin{cases} \mathfrak{a} < 0 \\ \mathfrak{b} < 0 \end{cases} = \begin{cases} 0 < L_z^2 < A \ \vee \ L_z^2 > B \\ 0 < L_z^2 < C \end{cases}, \tag{2.65a}$$

$$\begin{cases} \mathfrak{a} > 0 \\ \mathfrak{b} < 0 \end{cases} = \begin{cases} A < L_z^2 < B \\ 0 < L_z^2 < C \end{cases}, \qquad \begin{cases} \mathfrak{a} < 0 \\ \mathfrak{b} > 0 \end{cases} = \begin{cases} 0 < L_z^2 < A \ \vee \ L_z^2 > B \\ L_z^2 > C \end{cases}; \tag{2.65b}$$

then, we have to understand the position of the value C with respect to A and B.

Case 1 : $C < A$

$$C < A \quad \Longleftrightarrow \quad \sqrt{L_2^2 + 60L_3^2(1-\mathrm{e}_3^2)} < -L_2 + \frac{20L_3^2}{L_2}(1-\mathrm{e}_3^2)$$

i.e.

$$\begin{cases} -L_2 + \frac{20L_3^2}{L_2}(1-\mathrm{e}_3^2) \ge 0 \\ L_2^2 + 60L_3^2(1-\mathrm{e}_3^2) < L_2^2 + \frac{400L_3^4}{L_2^2}(1-\mathrm{e}_3^2)^2 - 40L_3^2(1-\mathrm{e}_3^2) \end{cases} \Longleftrightarrow \quad \begin{cases} \mathrm{e}_3^2 \le 1 - \frac{L_2^2}{20L_3^2} \\ \mathrm{e}_3^2 < 1 - \frac{L_2^2}{4L_3^2}, \end{cases}$$

then if $\mathrm{e}_3^2 < 1 - \frac{L_2^2}{4L_3^2}$. The last inequality makes sense if $1 - \frac{L_2^2}{4L_3^2} > 0$, that is $0 \leq L_2 < 2L_3$. Remembering that we are in the case ii), it follows that

$$C < A \iff \left(0 < L_2 < \sqrt{3}L_3 \ \wedge \ \sqrt{1 - \frac{L_2^2}{3L_3^2}} < \mathrm{e}_3 < \sqrt{1 - \frac{L_2^2}{4L_3^2}}\right) \vee \left(\sqrt{3}L_3 \leq L_2 < 2L_3 \ \wedge \ 0 \leq \mathrm{e}_3 < \sqrt{1 - \frac{L_2^2}{4L_3^2}}\right).$$

Therefore, studying (2.65a) and (2.65b), we can conclude that if $\left(0 < L_2 < \sqrt{3}L_3 \ \wedge \ \sqrt{1 - \frac{L_2^2}{3L_3^2}} < \mathrm{e}_3 < \sqrt{1 - \frac{L_2^2}{4L_3^2}}\right) \vee \left(\sqrt{3}L_3 \leq L_2 < 2L_3 \ \wedge \ 0 \leq \mathrm{e}_3 < \sqrt{1 - \frac{L_2^2}{4L_3^2}}\right)$, then the eigenvalues are real and opposite if $0 < L_z^2 < C$ (see the second of (2.65a)), purely immaginary and coniugates if $C < L_z^2 < A$ (see the second of (2.65b)), real and opposite if $A < L_z^2 < B$ (see the first of (2.65a)) and again purely immaginary and coniugates if $L_z^2 > B$ (see the second of (2.65b)), proving the **Case ii)** of the Proposition.

Case 2 : $C = A$

Following the same calculations done for the previous case ($C < A$), it easily follows that

$$C = A \iff \left(0 < L_2 \leq 2L_3 \ \wedge \ \mathrm{e}_3 = \sqrt{1 - \frac{L_2^2}{4L_3^2}}\right);$$

in this case, studying (2.65a) and (2.65b), we can conclude that the eigenvalues are real and opposite if $0 < L_z^2 < C = A$ (see the second of (2.65a)), again real and opposite if $C = A < L_z^2 < B$ (see the first of (2.65a)) (i.e. are real and opposite if $0 < L_z^2 < B$, passing from 0 if $L_z^2 = A = C$) and purely immaginary and coniugates if $L_z^2 > B$ (see the second of (2.65b)). This proves the **Case iii)** of the Proposition.

Case 3 : $A < C < B$

$$C > A \iff \sqrt{L_2^2 + 60L_3^2(1 - \mathrm{e}_3^2)} > -L_2 + \frac{20L_3^2}{L_2}(1 - \mathrm{e}_3^2) \tag{2.66}$$

$$C < B \iff \sqrt{L_2^2 + 60L_3^2(1 - \mathrm{e}_3^2)} > L_2 - \frac{20L_3^2}{L_2}(1 - \mathrm{e}_3^2). \tag{2.67}$$

Let us start from (2.66); we have to solve the following

$$\begin{cases} -L_2 + \frac{20L_3^2}{L_2}(1 - \mathrm{e}_3^2) \geq 0 \\ L_2^2 + 60L_3^2(1 - \mathrm{e}_3^2) > L_2^2 + \frac{400L_3^4}{L_2^2}(1 - \mathrm{e}_3^2)^2 - 40L_3^2(1 - \mathrm{e}_3^2) \end{cases} \wedge \begin{cases} -L_2 + \frac{20L_3^2}{L_2}(1 - \mathrm{e}_3^2) < 0 \\ \end{cases}$$

that gives

$$\left(\begin{cases} \mathrm{e}_3^2 \leq 1 - \frac{L_2^2}{20L_3^2} \\ \mathrm{e}_3^2 > 1 - \frac{L_2^2}{4L_3^2} \end{cases} \wedge \begin{cases} \mathrm{e}_3^2 > 1 - \frac{L_2^2}{20L_3^2} \\ \end{cases}\right) \implies \mathrm{e}_3^2 > 1 - \frac{L_2^2}{4L_3^2}. \tag{2.68}$$

Similarly, we can solve (2.67), having the following

$$\begin{cases} L_2 - \frac{20L_3^2}{L_2}(1 - \mathrm{e}_3^2) \geq 0 \\ L_2^2 + 60L_3^2(1 - \mathrm{e}_3^2) > L_2^2 + \frac{400L_3^4}{L_2^2}(1 - \mathrm{e}_3^2)^2 - 40L_3^2(1 - \mathrm{e}_3^2) \end{cases} \wedge \begin{cases} L_2 - \frac{20L_3^2}{L_2}(1 - \mathrm{e}_3^2) < 0 \\ \end{cases}$$

that gives

$$\left(\begin{cases} \mathrm{e}_3^2 \geq 1 - \dfrac{L_2^2}{20L_3^2} \\ \mathrm{e}_3^2 > 1 - \dfrac{L_2^2}{4L_3^2} \end{cases} \quad \wedge \quad \begin{cases} \mathrm{e}_3^2 < 1 - \dfrac{L_2^2}{20L_3^2} \\ \end{cases} \right) \quad \Longrightarrow \quad \forall\, \mathrm{e}_3. \tag{2.69}$$

Finally, putting together (2.68) and (2.69), we get $\mathrm{e}_3^2 > 1 - \frac{L_2^2}{4L_3^2}$. Let us observe that if $1 - \frac{L_2^2}{4L_3^2} < 0$, i.e. $L_2 > 2L_3$, then the last inequality for e_3 is automatically satisfy. Then, remembering that we are in the case ii) and putting togheter the results, it follows that

$$A < C < B \quad \Longleftrightarrow \quad \left(0 < L_2 \leq 2L_3 \ \wedge \ \mathrm{e}_3 > \sqrt{1 - \frac{L_2^2}{4L_3^2}} \right) \ \vee \ L_2 > 2L_3\,.$$

Again, studying (2.65a) and (2.65b), we can conclude that if $\left(0 < L_2 \leq 2L_3 \ \wedge \ \mathrm{e}_3 > \sqrt{1 - \frac{L_2^2}{4L_3^2}} \right) \vee L_2 > 2L_3$, then the eigenvalues are real and opposite if $0 < L_z^2 < A$ (see the second of (2.65a)), purely immaginary and coniugates if $A < L_z^2 < C$ (see the first of (2.65b)), real and opposite if $C < L_z^2 < B$ (see the first of (2.65a)) and again purely immaginary and coniugates if $L_z^2 > B$ (see the second of (2.65b)). This proves the last **Case iv)** of the Proposition.

Actually, there is a last case to be analyzed, that will not give any contribution, i.e.

Case 4 : $C \geq B$

$$C \geq B \quad \Longleftrightarrow \quad \sqrt{L_2^2 + 60L_3^2(1 - \mathrm{e}_3^2)} \leq L_2 - \frac{20L_3^2}{L_2}(1 - \mathrm{e}_3^2)$$

i.e.

$$\begin{cases} L_2 - \dfrac{20L_3^2}{L_2}(1 - \mathrm{e}_3^2) \geq 0 \\ L_2^2 + 60L_3^2(1 - \mathrm{e}_3^2) \leq L_2^2 + \dfrac{400L_3^4}{L_2^2}(1 - \mathrm{e}_3^2)^2 - 40L_3^2(1 - \mathrm{e}_3^2) \end{cases} \quad \Longleftrightarrow \quad \begin{cases} \mathrm{e}_3^2 \geq 1 - \dfrac{L_2^2}{20L_3^2} \\ \mathrm{e}_3^2 \leq 1 - \dfrac{L_2^2}{4L_3^2} \end{cases}$$

that has no solutions. This concludes the proof of the Proposition.

□

We readily find that in the limit $m_2 \to 0$, $e_3 \to 0$, the Kozai angles $\mathrm{i} = 39.2°$ and $\mathrm{i} = 140.77°$ are recovered (see [88]). In fact, for $\mathrm{e}_3 = 0$, the critical values A, B and C become

$$A = \frac{1}{5}\left(4L_2^2 + 5L_3^2 - L_2\sqrt{L_2^2 + 60L_3^2} \right), \quad B = \frac{1}{5}\left(4L_2^2 + 5L_3^2 + L_2\sqrt{L_2^2 + 60L_3^2} \right), \quad C = L_2^2 - 3\,L_3^2\,. \tag{2.70}$$

Then, at the limit $m_2 \to 0$ we readily obtain that

$$\begin{aligned} (\cos i_{mut})_{Lz^2=A} &= \frac{A - L_2^2 - L_3^2}{2L_2L_3} = -\frac{\sqrt{L_2^2 + 60\,L_3^2} + L_2}{10\,L_3} \xrightarrow{L_2 \to 0} -\sqrt{\frac{3}{5}} \\ (\cos i_{mut})_{Lz^2=B} &= \frac{B - L_2^2 - L_3^2}{2L_2L_3} = \frac{\sqrt{L_2^2 + 60\,L_3^2} - L_2}{10\,L_3} \xrightarrow{L_2 \to 0} \sqrt{\frac{3}{5}}\,. \end{aligned}$$

An interesting analysis of the Kozai mechanism and of the dynamics of a three-body problem on the S^3 sphere, in the framework of the quadrupolar approximation, can be found in [22].

Note that, while the above proposition strictly establishes the limit of $\mathcal{E}_{C,2}$ only in the quadrupolar approximation, in practice we find that the estimate is quite precise when the full Hamiltonian with higher order multipoles is considered. For example, applying the above criterion in the numerical example of Fig. 2.8 yields the estimate $\mathcal{E}_{C,2} \approx -2.2 \cdot 10^{-6}$, which is in agreement with the value of the energy where the transition is observed in the numerical phase portraits. On the other hand, since the quadrupolar approximation yields an integrable Hamiltonian, for any value of the energy $\mathcal{E} > \mathcal{E}_{C,2}$ $\mathcal{H}_{quad}$ yields a figure-8 phase portraits with invariant curves surrounding the 'frozen' (stable) orbits on both sides of the unstable orbit $\mathrm{e}_2 = 0$. However, this picture changes by adding just the octupolar terms to the model, given by

$$\mathcal{H}_{oct} = \mathcal{H}_{quad} + \tilde{\mathcal{H}}_{oct}\,, \tag{2.71}$$

where

$$\tilde{\mathcal{H}}_{oct} = \frac{75\,\mathcal{G}\,m_2\,m_3}{64\,a_3}\left(\frac{a_2}{a_3}\right)^3 \frac{1}{(1-\mathrm{e}_3^2)^{5/2}}\,\mathrm{e}_2\,\mathrm{e}_3\,\mathcal{F}_{oct} \tag{2.72}$$

with

$$\begin{aligned}\mathcal{F}_{oct} =& \frac{1}{40}\left(3\,\mathrm{e}_2^2+4\right)\left(1+11\theta-5\theta^2-15\,\theta^3\right)\cos(\omega_2-\omega_3)\\ &+\frac{1}{40}\left(3\,\mathrm{e}_2^2+4\right)\left(1-11\theta-5\theta^2+15\,\theta^3\right)\cos(\omega_2+\omega_3)\\ &+\frac{7}{8}\,\mathrm{e}_2^2(\theta^2-1)(1+\theta)\cos(3\omega_2-\omega_3)+\frac{7}{8}\,\mathrm{e}_2^2(\theta^2-1)(1-\theta)\cos(3\omega_2+\omega_3)\,,\end{aligned} \tag{2.73}$$

with $\theta = \cos(\mathrm{i}_2+\mathrm{i}_3)$. Note that the above formula is equivalent, after some algebraic operations, to the formulas given in [83] and [88], see also [67], [89], [26]. As depicted in Fig. 2.13, the addition of more harmonics besides $\cos(2\omega_2)$ via the octupole approximation implies the creation of a large domain of resonance overlap, mostly between the islands around the frozen orbits and the island of the C_1 orbit, which appears already in the octupole approximation. This implies, in turn, the disappearance of most quasi-periodic trajectories around the frozen orbits, and the appearance, instead, of a large domain of chaotic orbits, in accordance to what is observed in the last two panels of Fig. 2.8 for the full model.

Finally, we note that the use of the above proposition for the determination of critical values for the transition to instability has to be done in conjunction with the test that $\cos(\max i_{mut})$ does not produce unphysical values $|\cos(i_{mut})| > 1$. Such an unphysical value can occur in **case ii)**, for the critical value $L_z^2 = C$ and in **case iv)**, for the critical value $L_z^2 = A$. For example, in the second case of ii), setting $\sqrt{3}L_3 \le L_2 < 2\,L_3$ and $\mathrm{e}_3 = 0$, we find $C = L_2^2 - 3\,L_3^2$ which, together with $L_z^2 = C$, leads to $\cos(\max i_{mut}) = -2\,L_3/L_2 < -1$ iff $L_2 < 2\,L_3$. Similarly, in the second case of iv), where $L_2 > 2\,L_3$, setting $\mathrm{e}_3 = 0$, by the relation $L_z^2 = A = \frac{1}{5}\left(4L_2^2+5L_3^2-L_2\sqrt{L_2^2+60L_3^2}\right)$, we obtain $\cos(\max i_{mut}) = -(\sqrt{L_2+60\,L_3^2}+L_2)/(10\,L_3)$, which is physical only iff $L_2 \le 2\,L_3$.

2.3.5 Where does the $\upsilon-$Andromedae system lie in phase space?

We finally comment on the implications of the above analysis of the phase space structure on the interpretation of the data given by astronomical observations. Figure 2.14 shows the phase portrait (surface of section) for the value of the energy $\mathcal{E} = -2.081 \cdot 10^{-5}$, corresponding to the one found after reducing to the Laplace plane the data for the observed υ-Andromedae system (see subsection 2.2.3.2). The invariant curve (1) (marked in red) corresponds to the actual initial conditions of the system. According to the figure, this is a quasi-periodic orbit surrounding the family C_2. We note, however, that the orbit is very close to the separatrix between the C_2 librational domain and the domain of stability surrounding the fixed point of the mode B orbit. As a consequence, a change of the initial conditions (e_2, ω_2) by less than 10% results in a trajectory ((2), black curve) which undergoes quasi-periodic oscillations around the (aligned) apsidal corotation orbit of the system.

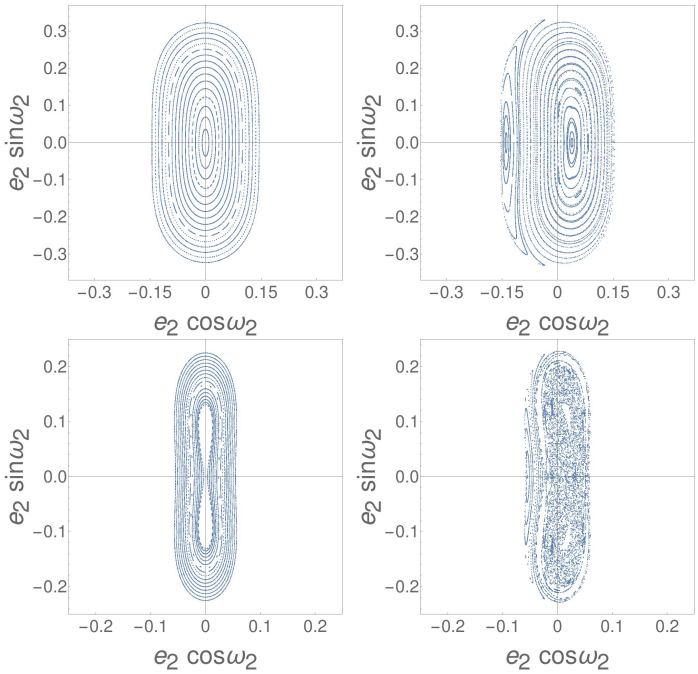

Figure 2.13: Comparison between the phase portraits (Poincaré surfaces of section) obtained with the quadrupolar approximation $\mathcal{H}_{quad}$ (left column) and the octupolar approximation $\mathcal{H}_{oct}$ (right column), at the energy levels $\mathcal{E} = -4.9 \cdot 10^{-6}$ (top), and $\mathcal{E} = -6.9 \cdot 10^{-7}$ (bottom). The quadrupolar approximation yields the phase portrait of an integrable system, which contains a figure-8 separatrix for energies beyond $\mathcal{E}_{C,2}$. The octupolar approximation is necessary to obtain both periodic orbits C_1 and C_2, as well as the chaotic zone around C_2 caused by the overlapping of resonances in the neighborhood of this orbit.

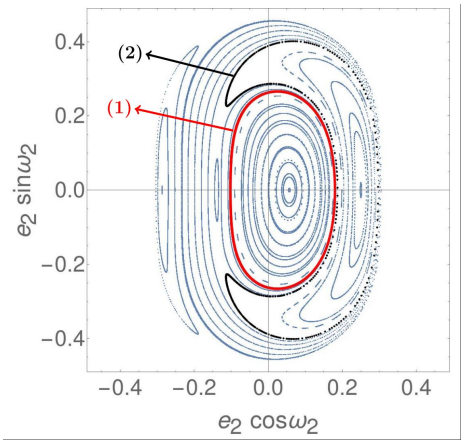

Figure 2.14: Poincaré surface of section for the energy $\mathcal{E} = -2.081 \cdot 10^{-5}$. The red curve (1) shows the orbit obtained by adopting our basic assumption as regards the initial conditions of the $\upsilon-$Andromedae system (see subsection 2.2.3.2), i.e. (after reduction to the Laplace plane) $e_2 = 0.2445$, $e_3 = 0.316$, $\omega_2 = 289.049°$, $\omega_3 = 235.464°$. The black curve (2) shows the trajectory obtained by changing by only about 10% the eccentricity e_2 and argument of the periastron ω_2, while maintaining the energy and argument of periastron of the outer planet invariant ($e_2 = 0.269$, $\omega_2 = 296.1°$, $\omega_3 = 235.464°$, $e_3 = 0.299$).

The proximity of the real trajectory to one of the separatrices generated by the families C_1, C_2 is noteworthy, as it is in contrast with the basic scenario of evolution of planetary orbits, according to which the dissipative phase of planetary migration should lead to an endstate close to one of the stable fixed points of the system (see, for example, [3]).

2.4 Parametric study

The present section provides an overview of how the form of the phase portraits (Poincaré sections) is varied with the energy $\mathcal{E}$, and hence with an increase in the level of mutual inclination, in various types of planetary systems differing from our so far main example as regards the choice of mass ratio m_2/m_3 as well as of semi-major axis ratio a_2/a_3 between the two planets. A thorough parametric study of the latter question is beyond our present scope. Instead, here we focus on only one central aspect of this study, namely the question of how generic is the description, as in section 2.3, of the transition from the planar-like to the Lidov Kozai regime, when either the mass ratio m_2/m_3 or the semi-major axis ratio a_2/a_3 are altered, including the so-called *hierarchical* limits, which correspond to mass ratio limits $m_2/m_3 \to 0$ (restricted three-body problem with the inner planet being a test particle), or $m_2/m_3 \to \infty$ (the outer planet is a test particle), and semi-major axis ratio $a_2/a_3 << 1$ (outer planet way further from the star than inner planet). To produce a suite of numerical experiments covering most cases of practical interest, we consider in the sequel five different values of the mass ratio m_2/m_3 representative of all possible mass hierarchies (or lack thereof) namely $m_2/m_3 = 1/10,\ 1/3,\ 1,\ 3,\ 10$, produced by the corresponding combination of the masses $m_0 = 1M_\odot$ and $1\,M_J$, $3\,M_J$ or $10\,M_J$ for m_2 and m_3 , while we consider the semimajor axes ratio $a_2/a_3 = 1/7$ ($a_2 = 1\,AU$, $a_3 = 7\,AU$) as a case representing distance hierarchy, or $a_2/a_3 = 1/3$ ($a_2 = 1\,AU$, $a_3 = 3\,AU$) as a case of no distance hierarchy. In each one of the previous cases, a comparison with the analysis of section 2.3 requires keeping fixed the value of the AMD (or L_z) while computing phase portraits with a varying value of the energy $\mathcal{E}$. To find a relevant value for L_z in each experiment, we consider a uniform value of the maximum possible mutual inclination i_{max} (Eq. (2.29)) in all the experiments, set as $\mathrm{i}_{mut} = 45°$. This typically proves to be slightly above the limit of the Lidov-Kozai instability (which is equal to $39.2°$ in the quadrupolar approximation of the restricted three body problem with $m_2 = 0$ and turns to be about $\sim 42.5°$ in our main numerical example of section 2.3). By Eq. (2.29), this implies setting

$$L_z = \sqrt{\Lambda_2^2 + \Lambda_3^2 + \sqrt{2}\Lambda_2\Lambda_3}$$

with Λ_2, Λ_3 specified by the choice of masses and semi-major axes in each experiment. Finally, in order to get some safety from any accuracy issues, we make computations with a Hamiltonian expanded at slightly larger orders with respect to those of the main numerical example of the previous section, i.e. multipole order 6, and order 12 in the eccentricities. To arrive at the final secular model, all Hamiltonians are processed, and their phase portraits computed, in the same way as in section 2.2.

Figure 2.15 shows the phase portraits obtained for increasing energy $\mathcal{E}$ in the case $a_2/a_3 = 1/3$, and in various mass hierarchy scenarios, namely, for the values m_2/m_3 (from top to bottom row) 1/10, 1/3, 1/1, 3/1, 10/1. The values of the energies whose corresponding phase portraits are shown are selected in each panel of Fig. 2.15 so as to visualize the most important changes observed in the phase-space structure as the energy increases.

Our main numerical example (Fig. 2.8) exhibits a similar structural change in the phase portraits, with increasing energy, as in the fully non-hierarchical case $m_2/m_3 = 1$ illustrated in the third row of Fig. 2.15. However, in Fig. 2.15 it is clear that the transition from the planar-like regime, where the modes A and B dominate the phase space, through the saddle-node bifurcation giving rise to the orbits C_1 and C_2 (transition regime), and, finally, the Lidov-Kozai regime (orbit C_2 becomes unstable and surrounded by a chaotic figure-8 separatrix-like layer) is generic in all cases $m_2/m_3 \leq 1$ (top three rows of Fig. 2.15) and follows by the same sequence of bifurcations. As the ratio m_2/m_3

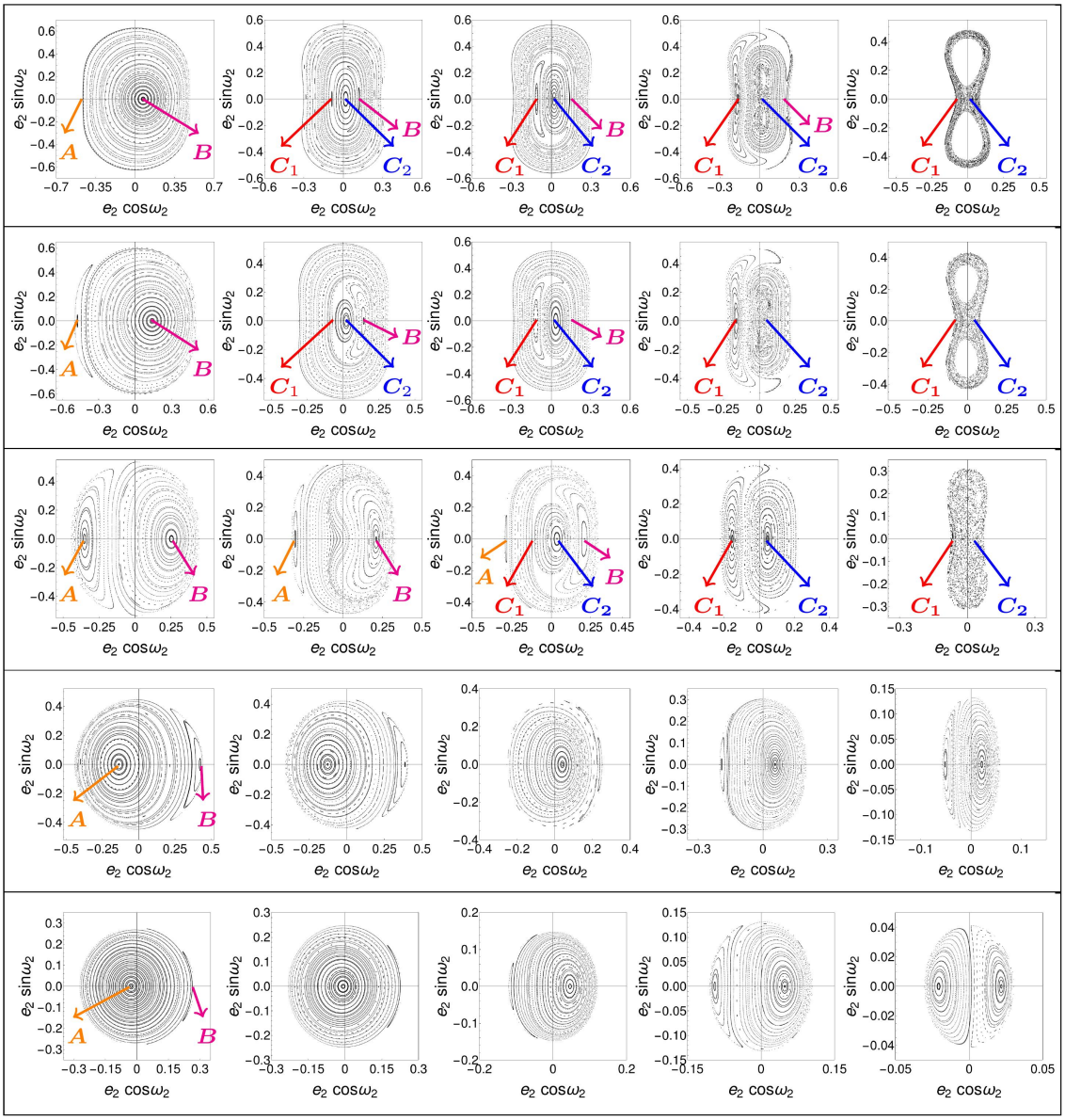

Figure 2.15: Poincaré surfaces of section in the plane $(\mathrm{e}_2\cos(\omega_2), \mathrm{e}_2\sin(\omega_2))$ with L_z fixed such that $\max i_{mut}$ is 45° and different values of energy. We consider the models $a_2/a_3 = 1/3$ and (from top to bottom) $m_2/m_3 = 1/10,\ 1/3,\ 1,\ 3,\ 10$. The values of the energy (from top to bottom) are (from left to right), top $\mathcal{E} = -2.71\cdot10^{-6}, -1.01\cdot10^{-6}, -9.24\cdot10^{-7}, -5.73\cdot10^{-7}, -8.23\cdot10^{-8}$, $\mathcal{E} = -9.03\cdot10^{-7}, -3.37\cdot10^{-7}, -2.87\cdot10^{-7}, -1.76\cdot10^{-7}, -2.35\cdot10^{-8}$, $\mathcal{E} = -2.68\cdot10^{-7}, -1.39\cdot10^{-7}, -1.14\cdot10^{-7}, -6.37\cdot10^{-8}, -6.98\cdot10^{-9}$, $\mathcal{E} = -1.12\cdot10^{-6}, -9.26\cdot10^{-7}, -3.37\cdot10^{-7}, -2.08\cdot10^{-7}, -1.67\cdot10^{-8}$, bottom $\mathcal{E} = -2.75\cdot10^{-6}, -1.91\cdot10^{-6}, -4.72\cdot10^{-7}, -3.54\cdot10^{-7}, -2.91\cdot10^{-8}$. The surfaces of section have been computed by a numerical integration of trajectories in a Hamiltonian averaged in closed form with a multipolar expansion truncated at degree 6 and expanded up to order 12 in the eccentricities.

tends to small values, the main differences observed with respect to the non-hierarchical case are: i) in the planar like regime (i.e. top row, first panel), the domain of quasi-periodic orbits around the aligned apsidal corotation orbit (B-mode) occupies most of the available phase space, and ii) at energies beyond the one of the Lidov-Kozai instability, there is a significant domain of regular orbits obtained around two stable periodic orbits of non-zero eccentricity e_2 with fixed points along the axes $\omega_2 = \pm\pi/2$ in the surface of section (the so-called 'frozen orbits'). Both properties (i) and (ii) can be interpreted by analogy with the restricted three-body problem ($m_2 = 0$), in which, for low inclinations, the only fixed point of the quadratic (Laplace-Lagrange) secular Hamiltonian is associated with an eccentric orbit of eccentricity e_2 equal to the forced value induced by the outer perturber and pericenter aligned with the one of the outer perturber (see [23]). On the other hand, in the cases $m_2/m_3 > 1$ we do not observe at all the transition to the Lidov-Kozai regime. Again, this can be interpreted in analogy with the RTBP, in which the outer Lidov-Kozai instability ($m_3 \to 0$) occurs at an inclination ($\approx 63°$; see [101]) much higher than the maximum mutual inclination $i_{max} = 45°$ considered in our examples. The case of a very high mutual inclination has been considered in the literature (see for example [40] and references therein), but it appears of rather theoretical interest compared to available observations on the orbital inclinations in exoplanetary systems.

Fig. 2.16, now, shows how the phase portraits evolve with the energy when, in addition to altering the mass ratio m_2/m_3, the limit of distance hierarchy is also approached ($a_2/a_3 = 1/7$). As an overall observation, we note again that the full sequence of bifurcations leading from the planar-like to the Lidov-Kozai regime is realized only in the cases $m_2/m_3 \leq 1$. However, the main difference, with respect to the case $a_2/a_3 = 1/3$, is that in the hierarchical in distance case the phase portraits contain many more regular orbits, with a cosiderably large domain of stability around the frozen orbits surviving the system's perturbations even at the mass ratio $m_2/m_3 = 1$ (third row of Fig. 2.16. This can be interpreted by the fact that the distance hierarchy brings the system closer to the dynamics of the integrable Hamiltonian $\mathcal{H}_{quad}$ (Eq. (2.56)), reducing the relative importance of perturbations including and beyond the octupolar one.

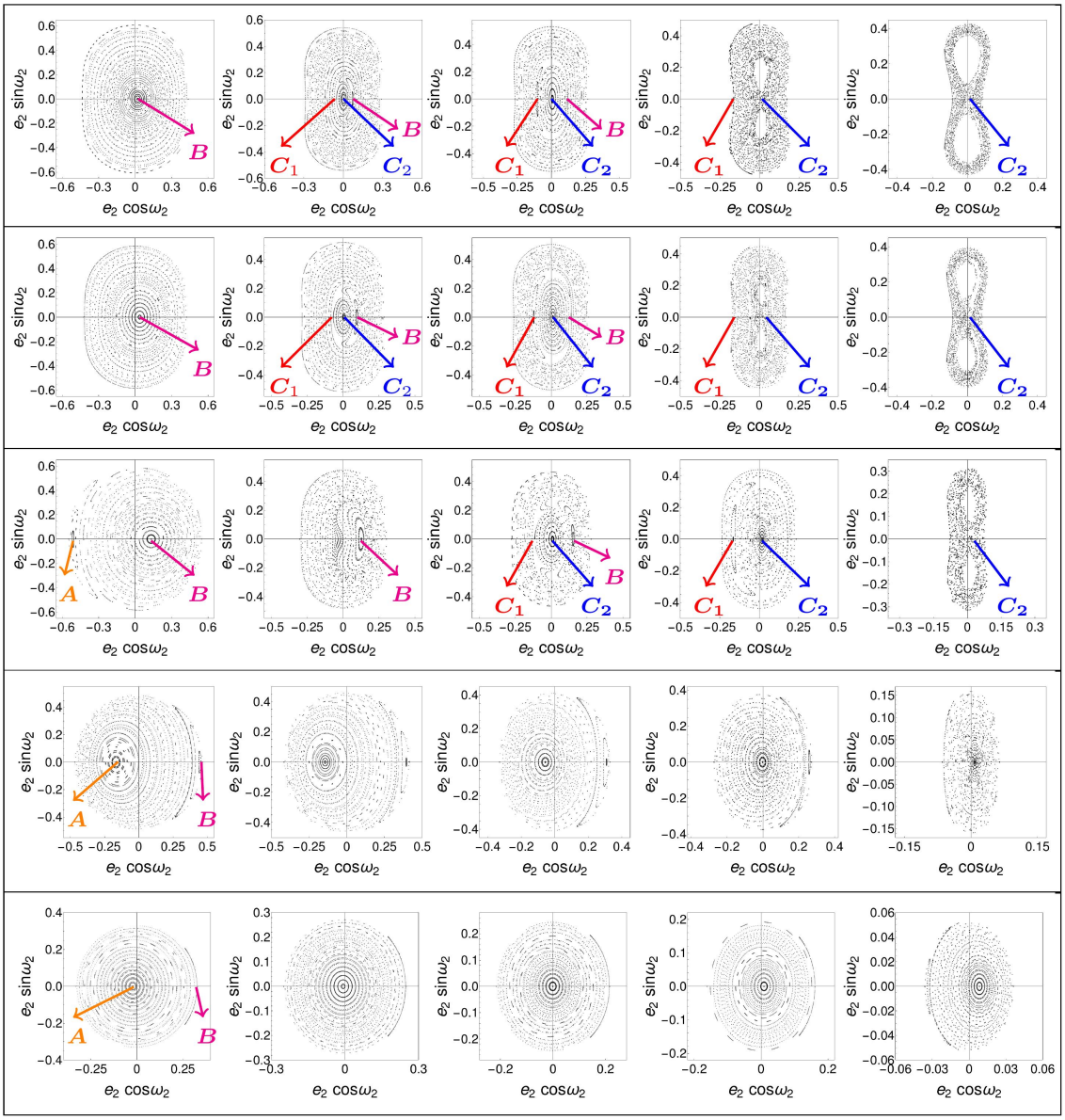

Figure 2.16: Poincaré surfaces of section in the plane $(\mathrm{e}_2\cos(\omega_2), \mathrm{e}_2\sin(\omega_2))$ with L_z fixed such that $\max i_{mut}$ is 45° and different values of energy. We consider the models $a_2/a_3 = 1/7$ and (from top to bottom) $m_2/m_3 = 1/10,\ 1/3,\ 1,\ 3,\ 10$. The values of the energy (from top to bottom) are (from left to right), top $\mathcal{E} = -1.54\cdot10^{-7}, -6.71\cdot10^{-8}, -5.78\cdot10^{-8}, -2.46\cdot10^{-8}, -6.15\cdot10^{-9}$, $\mathcal{E} = -4.5\cdot10^{-8}, -2.05\cdot10^{-8}, -1.7\cdot10^{-8}, -7.16\cdot10^{-9}, -1.79\cdot10^{-9}$, $\mathcal{E} = -2.75\cdot10^{-8}, -8.25\cdot10^{-9}, -7.01\cdot10^{-9}, -4.97\cdot10^{-9}, -5.51\cdot10^{-10}$, $\mathcal{E} = -7.5\cdot10^{-8}, -5.94\cdot10^{-8}, -3.69\cdot10^{-8}, -2.5\cdot10^{-8}, -1.38\cdot10^{-9}$, bottom $\mathcal{E} = -2.22\cdot10^{-7}, -1.21\cdot10^{-7}, -8.96\cdot10^{-8}, -4.91\cdot10^{-8}, -2.42\cdot10^{-9}$. The surfaces of section have been computed by a numerical integration of trajectories in a Hamiltonian averaged in closed form with a multipolar expansion truncated at degree 6 and expanded up to order 12 in the eccentricities.

3. Semi-analytical computation of periodic and quasi-periodic orbits

In subsection 2.3.2.2 we have seen how the existence of the A and B modes, which generalize the apsidal corotation periodic orbits of the model $\mathcal{H}_{planar}$ to the spatial case, can be established within the framework of the integrable model $\mathcal{H}_{int} = \mathcal{H}_{planar} + \mathcal{H}_{0,space}$. In the present Chapter we discuss how to recover semi-analytically the periodic orbits A and B under the full Hamiltonian $\mathcal{H}_{sec} = \mathcal{H}_{int} + \mathcal{H}_{1,space}$ (Eq. (2.44)). Besides its relevance in establishing the existence of these orbits in the full model (up to an exponentially small remainder), a computation of the orbits A and B using normal forms allows to obtain a semi-analitycal representation of the long term time series of the orbital elements for these planetary trajectories. Since the modes A and B are among the most probable expected endstates of the formation process for exoplanetary systems, such a representation can be of use also in the interpretation of the observational data regarding the planetary orbital configurations in such systems. Moreover, we discuss also how to recover semi-analytically the quasi-periodic orbits around both the 3D apsidal corotations A and B.

3.1 Semi-analytical (normal form) determination of the periodic orbits A and B

Let (ψ_*, Γ_*, J_*) be a fixed point of the integrable Hamiltonian $\mathcal{H}_{int}(\psi, \Gamma; J)$ (Eq. (2.42)), corresponding to one of the modes A or B. Introduce the translation

$$\psi = \psi_* + \delta\psi, \quad \Gamma = \Gamma_* + \delta\Gamma, \quad J = J_* + \delta J. \tag{3.1}$$

The transformation $(\psi, \varphi, \Gamma, J) \to (\delta\psi, \varphi, \delta\Gamma, \delta J)$ is canonical. The Hamiltonian $\mathcal{H}_{sec}$ in the new variables reads:

$$\mathcal{H}_{sec}(\delta\psi, \varphi, \delta\Gamma, \delta J) = \mathcal{H}_{int}(\delta\psi, \delta\Gamma, \delta J) + \mathcal{H}_{1,space}(\delta\psi, \varphi, \delta\Gamma, \delta J)\,. \tag{3.2}$$

More precisely, the development of the Hamiltonian around the apsidal solution of the integrable part $\mathcal{H}_{int}$ follows this procedure: Let $(\psi_*,\, \Gamma_*,\, J_*)$ be one of the two fixed points (apsidal corotation solutions) of the integrable Hamiltonian $\mathcal{H}_{int}(\psi,\, \Gamma\,;\, J)$. We consider the translations

$$\psi = \psi_* + \varepsilon_* \delta\psi\,, \qquad \Gamma = \Gamma_* + \varepsilon_*\, \delta\Gamma\,, \qquad J = J_* + \varepsilon_{J_*}\, \delta J\,, \tag{3.3}$$

where $\varepsilon_*,\, \varepsilon_{J_*}$ are both book-keeping symbols with numerical value equal to one. We then perform the following algebraic operations:

- substitute (3.3) into the Hamiltonian $\mathcal{H}_{sec}(\psi, \varphi, \Gamma, J)$ and expand the Hamiltonian in powers of the symbols $\varepsilon_*,\, \varepsilon_{J_*}$;

- in the resulting expression, replace $\cos(\varphi)$ and $\sin(\varphi)$ with $\varepsilon_* \cos(\varphi)$ and $\varepsilon_* \sin(\varphi)$ respectively;
- assign a unique book-keeping symbol to the expanded Hamiltonian $\mathcal{H}_{sec}(\delta\psi,\, \varphi,\, \delta\Gamma,\, \delta J\,)$, by setting $\varepsilon_{J_*}^a \rightsquigarrow \lambda^{a-1}\ a \geq 1\,,\ \varepsilon_* \rightsquigarrow \lambda\,;$
- truncate the resulting expression at a maximum order N_t in the book-keeping symbol λ.

After performing the above algebraic steps, the Hamiltonian resumes the form

$$\begin{aligned}\mathcal{H}^{(0)} = \mathcal{H}_{sec} &= c_1 + Z_0 + \sum_{s=1}^{N_t} \lambda^s h_s^{(0)}(\delta\psi,\, \varphi,\, \delta\Gamma,\, \delta J\,) \\ &= c_1 + \nu_*^{(0)} \delta J + \sum_{s=1}^{N_t} \lambda^s \left(\sum_{m,\,k,\,n,\,l} \theta^{(0)}_{m,k,n,l}\, \delta\psi^m \delta\Gamma^n \delta J^l\, e^{i\,k\,\varphi} \right)\end{aligned} \tag{3.4}$$

where c_1 is a constant term, $\theta^{(0)}_{m,k,n,l}$ are constant coefficients, and $\nu_*^{(0)} < 0$ is the (also constant) unperturbed frequency of the apsidal periodic orbit in the integrable approximation.

The Hamiltonian (3.4) can now be normalized by iterative steps using the method of composition of Lie series (subsection 1.1.3). The normalization algorithm is defined recursively, for $r = 1, 2, ...$ by the relations:

$$\mathcal{H}^{(r-1)} = c_1 + Z_0 + \sum_{s=1}^{r-1} \lambda^s Z_s(\delta\psi, \delta\Gamma, \delta J) + \sum_{s=r}^{N_t} \lambda^s \left(\sum_{m,\,k,\,n,\,l} \theta^{(r-1)}_{m,k,n,l}\, \delta\psi^m \delta\Gamma^n \delta J^l\, e^{i\,k\,\varphi} \right), \tag{3.5}$$

$$\chi^{(r)} = \lambda^r \sum_{\substack{m,\,k,\,n,\,l \\ k \neq 0}} \frac{\theta^{(r-1)}_{m,k,n,l}}{i\,\nu_*^{(0)}\,k}\, \delta\psi^m \delta\Gamma^n \delta J^l\, e^{i\,k\,\varphi}\,, \tag{3.6}$$

$$\mathcal{H}^{(r)} = \left[\exp(L_{\chi^{(r)}}) \mathcal{H}^{(r-1)} \right]^{\leq N_t}, \tag{3.7}$$

where $L_{\chi^{(r)}}$ denotes the Poisson bracket operator $L_{\chi^{(r)}} \cdot = \{\cdot, \chi^{(r)}\}$, and $[\cdot]^{\leq N_t}$ means truncation at the order N_t in the book-keeping parameter λ.

The normalizing transformation $\Phi^{(r)}$ is defined by:

$$\begin{aligned}(\delta\psi, \varphi, \delta\Gamma, \delta J) &= \Phi^{(r)}(\delta\tilde{\psi}, \tilde{\varphi}, \delta\tilde{\Gamma}, \delta\tilde{J}) \\ &= \left[\left(\exp\left(L_{\chi^{(r)}}\right) \exp\left(L_{\chi^{(r-1)}}\right) \ldots \exp\left(L_{\chi^{(1)}}\right) (\delta\psi, \varphi, \delta\Gamma, \delta J) \right) \Big|_{\substack{\delta\psi = \delta\tilde{\psi} \\ \varphi = \tilde{\varphi} \\ \delta\Gamma = \delta\tilde{\Gamma} \\ \delta J = \delta\tilde{J}}} \right]^{\leq N_t}.\end{aligned} \tag{3.8}$$

The inverse transformation

$$(\delta\tilde{\psi}, \tilde{\varphi}, \delta\tilde{\Gamma}, \delta\tilde{J}) = \left(\Phi^{(r)}\right)^{-1} (\delta\psi, \varphi, \delta\Gamma, \delta J)\ \ , \tag{3.9}$$

can be computed by the formula

$$(\delta\tilde{\psi}, \tilde{\varphi}, \delta\tilde{\Gamma}, \delta\tilde{J}) = \left[\exp\left(-L_{\chi^{(1)}}\right) \ldots \exp\left(-L_{\chi^{(r-1)}}\right) \exp\left(-L_{\chi^{(r)}}\right) (\delta\psi, \varphi, \delta\Gamma, \delta J) \right]^{\leq N_t}.$$

The final Hamiltonian takes the form

$$\begin{aligned}\mathcal{H}^{(r)} &= \left[\left(\exp\left(L_{\chi^{(r)}}\right)\exp\left(L_{\chi^{(r-1)}}\right)\ldots\exp\left(L_{\chi^{(1)}}\right)\mathcal{H}^{(0)}\right)\Big|_{\substack{\delta\psi=\delta\tilde{\psi}\\ \varphi=\tilde{\varphi}\\ \delta\Gamma=\delta\tilde{\Gamma}\\ \delta J=\delta\tilde{J}}}\right]^{\leq N_t} \\ &= Z^{(r)}(\delta\tilde{\psi},\,\delta\tilde{\Gamma},\,\delta\tilde{J}\,) + R^{(r)}(\delta\tilde{\psi},\,\tilde{\varphi},\,\delta\tilde{\Gamma},\,\delta\tilde{J}\,)\,.\end{aligned} \tag{3.10}$$

The functions $Z^{(r)}$ and $R^{(r)}$ are hereafter called the 'normal form' and 'remainder' respectively. The normalization order r is chosen so that the normal form term $Z^{(r)}(\delta\tilde{\psi},\,\delta\tilde{\Gamma},\,\delta\tilde{J}\,)$ yields the best possible approximation to the dynamics. In particular, we choose r so as to minimize the remainder $||R^{(r)}||$ with respect to r in the range $1 \leq r \leq N_t$.

In summary, this is a classical Birkhoff-like normalization procedure by which the angle φ is eliminated from the Hamiltonian via a sequence of Lie canonical transformations (see [19]).

The physical meaning of the above normalization procedure is the following: in the planar-like regime, we have $||\mathcal{H}_{1,space}|| << \mathcal{H}_{int}$. Then, through the normalization we find a new set of variables in which, except for a very small remainder, the dynamics locally (around the equilibrium (ψ_*, Γ_*, J_*)) is given by the normal form $Z^{(r)}(\tilde{\psi}, \tilde{\Gamma}, \tilde{J})$, with

$$\tilde{\psi} = \psi_* + \delta\tilde{\psi}, \quad \tilde{\Gamma} = \Gamma_* + \delta\tilde{\Gamma}, \quad \tilde{J} = J_* + \delta\tilde{J} \quad . \tag{3.11}$$

The phase flow induced by the integrable Hamiltonian $Z^{(r)}$ has the same structure as the one of the Hamiltonian $\mathcal{H}_{int}$ analyzed in the previous subsection, differing by it just in the fact that $Z^{(r)}$ contains terms arising from the normalization of $\mathcal{H}_{1,space}$ up to a very small remainder. In particular, Hamilton's flow under the normal form in the transformed variables admits a periodic orbit given by

$$\begin{aligned}\tilde{\psi}_* &= \psi_* + \delta\tilde{\psi}_* \quad , \\ \tilde{\Gamma}_* &= \Gamma_* + \delta\tilde{\Gamma}_* \quad , \\ \tilde{J}_* &= J_* + \delta\tilde{J}_* \quad , \\ \tilde{\varphi}(t) &= \tilde{\varphi}(0) + \nu_* t \quad ,\end{aligned} \tag{3.12}$$

where $(\tilde{\psi}_*,\, \tilde{\Gamma}_*, \tilde{J}_*)$ are computed by the system of algebraic equations

$$\begin{cases}\dot{\tilde{\psi}} = \dfrac{\partial Z^{(r)}}{\partial\tilde{\Gamma}} = 0 \\ \dot{\tilde{\Gamma}} = -\dfrac{\partial Z^{(r)}}{\partial\tilde{\psi}} = 0 \\ Z^{(r)}(\tilde{\psi},\,\tilde{\Gamma},\,\tilde{J}\,) = \mathcal{E}\end{cases} \tag{3.13}$$

and the frequency ν_* is given by

$$\nu_* = \left(\frac{\partial Z^{(r)}}{\partial\tilde{J}}\right)_{\tilde{\psi}=\tilde{\psi}_*,\tilde{\Gamma}=\tilde{\Gamma}_*,\tilde{J}=\tilde{J}_*} \quad . \tag{3.14}$$

Note that the constant term c_1 produced in Eq. (3.4) has to be carried along all the successive Hamiltonians $\mathcal{H}^{(r)}$ produced through the normalization process, being eventually included in the normal form $Z^{(r)}$. This is necessary, since this constant appears in the third of the algebraic equations (3.13) by which the fixed point corresponding to the apsidal periodic orbit is computed in the new canonical variables.

Figure 3.1 shows an example of the comparison between the semi-analytical computation of the periodic orbits A, B on the basis of the normal form flow of $Z^{(r)}$, and a full numerical computation

of the same orbits. The semi-analytical computation of the periodic orbits proceeds by the following steps:

i) we use the tangency method of subsection 2.3.2.2 to compute the fixed points of the integrable Hamiltonian $\mathcal{H}_{int}$, first in the Hopf variables and then in the variables $(\psi,\, \Gamma,\, J)$, obtaining ψ_*, Γ_*, J_*.

ii) Using an appropriate expansion of the Hamiltonian, as well as the method of composition of Lie series, we then obtain the transformation $\Phi^{(r)}$ and its inverse $\left(\Phi^{(r)}\right)^{-1}$, as well as the normal form $Z^{(r)}$ representation of the full Hamiltonian.

iii) Implementing a Newton method, we then compute the root $(\tilde{\psi}_*,\, \tilde{\Gamma}_*, \tilde{J}_*)$ of the system of algebraic equations (3.13), as well as the frequency (3.14). This yields the time evolution of all four quantities $(\delta\tilde{\psi} = \tilde{\psi}_* - \psi_*, \delta\tilde{\Gamma} = \tilde{\Gamma}_* - \Gamma_*, \delta\tilde{J} = \tilde{J}_* - J_*)$ (fixed) and $\tilde{\varphi}(t)$ as in Eq.(3.12).

iv) We finally obtain the semi-analytical approximation to the time flow of all four variables $\psi(t) = \psi_* + \delta\psi(t)$, $\varphi(t)$, $\Gamma(t) = \Gamma_* + \delta\Gamma(t)$, $J(t) = J_* + \delta J(t)$, through the normalizing transformation

$$(\delta\psi(t), \varphi(t), \delta\Gamma(t), \delta J(t)) = \left(\Phi^{(r)}(\delta\tilde{\psi}, \tilde{\varphi}, \delta\tilde{\Gamma}, \delta\tilde{J})\right)_{\delta\tilde{\psi}=\delta\tilde{\psi}_*, \tilde{\varphi}=\tilde{\varphi}(t), \delta\tilde{\Gamma}=\delta\tilde{\Gamma}_*, \delta\tilde{J}=\delta\tilde{J}_*} \quad . \tag{3.15}$$

This can be further transformed into a time series of the evolution of the orbital elements along the periodic orbit through the equations

$$\begin{aligned} \omega_2 &= \frac{-\psi - \varphi}{2}\,, \quad W_2 = J + \Gamma\,, \\ \omega_3 &= \frac{\psi - \varphi}{2}\,, \qquad W_3 = J - \Gamma\,, \end{aligned} \tag{3.16}$$

which allow to recover the evolution of the arguments of perihelia and eccentricities

$$\mathrm{e}_j = \sqrt{1 - (1 - W_j/\Lambda_j)^2}, \quad j = 2, 3 \tag{3.17}$$

as well as (equivalently to Eq. (2.16))

$$\begin{aligned} \Theta_2 &= \frac{(\mathrm{AMD} - W_2 - W_3)(2\Lambda_3 + W_2 - W_3 - \mathrm{AMD})}{2(\Lambda_2 + \Lambda_3 - \mathrm{AMD})} \\ \Theta_3 &= \frac{(\mathrm{AMD} - W_2 - W_3)(2\Lambda_2 - W_2 + W_3 - \mathrm{AMD})}{2(\Lambda_2 + \Lambda_3 - \mathrm{AMD})} \end{aligned} \tag{3.18}$$

which allow to compute the time series for the inclinations

$$\mathrm{i}_j = \cos^{-1}\left(1 - \frac{\Theta_j}{\Lambda_j - W_j}\right) \tag{3.19}$$

of the planetary periodic orbits.

As shown in Fig. 3.1, the semi-analytical representation of the periodic orbits fits with precision the numerical ones for both the modes A and B. As regards the physical interpretation, we note that the main effect of the perturbation $\mathcal{H}_{1,space}$ is to induce a periodic oscillation in the eccentricities (and, hence, also the inclinations) of both planets, which are no longer constant, contrary to what holds for the classical apsidal corotation orbits in the planar case, or for the orbits of the integrable approximation $\mathcal{H}_{int}$. From Fig. 3.1 it is evident that the amplitude of the oscillation of the eccentricities of both planets increases with the energy $\mathcal{E}$, and, hence, with the mutual inclination. Most notably we point out the ability of the semi-analytical theory to well represent the orbits of both modes A and B in the regime *after* the onset of the saddle-node bifurcation giving rise to the periodic orbits C_1 and C_2, as in the third panel of Fig. 3.1 (see subsection 2.3.1). This implies that, while at the corresponding level of energies the structure of the phase portraits is altered considerably with respect to the one of $\mathcal{H}_{int}$, the representation of the motions by a local normal form computed in the neighborhood of each of the modes A or B yields the correct picture of the dynamics, both qualitatively and quantitatively.

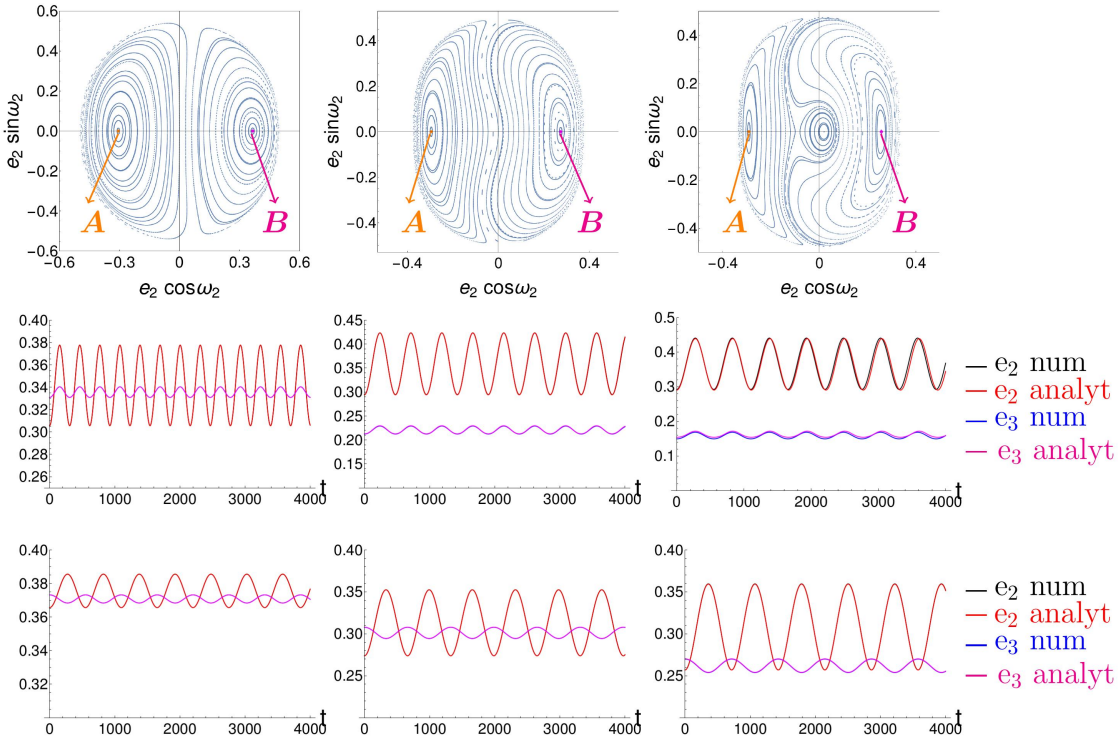

Figure 3.1: First row: Poincaré surfaces of section for the values of the energy (from left to right), $\mathcal{E} = -5.72 \cdot 10^{-5}$, $-3.19 \cdot 10^{-5}$, $-2.53 \cdot 10^{-5}$. Second and third rows: time series of the evolution of the eccentricities for both planets along the mode A (*anti-apsidal*, second row) and B (*apsidal*, third row). The curves in red and in magenta show the time series for the eccentricities e_2 and e_3 respectively as computed semi-analytically. The black and blue curves, instead, show the time series e_2 and e_3 as computed through a numerical evaluation of the periodic orbits.

3.2 Semi-analytical determination of the quasi-periodic orbits around the periodic orbits A or B

In the previous subsection we have seen the procedure allowing to semi-analitycally recover the periodic orbits A and B under the full Hamiltonian $\mathcal{H}_{sec} = \mathcal{H}_{int} + \mathcal{H}_{1,space}$. In particular, we computed a near-to-identity canonical transformation $(\delta\psi, \varphi, \delta\Gamma, \delta J) = \Phi^{(r)}(\delta\tilde{\psi}, \tilde{\varphi}, \delta\tilde{\Gamma}, \delta\tilde{J})$, (Eq. (3.8)) such that the Hamiltonian in the variables $(\delta\tilde{\psi}, \tilde{\varphi}, \delta\tilde{\Gamma}, \delta\tilde{J})$ takes the form (after resetting the numerical value $\lambda = 1$ of the book-keeping parameter)

$$\mathcal{H}^{(r)}_{sec}(\delta\tilde{\psi}, \tilde{\varphi}, \delta\tilde{\Gamma}, \delta\tilde{J}) = Z^{(r)}(\delta\tilde{\psi}, \delta\tilde{\Gamma}, \delta\tilde{J}) + R^{(r)}(\delta\tilde{\psi}, \tilde{\varphi}, \delta\tilde{\Gamma}, \delta\tilde{J})$$

with $||R^{(r)}|| << ||Z^{(r)}||$ and r is chosen so that the normal form $Z^{(r)}$ yields the best possible approximation to the dynamics. We define the 'secular local normal form Hamiltonian' $\tilde{\mathcal{H}}_{sec}$ as

$$\tilde{\mathcal{H}}_{sec} := \tilde{Z}(\delta\tilde{\psi}, \delta\tilde{\Gamma}, \delta\tilde{J}), \tag{3.20}$$

where $\tilde{Z} = Z^{(r)}$ with r fixed at a pre-selected (optimal) normalization order. The term 'local' referes to the fact that the Hamiltonian $\tilde{\mathcal{H}}_{sec}$ represents a local trigonometric polynomial expansion of an integrable approximation to the full Hamiltonian $\mathcal{H}_{sec}$ around one of the modes, A or B. In the present subsection we discuss how to determine quasi-period orbits for the Hamiltonian $\tilde{\mathcal{H}}_{sec}$ around these modes. The computation of such orbits using normal forms allows (up to a neglected small

remainder) to obtain a semi-analitycal representation of the long term time series of the orbital elements for these planetary trajectories. To this end, the following procedure is implemented:

I) Premilinary expansion of the Hamiltonian: development around the apsidal solutions of the full Hamiltonian $\mathcal{H}_{sec}$
Let $(\delta\tilde{\psi}_*, \delta\tilde{\Gamma}_*, \delta\tilde{J}_*)$ be a fixed point of the integrable normal form $\tilde{Z}(\delta\tilde{\psi}, \delta\tilde{\Gamma}, \delta\tilde{J})$, corresponding to the selected periodic orbit (A or B) around which the expansion is considered. Introduce the translation

$$\delta\tilde{\psi} = \delta\tilde{\psi}_* + \Delta\delta\tilde{\psi}, \quad \delta\tilde{\Gamma} = \delta\tilde{\Gamma}_* + \Delta\delta\tilde{\Gamma}, \quad \delta\tilde{J} = \delta\tilde{J}_* + \Delta\delta\tilde{J}. \tag{3.21}$$

The transformation $(\delta\tilde{\psi}, \tilde{\varphi}, \delta\tilde{\Gamma}, \delta\tilde{J}) \to (\Delta\delta\tilde{\psi}, \tilde{\varphi}, \Delta\delta\tilde{\Gamma}, \Delta\delta\tilde{J})$ is canonical. The Hamiltonian $\tilde{\mathcal{H}}_{sec}$ in the new variables reads:

$$\tilde{\mathcal{H}}_{sec}(\Delta\delta\tilde{\psi}, \Delta\delta\tilde{\Gamma}, \Delta\delta\tilde{J}) = \tilde{Z}(\Delta\delta\tilde{\psi}, \Delta\delta\tilde{\Gamma}, \Delta\delta\tilde{J})\,. \tag{3.22}$$

Technically, we introduce a book-keeping expansion of the Hamiltonian $\tilde{\mathcal{H}}_{sec}$ by the following steps. We consider the translations

$$\delta\tilde{\psi} = \delta\tilde{\psi}_* + \tilde{\varepsilon}_*\Delta\delta\tilde{\psi}, \quad \delta\tilde{\Gamma} = \delta\tilde{\Gamma}_* + \tilde{\varepsilon}_*\Delta\delta\tilde{\Gamma}, \quad \delta\tilde{J} = \delta\tilde{J}_* + \tilde{\varepsilon}_{J_*}\Delta\delta\tilde{J}, \tag{3.23}$$

where $\tilde{\varepsilon}_*$, $\tilde{\varepsilon}_{J_*}$ are both book-keeping symbols with numerical value equal to one. We then perform the following algebraic operations:

- substitute (3.23) into the Hamiltonian $\tilde{\mathcal{H}}_{sec}(\delta\tilde{\psi}, \delta\tilde{\Gamma}, \delta\tilde{J})$ (Eq. (3.20)) and expand the Hamiltonian in powers of the symbols $\tilde{\varepsilon}_*$, $\tilde{\varepsilon}_{J_*}$;
- assign a unique book-keeping symbol to the expanded Hamiltonian $\tilde{\mathcal{H}}_{sec}(\Delta\delta\tilde{\psi}, \Delta\delta\tilde{\Gamma}, \Delta\delta\tilde{J})$, by setting[1], first $\tilde{\varepsilon}_{J_*} \rightsquigarrow \tilde{\varepsilon}_*^3$, and then $\tilde{\varepsilon}_*^a \rightsquigarrow \lambda^{a-2}$;
- truncate the resulting expression at a maximum order $\tilde{N}_t$ in the book-keeping symbol λ.

After performing the above algebraic steps, the Hamiltonian (apart for a constant) resumes the form

$$\tilde{\mathcal{H}}^{(0)}(\Delta\delta\tilde{\psi}, \Delta\delta\tilde{\Gamma}, \Delta\delta\tilde{J}) = \tilde{\mathcal{H}}_{sec} = \tilde{Z}_0(\Delta\delta\tilde{\psi}, \Delta\delta\tilde{\Gamma}) + \sum_{s=1}^{\tilde{N}_t} \lambda^s \tilde{h}_s(\Delta\delta\tilde{\psi}, \Delta\delta\tilde{\Gamma}, \Delta\delta\tilde{J}) \tag{3.24}$$

where the zero-order (in the book-keeping parameter λ) term $\tilde{Z}_0$ is

$$\tilde{Z}_0(\Delta\delta\tilde{\psi}, \Delta\delta\tilde{\Gamma}) = -a\Delta\delta\tilde{\Gamma}^2 - b\Delta\delta\tilde{\psi}^2\,, \tag{3.25}$$

with a, $b > 0$ and $\tilde{h}_s$ are polynomal function in the variables $(\Delta\delta\tilde{\psi}, \Delta\delta\tilde{\Gamma}, \Delta\delta\tilde{J})$.

II) Diagonalization of the quadratic (in $(\Delta\delta\tilde{\psi}, \Delta\delta\tilde{\Gamma})$) term $\tilde{Z}_0$
Before providing the Birkhoff normal form for the construction of the quasi-periodic orbits around modes A and B we need to diagonalize the quadratic (in $(\Delta\delta\tilde{\psi}, \Delta\delta\tilde{\Gamma})$ term $\tilde{Z}_0$ of the Hamiltonian $\tilde{\mathcal{H}}^{(0)}$ Eq. (3.24). We recall the following lemma:

Lemma 3.2.1. (Diagonalization) *There exists a canonical transformation*

$$(\Delta\delta\tilde{\psi}, \Delta\delta\tilde{\Gamma}) = \mathscr{C}(\tilde{Q}, \tilde{P}) \tag{3.26}$$

[1]The substitution $\tilde{\varepsilon}_*^a \rightsquigarrow \lambda^{a-2}$ does not generate any λ with negative powers, being $\tilde{\varepsilon}_*^a$ such that $a \geq 2$.

such that the Hamiltonian $\tilde{\mathcal{H}}^{(0)}$ (Eq. (3.24)) in the variables $(\tilde{Q}, \tilde{P}, \Delta\delta\tilde{J})$ takes the form:

$$\begin{aligned}\tilde{\mathcal{H}}^{(0)}(\tilde{Q}, \tilde{P}, \Delta\delta\tilde{J}) &= \tilde{Z}_0(\tilde{Q}, \tilde{P}) + \sum_{s=1}^{\tilde{N}_t} \lambda^s \tilde{h}_s(\tilde{Q}, \tilde{P}, \Delta\delta\tilde{J}) \\ &= i\omega\, \tilde{Q}\tilde{P} + \sum_{s=1}^{\tilde{N}_t} \lambda^s \tilde{h}_s(\tilde{Q}, \tilde{P}, \Delta\delta\tilde{J})\,,\end{aligned} \tag{3.27}$$

with $\omega = 2\sqrt{ab}$ (a, b described by Eq. (3.25)).

Proof. First, we recall that the Hamiltonian vector field of $\tilde{Z}_0 = -a\,\Delta\delta\tilde{\Gamma}^2 - b\,\Delta\delta\tilde{\psi}^2$ is given by $\mathcal{X}_{\tilde{Z}_0} = \mathbb{J}\nabla\tilde{Z}_0$, where $\mathbb{J}$ is the symplectic matrix $\mathbb{J} = \begin{pmatrix} 0 & 1 \\ -1 & 0 \end{pmatrix}$. Thus, we can write

$$\dot{\boldsymbol{x}} = \mathcal{X}_{\tilde{Z}_0}(\boldsymbol{x}) = M\boldsymbol{x}\,,$$

where the vector $\boldsymbol{x}$ and the matrix M are defined as

$$\boldsymbol{x} = \begin{pmatrix} \Delta\delta\tilde{\psi} \\ \Delta\delta\tilde{\Gamma} \end{pmatrix}, \qquad M = \begin{pmatrix} \dfrac{\partial^2\tilde{Z}_0}{\partial\,\Delta\delta\tilde{\psi}\,\partial\,\Delta\delta\tilde{\Gamma}} & \dfrac{\partial^2\tilde{Z}_0}{\partial^2\,\Delta\delta\tilde{\Gamma}} \\ -\dfrac{\partial^2\tilde{Z}_0}{\partial^2\,\Delta\delta\tilde{\psi}} & -\dfrac{\partial^2\tilde{Z}_0}{\partial\,\Delta\delta\tilde{\Gamma}\,\partial\,\Delta\delta\tilde{\psi}} \end{pmatrix} = \begin{pmatrix} 0 & -2\,a \\ 2\,b & 0 \end{pmatrix}.$$

Now the aim is to find a canonical change of coordinates

$$\mathscr{C} : \boldsymbol{z} = \begin{pmatrix} \tilde{Q} \\ \tilde{P} \end{pmatrix} \longmapsto \boldsymbol{x} = \begin{pmatrix} \Delta\delta\tilde{\psi} \\ \Delta\delta\tilde{\Gamma} \end{pmatrix} = \mathscr{C}(\boldsymbol{z}) := A\,\boldsymbol{z}$$

such that the variables $\boldsymbol{z}$ satisfies $\dot{\boldsymbol{z}} = D\,\boldsymbol{z}$, with D a diagonal matrix.

It is easy to observe that it is sufficient to define A as the matrix having the eigenvectors of the matrix M as colums and D as the diagonal matrix composed by the relative eigenvalues. In fact, from the equalities $\boldsymbol{x} = A\,\boldsymbol{z}$ and $\dot{\boldsymbol{x}} = M\,\boldsymbol{x}$ it follows that

$$A\,\dot{\boldsymbol{z}} = \dot{\boldsymbol{x}} = M\,\boldsymbol{x} = M\,A\,\boldsymbol{z} \quad \Rightarrow \quad \dot{\boldsymbol{z}} = A^{-1}\,M\,A\,\boldsymbol{z} = D\,\boldsymbol{z} \quad \Rightarrow \quad M\,A = A\,D\,;$$

the last relation prove that the i-th colum of A correspond to the eigenvector of the matrix M and that its eigenvalues λ_i is in the i-th position of the diagonal matrix D.

Thus, observing that the eigenvalues of M are $\lambda_1 = 2\,i\sqrt{\mathrm{ab}}$ and $\lambda_2 = -\lambda_1$, we define $\omega = 2\sqrt{\mathrm{ab}}$, having

$$D = \begin{pmatrix} i\omega & 0 \\ 0 & -i\omega \end{pmatrix}, \qquad A = \begin{pmatrix} c\,v_{1,1} & c\,v_{2,1} \\ c\,v_{1,2} & c\,v_{2,2} \end{pmatrix} = \begin{pmatrix} c\,\boldsymbol{v}_1 & c\,\boldsymbol{v}_2 \end{pmatrix}$$

where the vector $\boldsymbol{v}_i = (v_{i,1}, v_{i,2})$, $i = 1, 2$, are the eigenvector of the matrix M (i.e. $M\,\boldsymbol{v}_i = \lambda_i \boldsymbol{v}_i$) and c is a constant making the transformation canonical, (i.e., by Definition (1.1.3), such that $A\,\mathbb{J}\,A^T = \mathbb{J}$).

It is easy to verify that, in the canonical variables $(\tilde{Q}, \tilde{P})$, the $\tilde{Z}_0$ term can be written as $\tilde{Z}_0 = i\omega\,\tilde{P}\tilde{Q}$; in fact, by Eq. (3.25) and using the relations $\boldsymbol{x} = A\boldsymbol{z}$, it follows

$$\tilde{Z}_0 = -a\Delta\delta\tilde{\Gamma}^2 - b\Delta\delta\tilde{\psi}^2 = \boldsymbol{x}^T \begin{pmatrix} -b & 0 \\ 0 & -a \end{pmatrix} \cdot \boldsymbol{x} = \frac{1}{2}\boldsymbol{x}^T\mathbb{J}^{-1}M \cdot \boldsymbol{x} = \frac{1}{2}\boldsymbol{z}^T A^T\mathbb{J}^{-1}MA \cdot \boldsymbol{z}\,.$$

On the other hand,

$$A^T\,\mathbb{J}^{-1}M\,A = \mathbb{J}^{-1}A^{-1}\,M\,A = \mathbb{J}^{-1}D$$

being $A\,\mathbb{J}\,A^T = \mathbb{J}$ and $M\,A = D\,A$, concluding (by Eqs. above) that

$$\tilde{Z}_0 = \frac{1}{2}\boldsymbol{z}^T A^T \mathbb{J}^{-1} M A \cdot \boldsymbol{z} = \frac{1}{2}\boldsymbol{z}^T \mathbb{J}^{-1} D \cdot \boldsymbol{z} = \boldsymbol{z}^T \begin{pmatrix} 0 & \frac{i\omega}{2} \\ \frac{i\omega}{2} & 0 \end{pmatrix} \cdot \boldsymbol{z} = i\omega\, \tilde{P}\tilde{Q}\,.$$

□

III) Birkhoff normal form around the modes A and B
Given the Hamiltonian (Eq. (3.27))

$$\tilde{\mathcal{H}}^{(0)}(\tilde{Q},\tilde{P},\Delta\delta\tilde{J}) = \tilde{Z}_0(\tilde{Q},\tilde{P}) + \sum_{s=1}^{\tilde{N}_t} \lambda^s \tilde{h}_s(\tilde{Q},\tilde{P},\Delta\delta\tilde{J}) = i\omega\,\tilde{Q}\tilde{P} + \sum_{s=1}^{\tilde{N}_t} \lambda^s \tilde{h}_s(\tilde{Q},\tilde{P},\Delta\delta\tilde{J})\,,$$

we now define a near-to-identity canonical transformation

$$(\tilde{Q},\tilde{\varphi},\tilde{P},\Delta\delta\tilde{J}) = \Psi^{(r)}(\widehat{Q},\widehat{\varphi},\widehat{P},\Delta\delta\widehat{J}) \quad , \tag{3.28}$$

obtained by a composition of r Lie canonical transformations, with r a sufficiently high integer, such that the Hamiltonian in the variables[2] $(\widehat{Q},\widehat{\varphi},\widehat{P},\Delta\delta\widehat{J})$ takes the form:

$$\tilde{\mathcal{H}}^{(r)}(\widehat{Q},\widehat{P},\Delta\delta\widehat{J}) = \tilde{Z}^{(r)}(\widehat{P}\widehat{Q},\Delta\delta\widehat{J}) + \tilde{R}^{(r)}(\widehat{Q},\widehat{P},\Delta\delta\widehat{J}) \tag{3.29}$$

with $||\tilde{R}^{(r)}|| << ||\tilde{Z}^{(r)}||$ for a suitably defined norm in the domain of the transformation. The superscript (r) in the above expressions means the expression derived after substituting the original variables $(\tilde{Q},\tilde{\varphi},\tilde{P},\Delta\delta\tilde{J})$ with the new canonical variables obtained by the transformation inverse to the r-step transformation (3.28):

$$(\widehat{Q},\widehat{\varphi},\widehat{P},\Delta\delta\widehat{J}) = \left(\Psi^{(r)}\right)^{-1}(\tilde{Q},\tilde{\varphi},\tilde{P},\Delta\delta\tilde{J}) \quad . \tag{3.30}$$

The Hamiltonian $\tilde{\mathcal{H}}^{(0)}(\tilde{Q},\tilde{P},\Delta\delta\tilde{J})$ (Eq. (3.27)) can be written as

$$\begin{aligned} \tilde{\mathcal{H}}^{(0)} &= \tilde{Z}_0(\tilde{Q},\tilde{P}) + \sum_{s=1}^{\tilde{N}_t} \lambda^s \tilde{h}_s(\tilde{Q},\tilde{P},\Delta\delta\tilde{J}) \\ &= i\omega\,\tilde{Q}\tilde{P} + \sum_{s=1}^{\tilde{N}_t} \lambda^s \left(\sum_{m,\,n,\,l} \zeta^{(0)}_{m,n,l}\, \tilde{Q}^m \tilde{P}^n \Delta\delta\tilde{J}^{\,l} \right) \end{aligned} \tag{3.31}$$

where $\zeta^{(0)}_{m,n,l}$ are constant coefficients, and $\omega = 2\sqrt{ab} > 0$ is the (constant) frequency.

Normal form to eliminate the power dependence on $\tilde{Q}^m\tilde{P}^n$ with $m \neq n$: The Hamiltonian (3.31) is normalized by iterative steps using the method of composition of Lie series. The normalization algorithm is defined recursively, for $r = 1, 2, ...$ by the relations:

$$\tilde{\mathcal{H}}^{(r-1)} = \tilde{Z}_0 + \sum_{s=1}^{r-1} \lambda^s \tilde{Z}_s(\tilde{Q}\tilde{P},\,\Delta\delta\tilde{J}) + \sum_{s=r}^{\tilde{N}_t} \lambda^s \left(\sum_{m,\,n,\,l} \zeta^{(r-1)}_{m,n,l}\, \tilde{Q}^m \tilde{P}^n \Delta\delta\tilde{J}^{\,l} \right), \tag{3.32}$$

$$\tilde{\chi}^{(r)} = \lambda^r \sum_{\substack{m,\,n,\,l \\ m\neq n}} \frac{\zeta^{(r-1)}_{m,n,l}}{i\,\omega(m-n)}\, \tilde{Q}^m \tilde{P}^n \Delta\delta\tilde{J}^{\,l}\,, \tag{3.33}$$

[2]Actually, due to the non-dependence of the generating functions $\tilde{\chi}^{(r)}$ on the $\tilde{\varphi}$ variable, it follows that $\Delta\delta\widehat{J} = \Delta\delta\tilde{J}$.

$$\tilde{\mathcal{H}}^{(r)} = \left[\exp(L_{\tilde{\chi}^{(r)}}) \tilde{\mathcal{H}}^{(r-1)} \right]^{\leq \tilde{N}_t} , \tag{3.34}$$

(where $[\cdot]^{\leq \tilde{N}_t}$ means truncation at the order $\tilde{N}_t$ in the book-keeping parameter λ).

Final Hamiltonian and normalizing transformation: the normalizing transformation $\Psi^{(r)}$ is defined by:

$$\begin{aligned} (\tilde{Q}, \tilde{\varphi}, \tilde{P}, \Delta\delta\tilde{J}) &= \Psi^{(r)}(\widehat{Q}, \widehat{\varphi}, \widehat{P}, \Delta\delta\widehat{J}) \qquad (3.35) \\ &= \left[\left(\exp\left(L_{\tilde{\chi}^{(r)}}\right) \exp\left(L_{\tilde{\chi}^{(r-1)}}\right) \dots \exp\left(L_{\tilde{\chi}^{(1)}}\right) (\tilde{Q}, \tilde{\varphi}, \tilde{P}, \Delta\delta\tilde{J}) \right) \Big|_{\substack{\tilde{Q}=\widehat{Q} \\ \tilde{\varphi}=\widehat{\varphi} \\ \tilde{P}=\widehat{P} \\ \Delta\delta\tilde{J}=\Delta\delta\widehat{J}}} \right]^{\leq \tilde{N}_t} \end{aligned}$$

and the final Hamiltonian

$$\begin{aligned} \tilde{\mathcal{H}}^{(r)} &= \left[\left(\exp\left(L_{\tilde{\chi}^{(r)}}\right) \exp\left(L_{\tilde{\chi}^{(r-1)}}\right) \dots \exp\left(L_{\tilde{\chi}^{(1)}}\right) \tilde{\mathcal{H}}^{(0)} \right) \Big|_{\substack{\tilde{Q}=\widehat{Q} \\ \tilde{\varphi}=\widehat{\varphi} \\ \tilde{P}=\widehat{P} \\ \Delta\delta\tilde{J}=\Delta\delta\widehat{J}}} \right]^{\leq N_t} \qquad (3.36) \\ &= \tilde{Z}^{(r)}(\widehat{Q}\widehat{P},\, \Delta\delta\widehat{J}) + \tilde{R}^{(r)}(\widehat{Q},\, \widehat{P},\, \Delta\delta\widehat{J}) , \end{aligned}$$

where $1 \leq r \leq \tilde{N}_t$ is chosen so that the normal form term $\tilde{Z}^{(r)}(\widehat{Q}\widehat{P},\, \Delta\delta\widehat{J})$ yields the best possible approximation to the dynamics.

Through the normalization procedure described above we find a new set of variables in which, except for a small remainder, the dynamics locally (around the apsidal solutions $(\delta\tilde{\psi}_*, \delta\tilde{\Gamma}_*, \delta\tilde{J}_*)$) is given by the normal form $\tilde{Z}^{(r)}(\widehat{Q}\widehat{P}, \Delta\delta\widehat{J})$. In particular Hamilton's flow under the normal form in the transformed variables, reads

$$\begin{cases} \dot{\widehat{Q}} = \dfrac{\tilde{Z}^{(r)}(\widehat{P}\widehat{Q},\, \Delta\delta\widehat{J})}{\partial\widehat{P}} = \widehat{Q}\, \mathcal{F}(\widehat{P}\widehat{Q},\, \Delta\delta\widehat{J}) \\ \dot{\widehat{\varphi}} = \dfrac{\tilde{Z}^{(r)}(\widehat{P}\widehat{Q},\, \Delta\delta\widehat{J})}{\partial\Delta\delta\tilde{J}} \\ \dot{\widehat{P}} = -\dfrac{\tilde{Z}^{(r)}(\widehat{P}\widehat{Q},\, \Delta\delta\widehat{J})}{\partial\widehat{Q}} = -\widehat{P}\, \mathcal{F}(\widehat{P}\widehat{Q},\, \Delta\delta\widehat{J}) \\ \dot{\Delta\delta\widehat{J}} = -\dfrac{\tilde{Z}^{(r)}(\widehat{P}\widehat{Q},\, \Delta\delta\widehat{J})}{\partial\Delta\delta\widehat{\varphi}} = 0 \end{cases} , \tag{3.37}$$

where $\mathcal{F}$ is a function of $(\widehat{P}\widehat{Q},\, \Delta\delta\widehat{J})$. From the previous system it is easy to observe that the quantities $\widehat{Q}\widehat{P}$ and $\Delta\delta\widehat{J}$ are constants (being their derivative equal to zero); thus $\widehat{Q}(t)\widehat{P}(t) = \widehat{Q}(0)\widehat{P}(0)$ and $\Delta\delta\widehat{J}(t) = \Delta\delta\widehat{J}(0)$. Thus, the solutions, in the transformed variables, are described by

$$\begin{aligned} \widehat{Q}(t) &= \widehat{Q}(0)\, e^{ft} , \\ \widehat{P}(t) &= \widehat{P}(0)\, e^{-ft} , \\ \widehat{\varphi}(t) &= \widehat{\varphi}(0) + \omega_{\widehat{\varphi}} t , \\ \Delta\delta\widehat{J}(t) &= \Delta\delta\widehat{J}(0) , \end{aligned} \tag{3.38}$$

where

$$f = \mathcal{F}(\widehat{P}\widehat{Q},\, \Delta\delta\widehat{J})\Big|_{\substack{\widehat{P}\widehat{Q}=\widehat{P}(0)\widehat{Q}(0) \\ \Delta\delta\widehat{J}=\Delta\delta\widehat{J}(0)}} , \qquad \omega_{\widehat{\varphi}} = \dot{\widehat{\varphi}}(\widehat{P}\widehat{Q},\, \Delta\delta\widehat{J})\Big|_{\substack{\widehat{P}\widehat{Q}=\widehat{P}(0)\widehat{Q}(0) \\ \Delta\delta\widehat{J}=\Delta\delta\widehat{J}(0)}} .$$

3.2 Semi-analytical determination of the quasi-periodic orbits around the periodic orbits A or B

Figure 3.2 shows an example of the comparison between the semi-analytical computation of some quasi-periodic orbits (surrounding the 3D apsidal corotations A and B) on the basis of the normal form flow of $\tilde{Z}^{(r)}$, and a full numerical computation of the same orbits.

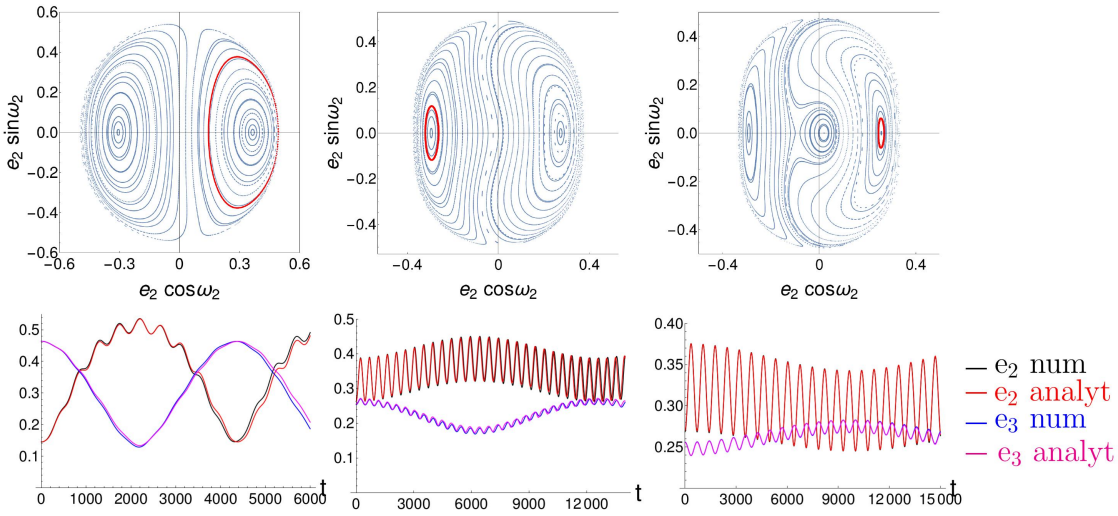

Figure 3.2: First row: Poincaré surfaces of section for the values of the energy (from left to right), $\mathcal{E} = -5.72 \cdot 10^{-5}$, $-3.19 \cdot 10^{-5}$, $-2.53 \cdot 10^{-5}$. The red close curves (from left to right, around, respectively, the mode B, A and B) represent a selected quasi-periodic orbit. Second row: time series of the evolution of the eccentricities for both planets along the quasi-periodic solutions (in red in the first row). The curves in red and in magenta show the time series for the eccentricities e_2 and e_3 respectively as computed semi-analytically. The black and blue curves, instead, show the time series e_2 and e_3 as computed through a numerical evaluation of the quasi-periodic orbits.

We resume the semi-analytical computation of the quasi-periodic orbits by the following steps:

i) we apply i)-iii) of section 3.1 so to semi-analytically compute the 3D apsidal corotations; this allows to determine the fixed point of the integrable Hamiltonian (ψ_*, Γ_*, J_*) (through the tangency method), the transformation $\Phi^{(r)}$ (see Eq. (3.8)) and the time evolution (in the tranformed variables) for the 3D apsidal solutions, given by $(\delta\tilde{\psi}_*, \delta\tilde{\Gamma}_*, \delta\tilde{J}_*, \tilde{\varphi}(t) = \tilde{\varphi}(0) + \nu_* t)$;

ii) following **I)**, perform an expansion of the Hamiltonian $\tilde{\mathcal{H}}_{sec}$ (see Eq. (3.20)) around the 3D apsidal solutions, through the traslation $\delta\tilde{\psi} = \delta\tilde{\psi}_* + \Delta\delta\tilde{\psi}$, $\delta\tilde{\Gamma} = \delta\tilde{\Gamma}_* + \Delta\delta\tilde{\Gamma}$, $\delta\tilde{J} = \delta\tilde{J}_* + \Delta\delta\tilde{J}$, described by Eq. (3.21);

iii) as in **II)**, apply the change of variables $(\Delta\delta\tilde{\psi}, \Delta\delta\tilde{\Gamma}) = \mathscr{C}(\tilde{Q}, \tilde{P})$ (Eq. (3.26)) diagonalizing the $\tilde{Z}_0$ term (Eq. (3.25);

iv) complete the procedure following **III)**, i.e. computing the change of variables $\Psi^{(r)}$ (given by Eq. (3.35)) and the solutions, in the trasformed variables, $\widehat{Q}(t) = \widehat{Q}(0)\, e^{ft}$, $\widehat{P}(t) = \widehat{P}(0)\, e^{-ft}$, $\widehat{\varphi}(t) = \widehat{\varphi}(0) + \omega_{\widehat{\varphi}} t$, $\Delta\delta\widehat{J}(t) = \Delta\delta\widehat{J}(0)$ (see Eq. (3.38));

v) finally, in order to recover the original dynamics $(\psi(t) = \psi_* + \delta\psi(t), \varphi(t), \Gamma(t) = \Gamma_* + \delta\Gamma(t), J(t) = J_* + \delta J(t))$, it is sufficient to back transform the new variables $(\widehat{Q}, \widehat{\varphi}, \widehat{P}, \Delta\delta\widehat{J}) \mapsto (\delta\psi, \varphi, \delta\Gamma, \delta J)$; we compute this change of variables using the Exchange Theorem 1.1.6, i.e. applying the canonical transformations $\Phi^{(r)}$ (Eq. (3.8)), the translation given by Eq. (3.23), $\mathscr{C}$ (Eq. (3.26)

and $\Psi^{(r)}$ (Eq. (3.35)) according to

$$(\delta\psi,\varphi,\delta\Gamma,\delta J) = \left[\Psi^{(r)}\left(\left(\Phi^{(r)}(\delta\psi,\varphi,\delta\Gamma,\delta J)\Big|_{\substack{\delta\psi=\delta\tilde{\psi}_*+\Delta\delta\tilde{\psi}\\ \delta\Gamma=\delta\tilde{\Gamma}_*+\Delta\delta\tilde{\Gamma}\\ \delta J=\delta\tilde{J}_*+\Delta\delta\tilde{J}\\ \varphi=\tilde{\varphi}}}\right)_{\binom{\Delta\delta\tilde{\psi}}{\Delta\delta\tilde{\Gamma}}=\mathscr{C}\binom{\tilde{Q}}{\tilde{P}}}\right)\right]_{\substack{\tilde{Q}=\widehat{Q}\\ \tilde{\varphi}=\widehat{\varphi}\\ \tilde{P}=\widehat{P}\\ \Delta\delta\tilde{J}=\Delta\delta\widehat{J}}}$$

Otherwise, it is possible to compute the above change of variables 'step-by-step', i.e. determining all the variables involved in each step i)-iv) and composing them in the end.

As for the semi-analytical determination of the 3D apsidal solutions, it is possible to compute the time series evolution of the perihelia, eccentricities and the inclinations by Eq. (3.16)– (3.19). As shown in Fig. 3.1, the semi-analytical representation of the selected quasi-periodic orbits (red curves of the first row) fits with precision the numerical ones for both the quasi-periodic orbits aroud the modes A and B. Moreover, as in the case of the semi-analytical computation of the periodc orbits, we point out the ability of the semi-analytical theory to well represent the orbits of the quasi-periodic orbits around A and B *after* the onset of the saddle-node bifurcation giving rise to the periodic orbits C_1 and C_2, as in the third panel of Fig. 3.2 (see subsection 2.3.1). Finally, concerning the choice of the quasi-periodic orbits, Fig. 3.2 shows only some possibilities; other choices are at priori possible. However, the more the energy increases the smaller is the domain of convergence of the normalization method (as it can be seen by the third panel of the first row of Fig. 3.2); thus it is convenient to choice quasi-periodic orbits close to the 3D apsidal corotations A and B .

4. Secular orbital dynamics of the innermost exoplanet of the υ-Andromedæ system

4.1 Introductory remarks

The available data for the orbital parameters of an extrasolar system are typically affected by wide observational error bars, because of the limitations in present detection methods. Most common is a lack of knowledge on the inclinations and nodes, and, consequently, only minimum limits for the planetary masses can be deduced by the observations. Through numerical integration of the full equations of motion, it is possible to explore the long-term stability of the orbits corresponding to various choices of the initial orbital parameters, thus providing dynamical information that helps to constrain the uncertainties on the unknown orbital parameters. Nevertheless, numerical integrations of the full planetary N-body problem are not always easy to perform, expecially when a large number of planets is involved. The aim of this Chapter is to introduce an "easier" Hamiltonian model (obtained by the secular approximation and by a double normalization procedure) whose long-term stability is compatible with the one of the full problem; in this way, it is sufficient to perform numerical integrations of a simple Hamiltonian model, with results that can be used reliably to recover information about the unknown orbital parameters also in the full problem.

More specifically, we want to describe the secular motion of a small-mass planet in a multi-planetary system through the introduction of a, so called, *secular quasi-periodic restricted Hamiltonian*. To fix the ideas, as a representative example, we refer to the motion of υ-And **b**, which is the innermost planet among those discovered in the extrasolar system orbiting around the υ-Andromedæ A star. Since (in our modelization) the mass of the innermost planet **b** is much smaller than the masses of the planets **c** and **d**, the motion of **b** can be modeled with a good approximation via a restricted four-body problem (with planets **c**, **d** providing the main perturbations). More precisely, in order to study its motion, we preassign the orbits of the Super-Jupiter exoplanets **c** and **d** ensuring that they correspond to a stable configuration. The Fourier decompositions of the secular motions of **c** and **d** are then reconstructed by using the well known technique of the (so called) Frequency Analysis (see e.g. [51]) and are injected in the equations describing the orbital dynamics of υ-And **b** under the gravitational effects exerted by those two external exoplanets (that are expected to be major ones in such an extrasolar system). This way to introduce a quasi-periodic restricted model has been recently used to study the long-term dynamics of our Solar System (see [85] and [43]). In our present case (referring to the υ-Andromedæ system with planets **b**, **c**, **d**), we start with a Hamiltonian having 9 degrees of freedom, ending up with a simpler Hamiltonian model, having $2 + 3/2$ degrees of freedom. In order to validate such a kind of

model, we perform a comparison with several numerical integrations of the complete 4-body problem, establishing the reliability of our secular quasi-periodic restricted model as regards predictions of the *stability domain* for secular motions.

The content of the following sections is largely based on the article [77].

4.2 Determination of the outer planets' motion

To prescribe the orbits of the giant planets υ-And **c** and υ-And **d**, we start from the Hamiltonian of the three-body problem in Poincaré heliocentric canonical variables, using this time the formulation based on the reduced masses β_2 , β_3 (see (1.9)), that is

$$\mathcal{H} = \sum_{j=2}^{3} \left(\frac{\boldsymbol{p}_j{}^2}{2\,\beta_j} - \frac{\mathcal{G}\,m_0\,m_j}{r_j} \right) + \frac{\boldsymbol{p}_2 \cdot \boldsymbol{p}_3}{m_0} - \frac{\mathcal{G}\,m_2\,m_3}{|\boldsymbol{r}_2 - \boldsymbol{r}_3|}\,, \tag{4.1}$$

where m_0 = mass of the star, m_j , $\boldsymbol{p}_j$, $\boldsymbol{r}_j$, $j = 2, 3$ are the masses, barycentric momenta and heliocentric position vectors of the planets, $\mathcal{G}$ is the gravitational constant and $\beta_j = m_0 m_j/(m_0 + m_j)$ $j = 2, 3$ are the reduced masses. Let us remark that, in the following, we will use the subindexes 2 and 3 respectively, for the 'inner' (υ-And **c**) and 'outer' (υ-And **d**) planets between the giant ones, while the subindex 1 will be used to refer to υ-And **b**.

In order to set up a quasi-periodic restricted model for the description of the motion of υ-And **b**, we need to characterize the motion of the giant planets; this can be done through the *Frequency Analysis* method, starting from the numerical integration of

i) the complete 3BP Hamiltonian, reported in equation (4.1) (i.e. before any expansions and averaging);

ii) the secular 3BP Hamiltonian at order two in masses (see Appendix C, Section C.1).

Concerning ii), as already explained in the Introduction (Subsection 1.4.5), in order to compute the secular Hamiltonian we need to remove the dependence on the 'fast' angles λ_2, λ_3 . This can be done by "averaging by scissors" (subsection 1.4.5), yielding a Hamiltonian equivalent to the one found after first order (in the mass ratios) averaging[1]. A more accurate secular model can be found by elimination of the fast angles through a canonical transformation, corresponding to a second order (in the mass ratios) averaging[2].

Referring to the model i), we numerically integrate the complete Hamiltonian (4.1) using a symplectic method of type $\mathcal{SBAB}_3$, which is described in [55]. As initial orbital parameters for the outer planets, we adopt those reported in Table 4.1, corresponding to the most robust planetary orbit compatible with the observed data available for υ-And **c** and υ-And **d** (see [78]), according to the criterion of "minimal area" explained in [72].

Having fixed as initial orbital parameters the ones described in Table 4.1, it is possible to compute their correspondent values in the Laplace reference frame (i.e., the invariant reference frame orthogonal to the total angular momentum vector $\boldsymbol{r}_2 \times \boldsymbol{p}_2 + \boldsymbol{r}_3 \times \boldsymbol{p}_3$, already introduced in Subsection 1.4.4 of the Introduction 1) and to perform the numerical integration of the full 3BP corrisponding to these initial values. Then, it is possible to express the *discrete* results produced by the numerical integrations in the canonical Poincaré variables (ξ_j, η_j), (P_j, Q_j) (momenta-coordinates,

[1] This simply means to remove from the Hamiltonian the terms depending upon the mean anomalies of the planets.

[2] Therefore, we have first tried to perform the *Frequency Analysis* on the signals obtained by the numerical integrations of the secular approximation at order two in masses of the problem (without performing the Jacobi's reduction of nodes on the Hamiltonian); however, as shown in Section C.2 of Appendix C, in order to study the secular motion of the small-mass planet υ-And **b**, a more accurate approximation of the orbits of the outer giant planets υ-And **c**, υ-And **d** is required.

	υ-And **c**	υ-And **d**
$m\,[M_J]$	15.9792	9.9578
$a(0)\,[AU]$	0.829	2.53
$\mathrm{e}(0)$	0.239	0.31
$\mathrm{i}(0)\,[^\circ]$	6.865	25.074
$M(0)\,[^\circ]$	355	335
$\omega(0)\,[^\circ]$	245.809	254.302
$\Omega(0)\,[^\circ]$	229.325	7.374

Table 4.1: Chosen values of the masses and of the initial orbital parameters for υ-And **c** and υ-And **d**, compatible with the observed data available, reported in [78].

already introduced in Subsection (1.4.3), equation (1.21)) given by

$$\begin{aligned}
\xi_j &= \sqrt{2\Gamma_j}\cos(\gamma_j) = \sqrt{2\Lambda_j}\sqrt{1-\sqrt{1-\mathrm{e}_j^2}}\cos(\varpi_j)\,,\\
\eta_j &= \sqrt{2\Gamma_j}\sin(\gamma_j) = -\sqrt{2\Lambda_j}\sqrt{1-\sqrt{1-\mathrm{e}_j^2}}\sin(\varpi_j)\,, \qquad\qquad j=2,3\,,\\
P_j &= \sqrt{2\Theta_j}\cos(\theta_j) = 2\sqrt{\Lambda_j}\sqrt[4]{1-\mathrm{e}_j^2}\,\sin\left(\frac{\mathrm{i}_j}{2}\right)\cos(\Omega_j)\,,\\
Q_j &= \sqrt{2\Theta_j}\sin(\theta_j) = -2\sqrt{\Lambda_j}\sqrt[4]{1-\mathrm{e}_j^2}\,\sin\left(\frac{\mathrm{i}_j}{2}\right)\sin(\Omega_j)
\end{aligned} \tag{4.2}$$

where $\Lambda_j = \beta_j\sqrt{\mu_j a_j}$ (see equation (1.20) for the modified Delaunay variables).

However, the numerical integrations do not allow to obtain a complete knowledge of the motion laws $t \mapsto (\xi_j(t), \eta_j(t))$, $t \mapsto (P_j(t), Q_j(t))$ $(j = 2, 3)$, producing only discrete time series made by sets of finite points computed on a regular grid in the interval $[0, T]$. The computational method of *Frequency Analysis* (hereafter, FA), allows however to reconstruct with a good accuracy the motion laws by using suitable continuous in the time variable t functions. For this purpose, we introduce the following convenient class of functions, that are comfortable to work with:

Definition 4.2.1. *We say that the law of the motion $z(t)$ is quasi-periodic if there exist*

- $\boldsymbol{\omega} \in \mathbb{R}^n$ *such that* $\boldsymbol{k}\cdot\boldsymbol{\omega} \neq 0\ \forall\,\boldsymbol{k} \in \mathbb{Z}^n \setminus \{\mathbf{0}\}$ *;*
- *a function with angular variables* $g = g(\boldsymbol{\vartheta})$*, where* $\boldsymbol{\vartheta} \in \mathbb{T}^n$*, such that* $z(t) = g(\omega_1 t, \ldots, \omega_n t)$*.*

Moreover, we say that g admits a Fourier decomposition

$$g(\boldsymbol{\vartheta}) = \sum_{\boldsymbol{k}\in\mathbb{Z}^n} a_{\boldsymbol{k}} e^{i\,\boldsymbol{k}\cdot\boldsymbol{\vartheta}}$$

with exponentially decaying coefficients $a_{\boldsymbol{k}}$ if there exists two parameters $c > 0$ and $\sigma > 0$ such that the following inequality is fulfilled

$$|a_{\boldsymbol{k}}| \leq c\, e^{-|\boldsymbol{k}|\sigma} \quad \forall\,\boldsymbol{k} \in \mathbb{Z}^n\,.$$

Given the following Fourier series decomposition

$$z(t) = \sum_{\boldsymbol{k}\in\mathbb{Z}^n} a_{\boldsymbol{k}} e^{i(\boldsymbol{k}\cdot\boldsymbol{\omega}t+\vartheta_{\boldsymbol{k}})}\,, \tag{4.3}$$

with $\boldsymbol{\omega} \in \mathbb{R}^n$ the fundamental frequency vector, $a_{\boldsymbol{k}} \in \mathbb{R}_+ \cup \{0\}$ and $\vartheta_{\boldsymbol{k}} \in \mathbb{T}$, $\forall\,\boldsymbol{k} \in \mathbb{Z}^n$, with the sequence $\{a_k\}_{\boldsymbol{k}\in\mathbb{Z}^n}$ satisfying a decay law of the same type of that described above, the FA allows to find an approximation of $z(t)$ of the form

$$z(t) \simeq \sum_{s=1}^{\mathcal{N}_C} a_{s;T} e^{i(\nu_T^{(s)}t+\vartheta_{s;T})} \tag{4.4}$$

where $\mathcal{N}_C$ is the number of components we want to consider. The equation (4.4) is an approximation of the motion $z(t)$ in the sense that if $\mathcal{N}_C \to +\infty$ and $T \to +\infty$, the right hand side of (4.4) converges to (4.3). Moreover, $a_{s;T} \in \mathbb{R}_+$ and $\vartheta_{s;T} \in [0, 2\pi)$ are called respectively the amplitude and the initial phase of the s-th component, while $\nu_T^{(s)}$ is a local maximum point of the function

$$\nu \mapsto \mathcal{A}(\nu) = \frac{1}{T} \left| \int_0^T z(t)\, e^{-i\nu t}\, \mathcal{W}(t)\, dt \right| , \tag{4.5}$$

where $\mathcal{W}$ is a suitable weight function such that $\int_0^T \mathcal{W}(t)\, dt = T$. We have used the so-called "Hanning filter", defined (in $[0, T]$) as $\mathcal{W}(t) = 1 - \cos[\pi(2t/T - 1)]$. For further details about the FA see [51] and [68].

The numerical integration of the 3BP (equation (4.1)) produces a discretization of the signals[3] $t \mapsto \xi_j(t) + i\eta_j(t)$ and $t \mapsto P_j(t) + iQ_j(t)$, i.e., the discrete time series $\{(\xi_j(s\Delta), \eta_j(s\Delta))\}_{s=0}^{\mathcal{N}_P}$ and $\{(P_j(s\Delta), Q_j(s\Delta))\}_{s=0}^{\mathcal{N}_P}$ $(j = 2, 3)$, where $s = 0, \ldots, \mathcal{N}_P$, and the timestep (or sampling time) is $\Delta = T/\mathcal{N}_P$. These discretizations allow to compute (by numerical quadrature) the integral in (4.5) and, consequently, a few of local maximum points of the function (4.5) considering, as $z(t)$, $\xi_2(t) + i\eta_2(t)$, $\xi_3(t) + i\eta_3(t)$, $P_2(t) + iQ_2(t)$ and $P_3(t) + iQ_3(t)$.

s	$\nu_T^{(s)}$	$k_3^{(s)}$	$k_4^{(s)}$	$k_5^{(s)}$	$\lvert\nu_T^{(s)} - \boldsymbol{k}^{(s)} \cdot \boldsymbol{\omega}\rvert$	A_s	ϑ_s
0	$-2.43699358194622660 \cdot 10^{-3}$	1	0	0	0.0000	$3.8182 \cdot 10^{-1}$	4.611
1	$-1.04274752029517815 \cdot 10^{-3}$	0	1	0	$3.9608 \cdot 10^{-8}$	$1.4219 \cdot 10^{-1}$	2.434
2	$1.22065297958166112 \cdot 10^{-2}$	−1	0	2	$9.2959 \cdot 10^{-9}$	$9.0935 \cdot 10^{-2}$	3.898
3	$-3.83123872535040154 \cdot 10^{-3}$	2	−1	0	$3.8689 \cdot 10^{-8}$	$4.0358 \cdot 10^{-2}$	3.593

Table 4.2: Decomposition of the signal $\xi_2(t) + i\,\eta_2(t)$ as it is provided by the FA.

s	$\nu_T^{(s)}$	$k_3^{(s)}$	$k_4^{(s)}$	$k_5^{(s)}$	$\lvert\nu_T^{(s)} - \boldsymbol{k}^{(s)} \cdot \boldsymbol{\omega}\rvert$	A_s	ϑ_s
0	$-2.43699698221569363 \cdot 10^{-3}$	1	0	0	$3.4003 \cdot 10^{-9}$	$5.6387 \cdot 10^{-1}$	1.469
1	$-1.04278712796661375 \cdot 10^{-3}$	0	1	0	0.0000	$1.1039 \cdot 10^{-1}$	2.437
2	$-3.83100979083359590 \cdot 10^{-3}$	2	−1	0	$1.9025 \cdot 10^{-7}$	$2.7811 \cdot 10^{-2}$	3.566
3	$1.22065393849870793 \cdot 10^{-2}$	−1	0	2	$2.9324 \cdot 10^{-10}$	$2.4050 \cdot 10^{-3}$	$7.556 \cdot 10^{-1}$

Table 4.3: Decomposition of the signal $\xi_3(t) + i\,\eta_3(t)$ as it is provided by the FA.

s	$\nu_T^{(s)}$	$\tilde{k}_3^{(s)}$	$\tilde{k}_4^{(s)}$	$\tilde{k}_5^{(s)}$	$\lvert\nu_T^{(s)} - \tilde{\boldsymbol{k}}^{(s)} \cdot \boldsymbol{\omega}\rvert$	$\tilde{A}_s$	$\tilde{\vartheta}_s$
0	$4.88477275490260560 \cdot 10^{-3}$	0	0	1	0.0000	$5.5389 \cdot 10^{-1}$	2.670
1	$-9.75856551797929864 \cdot 10^{-3}$	2	0	−1	$1.944 \cdot 10^{-7}$	$4.9772 \cdot 10^{-2}$	$1.914 \cdot 10^{-1}$
2	$-8.36452054946431114 \cdot 10^{-3}$	1	1	−1	$3.2915 \cdot 10^{-8}$	$2.2433 \cdot 10^{-2}$	4.351
3	$6.27899221605471031 \cdot 10^{-3}$	−1	1	1	$1.3007 \cdot 10^{-8}$	$1.2854 \cdot 10^{-2}$	$5.208 \cdot 10^{-1}$
4	$3.49055804503076465 \cdot 10^{-3}$	1	−1	1	$8.2559 \cdot 10^{-9}$	$1.0041 \cdot 10^{-2}$	1.678

Table 4.4: Decomposition of the signal $P_2(t) + i\,Q_2(t)$ as it is provided by the FA.

s	$\nu_T^{(s)}$	$\tilde{k}_3^{(s)}$	$\tilde{k}_4^{(s)}$	$\tilde{k}_5^{(s)}$	$\lvert\nu_T^{(s)} - \tilde{\boldsymbol{k}}^{(s)} \cdot \boldsymbol{\omega}\rvert$	$\tilde{A}_s$	$\tilde{\vartheta}_s$
0	$4.88477277322339754 \cdot 10^{-3}$	0	0	1	$1.8321 \cdot 10^{-11}$	$5.6348 \cdot 10^{-1}$	5.812
1	$-9.75856522554671181 \cdot 10^{-3}$	2	0	−1	$1.9469 \cdot 10^{-7}$	$5.1543 \cdot 10^{-2}$	3.333
2	$-8.36452090216070580 \cdot 10^{-3}$	1	1	−1	$3.2563 \cdot 10^{-8}$	$2.3352 \cdot 10^{-2}$	1.209
3	$3.49054260511432292 \cdot 10^{-3}$	1	−1	1	$2.3696 \cdot 10^{-8}$	$1.3434 \cdot 10^{-2}$	4.821
4	$6.27897429080374707 \cdot 10^{-3}$	−1	1	1	$4.9181 \cdot 10^{-9}$	$9.7673 \cdot 10^{-3}$	3.664

Table 4.5: Decomposition of the signal $P_3(t) + i\,Q_3(t)$ as it is provided by the FA.

Then, we use the FA to compute a quasi-periodic approximation of the secular dynamics of the giant planets υ-And **c** and υ-And **d**, i.e.

$$\xi_j(t) + i\eta_j(t) \simeq \sum_{s=1}^{\mathcal{N}_C} A_{j,s} e^{i(\boldsymbol{k}_{j,s} \cdot \boldsymbol{\theta}(t) + \vartheta_{j,s})}\,, \quad P_j(t) + iQ_j(t) \simeq \sum_{s=1}^{\widetilde{\mathcal{N}}_C} \tilde{A}_{j,s} e^{i(\tilde{\boldsymbol{k}}_{j,s} \cdot \boldsymbol{\theta}(t) + \tilde{\vartheta}_{j,s})}\,, \quad j = 2, 3\,, \tag{4.6}$$

where the angular vector

$$\boldsymbol{\theta}(t) = (\theta_3(t), \theta_4(t), \theta_5(t)) = (\omega_3\, t, \omega_4\, t, \omega_5\, t) := \boldsymbol{\omega}\, t \tag{4.7}$$

[3] Actually, the numerical integration of the complete problem allows to determine also a discretization of the 'fast' variables $\sqrt{2\Lambda_2}\cos(\lambda_2) + i\sqrt{2\Lambda_2}\sin(\lambda_2)$ and $\sqrt{2\Lambda_3}\cos(\lambda_3) + i\sqrt{2\Lambda_3}\sin(\lambda_3)$; however we are not interested in these variables. Thus, we do not report their decompositions as they are provided by the FA.

depends *linearly on time* and the fundamental frequency vector $\boldsymbol{\omega} \in \mathbb{R}^3$ has the components:

$$\begin{aligned} \omega_3 &= -2.4369935819462266 \cdot 10^{-3}\,, \\ \omega_4 &= -1.04278712796661375 \cdot 10^{-3}\,, \\ \omega_5 &= \;\; 4.88477275490260560 \cdot 10^{-3}\,. \end{aligned} \tag{4.8}$$

Thus, from now on, the motion of the outer planets $t \mapsto (\xi_j(t), \eta_j(t), P_j(t), Q_j(t))$, $j = 2, 3$, is approximated as it is written in both the r.h.s. of formula (4.6). The numerical values of the coefficients which appear in the quasi-periodic decompositions[4] of the motions laws are reported in Tables 4.2, 4.3, 4.4 and 4.5.

In order to verify that the numerical solutions are well approximated by the quasi-periodic decompositions computed above, we compare the time evolution of the variables ξ_2, ξ_3, η_2, η_3, P_2, P_3, Q_2, Q_3 as obtained by the numerical integration and by the FA. Figure (4.1) shows that the quasi-periodic approximations nearly perfectly superpose to the plots of the numerical solutions.

For the sake of completeness, we have also compared the Poincaré sections (corresponding to $\omega_3 = 0\,,\, \dot{\omega}_3 \geq 0\,$) as produced by the numerical integration or the quasi-periodic approximation of the motion. More precisely, after having introduced the variables[5]

$$\widehat{\xi}_j = \sqrt{2\Lambda_j}\,\sqrt{1-\sqrt{1-\mathrm{e}_j^2}}\,\cos(\omega_j)\,, \quad \widehat{\eta}_j = -\sqrt{2\Lambda_j}\,\sqrt{1-\sqrt{1-\mathrm{e}_j^2}}\,\sin(\omega_j)\,, \qquad j = 2, 3, \tag{4.9}$$

we report in Figure 4.2 the Poincaré sections, with respect to the representative coordinates $(\widehat{\xi}_2, \widehat{\eta}_2)\,$, in correspondence with the hyperplane $\widehat{\eta}_3 = 0\,,\, \widehat{\xi}_3 > 0\,$.

4.3 The secular quasi-periodic restricted (SQPR) Hamiltonian

Having preassigned the motion of the two outer planets υ-And **c** and υ-And **d**, it is now possible to properly define the secular model for a quasi-periodic restricted four-body problem (hereafter, 4BP). Starting from the Hamiltonian of the 4BP (see equation (1.9)), given by

$$\mathcal{H}_{4BP} = \sum_{j=1}^{3} \left(\frac{\boldsymbol{p}_j^{\,2}}{2\,\beta_j} - \frac{\mathcal{G}\,m_0\,m_j}{r_j} \right) + \sum_{1 \leq i < j \leq 3} \frac{\boldsymbol{p}_i \cdot \boldsymbol{p}_j}{m_0} - \sum_{1 \leq i < j \leq 3} \frac{\mathcal{G}\,m_i\,m_j}{|\boldsymbol{r}_i - \boldsymbol{r}_j|}\,, \tag{4.10}$$

(where the subindexes $1, 2, 3$ are referred, respectively, to υ-And **b**, υ-And **c** and υ-And **d**), the secular model of first order in the planetary masses is given by scissor-averaging with respect to the mean longitudes, i.e.,

$$\mathcal{H}_{sec}(\boldsymbol{\xi}, \boldsymbol{\eta}, \boldsymbol{P}, \boldsymbol{Q}) = \int_{\mathbb{T}^3} \frac{\mathcal{H}_{4BP}(\boldsymbol{\Lambda}, \boldsymbol{\lambda}, \boldsymbol{\xi}, \boldsymbol{\eta}, \boldsymbol{P}, \boldsymbol{Q})}{8\pi^3}\, d\lambda_1 d\lambda_2 d\lambda_3\,. \tag{4.11}$$

In the l.h.s. of the equation above, we disregarded the dependence on the actions Λ_j, because in the secular approximation of order one in the masses their values $\Lambda_j = \beta_j \sqrt{\mu_j\, a_j}\,$, $j = 1, 2, 3$, are

[4] Of course, the exact quasi-periodic decompositions include infinite terms in the Fourier series. In order to reduce the computational effort, we limit ourselves to consider just a few components, which are the main and most reliable ones, according to the following criteria. We take into account those terms corresponding to low order Fourier armonics, i.e., $\sum_{j=3}^{5} |k_j| \leq 5$ or $\sum_{j=3}^{5} |\tilde{k}_j| \leq 5\,$, and such that there are small uncertainties on the determination of the frequencies as linear combinations of the fundamental ones, i.e., $|\nu_T^{(s)} - \boldsymbol{k}^{(s)} \cdot \boldsymbol{\omega}| \leq 2 \cdot 10^{-7}$ or $|\nu_T^{(s)} - \tilde{\boldsymbol{k}}^{(s)} \cdot \boldsymbol{\omega}| \leq 2 \cdot 10^{-7}\,$.

[5] They are commonly used when the Jacobi's reduction of nodes is performed on the secular Hamiltonian, being $-\omega$ conjugated to $\Gamma\,$.

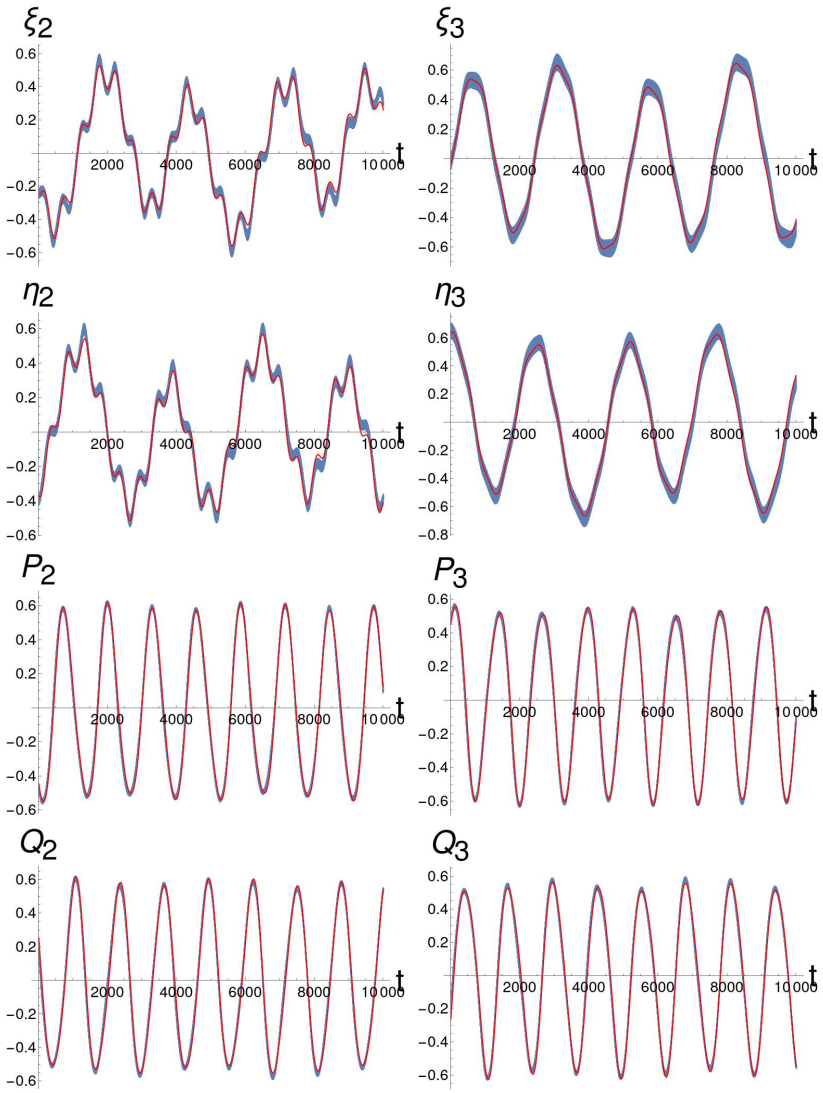

Figure 4.1: Dynamical-behaviour of the variables ξ_2, ξ_3, η_2, η_3, P_2, P_3, Q_2, Q_3 (their definition is reported in (4.2)) as it is computed by numerical integration of the complete (non secular) three-body problem and by the quasi-periodic approximation provided by the FA; the corresponding plots are in blue and red, respectively.

constant. Due to the D'Alembert rules ([87], [86]), it is well known that the secular Hamiltonian can be expanded in the following way:

$$\mathcal{H}_{sec}(\boldsymbol{\xi},\boldsymbol{\eta},\boldsymbol{P},\boldsymbol{Q}) = \sum_{s=0}^{\mathcal{N}/2} \sum_{\substack{|\boldsymbol{i}|+|\boldsymbol{l}|+\\ |\boldsymbol{m}|+|\boldsymbol{n}|=2s}} c_{\boldsymbol{i},\boldsymbol{l},\boldsymbol{m},\boldsymbol{n}} \prod_{j=1}^{3} \xi_j^{i_j} \eta_j^{l_j} P_j^{m_j} Q_j^{n_j} \,, \tag{4.12}$$

where $\mathcal{N}$ is the order of truncation in powers of eccentricity and inclination. We fix $\mathcal{N} = 8$ in all our computations.

Since we aim at describing the dynamical secular evolution of the innermost planet υ-And **b**, it is sufficient to consider the interactions between the two pairs υ-And **b**, υ-And **c** and υ-And **b**, υ-And **d**. In more details, let $\mathcal{H}_{sec}^{\mathrm{i-j}}$ be the secular Hamiltonian derived from the three-body problem for the planets i and j, averaging with respect to the mean longitudes λ_{i} , λ_{j} . Its expansion writes as

$$\mathcal{H}_{sec}^{\mathrm{i-j}}(\xi_{\mathrm{i}},\eta_{\mathrm{i}},P_{\mathrm{i}},Q_{\mathrm{i}},\xi_{\mathrm{j}},\eta_{\mathrm{j}},P_{\mathrm{j}},Q_{\mathrm{j}}) = \sum_{s=0}^{\mathcal{N}/2} \sum_{\substack{|\boldsymbol{i}|+|\boldsymbol{l}|+\\ |\boldsymbol{m}|+|\boldsymbol{n}|=2s}} c_{\boldsymbol{i},\boldsymbol{l},\boldsymbol{m},\boldsymbol{n}} \prod_{j=\mathrm{i,j}} \xi_j^{i_j} \eta_j^{l_j} P_j^{m_j} Q_j^{n_j} \,. \tag{4.13}$$

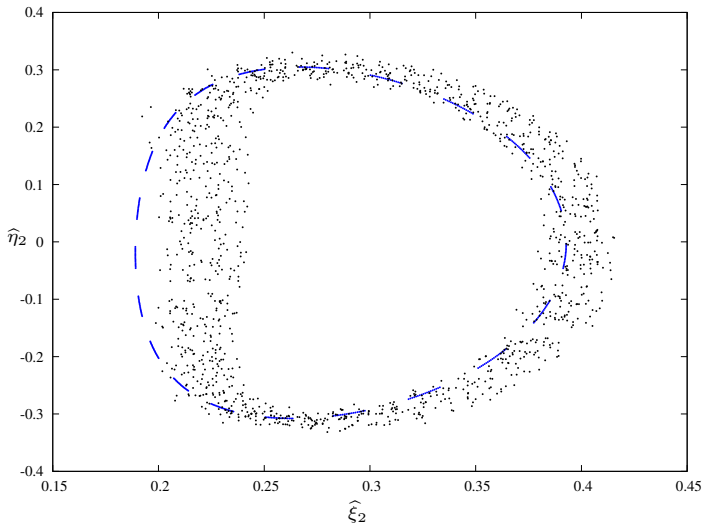

Figure 4.2: Poincaré surfaces of section with respect to the representative coordinates $(\widehat{\xi}_2, \widehat{\eta}_2)$ (as defined in equation (4.9)). The blue curve is obtained considering the quasi-periodic approximation of motion as computed by using the FA technique. Instead, the black dots are obtained taking into account the numerical integration of the complete three-body problem.

Therefore, a restricted non-autonomus model which approximates the secular dynamics of υ-And **b** could be defined by considering the terms

$$\begin{aligned}&\mathcal{H}^{1-2}_{sec}(\xi_1, \eta_1, P_1, Q_1, \xi_2(t), \eta_2(t), P_2(t), Q_2(t))\\ &+\mathcal{H}^{1-3}_{sec}(\xi_1, \eta_1, P_1, Q_1, \xi_3(t), \eta_3(t), P_3(t), Q_3(t))\,,\end{aligned}$$

where $\xi_2(t)$, $\eta_2(t)$, $\dots P_3(t)$, $Q_3(t)$ are replaced with the corresponding quasi-periodic approximations written in both the r.h.s. appearing in formula (4.6). Let us stress that, having prescribed the motion of the two outermost planets υ-And **c** and υ-And **d**, at this stage the Hamiltonian $\mathcal{H}^{2-3}_{sec}$ does not need to be reconsidered; indeed, it would introduce additional terms that disappear in the equations of motion (see formula (4.16) which is written below).

We can finally introduce the quasi-periodic restricted Hamiltonian model for the secular dynamics of υ-And **b**; it is given by the following $2 + 3/2$ degrees of freedom Hamiltonian:

$$\begin{aligned}\mathcal{H}_{sec,\,2+\frac{3}{2}}\,(\boldsymbol{p}, \boldsymbol{q}, \xi_1, \eta_1, P_1, Q_1) &= \omega_3\, p_3 + \omega_4\, p_4 + \omega_5\, p_5\\ &+\mathcal{H}^{1-2}_{sec}(\xi_1, \eta_1, P_1, Q_1, \xi_2(\boldsymbol{q}), \eta_2(\boldsymbol{q}), P_2(\boldsymbol{q}), Q_2(\boldsymbol{q}))\\ &+\mathcal{H}^{1-3}_{sec}(\xi_1, \eta_1, P_1, Q_1, \xi_3(\boldsymbol{q}), \eta_3(\boldsymbol{q}), P_3(\boldsymbol{q}), Q_3(\boldsymbol{q}))\,,\end{aligned} \tag{4.14}$$

where the pairs of canonical coordinates referring to the planets υ-And **c** and υ-And **d** (that are ξ_2, η_2, $\dots P_3$, Q_3) are replaced by the corresponding finite Fourier decomposition written in formula (4.6) as a function of the angles $\boldsymbol{\theta}$, renamed[6] as $\boldsymbol{q}$, i.e.,

$$\boldsymbol{q} = (q_3\,,\, q_4\,,\, q_5) := (\theta_3\,,\, \theta_4\,,\, \theta_5) = \boldsymbol{\theta}\,. \tag{4.15}$$

Let us focus on the summands appearing in the first row of (4.14), i.e., the Hamiltonian term $\boldsymbol{\omega}\cdot\boldsymbol{p}$, where $\boldsymbol{\omega}$ is the fundamental frequency vector (defined in formula (4.8)) and $\boldsymbol{p} = (p_3, p_4, p_5)$ is made by three so called "dummy variables", which are conjugated to the angles $\boldsymbol{q}$. The role they play is made clear by the equations of motion for the innermost planet, which write in the following way

[6]This replacement of symbols has been done just in order to write three pairs of canonical coordinates as (p_j, q_j), $j = 3,\, 4,\, 5$, in agreement with the traditional notation that is adopted in many treatises about Hamiltonian mechanics.

in the framework of the restricted quasi-periodic secular approximation:

$$\begin{cases} \dot{q}_3 = \partial \mathcal{H}_{sec,\,2+\frac{3}{2}}/\partial p_3 = \omega_3 \\ \dot{q}_4 = \partial \mathcal{H}_{sec,\,2+\frac{3}{2}}/\partial p_4 = \omega_4 \\ \dot{q}_5 = \partial \mathcal{H}_{sec,\,2+\frac{3}{2}}/\partial p_5 = \omega_5 \\ \dot{\xi}_1 = -\partial \mathcal{H}_{sec,\,2+\frac{3}{2}}/\partial \eta_1 = -\partial\big(\mathcal{H}^{1-2}_{sec} + \mathcal{H}^{1-3}_{sec}\big)/\partial \eta_1 \\ \dot{\eta}_1 = \partial \mathcal{H}_{sec,\,2+\frac{3}{2}}/\partial \xi_1 = \partial\big(\mathcal{H}^{1-2}_{sec} + \mathcal{H}^{1-3}_{sec}\big)/\partial \xi_1 \\ \dot{P}_1 = -\partial \mathcal{H}_{sec,\,2+\frac{3}{2}}/\partial Q_1 = -\partial\big(\mathcal{H}^{1-2}_{sec} + \mathcal{H}^{1-3}_{sec}\big)/\partial Q_1 \\ \dot{Q}_1 = \partial \mathcal{H}_{sec,\,2+\frac{3}{2}}/\partial P_1 = \partial\big(\mathcal{H}^{1-2}_{sec} + \mathcal{H}^{1-3}_{sec}\big)/\partial P_1 \end{cases} . \tag{4.16}$$

Due to the occurrence of the term $\boldsymbol{\omega} \cdot \boldsymbol{p}$ in the Hamiltonian $\mathcal{H}_{sec,\,2+\frac{3}{2}}$, the first three equations admit $\boldsymbol{q}(t) = \boldsymbol{\omega} t$ as a solution, in agreement with formulæ (4.7) and (4.15). This allows to reinject the wanted quasi-periodic time-dependence in the Fourier approximations $\xi_2(\boldsymbol{q})$, $\eta_2(\boldsymbol{q})$, ... $P_3(\boldsymbol{q})$, $Q_3(\boldsymbol{q})$. As a matter of fact, we do not need to compute the evolution of $(p_3(t), p_4(t), p_5(t))$ because they do not exert any influence on the motion of υ-And **b**; they are needed just if one is interested in checking that the energy is preserved, because it is given by the evaluation of $\mathcal{H}_{sec,\,2+\frac{3}{2}}$.

Finally, note that, in order to produce a restricted quasi-periodic secular model, it is also possible to apply a *closed-form averaging* (Chapter 2, subsection 2.2.1) instead of the method previously described in the present section. In Appendix D there is a comparison between the dynamics of the innermost planet as obtained from the numerical integrations of the system of equations (4.16) with the corresponding one generated by a multipolar expansion of the Hamiltonian jointly with closed-form averaging. The good agreement between these two methods allows us to conclude that both of them can be used in the preliminary definitions of the model yielding essentially equivalent results for what concerns the stability of the secular dynamics of υ-And **b**.

4.3.1 Numerical validation of the SQPR model

In order to validate our secular quasi-periodic restricted (hereafter SQPR) model describing the dynamics of υ-And **b**, we want to compare the numerical integrations of the complete 4BP with the ones of the equations of motions (4.16). Let us recall that the chosen values of parameters and initial conditions for the two outer planets are given in Table 4.1. For what concerns the orbital elements of the innermost planet υ-And **b**, both the inclination i_1 and the longitude of the ascending node Ω_1 are unknown (see, e.g., [78]). The available data for υ-And **b** are reported in Table 4.6. Among the possible values of the initial orbital parameters of υ-And **b**, we have chosen a_1, e_1, M_1 and ω_1 as in the stable prograde trial PRO2 described in [18]. They are reported in Table 4.7 and are compatible with the available ranges of values appearing in Table 4.6. Let us recall that the dynamical evolution of the SQPR model does not depend on the mass of υ-And **b**, therefore, the choice about its value is not reported in Table 4.7. For what concerns the unknown initial values of the inclination and of the longitude of nodes, we have decided to vary them so as to cover a 2D regular grid of values $(\mathrm{i}_1(0), \Omega_1(0)) \in I_\mathrm{i} \times I_\Omega = [6.865°, 34°] \times [0°, 360°]$, dividing I_i and I_Ω, respectively, in 20 and 60 sub-intervals; this means that the widths of the grid-steps are equal to 1.35675° and 6° in inclination and longitude of nodes, respectively. Let us recall that the lowest possible value of the interval I_i, i.e. $\mathrm{i}_2(0) = 6.865°$, corresponds to the inclination of υ-And **c**. Considering values smaller than $\mathrm{i}_2(0)$ could be incoherent with the assumptions leading to the SPQR model we have just introduced; indeed, the factor $1/\sin(\mathrm{i}_1(0))$ increases the mass of the exoplanet by one order of magnitude with respect to the minimal one. Therefore, for small values of $\mathrm{i}_1(0)$ the mass of υ-And **b** could become so large that the effects exerted by its gravitational attraction on the outer exoplanets could not be neglected anymore. On the other hand, it will be shown in the sequel that the stability region for the orbital motion of υ-And **b** nearly completely disappears for values of $i_1(0)$ larger than 34°. These are the reasons behind our choice about the lower and upper limits of I_i.

We emphasize that the study of the stability domain, as is deduced by the numerical integrations, can help us to obtain information about the possible ranges of the unknown values $(\mathrm{i}_1(0), \Omega_1(0))$. Moreover, the comparisons between the numerical integrations of the complete 4BP and the ones of the SQPR model aim to demonstrate that the agreement is sufficiently good so that it becomes possible to directly work with the latter Hamiltonian model, that has to be considered easier than the former, because the degrees of freedom are $2 + 3/2$ instead of 9.

	υ-And **b**
$m \sin(\mathrm{i})\,[M_J]$	0.69 ± 0.016
$a(0)\,[AU]$	0.0594 ± 0.0003
$\mathrm{e}(0)$	0.012 ± 0.005
$\omega(0)\,[^\circ]$	44.106 ± 25.561

Table 4.6: Available data for the orbital parameters of the exoplanet υ-And **b**. The values above are reported from Table 13 of [78].

	υ-And **b**
$a(0)\,[AU]$	0.0594
$\mathrm{e}(0)$	0.011769
$M(0)\,[^\circ]$	103.53
$\omega(0)\,[^\circ]$	51.14

Table 4.7: Values of the initial orbital parameters for υ-And **b** as they have been selected in the stable prograde trial PRO2 of [18].

4.3.1.1 Numerical integration of the complete 4-body problem

For each pair of values $(\mathrm{i}_1(0), \Omega_1(0)) \in I_\mathrm{i} \times I_\Omega$ ranging in the 20×60 regular grid we have previously prescribed, we first compute the corresponding initial orbital elements of the three exoplanets in the Laplace-reference frame, then we perform the numerical integration of the complete 4BP Hamiltonian (4.10) by using the symplectic method of type $\mathcal{SBAB}_3$. Contrary to the SPQR model, the numerical integrations in the full 4BP are affected by the mass of υ-And **b**; its value is simply fixed in such a way that $m_1 = 0.674/\sin(\mathrm{i}_1(0))$.

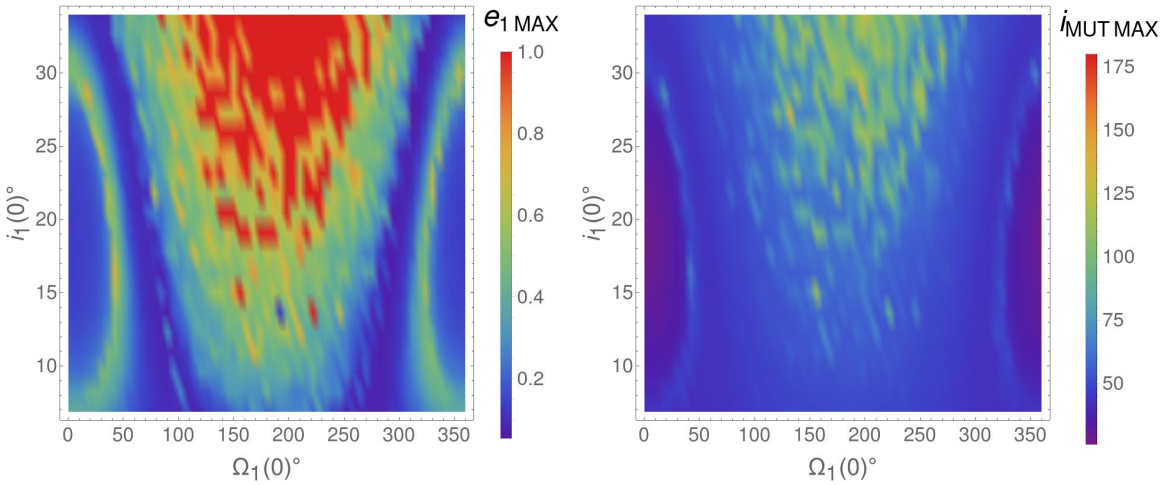

Figure 4.3: Color-grid plots of the maximal value reached by the eccentricity of υ-And **b** (on the left) and by the mutual inclination between υ-And **b** and υ-And **c** (on the right). The maxima are computed during the symplectic numerical integrations of the 4BP which cover a timespan of 10^5 yr.

The largest value reached by the eccentricity can be considered as a very simple numerical indicator about the stability of the orbital configurations. The maximum eccentricity obtained along each of the 21×60 numerical integrations is reported in the left panel of Figure 4.3. In particular, since we are interested in initial conditions leading to regular behaviour, i.e. avoiding

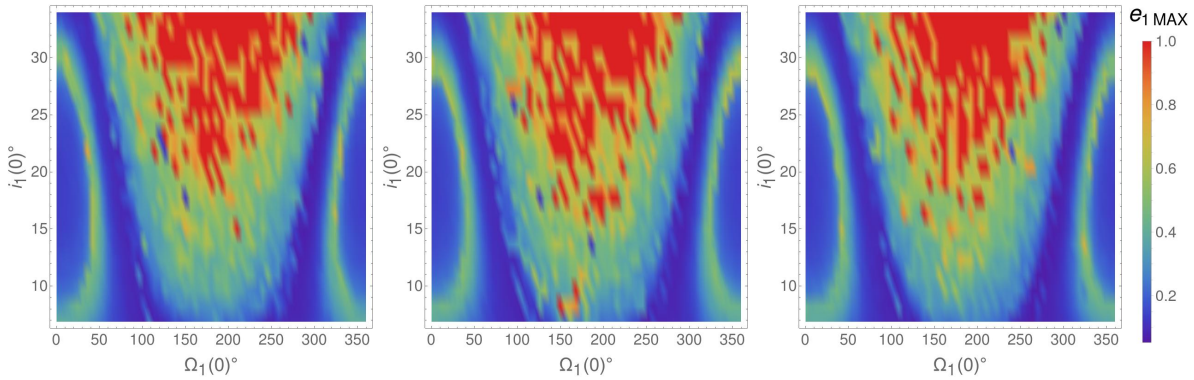

Figure 4.4: Color-grid plots of the maximal value reached by the eccentricity of υ-And **b**. The maxima are computed during the symplectic numerical integrations of the 4BP which cover a timespan of 10^5 yr. The results are obtained by numerical integrations which refer to sets of initial conditions that differ (passing from one panel to another) just because of the choice of the initial values of the mean anomaly; from left to right the plots refer to $M_1(0)$ equal to 51.4286°, 205.714°, and 308.571°, respectively.

quasi-collisions, every time that the eccentricity e_1 exceeds a threshold value (fixed to be equal to 0.85), in the color-code plots its maximal value is arbitrarily set equal to one. Moreover, since we expect that υ-And **c** is the most massive planet in that extrasolar system and being it the closest one to υ-And **b**, it is natural to focus the attention also on the mutual inclination between υ-And **b** and υ-And **c**. Let us recall that it is defined in such a way that

$$\cos(\mathrm{i}_{mut_{\mathbf{bc}}}) = \cos(\mathrm{i}_1)\cos(\mathrm{i}_2) + \sin(\mathrm{i}_1)\sin(\mathrm{i}_2)\cos(\Omega_1 - \Omega_2)\,; \tag{4.17}$$

therefore, for each numerical integration it is also possible to compute the maximal value reached by $\mathrm{i}_{mut_{\mathbf{bc}}}$. The results are reported in the right panel of Figure 4.3. In both those panels the color-grid plots are provided as functions of the initial values of the longitude of nodes Ω_1 and the inclination i_1, which are reported on the x and y axes, respectively. By comparing the two plots in the Figure panels 4.3a and 4.3b, one can easily distinguish the regions which have to be considered as dynamically unstable because the eccentricity e_1 can grow to large values corresponding also to large mutual inclinations of the planetary orbits of υ-And **b** and υ-And **c**.

We remark that the value of the initial mean anomaly $M_1(0)$ is missing among the available observational data reported in Table 4.6. As a matter of fact, mean anomalies of exoplanets are in general so poorly known that usually their values are not reported in the public databases.[7] However, in order to understand if (and up to what extent) the initial value $M_1(0)$ can affect the dynamics of υ-And **b**, we repeat all the numerical integrations of the 4BP for four different initial values of M_1, chosen so as to have one of them belonging to each of the quadrants $[0°, 90°]$, $[90°, 180°]$, $[180°, 270°]$ and $[270°, 360°]$. In Figure 4.4 we report three examples; in particular, they show the color-grid plots of the maximal value reached by the eccentricity e_1, taking $M_1(0)$ as $360°/7 = 51.4286°$, $4 \cdot 360°/7 = 205.714°$ and $6 \cdot 360°/7 = 308.571°$, respectively. For what concerns the region $[90°, 180°]$, let us recall that Figure 4.3a refers to $M_1(0) = 103.53°$. The comparison between Figures 4.3a and 4.4 shows that the choice of the value of $M_1(0)$ does not seem to produce any remarkable impact on the global structure of the dinamical stability of these exoplanetary orbits. Moreover, the same conclusion applies also to the increasing factor $1/\sin(\mathrm{i}_1(0))$ (with $\mathrm{i}_1(0) \in I_\mathrm{i}$) which multiplies the minimal mass of υ-And **b** in such a way to determine the value of m_1. In fact, substantial differences are not observed between Figures 4.3 and 4.5.

[7] See, e.g., `http://exoplanet.eu/`

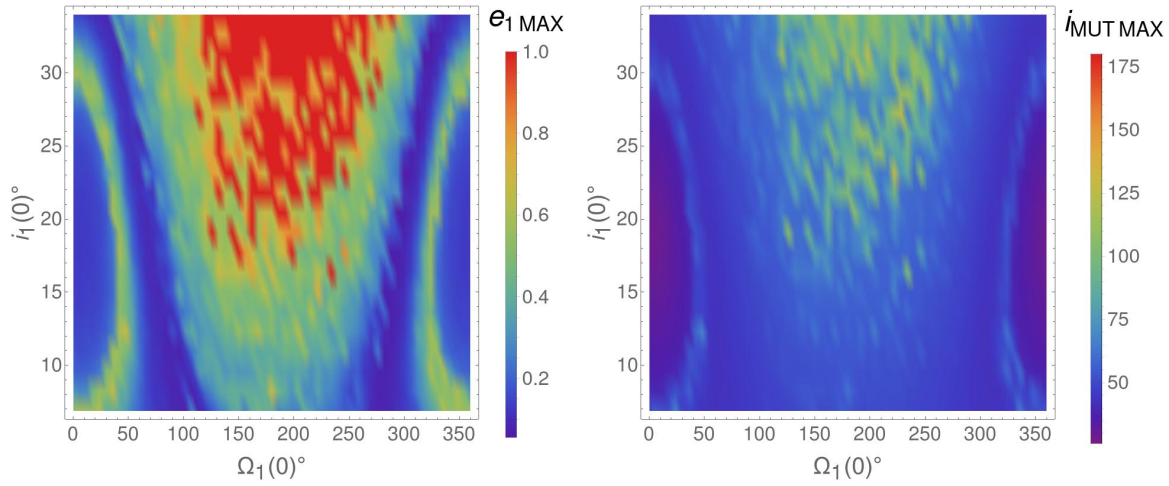

Figure 4.5: Color-grid plots of the maximal value reached by the eccentricity of υ-And **b** (on the left) and by the mutual inclination between υ-And **b** and υ-And **c** (on the right). The maxima are computed during the symplectic numerical integrations of the 4BP which cover a timespan of 10^5 yr. As the only difference with respect to the numerical integration whose results are reported in Figure 4.3, here the mass of υ-And **b** is always kept fixed so as to be equal to its minimal value $m_1 = 0.674$.

4.3.1.2 Numerical integration of the secular quasi-periodic restricted model

We want now to compare the previous results with those found in the SQPR approximation of the 4-body problem, performing numerical integrations of the system of equations (4.16). In order to make these comparisons coherent, also here we consider the data listed in Table 4.7 as initial conditions for the orbital elements of υ-And **b** which are completed with the values of $(\mathrm{i}_1(0)\,, \Omega_1(0))$ ranging in the regular 20×60 grid that covers $I_\mathrm{i} \times I_\Omega = [6.865°, 34°] \times [0°, 360°]$. At the beginning of the computational procedure, the initial values of the orbital elements are determined in the Laplace reference frame, which is fixed by taking into account *only* of the two outermost planets (i.e., the total angular momentum of the system is given *only* by the sum of the angular momentum of υ-And **c** and υ-And **d**). Of course, this is made in agreement with our choice to consider a *restricted* framework, because we are assuming that the mass of υ-And **b** is so small that can be neglected.

For each numerical integration we compute the maximal value reached by the eccentricity e_1 and the mutual inclination $\mathrm{i}_{mut_{\mathbf{bc}}}$. The results are reported in the color-grid plots of the left and right panels of Figure 4.6, respectively. Once again, they are provided as functions of $\Omega_1(0)$ and $\mathrm{i}_1(0)$, whose values appear on the x and y axes, respectively.

Comparing Figures 4.3a with 4.6a and 4.3b with 4.6b, respectively, we can immediately conclude the striking similarity of the color-grid plots, implying the same dependence of the dynamics on the initial values of the orbital elements $\mathrm{i}_1(0)$ and $\Omega_1(0)$ in either model. In particular, the regions of stability located at the two lateral sides of the plots are the same, where the orbit of υ-And **b** does not become very eccentric. This occurs also for what concerns the plots of the maximal mutual inclination. However, some discrepancies are evident in the central parts of the panels i.e., for values of $\Omega_1(0)$ ranging between 90° and 270°. We stress that this lack of agreement between the results provided by the two models is expected in these central regions of the panels. Indeed, let us recall that the SQPR model has been introduced starting from some classical expansions in powers of eccentricities and inclinations. Therefore, it is reasonable to expect a deterioration of the accuracy of the SQPR model in the orbital dynamics depicted in the central regions of the plots where large values of the eccentricity e_1 and the mutual inclination are attained. We emphasize that similar

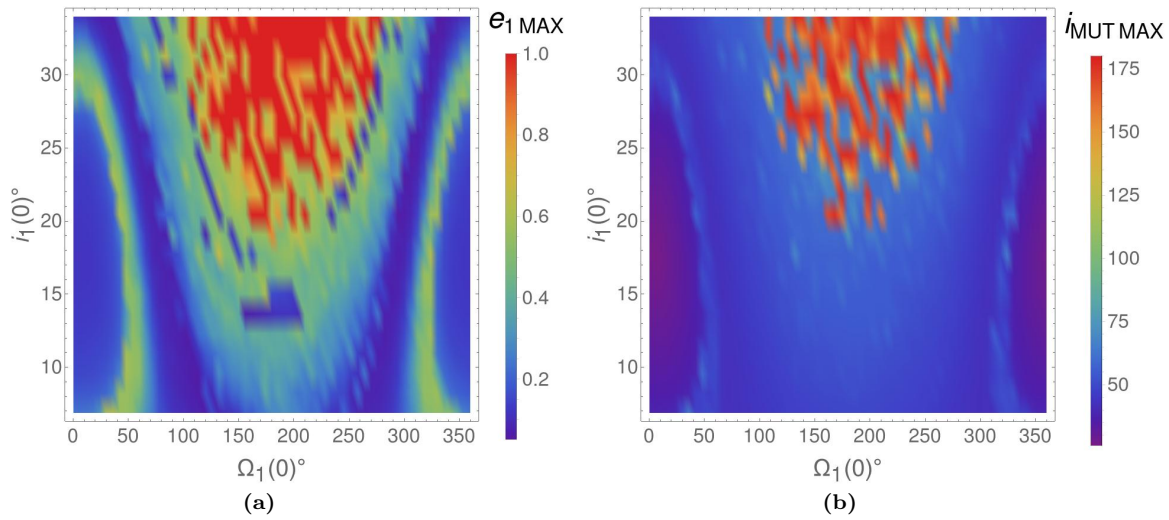

Figure 4.6: Color-grid plots of the maximal value reached by the eccentricity of υ-And **b** (on the left) and by the mutual inclination between υ-And **b** and υ-And **c** (on the right). The maxima are computed along the RK4 numerical integrations of the equations of motion (4.16) of the SQPR model, covering a timespan of 10^5 yr.

remarks about the very strong impact of the initial value $\Omega_1(0)$ on the orbital stability of υ-And **b** can be found in section 4.2 of [93].

A further exploration of the stable and chaotic regions of Figure 4.6a can be done by applying the so called Frequency Map Analysis method (see, e.g., [49]), in order to study the signal $\xi_1(t) + i\eta_1(t)$ produced by the numerical integration of the system (4.16), i.e., in the SQPR approximation. We perform the numerical integrations as prescribed at the beginning of the present section, taking into account only a few values in I_{i} for the initial inclinations, i.e., $\mathrm{i}_1(0) = 6.865°, 8.22175°, 9.5785°, 10.9353°$ and $\Omega_1(0) \in I_\Omega$. In Figure 4.7 we report the behaviour of the angular velocity corresponding to the first component of the approximation of $\xi_1(t) + i\eta_1(t)$, as obtained by applying the FA computational algorithm; therefore, this quantity is related to the precession rate of ϖ_1. As initial value for the inclination $\mathrm{i}_1(0)$ we fix $6.865°$ for Figure 4.7a and $10.9353°$ for Figure 4.7b. We do not report the cases $(\mathrm{i}_1(0), \Omega_1(0)) \in \{8.22175°, 9.5785°\} \times I_\Omega$, since the behaviour of those plots is similar to the ones in Figure 4.7.

The situation is well described in Figure 4.7b and analogous considerations can be done for Figure 4.7a. For what concerns the values of $\Omega_1(0)$ in the range $[0, \sim 50°]$ and $[\sim 325°, 360°]$ we can observe a regular behaviour of the angular velocity ν which is also monotone with the only exception of the local minimum. According to the interpretation of the Frequency Map Analysis (in the light of KAM theory), such a regular regime is due to the presence of many invariant tori which fill the stability region located at the two lateral sides of the plot 4.6a. Instead for values of $\Omega_1(0)$ in $[\sim 50°, \sim 70°]$ and $[\sim 300°, \sim 325°]$ and $\Omega_1(0)$ in $[\sim 120°, \sim 270°]$ we observe a strongly irregular behaviour, which corresponds to the lateral green stripes and the internal region of Figure 4.6a. Thus, they represent chaotic regions in proximity of a secular resonance. Indeed, in Figure 4.7b the angular velocity is constant for values of $\Omega_1(0)$ in $[\sim 70°, \sim 85°]$ and $[\sim 280°, \sim 300°]$ (corresponding to part of the blue central stripes of Figure 4.6a). More precisely, the value of ν is equal to $\simeq -1.04 \cdot 10^{-3}$, that is ω_4, i.e., one of the fundamental angular velocities which characterize the quasi-periodic motion of the outer planets (see Eq. (4.8)). This allows us to conclude that they represent the stable central part of a resonant region.

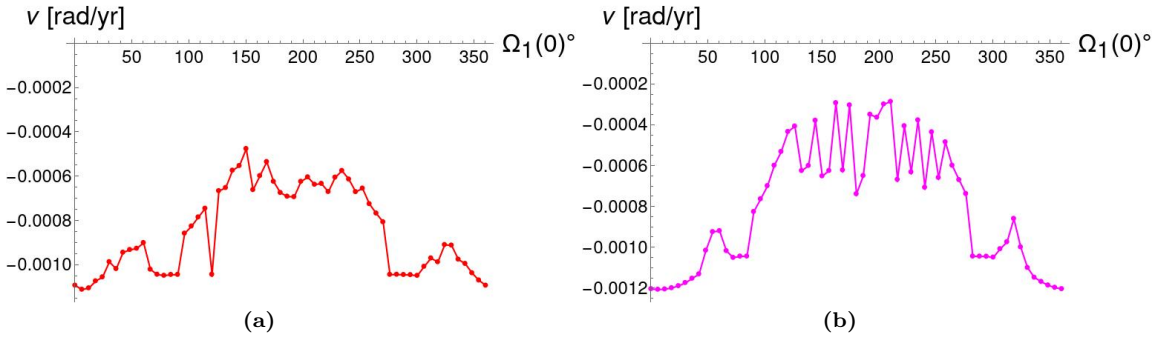

Figure 4.7: Behaviour of the fundamental angular velocity ν as obtained by applying the Frequency Map Analysis method to the signal $\xi_1(t) + i\eta_1(t)$, computed through the RK4 numerical integration of the SQPR model (4.16), covering a timespan of $1.31072 \cdot 10^5$ yr. We take, as initial conditions, $(\mathrm{i}_1(0), \Omega_1(0)) \in \{6.865^\circ\} \times I_\Omega$ for the left panel and $(\mathrm{i}_1(0), \Omega_1(0)) \in \{10.9353^\circ\} \times I_\Omega$ for the right one.

4.4 Introduction of a secular model by a normal form approach

This section aims at manipulating the Hamiltonian with normal form algorithms in order to define a new model that is more compact; this will allow us to simulate the secular dynamics of υ-And **b** with much faster numerical integrations. In fact, we are going to describe a reduction of the number of degrees of freedom (DOF) of our Hamiltonian models. For such a purpose, we apply two normal form methods: first, we will perform the construction of an *elliptic torus*, hence, we will proceed removing the angles (q_3, q_4, q_5) whose evolution is linearly depending on time. The latter elimination will be made by applying a normalization method *à la* Birkhoff in such a way to introduce a so called resonant normal form[8] that includes, at least partially, the long-term effects due to the outer planets' motion.

4.4.1 Normal form algorithm of construction of invariant elliptic tori

In [34] the existence of elliptic tori in 3D planetary problems with n bodies has been proved by using a normal form method which is explicitly constructive. However, such an approach does not look suitable to be directly applied to Hamiltonian secular models, because in this latter case the separation between fast and slow dynamics is lost. Therefore, we follow the explanatory notes [71], where the algorithm constructing the normal form for elliptic tori is compared with the classical one *à la Kolmogorov*, which is at the basis of the original proof scheme of the KAM theorem. We first summarize this general procedure leading to the construction of elliptic tori. We then add some comments explaining how this general method can be suitably adapted to our problem.

We start considering a Hamiltonian $\mathcal{H}^{(0)}$ written as follows:

$$\begin{aligned}\mathcal{H}^{(0)}(\boldsymbol{p},\boldsymbol{q},\boldsymbol{I},\boldsymbol{\alpha}) = \mathcal{E}^{(0)} + \boldsymbol{\omega}^{(0)}\cdot\boldsymbol{p} + \boldsymbol{\Omega}^{(0)}\cdot\boldsymbol{I} + \sum_{s\geq 0}\sum_{l\geq 3} f_l^{(0,s)}(\boldsymbol{p},\boldsymbol{q},\boldsymbol{I},\boldsymbol{\alpha}) \\ + \sum_{s\geq 1} f_0^{(0,s)}(\boldsymbol{q}) + \sum_{s\geq 1} f_1^{(0,s)}(\boldsymbol{q},\boldsymbol{I},\boldsymbol{\alpha}) + \sum_{s\geq 1} f_2^{(0,s)}(\boldsymbol{p},\boldsymbol{q},\boldsymbol{I},\boldsymbol{\alpha}),\end{aligned} \tag{4.18}$$

where $\mathcal{E}^{(0)}$ is a constant term, representing the energy, $(\boldsymbol{p},\boldsymbol{q}) \in \mathbb{R}^{n_1}\times\mathbb{T}^{n_1}$, $(\boldsymbol{I},\boldsymbol{\alpha}) \in \mathbb{R}^{n_2}_{\geq 0}\times\mathbb{T}^{n_2}$ are action-angle variables and $(\boldsymbol{\omega}^{(0)},\boldsymbol{\Omega}^{(0)}) \in \mathbb{R}^{n_1}\times\mathbb{R}^{n_2}$ is the angular velocity vector. The symbol

[8] Resonant normal forms play a relevant role in the proof of the celebrated Nekhoroshev theorem (see, e.g., [31]).

$f_l^{(r,s)}$ is used to denote a function of the variables $(\boldsymbol{p},\boldsymbol{q},\boldsymbol{I},\boldsymbol{\alpha})$, such that l is the total degree in the square root of the actions $(\boldsymbol{p},\boldsymbol{I})$, s is the index such that the maximum trigonometric degree, in the angles $(\boldsymbol{q},\boldsymbol{\alpha})$, is sK (for a fixed positive integer K) and r refers to the normalization step. In more details, we can say that $f_l^{(0,s)} \in \mathfrak{B}_{l,sK}$, which is a class of functions that we introduce as follows.

Definition 4.4.1. *We say that* $g \in \mathfrak{B}_{l,sK}$ *if* $g \in \bigcup_{\substack{\widehat{m}\geq 0,\,\widehat{l}\geq 0\\ 2\widehat{m}+\widehat{l}=l}} \widehat{\mathfrak{B}}_{\widehat{m},\widehat{l},sK}$, *where*

$$\widehat{\mathfrak{B}}_{\widehat{m},\widehat{l},sK} = \Bigg\{ g : \mathbb{R}^{n_1}\times\mathbb{T}^{n_1}\times\mathbb{R}^{n_2}_{\geq 0}\times\mathbb{T}^{n_2}\to\mathbb{R} \;:\; g(\boldsymbol{p},\boldsymbol{q},\boldsymbol{I},\boldsymbol{\alpha}) = \sum_{\substack{\boldsymbol{m}\in\mathbb{N}^{n_1}\\ |\boldsymbol{m}|=\widehat{m}}} \sum_{\substack{\boldsymbol{l}\in\mathbb{N}^{n_2}\\ |\boldsymbol{l}|=\widehat{l}}} \sum_{\substack{\boldsymbol{k}\in\mathbb{Z}^{n_1}\\ |\boldsymbol{k}|+|\widehat{\boldsymbol{l}}|\leq sK}} \sum_{\substack{\widehat{l}_j=-l_j,-l_j+2,\ldots,l_j\\ j=1,\ldots,n_2}} c_{\boldsymbol{m},\boldsymbol{l},\boldsymbol{k},\widehat{\boldsymbol{l}}}\; \boldsymbol{p}^{\boldsymbol{m}} \left(\sqrt{\boldsymbol{I}}\right)^{\boldsymbol{l}} e^{i(\boldsymbol{k}\cdot\boldsymbol{q}+\widehat{\boldsymbol{l}}\cdot\boldsymbol{\alpha})} \Bigg\}.$$

A few remarks about the above definition are in order. First, since we deal with *real* functions, the complex coefficients must be such that $c_{\boldsymbol{m},\boldsymbol{l},-\boldsymbol{k},-\widehat{\boldsymbol{l}}} = \bar{c}_{\boldsymbol{m},\boldsymbol{l},\boldsymbol{k},\widehat{\boldsymbol{l}}}$. Moreover, the rules about the integer coefficients vector $\widehat{\boldsymbol{l}}$ are such that, $\forall\, j = 1,\ldots,n_2$, the j-th component of the Fourier harmonic $\widehat{l}_j$ (that refers to the angle α_j) must have the same parity with respect to the corresponding degree l_j of $\sqrt{I_j}$ and must satisfy the inequality[9] $|\widehat{l}_j| \leq l_j$.

Let us here emphasize that our SQPR model of the secular dynamics of υ-And **b** can be reformulated in such a way as to be described by a Hamiltonian of the type (4.18); this will be explained in detail at the beginning of Section 4.5.

The following statement plays a substantial role, since it ensures that the structure of the functions $f_l^{(r,s)}$ is preserved while the normalization algorithm is iterated.

Lemma 4.4.2. *Let us consider two generic functions* $g \in \mathfrak{B}_{l,sK}$ *and* $h \in \mathfrak{B}_{m,rK}$, *where* K *is a fixed positive integer number. Then*

$$\{g,h\} = L_h\, g \;\in\; \mathfrak{B}_{l+m-2,\,(r+s)K} \qquad \forall\, l,\, m,\, r,\, s \;\in\; \mathbb{N},$$

where we trivially extend the definition 4.4.1 in such a way that $\mathfrak{B}_{-2,\,sK} = \mathfrak{B}_{-1,\,sK} = \{0\}\ \forall\ s \in \mathbb{N}$.

The algorithm constructing the normal form for elliptic tori is applied to Hamiltonians of the type (4.18), where the terms appearing in the second row (namely, $\sum_{s\geq 1}\sum_{l=0}^{2} f_l^{(0,s)}(\boldsymbol{p},\boldsymbol{q},\boldsymbol{I},\boldsymbol{\alpha})$) are considered as the perturbation to remove. Therefore, one can easily realize that such a perturbation must be sufficiently small so that the procedure behaves well as regards convergence. There are general situations where this essential smallness condition is satisfied. For instance, this occurs for Hamiltonian systems in the neighborhood of a stable equilibrium point; in fact, it is possible to prove that, $f_l^{(0,s)} = \mathcal{O}(\varepsilon^s)$, where ε is a small parameter which denotes the first approximation of the distance (expressed in terms of the actions) between the elliptic torus and the stable equilibrium point. The elimination of the small perturbing terms can be done through a sequence of canonical transformations, leading the Hamiltonian in the following final form:

$$\mathcal{H}^{(\infty)}(\tilde{\boldsymbol{p}},\tilde{\boldsymbol{q}},\tilde{\boldsymbol{I}},\tilde{\boldsymbol{\alpha}}) = \mathcal{E}^{(\infty)} + \boldsymbol{\omega}^{(\infty)}\cdot\tilde{\boldsymbol{p}} + \boldsymbol{\Omega}^{(\infty)}\cdot\tilde{\boldsymbol{I}} + \sum_{s\geq 0}\sum_{l\geq 3} f_l^{(\infty,s)}(\tilde{\boldsymbol{p}},\tilde{\boldsymbol{q}},\tilde{\boldsymbol{I}},\tilde{\boldsymbol{\alpha}}), \tag{4.19}$$

[9] These rules are inherited from the polynomial structure of the canonical coordinates describing the small oscillations that are transverse to the elliptic torus. For istance, it is easy to verify that the restrictions on the indexes appearing in definition 4.4.1 is satisfied when the change of variables (4.52) is plugged into the Hamiltonian (4.14).

with $f_l^{(\infty,s)} \in \mathfrak{B}_{l,sK}$. Therefore, for any initial conditions of type $(\mathbf{0}, \tilde{\boldsymbol{q}}_0, \mathbf{0}, \tilde{\boldsymbol{\alpha}})$ (where $\tilde{\boldsymbol{q}}_0 \in \mathbb{T}^{n_1}$ and the value of $\tilde{\boldsymbol{\alpha}} \in \mathbb{T}^{n_2}$ does not play any role[10]), the motion law $(\tilde{\boldsymbol{p}}(t), \tilde{\boldsymbol{q}}(t), \tilde{\boldsymbol{I}}(t), \tilde{\boldsymbol{\alpha}}(t)) = (\mathbf{0}, \tilde{\boldsymbol{q}}_0 + \boldsymbol{\omega}^{(\infty)} t, \mathbf{0}, \tilde{\boldsymbol{\alpha}})$ is a solution of the Hamilton's equations related to $\mathcal{H}^{(\infty)}$. This quasi-periodic solution (having $\boldsymbol{\omega}^{(\infty)}$ as constant angular velocity vector) lies on the n_1-dimensional invariant torus such that the values of the action coordinates are $\tilde{\boldsymbol{p}} = \mathbf{0}$, $\tilde{\boldsymbol{I}} = \mathbf{0}$.

The generic r-th step of the algorithm is defined as follows. Let us assume that after $r-1$ normalization steps the expansion of the Hamiltonian can be written as

$$\begin{aligned}\mathcal{H}^{(r-1)}(\boldsymbol{p},\boldsymbol{q},\boldsymbol{I},\boldsymbol{\alpha}) = \mathcal{E}^{(r-1)} + \boldsymbol{\omega}^{(r-1)}\cdot\boldsymbol{p} + \boldsymbol{\Omega}^{(r-1)}\cdot\boldsymbol{I} + \sum_{s\geq 0}\sum_{l\geq 3} f_l^{(r-1,s)}(\boldsymbol{p},\boldsymbol{q},\boldsymbol{I},\boldsymbol{\alpha}) \\ + \sum_{s\geq r} f_0^{(r-1,s)}(\boldsymbol{q}) + \sum_{s\geq r} f_1^{(r-1,s)}(\boldsymbol{q},\boldsymbol{I},\boldsymbol{\alpha}) + \sum_{s\geq r} f_2^{(r-1,s)}(\boldsymbol{p},\boldsymbol{q},\boldsymbol{I},\boldsymbol{\alpha})\,,\end{aligned} \tag{4.20}$$

with $f_l^{(r-1,s)} \in \mathfrak{B}_{l,sK}$. For a better understanding of the normalization algorithm, we think it is convenient to refer to a graphical scheme of the expansion, that can be easily visualized as in Table 4.8. By comparing formula (4.18) with (4.20) (and also with the scheme in Table 4.8), one immediately realizes that the assumption above is satisfied in the case with $r = 1$ for what concerns the expansion of the initial Hamiltonian $\mathcal{H}^{(0)}$.

$$\mathcal{H}^{(r-1)} = \sum \begin{array}{|ccccccc|c}
\vdots & \vdots & \vdots & \vdots & \vdots & \vdots & \vdots & \vdots \\
f_4^{(r-1,0)} & f_4^{(r-1,1)} & \dots & f_4^{(r-1,r-1)} & f_4^{(r-1,r)} & f_4^{(r-1,r+1)} & \dots & \leftarrow 4 \\
f_3^{(r-1,0)} & f_3^{(r-1,1)} & \dots & f_3^{(r-1,r-1)} & f_3^{(r-1,r)} & f_3^{(r-1,r+1)} & \dots & \leftarrow 3 \\
\boldsymbol{\omega}^{(r-1)}\cdot\boldsymbol{p} + \boldsymbol{\Omega}^{(r-1)}\cdot\boldsymbol{I} & 0 & \dots & 0 & f_2^{(r-1,r)} & f_2^{(r-1,r+1)} & \dots & \leftarrow 2 \\
0 & 0 & \dots & 0 & f_1^{(r-1,r)} & f_1^{(r-1,r+1)} & \dots & \leftarrow 1 \\
\mathcal{E}^{(r-1)} & 0 & \dots & 0 & f_0^{(r-1,r)} & f_0^{(r-1,r+1)} & \dots & \leftarrow 0 \\
\hline
\uparrow & \uparrow & \dots & \uparrow & \uparrow & \uparrow & \dots & \\
0 & 1 & & r-1 & r & r+1 & &
\end{array}$$

Degree in square root of the actions:

Trigonometric degree/K:

Table 4.8: Graphical representation of the expansion of the Hamiltonian after $r-1$ normalization steps.

The r-th normalization step consists of three substeps, each of them is involving a canonical transformation which is expressed in terms of the Lie series having $\chi_0^{(r)}$, $\chi_1^{(r)}$, $\chi_2^{(r)}$ as generating function, respectively. Therefore, the new Hamiltonian that is introduced at the end of the r-th normalization step is defined as follows:

$$\mathcal{H}^{(r)} = \exp\left(L_{\chi_2^{(r)}}\right)\exp\left(L_{\chi_1^{(r)}}\right)\exp\left(L_{\chi_0^{(r)}}\right)\mathcal{H}^{(r-1)}\,. \tag{4.21}$$

First substep (of the r-th normalization step)

The first substep aims to remove the term depending only on the angles[11] $\boldsymbol{q}$ up to trigonometric degree rK, i.e., $f_0^{(r-1,r)}$ (included in the first sum of the second row of (4.20)), which has to be

[10] Indeed, when $\tilde{\boldsymbol{I}} = \mathbf{0}\ \forall\,\tilde{\boldsymbol{\alpha}} \in \mathbb{T}^{n_2}$, the canonical coordinates $(\sqrt{2\tilde{I}_j}\cos(\tilde{\alpha}_j)\,,\ \sqrt{2\tilde{I}_j}\sin(\tilde{\alpha}_j))$ are mapped into the origin of the j-th subspace that is transversal to the elliptic torus. This fictitious singularity of the action-angle variables $(\boldsymbol{I},\boldsymbol{\alpha})$ is completely harmless just because all the normalization algorithm can be performed working on Hamiltonians whose expansions are made by terms belonging to sets of functions of type $\mathfrak{B}_{l,sK}$. We stress that all the algorithm could be reformulated using polynomial canonical coordinates to describe the dynamics in the subspaces transversal to the elliptic torus; in particular, this is done with complex pairs of canonical coordinates in [7]. In the sequel, we adopt an exposition entirely based on the use of the action-angle coordinates, which makes the algorithm easier to understand.

[11] This first substep of the algorithm is basically useless when the explicit construction of the normal form related to an elliptic torus is started from the Hamiltonian $\mathcal{H}_{sec,\,2+3/2}$ described in (4.53). Indeed, in the case under study

considered as $\mathcal{O}(\varepsilon^r)$. The first generating function $\chi_0^{(r)}(\boldsymbol{q})$ is determined by solving the following homological equation:

$$\{\boldsymbol{\omega}^{(r-1)}\cdot\boldsymbol{p},\chi_0^{(r)}\}+f_0^{(r-1,r)}(\boldsymbol{q})=\left\langle f_0^{(r-1,r)}\right\rangle_{\boldsymbol{q}}\,. \tag{4.22}$$

Since $f_0^{(r-1,r)}\in\mathfrak{B}_{0,rK}$, its Fourier expansion can be written $f_0^{(r-1,r)}(\boldsymbol{q})=\sum_{|k|\leq rK}c_{\boldsymbol{k}}^{(r-1)}e^{i\boldsymbol{k}\cdot\boldsymbol{q}}$. Because of the homological equation (4.22), we find

$$\chi_0^{(r)}(\boldsymbol{q})=\sum_{0<|k|\leq rK}\frac{c_{\boldsymbol{k}}^{(r-1)}}{i\,\boldsymbol{k}\cdot\boldsymbol{\omega}^{(r-1)}}e^{i\boldsymbol{k}\cdot\boldsymbol{q}}\,; \tag{4.23}$$

the above solution is well defined if the non-resonance condition

$$\boldsymbol{k}\cdot\boldsymbol{\omega}^{(r-1)}\neq 0\qquad\forall\,0<\boldsymbol{k}\leq rK$$

is satisfied. We can now apply the Lie series operator $\exp\left(L_{\chi_0^{(r)}}\right)$ to $\mathcal{H}^{(r-1)}$. This allows us to write the expansion of the new intermediate Hamiltonian as follows:

$$\begin{aligned}\mathcal{H}^{(I;\,r)}(\boldsymbol{p},\boldsymbol{q},\boldsymbol{I},\boldsymbol{\alpha})&=\exp\left(L_{\chi_0^{(r)}}\right)\mathcal{H}^{(r-1)}\\&=\mathcal{E}^{(r)}+\boldsymbol{\omega}^{(r-1)}\cdot\boldsymbol{p}+\boldsymbol{\Omega}^{(r-1)}\cdot\boldsymbol{I}+\sum_{s\geq 0}\sum_{l\geq 3}f_l^{(I;\,r,s)}(\boldsymbol{p},\boldsymbol{q},\boldsymbol{I},\boldsymbol{\alpha})\\&\quad+\sum_{s\geq r}f_0^{(I;\,r,s)}(\boldsymbol{q})+\sum_{s\geq r}f_1^{(I;\,r,s)}(\boldsymbol{q},\boldsymbol{I},\boldsymbol{\alpha})+\sum_{s\geq r}f_2^{(I;\,r,s)}(\boldsymbol{p},\boldsymbol{q},\boldsymbol{I},\boldsymbol{\alpha})\,,\end{aligned} \tag{4.24}$$

where (by abuse of notation) for the new canonical coordinates we have adopted the same symbols as the old ones; moreover, new Hamiltonian terms appearing in the expansion above are defined so that

$$\begin{aligned}f_0^{(I;\,r,s)}&=f_0^{(I;\,r-1,s)}&&r+1\leq s\leq 2r-1\,,\\f_l^{(I;\,r,s)}&=\sum_{j=0}^{\lfloor s/r\rfloor}\frac{1}{j!}L^j_{\chi_0^{(r)}}f_{l+2j}^{(r-1,s-jr)}&&l=0,\ s\geq 2r\ \text{ or }\ l=1,2,\ s\geq r\ \text{ or }\ l\geq 3,\ s\geq 0\,,\end{aligned} \tag{4.25}$$

while, due to the homological equation (4.22), we set $f_0^{(I;\,r,r)}=0$ and update the energy value in such a way that $\mathcal{E}^{(r)}=\mathcal{E}^{(r-1)}+\left\langle f_0^{(r-1,r)}\right\rangle_{\boldsymbol{q}}$, where $\langle\cdot\rangle_{\boldsymbol{q}}$ is used to denote the angular average with respect to $\boldsymbol{q}$. From a practical point of view, it can be more comfortable to refer to another formulation of the definitions above, which is structured in such a way to mimic more closely what is usually done in any programming language. In fact, in can be convenient to first define the new summands as the old ones, so that $f_l^{(I;\,r,s)}=f_l^{(r-1,s)}\ \forall\,l\geq 0\,,\ s\geq 0$. Hence, each term generated by Lie derivatives with respect to $\chi_0^{(r)}$ is added to the corresponding class of functions. By a further abuse of notation, this is made by the following sequence[12] of redefinitions:

$$f_{l-2j}^{(I;\,r,s+jr)}\hookleftarrow\frac{1}{j!}L^j_{\chi_0^{(r)}}f_l^{(r-1,s)}\qquad\forall\,l\geq 0,\,1\leq j\leq\lfloor l/2\rfloor,\,s\geq 0\,, \tag{4.26}$$

where with the notation $a\hookleftarrow b$ we mean that the quantity a is redefined so as to be equal $a+b$. In fact, since $\chi_0^{(r)}\in\mathfrak{B}_{0,rK}$, Lemma 4.4.2 ensures that each application of the Lie derivative operator

just the so called dummy actions are affected by this kind of canonical change of variables, which is defined by a Lie series with a generating function depending on the angles $\boldsymbol{q}$ only. Aiming to make a rather general discussion of the computational procedure, we keep in the algorithm the description of this first normalization substep.

[12] From a practical point of view, since we have to deal with series truncated in such a way that the index s goes up to a fixed order called $\mathcal{N}_S$, we have to require also that $1\leq j\leq\min\left\{\lfloor l/2\rfloor,\lfloor(\mathcal{N}_S-s)/r\rfloor\right\}$.

$L_{\chi_0^{(r)}}$ decreases by 1 the degree in $\boldsymbol{p}$ (that is obviously equivalent to 2 in the square root of the actions), while the trigonometrical degree in the angles $\boldsymbol{q}$ is increased by rK. By using repeatedly such a simple rule, one can easily verify that $f_l^{(I;\,r,s)} \in \mathfrak{B}_{l,sK}\ \forall\, l \geq 0,\ s \geq 0$.

At the end of this first normalization substep, the new Hamiltonian can be easily visualized as in the scheme reported in Table 4.9.

$$\mathcal{H}^{(I;\,r)} = \sum$$

							Degree in square root of the actions:
$\vdots$	$\vdots$	$\vdots$	$\vdots$	$\vdots$	$\vdots$	$\vdots$	$\vdots$
$f_4^{(I;\,r,0)}$	$f_4^{(I;\,r,1)}$	$\dots$	$f_4^{(I;\,r,r-1)}$	$f_4^{(I;\,r,r)}$	$f_4^{(I;\,r,r+1)}$	$\dots$	$\leftarrow 4$
$f_3^{(I;\,r,0)}$	$f_3^{(I;\,r,1)}$	$\dots$	$f_3^{(I;\,r,r-1)}$	$f_3^{(I;\,r,r)}$	$f_3^{(I;\,r,r+1)}$	$\dots$	$\leftarrow 3$
$\boldsymbol{\omega}^{(r-1)}\cdot\boldsymbol{p}+\boldsymbol{\Omega}^{(r-1)}\cdot\boldsymbol{I}$	0	$\dots$	0	$f_2^{(I;\,r,r)}$	$f_2^{(I;\,r,r+1)}$	$\dots$	$\leftarrow 2$
0	0	$\dots$	0	$f_1^{(I;\,r,r)}$	$f_1^{(I;\,r,r+1)}$	$\dots$	$\leftarrow 1$
$\mathcal{E}^{(r)}$	0	$\dots$	0	0	$f_0^{(I;\,r,r+1)}$	$\dots$	$\leftarrow 0$
Trigonometric degree/K:							
$\uparrow$	$\uparrow$	$\dots$	$\uparrow$	$\uparrow$	$\uparrow$	$\dots$	
0	1		$r-1$	r	$r+1$		

Table 4.9: Graphical representation of the expansion of the Hamiltonian after the first substep (of the r-th normalization step).

Second substep (of the r-th normalization step)

The second substep aims to remove the term that is linear in $\sqrt{\boldsymbol{I}}$ and independent of $\boldsymbol{p}$, i.e., $f_1^{(I;r,r)}$, which is included in the second sum appearing in the second row of (4.24). The second generating function $\chi_1^{(r)}(\boldsymbol{q},\boldsymbol{I},\boldsymbol{\alpha})$ is determined solving the following homological[13] equation:

$$\{\boldsymbol{\omega}^{(r-1)}\cdot\boldsymbol{p}+\boldsymbol{\Omega}^{(r-1)}\cdot\boldsymbol{I},\chi_1^{(r)}\}+f_1^{(I;\,r,r)}(\boldsymbol{q},\boldsymbol{I},\boldsymbol{\alpha})=0\,. \tag{4.27}$$

Since $f_1^{(I;\,r,r)} \in \mathfrak{B}_{1,rK}$, we can write its expansion as

$$\begin{aligned} f_1^{(I;\,r,r)}(\boldsymbol{q},\boldsymbol{I},\boldsymbol{\alpha}) &= \sum_{\substack{\boldsymbol{l}\in\mathbb{N}^{n_2}\\ |\boldsymbol{l}|=1}} \sum_{\substack{\boldsymbol{k}\in\mathbb{Z}^{n_1}\\ |\boldsymbol{k}|+|\widehat{\boldsymbol{l}}|\leq rK}} \sum_{\substack{\widehat{l}_j=-l_j,l_j\\ j=1,\dots,n_2}} c_{\boldsymbol{l},\boldsymbol{k},\widehat{\boldsymbol{l}}}\left(\sqrt{\boldsymbol{I}}\right)^{\boldsymbol{l}} e^{i\left(\boldsymbol{k}\cdot\boldsymbol{q}+\widehat{\boldsymbol{l}}\cdot\boldsymbol{\alpha}\right)} \\ &= \sum_{0\leq|\boldsymbol{k}|\leq rK-1} \sum_{j=1}^{n_2} \sqrt{I_j}\left[c_{\boldsymbol{k},j}^{(+)} e^{i(\boldsymbol{k}\cdot\boldsymbol{q}+\alpha_j)} + c_{\boldsymbol{k},j}^{(-)} e^{i(\boldsymbol{k}\cdot\boldsymbol{q}-\alpha_j)}\right]; \end{aligned}$$

due to the homological equation (4.27), we find

$$\begin{aligned} \chi_1^{(r)}(\boldsymbol{q},\boldsymbol{I},\boldsymbol{\alpha}) = \sum_{0\leq\boldsymbol{k}\leq rK-1} \sum_{j=1}^{n_2} \sqrt{I_j}\Bigg[&\frac{c_{\boldsymbol{k},j}^{(+)}}{i\left(\boldsymbol{k}\cdot\boldsymbol{\omega}^{(r-1)}+\Omega_j^{(r-1)}\right)} e^{i(\boldsymbol{k}\cdot\boldsymbol{q}+\alpha_j)} \\ &+\frac{c_{\boldsymbol{k},j}^{(-)}}{i\left(\boldsymbol{k}\cdot\boldsymbol{\omega}^{(r-1)}-\Omega_j^{(r-1)}\right)} e^{i(\boldsymbol{k}\cdot\boldsymbol{q}-\alpha_j)}\Bigg]. \end{aligned} \tag{4.28}$$

[13] In the r.h.s. of (4.27) we do not need to put any term produced by an angular average (similar to that appearing, for instance, in the r.h.s. of the homological equation (4.22)), because $\left\langle f_1^{(I;\,r,r)}\right\rangle_{\boldsymbol{q},\boldsymbol{\alpha}} = 0$. In fact, since $f_1^{(I;\,r,r)}$ is linear in $\sqrt{\boldsymbol{I}}$ and belongs to $\mathfrak{B}_{1,rK}$, from definition (4.4.1) it easily follows that in the expansion of $f_1^{(I;\,r,r)}$ all the terms include the dependence on $e^{\pm i\alpha_j}$ with $j=1,\dots,n_2$, leading to a null mean over the angles.

The above expression is well defined provided that the first Melnikov non-resonance condition is satisfied, i.e.,

$$\min_{\substack{0<|\boldsymbol{k}|\leq rK-1\\ |\boldsymbol{l}|=1}} \left|\boldsymbol{k}\cdot\boldsymbol{\omega}^{(r-1)}+\boldsymbol{l}\cdot\boldsymbol{\Omega}^{(r-1)}\right| \geq \frac{\gamma}{(rK)^{\tau}} \qquad \text{and} \qquad \min_{|\boldsymbol{l}|=1}\left|\boldsymbol{l}\cdot\boldsymbol{\Omega}^{(r-1)}\right| \geq \gamma\,, \tag{4.29}$$

for a pair of fixed values of $\gamma>0$ and $\tau>n_1-1$ (see [71] and reference therein).

We can now apply the transformation $\exp\left(L_{\chi_1^{(r)}}\right)$ to the Hamiltonian $\mathcal{H}^{(I;\,r)}$. By the usual abuse of notation (i.e., the new canonical coordinates are denoted with the same symbols of the old ones), the expansion of the new Hamiltonian can be written as

$$\begin{aligned}\mathcal{H}^{(II;\,r)}(\boldsymbol{p},\boldsymbol{q},\boldsymbol{I},\boldsymbol{\alpha}) &= \exp\left(L_{\chi_1^{(r)}}\right)\mathcal{H}^{(I;\,r)}\\ &= \mathcal{E}^{(r)}+\boldsymbol{\omega}^{(r-1)}\cdot\boldsymbol{p}+\boldsymbol{\Omega}^{(r-1)}\cdot\boldsymbol{I}+\sum_{s\geq 0}\sum_{l\geq 3} f_l^{(II;\,r,s)}(\boldsymbol{p},\boldsymbol{q},\boldsymbol{I},\boldsymbol{\alpha})\\ &\quad+\sum_{s\geq r+1} f_0^{(II;\,r,s)}(\boldsymbol{q})+\sum_{s\geq r} f_1^{(II;\,r,s)}(\boldsymbol{q},\boldsymbol{I},\boldsymbol{\alpha})+\sum_{s\geq r} f_2^{(II;\,r,s)}(\boldsymbol{p},\boldsymbol{q},\boldsymbol{I},\boldsymbol{\alpha})\,,\end{aligned} \tag{4.30}$$

where in the last row of the previous formula, it is possible to start the first sum from $r+1$ instead of r, being $f_0^{(II;\,r,r)}=f_0^{(I;\,r,r)}=0$. In an analogous way as in the first substep, it is convenient to first define the new Hamiltonian terms as the old ones, i.e., $f_l^{(II;\,r,s)}=f_l^{(I;\,r,s)}\ \forall\, l\geq 0\,,\ s\geq 0$. Hence, each term generated by the Lie derivatives with respect to $\chi_1^{(r)}$ is added to the corresponding class of functions. This is made by the following sequence[14] of redefinitions:

$$\begin{aligned} f_{l-j}^{(II;\,r,s+jr)} &\hookleftarrow \frac{1}{j!}L^j_{\chi_1^{(r)}} f_l^{(I;\,r,s)} \qquad \forall\, l\geq 0,\ 1\leq j\leq l,\ s\geq 0\,,\\ f_0^{(II;\,r,2r)} &\hookleftarrow \frac{1}{2}L^2_{\chi_1^{(r)}}\left(\boldsymbol{\omega}^{(r-1)}\cdot\boldsymbol{p}+\Omega^{(r-1)}\cdot\boldsymbol{I}\right)\,.\end{aligned} \tag{4.31}$$

In fact, since $\chi_1^{(r)}\in\mathfrak{B}_{1,rK}$ is linear in $\sqrt{\boldsymbol{I}}$, each application of the Lie derivative operator $L_{\chi_1^{(r)}}$ decreases by 1 the degree in square root of the actions, while the trigonometrical degree in the angles is increased by rK; such a rule holds because of Lemma 4.4.2. Moreover, thanks to the homological equation (4.27), one can easily remark that $f_1^{(II;\,r,r)}=0$. A repeated application of Lemma 4.4.2 allows us to verify also that $f_l^{(II;\,r,s)}\in\mathfrak{B}_{l,sK}\,,\ \forall l\geq 0,\ s\geq 0$.

At the end of this second normalization substep, the new Hamiltonian can be easily visualized as in Table 4.10.

Third substep (of the r-th normalization step)

The last substep aims to remove the term $f_2^{(II;\,r,r)}$ which is quadratic in the square root of the actions (i.e., either quadratic in $\sqrt{\boldsymbol{I}}$ or linear in $\boldsymbol{p}$) and included in the third sum appearing in the second row of (4.30). The third generating function $\chi_2^{(r)}(\boldsymbol{p},\boldsymbol{q},\boldsymbol{I},\boldsymbol{\alpha})$ is determined by solving the following homological equation:

$$\{\boldsymbol{\omega}^{(r-1)}\cdot\boldsymbol{p}+\boldsymbol{\Omega}^{(r-1)}\cdot\boldsymbol{I},\chi_2^{(r)}\}+f_2^{(II;\,r,r)}(\boldsymbol{p},\boldsymbol{q},\boldsymbol{I},\boldsymbol{\alpha})=\left\langle f_2^{(II;\,r,r)}\right\rangle_{\boldsymbol{q},\boldsymbol{\alpha}}\,. \tag{4.32}$$

[14] From a practical point of view, since we have to deal again with series truncated in such a way that the index s goes up to a fixed order called $\mathcal{N}_S$, we have to require also that $1\leq j\leq \min\{l,\lfloor(\mathcal{N}_S-s)/r\rfloor\}$.

$$\mathcal{H}^{(II;\,r)} = \sum_{\boldsymbol{\omega}^{(r-1)}\cdot\boldsymbol{p}+\boldsymbol{\Omega}^{(r-1)}\cdot\boldsymbol{I}}$$

							Degree in square root of the actions:
$\vdots$	$\vdots$	$\vdots$	$\vdots$	$\vdots$	$\vdots$	$\vdots$	$\vdots$
$f_4^{(II;r,0)}$	$f_4^{(II;r,1)}$	$\dots$	$f_4^{(II;r,r-1)}$	$f_4^{(II;r,r)}$	$f_4^{(II;r,r+1)}$	$\dots$	$\leftarrow 4$
$f_3^{(II;r,0)}$	$f_3^{(II;r,1)}$	$\dots$	$f_3^{(II;r,r-1)}$	$f_3^{(II;r,r)}$	$f_3^{(II;r,r+1)}$	$\dots$	$\leftarrow 3$
0	0	$\dots$	0	$f_2^{(II;r,r)}$	$f_2^{(II;r,r+1)}$	$\dots$	$\leftarrow 2$
0	0	$\dots$	0	0	$f_1^{(II;r,r+1)}$	$\dots$	$\leftarrow 1$
$\mathcal{E}^{(r)}$	0	$\dots$	0	0	$f_0^{(II;r,r+1)}$	$\dots$	$\leftarrow 0$
$\uparrow$	$\uparrow$		$\uparrow$	$\uparrow$	$\uparrow$		
0	1	$\cdots$	$r-1$	r	$r+1$	$\cdots$	

Trigonometric degree/K:

Table 4.10: Graphical representation of the expansion of the Hamiltonian after the second substep (of the r-th normalization step).

Since $f_2^{(II;\,r,r)} \in \mathfrak{B}_{2,rK}$, we can write it (according to definition 4.4.1 with $2\widehat{m}+\widehat{l}=2$ and $s=r$) as follows:

$$\begin{aligned} f_2^{(II;\,r,r)}(\boldsymbol{p},\boldsymbol{q},\boldsymbol{I},\boldsymbol{\alpha}) = &\sum_{\substack{\boldsymbol{m}\in\mathbb{N}^{n_1}\\ |\boldsymbol{m}|=1}} \sum_{\substack{\boldsymbol{k}\in\mathbb{Z}^{n_1}\\ |\boldsymbol{k}|\le rK}} c_{\boldsymbol{m},\boldsymbol{k}}\, \boldsymbol{p}^{\boldsymbol{m}} e^{i\,\boldsymbol{k}\cdot\boldsymbol{q}} \\ &+ \sum_{\substack{\boldsymbol{l}\in\mathbb{N}^{n_2}\\ |\boldsymbol{l}|=2}} \sum_{\substack{\boldsymbol{k}\in\mathbb{Z}^{n_1}\\ |\boldsymbol{k}|+|\widehat{\boldsymbol{l}}|\le rK}} \sum_{\substack{\widehat{l}_j=-l_j,-l_j+2,\dots,l_j\\ j=1,\dots,n_2}} \tilde{c}_{\boldsymbol{l},\boldsymbol{k},\widehat{\boldsymbol{l}}}\, \left(\sqrt{\boldsymbol{I}}\right)^{\boldsymbol{l}} e^{i\left(\boldsymbol{k}\cdot\boldsymbol{q}+\widehat{\boldsymbol{l}}\cdot\boldsymbol{\alpha}\right)}\,, \end{aligned}$$

Due to the homological equation (4.32), we obtain

$$\begin{aligned} \chi_2^{(r)}(\boldsymbol{p},\boldsymbol{q},\boldsymbol{I},\boldsymbol{\alpha}) = &\sum_{\substack{\boldsymbol{m}\in\mathbb{N}^{n_1}\\ |\boldsymbol{m}|=1}} \sum_{\substack{\boldsymbol{k}\in\mathbb{Z}^{n_1}\\ 0<|\boldsymbol{k}|\le rK}} \frac{c_{\boldsymbol{m},\boldsymbol{k}}\, \boldsymbol{p}^{\boldsymbol{m}} e^{i\,\boldsymbol{k}\cdot\boldsymbol{q}}}{i\,\boldsymbol{k}\cdot\boldsymbol{\omega}^{(r-1)}} \\ &+ \sum_{\substack{\boldsymbol{l}\in\mathbb{N}^{n_2}\\ |\boldsymbol{l}|=2}} \sum_{\substack{\boldsymbol{k}\in\mathbb{Z}^{n_1}\\ 0<|\boldsymbol{k}|+|\widehat{\boldsymbol{l}}|\le rK}} \sum_{\substack{\widehat{l}_j=-l_j,-l_j+2,\dots,l_j\\ j=1,\dots,n_2}} \frac{\tilde{c}_{\boldsymbol{l},\boldsymbol{k},\widehat{\boldsymbol{l}}}\, \left(\sqrt{\boldsymbol{I}}\right)^{\boldsymbol{l}} e^{i\left(\boldsymbol{k}\cdot\boldsymbol{q}+\widehat{\boldsymbol{l}}\cdot\boldsymbol{\alpha}\right)}}{i\left(\boldsymbol{k}\cdot\boldsymbol{\omega}^{(r-1)}+\widehat{\boldsymbol{l}}\cdot\boldsymbol{\Omega}^{(r-1)}\right)}\,, \end{aligned} \tag{4.33}$$

provided that both the non-resonance condition and the Melnikov one of second kind are satisfied, i.e.,

$$\boldsymbol{k}\cdot\boldsymbol{\omega}^{(r-1)} \neq 0 \quad \forall\, 0<\boldsymbol{k}\le rK \qquad \text{and} \qquad \min_{\substack{0<|\boldsymbol{k}|\le rK-2\\ |\boldsymbol{l}|=2}} \left|\boldsymbol{k}\cdot\boldsymbol{\omega}^{(r-1)}+\boldsymbol{l}\cdot\boldsymbol{\Omega}^{(r-1)}\right| \ge \frac{\gamma}{(rK)^{\tau}}\,, \tag{4.34}$$

with the same values of the constant parameters $\gamma>0$ and $\tau>n_1-1$ appearing in (4.29).

We can now apply the transformation $\exp\left(L_{\chi_2^{(r)}}\right)$ to the Hamiltonian $\mathcal{H}^{(II;\,r)}$. By the usual abuse of notation (i.e., the new canonical coordinates are denoted with the same symbols of the old ones), the expansion[15] of the new Hamiltonian can be written as

$$\begin{aligned} \mathcal{H}^{(r)}(\boldsymbol{p},\boldsymbol{q},\boldsymbol{I},\boldsymbol{\alpha}) &= \exp\left(L_{\chi_2^{(r)}}\right)\mathcal{H}^{(II;\,r)} \\ &= \mathcal{E}^{(r)} + \boldsymbol{\omega}^{(r-1)}\cdot\boldsymbol{p} + \boldsymbol{\Omega}^{(r-1)}\cdot\boldsymbol{I} + \sum_{s\ge 0}\sum_{l\ge 3} f_l^{(r,s)}(\boldsymbol{p},\boldsymbol{q},\boldsymbol{I},\boldsymbol{\alpha}) \\ &\quad + \sum_{s\ge r+1} f_0^{(r,s)}(\boldsymbol{q}) + \sum_{s\ge r+1} f_1^{(r,s)}(\boldsymbol{q},\boldsymbol{I},\boldsymbol{\alpha}) + \sum_{s\ge r} f_2^{(r,s)}(\boldsymbol{p},\boldsymbol{q},\boldsymbol{I},\boldsymbol{\alpha})\,. \end{aligned} \tag{4.35}$$

[15] In the third row of (4.35), it is possible to start the second sum from $r+1$ instead of r, being $f_1^{(r,r)} = f_1^{(II;\,r,r)} = 0$.

Once again, it is convenient to first define the new Hamiltonian terms as the old ones, i.e., $f_l^{(r,s)} = f_l^{(II;\,r,s)}\ \forall\, l \geq 0\,,\ s \geq 0\,$. Hence, each term generated by the Lie derivatives with respect to $\chi_2^{(r)}$ is added to the corresponding class of functions. This is made by the following sequence[16] of redefinitions:

$$\begin{aligned} f_l^{(\,r,s+jr)} &\hookleftarrow \frac{1}{j!} L^j_{\chi_1^{(r)}} f_l^{(II;\,r,s)} \qquad \forall\, l \geq 0,\ j \geq 1,\ s \geq 0\,, \\ f_2^{(r,jr)} &\hookleftarrow \frac{1}{j!} L^j_{\chi_2^{(r)}} \left(\boldsymbol{\omega}^{(r-1)} \cdot \boldsymbol{p} + \boldsymbol{\Omega}^{(r-1)} \cdot \boldsymbol{I} \right) \qquad \forall\, j \geq 1\,. \end{aligned} \tag{4.36}$$

In fact, since $\chi_2^{(r)} \in \mathfrak{B}_{2,rK}$ is either quadratic in $\sqrt{\boldsymbol{I}}$ or linear in $\boldsymbol{p}$, each application of the Lie derivative operator $L^{(r)}_{\chi_2}$ does not modify the degree in the square root of the actions, while the trigonometric degree in the angles is increased by $rK\,$. By applying Lemma 4.4.2 one can verify also that $f_l^{(r,s)} \in \mathfrak{B}_{l,sK}\,,\ \forall l \geq 0,\ s \geq 0\,$.

Because of the homological equation (4.32), it immediately follows that the term that cannot be removed, that is $f_2^{(r,r)} = \left\langle f_2^{(II;\,r,r)} \right\rangle_{\boldsymbol{q},\boldsymbol{\alpha}} \in \mathfrak{B}_{2,0}\,$, is exactly of the same type with respect to the main term that is linear in the actions, i.e., $\boldsymbol{\omega}^{(r-1)} \cdot \boldsymbol{p} + \boldsymbol{\Omega}^{(r-1)} \cdot \boldsymbol{I}$. It looks then natural to update the angular velocity vectors so that

$$\boldsymbol{\omega}^{(r)} = \boldsymbol{\omega}^{(r-1)} + \nabla_{\boldsymbol{p}} \left(\left\langle f_2^{(II;\,r,r)} \right\rangle_{\boldsymbol{q},\boldsymbol{\alpha}} \right)\,, \qquad \boldsymbol{\Omega}^{(r)} = \boldsymbol{\Omega}^{(r-1)} + \nabla_{\boldsymbol{I}} \left(\left\langle f_2^{(II;\,r,r)} \right\rangle_{\boldsymbol{q},\boldsymbol{\alpha}} \right)\,, \tag{4.37}$$

where, as usual, the symbols $\nabla_{\boldsymbol{p}}$ and $\nabla_{\boldsymbol{I}}$ denote the gradient with respect to the action variables $\boldsymbol{p}$ and $\boldsymbol{I}$, respectively, and to set $f_2^{(r,r)} = 0\,$. Therefore, the expansion of the Hamiltonian $\mathcal{H}^{(r)}$ can be rewritten as

$$\begin{aligned} \mathcal{H}^{(r)}(\boldsymbol{p},\boldsymbol{q},\boldsymbol{I},\boldsymbol{\alpha}) = \mathcal{E}^{(r)} + \boldsymbol{\omega}^{(r)} \cdot \boldsymbol{p} + \boldsymbol{\Omega}^{(r)} \cdot \boldsymbol{I} + \sum_{s\geq 0} \sum_{l \geq 3} f_l^{(r,s)}(\boldsymbol{p},\boldsymbol{q},\boldsymbol{I},\boldsymbol{\alpha}) \\ + \sum_{s \geq r+1} \sum_{l=0}^{2} f_l^{(r,s)}(\boldsymbol{p},\boldsymbol{q},\boldsymbol{I},\boldsymbol{\alpha})\,, \end{aligned} \tag{4.38}$$

where $f_l^{(r,s)} \in \mathfrak{B}_{l,sK}$ and $\mathcal{E}^{(r)} \in \mathfrak{B}_{0,0}$ is a constant.

At the end of the r-th normalization step, the new Hamiltonian can be easily visualized as in Table 4.11. The comparison with Table 4.8 makes evident that it is now possible to iterate the algorithm, by performing the (next) $r+1$-th normalization step. The convergence of this normal form algorithm is proved in [6] and [7] under suitable conditions.

In order to implement such a kind of normalization algorithm with the aid of a computer, we have to deal with Hamiltonians including a finite number of summands in their expansions in Taylor-Fourier series. To fix the ideas, let us suppose that we set a truncation rule in such a way as to neglect all the terms with a trigonometric degree greater than $\mathcal{N}_S K$, for a fixed positive integer value of the parameter $\mathcal{N}_S\,$. After iteratively performing $\mathcal{N}_S$ steps of the constructive algorithm, we end up with an approximation of the Hamiltonian which is in the normal form corresponding to an elliptic torus, i.e.,

$$\mathcal{H}^{(\mathcal{N}_S)}(\boldsymbol{p},\boldsymbol{q},\boldsymbol{I},\boldsymbol{\alpha}) = \mathcal{E}^{(\mathcal{N}_S)} + \boldsymbol{\omega}^{(\mathcal{N}_S)} \cdot \boldsymbol{p} + \boldsymbol{\Omega}^{(\mathcal{N}_S)} \cdot \boldsymbol{I} + \sum_{s\geq 0}^{\mathcal{N}_S} \sum_{l \geq 3} f_l^{(\mathcal{N}_S,s)}(\boldsymbol{p},\boldsymbol{q},\boldsymbol{I},\boldsymbol{\alpha})\,, \tag{4.39}$$

which is visualized in Table 4.12.

The Hamiltonian $\mathcal{H}^{(\mathcal{N}_S)}$ represents the natural starting point for the application of a second (Birkhoff-like) algorithm, which will aim to produce a new normal form in such a way to remove the dependence on the angles $\boldsymbol{q}$, as explained in the next Subsection.

[16] From a practical point of view, since we have to deal with series truncated in such a way that the index s goes up to a fixed order called $\mathcal{N}_S$, we have to require also that $1 \leq j \leq \lfloor (\mathcal{N}_S - s)/r \rfloor\,$.

								Degree in square root of the actions:
	$\vdots$	$\vdots$	$\vdots$	$\vdots$	$\vdots$	$\vdots$	$\vdots$	$\vdots$
	$f_4^{(r,0)}$	$f_4^{(r,1)}$	$\dots$	$f_4^{(r,r-1)}$	$f_4^{(r,r)}$	$f_4^{(r,r+1)}$	$\dots$	$\leftarrow 4$
	$f_3^{(r,0)}$	$f_3^{(r,1)}$	$\dots$	$f_3^{(r,r-1)}$	$f_3^{(r,r)}$	$f_3^{(r,r+1)}$	$\dots$	$\leftarrow 3$
$\mathcal{H}^{(r)} = \sum$	$\boldsymbol{\omega}^{(r)} \cdot \boldsymbol{p} + \boldsymbol{\Omega}^{(r)} \cdot \boldsymbol{I}$	0	$\dots$	0	0	$f_2^{(r,r+1)}$	$\dots$	$\leftarrow 2$
	0	0	$\dots$	0	0	$f_1^{(r,r+1)}$	$\dots$	$\leftarrow 1$
	$\mathcal{E}^{(r)}$	0	$\dots$	0	0	$f_0^{(r,r+1)}$	$\dots$	$\leftarrow 0$
Trigonometric degree/K:	$\uparrow$ 0	$\uparrow$ 1	$\dots$	$\uparrow$ $r-1$	$\uparrow$ r	$\uparrow$ $r+1$	$\dots$	

Table 4.11: Graphical representation of the expansion of the Hamiltonian after the third and last substep (of the r-th normalization step).

								Degree in square root of the actions:
	$\vdots$	$\vdots$	$\vdots$	$\vdots$	$\vdots$	$\vdots$	$\vdots$	$\vdots$
	$f_4^{(\mathcal{N}_S,0)}$	$f_4^{(\mathcal{N}_S,1)}$	$\dots$	$f_4^{(\mathcal{N}_S,r)}$	$\dots$	$f_4^{(\mathcal{N}_S,\mathcal{N}_S-1)}$	$f_4^{(\mathcal{N}_S,\mathcal{N}_S)}$	$\leftarrow 4$
	$f_3^{(\mathcal{N}_S,0)}$	$f_3^{(\mathcal{N}_S,1)}$	$\dots$	$f_3^{(\mathcal{N}_S,r)}$	$\dots$	$f_3^{(\mathcal{N}_S,\mathcal{N}_S-1)}$	$f_3^{(\mathcal{N}_S,\mathcal{N}_S)}$	$\leftarrow 3$
$\mathcal{H}^{(\mathcal{N}_S)} = \sum$	$\boldsymbol{\omega}^{(\mathcal{N}_S)} \cdot \boldsymbol{p} + \boldsymbol{\Omega}^{(\mathcal{N}_S)} \cdot \boldsymbol{I}$	0	$\dots$	0	$\dots$	0	0	$\leftarrow 2$
	0	0	$\dots$	0	$\dots$	0	0	$\leftarrow 1$
	$\mathcal{E}^{(\mathcal{N}_S)}$	0	$\dots$	0	$\dots$	0	0	$\leftarrow 0$
Trigonometric degree/K:	$\uparrow$ 0	$\uparrow$ 1	$\dots$	$\uparrow$ r	$\dots$	$\uparrow$ $\mathcal{N}_S-1$	$\uparrow$ $\mathcal{N}_S$	

Table 4.12: Graphical representation of the Hamiltonian after $\mathcal{N}_S$ normalization steps whose expansion is truncated up to the maximal trigonometric degree $\mathcal{N}_S K$.

4.4.2 Construction of the resonant normal form in such a way to average with respect to the angles q

Consider a Hamiltonian[17] $\mathcal{H}_B^{(0)}$ of the form:

$$\mathcal{H}_B^{(0)}(\boldsymbol{p},\boldsymbol{q},\boldsymbol{I},\boldsymbol{\alpha}) = \mathcal{E}_B + \boldsymbol{\omega}_B \cdot \boldsymbol{p} + \boldsymbol{\Omega}_B \cdot \boldsymbol{I} + \sum_{s=0}^{\mathcal{N}_S} \sum_{l \geq 3} g_l^{(0,s)}(\boldsymbol{p},\boldsymbol{q},\boldsymbol{I},\boldsymbol{\alpha})\,, \tag{4.40}$$

where $\mathcal{E}_B$ is a constant term, representing the energy, $(\boldsymbol{p},\boldsymbol{q}) \in \mathbb{R}^{n_1} \times \mathbb{T}^{n_1}$, $(\boldsymbol{I},\boldsymbol{\alpha}) \in \mathbb{R}^{n_2}_{\geq 0} \times \mathbb{T}^{n_2}$ are action-angle variables, $(\boldsymbol{\omega}_B,\boldsymbol{\Omega}_B) \in \mathbb{R}^{n_1} \times \mathbb{R}^{n_2}$ are the frequencies, $\mathcal{N}_S$ is a fixed positive integer (ruling the truncations in the Fourier series) and $g_l^{(0,s)} \in \mathfrak{B}_{l,sK}$, $\forall\, l \geq 0$, $0 \leq s \leq \mathcal{N}_S$. In practice, we are starting from the normalized Hamiltonian of the previous Subsection $\mathcal{H}^{(\mathcal{N}_S)}$, given by equation (4.39), where we have defined $\mathcal{H}_B^{(0)} := \mathcal{H}^{(\mathcal{N}_S)}$, $\mathcal{E}_B := \mathcal{E}^{(\mathcal{N}_S)}$, $(\boldsymbol{\omega}_B,\boldsymbol{\Omega}_B) := (\boldsymbol{\omega}^{(\mathcal{N}_S)},\boldsymbol{\Omega}^{(\mathcal{N}_S)})$ and $g_l^{(0,s)} := f_l^{(\mathcal{N}_S,s)} \in \mathfrak{B}_{l,sK}$ $\forall\, l \geq 0$, $0 \leq s \leq \mathcal{N}_S$; this is done also in order to simplify the notation. By comparison with equation (4.39), it is easy to remark that $g_l^{(0,s)} := f_l^{(\mathcal{N}_S,s)} = 0$, $\forall\, 0 \leq l \leq 2$, $1 \leq s \leq \mathcal{N}_S$. The structure of $\mathcal{H}_B^{(0)}$ can be easily visualized as in Table 4.13.

[17] We use the symbol $\mathcal{H}_B^{(0)}$ instead of $\mathcal{H}^{(0)}$ to distinguish this starting Hamiltonian from the one of the previous normalization algorithm, which is written in equation (4.18).

$$\mathcal{H}_B^{(0)} = \sum \begin{array}{|ccccccc|l} \vdots & \vdots & \vdots & \vdots & \vdots & \vdots & \vdots & \vdots \\ g_n^{(0,0)}(\boldsymbol{p},\boldsymbol{I}) & g_n^{(0,1)}(\boldsymbol{p},\boldsymbol{q},\boldsymbol{I},\boldsymbol{\alpha}) & \dots & g_n^{(0,r)}(\boldsymbol{p},\boldsymbol{q},\boldsymbol{I},\boldsymbol{\alpha}) & \dots & g_n^{(0,\mathcal{N}_S-1)}(\boldsymbol{p},\boldsymbol{q},\boldsymbol{I},\boldsymbol{\alpha}) & g_n^{(0,\mathcal{N}_S)}(\boldsymbol{p},\boldsymbol{q},\boldsymbol{I},\boldsymbol{\alpha}) & \leftarrow n \\ \vdots & \vdots & \vdots & \vdots & \vdots & \vdots & \vdots & \vdots \\ g_3^{(0,0)}(\boldsymbol{p},\boldsymbol{I}) & g_3^{(0,1)}(\boldsymbol{p},\boldsymbol{q},\boldsymbol{I},\boldsymbol{\alpha}) & \dots & g_3^{(0,r)}(\boldsymbol{p},\boldsymbol{q},\boldsymbol{I},\boldsymbol{\alpha}) & \dots & g_3^{(0,\mathcal{N}_S-1)}(\boldsymbol{p},\boldsymbol{q},\boldsymbol{I},\boldsymbol{\alpha}) & g_3^{(0,\mathcal{N}_S)}(\boldsymbol{p},\boldsymbol{q},\boldsymbol{I},\boldsymbol{\alpha}) & \leftarrow 3 \\ \boldsymbol{\omega}_B\cdot\boldsymbol{p}+\boldsymbol{\Omega}_B\cdot\boldsymbol{I} & 0 & \dots & 0 & \dots & 0 & 0 & \leftarrow 2 \\ 0 & 0 & \dots & 0 & \dots & 0 & 0 & \leftarrow 1 \\ \mathcal{E}_B & 0 & \dots & 0 & \dots & 0 & 0 & \leftarrow 0 \\ \hline \uparrow & \uparrow & \dots & \uparrow & \dots & \uparrow & \uparrow & \\ 0 & 1 & & r & & \mathcal{N}_S-1 & \mathcal{N}_S & \end{array}$$

Table 4.13: Graphical representation of the starting Hamiltonian $\mathcal{H}_B^{(0)}$. The colored terms are those we want to remove the dependence on $\boldsymbol{q}$.

The aim of the present algorithm is to delete the dependence of $\mathcal{H}_B^{(0)}$ on the angles $\boldsymbol{q}$, reducing by n_1 the number of degrees of freedom. In order to do this, we have to act on the terms $g_l^{(0,s)}(\boldsymbol{p},\boldsymbol{q},\boldsymbol{I},\boldsymbol{\alpha})$ such that $s \geq 1$ and $l \geq 3$ (that are highlighted with gray color in Table 4.13), removing their dependence on $\boldsymbol{q}$; indeed, for $s = 0$, the sum $\sum_{l\geq 3} g_l^{(0,0)}(\boldsymbol{p},\boldsymbol{I})$ does not depend on the angles, thus it is already in normal form. This elimination can be done by a sequence of canonical transformations. If convergent, this would lead the Hamiltonian to the following final normal form:

$$\mathcal{H}_B^{(\infty)}(\tilde{\boldsymbol{p}},\tilde{\boldsymbol{I}},\tilde{\boldsymbol{\alpha}}) = \mathcal{E}_B + \boldsymbol{\omega}_B\cdot\tilde{\boldsymbol{p}} + \boldsymbol{\Omega}_B\cdot\tilde{\boldsymbol{I}} + \sum_{s=0}^{\infty}\sum_{l\geq 3} g_l^{(\infty,s)}(\tilde{\boldsymbol{p}},\tilde{\boldsymbol{I}},\tilde{\boldsymbol{\alpha}})\,, \tag{4.41}$$

where $(\tilde{\boldsymbol{p}},\tilde{\boldsymbol{I}},\tilde{\boldsymbol{\alpha}})$ denote the new variables; it is evident that, having removed the dependence on $\tilde{\boldsymbol{q}}$, the conjugate momenta vector $\tilde{\boldsymbol{p}}$ is constant. However, as typical of the computational procedures *à la* Birkhoff, the constructive algorithm produces divergent series if the normalization is iterated infinitely many times. For this reason, it is convenient to look for an optimal order of normalization to which the algorithm is stopped. In our approach, we have not to consider such a problem, because we are dealing with truncated series; this is done in order to keep our discussion as close as possible to the practical implementations where the maximal degree in actions of the expansions is usually rather low.

The generic r-th step of this new normalization algorithm is defined as follows. After $r-1$ steps, the Hamiltonian (4.40) takes the form

$$\begin{aligned}\mathcal{H}_B^{(r-1)}(\boldsymbol{p},\boldsymbol{q},\boldsymbol{I},\boldsymbol{\alpha}) = \mathcal{E}_B + \boldsymbol{\omega}_B\cdot\boldsymbol{p} + \boldsymbol{\Omega}_B\cdot\boldsymbol{I} + \sum_{l\geq 3} g_l^{(r-1,0)}(\boldsymbol{p},\boldsymbol{I}) \\ + \sum_{s=1}^{\mathcal{N}_S}\sum_{3\leq l\leq r+1} g_l^{(r-1,s)}(\boldsymbol{p},\boldsymbol{I},\boldsymbol{\alpha}) + \sum_{s=1}^{\mathcal{N}_S}\sum_{l\geq r+2} g_l^{(r-1,s)}(\boldsymbol{p},\boldsymbol{q},\boldsymbol{I},\boldsymbol{\alpha})\,,\end{aligned} \tag{4.42}$$

with $g_l^{(r-1,s)} \in \mathfrak{B}_{l,sK}$. The structure of the Hamiltonian can be easily visualized in Table 4.14.

The r-th normalization step consists of a sequence of $\mathcal{N}_S$ substeps, each of them is involving a canonical transformation which is expressed in terms of the Lie series having $\chi_B^{(j;\,r)}$ as generating function, with $j = 1, \dots, \mathcal{N}_S$. Therefore, the new Hamiltonian introduced at the end of the r-th normalization step of this algorithm is defined as follows:

$$\mathcal{H}_B^{(r)} = \exp\left(L_{\chi_B^{(\mathcal{N}_S;\,r)}}\right)\dots\exp\left(L_{\chi_B^{(3;\,r)}}\right)\exp\left(L_{\chi_B^{(2;\,r)}}\right)\exp\left(L_{\chi_B^{(1;\,r)}}\right)\mathcal{H}_B^{(r-1)}\,. \tag{4.43}$$

The generating functions $\chi_B^{(j;\,r)}$ are defined so as to remove the dependence on $\boldsymbol{q}$ from the perturbing term of lowest order in the square root of the actions, i.e., $\sum_{s=1}^{\mathcal{N}_S} g_{r+2}^{(r-1,s)}(\boldsymbol{p},\boldsymbol{q},\boldsymbol{I},\boldsymbol{\alpha})$.

$$\mathcal{H}_B^{(r-1)} = \sum$$

$\vdots$	$\vdots$	$\vdots$	$\vdots$	$\vdots$	$\vdots$	$\vdots$
$g_{r+3}^{(r-1,0)}(\boldsymbol{p},\boldsymbol{I})$	$g_{r+3}^{(r-1,1)}(\boldsymbol{p},\boldsymbol{q},\boldsymbol{I},\boldsymbol{\alpha})$	$\dots$	$g_{r+3}^{(r-1,r)}(\boldsymbol{p},\boldsymbol{q},\boldsymbol{I},\boldsymbol{\alpha})$	$\dots$	$g_{r+3}^{(r-1,\mathcal{N}_S-1)}(\boldsymbol{p},\boldsymbol{q},\boldsymbol{I},\boldsymbol{\alpha})$	$g_{r+3}^{(r-1,\mathcal{N}_S)}(\boldsymbol{p},\boldsymbol{q},\boldsymbol{I},\boldsymbol{\alpha})$	$\leftarrow r+3$
$g_{r+2}^{(r-1,0)}(\boldsymbol{p},\boldsymbol{I})$	$g_{r+2}^{(r-1,1)}(\boldsymbol{p},\boldsymbol{q},\boldsymbol{I},\boldsymbol{\alpha})$	$\dots$	$g_{r+2}^{(r-1,r)}(\boldsymbol{p},\boldsymbol{q},\boldsymbol{I},\boldsymbol{\alpha})$	$\dots$	$g_{r+2}^{(r-1,\mathcal{N}_S-1)}(\boldsymbol{p},\boldsymbol{q},\boldsymbol{I},\boldsymbol{\alpha})$	$g_{r+2}^{(r-1,\mathcal{N}_S)}(\boldsymbol{p},\boldsymbol{q},\boldsymbol{I},\boldsymbol{\alpha})$	$\leftarrow r+2$
$g_{r+1}^{(r-1,0)}(\boldsymbol{p},\boldsymbol{I})$	$g_{r+1}^{(r-1,1)}(\boldsymbol{p},\boldsymbol{I},\boldsymbol{\alpha})$	$\dots$	$g_{r+1}^{(r-1,r)}(\boldsymbol{p},\boldsymbol{I},\boldsymbol{\alpha})$	$\dots$	$g_{r+1}^{(r-1,\mathcal{N}_S-1)}(\boldsymbol{p},\boldsymbol{I},\boldsymbol{\alpha})$	$g_{r+1}^{(r-1,\mathcal{N}_S)}(\boldsymbol{p},\boldsymbol{I},\boldsymbol{\alpha})$	$\leftarrow r+1$
$\vdots$	$\vdots$	$\vdots$	$\vdots$	$\vdots$	$\vdots$	$\vdots$	$\vdots$
$g_3^{(r-1,0)}(\boldsymbol{p},\boldsymbol{I})$	$g_3^{(r-1,1)}(\boldsymbol{p},\boldsymbol{I},\boldsymbol{\alpha})$	$\dots$	$g_3^{(r-1,r)}(\boldsymbol{p},\boldsymbol{I},\boldsymbol{\alpha})$	$\dots$	$g_3^{(r-1,\mathcal{N}_S-1)}(\boldsymbol{p},\boldsymbol{I},\boldsymbol{\alpha})$	$g_3^{(r-1,\mathcal{N}_S)}(\boldsymbol{p},\boldsymbol{I},\boldsymbol{\alpha})$	$\leftarrow 3$
$\boldsymbol{\omega}_B\cdot\boldsymbol{p}+\boldsymbol{\Omega}_B\cdot\boldsymbol{I}$	0	$\dots$	0	$\dots$	0	0	$\leftarrow 2$
0	0	$\dots$	0	$\dots$	0	0	$\leftarrow 1$
$\mathcal{E}_B$	0	$\dots$	0	$\dots$	0	0	$\leftarrow 0$
$\uparrow$	$\uparrow$	$\dots$	$\uparrow$	$\dots$	$\uparrow$	$\uparrow$	
0	1		r		$\mathcal{N}_S-1$	$\mathcal{N}_S$	

Table 4.14: Graphical representation of the expansion of the Hamiltonian after $r-1$ normalization steps of the algorithm constructing the resonant normal form.

j-th substep of the r-th step of the algorithm constructing the resonant normal form

After $j-1$ substeps, the Hamiltonian can be written as follows:

$$\begin{aligned}\mathcal{H}_B^{(j-1;\,r)}(\boldsymbol{p},\boldsymbol{q},\boldsymbol{I},\boldsymbol{\alpha}) = \mathcal{E}_B + \boldsymbol{\omega}_B\cdot\boldsymbol{p}+\boldsymbol{\Omega}_B\cdot\boldsymbol{I} + \sum_{l\geq 3} g_l^{(j-1;\,r,0)}(\boldsymbol{p},\boldsymbol{I}) \\ + \sum_{s=1}^{\mathcal{N}_S}\sum_{3\leq l\leq r+1} g_l^{(j-1;\,r,s)}(\boldsymbol{p},\boldsymbol{I},\boldsymbol{\alpha}) + \sum_{s=1}^{j-1} g_{r+2}^{(j-1;\,r,s)}(\boldsymbol{p},\boldsymbol{I},\boldsymbol{\alpha}) \\ + \sum_{s=j}^{\mathcal{N}_S} g_{r+2}^{(j-1;\,r,s)}(\boldsymbol{p},\boldsymbol{q},\boldsymbol{I},\boldsymbol{\alpha}) + \sum_{s=1}^{\mathcal{N}_S}\sum_{l\geq r+3} g_l^{(j-1;\,r,s)}(\boldsymbol{p},\boldsymbol{q},\boldsymbol{I},\boldsymbol{\alpha})\,,\end{aligned} \tag{4.44}$$

where, for $j=1$, we set $\mathcal{H}_B^{(0;\,r)} := \mathcal{H}_B^{(r-1)}$ and $g_l^{(0;\,r,s)} = g_l^{(n-1,s)}$, $\forall l\geq 0$, $\forall\, 0\leq s\leq \mathcal{N}_S$. To fix the ideas, the Hamiltonian (4.44) is graphically represented in Table 4.15.

$$\mathcal{H}_B^{(j-1;\,r)} = \sum$$

$\vdots$	$\vdots$	$\vdots$	$\vdots$	$\vdots$	$\vdots$	$\vdots$	$\vdots$
$g_{r+3}^{(j-1;\,r,0)}(\boldsymbol{p},\boldsymbol{I})$	$g_{r+3}^{(j-1;\,r,1)}(\boldsymbol{p},\boldsymbol{q},\boldsymbol{I},\boldsymbol{\alpha})$	$\dots$	$g_{r+3}^{(j-1;\,r,j-1)}(\boldsymbol{p},\boldsymbol{q},\boldsymbol{I},\boldsymbol{\alpha})$	$g_{r+3}^{(j-1;\,r,j)}(\boldsymbol{p},\boldsymbol{q},\boldsymbol{I},\boldsymbol{\alpha})$	$\dots$	$g_{r+3}^{(j-1;\,r,\mathcal{N}_S)}(\boldsymbol{p},\boldsymbol{q},\boldsymbol{I},\boldsymbol{\alpha})$	$\leftarrow r+3$
$g_{r+2}^{(j-1;\,r,0)}(\boldsymbol{p},\boldsymbol{I})$	$g_{r+2}^{(j-1;\,r,1)}(\boldsymbol{p},\boldsymbol{I},\boldsymbol{\alpha})$	$\dots$	$g_{r+2}^{(j-1;\,r,j-1)}(\boldsymbol{p},\boldsymbol{I},\boldsymbol{\alpha})$	$g_{r+2}^{(j-1;\,r,j)}(\boldsymbol{p},\boldsymbol{q},\boldsymbol{I},\boldsymbol{\alpha})$	$\dots$	$g_{r+2}^{(j-1;\,r,\mathcal{N}_S)}(\boldsymbol{p},\boldsymbol{q},\boldsymbol{I},\boldsymbol{\alpha})$	$\leftarrow r+2$
$g_{r+1}^{(j-1;\,r,0)}(\boldsymbol{p},\boldsymbol{I})$	$g_{r+1}^{(j-1;\,r,1)}(\boldsymbol{p},\boldsymbol{I},\boldsymbol{\alpha})$	$\dots$	$g_{r+1}^{(j-1;\,r,j-1)}(\boldsymbol{p},\boldsymbol{I},\boldsymbol{\alpha})$	$g_{r+1}^{(j-1;\,r,j)}(\boldsymbol{p},\boldsymbol{I},\boldsymbol{\alpha})$	$\dots$	$g_{r+1}^{(j-1;\,r,\mathcal{N}_S)}(\boldsymbol{p},\boldsymbol{I},\boldsymbol{\alpha})$	$\leftarrow r+1$
$\vdots$	$\vdots$	$\vdots$	$\vdots$	$\vdots$	$\vdots$	$\vdots$	$\vdots$
$g_3^{(j-1;\,r,0)}(\boldsymbol{p},\boldsymbol{I})$	$g_3^{(j-1;\,r,1)}(\boldsymbol{p},\boldsymbol{I},\boldsymbol{\alpha})$	$\dots$	$g_3^{(j-1;\,r,j-1)}(\boldsymbol{p},\boldsymbol{I},\boldsymbol{\alpha})$	$g_3^{(j-1;\,r,j)}(\boldsymbol{p},\boldsymbol{I},\boldsymbol{\alpha})$	$\dots$	$g_3^{(j-1;\,r,\mathcal{N}_S)}(\boldsymbol{p},\boldsymbol{I},\boldsymbol{\alpha})$	$\leftarrow 3$
$\boldsymbol{\omega}_B\cdot\boldsymbol{p}+\boldsymbol{\Omega}_B\cdot\boldsymbol{I}$	0	$\dots$	0	0	$\dots$	0	$\leftarrow 2$
0	0	$\dots$	0	0	$\dots$	0	$\leftarrow 1$
$\mathcal{E}_B$	0	$\dots$	0	0	$\dots$	0	$\leftarrow 0$
$\uparrow$	$\uparrow$	$\dots$	$\uparrow$	$\uparrow$	$\dots$	$\uparrow$	
0	1		$j-1$	j		$\mathcal{N}_S$	

Table 4.15: Graphical representation of the expansion of the Hamiltonian after after $j-1$ substeps (of the r-th normalization step of the algorithm constructing the resonant normal form).

The j-th substep generating function $\chi_B^{(j;\,r)}$ is determined by the following homological equation:

$$\{\boldsymbol{\omega}_B\cdot\boldsymbol{p}+\boldsymbol{\Omega}_B\cdot\boldsymbol{I}\,,\chi_B^{(j;\,r)}\} + g_{r+2}^{(j-1;\,r,j)}(\boldsymbol{p},\boldsymbol{q},\boldsymbol{I},\boldsymbol{\alpha}) = \left\langle g_{r+2}^{(j-1;\,r,j)}\right\rangle_{\boldsymbol{q}}. \tag{4.45}$$

Proceeding in a similar way as in the description of the third substep of the previous Subsection 4.4.1, first we write the expansion of the perturbing function in the form

$$g_{r+2}^{(j-1;\,r,j)}(\boldsymbol{p},\boldsymbol{q},\boldsymbol{I},\boldsymbol{\alpha}) = \sum_{2|\boldsymbol{m}|+|\boldsymbol{l}|=r+2} \sum_{\boldsymbol{m}\in\mathbb{N}^{n_1}} \sum_{\boldsymbol{l}\in\mathbb{N}^{n_2}} \sum_{\substack{\boldsymbol{k}\in\mathbb{Z}^{n_1} \\ |\boldsymbol{k}|+|\widehat{\boldsymbol{l}}|\le jK}} \sum_{\substack{\widehat{l}_{j_2}=-l_{j_2},-l_{j_2}+2,\ldots,l_{j_2} \\ j_2=1,\ldots,n_2}} c_{\boldsymbol{m},\boldsymbol{l},\boldsymbol{k},\widehat{\boldsymbol{l}}}\, \boldsymbol{p}^{\boldsymbol{m}} \left(\sqrt{\boldsymbol{I}}\right)^{\boldsymbol{l}} e^{i\left(\boldsymbol{k}\cdot\boldsymbol{q}+\widehat{\boldsymbol{l}}\cdot\boldsymbol{\alpha}\right)} . \tag{4.46}$$

The solution of the homological equation (4.45) is then

$$\chi_B^{(j;\,r)}(\boldsymbol{p},\boldsymbol{q},\boldsymbol{I},\boldsymbol{\alpha}) = \sum_{2|\boldsymbol{m}|+|\boldsymbol{l}|=r+2} \sum_{\boldsymbol{m}\in\mathbb{N}^{n_1}} \sum_{\boldsymbol{l}\in\mathbb{N}^{n_2}} \sum_{\substack{\boldsymbol{k}\in\mathbb{Z}^{n_1},\,|\boldsymbol{k}|>0 \\ |\boldsymbol{k}|+|\widehat{\boldsymbol{l}}|\le jK}} \sum_{\substack{\widehat{l}_{j_2}=-l_{j_2},-l_{j_2}+2,\ldots,l_{j_2} \\ j_2=1,\ldots,n_2}} \frac{c_{\boldsymbol{m},\boldsymbol{l},\boldsymbol{k},\widehat{\boldsymbol{l}}}}{i\left(\boldsymbol{k}\cdot\boldsymbol{\omega}_B+\widehat{\boldsymbol{l}}\cdot\boldsymbol{\Omega}_B\right)}\ \boldsymbol{p}^{\boldsymbol{m}} \left(\sqrt{\boldsymbol{I}}\right)^{\boldsymbol{l}} e^{i\left(\boldsymbol{k}\cdot\boldsymbol{q}+\widehat{\boldsymbol{l}}\cdot\boldsymbol{\alpha}\right)} . \tag{4.47}$$

We can now apply the transformation $\exp\left(L_{\chi_B^{(j;\,r)}}\right)$ to the Hamiltonian $\mathcal{H}_B^{(j-1;\,r)}$. By the usual abuse of notation (i.e., the new canonical coordinates are denoted with the same symbols of the old ones), the expansion of the new Hamiltonian can be written as

$$\begin{aligned}
\mathcal{H}_B^{(j;\,r)}(\boldsymbol{p},\boldsymbol{q},\boldsymbol{I},\boldsymbol{\alpha}) &= \exp\left(L_{\chi_B^{(j;\,r)}}\right)\mathcal{H}_B^{(j-1;\,r)} \\
&= \mathcal{E}_B + \boldsymbol{\omega}_B\cdot\boldsymbol{p} + \boldsymbol{\Omega}_B\cdot\boldsymbol{I} + \sum_{l\ge 3} g_l^{(j;\,r,0)}(\boldsymbol{p},\boldsymbol{I}) \\
&\quad + \sum_{s=1}^{\mathcal{N}_S} \sum_{3\le l\le r+1} g_l^{(j;\,r,s)}(\boldsymbol{p},\boldsymbol{I},\boldsymbol{\alpha}) + \sum_{s=1}^{j} g_{r+2}^{(j;\,r,s)}(\boldsymbol{p},\boldsymbol{I},\boldsymbol{\alpha}) \\
&\quad + \sum_{s=j+1}^{\mathcal{N}_S} g_{r+2}^{(j;\,r,s)}(\boldsymbol{p},\boldsymbol{q},\boldsymbol{I},\boldsymbol{\alpha}) + \sum_{s=1}^{\mathcal{N}_S} \sum_{l\ge r+3} g_l^{(j;\,r,s)}(\boldsymbol{p},\boldsymbol{q},\boldsymbol{I},\boldsymbol{\alpha}) .
\end{aligned} \tag{4.48}$$

In a similar way to what has been done previously, it is convenient to first define the new Hamiltonian terms as the old ones, i.e., $g_l^{(j;\,r,s)} = g_l^{(j-1;\,r,s)}\ \forall\, l\ge 0\,,\ 0\le s\le \mathcal{N}_S$; hence, each term generated by the Lie derivatives with respect to $\chi_B^{(j;\,r)}$ is added to the corresponding class of functions. This is made by the following sequence[18] of redefinitions

$$\begin{aligned}
&g_{l+mr}^{(j;\,r,s+mj)} \hookleftarrow \frac{1}{m!} L^m_{\chi_B^{(j;\,r)}} g_l^{(j;\,r,s)} \qquad \forall\, l\ge 0,\ 1\le m\le \lfloor(\mathcal{N}_S-s)/j\rfloor,\ 0\le s\le\mathcal{N}_S\,, \\
&g_{2+mr}^{(j;\,r,mj)} \hookleftarrow \frac{1}{m!} L^m_{\chi_B^{(j;\,r)}} \left(\boldsymbol{\omega}_B\cdot\boldsymbol{p}+\Omega_B\cdot\boldsymbol{I}\right) \qquad \forall\, 1\le m\le\lfloor\mathcal{N}_S/j\rfloor\,.
\end{aligned} \tag{4.49}$$

In fact, since $\chi_B^{(j;\,r)} \in \mathfrak{B}_{r+2,jK}$, each application of the Lie derivative operator $L_{\chi_B^{(j;\,r)}}$ increases the degree in square root of the actions and the trigonometrical degree in the angles by r and jK, respectively. Moreover, thanks to the homological equation (4.45) and the second rule included in formula (4.49) (in the case with $m=1$), one can easily remark that $g_{r+2}^{(j;\,r,j)} = \left\langle g_{r+2}^{(j-1;\,r,j)}\right\rangle_{\boldsymbol{q}}$. By applying Lemma 4.4.2 one can verify also that $g_l^{(j;\,r,s)} \in \mathfrak{B}_{l,sK}\,,\ \forall l\ge 0,\ s\ge 0$.

[18] From a practical point of view, since we have to deal with finite series, that are truncated in such a way that the indexes s and l do not exceed the threshold values $\mathcal{N}_S$ and $\mathcal{N}_L$, respectively, then we have to require that $1\le m\le \min\left((\mathcal{N}_L-l)/r,\lfloor(\mathcal{N}_S-s)/j\rfloor\right)$, which is more restrictive with respect to the corresponding rule appearing in (4.49).

The r-th step of the algorithm constructing the resonant normal form is completed at the end of the iterative repetition of the j-th substep for $j = 1, \dots, \mathcal{N}_S$. Therefore, the expansion of the Hamiltonian can be written in the following form:

$$\begin{aligned}\mathcal{H}_B^{(r)}(\boldsymbol{p},\boldsymbol{q},\boldsymbol{I},\boldsymbol{\alpha}) &= \exp\left(L_{\chi_B^{(\mathcal{N}_S;\,r)}}\right)\cdots\exp\left(L_{\chi_B^{(1;\,r)}}\right)\mathcal{H}_B^{(r-1)} \\ &= \mathcal{E}_B + \boldsymbol{\omega}_B\cdot\boldsymbol{p} + \boldsymbol{\Omega}_B\cdot\boldsymbol{I} + \sum_{l\geq 3} g_l^{(r,0)}(\boldsymbol{p},\boldsymbol{I}) \\ &\quad + \sum_{s=1}^{\mathcal{N}_S}\sum_{3\leq l\leq r+2} g_l^{(r,s)}(\boldsymbol{p},\boldsymbol{I},\boldsymbol{\alpha}) + \sum_{s=1}^{\mathcal{N}_S}\sum_{l\geq r+3} g_l^{(r,s)}(\boldsymbol{p},\boldsymbol{q},\boldsymbol{I},\boldsymbol{\alpha})\,,\end{aligned} \tag{4.50}$$

where $g_l^{(r,s)} := g_l^{(\mathcal{N}_S;\,r,s)}\,, \forall\, l \geq 0\,, 0 \leq s \leq \mathcal{N}_S$. Then, the normalization algorithm can be iteratively repeated. Since we are interested in the computer implementation, we consider finite sequences of Hamiltonians whose expansion is truncated up to a finite degree, say, $\mathcal{N}_L$ in the square root of the actions. Therefore, the iteration of $\mathcal{N}_L - 2$ normalization steps of the algorithm constructing the resonant normal form are sufficient to obtain

$$\mathcal{H}_B^{(\mathcal{N}_L-2)}(\boldsymbol{p},\boldsymbol{I},\boldsymbol{\alpha}) = \mathcal{E}_B + \boldsymbol{\omega}_B\cdot\boldsymbol{p} + \boldsymbol{\Omega}_B\cdot\boldsymbol{I} + \sum_{s=0}^{\mathcal{N}_S}\sum_{l=3}^{\mathcal{N}_L} g_l^{(\mathcal{N}_L-2,s)}(\boldsymbol{p},\boldsymbol{I},\boldsymbol{\alpha})\,. \tag{4.51}$$

The Hamiltonian (4.51) does not depend on the angles $\boldsymbol{q}$. Therefore, the corresponding actions $\boldsymbol{p}$ are constant and they can be considered as parameters whose values are fixed by the initial conditions; this allows us to decrease the number of degrees of freedom by n_1, passing from $n_1 + n_2$ to n_2.

4.5 Application of the normalization algorithms to the secular quasi-periodic restricted model of the dynamics of υ-And b

The SQPR model can be reformulated in such a way as to resume the form of a Hamiltonian of the type (4.18), to which we can sequentially apply both normalization procedures described in the two previous subsections. In fact, the canonical change of variables

$$\begin{aligned}\xi_1 &= \sqrt{2I_1}\cos(\alpha_1)\,, & \eta_1 &= \sqrt{2I_1}\sin(\alpha_1)\,, \\ P_1 &= \sqrt{2I_2}\cos(\alpha_2)\,, & Q_1 &= \sqrt{2I_2}\sin(\alpha_2)\,,\end{aligned} \tag{4.52}$$

allows to rewrite the expansion of the SQPR Hamiltonian (4.14) as follows:

$$\begin{aligned}\mathcal{H}_{sec,\,2+3/2}(\boldsymbol{p},\boldsymbol{q},\boldsymbol{I},\boldsymbol{\alpha}) &= \omega_3\,p_3 + \omega_4\,p_4 + \omega_5\,p_5 \\ &+ \sum_{\substack{l_1+l_2=0\\(l_1\,,\,l_2)\in\mathbb{N}^2}}^{\mathcal{N}_L}\ \sum_{\substack{(k_3\,,\,k_4\,,\,k_5)\in\mathbb{Z}^3\\|\boldsymbol{k}|\leq\mathcal{N}_S K}}\ \sum_{\substack{k_j=-l_j,-l_j+2,\dots,l_j\\j=1,\,2}} c_{\boldsymbol{l},\boldsymbol{k}}(\sqrt{I_1})^{l_1}(\sqrt{I_2})^{l_2}e^{i(k_1\alpha_1+k_2\alpha_2+k_3q_3+k_4q_4+k_5q_5)}\,,\end{aligned} \tag{4.53}$$

where $\boldsymbol{k} = (k_1, \dots, k_5) \in \mathbb{Z}^5$. The r.h.s. of the above equation can be expressed in the general and more compact form described in equation (4.18), by setting $n_1 = 3$, $n_2 = 2$, $\boldsymbol{\omega}^{(0)} = \boldsymbol{\omega} = (\omega_3, \omega_4, \omega_5) \in \mathbb{R}^3$, that are the fundamental frequencies of the two outer planets (described in equation (4.8)), while $\boldsymbol{\Omega}^{(0)} \in \mathbb{R}^2$ can be easily determined by performing the so called diagonalization of the Hamiltonian part quadratic in the square root of the actions $\boldsymbol{I}$ and not depending on the

angles $\boldsymbol{q}$ (see, e.g., in [32]). In the equation above, the parameters $\mathcal{N}_L$ and $\mathcal{N}_S$ define the truncation order of the expansions in Taylor and Fourier series, respectively, in such a way to represent on the computer just a finite number of terms that are not too many to handle with; in our computations we have fixed $\mathcal{N}_L = 6$ as maximal power degree in square root of the actions and we have decided to include Fourier terms up to a maximal trigonometric degree of 8, putting $\mathcal{N}_S = 4$, $K = 2$. We recall that setting $K = 2$ is quite natural for Hamiltonian systems close to stable equilibria as it is for models describing the secular planetary dynamics, see, e.g., [35]. Let us also remark that a simple reordering of the summands according to the total trigonometric degree $|\boldsymbol{k}|$ in the angles $(\boldsymbol{q}, \boldsymbol{\alpha})$ allows us to represent the second row of formula (4.53) as a sum of Hamiltonian terms each of them is belonging to a functions class of type $\mathfrak{B}_{l,sK}$, which is unique for any positive integer K if we ask for the minimality of the index s. These comments can be used all together in order to formally verify that the new expansion of $\mathcal{H}_{sec,\,2+3/2}$ in (4.53) can be finally reexpressed in the same form as $\mathcal{H}^{(0)}$ in (4.18).

Furthermore, in the case of our SQPR model of the secular dynamics of υ-And **b**, the only term depending on the action variables $\boldsymbol{p}$ (that are the so called dummy variables) is $\boldsymbol{\omega}^{(0)} \cdot \boldsymbol{p}$; thus, none of the Hamiltonian term $f_l^{(0,s)}$ is depending on $\boldsymbol{p}$. This fact would allow to introduce some simplification in the computational algorithm. For instance, the value of the angular velocity vector $\boldsymbol{\omega}^{(0)}$ is not modified during the first normalization procedure (i.e. the algorithmic construction of the elliptic tori) and it will remain equal to its initial value, given by the fundamental frequencies described in (4.8). Therefore, the expansion of the starting Hamiltonian in the special case of our SQPR model could have been rewritten as

$$\mathcal{H}^{(0)}(\boldsymbol{p},\boldsymbol{q},\boldsymbol{I},\boldsymbol{\alpha}) = \mathcal{E}^{(0)} + \boldsymbol{\omega}^{(0)} \cdot \boldsymbol{p} + \boldsymbol{\Omega}^{(0)} \cdot \boldsymbol{I} + \sum_{s=0}^{\mathcal{N}_S} \sum_{l=3}^{\mathcal{N}_L} f_l^{(0,s)}(\boldsymbol{q},\boldsymbol{I},\boldsymbol{\alpha}) + \sum_{s=1}^{\mathcal{N}_S} \sum_{l=0}^{2} f_l^{(0,s)}(\boldsymbol{q},\boldsymbol{I},\boldsymbol{\alpha})\,;$$

however, in our opinion, for what concerns the general description of the previous subsections it has been worth to consider also an eventual dependence of $f_l^{(0,s)}$ on $\boldsymbol{p}$ in order to keep the discussion of the constructive procedure as general as possible.

The first algorithm to be applied aims to construct the normal form corresponding to an invariant elliptic torus. It starts from the Hamiltonian $\mathcal{H}_{sec,\,2+3/2}$ rewritten in the same form as $\mathcal{H}^{(0)}$ in (4.18) and its computational procedure is fully detailed in Subsection 4.4.1. Therefore, we perform $\mathcal{N}_S$ normalization steps of this first normalization algorithm. This allows us to bring the Hamiltonian in the following (intermediate) normal form:

$$\mathcal{H}^{(\mathcal{N}_S)}(\boldsymbol{p},\boldsymbol{q},\boldsymbol{I},\boldsymbol{\alpha}) = \mathcal{E}^{(\mathcal{N}_S)} + \boldsymbol{\omega}^{(\mathcal{N}_S)} \cdot \boldsymbol{p} + \boldsymbol{\Omega}^{(\mathcal{N}_S)} \cdot \boldsymbol{I} + \sum_{s=0}^{\mathcal{N}_S} \sum_{l\geq 3}^{\mathcal{N}_L} f_l^{(\mathcal{N}_S,s)}(\boldsymbol{q},\boldsymbol{I},\boldsymbol{\alpha})\,,$$

where $f_l^{(\mathcal{N}_S,s)} \in \mathfrak{B}_{l,sK}$ and $\forall\, l = 3, \ldots, \mathcal{N}_L$, $s = 0, \ldots, \mathcal{N}_S$ and the angular velocity vector related to the angles $\boldsymbol{q}$ is such that $\boldsymbol{\omega}^{(\mathcal{N}_S)} = \boldsymbol{\omega}^{(0)} = (\omega_3, \omega_4, \omega_5)$, whose components are given in (4.8).

It is now possible to apply the second algorithm aiming to construct a resonant normal form where the dependence on the angles $\boldsymbol{q} = (q_3, q_4, q_5)$ is completely removed. Such a normalization starts from the Hamiltonian $\mathcal{H}^{(\mathcal{N}_S)}$ obtained after the first normalization procedure. Therefore, we perform $\mathcal{N}_L - 2$ normalization steps of the above algorithm, each of them involving $\mathcal{N}_S$ substeps as described in Subsection 4.4.2; this allows us to bring the Hamiltonian in the following (final) normal form:

$$\mathcal{H}_{2DOF}(\boldsymbol{p},\boldsymbol{I},\boldsymbol{\alpha}) = \mathcal{E}_B + \boldsymbol{\omega}_B \cdot \boldsymbol{p} + \boldsymbol{\Omega}_B \cdot \boldsymbol{I} + \sum_{l=3}^{\mathcal{N}_L} g_l^{(\mathcal{N}_L-2,0)}(\boldsymbol{I}) + \sum_{s=1}^{\mathcal{N}_S} \sum_{l=3}^{\mathcal{N}_L} g_l^{(\mathcal{N}_L-2,s)}(\boldsymbol{I},\boldsymbol{\alpha})\,, \qquad (4.54)$$

where $g_l^{(\mathcal{N}_L-2,s)} \in \mathfrak{B}_{l,sK}$ $\forall\, l = 3, \ldots, \mathcal{N}_L$, $s = 0, \ldots, \mathcal{N}_S$ and it still holds true that $\boldsymbol{\omega}_B = \boldsymbol{\omega}^{(0)}$.

All the algebraic manipulations that are prescribed by the normal form algorithms have been performed by using the symbolic manipulator `Mathematica` as a programming framework.

4.5 Application of the normalization algorithms to the secular quasi-periodic restricted model of the dynamics of υ-And b

In view of the numerical explorations of the dynamical evolution of our new model described by the Hamiltonian $\mathcal{H}_{2DOF}(\boldsymbol{p},\boldsymbol{I},\boldsymbol{\alpha})$, it is convenient to introduce the canonical transformations related to the so called semianalytic method of integration for the equations of motion (see, e.g., [35]). In order to fix the ideas, let us focus on the second algorithm, designed to construct a resonant normal form. This normalization procedure can be summarized by the transformation that is obtained by iteratively applying all the Lie series to the canonical variables; this is done as follows:

$$\begin{aligned} I_i = &\exp\left(L_{\chi_B^{(\mathcal{N}_S;\,\mathcal{N}_L-2)}}\right)\ldots\exp\left(L_{\chi_B^{(2;\,\mathcal{N}_L-2)}}\right)\exp\left(L_{\chi_B^{(1;\,\mathcal{N}_L-2)}}\right)\ldots\ldots \\ &\qquad\ldots\exp\left(L_{\chi_B^{(\mathcal{N}_S;\,1)}}\right)\ldots\exp\left(L_{\chi_B^{(2;\,1)}}\right)\exp\left(L_{\chi_B^{(1;\,1)}}\right) I_i\Big|_{\substack{\boldsymbol{I}=\tilde{\boldsymbol{I}}\\ \boldsymbol{\alpha}=\tilde{\boldsymbol{\alpha}}}}\,, \\ \alpha_i = &\exp\left(L_{\chi_B^{(\mathcal{N}_S;\,\mathcal{N}_L-2)}}\right)\ldots\exp\left(L_{\chi_B^{(2;\,\mathcal{N}_L-2)}}\right)\exp\left(L_{\chi_B^{(1;\,\mathcal{N}_L-2)}}\right)\ldots\ldots \\ &\qquad\ldots\exp\left(L_{\chi_B^{(\mathcal{N}_S;\,1)}}\right)\ldots\exp\left(L_{\chi_B^{(2;\,1)}}\right)\exp\left(L_{\chi_B^{(1;\,1)}}\right) \alpha_i\Big|_{\substack{\boldsymbol{I}=\tilde{\boldsymbol{I}}\\ \boldsymbol{\alpha}=\tilde{\boldsymbol{\alpha}}}}\,, \end{aligned} \tag{4.55}$$

for $i=1,2$. We introduce the symbol $\mathscr{C}_B$ to denote the change of coordinates[19] defined by the above expressions, i.e., $(\boldsymbol{I},\boldsymbol{\alpha})=\mathscr{C}_B(\boldsymbol{q},\tilde{\boldsymbol{I}},\tilde{\boldsymbol{\alpha}})$. We can proceed in the same way for what concerns the algorithm constructing the normal form corresponding to an invariant elliptic torus. In fact, we first introduce the application of all the Lie series to the canonical variables in such a way to write, $\forall\ i=1,2$,

$$\begin{aligned} I_i =&\exp\left(L_{\chi_2^{(\mathcal{N}_S)}}\right)\exp\left(L_{\chi_1^{(\mathcal{N}_S)}}\right)\exp\left(L_{\chi_0^{(\mathcal{N}_S)}}\right)\ldots\exp\left(L_{\chi_2^{(1)}}\right)\exp\left(L_{\chi_1^{(1)}}\right)\exp\left(L_{\chi_0^{(1)}}\right) I_i\Big|_{\substack{\boldsymbol{I}=\hat{\boldsymbol{I}}\\ \boldsymbol{\alpha}=\hat{\boldsymbol{\alpha}}}}\,, \\ \alpha_i =&\exp\left(L_{\chi_2^{(\mathcal{N}_S)}}\right)\exp\left(L_{\chi_1^{(\mathcal{N}_S)}}\right)\exp\left(L_{\chi_0^{(\mathcal{N}_S)}}\right)\ldots\exp\left(L_{\chi_2^{(1)}}\right)\exp\left(L_{\chi_1^{(1)}}\right)\exp\left(L_{\chi_0^{(1)}}\right) \alpha_i\Big|_{\substack{\boldsymbol{I}=\hat{\boldsymbol{I}}\\ \boldsymbol{\alpha}=\hat{\boldsymbol{\alpha}}}}\,; \end{aligned} \tag{4.56}$$

finally, we use the symbol $\mathscr{C}$ to summarize the whole change of coordinates that is defined by the whole expression above, i.e., $(\boldsymbol{I},\boldsymbol{\alpha})=\mathscr{C}(\boldsymbol{q},\hat{\boldsymbol{I}},\hat{\boldsymbol{\alpha}})$. Let us now introduce the function $\mathscr{F}:\mathbb{T}^3\times\mathbb{R}^2_{\geq 0}\times\mathbb{T}^2\to\mathbb{R}^2_{\geq 0}\times\mathbb{T}^2$, which is defined so that

$$\mathscr{F}(\boldsymbol{q},\tilde{\boldsymbol{I}},\tilde{\boldsymbol{\alpha}})=\mathscr{C}\big(\boldsymbol{q},\mathscr{C}_B(\boldsymbol{q},\tilde{\boldsymbol{I}},\tilde{\boldsymbol{\alpha}})\big)\,, \tag{4.57}$$

where we have omitted to put the $\tilde{}$ symbol on top of $\boldsymbol{q}$ in order to stress that the angles $\boldsymbol{q}$ are not affected by the change of coordinates. Moreover, let also introduce the symbol $\mathcal{A}$ to denote the usual canonical transformation defining the action-angle variables for the harmonic oscillator, i.e., by equation (4.52), in our case this means that

$$\mathcal{A}(\boldsymbol{I},\boldsymbol{\alpha})=\big(\sqrt{2I_1}\cos(\alpha_1),\,\sqrt{2I_1}\sin(\alpha_1),\,\sqrt{2I_2}\cos(\alpha_2),\,\sqrt{2I_2}\sin(\alpha_2)\big)\,. \tag{4.58}$$

By applying the Exchange Theorem 1.1.6 (subsection 1.1.3 (see also [36] and [30]), the solutions of the equations of motions related to $\mathcal{H}_{2DOF}$ can be mapped to those for $\mathcal{H}_{sec,\,2+3/2}$. Indeed, assume that $t\mapsto\big(\tilde{\boldsymbol{p}}(t),\,\tilde{\boldsymbol{q}}(t),\,\tilde{\boldsymbol{I}}(t),\,\tilde{\boldsymbol{\alpha}}(t)\big)$ is an orbit corresponding to the flow induced by $\mathcal{H}_{2DOF}$; in particular, in our model we have that $\tilde{\boldsymbol{q}}(t)=\boldsymbol{\omega}_B t=\boldsymbol{\omega}t$, where the components of the angular velocity vector $\boldsymbol{\omega}$ are given in equation (4.8). Then, the orbit

$$t\mapsto\big(\boldsymbol{\omega}t\,,\,\mathcal{A}\big(\mathscr{F}(\boldsymbol{\omega}t,\tilde{\boldsymbol{I}}(t),\tilde{\boldsymbol{\alpha}}(t))\big)\big) \tag{4.59}$$

[19] Since none of the generating functions $\chi_B^{(j;\,r)}$ depends on $\boldsymbol{p}$, the way that these dummy variables are modified by the application of the Lie series does not really matter, because they do not enter in Hamilton's equations of motion (4.16), under the Hamiltonian $\mathcal{H}_{sec,\,2+3/2}$. Since, however, the generating functions do depend on $\boldsymbol{q}$ (but not on their conjugate actions $\boldsymbol{p}$, as we have remarked just above) in the arguments of $\mathscr{C}_B$ we have included also the angles $\boldsymbol{q}$ that are not affected by any modification due to the application of the Lie series.

is an approximate[20] solution of the Hamilton's equations (4.16).

For our purposes, it is also useful to construct the inverse of the function $\mathscr{F}$, which maps from the original canonical coordinates to the ones referring to the resonant normal form. Therefore, it is convenient to replace all the compositions of Lie series appearing in the r.h.s. (4.56) with the following expressions, $\forall\ i = 1, 2$:

$$\begin{aligned}\hat{I}_i &= \exp\left(L_{-\chi_0^{(1)}}\right)\exp\left(L_{-\chi_1^{(1)}}\right)\exp\left(L_{-\chi_2^{(1)}}\right)\ldots\exp\left(L_{-\chi_0^{(\mathcal{N}_S)}}\right)\exp\left(L_{-\chi_1^{(\mathcal{N}_S)}}\right)\exp\left(L_{-\chi_2^{(\mathcal{N}_S)}}\right) I_i\,,\\ \hat{\alpha}_i &= \exp\left(L_{-\chi_0^{(1)}}\right)\exp\left(L_{-\chi_1^{(1)}}\right)\exp\left(L_{-\chi_2^{(1)}}\right)\ldots\exp\left(L_{-\chi_0^{(\mathcal{N}_S)}}\right)\exp\left(L_{-\chi_1^{(\mathcal{N}_S)}}\right)\exp\left(L_{-\chi_2^{(\mathcal{N}_S)}}\right) \alpha_i;\end{aligned} \tag{4.60}$$

gathering all the corresponding changes of coordinates allows us to define[21] $\mathscr{C}^{-1}(\boldsymbol{q}, \boldsymbol{I}, \boldsymbol{\alpha})$. Proceeding in an analogous way, we can introduce the inverse function of $\mathscr{C}_B$; in more detail, we can start from formula (4.55), by reversing the order of all the Lie series and by changing the sign to all the generating functions, then we can define $\mathscr{C}_B^{-1}(\boldsymbol{q}, \boldsymbol{I}, \boldsymbol{\alpha})$. Therefore, we can introduce also

$$\mathscr{F}^{-1}(\boldsymbol{q}, \boldsymbol{I}, \boldsymbol{\alpha}) = \mathscr{C}_B^{-1}\big(\boldsymbol{q}, \mathscr{C}^{-1}(\boldsymbol{q}, \boldsymbol{I}, \boldsymbol{\alpha})\big)\,. \tag{4.61}$$

We are now ready to exploit the (fast) numerical integrations of the 2 DOF Hamiltonian, which is described in (4.54) when the dummy variables $\boldsymbol{p}$ are disregarded, in order to retrieve information about the secular dynamics of υ-And **b** through our SQPR model. This can be done thanks to the knowledge of the approximate solution (4.59). The initial conditions are selected in the same way as in Subsection 4.3.1.2: we consider the initial orbital elements reported in Table 4.7 and the minimal possible value of the mass of υ-And **b**, i.e., $m_1 = 0.674\ M_J$. These data are completed with the values of $(\mathrm{i}_1(0)\,, \Omega_1(0))$ ranging in the regular 20×60 grid that covers $I_\mathrm{i} \times I_\Omega = [6.865°, 34°] \times [0°, 360°]$; moreover, all these initial values of the orbital elements are translated in the Laplace frame, which refers only to the two outermost exoplanets. Hence, we can compute a set of 21×60 initial conditions of type $\big(\boldsymbol{I}(0), \boldsymbol{\alpha}(0)\big) = \mathcal{A}^{-1}\big(\xi_1(0), \eta_1(0), P_1(0), Q_1(0)\big)$, by using formula (4.2) with $j = 1$, and using the definition (4.58). Finally, we can translate the initial conditions to initial values of the canonical coordinates found after the resonant normal form, by computing $\big(\tilde{\boldsymbol{I}}(0), \tilde{\boldsymbol{\alpha}}(0)\big) = \mathscr{F}^{-1}\big(\boldsymbol{0}, \boldsymbol{I}(0), \boldsymbol{\alpha}(0)\big)$.

As shown below, an important information is obtained by a criterion allowing to identify those domains of initial conditions in which the series are either divergent or slowly converging. We introduce such a criterion to preselect initial conditions that are admissible. From a mathematical point of view, the identity $(\boldsymbol{I}(0), \boldsymbol{\alpha}(0)) = (\boldsymbol{I}^O(0), \boldsymbol{\alpha}^O(0)) = \mathscr{F}\big(\boldsymbol{0}, \mathscr{F}^{-1}\big(\boldsymbol{0}, \boldsymbol{I}(0), \boldsymbol{\alpha}(0)\big)\big)$ holds in a domain where the normalization procedure is convergent, provided that no truncations are applied to the series $\mathscr{F}$ and $\mathscr{F}^{-1}$ and that the computation of the series is not affected by any round-off errors. Due to the errors and truncations introduced in the computation, however, in general we

[20] There are at least two substantial reasons for which this motion law, which has been produced by a (so called) semi-analytic integration scheme, is not an *exact* solution of the equations (4.16). Let us recall that Lie series define near-to-the-identity canonical transformations that are well defined on suitable restrictions of the phase space. However, we are always working with finite truncated series; therefore, the corresponding changes of variables cannot preserve exactly the solutions because infinite tails of summands are neglected. Moreover, in the resonant normal form $\mathcal{H}_{2DOF}$ described in (4.54) we have not included the remainder terms; let us recall that they become dominant if the Birkhoff algorithm is iterated infinitely many times, making the series expansion of the normal form to be divergent. Therefore, the semi-analytic solutions are prevented to be exact also because of this second source of truncations acting on the series expansion of the Hamiltonians (instead of the Lie series defining the canonical transformations). As a final remark, let us also recall that in order to be canonical the change of coordinates should include also the dummy actions $\boldsymbol{p}$, in which we are not intested at all because they do not exert any role in the equations of motion (4.16).

[21] Of course, since also $\mathscr{C}^{-1} : \mathbb{T}^3 \times \mathbb{R}^2_{\geq 0} \times \mathbb{T}^2 \to \mathbb{R}^2_{\geq 0} \times \mathbb{T}^2$ (i.e., $\mathscr{C}$ and $\mathscr{C}^{-1}$ share the same domains and codomains,which are different between them), then $\mathscr{C}^{-1}$ cannot be considered as the inverse function in a strict sense. However, if we extend trivially both these functions, in such a way to introduce $\hat{\mathscr{C}}(\boldsymbol{q}, \boldsymbol{I}, \boldsymbol{\alpha}) = \big(\boldsymbol{q}, \mathscr{C}(\boldsymbol{q}, \boldsymbol{I}, \boldsymbol{\alpha})\big)$ and $\hat{\mathscr{C}}^{-1}(\boldsymbol{q}, \boldsymbol{I}, \boldsymbol{\alpha}) = \big(\boldsymbol{q}, \mathscr{C}^{-1}(\boldsymbol{q}, \boldsymbol{I}, \boldsymbol{\alpha})\big)$, then $\hat{\mathscr{C}}^{-1}$ would really be the inverse function of $\hat{\mathscr{C}}$ (where elementary properties of the Lie series described in Chap. 4 of [30] are also used and the small effects due to the truncations are neglected). Therefore, it is by a harmless abuse of notation that we are adopting the symbol $\mathscr{C}^{-1}$. The same abuse will be made for what concerns the symbols $\mathscr{C}_B^{-1}$ and $\mathscr{F}^{-1}$.

obtain that $(\boldsymbol{I}(0),\boldsymbol{\alpha}(0)) \neq (\boldsymbol{I}^O(0),\boldsymbol{\alpha}^O(0))$. In the domain where the series expansions are rapidly converging the difference $(\boldsymbol{I}(0),\boldsymbol{\alpha}(0)) - (\boldsymbol{I}^O(0),\boldsymbol{\alpha}^O(0))$ is small. When, instead, we obtain a large difference, this is an indicator that we are outside the domain of convergence of the series. The situation is represented graphically below.

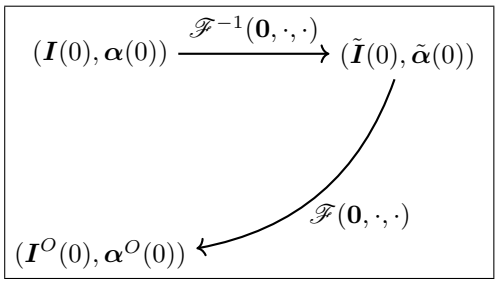

Figure 4.8: Graphical representation of the definitions about the initial conditions.

In view of the above, we define the following preselection criterion of *admissible initial conditions*. For any initial condition $(\boldsymbol{I}(0),\boldsymbol{\alpha}(0))$ we compute the quantities

$$\mathfrak{r}_1 = \frac{\sqrt{I_1(0)} - \sqrt{I_1^O(0)}}{\sqrt{I_1(0)}}\,, \qquad \mathfrak{r}_2 = \frac{\sqrt{I_2(0)} - \sqrt{I_2^O(0)}}{\sqrt{I_2(0)}}\,. \tag{4.62}$$

The use of the quantities $\sqrt{I_1}$ and $\sqrt{I_2}$ is motivated by the fact that they are of the same order of magnitude as the eccentricity and the inclination of υ-And **b**, respectively. Moreover, it is useful to define also the following ratios

$$\mathfrak{R}_1(t) = \frac{\sqrt{\big(\tilde{\xi}_1(t)\big)^2 + \big(\tilde{\eta}_1(t)\big)^2}}{\sqrt{\big(\tilde{\xi}_1(0)\big)^2 + \big(\tilde{\eta}_1(0)\big)^2}}\,, \qquad \mathfrak{R}_2(t) = \frac{\sqrt{\big(\tilde{P}_1(t)\big)^2 + \big(\tilde{Q}_1(t)\big)^2}}{\sqrt{\big(\tilde{P}_1(0)\big)^2 + \big(\tilde{Q}_1(0)\big)^2}}\,, \tag{4.63}$$

where

$$t \mapsto \big(\boldsymbol{\omega}t,\, \tilde{\xi}_1(t), \tilde{\eta}_1(t), \tilde{P}_1(t), \tilde{Q}_1(t)\big) := \big(\boldsymbol{\omega}t\,,\, \mathcal{A}\big(\mathscr{F}(\boldsymbol{\omega}t, \tilde{\boldsymbol{I}}(t), \tilde{\boldsymbol{\alpha}}(t))\big)\big)$$

is the approximate solution of Hamilton's equations (4.16), as produced by the semi-analytic integration scheme summarized in formula (4.59). Comparing formula (4.63) with the definition of the Poincaré canonical variables in (4.2), it is easy to realize that $\mathfrak{R}_1$ and $\mathfrak{R}_2$ are functions of the time that describe the behavior of the orbital excursions with respect to the eccentricity and the inclination of υ-And **b**, respectively. We then investigate the behaviour of the following function:

$$\tilde{\mathrm{e}}_1(t) = \sqrt{\frac{2\tilde{I}_1(t)}{\Lambda_1} - \frac{\tilde{I}_1^2(t)}{\Lambda_1^2}}\,. \tag{4.64}$$

Note that $\tilde{\mathrm{e}}_1$ would be equal to the eccentricity of υ-And **b** if $\tilde{I}_1$ was replaced by $\big(\xi_1^2+\eta_1^2\big)/2$, with $(\xi_1\,,\,\eta_1)$ defined in (4.2). However, the new action $\tilde{I}_1$ is conjugated to $\big(\tilde{\xi}_1^2+\tilde{\eta}_1^2\big)/2$ wich is only nearly equal to $\big(\xi_1^2+\eta_1^2\big)/2$, since the composition of the transformations $\mathscr{C}$ and $\mathscr{C}_B$ is near-to-identity. Therefore, we can consider $\tilde{\mathrm{e}}_1$ as an approximate evaluation of the eccentricity under the resonant normal form model. Let us also recall that since Λ_1 is a constant of motion in the secular model, the computation of the value of $\tilde{\mathrm{e}}_1$ is intrinsically faster with respect to the ones of the ratios defined in (4.64), because the former does not even require any evaluation of the change of coordinates $\mathscr{C}$ and $\mathscr{C}_B$, which are defined by rather cumbersome series expansions.

For each pair $\big(\mathrm{i}_1(0),\Omega_1(0)\big)$ of the 21×60 points definining the grid which covers $I_{\mathrm{i}}\times I_\Omega = [6.865^\circ, 34^\circ]\times[0^\circ, 360^\circ]$ we determine the corresponding initial conditions of type $(\boldsymbol{I}(0),\boldsymbol{\alpha}(0))$, as explained above, and we proceed as follows:

- if $\max\{\mathfrak{r}_1\,,\,\mathfrak{r}_2\} > 1$, then the corresponding initial condition is considered as "non-admissible", i.e. outside the domain of applicability of the series. Then, we skip the step below and pass directly to consider the next initial conditions of the grid;
- If the initial conditions is admissible, we numerically integrate the equations of motion by the 2 DOF Hamiltonian model (4.54), using a RK4 method and starting from $\big(\mathbf{0},\,\tilde{\boldsymbol{I}}(0),\tilde{\boldsymbol{\alpha}}(0)\big)$; during such a numerical integration, we compute the maximal values attained by the three previously defined numerical indicators, that are

$$\mathfrak{R}_{1\,\mathrm{MAX}} = \max_t\{\mathfrak{R}_1(t)\}\ , \qquad \mathfrak{R}_{2\,\mathrm{MAX}} = \max_t\{\mathfrak{R}_2(t)\}\ , \qquad \tilde{\mathrm{e}}_{1\,\mathrm{MAX}} = \max_t\{\tilde{\mathrm{e}}_1(t)\}\ .$$

The results about the maxima of the functions defined in (4.63)–(4.64) are reported in Figures 4.9–4.10. The white central regions of those pictures correspond to those pairs $\big(\mathrm{i}_1(0),\Omega_1(0)\big)$ for which we obtain failure of the preliminary test, i.e. $\max\{\mathfrak{r}_1\,,\,\mathfrak{r}_2\} > 1$. We immediately recognize that the missing part of the plots (where the determination of the initial conditions is considered so unreliable that the corresponding numerical integrations are not performed at all) nearly coincides with the central region of Figure 4.3a, where the orbital eccentricity of υ-And **b** reaches critical values. We conclude that the stability domain in the space of the initial values of $\mathrm{i}_1(0)$ and $\Omega_1(0)$ (which are unknown observational data) can be reconstructed in a reliable way through the application of the above criterion, which only involves the series transformations, as well as through the numerical integrations of our 2 DOF secular model. We emphasize that this allows to reduce significantly the computational cost with respect to the long-term symplectic integrations of the complete 4-body problem, which is a 9 DOF Hamiltonian system.

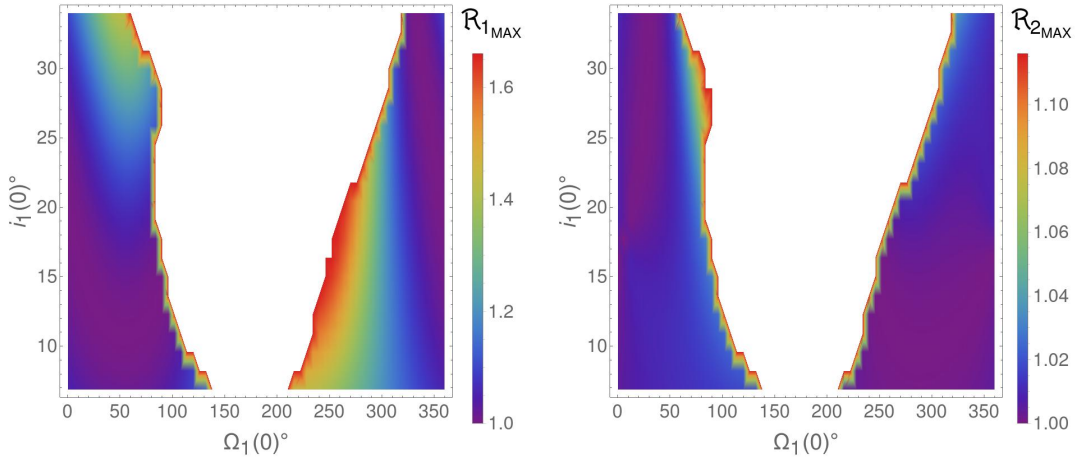

Figure 4.9: Color-grid plots of the maximal values reached by the ratio $\mathfrak{R}_1$ (on the left) and $\mathfrak{R}_2$ (on the right); see the text for more details.

Comparing the regions of the stability domain at the border near the (white) central ones, we see that all three numerical indicators plotted in Figures 4.9–4.10 increase their values when the unstable zone is approached. This is in agreement with the expectations and the comparison with Figure 4.3a. On the other hand, the 2 DOF secular model is unable to capture the region of instability internal to the stable one, highlighted by two green stripes starting from the bottom of Figure 4.3a in correspondence with $\Omega_1(0) = 0° = 360°$. The two curved stripes look rather symmetric and they join each other around the point $\big(\mathrm{i}_1(0)\,,\,\Omega_1(0)\big) \simeq \big(30°,\,0°\big) = \big(30°,\,360°\big)$. Since the dependence of the Hamiltonian on the angles $\boldsymbol{q}$ (which describes the dynamics of the outer exoplanets) was removed from the 2DOF model, it seems reasonable that some of the resonances are not present in the normal form generated by the algorithm *à la* Birkhoff, although they play a remarkable role in the dynamics of more complex models.

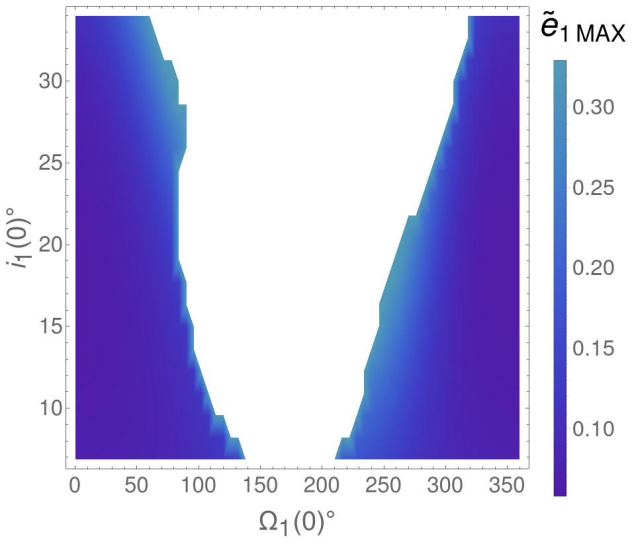

Figure 4.10: Color-grid plots of the maximum of the function $\tilde{\mathrm{e}}(t)$, which is defined in (4.64).

4.6 Secular orbital evolution of υ-And b taking also into account relativistic effects

In this section we study the dynamics of υ-And **b** in the framework of a secular quasi-periodic restricted Hamiltonian model where also corrections due to general relativity are taken into account. However, we still neglect relativistic effects on the orbital motion of the two outermost planets, whose dynamical evolution is preassigned as described in (4.6)–(4.8). In fact, let us recall that, in the Solar System, the general relativity contributes to the secular precession of the Mercury perihelion with an additional angular velocity term that is evaluated as $43''$ per century. Mercury is the planet for which such a relativistic effect is the most remarkable, due to its vicinity to the Sun (it is well known that its semi-major axis is approximately equal to 0.387 AU). Since in the υ-Andromedæ system we are focusing on the orbital dynamics of the innermost planet and it is very close to a star that is about 30% more massive than the Sun (let us recall that the value of the semi-major axis of υ-And **b** is reported in Table 4.7, i.e., $a_1 = 0.0594$ AU), it is natural to expect that the corrections due to general relativity can play a relevant role for the system under consideration.

Similarly as in the previous sections, we study these effects in the framework of a 2 DOF secular model. We start by considering the following Hamiltonian:

$$\mathcal{H} = \mathcal{H}_{4BP} + \mathcal{H}_{GR}\,,$$

where $\mathcal{H}_{4BP}$ defines the four body problem (see Eq. (4.10)) and $\mathcal{H}_{GR}$ describes the general (post-Newtonian) relativistic corrections to the Newtonian mechanics (see Eq. E.1 in Appendix E). Following [82], the secular quasi-periodic restricted Hamiltonian which includes corrections due to the General Relativity (hereafter, GR) is obtained by removing the dependence of the Hamiltonian on the fast angles. Therefore, we introduce

$$\mathcal{H}^{(GR)}_{sec} = \int_{\mathbb{T}^3} \frac{\mathcal{H}_{4BP}}{8\pi^3}\, d\lambda_1 d\lambda_2 d\lambda_3 + \int_{\mathbb{T}} \frac{\mathcal{H}_{GR}}{2\pi}\, dM_1 \;:= \mathcal{H}^{(NG)}_{sec} + \langle \mathcal{H}_{GR} \rangle_{M_1}\,, \tag{4.65}$$

where the expansions of the mean of the $4BP$ Hamiltonian (recall definition (4.11)) are explicitely written in equation (4.12), while the average of the GR contribution with respect to the mean anomaly of υ-And **b** is given by

$$\langle \mathcal{H}_{GR} \rangle_{M_1} = -\frac{3\,\mathcal{G}^2\, m_0^2\, m_1}{a_1^2 c^2 \sqrt{1-\mathrm{e}_1^2}} + \frac{15\,\mathcal{G}^2\, m_0^2\, m_1}{8 a_1^2 c^2} - \frac{\mathcal{G}^2\, m_0\, m_1^2}{8 a_1^2 c^2}\,, \tag{4.66}$$

c being the velocity of light in vacuum. In the above expression of $\langle \mathcal{H}_{GR} \rangle_{M_1}$, the summand where the eccentricity of υ-And **b** (i.e., e_1) occurs in the denominator is the only to be untrivial, in the sense that the other two give additional *constant* contribution to the secular Hamiltonian and, then, they can be disregarded. By proceeding in a similar way to what has been already done for the classical expansions of the initial Hamiltonian (4.1), it is possible to express $\langle \mathcal{H}_{GR} \rangle$ in the Poincaré variables (ξ_1, η_1), described in equation (4.2). More details on the computation of $\langle \mathcal{H}_{GR} \rangle$ are given in the Appendix E.

Thus, keeping in mind the procedure explained in Section 4.3, one easily realizes that the secular quasi-periodic restricted model of the dynamics of υ-And **b** which includes relativistic corrections (hereafter, SQPR-GR) can be described by the following $2 + 3/2$ DOF Hamiltonian:

$$\begin{aligned} \mathcal{H}^{(GR)}_{sec,\,2+\frac{3}{2}}(\boldsymbol{p}, \boldsymbol{q}, \xi_1, \eta_1, P_1, Q_1) &= \omega_3\, p_3 + \omega_4\, p_4 + \omega_5\, p_5 \\ &\quad + \mathcal{H}^{(NG)}_{sec}(q_3, q_4, q_5, \xi_1, \eta_1, P_1, Q_1) + \langle \mathcal{H}_{GR} \rangle_{M_1}(\xi_1, \eta_1)\,, \end{aligned} \tag{4.67}$$

where the angular velocity vector $\boldsymbol{\omega} = (\omega_3, \omega_4, \omega_5\,)$ is given in (4.8). Finally, in the framework of this SQPR-GR model the equations for the orbital motion of the innermost planet can be written as

$$\begin{cases} \dot{q_3} = \partial \mathcal{H}^{(GR)}_{sec,2+\frac{3}{2}} / \partial p_3 = \omega_3 \\ \dot{q_4} = \partial \mathcal{H}^{(GR)}_{sec,2+\frac{3}{2}} / \partial p_4 = \omega_4 \\ \dot{q_5} = \partial \mathcal{H}^{(GR)}_{sec,2+\frac{3}{2}} / \partial p_5 = \omega_5 \\ \dot{\xi}_1 = -\partial \left(\mathcal{H}^{(NG)}_{sec}(q_3, q_4, q_5, \xi_1, \eta_1, P_1, Q_1) + \langle \mathcal{H}_{GR} \rangle_{M_1}(\xi_1, \eta_1) \right) / \partial \eta_1 \\ \dot{\eta}_1 = \partial \left(\mathcal{H}^{(NG)}_{sec}(q_3, q_4, q_5, \xi_1, \eta_1, P_1, Q_1) + \langle \mathcal{H}_{GR} \rangle_{M_1}(\xi_1, \eta_1) \right) / \partial \xi_1 \\ \dot{P}_1 = -\partial \mathcal{H}^{(NG)}_{sec}(q_3, q_4, q_5, \xi_1, \eta_1, P_1, Q_1) / \partial Q_1 \\ \dot{Q}_1 = \partial \mathcal{H}^{(NG)}_{sec}(q_3, q_4, q_5, \xi_1, \eta_1, P_1, Q_1) / \partial P_1 \end{cases} . \tag{4.68}$$

4.6.1 Numerical integration of the SQPR-GR model

Similarly as in subsection 4.3.1.2, we numerically integrate the equations of motion for the secular quasi-periodic restricted Hamiltonian with general relativistic corrections, defined in formula (4.68). As initial values of the orbital parameters $a_1(0)$, $\mathrm{e}_1(0)$, $M_1(0)$ and $\omega_1(0)$ we take those reported in Table 4.7; moreover, we set $m_1 = 0.674$ as value for the mass of υ-And **b** and $(\mathrm{i}_1(0)\,, \Omega_1(0))$ ranging in the regular 20×60 grid that covers $I_\mathrm{i} \times I_\Omega = [6.865°, 34°] \times [0°, 360°]$. Hence, it is possible to compute the corresponding initial values of the orbital elements in the Laplace reference frame (which is determined taking into account υ-And **c** and υ-And **d** only) and to perform 21×60 numerical integrations starting from all these initial data. Once again, for each numerical integration, we are interested in determining the maximal values reached by the eccentricity of υ-And **b** and by the maximal mutual inclination between υ-And **b** and υ-And **c** . The results are reported in the color-grid plots of Figure 4.11.

By comparing Figure 4.11a with Figure 4.6a, one can immediately realize that the regions colored in blue are much wider in the former than in the latter one. Indeed, the darker regions refer to initial conditions which generate motions with maximal values of the eccentricity of υ-And **b** that are relatively low, while the zones colored in red or yellow correspond to such large values of the eccentricity implying that those orbits have to be considered unstable. Therefore, our numerical explorations highlight that the effects due to general relativity play a stabilizing role on the orbital dynamics of the innermost planet. This conclusion is in agreement with was already remarked about the past evolution of our Solar System, in particular for what concerns the orbital eccentricity of Mercury (see [52]).

Moreover, as already done in section 4.3.1.2, in order to further explore the stable and chaotic regions of Figure 4.11a, we apply the Frequency Map Analysis method to the signal $\xi_1(t) + i\eta_1(t)$

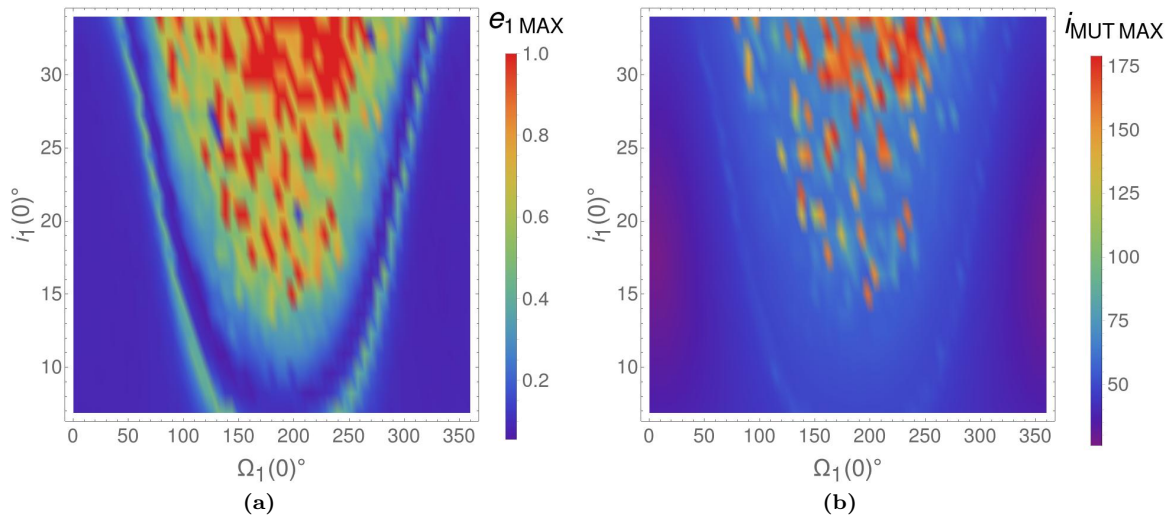

Figure 4.11: Color-grid plots of the maximal value reached by the eccentricity of υ-And **b** (on the left) and by the mutual inclination between υ-And **b** and υ-And **c** (on the right). The maxima are computed during the RK4 numerical integrations (each of them covering a timespan of 10^5 yr) of the SQPR-GR equations of motion (4.68).

as produced by the numerical integration of the system (4.68), i.e., in the SQPR-GR approximation. We perform the numerical integrations as described at the beginning of the present section, taking into account only a few values in I_{i} for the initial inclinations, i.e. $\mathrm{i}_1(0) = 6.865°, 8.22175°, 9.5785°, 10.9353°$ and $\Omega_1(0) \in I_\Omega$. In Figure 4.12 we report the behaviour of the angular velocity ν corresponding to the first component of the approximation of $\xi_1(t)+i\eta_1(t)$, as obtained by applying the FA computational algorithm; therefore, this quantity is related to the precession rate of ϖ_1. As initial value for the inclination $\mathrm{i}_1(0)$ we fix $6.865°$ for Figure 4.12a and $10.9353°$ for Figure 4.12b. Also here, we do not report the cases $(\mathrm{i}_1(0), \Omega_1(0)) \in \{8.22175°, 9.5785°\} \times I_\Omega$, since the behaviour of these plots is similar to the ones in Figure 4.12.

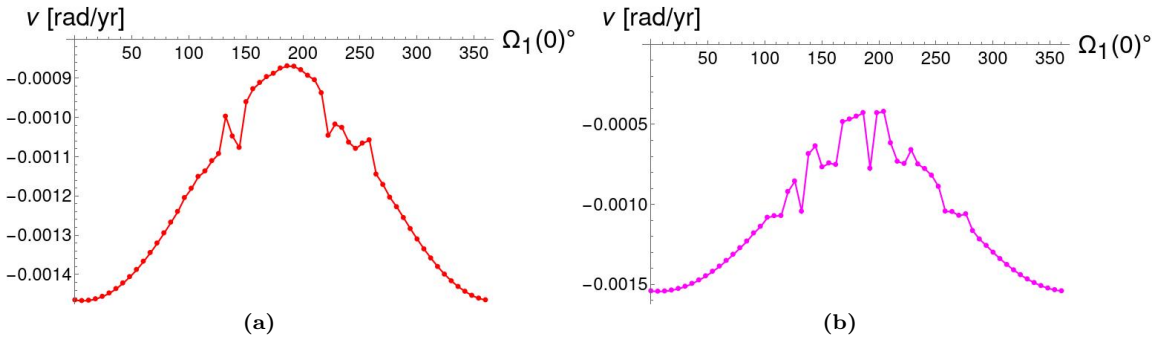

Figure 4.12: Behaviour of the fundamental angular velocity ν as obtained by applying the Frequency Map Analysis method to the signal $\xi_1(t)+i\eta_1(t)$, computed through the RK4 numerical integration of the SQPR-GR model (4.68), covering a timespan of $1.31072 \cdot 10^5$ yr. We take, as initial conditions, $(\mathrm{i}_1(0), \Omega_1(0)) \in \{6.865°\} \times I_\Omega$ for the left panel and $(\mathrm{i}_1(0), \Omega_1(0)) \in \{10.9353°\} \times I_\Omega$ for the right one.

The situation is well described by Figure 4.12a and analogous considerations hold for Figure 4.12b apart from a few main differences which will be highlighted in the following discussion. When the values of $\Omega_1(0)$ are ranging in $[0, \sim 120°]$ and $[\sim 260°, 360°]$ we can observe a regular

behaviour of the angular velocity ν which is also nearly monotone, with the only exception around a local minimum. According to the Frequency Map Analysis method, such a regular regime is due to the presence of many invariant tori which fill the stability region located at the two lateral sides of the plot 4.11a. In the case of Figure 4.12a, this also applies when $\Omega_1(0)$ is ranging in $[\sim 150^\circ, \sim 220^\circ]$, which corresponds to the stable blue internal area of Figure 4.11a. On the other hand, in the case of Figure 4.12b, for the same range of initial values of the node longitude of υ-And **b**, the behaviour is not so regular; this is in agreement with the fact that in correspondence with $\mathrm{i}_1(0) \sim 11^\circ$ the plot of the maximal values of e_1 in the central region highlights the occurrence of chaotical phenomena. Moreover, for what concerns values of $\Omega_1(0)$ in $[\sim 120^\circ, \sim 150^\circ]$ and $[\sim 220^\circ, \sim 260^\circ]$ (corresponding to the green stripes of Figure 4.11a), Figure 4.12a shows a behaviour typical of the crossing of a resonance in the chaotic region surrounding a separatrix. The value of the angular velocity for which this phenomenon takes place is, again, related to $\omega_4 \simeq -1.04 \cdot 10^{-3}$ (as it can be easily appreciated looking to the small plateau appearing in Figure 4.12b).

Comparing Figure 4.12 with Figure 4.7 the enlargement of the stable region is evident. Moreover, we can also see how the modification of the pericenter precession rate of the inner planet by relativistic effects influences the phenomenon. Indeed, looking at the values reported on the y-axis of Figures 4.12 and 4.7, one can appreciate that the fundamental angular velocity, in the case of the SQPR model, takes values remarkably closer to zero with respect to those assumed in the case of the SQPR-GR model.

4.6.2 Application of the normalization algorithms to the secular quasi-periodic restricted model of the dynamics of υ-And b with relativistic corrections

Starting from Hamiltonian (4.67), we can reapply the normalization algorithms described in Subsections 4.4.1 and 4.4.2. All this computational procedure ends up with the introduction of a new 2 DOF Hamiltonian[22] model which can be written in the following form (analogous to the one reported in formula (4.54)):

$$\mathcal{H}_{2DOF}^{(GR)}(\boldsymbol{I},\boldsymbol{\alpha}) = \mathcal{E}_{B;GR} + \boldsymbol{\Omega}_{B;GR}\cdot\boldsymbol{I} + \sum_{l=3}^{\mathcal{N}_L} h_l^{(\mathcal{N}_L-2,0)}(\boldsymbol{I}) + \sum_{s=1}^{\mathcal{N}_S}\sum_{l=3}^{\mathcal{N}_L} h_l^{(\mathcal{N}_L-2,s)}(\boldsymbol{I},\boldsymbol{\alpha})\,, \tag{4.69}$$

where $\mathcal{E}_{B;GR} \in \mathbb{R}$, $\boldsymbol{\Omega}_{B;GR} \in \mathbb{R}^2$ and $h_l^{(\mathcal{N}_L-2,s)} \in \mathfrak{B}_{l,2s}\ \forall\ l = 3,\ \ldots\ ,\mathcal{N}_L\ ,\ s = 0\,,\ \ldots\ ,\mathcal{N}_S\,.$

Moreover, also for this new model we can reproduce the same kind of numerical exploration described in Section 4.5. In particular, we can compute the values of the numerical indicators $\mathfrak{R}_{1\,\mathrm{MAX}}$, $\mathfrak{R}_{2\,\mathrm{MAX}}$ and $\tilde{\mathrm{e}}_{1\,\mathrm{MAX}}$ corresponding to each pair $\big(\mathrm{i}_1(0),\Omega_1(0)\big)$ of the 21×60 points defining the regular grid which covers $I_\mathrm{i}\times I_\Omega = [6.865^\circ, 34^\circ]\times[0^\circ, 360^\circ]$. In the following, we analyze the color-grid plots for a few different values of the parameter ruling the truncation in the trigonometric degree, namely $\mathcal{N}_S$, and in the square root of the action, i.e., $\mathcal{N}_L$. The color-grid plots for the maximal value reached by $\mathfrak{R}_1$, $\mathfrak{R}_2$ and $\tilde{\mathrm{e}}_1$ are reported in Figures 4.13–4.15.

Let us recall that $\mathfrak{R}_{2\,\mathrm{MAX}}$ is an evaluation of the maximal excursion of the inclination of υ-And **b**. For the sake of completeness, its plots are reported in the mid panels of Figures 4.13–4.15, but the ranges of values experienced by $\mathfrak{R}_{2\,\mathrm{MAX}}$ are so narrow that the details about the regions that are colored differently do not look so significant. Therefore, it is better to focus on the left and right panels, which include the plots of $\mathfrak{R}_{1\,\mathrm{MAX}}$ and $\tilde{\mathrm{e}}_{1\,\mathrm{MAX}}$ (respectively, both of them referring to the eccentricity of υ-And **b**). By comparing Figures 4.13–4.15, one can appreciate a well known phenomenon concerning the constructive algorithms *à la* Birkhoff: the greater the number of normalization steps (i.e., $\mathcal{N}_L - 2$), the smaller the domain of applicability (see, e.g., [30] for the discussion about the determination of the optimal step).

[22] In the expansion (4.69), the term that is linear in the dummy actions (i.e., $\boldsymbol{\omega}_B\cdot\boldsymbol{p}$) is removed, because it is irrelevant for the present discussion.

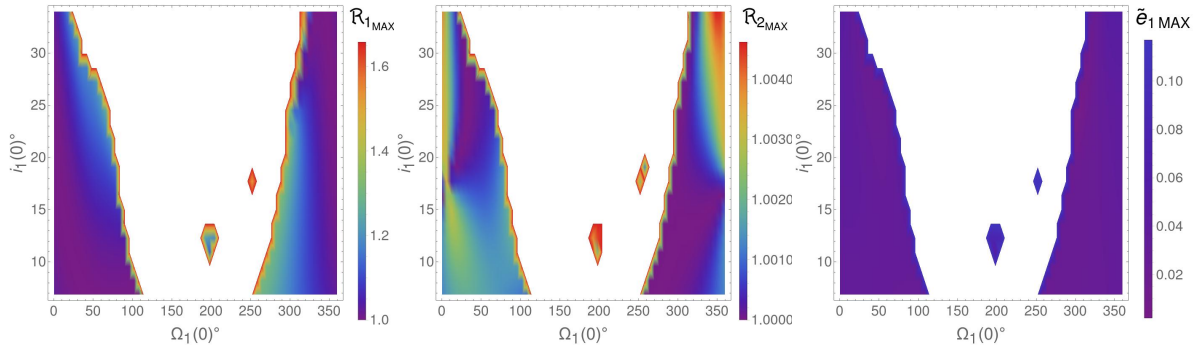

Figure 4.13: Color-grid plots of the maximal values reached by the ratios $\mathfrak{R}_1(t)$ (on the left), $\mathfrak{R}_2(t)$ (in the mid) and the function $\tilde{\mathrm{e}}(t)$ (on the right), which are defined in (4.63)–(4.64). These laws of motion are computed along the flow induced by the 2 DOF Hamiltonian $\mathcal{H}^{(GR)}_{2DOF}$ which takes into account also GR corrections and is defined in (4.69), in the particular case with $\mathcal{N}_S = 5$ and $\mathcal{N}_L = 6$.

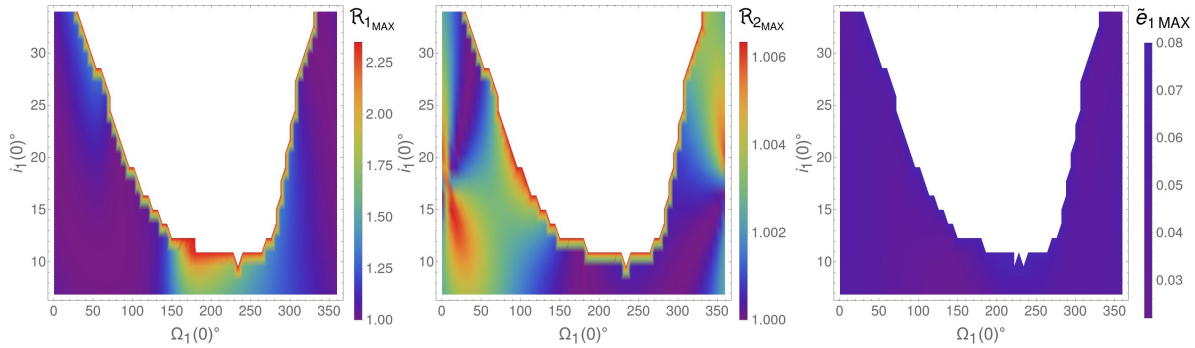

Figure 4.14: Same as in Figure 4.13, in the case with $\mathcal{N}_S = 6$ and $\mathcal{N}_L = 5$.

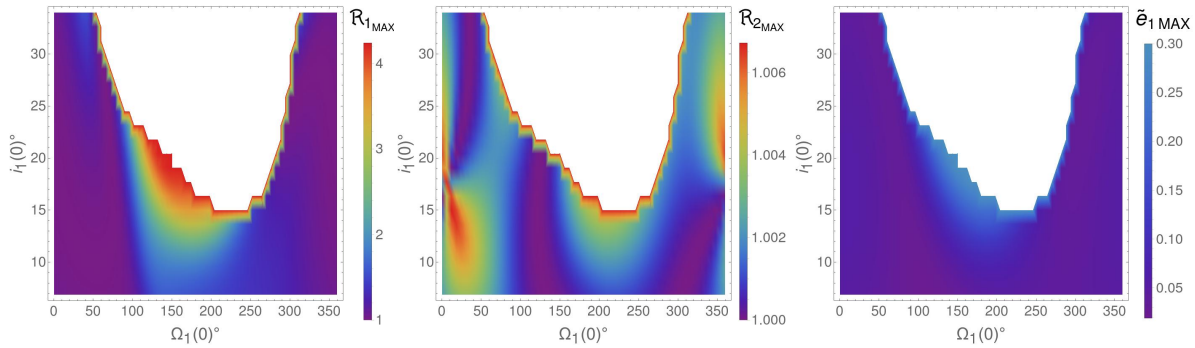

Figure 4.15: Same as in Figure 4.13, in the case with $\mathcal{N}_S = 6$ and $\mathcal{N}_L = 4$.

By comparing Figures 4.14–4.15 also with Figure 4.11a, we observe that in the cases with $\mathcal{N}_L = 4, 5$ our computational procedure is able to reconstruct with a good accuracy the U–shaped border of the stability domain. Note that the horizontal strip at the bottom of the plots[23] corresponds to orbital motions which look stable, since the eccentricity of υ-And **b** does not reach large values (with the eventual exception of the narrow green areas that in Figure 4.11a are expected to correspond to resonant regions). This highlights a main difference with the non-relativistic model discussed in Section 4.5, because in that case there is an interval of values of $\Omega_1(0)$ centered about 180° for which none of the initial inclinations $\mathrm{i}_1(0) \in [6.865°, 34°]$ is corresponding to a stable orbital

[23]This means that we are considering initial values of the inclination $\mathrm{i}_1(0)$ that are close to that of υ-And **c**.

configuration (see Figure 4.6a). The reliability of our simplified 2 DOF Hamiltonian model (which is defined in formula (4.69) and takes into account also GR corrections) is enforced also by the fact that it is able to capture also this phenomenon.

5. KAM stability of 2 DOF secular models of the innermost exoplanet orbiting in the υ-Andromedæ system

The secular quasi-periodic restricted model with 2 DOF which has been introduced in the previous Chapter is reconsidered in the present one. For both the versions of such a model (taking into account, or not, the general relativity corrections), we aim to study the convergence of a classical formulation of the algorithm constructing the Kolmogorov normal form. Let us recall that this is ensured by the (well known KAM) Theorem 1.3.1 under rather suitable hypotheses, which unfortunately require that the perturbation is extremely small. Indeed, this assumption is so restrictive to prevent applications to realistic physical systems for what concerns any KAM-like formal statement, the proof of which is made by using purely analytical methods. However, this problem can be overcome by adopting an approach based on a *Computer-Assisted Proof* (hereafter, CAP). For instance, interesting applications are produced by implementing a strategy that can be summarized as follows. First, the perturbation is reduced by iterating the normalization procedure for a finite number of steps, that are explicitly performed on a computer. We emphasize that this preliminar stage is really effective if and only if the original perturbation is small enough. Moreover, all the Hamiltonian terms which are generated by this first part of the computational procedure can be estimated *rigorously* by exploiting the, so called, *validated numerics* (which includes also *interval arithmetics*; see, e.g., Appendix A of [8] for a gentle introduction to these topics). Finally, if the perturbation has been squeezed so much that we can apply a suitable version of the KAM theorem to the last Hamiltonian that has been produced by the preliminar part of the above computational procedure, then the convergence of the whole normalization algorithm is definitely ensured (see, e.g., [10]).

In the present Chapter, we aim to prove the existence of KAM tori which are invariant with respect to the secular dynamics of υ-And **b** (in the framework of the quasi-periodic restricted models with 2 DOF, that have been introduced previously), by adopting an approach based on a CAP which follows the strategy summarized above.

5.1 Algorithmic construction of the Kolmogorov normal form keeping fixed the angular velocity

Let us start considering the following initial Hamiltonian:

$$\mathcal{H}_K^{(0)} = \mathcal{E}^{(0)} + \widetilde{\boldsymbol{\omega}} \cdot \boldsymbol{p} + \sum_{s\geq 0} \sum_{l\geq 2} f_l^{(0,s)}(\boldsymbol{p},\boldsymbol{q}) + \sum_{s\geq 1} \sum_{l=0}^{1} f_l^{(0,s)}(\boldsymbol{p},\boldsymbol{q})\,, \tag{5.1}$$

where $(\boldsymbol{p}, \boldsymbol{q})$ are action-angle canonical coordinates, $\widetilde{\boldsymbol{\omega}}$ is the angular velocity vector, $\mathcal{E}^{(0)} \in \mathcal{P}_{0,0}$ (i.e., $\mathcal{E}^{(0)} \in \mathbb{R}$) denotes an energy value and every term $f_l^{(0,s)} \in \mathcal{P}_{l,s\tilde{K}}$. Moreover, for a fixed positive integer $\tilde{K}$ and $\forall\, l \geq 0$, $s \geq 0$, the class of function $\mathcal{P}_{l,s\tilde{K}}$ is defined in such a way that

$$\mathcal{P}_{l,s\tilde{K}} = \left\{ f : \mathbb{R}^n \times \mathbb{T}^n \to \mathbb{R} \,:\, f(\boldsymbol{p}, \boldsymbol{q}) = \sum_{\substack{\boldsymbol{j} \in \mathbb{N}^n \\ |\boldsymbol{j}| = l}} \sum_{\substack{\boldsymbol{k} \in \mathbb{Z}^n \\ |\boldsymbol{k}| \leq s\tilde{K}}} c_{\boldsymbol{j},\boldsymbol{k}}\, \boldsymbol{p}^{\boldsymbol{j}}\, e^{i\,\boldsymbol{k}\cdot\boldsymbol{q}} \right\}; \tag{5.2}$$

since every coefficient $c_{\boldsymbol{j},\boldsymbol{k}} \in \mathbb{C}$, then the following relation holds true: $c_{\boldsymbol{j},-\boldsymbol{k}} = \bar{c}_{\boldsymbol{j},\boldsymbol{k}}$. Let us also recall that in the symbol $f_l^{(0,s)}$ the first upper index denotes the normalization step (in accordance with the notation adopted in the previous chapters).

We are going to describe an algorithm that aims to bring the initial Hamiltonian $\mathcal{H}_K^{(0)}$ in *Kolmogorov normal form*; this means that we want to remove the last series appearing in the expansion (5.1), i.e., $\sum_{s\geq 1} \sum_{l=0}^{1} f_l^{(0,s)}(\boldsymbol{p}, \boldsymbol{q})$ which has to be considered smaller than the rest of the Hamiltonian. In fact, because of the Fourier decay of $f_l^{(0,s)} \in \mathcal{P}_{l,s\tilde{K}}$ (whose expansion is generically described in (5.2)), a suitable choice of the positive integer parameter $\tilde{K}$ and an eventual reordering of the monomials allow to write the expansion (5.1) (starting from the general problem of the dynamics (1.1)) in such a way that $f_l^{(0,s)} = \mathcal{O}(\varepsilon^s)$.

In order to check how the structure of the classes of functions is preserved by the normalization algorithm, the following statement plays an essential role.

Lemma 5.1.1. *Let us consider two generic functions $g \in \mathcal{P}_{l,s\tilde{K}}$ and $h \in \mathcal{P}_{m,r\tilde{K}}$, where $\tilde{K}$ is a fixed positive integer number. Then*

$$\{g, h\} = L_h\, g \,\in\, \mathcal{P}_{l+m-1,\,(r+s)\tilde{K}} \qquad \forall\, l,\, m,\, s \,\in\, \mathbb{N},$$

where we trivially extend the definition (5.2) *in such a way that $\mathcal{P}_{-1,\,s\tilde{K}} = \{0\}$ $\forall\ s \in \mathbb{N}$.*

We can now explain the generic r-th step of the algorithm. Let us assume that, after $r-1$ normalization steps, the Hamiltonian can be written in the following form:

$$\mathcal{H}_K^{(r-1)}(\boldsymbol{p}, \boldsymbol{q}) = \mathcal{E}^{(r-1)} + \widetilde{\boldsymbol{\omega}} \cdot \boldsymbol{p} + \sum_{s\geq 0} \sum_{l\geq 2} f_l^{(r-1,s)}(\boldsymbol{p}, \boldsymbol{q}) + \sum_{s\geq r} \sum_{l=0}^{1} f_l^{(r-1,s)}(\boldsymbol{p}, \boldsymbol{q}), \tag{5.3}$$

where $\mathcal{E}^{(r-1)} \in \mathbb{R}$, $f_l^{(r-1,s)} \in \mathcal{P}_{l,s\tilde{K}}$ and $f_l^{(r-1,s)} = \mathcal{O}(\varepsilon^s)$. Of course, the expansion of the initial Hamiltonian $\mathcal{H}_K^{(0)}$ (which is reported in (5.1)) perfectly fits with the previous one of $\mathcal{H}_K^{(r-1)}$ when $r = 1$. Also in the case of the construction of the Kolmogorov normal form, for a better understanding of the algorithm, we think it is convenient to refer to a graphical scheme of the expansion, that can be easily visualized as in Table 5.1.

The r-th normalization step consists of three substeps, each of them involves a canonical transformation, whose generating function is correspondingly denoted with $\chi_1^{(r)}(\boldsymbol{q})$, $\boldsymbol{\xi}^{(r)} \cdot \boldsymbol{q}$ and $\chi_2^{(r)}(\boldsymbol{p}, \boldsymbol{q})$, respectively. The new Hamiltonian, at the end of the r-th normalization step, can be defined as

$$\mathcal{H}_K^{(r)} = \exp\left(L_{\chi_2^{(r)}}\right) \exp\left(L_{\boldsymbol{\xi}^{(r)}\cdot\boldsymbol{q}}\right) \exp\left(L_{\chi_1^{(r)}}\right) \mathcal{H}_K^{(r-1)}. \tag{5.4}$$

Let us here remark that the first substep and the second one could be unified, in a completely equivalent way for what concerns the normalization procedure, by considering the sum of the corresponding generating functions, i.e., $\chi_1^{(r)}(\boldsymbol{q}) + \boldsymbol{\xi}^{(r)} \cdot \boldsymbol{q}$. However, in our opinion the explanation of the algorithm looks more clear, when it is based on three separate substeps; moreover, this will allow us to discuss some suitable modifications (that will be necessary to introduce in the next Chapter) in a more elegant way.

$$\mathcal{H}_K^{(r-1)} = \sum$$

							Degree in actions:
$\vdots$	$\vdots$	$\vdots$	$\vdots$	$\vdots$	$\vdots$	$\vdots$	$\vdots$
$f_3^{(r-1,0)}$	$f_3^{(r-1,1)}$	$\dots$	$f_3^{(r-1,r-1)}$	$f_3^{(r-1,r)}$	$f_3^{(r-1,r+1)}$	$\dots$	$\leftarrow 3$
$f_2^{(r-1,0)}$	$f_2^{(r-1,1)}$	$\dots$	$f_2^{(r-1,r-1)}$	$f_2^{(r-1,r)}$	$f_2^{(r-1,r+1)}$	$\dots$	$\leftarrow 2$
$\widetilde{\boldsymbol{\omega}} \cdot \boldsymbol{p}$	0	$\dots$	0	$f_1^{(r-1,r)}$	$f_1^{(r-1,r+1)}$	$\dots$	$\leftarrow 1$
$\mathcal{E}^{(r-1)}$	0	$\dots$	0	$f_0^{(r-1,r)}$	$f_0^{(r-1,r+1)}$	$\dots$	$\leftarrow 0$
Trigonometric degree/$\widetilde{K}$:							
$\uparrow$	$\uparrow$		$\uparrow$	$\uparrow$	$\uparrow$		
0	1	$\dots$	$r-1$	r	$r+1$	$\dots$	

Table 5.1: Graphical representation of the expansion of the Hamiltonian after $r-1$ normalization steps of the algorithm contructing the Kolmogorov normal form.

First substep (of the r-th normalization step)

The first substep aims to remove the term $f_0^{(r-1,r)}$; thus, the first generating function $\chi_1^{(r)}(\boldsymbol{q})$ is determined by solving the following homological equation:

$$\{\widetilde{\boldsymbol{\omega}} \cdot \boldsymbol{p}\,,\, \chi_1^{(r)}\} + f_0^{(r-1,r)}(\boldsymbol{q}) = \left\langle f_0^{(r-1,r)} \right\rangle_{\boldsymbol{q}} . \tag{5.5}$$

Since $f_0^{(r-1,r)} \in \mathcal{P}_{0,r\tilde{K}}$, we can write it as $f_0^{(r-1,r)}(\boldsymbol{q}) = \sum_{|k|\le r\tilde{K}} c_{\boldsymbol{k}}^{(r-1)} e^{i\boldsymbol{k}\cdot\boldsymbol{q}}$, (where $c_{-\boldsymbol{k}}^{(r-1)} = \overline{c}_{\boldsymbol{k}}^{(r-1)}$); therefore, due to the homological equation (5.5), we obtain that $\left\langle f_0^{(r-1,r)} \right\rangle_{\boldsymbol{q}} = c_{\boldsymbol{0}}^{(r-1)} \in \mathbb{R}$ and

$$\chi_1^{(r)}(\boldsymbol{q}) = \sum_{0<|k|\le r\tilde{K}} \frac{c_{\boldsymbol{k}}^{(r-1)}}{i\,\boldsymbol{k}\cdot\widetilde{\boldsymbol{\omega}}} e^{i\boldsymbol{k}\cdot\boldsymbol{q}}\,; \tag{5.6}$$

the above solution is well defined provided that the non-resonance condition

$$\boldsymbol{k}\cdot\widetilde{\boldsymbol{\omega}} \neq 0 \qquad \forall\ 0 < |\boldsymbol{k}| \le r\tilde{K}$$

is satisfied.

We can now introduce the first intermediate Hamiltonian so that $\widehat{\mathcal{H}}_K^{(r)} = \exp\left(L_{\chi_1^{(r)}}\right) \mathcal{H}_K^{(r-1)}$. By the usual abuse of notation (which is common in the Lie series formalism, i.e., the new canonical coordinates are denoted with the same symbols as the old ones), the expansion of $\widehat{\mathcal{H}}_K^{(r)}$ can be written as

$$\widehat{\mathcal{H}}_K^{(r)}(\boldsymbol{p},\boldsymbol{q}) = \mathcal{E}^{(r)} + \widetilde{\boldsymbol{\omega}}\cdot\boldsymbol{p} + \sum_{s\ge 0}\sum_{l\ge 2} \widehat{f}_l^{(r,s)}(\boldsymbol{p},\boldsymbol{q}) + \sum_{s\ge r}\sum_{l=0}^{1} \widehat{f}_l^{(r,s)}(\boldsymbol{p},\boldsymbol{q})\,. \tag{5.7}$$

Also the new Hamiltonian terms can be conveniently defined, by abusing of the notation in another suitable way. Indeed, first, we set $\widehat{f}_l^{(r,s)} = f_l^{(r-1,s)}$, $\forall\, l \ge 0$, $s \ge 0$ and then we include the contributions that are generated by the Lie derivatives with respect to $\chi_1^{(r)}$, so as to respect the structure of the classes of functions. This means that, by abuse, we redefine the new Hamiltonian terms in such a way that[1]

$$\widehat{f}_{l-j}^{(r,s+jr)} \hookleftarrow \frac{1}{j!} L^j_{\chi_1^{(r)}} f_l^{(r-1,s)} \qquad \forall\, l \ge 1,\ 1 \le j \le l,\ s \ge 0\,. \tag{5.8}$$

[1]From a practical point of view, if we have to deal with finite sum (for istance, in Eq. (5.1)), such that the index s goes up to a fixed order called $\tilde{\mathcal{N}}_S$, then we have to require also that $1 \le j \le \min\left(l, \lfloor(\tilde{\mathcal{N}}_S - s)/r\rfloor\right)$.

Let us recall that with the notation $a \hookleftarrow b$ we mean that the quantity a is redefined so as to be equal $a + b$.

It is easy to see that, since $\chi_1^{(r)}$ depends on $\boldsymbol{q}$ only, then its Lie derivative decreases by 1 the degree in $\boldsymbol{p}$, while the trigonometrical degree in the angles $\boldsymbol{q}$ is increased by $r\tilde{K}$, because of Lemma 5.1.1. For what concerns the special case of the following redefinition:

$$\widehat{f}_0^{(r,r)} \hookleftarrow L_{\chi_1^{(r)}}(\widetilde{\boldsymbol{\omega}} \cdot \boldsymbol{p}),$$

the homological equation (5.5) allows us to put $\widehat{f}_0^{(r,r)} = 0$ and update the energy in such a way that $\mathcal{E}^{(r)} = \mathcal{E}^{(r-1)} + \left\langle f_0^{(r-1,r)} \right\rangle_{\boldsymbol{q}}$.

By applying repeatedly Lemma 5.1.1 to the formulæ above, one can easily verify that for all the Hamiltonian terms appearing in the expansion (5.7) it holds true that $\widehat{f}_l^{(r,s)} \in \mathcal{P}_{l,s\tilde{K}}$; moreover, it is also very easy to check (by induction) that $\widehat{f}_l^{(r,s)} = \mathcal{O}(\varepsilon^s)$. At the end of this first normalization substep, the expansion of the new Hamiltonian can be easily visualized as in the scheme reported in Table 4.9.

$$\widehat{\mathcal{H}}_K^{(r)} = \sum$$

							Degree in actions:
$\vdots$	$\vdots$	$\vdots$	$\vdots$	$\vdots$	$\vdots$	$\vdots$	$\vdots$
$\widehat{f}_3^{(r,0)}$	$\widehat{f}_3^{(r,1)}$	$\dots$	$\widehat{f}_3^{(r,r-1)}$	$\widehat{f}_3^{(r,r)}$	$\widehat{f}_3^{(r,r+1)}$	$\dots$	$\leftarrow 3$
$\widehat{f}_2^{(r,0)}$	$\widehat{f}_2^{(r,1)}$	$\dots$	$\widehat{f}_2^{(r,r-1)}$	$\widehat{f}_2^{(r,r)}$	$\widehat{f}_2^{(r,r+1)}$	$\dots$	$\leftarrow 2$
$\widetilde{\boldsymbol{\omega}} \cdot \boldsymbol{p}$	0	$\dots$	0	$\widehat{f}_1^{(r,r)}$	$\widehat{f}_1^{(r,r+1)}$	$\dots$	$\leftarrow 1$
$\mathcal{E}^{(r)}$	0	$\dots$	0	0	$\widehat{f}_0^{(r,r+1)}$	$\dots$	$\leftarrow 0$
Trigonometric degree/$\widetilde{K}$:							
$\uparrow$	$\uparrow$		$\uparrow$	$\uparrow$	$\uparrow$		
0	1	$\dots$	$r-1$	r	$r+1$	$\dots$	

Table 5.2: Graphical representation of the expansion of the Hamiltonian after the first substep (of the r-th normalization step).

Second substep (of the r-th normalization step)

The second substep aims to keep constant the angular velocity vector $\widetilde{\boldsymbol{\omega}}$ by removing the average term $\left\langle \widehat{f}_1^{(r,r)} \right\rangle_{\boldsymbol{q}} \in \mathcal{P}_{1,0}$, which is linear in the actions $\boldsymbol{p}$ and independent on the angles $\boldsymbol{q}$; this means that it is exactly in the same class of function as $\widetilde{\boldsymbol{\omega}} \cdot \boldsymbol{p}$. For such a purpose, we determine the generating function $\boldsymbol{\xi}^{(r)} \cdot \boldsymbol{q}$ in such a way that

$$\{\widehat{f}_2^{(r,0)}, \boldsymbol{\xi}^{(r)} \cdot \boldsymbol{q}\} + \left\langle \widehat{f}_1^{(r,r)} \right\rangle_{\boldsymbol{q}} = 0\,. \tag{5.9}$$

Since $\widehat{f}_2^{(r,0)} = f_2^{(r-1,0)} \in \mathcal{P}_{2,0}$, then the part of the Hamiltonian $\widehat{\mathcal{H}}_K^{(r)}$ that is integrable and quadratic in the actions can be written as follows:

$$\widehat{f}_2^{(r,0)} = f_2^{(r-1,0)} = \frac{1}{2}(C^{(r-1)}\boldsymbol{p}) \cdot \boldsymbol{p}\,, \tag{5.10}$$

where $C^{(r-1)}$ represents the Hessian matrix of $f_2^{(r-1,0)}$. Therefore, the real vector $\boldsymbol{\xi}^{(r)}$ is such that

$$C^{(r-1)}\boldsymbol{\xi}^{(r)} = \nabla_{\boldsymbol{p}} \left\langle \widehat{f}_1^{(r,r)} \right\rangle_{\boldsymbol{q}}.$$

The linear equation above can be easily solved provided that the Hessian matrix $C^{(r-1)}$ is non-degenerate. Under this assumption, then, the generating function $\boldsymbol{\xi}^{(r)} \cdot \boldsymbol{q}$ is fully determinated.

We can now introduce the second intermediate Hamiltonian so that $\widehat{\widehat{\mathcal{H}}}_K^{(r)} = \exp\left(L_{\boldsymbol{\xi}^{(r)} \cdot \boldsymbol{q}}\right) \widehat{\mathcal{H}}_K^{(r)}$. By the usual abuse of notation (i.e., the new canonical coordinates are denoted with the same symbols as the old ones), the expansion of the new intermediate Hamiltonian can be written as

$$\widehat{\widehat{\mathcal{H}}}_K^{(r)}(\boldsymbol{p}, \boldsymbol{q}) = \mathcal{E}^{(r)} + \widetilde{\boldsymbol{\omega}} \cdot \boldsymbol{p} + \sum_{s \geq 0} \sum_{l \geq 2} \widehat{\widehat{f}}_l^{(r,s)}(\boldsymbol{p}, \boldsymbol{q}) + \widehat{\widehat{f}}_1^{(r,r)}(\boldsymbol{p}, \boldsymbol{q}) + \sum_{s \geq r+1} \sum_{l=0}^{1} \widehat{\widehat{f}}_l^{(r,s)}(\boldsymbol{p}, \boldsymbol{q}) \,. \tag{5.11}$$

In analogy with what has been done in the description of the first substep, we can introduce the new Hamiltonian terms appearing in the expansion above, by initially setting $\widehat{\widehat{f}}_l^{(r,s)} = \widehat{f}_l^{(r,s)}$, $\forall\, l \geq 0$, $s \geq 0$. Hence, we include the contributions to each corresponding class of functions which are generated by the Lie derivatives with respect to $\boldsymbol{\xi}^{(r)} \cdot \boldsymbol{q}$; this means that (by abuse of notation) we redefine the new Hamiltonian terms[2] in such a way that

$$\widehat{\widehat{f}}_{l-j}^{(r,s+jr)} \hookleftarrow \frac{1}{j!} L^j_{\boldsymbol{\xi}^{(r)} \cdot \boldsymbol{q}} \widehat{f}_l^{(r,s)} \qquad \forall\, l \geq 1,\ 1 \leq j \leq l,\ s \geq 0 \,. \tag{5.12}$$

By an easy induction argument, one can verify that for all the Hamiltonian terms appearing in the expansion (5.11) it holds true that $\widehat{\widehat{f}}_l^{(r,s)} \in \mathcal{P}_{l, s\tilde{K}}$; moreover, one can also check that $\widehat{\widehat{f}}_l^{(r,s)} = \mathcal{O}(\varepsilon^s)$. At the end of this second normalization substep, the schematic visualization of the expansion of the new Hamiltonian $\widehat{\widehat{\mathcal{H}}}^{(r)}$ can be produced by replacing all the symbols $\widehat{f}$ with $\widehat{\widehat{f}}$ in Table 5.2. Moreover, since

$$\widehat{\widehat{f}}_1^{(r,r)} = \widehat{f}_1^{(r,r)} + L_{\boldsymbol{\xi}^{(r)} \cdot \boldsymbol{q}} \widehat{f}_2^{(r,0)},$$

equation (5.9) allows us to conclude that $\left\langle \widehat{\widehat{f}}_1^{(r,r)} \right\rangle_{\boldsymbol{q}} = 0$; this remark will be very useful in view of the next substep.

Third substep (of the r-th normalization step)

The third substep aims to completely remove the term $\widehat{\widehat{f}}_1^{(r,r)}$; thus, the generating function $\chi_2^{(r)}(\boldsymbol{p}, \boldsymbol{q})$ is determined by solving the following homological equation:

$$\{\widetilde{\boldsymbol{\omega}} \cdot \boldsymbol{p}, \chi_2^{(r)}\} + \widehat{\widehat{f}}_1^{(r,r)}(\boldsymbol{p}, \boldsymbol{q}) = 0 \,, \tag{5.13}$$

with $\left\langle \widehat{\widehat{f}}_1^{(r,r)} \right\rangle_{\boldsymbol{q}} = 0$ (as it has been remarked at the end of the description of the previous substep). Therefore, we can write the Taylor–Fourier expansion of the perturbing term to remove as $\widehat{\widehat{f}}_1^{(r,r)} = \sum_{|\boldsymbol{j}|=1} \sum_{0<|k|\leq r\tilde{K}} c^{(r)}_{\boldsymbol{j},\boldsymbol{k}} \boldsymbol{p}^{\boldsymbol{j}} e^{i\boldsymbol{k}\cdot\boldsymbol{q}}$, with $c_{\boldsymbol{j},-\boldsymbol{k}} = \bar{c}_{\boldsymbol{j},\boldsymbol{k}}$; hence, from the homological equation (5.13) it follows that

$$\chi_2^{(r)}(\boldsymbol{p}, \boldsymbol{q}) = \sum_{|\boldsymbol{j}|=1} \sum_{0<|k|\leq r\tilde{K}} \frac{c^{(r)}_{\boldsymbol{j},\boldsymbol{k}}}{i\,\boldsymbol{k} \cdot \widetilde{\boldsymbol{\omega}}} \boldsymbol{p}^{\boldsymbol{j}} e^{i\boldsymbol{k}\cdot\boldsymbol{q}} \,. \tag{5.14}$$

[2] As for the first substep, if we have to deal with finite sum (for istance in Eq. (5.1)), such that the index s goes up to a fixed order called $\tilde{\mathcal{N}}_S$, then we have to require also that $1 \leq j \leq \min\left(l, \lfloor(\tilde{\mathcal{N}}_S - s)/r\rfloor\right)$.

Once again, the above solution is well defined provided that it is satisfied the same non-resonance condition that has already been assumed during the description of the first substep, i.e., $\boldsymbol{k}\cdot\widetilde{\boldsymbol{\omega}} \neq 0$ $\forall\ 0 < |\boldsymbol{k}| \leq r\tilde{K}$.

According to equation (5.4), we can define the new Hamiltonian at the end of the r-th step so that $\mathcal{H}_K^{(r)} = \exp\left(L_{\chi_2^{(r)}}\right)\widehat{\widetilde{\mathcal{H}}}_K^{(r)}$. By the usual abuse of notation (such that the new canonical coordinates are denoted with the same symbols as the old ones), the expansion of the new Hamiltonian can be written as

$$\begin{aligned}\mathcal{H}_K^{(r)}(\boldsymbol{p},\boldsymbol{q}) &= \exp\left(L_{\chi_2^{(r)}}\right)\widehat{\widetilde{\mathcal{H}}}_K^{(r)} \\ &= \mathcal{E}^{(r)} + \widetilde{\boldsymbol{\omega}}\cdot\boldsymbol{p} + \sum_{s\geq 0}\sum_{l\geq 2} f_l^{(r,s)}(\boldsymbol{p},\boldsymbol{q}) + \sum_{s\geq r+1}\sum_{l=0}^{1} f_l^{(r,s)}(\boldsymbol{p},\boldsymbol{q})\,.\end{aligned} \tag{5.15}$$

Once again, we can introduce the new Hamiltonian terms appearing in the expansion above, by initially setting $f_l^{(r,s)} = \widehat{\widetilde{f}}_l^{(r,s)}$, $\forall\, l \geq 0$, $s \geq 0$; hence, we update these terms according to the following[3] prescriptions:

$$\begin{aligned} f_l^{(r,s+jr)} &\hookleftarrow \frac{1}{j!}L^j_{\chi_2^{(r)}}\widehat{\widetilde{f}}_l^{(r,s)} && \forall\, l\geq 0,\ j\geq 1,\ s\geq 0\,, \\ f_1^{(r,jr)} &\hookleftarrow \frac{1}{j!}L^j_{\chi_2^{(r)}}\left(\widetilde{\boldsymbol{\omega}}\cdot\boldsymbol{p}\right) && \forall\, j\geq 1\,. \end{aligned} \tag{5.16}$$

By applying repeatedly Lemma 5.1.1 to the formulæ above, one can easily verify that for all the Hamiltonian terms appearing in the expansion (5.15) it holds true that $f_l^{(r,s)} \in \mathcal{P}_{l,s\tilde{K}}$; moreover, it is also very easy to check (by induction) that $f_l^{(r,s)} = \mathcal{O}(\varepsilon^s)$. Moreover, thanks to homological equation (5.13), one can immediately realize that $f_1^{(r,r)} = 0$. It is also convenient to update the term that is integrable and quadratic in the actions in such a way that

$$f_2^{(r,0)} = f_2^{(r,0)} + \left\langle f_2^{(r,r)}\right\rangle_{\boldsymbol{q}}$$

and, consequently, we redefine $f_2^{(r,r)} = f_2^{(r,r)} - \left\langle f_2^{(r,r)}\right\rangle_{\boldsymbol{q}}$. Therefore, from the new definition above of $f_2^{(r,0)}$, it is possible to compute the new Hessian matrix $C^{(r)}$ whose non-degeneracy is essential in order to successfully perform the next $(r+1)$-th normalization step, since $f_2^{(r,0)} = (C^{(r)}\boldsymbol{p})\cdot\boldsymbol{p}/2$ (see Eq. (5.10)).

As a final comment ending the description of the generic r-th normalization step of the classical algorithm constructing the Kolmogorov normal form, let us also remark that the expansion (5.15) of the Hamiltonian $\mathcal{H}_K^{(r)}$ can be visualized as in the scheme reported in Table 5.1, by replacing everywhere r with $r+1$.

5.2 Application to the 2 DOF Hamiltonian model of the secular orbital dynamics of υ-And b

Let us start from the model defined by the following Hamiltonian:

$$\mathcal{H}_{2DOF}(\boldsymbol{I},\boldsymbol{\alpha}) = \mathcal{E}_B + \boldsymbol{\Omega}_B\cdot\boldsymbol{I} + \sum_{l=3}^{\mathcal{N}_L} g_l^{(\mathcal{N}_L-2,0)}(\boldsymbol{I}) + \sum_{s=1}^{\mathcal{N}_S}\sum_{l=3}^{\mathcal{N}_L} g_l^{(\mathcal{N}_L-2,s)}(\boldsymbol{I},\boldsymbol{\alpha})\,,$$

[3] From a practical point of view, if we have to deal with finite sum, such that the index s goes up to a fixed order called $\tilde{\mathcal{N}}_S$, then we have to require also that $1 \leq j \leq \lfloor(\tilde{\mathcal{N}}_S - s)/r\rfloor$.

which is obtained as the reduction of the resonant normal form described in equation (4.54) to a problem with 2 DOF; according to what has been discussed in Section 4.5, we define the values of the parameters ruling the truncations so that $\mathcal{N}_L = 6$, $K = 2$ and $\mathcal{N}_S = 4$. We now perform a first change of variables inducing a shift of the origin of the actions, i.e.,

$$\begin{aligned} p_1 &= I_1 - I_{1_*}\,, \quad & p_2 &= I_2 - I_{2_*}\,, \\ q_1 &= \alpha_1\,, & q_2 &= \alpha_2\,. \end{aligned} \tag{5.17}$$

Moreover, we expand the 2 DOF Hamiltonian around $(p_1\,,\,p_2) = (0,0)$ and we can write it in the following compact form:

$$\mathcal{H}_{2DOF}(\boldsymbol{p},\boldsymbol{q};\boldsymbol{I}_*) = \sum_{s\geq 0}\sum_{l\geq 0} f_l^{(0,s)}(\boldsymbol{p},\boldsymbol{q};\boldsymbol{I}_*)\,, \tag{5.18}$$

where the terms $f_l^{(0,s)}$ are determined by the substitution of the old variables $(\boldsymbol{I},\boldsymbol{\alpha})$ with the new ones in the functions $g_l^{(\mathcal{N}_L-2,s)}$; moreover, the summands have to be rearranged in such a way that $f_l^{(0,s)} \in \mathcal{P}_{l,s\tilde{K}}$ (defined in (5.2)). The translation vector $\boldsymbol{I}_* = (I_{1_*}, I_{2_*})$ is determined so that the torus $\boldsymbol{p} = \boldsymbol{0}$ provides a first approximation of the real wanted orbit; indeed, $\boldsymbol{I}_*$ is chosen so as to optimize the agreement with respect to the angular velocities. Therefore, first we numerically integrate the 2+3/2 DOF Hamiltonian model (whose equations of motion are described in (4.16)) and, then, we apply the frequency analysis method to the signals the $t \mapsto \xi_1(t) + i\eta_1(t)$ and $t \mapsto P_1(t) + iQ_1(t)$ (see, e.g., [51] and [68]). This allows us to numerically determine the fundamental angular velocity vector for the proper secular motion of υ-And **b**, that we denote as $\widetilde{\boldsymbol{\omega}} = (\widetilde{\omega}_1\,,\,\widetilde{\omega}_2)$. Hence, $\boldsymbol{I}_*$ is fixed in such a way to solve the following equation, which involves the part of the Hamitonian that is integrable and linear in the actions, i.e.,

$$F(\boldsymbol{I}_*) := \nabla_{p_1,p_2}\left(f_1^{(0,0)}(\boldsymbol{p};\boldsymbol{I}_*)\right) = \widetilde{\boldsymbol{\omega}}\,. \tag{5.19}$$

The numerical solution of the equation $F(\boldsymbol{I}_*) = \widetilde{\boldsymbol{\omega}}$ can be found by applying the Newton method, using the values of $\big(I_1(0)\,,\,I_2(0)\big)$ (that are given by the initial condition) as a first approximation of the unknown $\boldsymbol{I}_*$.

After having replaced the numerical value of $\boldsymbol{I}_*$ in the Hamiltonian (5.18), we can write its expansion as follows:

$$\mathcal{H}_K^{(0)} = \mathcal{E}^{(0)} + \widetilde{\boldsymbol{\omega}}\cdot\boldsymbol{p} + \sum_{s=0}^{\tilde{\mathcal{N}}_S}\sum_{l=2}^{\tilde{\mathcal{N}}_L} f_l^{(0,s)}(\boldsymbol{p},\boldsymbol{q}) + \sum_{s=1}^{\tilde{\mathcal{N}}_S}\sum_{l=0}^{1} f_l^{(0,s)}(\boldsymbol{p},\boldsymbol{q})\,,$$

where $\mathcal{E}^{(0)} \in \mathbb{R}$, $f_l^{(0,s)} \in \mathcal{P}_{l,s\tilde{K}}$ and the parameters $\tilde{\mathcal{N}}_L\,,\,\tilde{\mathcal{N}}_S$ rule the truncations of the series with respect to the actions $\boldsymbol{p}$ and the angles $\boldsymbol{q}$, respectively. We emphasize that the expansion above fits with the one written in (5.1), therefore, $\mathcal{H}_K^{(0)}$ can be used as the initial Hamiltonian in order to perform the classical algorithm à la Kolmogorov that has been described in detail in the previous Section 5.1. Thus, after having performed $\tilde{\mathcal{N}}_S$ steps of such a normalization algorithm, according to (5.15) we can write the truncated expansion of the final Hamiltonian as follows:

$$\mathcal{H}_K^{(\tilde{\mathcal{N}}_S)}(\widehat{\boldsymbol{p}},\widehat{\boldsymbol{q}}) = \mathcal{E}^{(\tilde{\mathcal{N}}_S)} + \widetilde{\boldsymbol{\omega}}\cdot\widehat{\boldsymbol{p}} + \sum_{s=0}^{\tilde{\mathcal{N}}_S}\sum_{l=2}^{\tilde{\mathcal{N}}_L} f_l^{(\tilde{\mathcal{N}}_S,s)}(\widehat{\boldsymbol{p}},\widehat{\boldsymbol{q}}) = \mathcal{E}^{(\tilde{\mathcal{N}}_S)} + \widetilde{\boldsymbol{\omega}}\cdot\widehat{\boldsymbol{p}} + \mathcal{O}(||\widehat{\boldsymbol{p}}||^2)\,,$$

with $f_l^{(\tilde{\mathcal{N}}_S,s)} \in \mathcal{P}_{l,s\tilde{K}}$. For the purposes of the present Section, let us stress that for the final Hamiltonian $\mathcal{H}_K^{(\tilde{\mathcal{N}}_S)}$ it is convenient to adopt new symbols to denote the so called normalized coordinates (i.e., $\widehat{\boldsymbol{p}}$ and $\widehat{\boldsymbol{q}}$), which are different with respect to the usual ones ($\boldsymbol{p}$ and $\boldsymbol{q}$) that refer to the canonical variables of the initial Hamiltonian. Since the equations of motion corresponding to

$\mathcal{H}_K^{(\tilde{\mathcal{N}}_S)}$ can be written as $\dot{\widehat{\boldsymbol{p}}} = -\partial\mathcal{H}_K^{(\tilde{\mathcal{N}}_S)}/\partial\widehat{\boldsymbol{q}} = \mathcal{O}(||\widehat{\boldsymbol{p}}||^2)$ and $\dot{\widehat{\boldsymbol{q}}} = \partial\mathcal{H}_K^{(\tilde{\mathcal{N}}_S)}/\partial\widehat{\boldsymbol{p}} = \widetilde{\boldsymbol{\omega}} + \mathcal{O}(||\widehat{\boldsymbol{p}}||)$, then it immediately follows that the torus $\{\,(\widehat{\boldsymbol{p}},\widehat{\boldsymbol{q}}) \in \mathbb{R}^2 \times \mathbb{T}^2 \,:\, \widehat{\boldsymbol{p}} = \boldsymbol{0}\}$ is invariant and is travelled by the following quasi-periodic solution:

$$t \mapsto \left(\widehat{\boldsymbol{p}}(t) = \boldsymbol{0}\,,\, \widehat{\boldsymbol{q}}(t) = \widehat{\boldsymbol{q}}_0 + \widetilde{\boldsymbol{\omega}} t\right). \tag{5.20}$$

In order to fix the ideas, we report the values of the truncation parameters; by using `Mathematica` as a programming framework, we have explicitly performed all the normalization steps *à la* Kolmogorov, in such a way to compute the expansion of $\mathcal{H}_K^{(\tilde{\mathcal{N}}_S)}$ with $\tilde{\mathcal{N}}_L = 3$, $\tilde{K} = 4$ and $\tilde{\mathcal{N}}_S = 16$. That same code using `Mathematica` as an algebraic manipulator allows us to explicitly compute the expansions of the following change of coordinates:

$$\begin{aligned}
\boldsymbol{p} &= \exp\left(L_{\chi_2^{(\tilde{\mathcal{N}}_S)}}\right) \exp\left(L_{\boldsymbol{\xi}^{(\tilde{\mathcal{N}}_S)}\cdot\boldsymbol{q}}\right) \exp\left(L_{\chi_1^{(\tilde{\mathcal{N}}_S)}}\right) \ldots \exp\left(L_{\chi_2^{(1)}}\right) \exp\left(L_{\boldsymbol{\xi}^{(1)}\cdot\boldsymbol{q}}\right) \exp\left(L_{\chi_1^{(1)}}\right) \boldsymbol{p}\Big|_{\substack{\boldsymbol{p}=\widehat{\boldsymbol{p}}\\ \boldsymbol{q}=\widehat{\boldsymbol{q}}}}\,, \\
\boldsymbol{q} &= \exp\left(L_{\chi_2^{(\tilde{\mathcal{N}}_S)}}\right) \exp\left(L_{\boldsymbol{\xi}^{(\tilde{\mathcal{N}}_S)}\cdot\boldsymbol{q}}\right) \exp\left(L_{\chi_1^{(\tilde{\mathcal{N}}_S)}}\right) \ldots \exp\left(L_{\chi_2^{(1)}}\right) \exp\left(L_{\boldsymbol{\xi}^{(1)}\cdot\boldsymbol{q}}\right) \exp\left(L_{\chi_1^{(1)}}\right) \boldsymbol{q}\Big|_{\substack{\boldsymbol{p}=\widehat{\boldsymbol{p}}\\ \boldsymbol{q}=\widehat{\boldsymbol{q}}}}\,.
\end{aligned} \tag{5.21}$$

This can be used to produce the following semi-analytical solution for the flow induced by the model described by the Hamiltonian $\mathcal{H}_{2DOF}$:

$$t \mapsto \left(\tilde{\boldsymbol{I}}(t) = \boldsymbol{p}(t) + \boldsymbol{I}_*\,,\, \tilde{\boldsymbol{\alpha}}(t) = \boldsymbol{q}(t)\right)\,, \tag{5.22}$$

where we have used the inverse of the canonical transformation (5.17) and the expression of $\left(\boldsymbol{p}(t)\,,\,\boldsymbol{q}(t)\right)$ is given by (5.21), when $\left(\widehat{\boldsymbol{p}}\,,\,\widehat{\boldsymbol{q}}\right)$ is replaced by the quasi-periodic solution (5.20). Furthermore, we can also approximate the solution of the Hamilton equations (4.16) by a semi-analytic scheme, by plugging the motion law $t \mapsto \left(\tilde{\boldsymbol{I}}(t), \tilde{\boldsymbol{\alpha}}(t)\right)$ into the one written in (4.59). Let us recall that such an approximate semi-analytic solution refers to the SQPR model with $2+3/2$ DOF that is defined by the Hamiltonian (4.14); this is written in canonical variables including also $(\xi_1, \eta_1, P_1, Q_1)$, from which we can compute the secular evolution of most of the orbital elements of υ-And **b**.

Let us focus on an application for a very specific case. We start from a $2 + 3/2$ DOF SQPR model described by the Hamiltonian $\mathcal{H}_{sec,\,2+3/2}$ whose expansion (4.53) is finite, with truncation parameters fixed so that $\mathcal{N}_L = 6$, $K = 2$ and $\mathcal{N}_S = 4$. The corresponding equations of motion are reported in formula (4.16) (recall also the canonical transformation (4.52)). Most of the values of the initial orbital parameters, that are $a_1(0)$, $\mathrm{e}_1(0)$, $M_1(0)$ and $\omega_1(0)$, are reported in Table 4.7; they are completed with $m_1 = 0.674$ (i.e., the value of the mass of υ-And **b**) and $(\mathrm{i}_1(0), \Omega_1(0)) = (17^\circ, 5^\circ)$. In words, the reason of this choice about the initial values of the inclination and the longitude of the node can be explained as follows: $(\mathrm{i}_1(0), \Omega_1(0)) = (17^\circ, 5^\circ)$ is in the mid of the egg–shaped region that is colored in blue and contoured by green curved strips in Figure 4.6a (let us remark that such a region is not splitted in two separate parts, because the left vertical axis corresponding to $\Omega_1(0) = 0^\circ$ coincides with the right one at $\Omega_1(0) = 360^\circ$). Therefore, since $(\mathrm{i}_1(0), \Omega_1(0)) = (17^\circ, 5^\circ)$ is close to the center of an area of initial conditions that generate stable orbits, it is expected to be related to a configuration that is very robust from a dynamical point of view, in the sense that the perturbing terms are relatively small with respect to the situations corresponding to other initial conditions. Moreover, we compute the expansion of the Hamiltonian $\mathcal{H}_{2DOF}$ defininig the 2 DOF model by following the algorithms explained in Section 4.4; hence, we determine numerically the angular velocity vector $\widetilde{\boldsymbol{\omega}}$ by using the frequency analysis method and we perform the construction of the corresponding KAM torus by following the procedure that has been previously described in the present Chapter. Looking at Figure 5.1, one can appreciate that the decay of the norms of the generating functions $\chi_1^{(r)}$ and $\chi_2^{(r)}$ is fast and sharp; this gives the numerical evidence that the normalization algorithm is convergent. Finally, we compute the secular evolution of both the eccentricity and the inclination of υ-And **b** according to the semi-analytic integration scheme corresponding to the quasi-periodic solution, which is generated when the motion law (5.22) is

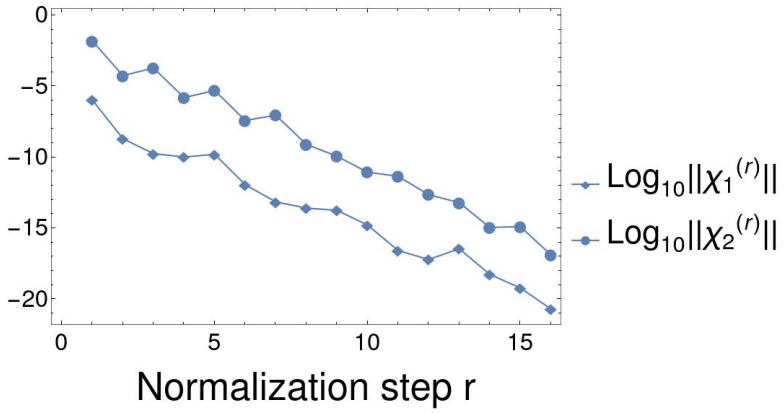

Figure 5.1: Convergence of the generating functions $\chi_1^{(r)}$ and $\chi_2^{(r)}$ defined by the classical normalization algorithm à la Kolmogorov, when it is performed in the case corresponding to $(\mathrm{i}_1(0), \Omega_1(0)) = (17°, 5°)$. The Log_{10} of their norms are reported as a function of the normalization step r.

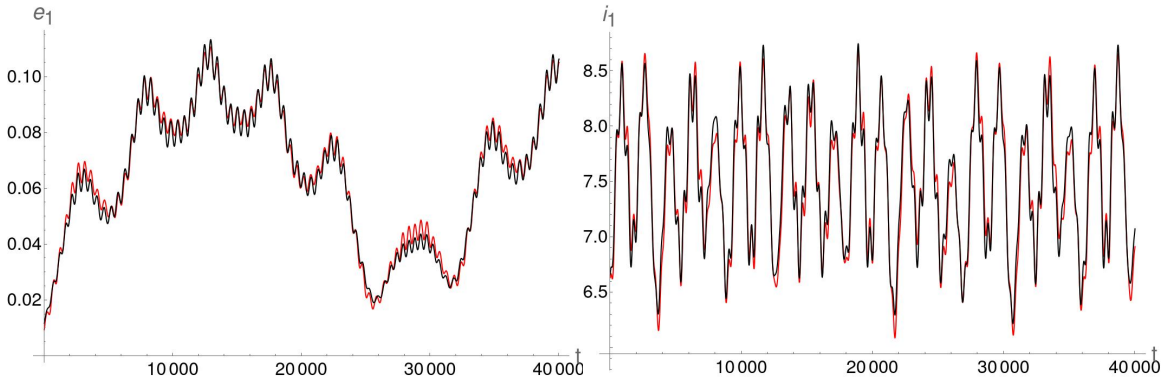

Figure 5.2: Comparisons between the eccentricity e_1 (on the left) and the inclination i_1 (on the right) as obtained through the semi-analytical approach (in red) and the numerical one (in black). Both the integration methods consider the case with initial conditions with $(\mathrm{i}_1(0), \Omega_1(0)) = (17°, 5°)$.

plugged into the one written in (4.59). Such a quasi-periodic evolution is plotted in Figure 5.2, where one can appreciate the nice agreement with the numerical integrations of the motion for what concerns the behavior of both the eccentricity and the inclination of υ-And **b**.

Let us also discuss the application of the algorithm constructing KAM tori for different initial conditions. We consider two sets of values of $(\mathrm{i}_1(0), \Omega_1(0))$ which cross the stable egg–shaped region (colored in blue) in the vertical direction and in the horizontal one; they are defined so that $\mathcal{I}_1 = \{\Omega_1(0) = 5°, \mathrm{i}_1(0) = 6.865°, 10°, 15°, 20°, 25°, 28°\}$ and $\mathcal{I}_2 = \{\mathrm{i}_1(0) = 17°, \Omega_1(0) = 0°, 5°, 10°, 20°, 30°, 40°, 330°, 340°, 350°\}$, respectively. All the points corresponding to the cartesian coordinates listed in the sets $\mathcal{I}_1$, $\mathcal{I}_2$ are marked by a red dot in Figure 5.3, with the exceptions of the two particular cases that are considered in the two pairs of Figures 5.1–5.2 and 5.4–5.5, because in correspondence with $(\mathrm{i}_1(0), \Omega_1(0)) = (17°, 5°)$ and $(\mathrm{i}_1(0), \Omega_1(0)) = (17°, 40°)$ we have plotted a yellow star and a light blue one, respectively. For all the initial conditions which include the values of $(\mathrm{i}_1(0), \Omega_1(0))$ listed in the above sets $\mathcal{I}_1$, $\mathcal{I}_2$ we have repeated the computational procedure that we have already detailed in the special case of $(\mathrm{i}_1(0), \Omega_1(0)) = (17°, 5°)$. We have remarked that the convergence of the generating functions is faster in the inner part of the stable egg–shaped region of Figure 5.3; on the other hand, the more we get closer to the green edge, the slower is the decay of the norms of the generating functions $\chi_1^{(r)}$ and $\chi_2^{(r)}$. This confirms the expectation that the innermost part of the egg–shaped blue region is the most robust from a dynamical point of view (see [72]).

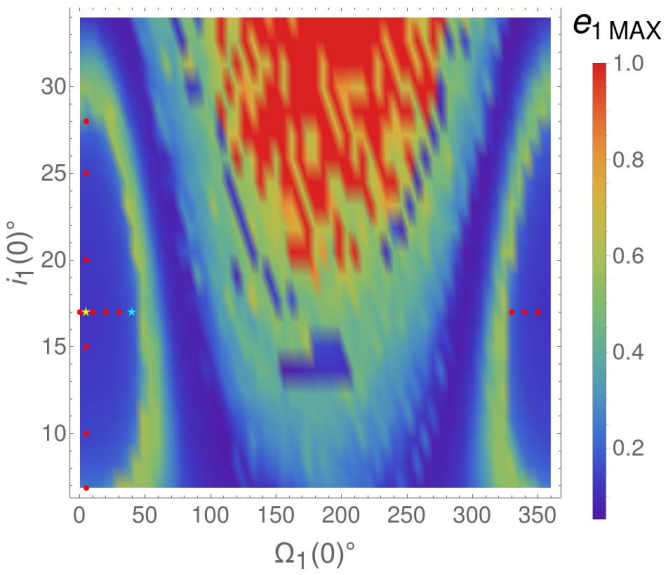

Figure 5.3: The pairs of values $(\mathrm{i}_1(0), \Omega_1(0))$ making part of the initial conditions for which we apply the Kolmogorov normalization algorithm are outlined by a red dot or a yellow / light blue star. The colors in background are exactly as in Figure 4.6a.

For the sake of brevity, we do not include a detailed description of the results that we have obtained for each different pair of initial values of $(\mathrm{i}_1(0), \Omega_1(0))$, in all the cases to which our computational algorithm has been applied. Indeed, we limit ourselves to discuss an example showing the relatively slow decay of the norms of the generating functions for initial conditions close to the green border. We focus our attention on the case with $(\mathrm{i}_1(0), \Omega_1(0)) = (17°, 40°)$, which is marked by a light blue star in Figure 5.3. By comparing Figures 5.4 and 5.1, one can remark that the norm of the last generating functions that are computed, that are $\chi_1^{(16)}$ and $\chi_2^{(16)}$, are larger in the former case by at least five orders of magnitude; this makes evident that the convergence of the normalization algorithm is much slower in the case with $(\mathrm{i}_1(0), \Omega_1(0)) = (17°, 40°)$. Such a remark is also in agreement with the comparison between Figure 5.5 and 5.2: one can appreciate that the agreement between the semi-analytic integration and the numerical one significantly deteriorates when the case with $(\mathrm{i}_1(0), \Omega_1(0)) = (17°, 40°)$ is considered instead of the one referring to $(\mathrm{i}_1(0), \Omega_1(0)) = (17°, 5°)$.

Finally, for all the pairs of values $(\mathrm{i}_1(0), \Omega_1(0))$ listed in the sets $\mathcal{I}_1$, $\mathcal{I}_2$, we have performed also the Computer-Assisted Proofs, in order to ensure the convergence of the Kolmogorov normalization algorithm that is applied to the 2 DOF Hamiltonian model we are studying. The package that allows to deal with this kind of CAPs is publicly available (see [69]). We have run the codes which can be downloaded from this website, for all the expansions (5.1) of the Hamiltonians $\mathcal{H}_K^{(0)}$ corresponding to the different[4] initial conditions. For all of them, the CAP has been successful[5] and so it has been rigorously proved the existence of KAM tori corresponding to angular velocity vectors which are Diophantine and in an extremely small neighborhood of $\widetilde{\boldsymbol{\omega}}$.

As a further comment, it is also worth to remark that none of the application of the CAP worked

[4]Let us recall that the angular velocity vector $\widetilde{\boldsymbol{\omega}}$ is determined by applying the frequency analysis method to signals that are generated by numerical integrations, which in turn do depend on the initial conditions. Therefore, this holds true also for the translation vector $\boldsymbol{I}_*$ that is determined by solving the equation (5.19). Since the truncated expansion of $\mathcal{H}_K^{(0)}$ is obtained by applying the canonical transformation (5.17) to the Hamiltonian $\mathcal{H}_{2DOF}$, then $\mathcal{H}_K^{(0)}$ definitely depends on the initial conditions.

[5]In the codes that are publicly available from [69] and automatically perform the CAP of existence of KAM tori, there are two internal parameters playing a fundamental role. R_I refers to the number of normalization steps for which the expansions of the generating functions are explicitly computed, while R_{II} corresponds to the last step for which just their upper bounds are estimated. Their impact on the performances of this kind of CAPs is widely discussed in [10]. For what concerns the cases discussed in the present Section, all the successful CAPs can be performed with $R_I = 25$ and $R_{II} = 650$; each of them requires less than 2 minutes of CPU–time on a computer equipped with an `Intel i5` processor of 7-th generation.

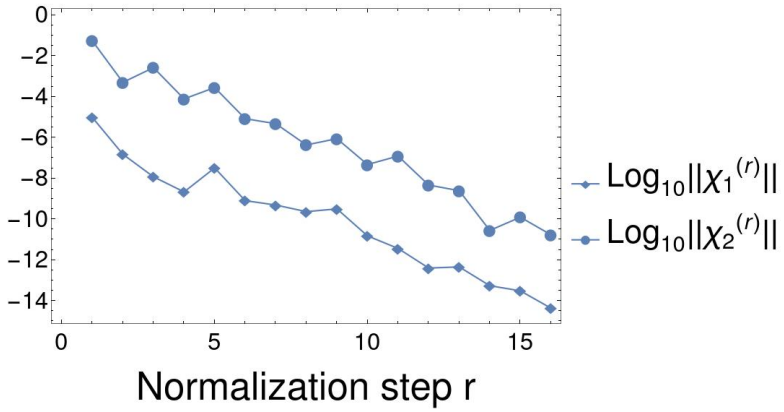

Figure 5.4: Convergence of the generating functions $\chi_1^{(r)}$ and $\chi_2^{(r)}$ defined by the classical normalization algorithm à la Kolmogorov, when it is performed in the case corresponding to $(\mathrm{i}_1(0), \Omega_1(0)) = (17^\circ, 40^\circ)$. The Log_{10} of their norms are reported as a function of the normalization step r.

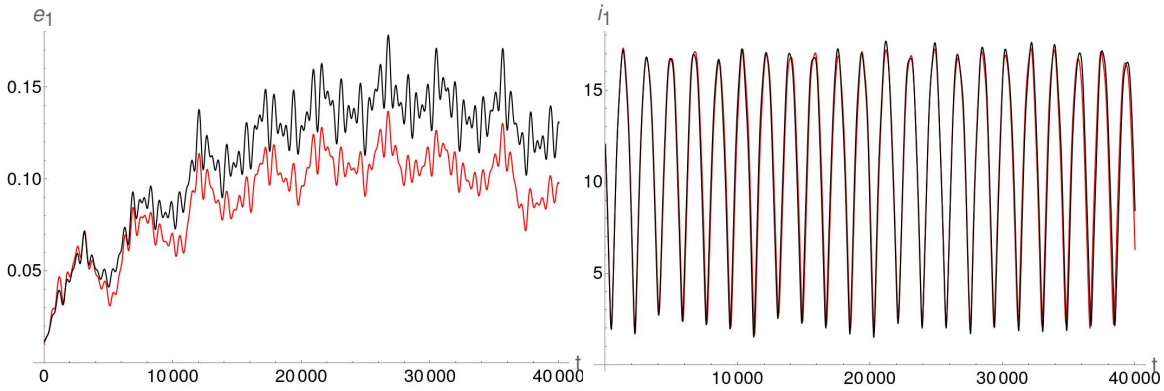

Figure 5.5: Comparisons between the eccentricity e_1 (on the left) and the inclination i_1 (on the right) as obtained through the semi-analytical approach (in red) and the numerical one (in black). Both the integration methods consider the case with initial conditions with $(\mathrm{i}_1(0), \Omega_1(0)) = (17^\circ, 40^\circ)$.

for initial conditions corresponding to pairs of values of $(\mathrm{i}_1(0), \Omega_1(0))$ located outside the blue egg–shaped region of Figure 5.3. This enforces the conviction that our computational procedure used in junction with CAPs can produce rigorous results that are nicely in agreement with the ones provided by numerical explorations.

5.3 Application to the 2 DOF Hamiltonian model of the secular orbital dynamics of υ-And b taking into account relativistic corrections

In analogy with what has been done in the Section 5.2, we reapply the computational procedure described previously to the 2 DOF model that is obtained by constructing the resonant normal form in such a way to take into account also the corrections due to General Relativity (hereafter, GR). Thus, the starting point is now represented by the Hamiltonian $\mathcal{H}^{(GR)}_{2DOF}(\boldsymbol{I}, \boldsymbol{\alpha})$ whose expansion is written in (4.69), where the parameters ruling the truncations are fixed in such a way that $\mathcal{N}_L = 6$, $K = 2$ and $\mathcal{N}_S = 5$. Hence, we perform the canonical change of variables defined in formula (5.17) and we introduce the new Hamiltonian $\mathcal{H}^{(0)}_K(\boldsymbol{p}, \boldsymbol{q}) = \mathcal{H}^{(GR)}_{2DOF}(\boldsymbol{p}+\boldsymbol{I}_*, \boldsymbol{q})$, where the translation vector

$\boldsymbol{I}_*$ is determined by solving the following equation (that is analogous to the one written in (5.19)):

$$\nabla_{I_1,I_2}\left(\left\langle \mathcal{H}^{(GR)}_{2DOF}\right\rangle_{\boldsymbol{\alpha}}\right)\Big|_{\boldsymbol{I}=\boldsymbol{I}_*} = \widetilde{\boldsymbol{\omega}}^{(GR)} \ .$$

In the equation above, the angular velocity vector $\widetilde{\boldsymbol{\omega}}^{(GR)} = (\widetilde{\omega}^{(GR)}_1, \widetilde{\omega}^{(GR)}_2)$ is determined by applying the frequency analysis method to the signals $t \mapsto \xi_1(t) + i\eta_1(t)$ and $t \mapsto P_1(t) + iQ_1(t)$, which are generated by the numerical integration of the corresponding $2+3/2$ DOF Hamiltonian model with GR corrections, whose equations of motion are described in (4.68). Let us write the expansion of $\mathcal{H}^{(0)}_K(\boldsymbol{p},\boldsymbol{q}) = \mathcal{H}^{(GR)}_{2DOF}(\boldsymbol{p}+\boldsymbol{I}_*\,,\,\boldsymbol{q})$ as follows:

$$\mathcal{H}^{(0)}_K = \mathcal{E}^{(0)} + \widetilde{\boldsymbol{\omega}}^{(GR)}\cdot\boldsymbol{p} + \sum_{s=0}^{\tilde{\mathcal{N}}_S}\sum_{l=2}^{\tilde{\mathcal{N}}_L} f^{(0,s)}_l(\boldsymbol{p},\boldsymbol{q}) + \sum_{s=1}^{\tilde{\mathcal{N}}_S}\sum_{l=0}^{1} f^{(0,s)}_l(\boldsymbol{p},\boldsymbol{q})\,, \tag{5.23}$$

where $\mathcal{E}^{(0)} \in \mathbb{R}$, $f^{(0,s)}_l \in \mathcal{P}_{l,s\tilde{K}}$ and the parameters ruling the truncations are fixed so that $\tilde{\mathcal{N}}_L = 3$, $\tilde{K} = 4$ and $\tilde{\mathcal{N}}_S = 16$. Let us remark that the expansion above fits with the one written in (5.1), therefore, it can be used as the starting point to perform the constructive algorithm à la Kolmogorov that has been described in Section 5.1.

As a first application to the SQPR model of the dynamics of υ-And **b** which has 2 DOF and takes into account also the effects due to GR, we repeat all the computations that in the non-relativistic case allowed us to obtain the results reported in Figures 5.1–5.2. Thus, we consider the values of $a_1(0)$, $\mathrm{e}_1(0)$, $M_1(0)$ and $\omega_1(0)$ that are reported in Table 4.7, $m_1 = 0.674$ and $(\mathrm{i}_1(0), \Omega_1(0)) = (17^\circ, 5^\circ)$; then, we compute the corresponding expansion (5.23) of $\mathcal{H}^{(0)}_K$ to which we apply $\tilde{\mathcal{N}}_S = 16$ steps of the Kolmogorov normalization algorithm. The norms of the generating functions $\chi^{(r)}_1$ and $\chi^{(r)}_2$ are plotted in a semi-log scale in Figure 5.6, where their sharp decay can be appreciated; once again, this gives the numerical evidence that the normalization algorithm is convergent. Moreover, the comparison between Figures 5.1 and 5.6 shows that the addition of the GR correction makes the decay of the generating functions even faster. Following once more the approach described in Section 5.2, we can use the semi-analytic integration scheme to compute the secular evolution of both the eccentricity and the inclination of υ-And **b** (for the dynamical model including the effects due to GR). This quasi-periodic (approximate) solution is plotted in Figure 5.7, where one can appreciate the rather good agreement with the numerical integrations of the motion for what concerns the evolution of both the eccentricity and the inclination of υ-And **b**. By comparing Figures 5.2 and 5.7, we can also remark that that the maximal value reached by the eccentricity in the case of the SQPR model with GR corrections (that is 0.0836) is significantly smaller with respect to the one reached in the SQPR model without GR corrections (that is 0.1105). These remarks further confirm that the effects due to GR play a stabilizing role from the dynamical point of view.

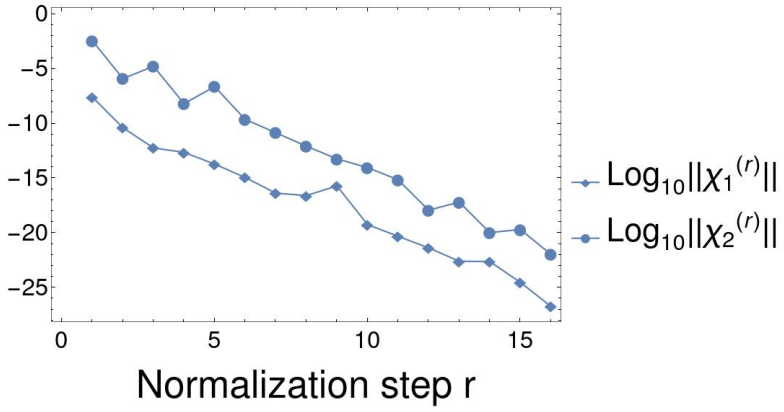

Figure 5.6: Convergence of the generating functions $\chi^{(r)}_1$ and $\chi^{(r)}_2$ defined by the classical normalization algorithm à la Kolmogorov, when it is applied to the 2 DOF SQPR model with GR corrections and is performed in the case corresponding to $(\mathrm{i}_1(0), \Omega_1(0)) = (17^\circ, 5^\circ)$. The Log_{10} of their norms are reported as a function of the normalization step r.

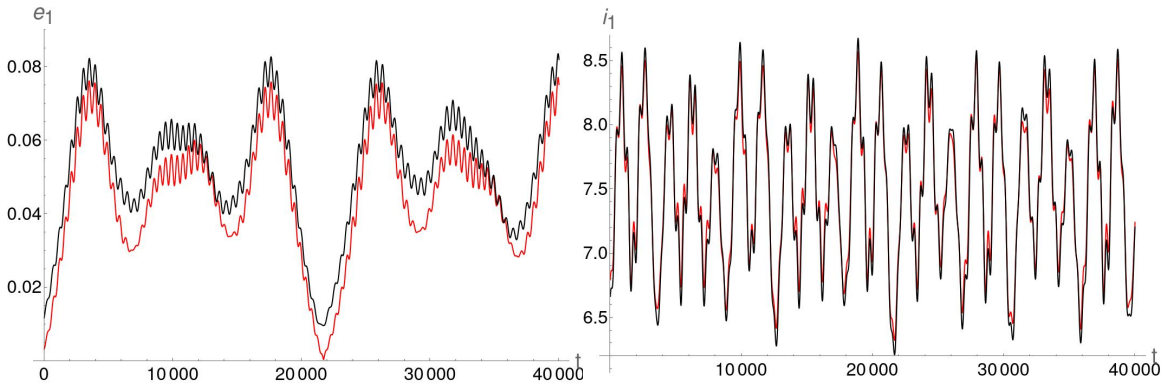

Figure 5.7: Comparisons between the eccentricity e_1 (on the left) and the inclination i_1 (on the right) as obtained through the semi-analytical approach (in red) and the numerical one (in black). Both the integration methods consider the case with initial conditions with $(i_1(0), \Omega_1(0)) = (17°, 5°)$ and they are applied to models which take into account the effects due to GR.

Now, also for the model including the GR effects, we are going to discuss the application of the algorithm constructing KAM tori for different initial conditions. We consider four sets of values of $(i_1(0), \Omega_1(0))$ that cross the stable trapezoidal region (which is colored in blue and is contoured by the U–shaped green strips) in the vertical direction of Figure 4.11a, namely, $\mathcal{J}_{1,2} = \{\Omega_1 = 15°, 340°, i_1 = 6.865°, 13°, 20°, 27°\}$ and in the horizontal one, i.e., $\mathcal{I}_3 = \{i_1 = 6.865°, \Omega_1 = 0°, 50°, 80°, 300°, 320°\}$, $\mathcal{I}_4 = \{i_1 = 20°, \Omega_1 = 0°, 40°, 320°, 330°, 340°\}$. All the points corresponding to the cartesian coordinates $(i_1(0), \Omega_1(0)) = (33°, 0°)$ and listed in the sets $\mathcal{J}_{1,2}$ and $\mathcal{I}_{3,4}$ are marked by a symbol in Figure 5.8. In particular, a yellow star is used in Figure 5.8 to outline $(i_1(0), \Omega_1(0)) = (17°, 5°)$, whose corresponding results have been reported in Figures 5.6–5.7 and already commented. Another green star marks $(i_1(0), \Omega_1(0)) = (20°, 0°)$, whose corresponding plots are omitted because they are quite similar to those of the case $(i_1(0), \Omega_1(0)) = (17°, 5°)$ above. For all the initial conditions which include the values of $(i_1(0), \Omega_1(0)) = (33°, 0°)$ and those listed in the sets $\mathcal{J}_{1,2}$ and $\mathcal{I}_{3,4}$ we have repeated the computational procedure that we have already described in the special case of $(i_1(0), \Omega_1(0)) = (17°, 5°)$. Moreover, we have remarked that the convergence of the generating functions is faster in the inner part of the stable trapezoidal region of Figure 5.8. Therefore, also in the present case dealing with the SQPR model with GR corrections, this kind of remarks confirms the expectation that the innermost part of the trapezoidal blue region is the most robust from a dynamical point of view (once again we refer to the discussions in [72] for more details).

For the sake of brevity, we do not include a detailed description of the results that we have obtained for each different pair of initial values of $(i_1(0), \Omega_1(0))$, in all the cases to which our computational algorithm has been applied. Indeed, we limit ourselves to discuss an example showing the relatively slow decay of the norms of the generating functions for initial conditions relatively close to the green border. We focus our attention on the case with $(i_1(0), \Omega_1(0)) = (20°, 40°)$, which is marked by an orange star in Figure 5.8. By comparing Figures 5.9 and 5.6, one can remark that the norm of the last generating functions that are computed, that are $\chi_1^{(16)}$ and $\chi_2^{(16)}$, are larger in the former case by at least ten orders of magnitude; this makes evident that the convergence of the normalization algorithm is much slower in the case with $(i_1(0), \Omega_1(0)) = (20°, 40°)$. Such a remark is also in agreement with the comparison between Figure 5.10 and 5.7: one can appreciate that the agreement between the semi-analytic integration and the numerical one significantly deteriorates when the case with $(i_1(0), \Omega_1(0)) = (20°, 40°)$ is considered instead of the one referring to $(i_1(0), \Omega_1(0)) = (17°, 5°)$.

Red dots and colored stars are used in Figure 5.8 to mark all the initial conditions which include $(i_1(0), \Omega_1(0)) = (33°, 0°)$ and those listed in the sets $\mathcal{J}_{1,2}$ and $\mathcal{I}_{3,4}$; for all of them, we have

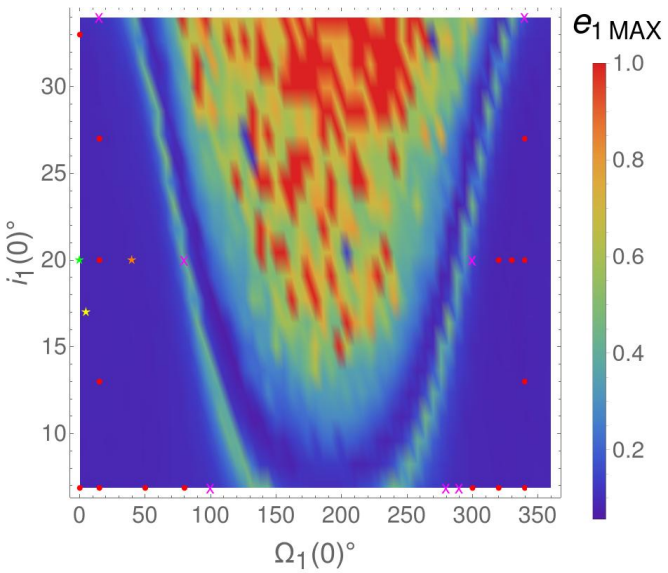

Figure 5.8: The pairs of values $(i_1(0), \Omega_1(0))$ making part of the initial conditions for which we successfully apply the CAP (ensuring the convergence of the Kolmogorov normalization algorithm) are outlined by a red dot or a yellow / green / orange star. The pairs $(i_1(0), \Omega_1(0))$ for which the CAP does not work are denoted with a magenta cross. The colors in background are exactly as in Figure 4.11a.

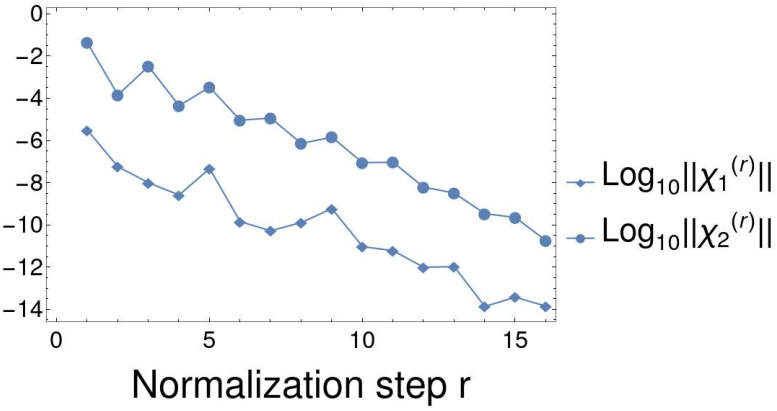

Figure 5.9: Convergence of the generating functions $\chi_1^{(r)}$ and $\chi_2^{(r)}$ defined by the classical normalization algorithm à la Kolmogorov, when it is applied to the 2 DOF SQPR model with GR corrections and is performed in the case corresponding to $(i_1(0), \Omega_1(0)) = (20°, 40°)$. The Log_{10} of their norms are reported as a function of the normalization step r.

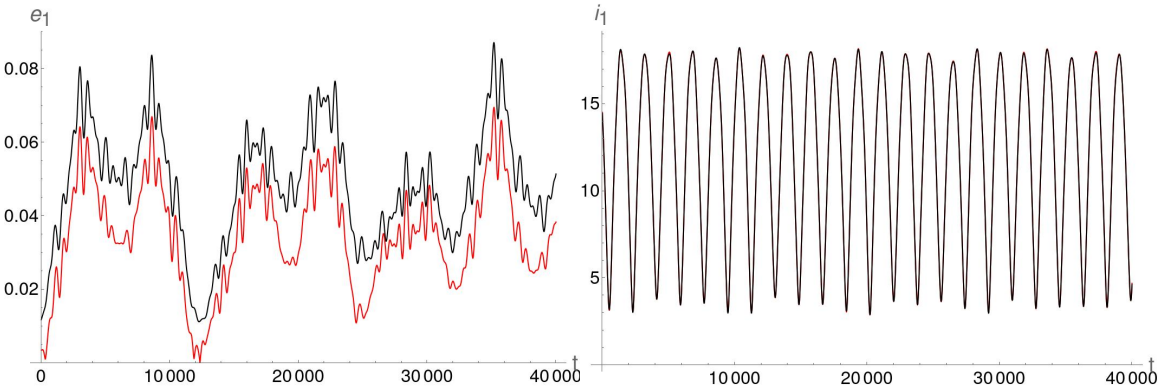

Figure 5.10: Comparisons between the eccentricity e_1 (on the left) and the inclination i_1 (on the right) as obtained through the semi-analytical approach (in red) and the numerical one (in black). Both the integration methods consider the case with initial conditions with $(i_1(0), \Omega_1(0)) = (20°, 40°)$ and they are applied to models which take into account the effects due to GR.

performed Computer-Assisted Proofs, in order to ensure the convergence of the Kolmogorov nor-

malization algorithm also when it is applied to the 2 DOF Hamiltonian model with GR corrections. We have run the codes which can be downloaded from the publicly available website [69], for all the expansions (5.23) of the Hamiltonians $\mathcal{H}_K^{(0)}$ corresponding to the different initial conditions. For each of them, the CAP has been successful[6] and so it has been rigorously proved the existence of KAM tori corresponding to angular velocity vectors which are Diophantine and in an extremely small neighborhood of $\widetilde{\boldsymbol{\omega}}^{(GR)}$.

Moreover, we have tested also other conditions that are internal to the stable trapezoidal region (which is colored in blue and is contoured by the U–shaped green strips), i.e., $(\mathrm{i}_1(0), \Omega_1(0)) = (6.865°, 100°)$, $(6.865°, 280°)$, $(6.865°, 290°)$, $(20°, 80°)$, $(20°, 300°)$, $(34°, 15°)$, $(34°, 340°)$; each of these pairs of cartesian coordinates is highlighted with a magenta cross in Figure 5.8. In none of these cases the codes were able to successfully complete the CAP. Therefore, we expect that it is possible to rigorously prove the existence of KAM tori (which are invariant with respect to the flow of the 2 DOF Hamiltonian model with GR corrections) in a region of triangular shape having the segment $\mathrm{i}_1 = 6.865°$, $\Omega_1 = [0°, 80°] \cup [300°, 360°]$ as base and $\Omega_1 = 0°$, $\mathrm{i}_1 = [6.865°, 33°]$ as height. Although the coverage of the stable (trapezoidal) region is not complete when the 2 DOF model takes into account also the relativistic corrections, the area for which the CAPs can produce rigorous results is so wide that, also in this case, their performances are nicely in agreement with the results provided by numerical explorations.

[6] For what concerns the cases discussed in the present Section, all the successful CAPs can be performed with $R_I = 60$ and $R_{II} = 5000$ in less than 70 minutes of CPU–time on a computer equipped with an `Intel i5` processor of 7-th generation. See footnote [5] for a short explanation of the meaning of the parameters R_I and R_{II}. Let us also stress that for initial conditions in the inner part of the stable trapezoidal region of Figure 5.8 (where the convergence of the generating functions is faster) the parameters R_I and R_{II} can be conveniently reduced in such a way to conclude the corresponding CAPs in a shorter time.

6. KAM stability of $2+3/2$ DOF secular models of the innermost exoplanet orbiting in the υ-Andromedæ system

In the present Chapter we aim to apply the algorithm constructing the Kolmogorov normal form to the Secular Quasi-Periodic Restricted system (taking into account, or not, the general relativity corrections) in its version with $2+3/2$ DOF. In fact, since we are going to reconsider the SQPR model of the orbital dynamics of υ-And **b** without starting the further normalization procedure described in Subection 4.4.2, then the model is defined by a Hamiltonian which also depends on the three angles describing the motion of the two outer planets υ-And **c** and υ-And **d**. The ultimate goal is again to perform some CAPs of existence of KAM tori corresponding to carefully selected orbits; this means that we will focus on the initial conditions that are related to the most robust configurations, according to some of the results discussed in Chapter 5. With respect to such a previous Chapter, dealing with CAPs is more complicated, since the number of DOF is now greater than two. In order to achieve our goal, it is convenient to adapt the Kolmogorov algorithm, in such a way to not keep fixed the angular velocity vector; such a slightly modified version of this classical normalization algorithm can be used in junction with a Newton-like method. As the main result of the present Chapter, we will show that the computational procedure above can be performed preliminarly in order to locate an approximation of the preselected orbit, which is a starting point good enough to successfully complete the CAP of existence of the wanted KAM tori.

6.1 Reduction of the angular momentum

After having performed $\mathcal{N}_S$ steps of the algorithm constructing the normal form for an elliptic torus (according to the prescriptions given in Subsection 4.4.1), the SQPR model of the orbital dynamics of υ-And **b** (taking into account, or not, the general relativity corrections) is described by the Hamiltonian written in (4.39). It is reported here for the convenience of the reader:

$$\mathcal{H}^{(\mathcal{N}_S)}(\boldsymbol{p},\boldsymbol{q},\boldsymbol{I},\boldsymbol{\alpha}) = \mathcal{E}^{(\mathcal{N}_S)} + \boldsymbol{\omega}\cdot\boldsymbol{p} + \boldsymbol{\Omega}^{(\mathcal{N}_S)}\cdot\boldsymbol{I} + \sum_{s\geq 0}^{\mathcal{N}_S}\sum_{l=3}^{\mathcal{N}_L} f_l^{(\mathcal{N}_S,s)}(\boldsymbol{p},\boldsymbol{q},\boldsymbol{I},\boldsymbol{\alpha})\,,$$

where the Taylor–Fourier expansion above is truncated[1] up to order $\mathcal{N}_L$ with respect to the square root of the actions $\boldsymbol{I}$ and to the trigonometric degree $\mathcal{N}_S K$ in the angles $(\boldsymbol{q},\boldsymbol{\alpha})$, while $\mathcal{E}^{(\mathcal{N}_S)} \in \mathbb{R}$

[1] We recall that the parameters ruling the truncation of the series expansion are fixed so that $\mathcal{N}_L = 6\,,\ \mathcal{N}_S = 4$ and $K = 2$ if we are not considering the GR correction on the SQPR model, $\mathcal{N}_L = 6\,,\ \mathcal{N}_S = 5$ and $K = 2$ if we are dealing with the SQPR model with GR corrections.

and the summands $f_l^{(0,s)} \in \mathfrak{B}_{l,sK}$, that is defined in (4.4.1). Let us also recall that the angular velocity vector $\boldsymbol{\omega}$ does not change during the normalization procedure described in Subsection 4.4.1, because all the Hamiltonian terms, but $\boldsymbol{\omega} \cdot \boldsymbol{p}$, do not depend on the dummy variables (p_3, p_4, p_5); thus, the components of $\boldsymbol{\omega} = (\omega_3, \omega_4, \omega_5) \in \mathbb{R}^3$ are written in formula (4.8), because they are still equal to the values corresponding to the fundamental periods of the secular dynamics of the outer exoplanets.

The Hamiltonian $\mathcal{H}^{(\mathcal{N}_S)}$ is invariant with respect to a class of rotations, therefore, it is convenient to reduce[2] the number of DOF as we are going to explain. We consider the canonical transformation expressed by the following generating function (in mixed coordinates):

$$S(I_1, I_2, p_3, p_4, p_5, Q_1, Q_2, Q_3, Q_4, Q_5) = \\ \big(I_1 - I_{1_*}\big)Q_1 + \big(I_2 - I_{2_*}\big)Q_2 + p_3 Q_3 + p_4 Q_4 + (I_1 + I_2 - I_{1_*} - I_{2_*} + p_3 + p_4 + p_5)Q_5 \,,$$

where the translation vector $\big(I_{1_*}\,,\, I_{2_*}\big)$ includes two constant parameters that will be determined as explained in the next Sections. In view of Proposition 1.1.4 (which is reported in Section 1.1.2), the corresponding canonical change of variables is explicitely given by

$$\begin{aligned} I_1 &= P_1 + I_{1_*}\,, & \alpha_1 &= Q_1 + Q_5, \\ I_2 &= P_2 + I_{2_*}\,, & \alpha_2 &= Q_2 + Q_5, \\ p_3 &= P_3, & q_3 &= Q_3 + Q_5, \\ p_4 &= P_4, & q_4 &= Q_4 + Q_5, \\ p_5 &= P_5 - P_1 - P_2 - P_3 - P_4, & q_5 &= Q_5\,. \end{aligned} \tag{6.1}$$

After having expressed the Hamiltonian $\mathcal{H}^{(\mathcal{N}_S)}$ as a function of the new canonical coordinates $(P_1, P_2, P_3, P_4, P_5, Q_1, Q_2, Q_3, Q_4, Q_5)$, then one can easily check that

$$\frac{\partial \mathcal{H}^{(\mathcal{N}_S)}}{\partial Q_5} = 0\,;$$

in words, this is equivalent to say that Q_5 is a cyclic angle and, therefore, its conjugate momentum $P_5 = I_1 - I_{1_*} + I_2 - I_{2_*} + p_3 + p_4 + p_5$ is a constant of motion. It is worth to add here some comments, in order to clarify the role of the pair $(P_5\,,\, Q_5)$. Apart the modifications introduced by all the near-to-identity canonical transformations[3] which define the normalization procedure described in Subsection 4.4.1, q_3 and q_4 correspond to the longitudes of the pericenters of υ-And **c** and υ-And **d**, respectively, while q_5 refers to the longitude of the nodes of υ-And **c** and υ-And **d** (that are opposite each other, in the Laplace frame determined by taking into account just these two exoplanets). This identification is due to the way we have determined (q_3, q_4, q_5) by decomposing some specific signals of the secular dynamics of the outer exoplanets (this is made by using the Frequency Analysis as it is explained in Section 4.2). Moreover, $q_1 = \alpha_1$ and $q_2 = \alpha_2$ correspond to the longitude of the pericenter and the longitude of the node of υ-And **b**, respectively. Therefore, it is not difficult to see that the dynamics of the model we are studying does depend just on the pericenters arguments of the three exoplanets and on the difference between the longitude of the nodes of υ-And **b** and υ-And **c**, i.e., $\Omega_1 - \Omega_2 = \Omega_1 - \Omega_3 - \pi$. Since the Hamiltonian is invariant with respect to any rotation of the same angle that is applied to all the longitudes of the nodes, then the total angular momentum is preserved. Thus, P_5 is constant because it describes the total angular momentum.

We focus our analysis on the 2+2/2 DOF Hamiltonian

$$\mathcal{H}^{(\mathcal{N}_S)}(P_1 + I_{1_*}, P_2 + I_{2_*}, P_3, P_4, P_5 - P_1 - P_2 - P_3 - P_4, Q_1 + Q_5, Q_2 + Q_5, Q_3 + Q_5, Q_4 + Q_5, Q_5)\,,$$

[2] In the previous Chapters 4–5, we have decided to not perform such a reduction, in order to make the role of the angular (canonical) variables more transparent, in such a way to clarify their meaning with respect to the positions of the exoplanets.

[3] It is not difficult to verify that the all Lie series introduced in Subsection 4.4.1 preserve the invariance with respect to Q_5.

where we have stressed the parametric role of the constant values of $I_* = \left(I_{1_*}, I_{2_*}\right)$ and the angular momentum P_5 is replaced by its constant value, which can be fixed according to the initial conditions, i.e., $P_5 = P_5(0) = I_1(0) - I_{1_*} + I_2(0) - I_{2_*} + p_3(0) + p_4(0) + p_5(0)$. The Taylor expansion around $P_1 = 0$, $P_2 = 0$ of the previous expression of $\mathcal{H}^{(\tilde{\mathcal{N}}_S)}$ can be written as follows:

$$\mathcal{H}_K^{(0)}(\boldsymbol{P},\boldsymbol{Q};\boldsymbol{I}_*) = \mathcal{E}^{(0)}(\boldsymbol{I}_*) + \left(\boldsymbol{\omega}^{(0)}(\boldsymbol{I}_*)\right)\cdot\boldsymbol{P} + \sum_{s=0}^{\tilde{\mathcal{N}}_S}\sum_{l=2}^{\tilde{\mathcal{N}}_L} f_l^{(0,s)}(\boldsymbol{P},\boldsymbol{Q};\boldsymbol{I}_*) + \sum_{s=1}^{\tilde{\mathcal{N}}_S}\sum_{l=0}^{1} f_l^{(0,s)}(\boldsymbol{P},\boldsymbol{Q};\boldsymbol{I}_*)\,, \quad (6.2)$$

where $(\boldsymbol{P},\boldsymbol{Q}) := (P_1,P_2,P_3,P_4,Q_1,Q_2,Q_3,Q_4)$, and $\boldsymbol{\omega}^{(0)}(\boldsymbol{I}_*) \in \mathbb{R}^4$ is defined so that

$$\omega_1^{(0)}(\boldsymbol{I}_*) = \left.\frac{\partial\left\langle\mathcal{H}_K^{(0)}\right\rangle_{\boldsymbol{Q}}}{\partial P_1}\right|_{\substack{P_1=0\\P_2=0}}, \quad \omega_2^{(0)}(\boldsymbol{I}_*) = \left.\frac{\partial\left\langle\mathcal{H}_K^{(0)}\right\rangle_{\boldsymbol{Q}}}{\partial P_2}\right|_{\substack{P_1=0\\P_2=0}}, \quad \omega_3^{(0)} = \omega_3 - \omega_5\,, \quad \omega_4^{(0)} = \omega_4 - \omega_5\,. \quad (6.3)$$

Moreover, $\mathcal{E}^{(0)} = \left\langle\mathcal{H}_K^{(0)}\right\rangle_{\boldsymbol{Q}}\Big|_{\boldsymbol{P}=\boldsymbol{0}} \in \mathbb{R}$ and the summands can be rearranged so that $f_l^{(0,s)} \in \mathcal{P}_{l,s\tilde{K}}$, which is defined in (5.2); therefore, $\tilde{\mathcal{N}}_L$ denotes the order of truncation with respect to the actions $\boldsymbol{P}$ and $\tilde{\mathcal{N}}_S\tilde{K}$ is the maximal trigonometric degree in the angles $\boldsymbol{Q}$.

6.2 Algorithmic construction of the Kolmogorov normal form without fixing the angular velocity vector

We describe the generic r-th normalization step, starting from the Hamiltonian

$$\mathcal{H}_K^{(r-1)}(\boldsymbol{P},\boldsymbol{Q}) = \mathcal{E}^{(r-1)} + \boldsymbol{\omega}^{(r-1)}\cdot\boldsymbol{P} + \sum_{s\geq 0}\sum_{l\geq 2} f_l^{(r-1,s)}(\boldsymbol{P},\boldsymbol{Q}) + \sum_{s\geq r}\sum_{l=0}^{1} f_l^{(r-1,s)}(\boldsymbol{P},\boldsymbol{Q})\,, \quad (6.4)$$

where $(\boldsymbol{P},\boldsymbol{Q})$ are action-angle variables, $\boldsymbol{\omega}^{(r-1)} \in \mathbb{R}^4$, $\mathcal{E}^{(r-1)} \in \mathbb{R}$ is an energy value and $f_l^{(r-1,s)} \in \mathcal{P}_{l,s\tilde{K}}$. The first upper index (i.e., $r-1$) denotes the number of normalization steps that has been already performed; therefore, the expansion (6.2) of $\mathcal{H}_K^{(0)}$ is coherent with the one of $\mathcal{H}_K^{(r-1)}$ in (6.4) when $r = 1$. Of course, in order to simplify the notation in the expansion (6.4), we have omitted to stress that all the Hamiltonian terms depend on the parameter $I_* = \left(I_{1_*}, I_{2_*}\right)$.

The approach of this new normalization procedure is very similar to the one already discussed in Section 5.1: in order to bring the Hamiltonian in *Kolmogorov normal form*, a sequence of canonical transformations is performed with the aim to remove the (small) perturbing terms, that are represented by the last series appearing in the expansion (6.4). Thus, the r-th normalization step consists of two substeps, each of them involving two canonical transformations, that are defined by Lie series. Their generating functions are $\chi_1^{(r)}(\boldsymbol{Q})$ and $\chi_2^{(r)}(\boldsymbol{P},\boldsymbol{Q})$, respectively; thus, the new Hamiltonian at the end of the r-th normalization step is defined as

$$\mathcal{H}_K^{(r)} = \exp\left(L_{\chi_2^{(r)}}\right)\exp\left(L_{\chi_1^{(r)}}\right)\mathcal{H}_K^{(r-1)}\,. \quad (6.5)$$

As the main difference with respect to the algorithm described in Section 5.1, we skip the intermediate substeps where small translations on the actions were performed with the aim of keeping fixed all the components of the angular velocity vector.

First substep (of the r-th normalization step)

The first substep aims to remove the perturbing term $f_0^{(r-1,r)}$; thus, the first generating function $\chi_1^{(r)}(\boldsymbol{Q})$ is determined solving the following homological equation:

$$\{\boldsymbol{\omega}^{(r-1)}\cdot\boldsymbol{P},\chi_1^{(r)}\} + f_0^{(r-1,r)}(\boldsymbol{Q}) = \left\langle f_0^{(r-1,r)}\right\rangle_{\boldsymbol{Q}}\,. \quad (6.6)$$

After having expanded the perturbing term as $f_0^{(r-1,r)}(\boldsymbol{Q}) = \sum_{|k|\le r\tilde{K}} c_{\boldsymbol{k}}^{(r-1)} e^{i\boldsymbol{k}\cdot\boldsymbol{Q}}$, one easily gets

$$\chi_1^{(r)}(\boldsymbol{Q}) = \sum_{0<|k|\le r\tilde{K}} \frac{c_{\boldsymbol{k}}^{(r-1)}}{i\,\boldsymbol{k}\cdot\boldsymbol{\omega}^{(r-1)}} e^{i\boldsymbol{k}\cdot\boldsymbol{Q}}\,,$$

which is well defined provided that the non-resonance condition $\boldsymbol{k}\cdot\boldsymbol{\omega}^{(r-1)} \neq 0$ is satisfied $\forall\ 0 < \boldsymbol{k} \le r\tilde{K}$. At the end of this first normalization substep, (by the abuse of notation that is usual in the Lie formalism, i.e., the new canonical coordinates are denoted with the same symbols as the old ones) the intermediate Hamiltonian can be written as follows:

$$\widehat{\mathcal{H}}^{(r)} = \exp L_{\chi_1^{(r)}} \mathcal{H}^{(r-1)} = \mathcal{E}^{(r)} + \boldsymbol{\omega}^{(r-1)}\cdot\boldsymbol{P} + \sum_{s\ge 0}\sum_{l\ge 2} \widehat{f}_l^{(r,s)}(\boldsymbol{P},\boldsymbol{Q}) + \sum_{s\ge r}\sum_{l=0}^{1} \widehat{f}_l^{(r,s)}(\boldsymbol{P},\boldsymbol{Q})\,,$$

where, first, we introduce $\widehat{f}_l^{(r,s)} = f_l^{(r-1,s)}\ \forall\, l\ge 0\,,\ s\ge 0$ and then, by abuse, we redefine[4] these new symbols so that

$$\widehat{f}_{l-j}^{(r,s+jr)} \hookleftarrow \frac{1}{j!} L^j_{\chi_1^{(r)}} f_l^{(r-1,s)} \qquad \forall\, l\ge 1,\ 1\le j\le l,\ s\ge 0\,;$$

in view of (6.6) we also set $\widehat{f}_0^{(r,r)} = 0$ and we update the energy so that $\mathcal{E}^{(r)} = \mathcal{E}^{(r-1)} + \left\langle f_0^{(r-1,r)} \right\rangle_{\boldsymbol{Q}}$.

Second substep (of the r-th normalization step)

The second substep aims to remove the perturbing term $\widehat{f}_1^{(r,r)}$; thus, the generating function $\chi_2^{(r)}(\boldsymbol{P},\boldsymbol{Q})$ can be determined by solving the following homological equation:

$$\{\boldsymbol{\omega}^{(r-1)}\cdot\boldsymbol{P}, \chi_2^{(r)}\} + \widehat{f}_1^{(r,r)}(\boldsymbol{P},\boldsymbol{Q}) = \left\langle \widehat{f}_1^{(r,r)} \right\rangle_{\boldsymbol{Q}}\,. \tag{6.7}$$

Since in the first substep the non-resonance condition has been assumed to be true, we get

$$\chi_2^{(r)}(\boldsymbol{P},\boldsymbol{Q}) = \sum_{|\boldsymbol{j}|=1}\ \sum_{0<|k|\le r\tilde{K}} \frac{c_{\boldsymbol{j},\boldsymbol{k}}^{(r)}}{i\,\boldsymbol{k}\cdot\boldsymbol{\omega}^{(r-1)}}\,\boldsymbol{P}^{\boldsymbol{j}} e^{i\boldsymbol{k}\cdot\boldsymbol{Q}}\,,$$

where $\widehat{f}_1^{(r,r)} = \sum_{|\boldsymbol{j}|=1}\sum_{0<|k|\le r\tilde{K}} c_{\boldsymbol{j},\boldsymbol{k}}^{(r)}\,\boldsymbol{P}^{\boldsymbol{j}} e^{i\boldsymbol{k}\cdot\boldsymbol{Q}}$. Thus, the Hamiltonian at the end of the r-th normalization step can be written (by the usual abuse of notation on the new variables, renamed as the old ones) as follows:

$$\begin{aligned}\mathcal{H}_K^{(r)} &= \exp L_{\chi_2^{(r)}} \widehat{\mathcal{H}}^{(r-1)} = \exp L_{\chi_2^{(r)}} \exp L_{\chi_1^{(r)}} \mathcal{H}^{(r-1)} \\ &= \mathcal{E}^{(r)} + \boldsymbol{\omega}^{(r)}\cdot\boldsymbol{P} + \sum_{s\ge 0}\sum_{l\ge 2} f_l^{(r,s)}(\boldsymbol{P},\boldsymbol{Q}) + \sum_{s\ge r+1}\sum_{l=0}^{1} f_l^{(r,s)}(\boldsymbol{P},\boldsymbol{Q})\,,\end{aligned} \tag{6.8}$$

where, first, we introduce $f_l^{(r,s)} = \widehat{f}_l^{(r,s)}\ \forall\, l\ge 0\,,\ s\ge 0$ and then, by abuse, we redefine[5] these new symbols so that

$$f_1^{(r,jr)} \hookleftarrow \frac{1}{j!} L^j_{\chi_2^{(r)}} \left(\boldsymbol{\omega}^{(r-1)}\cdot\boldsymbol{P}\right) \quad \text{and} \quad f_l^{(r,s+jr)} \hookleftarrow \frac{1}{j!} L^j_{\chi_2^{(r)}} \widehat{f}_l^{(r,s)} \quad \forall\, l\ge 0,\ j\ge 1,\ s\ge 0\,.$$

[4] From a practical point of view, if we have to deal with finite sums (as, for instance, in formula (6.4)), such that the index s goes up to a fixed order called $\tilde{\mathcal{N}}_S$, then we have to require also that $1\le j\le \min\left(l, \lfloor(\tilde{\mathcal{N}}_S - s)/r\rfloor\right)$.

[5] From a practical point of view, if we have to deal with finite sums such that the index s goes up to a fixed order called $\tilde{\mathcal{N}}_S$, then we have to require also that $1\le j\le \lfloor(\tilde{\mathcal{N}}_S - s)/r\rfloor$ and, in the case of $f_1^{(r,jr)} \hookleftarrow \frac{1}{j!} L^j_{\chi_2^{(r)}} \left(\boldsymbol{\omega}^{(r-1)}\cdot\boldsymbol{P}\right)$, $1\le j\le \lfloor\tilde{\mathcal{N}}_S/r\rfloor$.

In view of the previous homological equation (6.7) we also set $f_1^{(r,r)}=0$ and we redefine the angular velocity vector so that

$$\boldsymbol{\omega}^{(r)}\cdot\boldsymbol{P}=\boldsymbol{\omega}^{(r-1)}\cdot\boldsymbol{P}+\left\langle \widehat{f}_1^{(r,r)}\right\rangle_{\boldsymbol{Q}}\,.$$

Finally, if we denote with $(\boldsymbol{P}^{(r)},\boldsymbol{Q}^{(r)})$ the so called normalized coordinates after r normalization steps, i.e., $\mathcal{H}_K^{(r)}(\boldsymbol{P}^{(r)},\boldsymbol{Q}^{(r)})$, then they are related to the original ones (that are referring to $\mathcal{H}_K^{(0)}$, i.e. $(\boldsymbol{P}^{(0)},\boldsymbol{Q}^{(0)})=(\boldsymbol{P},\boldsymbol{Q})$) by the following equation:

$$(\boldsymbol{P}^{(0)},\boldsymbol{Q}^{(0)})=\exp L_{\chi_2^{(r)}}\exp L_{\chi_1^{(r)}}\ldots\exp L_{\chi_2^{(1)}}\exp L_{\chi_1^{(1)}}(\boldsymbol{P},\boldsymbol{Q})\Big|_{\substack{\boldsymbol{P}=\boldsymbol{P}^{(r)}\\ \boldsymbol{Q}=\boldsymbol{Q}^{(r)}}}\,, \tag{6.9}$$

that can be fully justified by using repeteadly the Exchange Theorem 1.1.6.

6.3 Applications of the Kolmogorov normalization algorithm to the SQPR Hamiltonian model with $2+2/2$ DOF

Here, we want to construct the Kolmogorov normal form, as it has been explained in the previous Section, starting from the Hamiltonian $\mathcal{H}_K^{(0)}(\boldsymbol{P},\boldsymbol{Q};\boldsymbol{I}_*)$. In its expansion, which is written in (6.2), the parametric dependency on the translation vector $I_*=\left(I_{1_*}\,,\,I_{2_*}\right)$ is emphasized for each Hamiltonian summand. The initial canonical transformation (6.1) is fully determined when the components of $\boldsymbol{I}_*$ are fixed. In our strategy, we aim to choose the values of I_{1_*} and I_{2_*} in such a way that, at the end of the algorithm *à la* Kolmogorov, the wanted angular velocity vector $\tilde{\boldsymbol{\omega}}_{new}$ is approached by the one that is updated at the end of each normalization step, i.e., $\boldsymbol{\omega}^{(r)}(\boldsymbol{I}_*)$ with $r=0,\,1,\,\ldots\,\tilde{\mathcal{N}}_S$. As already done in Section 5.1, we can determine the angular velocity vector of the selected orbit, by performing a numerical integration of the original $2+3/2$ DOF model (whose equations of motion are written in (4.16)) and applying the frequency analysis method to the discretized signals $t\mapsto\xi_1(t)+i\eta_1(t)$, $t\mapsto 2\sqrt{\Lambda_1}\sqrt[4]{1-\left(\mathrm{e}_1(t)\right)^2}\,\sin\left(\frac{\mathrm{i}_1(t)}{2}\right)e^{-i\Omega_1(t)}$ (recall the definition (4.2) of the Poincaré canonical variables). Let us denote with $\tilde{\omega}_1$ and $\tilde{\omega}_2$ the values of the fundamental angular velocities corresponding to these two signals, respectively. Taking into account the canonical transformation (6.1), then we can finally provide the values of the components of the angular velocity vector $\tilde{\boldsymbol{\omega}}_{new}$, i.e.,

$$\tilde{\omega}_{1_{new}}=\tilde{\omega}_1-\omega_5\,,\quad \tilde{\omega}_{2_{new}}=\tilde{\omega}_2-\omega_5\,,\quad \tilde{\omega}_{3_{new}}=\omega_3-\omega_5\,,\quad \tilde{\omega}_{4_{new}}=\omega_4-\omega_5\,, \tag{6.10}$$

where the values of $(\omega_3,\omega_4,\omega_5)\in\mathbb{R}^3$, are related to the fundamental periods of the two outer exoplanets and are given in equation (4.8). We remark that since the actions P_3 and P_4 play the role of dummy variables during the Kolmogorov normalization algorithm, just the first two components of the angular velocity vector are updated at the end of every r-th step of such a computational procedure, i.e., $\omega_1^{(r)}(\boldsymbol{I}_*)$ and $\omega_2^{(r)}(\boldsymbol{I}_*)$.

It is now convenient to explain how the Kolmogorov normalization algorithm can be used in junction with a Newton-like method. For the sake of definiteness, as a first approximation of the translation vector $\boldsymbol{I}_*$ we are looking for, let us consider the values at the time $t=0$ of the actions $\boldsymbol{I}_*^{(0)}=\left(I_{1_*}(0)\,,\,I_{2_*}(0)\right)$ in correspondence with the initial conditions[6] of the selected orbit. After having fixed a translation vector $\boldsymbol{I}_*^{(n_{\mathcal{N}})}$ (where the upper index $n_{\mathcal{N}}$ just counts the number of times the Newton method is iterated) we apply the algorithm for the construction of the Kolmogorov normal form as it has been explained in Section 6.2 and starting from the Hamiltonian (6.2). Such an algorithm is explicitly performed up to the $\tilde{\mathcal{N}}_S$-th normalization step by using `Mathematica` as

[6]Starting from the initial values of the orbital parameters that have been preselected, we can compute the corresponding actions values $\left(I_1(0)\,,\,I_2(0)\right)$ after the normalization procedure which is described in Subsection 4.4.1 and it has been designed in order to construct a suitable elliptic torus.

an algebraic manipulator. Thus, this part of the computational procedure provides us the expansion of $\mathcal{H}_K^{(\tilde{\mathcal{N}}_S)}(\boldsymbol{P},\boldsymbol{Q};\,\boldsymbol{I}_*^{(n_{\mathcal{N}})})$, which is of the same type with respect to that described in (6.8), but we rewrite it in such a way to emphasize its parametric dependence on the translation vector, i.e.,

$$\begin{aligned}\mathcal{H}_K^{(\tilde{\mathcal{N}}_S)}(\boldsymbol{P},\boldsymbol{Q};\,\boldsymbol{I}_*^{(n_{\mathcal{N}})}) &= \mathcal{E}^{(\tilde{\mathcal{N}}_S)}(\boldsymbol{I}_*^{(n_{\mathcal{N}})}) + \big(\boldsymbol{\omega}^{(\tilde{\mathcal{N}}_S)}(\boldsymbol{I}_*^{(n_{\mathcal{N}})})\big)\cdot\boldsymbol{P} + \sum_{s=0}^{\tilde{\mathcal{N}}_S}\sum_{l=2}^{\tilde{\mathcal{N}}_L} f_l^{(\tilde{\mathcal{N}}_S,s)}(\boldsymbol{P},\boldsymbol{Q};\,\boldsymbol{I}_*^{(n_{\mathcal{N}})}) \\ &= \mathcal{E}^{(\tilde{\mathcal{N}}_S)}(\boldsymbol{I}_*^{(n_{\mathcal{N}})}) + \big(\boldsymbol{\omega}^{(\tilde{\mathcal{N}}_S)}(\boldsymbol{I}_*^{(n_{\mathcal{N}})})\big)\cdot\boldsymbol{P} + \mathcal{O}\big(||\boldsymbol{P}||^2\big)\,.\end{aligned} \tag{6.11}$$

The truncated expansion above is in Kolmogorov normal form and refers to an (approximately) invariant torus whose energy level is equal to $\mathcal{E}^{(\tilde{\mathcal{N}}_S)}(\boldsymbol{I}_*^{(n_{\mathcal{N}})})$ and its angular velocity vector is $\boldsymbol{\omega}^{(\tilde{\mathcal{N}}_S)}(\boldsymbol{I}_*^{(n_{\mathcal{N}})}) = \big(\omega_1^{(\tilde{\mathcal{N}}_S)}(\boldsymbol{I}_*^{(n_{\mathcal{N}})})\,,\,\omega_2^{(\tilde{\mathcal{N}}_S)}(\boldsymbol{I}_*^{(n_{\mathcal{N}})})\,,\,\tilde{\omega}_{3_{new}}\,,\,\tilde{\omega}_{4_{new}}\big)$, where the last two components are defined in formula (6.10). Of course, if the $n_{\mathcal{N}}$-th numerical approximation $\boldsymbol{I}_*^{(n_{\mathcal{N}})}$ is close enough to the translation vector $\boldsymbol{I}_*$ we are looking for, then also $\boldsymbol{\omega}^{(\tilde{\mathcal{N}}_S)}(\boldsymbol{I}_*^{(n_{\mathcal{N}})})$ will be close to the angular velocity vector $\tilde{\boldsymbol{\omega}}_{new}$ we are targeting. In order to find a better approximation of the translation vector $\boldsymbol{I}_*$ (and, consequently, of the preselected quasi-periodic orbit) we can proceed by applying the Newton method. Thus, the approximations of the initial translation vector are iteratively computed so that

$$\boldsymbol{I}_*^{(n_{\mathcal{N}})} = \boldsymbol{I}_*^{(n_{\mathcal{N}}-1)} + \mathrm{d}\boldsymbol{I}_*^{(n_{\mathcal{N}}-1)}\,,\qquad n_{\mathcal{N}}\geq 1$$

where the correction $\mathrm{d}\boldsymbol{I}_*^{(n_{\mathcal{N}}-1)}$ is given by the following refinement formula:

$$\Delta\boldsymbol{\omega}(\boldsymbol{I}_*^{(n_{\mathcal{N}}-1)}) + \mathcal{J}(\boldsymbol{I}_*^{(n_{\mathcal{N}}-1)})\mathrm{d}\boldsymbol{I}_*^{(n_{\mathcal{N}}-1)} = 0\,,$$

where $\Delta\boldsymbol{\omega}(\boldsymbol{I}_*^{(n_{\mathcal{N}}-1)}) = \big(\omega_1^{(\tilde{\mathcal{N}}_S)}(\boldsymbol{I}_*^{(n_{\mathcal{N}}-1)}) - \tilde{\omega}_{1_{new}}\,,\,\omega_2^{(\tilde{\mathcal{N}}_S)}(\boldsymbol{I}_*^{(n_{\mathcal{N}}-1)}) - \tilde{\omega}_{2_{new}}\big)$ and the 2×2 Jacobian matrix $\mathcal{J}(\boldsymbol{I}_*^{(n_{\mathcal{N}}-1)})$ of the function $\boldsymbol{I}_*^{(n_{\mathcal{N}}-1)} \mapsto \big(\omega_1^{(\tilde{\mathcal{N}}_S)}(\boldsymbol{I}_*^{(n_{\mathcal{N}}-1)})\,,\,\omega_2^{(\tilde{\mathcal{N}}_S)}(\boldsymbol{I}_*^{(n_{\mathcal{N}}-1)})\big)$ is evaluated numerically by the finite difference method[7] since there is not an explicit analytic expression of such a function. As usual, the Newton method will be iterated until the discrepancy $\|\Delta\boldsymbol{\omega}(\boldsymbol{I}_*^{(n_{\mathcal{N}}-1)})\|$ is smaller than a prefixed tolerance threshold. Therefore, if such a condition is reached, we will have constructed a Kolmogorov normal form corresponding to an invariant torus approximating the preselected quasi-periodic orbit in a so accurate way that $\big(\omega_1^{(\tilde{\mathcal{N}}_S)}(\boldsymbol{I}_*^{(n_{\mathcal{N}}-1)})\,,\,\omega_2^{(\tilde{\mathcal{N}}_S)}(\boldsymbol{I}_*^{(n_{\mathcal{N}}-1)})\big) \simeq \big(\tilde{\omega}_{1_{new}}\,,\,\tilde{\omega}_{2_{new}}\big)$. In all our applications we are going to describe, the initial approximation provided by the initial conditions, i.e., $\boldsymbol{I}_*^{(0)} = \big(I_{1_*}(0)\,,\,I_{2_*}(0)\big)$ is good enough to successfully perform the Newton method that stops regularly with a final discrepancy that gets smaller than the tolerance threshold, which is fixed so to be equal to 10^{-10}.

6.3.1 Results produced by the semi-analytic integration of the SQPR Hamiltonian model with $2+2/2$ DOF and without GR corrections

As we have done in Section 5.2, we start from the secular quasi-periodic restricted Hamiltonian with $2+3/2$ DOF, namely $\mathcal{H}_{sec,\,2+3/2}$, whose expansion (4.53) is finite, with truncation parameters

[7] In practice, let us refer with the symbols $\boldsymbol{\omega}^{(\tilde{\mathcal{N}}_S)}(\boldsymbol{I}_*^{(n_{\mathcal{N}}-1)})$, $\boldsymbol{\omega}^{(\tilde{\mathcal{N}}_S)}(\tilde{\boldsymbol{I}}_1^{(n_{\mathcal{N}}-1)})$, $\boldsymbol{\omega}^{(\tilde{\mathcal{N}}_S)}(\tilde{\boldsymbol{I}}_2^{(n_{\mathcal{N}}-1)})$ to the angular velocity vectors as they are determined at the end of the Kolmogorov normalization algorithm which start from the initial translation vectors $\boldsymbol{I}_*^{(n_{\mathcal{N}}-1)} = (I_{1_*}^{(n_{\mathcal{N}}-1)}, I_{2_*}^{(n_{\mathcal{N}}-1)})$, $\tilde{\boldsymbol{I}}_1^{(n_{\mathcal{N}}-1)} = (I_{1_*}^{(n_{\mathcal{N}}-1)} + h_1\,,\, I_{2_*}^{(n_{\mathcal{N}}-1)})$, $\tilde{\boldsymbol{I}}_2^{(n_{\mathcal{N}}-1)} = (I_{1_*}^{(n_{\mathcal{N}}-1)}\,,\, I_{2_*}^{(n_{\mathcal{N}}-1)} + h_2)$, respectively; then

$$\mathcal{J}(\boldsymbol{I}_*^{(n_{\mathcal{N}}-1)}) = \begin{pmatrix} \frac{\omega_1^{(\tilde{\mathcal{N}}_S)}(\tilde{\boldsymbol{I}}_1^{(n_{\mathcal{N}}-1)}) - \omega_1^{(\tilde{\mathcal{N}}_S)}(\boldsymbol{I}_*^{(n_{\mathcal{N}}-1)})}{h_1} & \frac{\omega_1^{(\tilde{\mathcal{N}}_S)}(\tilde{\boldsymbol{I}}_2^{(n_{\mathcal{N}}-1)}) - \omega_1^{(\tilde{\mathcal{N}}_S)}(\boldsymbol{I}_*^{(n_{\mathcal{N}}-1)})}{h_2} \\ \frac{\omega_2^{(\tilde{\mathcal{N}}_S)}(\tilde{\boldsymbol{I}}_1^{(n_{\mathcal{N}}-1)}) - \omega_2^{(\tilde{\mathcal{N}}_S)}(\boldsymbol{I}_*^{(n_{\mathcal{N}}-1)})}{h_1} & \frac{\omega_2^{(\tilde{\mathcal{N}}_S)}(\tilde{\boldsymbol{I}}_2^{(n_{\mathcal{N}}-1)}) - \omega_2^{(\tilde{\mathcal{N}}_S)}(\boldsymbol{I}_*^{(n_{\mathcal{N}}-1)})}{h_2} \end{pmatrix}\,.$$

In all our applications we have set the small increments in such a way that $h_1 = I_{1_*}^{(n_{\mathcal{N}}-1)}/100$ and $h_2 = I_{2_*}^{(n_{\mathcal{N}}-1)}/100$.

fixed so that $\mathcal{N}_L = 6$, $K = 2$ and $\mathcal{N}_S = 4$. The corresponding equations of motion are reported in formula (4.16) (recall also the canonical transformation (4.52)). Most of the values of the initial orbital parameters, that are $a_1(0)$, $\mathrm{e}_1(0)$, $M_1(0)$ and $\omega_1(0)$, are reported in Table 4.7; they are completed with $m_1 = 0.674$ (i.e., the value of the mass of υ-And **b**) and $(\mathrm{i}_1(0), \Omega_1(0)) = (17°, 5°)$. Then, we perform $\mathcal{N}_S$ steps of the algorithm constructing the elliptic torus by applying the normalization procedure described in Subsection 4.4.1. Hence, we proceed as explained in the Sections 6.1, 6.2 and 6.3 (before the beginning of the present Subsection). Concerning the construction of the Kolmogorov normal form (without fixing the angular velocity vector), we adopt $\tilde{\mathcal{N}}_L = 2$, $\tilde{K} = 2$, $\tilde{\mathcal{N}}_S = 6$ as parameters ruling the truncations of the expansions. In particular, 4 iterations of the Newton method are enough to reach the condition $\|\boldsymbol{\omega}^{(\tilde{\mathcal{N}}_S)}(\boldsymbol{I}_*^{(4)}) - \tilde{\boldsymbol{\omega}}_{new}\| < 10^{-10}$, which allows us to successfully conclude the search for the initial translation vector that approximates well enough the one we are looking for, namely the unknown $\boldsymbol{I}_*$. We focus on the last Kolmogorov normalization that is performed at the end of the Newton method, i.e., the one corresponding to the initial translation vector $\boldsymbol{I}_*^{(4)}$. In spite of the fact that `Mathematica` allows to deal just with a few normalization steps in the case of a system with $2+2/2$ DOF, looking at Figure 6.1, one can appreciate that the decay of the norms of the generating functions $\chi_1^{(r)}$ and $\chi_2^{(r)}$ is rather regular and sharp. This numerical evidence suggest that the normalization algorithm should be convergent.

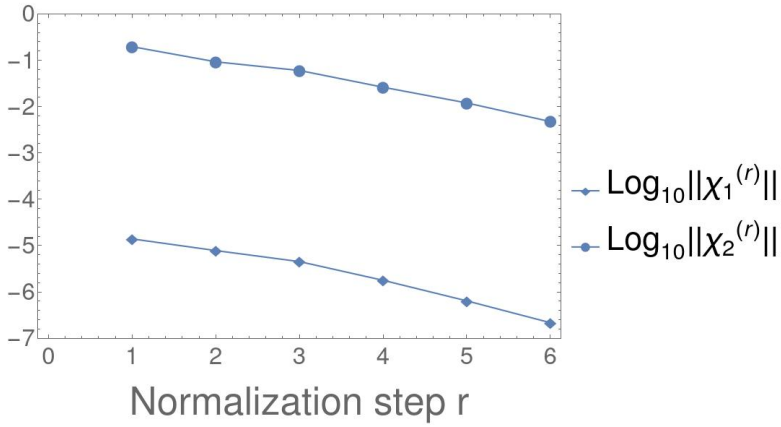

Figure 6.1: Convergence of the generating functions $\chi_1^{(r)}$ and $\chi_2^{(r)}$ defined by the normalization algorithm à la Kolmogorov without keeping fixed the angular velocity vector, when it is applied to the 2+2/2 DOF SQPR model *without* GR corrections and is performed in the case corresponding to $(\mathrm{i}_1(0), \Omega_1(0)) = (17°, 5°)$. The Log_{10} of their norms are reported as a function of the normalization step r.

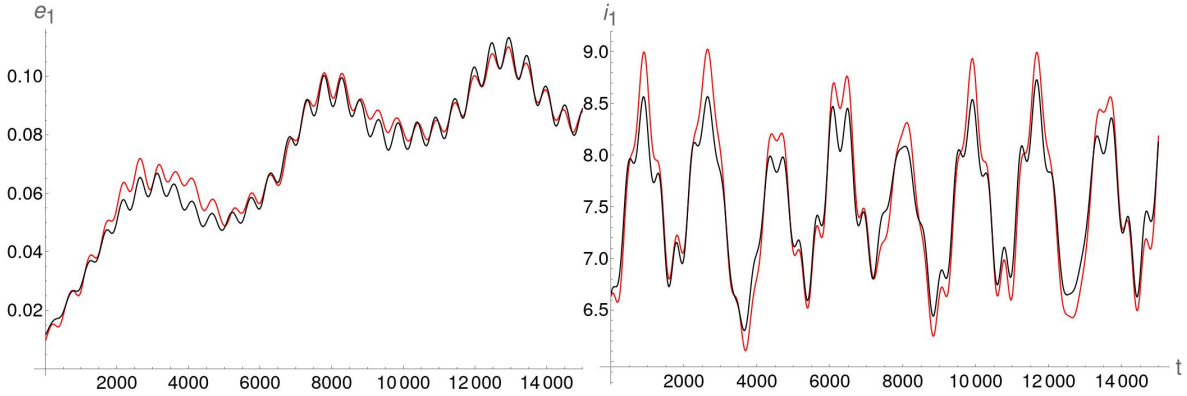

Figure 6.2: Comparisons between the eccentricity e_1 (on the left) and the inclination i_1 (on the right) as obtained through the semi-analytical approach (in red) and the numerical one (in black). Both the integration methods consider the case with initial conditions with $(\mathrm{i}_1(0), \Omega_1(0)) = (17°, 5°)$ and they are applied to $2+3/2$ DOF model which *does not* take into account the effects due to GR.

In order to express the change of canonical coordinates allowing us to express the original variables of our problem, i.e., the ones appearing as arguments of the Hamiltonian $\mathcal{H}_{sec,\,2+3/2}$, whose expansion is reported in (4.53), as a function of the normalized ones that are listed in the final form of the Hamiltonian (6.11), let us recall that is "just" matter of composing all the canonical transformations we have performed. Therefore, by using `Mathematica` as an algebraic manipulator, it has been possible to compute the expansions of such a composition of canonical transformations, described in formulæ (4.56), (6.1) and (6.9). This allows us to construct a semi-analytic (approximate) solution of the equations of motion (4.16) which corresponds to the invariant KAM torus that is travelled by quasi-periodic orbits characterized by the angular velocity vector $\tilde{\boldsymbol{\omega}}_{new}$. Such a quasi-periodic evolution is plotted in Figure 6.2, where one can appreciate the rather good agreement with the numerical integrations of the motion for what concerns the behavior of both the eccentricity and the inclination of υ-And **b**. It is particularly relevant that we arrived to the same conclusions discussed in Subsection 5.2 also when the final invariant torus is constructed for an Hamiltonian model with $2+2/2$ DOF, where just a few normalization steps can be effectively performed.

6.3.2 Results produced by the semi-analytic integration of the SQPR Hamiltonian model with $2+2/2$ DOF and GR corrections

We now start from the secular quasi-periodic restricted Hamiltonian which has $2+3/2$ DOF and takes into account the relativistic effects, namely $\mathcal{H}^{(GR)}_{sec,\,2+\frac{3}{2}}$ written in (4.67). The corresponding equations of motion are reported in formula (4.68). We consider initial conditions that are very similar to the one given in the previous Subsection 6.3.1, with the only difference that here we assume $(i_1(0), \Omega_1(0)) = (20^\circ, 0^\circ)$. The construction of the normal form for an elliptic torus by applying the procedure described in Subsection 4.4.1 is performed with the following values parameters ruling the truncation of the series expansions: $\mathcal{N}_L = 6$, $K = 2$, $\mathcal{N}_S = 5$. Hence, we proceed in a way very similar to the one that has been detailed in the previous Subsection 6.3.1 (for what concerns the construction of the Kolmogorov normal form without fixing the angular velocity vector, we adopt $\tilde{\mathcal{N}}_L = 2$, $\tilde{K} = 2$, $\tilde{\mathcal{N}}_S = 6$ as parameters ruling the truncations of the expansions). Here, 3 iterations of the Newton method are enough to reach the condition, which allows us to successfully conclude the search for a good enough approximation of the unknown initial translation vector, i.e., $\boldsymbol{I}_*$. We focus again on the last Kolmogorov normalization that is performed at the end of the Newton method, i.e., the one corresponding to the initial translation vector $\boldsymbol{I}^{(3)}_*$. Looking at Figure 6.3, once again we can appreciate a rather regular and sharp decay of the norms of the generating functions $\chi_1^{(r)}$ and $\chi_2^{(r)}$.

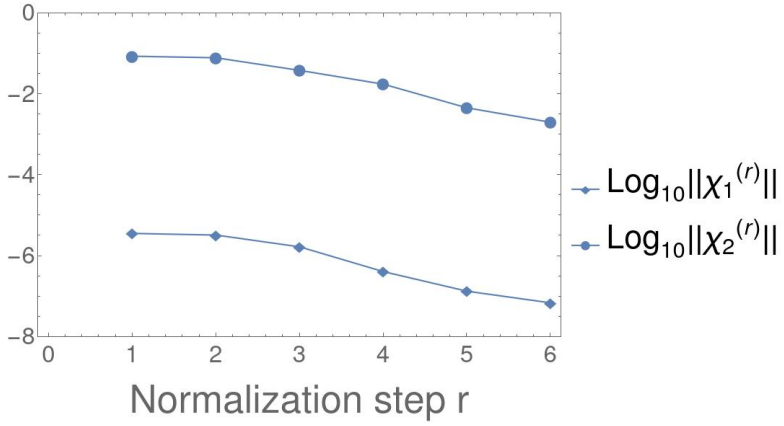

Figure 6.3: Convergence of the generating functions $\chi_1^{(r)}$ and $\chi_2^{(r)}$ defined by the normalization algorithm à la Kolmogorov without keeping fixed the angular velocity vector, when it is applied to the 2+2/2 DOF SQPR model *with* GR corrections and is performed in the case corresponding to $(i_1(0), \Omega_1(0)) = (20^\circ, 0^\circ)$. The Log_{10} of their norms are reported as a function of the normalization step r.

Following again the approach described in the previous Subsection 6.3.1, we can construct a semi-analytic (approximate) solution of the equations of motion (4.68) which here corresponds to a quasi-periodic orbit whose angular velocity vector is now denoted with $\tilde{\boldsymbol{\omega}}^{(GR)}_{new}$. Such a quasi-periodic evolution is plotted in Figure 6.4, where one can appreciate that there is rather good agreement with the numerical integrations of the motion for what concerns the behavior of both the eccentricity and the inclination of υ-And **b** (apart a small shift of the two plots reported in the left panel).

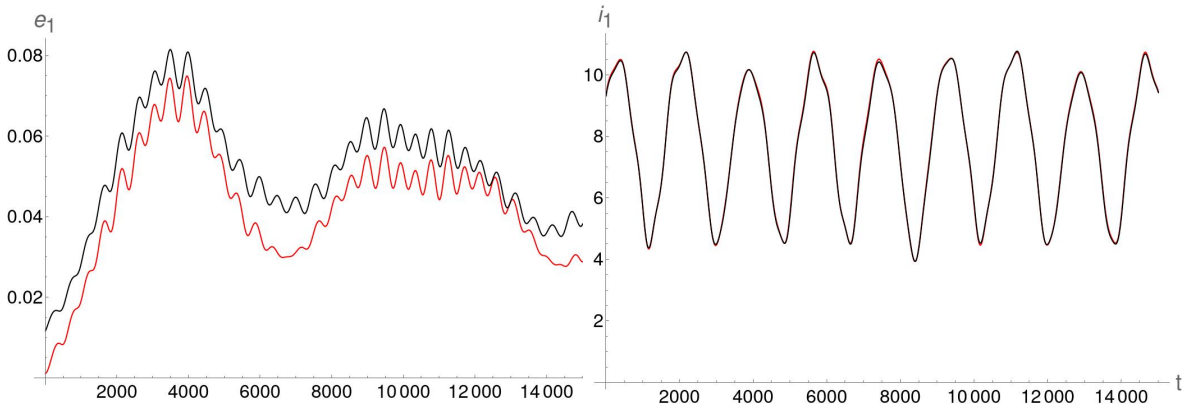

Figure 6.4: Comparisons between the eccentricity e_1 (on the left) and the inclination i_1 (on the right) as obtained through the semi-analytical approach (in red) and the numerical one (in black). Both the integration methods consider the case with initial conditions with $(\mathrm{i}_1(0), \Omega_1(0)) = (20^\circ, 0^\circ)$ and they are applied to $2+3/2$ DOF model taking into account the effects due to GR.

6.3.3 Computer-Assisted Proofs of existence of KAM tori for the SQPR Hamiltonian models with $2+2/2$ DOF

Since we have been able to perform the normalization procedure à la Kolmogorov just for very few steps of the algorithm, the expectation of its convergence is not supported in a very convincing way by the results discussed in the two previous Subsections 6.3.1–6.3.2. Therefore, we think it is particularly interesting to adopt an approach based on rigorous CAPs for both the cases described above.

We have run the codes which can be downloaded from the publicly available website [70]; such a software package is designed to prove the existence of KAM tori for Hamiltonian systems with a number of DOF $n \geq 2$ (while the one in [69] is limited to the case with 2 DOF). For what concerns the systems described in Subsections 6.3.1 and 6.3.2, we have applied the CAP to $\mathcal{H}^{(\tilde{\mathcal{N}}_S-1)}(\boldsymbol{P}, \boldsymbol{Q}; \boldsymbol{I}^{(4)}_*)$ and $\mathcal{H}^{(\tilde{\mathcal{N}}_S-1)}(\boldsymbol{P}, \boldsymbol{Q}; \boldsymbol{I}^{(3)}_*)$, respectively. This means that, in both cases, we are studying the last Kolmogorov algorithm started at the end of the Newton method, but we consider the Hamiltonian produced at the end of the next to last normalization step. Performing also the last step, of course, would completely remove all the perturbation terms that are represented in our *truncated* expansions. Therefore, an application of a CAP to $\mathcal{H}^{(\tilde{\mathcal{N}}_S)}$ would be completely pointless. Stopping the preliminary algebraic manipulations that are performed by using `Mathematica` at the next to last step allows us to consider the main perturbing terms that would make part also of an *infinite* series expansion of $\mathcal{H}^{(\tilde{\mathcal{N}}_S-1)}$; therefore, in our opinion this is significant and challenging.

In the case of the 2+2/2 DOF Hamiltonian model $\mathcal{H}^{(\tilde{\mathcal{N}}_S-1)}(\boldsymbol{P}, \boldsymbol{Q}; \boldsymbol{I}^{(4)}_*)$ (which does not consider any relativistic effect and is described in Subsection 6.3.1) the CAP succeeds in rigorously proving the existence of a set (with positive Lebesgue measure) of KAM tori whose corresponding angular velocity vectors are Diophantine and in an extremely small neighborhood of $\tilde{\boldsymbol{\omega}}_{new}$. Moreover, in the case of the Hamiltonian $\mathcal{H}^{(\tilde{\mathcal{N}}_S-1)}(\boldsymbol{P}, \boldsymbol{Q}; \boldsymbol{I}^{(3)}_*)$ (which takes into account the effects due to GR

and is described in Subsection 6.3.2) the CAP succeeds in rigorously proving the same statement about the local existence of Diophantine KAM tori in the vicinity of $\tilde{\boldsymbol{\omega}}_{new}^{(GR)}$. In the former case the CPU-time needed to complete the CAP[8] is about 53 days on a workstation equipped with processors of type `Intel XEON-GOLD 5220` (2.2 GHz), while in the latter case 22 days of CPU-time are requested on the same computer. We emphasize that, as far as we know, this is the first complete application of a CAP to a so realistic Hamiltonian model with more than 2 DOF. On the other hand, the CPU-time needed to run a single CAP of this kind is so huge that it strongly discourages any further exploration of its performances, in particular, for what concerns the eventual coverage of the dynamically stable region with an approach similar to the one discussed at the end of Chapter 5.

[8]For what concerns the non-relativistic case the values of the parameters that are internal to the CAP and affect the most the computational complexity are fixed so that $R_I = 40$ and $R_{II} = 12000$; while in the relativitic case they are defined as $R_I = 36$ and $R_{II} = 18000$. See footnote[5] in Chapter 5 for a short explanation of the meaning of the parameters R_I and R_{II}.

7. KAM theory for Hamiltonian systems with an isochronous integrable part

7.1 Motivation of the theory

As already explained in the Introduction (subsection 1.3.1), the Kolmogorov-Arnold-Moser (KAM) theorem refers to Hamiltonian systems of the form

$$\mathcal{H}(\boldsymbol{p},\boldsymbol{q}) = h(\boldsymbol{p}) + \varepsilon f(\boldsymbol{p},\boldsymbol{q})\,, \tag{7.1}$$

where $(\boldsymbol{p},\boldsymbol{q})$ are action-angle variables. In particular the Theorem 1.3.1 proves the existence of invariant tori in the phase space of the full Hamiltonian (7.1), for sufficiently small ε. In this Chapter we are interested in the study of Hamiltonian with "isochronous" integrable part, given by

$$\mathcal{H}(\boldsymbol{q},\boldsymbol{J}) \,=\, \boldsymbol{\omega}_0 \cdot \boldsymbol{J} + \sum_{i\geq 1}\sum_{s\geq 3} \varepsilon^i \tilde{h}_{i,\,s}(\boldsymbol{q},\boldsymbol{J})$$

where $\boldsymbol{q} \in \mathbb{T}^n$, $\boldsymbol{J} \in \mathcal{B} \subseteq \mathbb{R}^n$, $\tilde{h}_{i,\,s} = \mathcal{O}(||\boldsymbol{J}||^{\frac{s}{2}})$. More precisely, we are interested in finding quasi-periodic orbits, with a certain frequency $\boldsymbol{\omega}$ fixed in advance, given by the expression

$$\boldsymbol{\omega} = \boldsymbol{\omega}_0 - \sum_{i\geq 1} \varepsilon^i \boldsymbol{a}_i(\boldsymbol{J}_0)$$

where $\boldsymbol{J}_0$ is the initial condition for $\boldsymbol{J}$ of a trajectory on the torus with frequency $\boldsymbol{\omega}$.

The algorithm which gives a formal construction for the calculation of such a trajectory is explicitely given in Section 7.4. However, there exist different methods (direct or indirect) to approach in a perturbative way the problem of Hamiltonian systems with an isochronous integrable part. For this reason, before exposing our own Kolmogorov-like algorithm, we review in the present Chapter some of these methods, outlining differences and analogies between them as well as providing some explicit examples and applications.

The content of the following sections is largely based on the article [76].

7.2 Background: Lindstedt series and normal forms

In various contexts in the literature, the use of the term 'Lindstedt series' for isochronous Hamiltonian systems often refers to one of two *distinct* methods, both applicable to the perturbative study of the dynamics around systems with elliptic equilibria. The difference between these two methods

can be conveniently explained with the help of the following example: consider a 'Henon-Heiles' type Hamiltonian

$$\mathcal{H} = \frac{1}{2}(p_x^2 + p_y^2) + \frac{1}{2}\omega_{0,1}^2 x^2 + \frac{1}{2}\omega_{0,2}^2 y^2 + \varepsilon P_3(x,y) \tag{7.2}$$

where, contrary to the actual Hénon-Heiles model ([41]) (where $\omega_{0,1} = \omega_{0,2} = 1$), we first assume that the frequencies $(\omega_{0,1}, \omega_{0,2})$ satisfy no resonance condition. P_3 can be any polynomial cubic in x, y. Note that the first form of perturbation theory for systems of this type, called the 'third integral', was developed by Contopoulos and collaborators (see for istance [13], [14], [15]).

We are interested in constructing perturbative series solutions in the model (7.2) under the form:

$$x(t) = x_0(t) + \varepsilon x_1(t) + \varepsilon^2 x_2(t) + \ldots, \quad y(t) = y_0(t) + \varepsilon y_1(t) + \varepsilon^2 y_2(t) + \ldots, \tag{7.3}$$

where we adopt some periodic form for the functions $x_0(t), y_0(t)$ and compute iteratively all subsequent functions $x_i(t), y_i(t)$, $i = 1, 2, \ldots$. We further want to secure that the iterative scheme used to compute the functions $x_i(t), y_i(t)$ preserves the quasi-periodic character of the solutions, i.e., produces no secular terms (of the form $t\sin(\omega t)$, etc) for some frequencies ω obtained as discussed below. An elementary remark in this context is that the nonlinear coupling of the oscillators implies that quasi-periodic orbits in the above model are expected to evolve, in general, with frequencies ω_1, ω_2 different from those of the unperturbed oscillators, $\omega_{0,1}, \omega_{0,2}$. As it is well known (see, for example, [29]), recognition of this fact implies to introduce formal series also for the frequencies:

$$\begin{aligned} \omega_1(A_1, A_2) &= \omega_{0,1} + \varepsilon\omega_{1,1}(A_1, A_2) + \varepsilon^2\omega_{2,1}(A_1, A_2) + \ldots, \\ \omega_2(A_1, A_2) &= \omega_{0,2} + \varepsilon\omega_{1,2}(A_2, A_2) + \varepsilon^2\omega_{2,2}(A_1, A_2) + \ldots. \end{aligned} \tag{7.4}$$

The quantities $\omega_{i,1}(A_1, A_2), \omega_{i,2}(A_1, A_2)$ are functions depending on two parameters A_1, A_2, called hereafter the 'amplitudes' of the oscillations in x and y respectively. They enter into the calculation through the choice made for the zero-th order terms $x_0(t)$, $y_0(t)$, since the iterative procedure starts by setting

$$x_0(t) = A_1\cos(\omega_1 t + \phi_{x0}), \quad y_0(t) = A_2\cos(\omega_2 t + \phi_{y0}) \tag{7.5}$$

where the initial phases ϕ_{x0}, ϕ_{y0} can be arbitrary.

The above are common elements of the point of departure for both versions discussed below of the Lindstedt method. However, at this stage emerges an important bifurcation in the way we define the iterative scheme by which the functions $x_i(t), y_i(t), \omega_{i,1}, \omega_{i,2}$ are to be computed. We discuss two distinct possibilities, referred to below as (i) a Lindstedt scheme 'analogous to the Birkhoff series', or (ii) a Lindstedt scheme 'analogous to the Kolmogorov series'.

As typical in perturbation theory, the formal difference between the above two schemes actually reflects a real (physical) difference in the way we interpret the meaning of the series (7.4). In summary, the difference can be posed as follows (see section 7.3 for details):

(i) in the scheme called below 'analogous to Birkhoff', we seek to construct a quasi-periodic solution valid for any value of the amplitudes A_1, A_2 within a suitably defined open domain around the origin. Thus, the series (7.4) in this scheme are meant to answer the question of what are the values of the frequencies ω_1, ω_2 under which the motion takes place for *any given and pre-selected* sets of values of the amplitudes A_1, A_1 in the above domain. The reader is referred to [46] where a clear exposition of the method is given in the framework of special solutions of the three-body problem computed via Lindstedt series.

(ii) in the scheme called below 'analogous to Kolmogorov', instead, we *fix in advance* the values of the frequencies ω_1, ω_2 (see [29] for a clear exposition of the method in the context of the forced anharmonic oscillator); this is called by some authors a 'torus fixing method'. A relevant remark in the context of this last method is that the series (7.4) are actually purported to answer the question *reverse* to the one posed in (i) above. That is, the question now is: with given and pre-selected values of the frequencies ω_1, ω_2, invert the series (7.4) and compute which are the corresponding amplitudes A_1, A_2 for which we obtain quasi-periodic trajectories with the frequencies ω_1, ω_2. Thus,

in method (i) the series are parameterized by the amplitudes A_1, A_2, which can be selected at the beginning of the construction, while in method (ii) the solutions are parameterized by the frequencies ω_1, ω_2, which are the parameters to select at the beginning of the construction. Also, in the latter case the series inverse to (7.4) turn out to have the form (in the cubic case)

$$\varepsilon^2 A_1^2 = \sum_{i=1}^{\infty} C_{i,1}(\omega_1 - \omega_{0,1})^i, \quad \varepsilon^2 A_2^2 = \sum_{i=1}^{\infty} C_{i,2}(\omega_2 - \omega_{0,2})^i, \tag{7.6}$$

for some constant coefficients $C_{i,1}, C_{i,2}$ computable from the series (7.4). Thus, with all frequencies of the problem fixed in advance, establishing the convergence of the inverse series (7.6) suffices to answer the question posed at (ii).

The question of the convergence of the series is, of course, crucial, and related to the kind, and pattern of accumulation in the series terms, of small divisors appearing at successive perturbative steps. As regards the kind of divisors, we can readily see that:

- in scheme (i) we obtain divisors of the form $k_1\omega_{0,1} + k_2\omega_{0,2}$, with $(k_1, k_2) \in \mathbb{Z}^2$, $|k_1| + |k_2| \neq 0$. This follows from the kind of linear (non-homogeneous) equation to solve iteratively. Deferring details to the example treated in Section 2, we briefly recall that in scheme (i) we introduce the parametrization (modulo two unimportant phases) $\varphi_1 = \omega_1 t$, $\varphi_2 = \omega_2 t$, and after introducing the series expressions (7.3) and (7.4) to the equations of motion and separate terms of like orders we arrive at equations (to be solved iteratively) of the form:

$$\begin{aligned} &\left(\omega_{0,1}\frac{\partial}{\partial\varphi_1} + \omega_{0,2}\frac{\partial}{\partial\varphi_2}\right)^2 x_i + x_i = \Theta_{1,i}(\varphi_1, \varphi_2) \\ &\left(\omega_{0,1}\frac{\partial}{\partial\varphi_1} + \omega_{0,2}\frac{\partial}{\partial\varphi_2}\right)^2 y_i + y_i = \Theta_{2,i}(\varphi_1, \varphi_2) \quad i = 1, 2, \ldots \end{aligned} \tag{7.7}$$

where the functions $\Theta_{1,i}(\varphi_1, \varphi_2)$, $\Theta_{2,i}(\varphi_1, \varphi_2)$ contain trigonometric terms in the angles φ_1, φ_2 (see [46], section 4).

- In scheme (ii), instead, we obtain divisors of the form $k_1\omega_1 + k_2\omega_2$, i.e., depending on the (fixed) pre-selected new frequencies ω_1, ω_2. This follows from the fact that the linear non-homogeneous equations to solve are now of the form (see [29]):

$$\begin{aligned} &\ddot{x}_i + \omega_1^2 x_i = \Phi_{1,i}(\varphi_1, \varphi_2) \\ &\ddot{y}_i + \omega_2^2 y_i = \Phi_{2,i}(\varphi_1, \varphi_2) \quad i = 1, 2, \ldots \end{aligned} \tag{7.8}$$

again with functions $\Phi_{1,i}(\varphi_1, \varphi_2)$, $\Phi_{2,i}(\varphi_1, \varphi_2)$ containing trigonometric terms in the angles $\varphi_1 = \omega_1 t, \varphi_2 = \omega_2 t$. Note that since the divisors depend on the new frequencies ω_1, ω_2, choosing non-resonant values for the *latter* permits the formal construction to proceed; this, even when the unperturbed frequencies $\omega_{0,1}, \omega_{0,2}$ are, instead, resonant.

As regards convergence, in the case (i) Poincaré ([94], Ch.IX) already emphasizes that the Lindstedt series with divisors depending on the original harmonic frequencies $\omega_{0,1}, \omega_{0,2}$ are divergent, exhibiting the well known asymptotic character associated with the series computed via a Birkhoff normal form (see [20] for a review). Indeed, as shown by example in section 2 below, it possible to construct Birkhoff series yielding the same individual solutions as those of the Lindstedt series of scheme (i). We note here that the series originally introduced by Lindstedt ([64, 65, 66]), albeit somewhat different in structure, exhibit the same divisors as those of the scheme (i) above, thus, according to Poincaré, they are only asymptotic. On the other hand, Eliasson ([21]) and Gallavotti ([27, 28]) established the existence of convergent Lindstedt series by the 'torus fixing method' on the basis of the cancellations between terms with small divisors (see [33] for an instructive example). A proof of the convergence of scheme (ii) is actually possible by diagrammatic methods via the following theorem [16]:

Theorem 7.2.1 ([16]). *Consider the N coupled oscillator equations*

$$\ddot{x}_j + \omega_j^2 x_j + f_j(x_1, \ldots, x_N; \varepsilon) + (\omega_{0,j}^2 - \omega_j^2) x_j = 0, \qquad j = 1, \ldots, N \tag{7.9}$$

where ε is a real parameter, $\boldsymbol{f}(\boldsymbol{x}, \varepsilon)$ is real analytic at $\boldsymbol{x} = 0$, $\varepsilon = 0$, at least quadratic in $\boldsymbol{x}$ and such that $f(\boldsymbol{x}, 0) = 0$, and the frequency vector $\boldsymbol{\omega}$ is diophantine. Let

$$x_j^{(0)}(t) = c_j e^{i\omega_j t} + c_j^* e^{-i\omega_j t}, \quad j = 1, \ldots, N \tag{7.10}$$

which is a solution of (7.9) for any choice of the complex constants c_j, for $\varepsilon = 0$ and $\boldsymbol{\omega}_0 = \boldsymbol{\omega}$. Let $\Gamma(\boldsymbol{c}) = \max(|c_1|, \ldots, |c_N|, 1)$. Then, there exists a positive constant η_0 and a function $\boldsymbol{\eta}(\varepsilon, \boldsymbol{c})$ holomorphic in the domain $|\varepsilon|\Gamma^3(\boldsymbol{c}) \leq \eta_0$, real for real ε, such that the system

$$\ddot{x}_j + \omega_j^2 x_j + f_j(x_1, \ldots, x_N, \varepsilon) + \eta_j(\varepsilon, \boldsymbol{c}) x_j = 0, \qquad j = 1, \ldots, N \tag{7.11}$$

admits a solution of the form

$$\boldsymbol{x}(t, \varepsilon, \boldsymbol{c}) = \sum_{\boldsymbol{\nu} \in \mathbb{Z}^N} \boldsymbol{A}_{\boldsymbol{\nu}} \exp(i\boldsymbol{\nu} \cdot (\boldsymbol{\omega} t)) \tag{7.12}$$

holomorphic in the domain $|\varepsilon|\Gamma^3(\boldsymbol{c}) e^{3|\boldsymbol{\omega}||\Im t|} \leq \eta_0$ and real for real ε, t. The constants $\boldsymbol{A}_{\boldsymbol{\nu}}$ are $\mathcal{O}(\varepsilon)$, except for the constants $A_{1,0,\ldots,0}$, $A_{0,1,\ldots,0}$, $A_{0,0,\ldots,1}$, which are equal to c_1, c_2, $\ldots$, c_N respectively.

A similar proof in action-angle variables in the case $N = 2$ is discussed in [1].

As a final introductory remark, the series construction in the isochronous case finds a plethora of applications in various fields of physics. We mention in particular, the use of the Lindstedt method for the computation of solutions lying on low-dimensional tori ('q-tori') in the celebrated Fermi-Pasta-Ulam (FPU) problem ([11, 12]). The FPU model takes, in normal mode space, the form of N harmonic oscillators coupled with nonlinear terms:

$$\ddot{Q}_k + \Omega_k^2 Q_k = \varepsilon F_k(Q_1, \ldots, Q_N) \tag{7.13}$$

where the frequencies Ω_k, $k = 1, \ldots, N$ are given in terms of the FPU normal mode spectrum $\Omega_k = 2\sin(k\pi/(2(N+1)))$, the function F can be cubic or quartic in the variables Q_k, and the perturbation ε satisfies some scaling law with N.

Flach and co-workers ([24, 25]) emphasized the special role for dynamics played by solutions called 'q-breathers'. These are periodic orbits of the form $Q_q(t) = A_q \cos(\omega_q t + \phi_q)$, and $Q_k(t) = 0$ for $k \neq q$. For the frequencies ω_q we obtain series expressions of the form

$$\omega_q = \Omega_q + \Delta\omega_q(A_q; \varepsilon), \qquad \Delta\omega_q = \mathcal{O}(\varepsilon). \tag{7.14}$$

Then, for ε sufficiently small, the Lindstedt method (ii) above allows to represent the q-breathers via the Fourier expansion

$$\begin{aligned} Q_q(t) &= A_q \cos(\omega_q t + \phi_q) + \sum_{m=0}^{\infty} \tilde{f}_{q,m}(A_q; \varepsilon) \cos[m(\omega_q t + \phi_q)] \\ Q_k(t) &= \sum_{m=0}^{\infty} \tilde{f}_{k,m}(A_q; \varepsilon) \cos[m(\omega_q t + \phi_q)], \quad k \neq q, \end{aligned} \tag{7.15}$$

where $\tilde{f}_{k,m} = \mathcal{O}(\varepsilon^{p(k,q,m)})$, with integer exponent $p(k, q, m) \geq 1$. The relevant point for the FPU problem is that the rules of propagation of the amplitude A_q in the series terms for all modes allows to find an analytic formula explaining the phenomenon of 'energy localization' observed for particular initial excitations in the FPU model. In [12] and [11], on the other hand, it was shown that the q-breathers constitute only the first member in the hierarchy of special FPU solutions

that exhibit energy localization. More general members are the 'q-tori', i.e., special solutions with $M < N$ incommensurable frequencies satisfying

$$\omega_{q_i} = \Omega_{q_i} + \Delta\omega_{q_i}(A_{q_1}, A_{q_2}, \ldots, A_{q_M}; \varepsilon), \qquad \Delta\omega_{q_i} = \mathcal{O}(\varepsilon), \tag{7.16}$$

where $\mathcal{R}_q = (q_1, \ldots q_M) \in \{1, 2, ..., N\}^M$. The corresponding Fourier representation of these special solutions can again been computed using Lindstedt series, and it obtains the form

$$\begin{aligned} Q_k(t) &= A_k \cos(\omega_k t + \phi_k) + \sum_{|\mathbf{m}|=0}^{\infty} \tilde{f}_{k,\boldsymbol{m}}(\mathbf{A}; \varepsilon) \cos[\boldsymbol{m} \cdot (\boldsymbol{\omega} t + \boldsymbol{\phi})], \quad k \in \mathcal{R}_q \\ Q_k(t) &= 0 + \sum_{|\mathbf{m}|=0}^{\infty} \tilde{f}_{k,\boldsymbol{m}}(\mathbf{A}; \varepsilon) \cos[\boldsymbol{m} \cdot (\boldsymbol{\omega} t + \boldsymbol{\phi})], \quad k \notin \mathcal{R}_q \end{aligned} \tag{7.17}$$

with $\boldsymbol{m} \equiv (m_1, \ldots, m_M) \in \mathbb{Z}^M$, $\boldsymbol{A} \equiv (A_{q_1}, \ldots, A_{q_M})$, $\boldsymbol{\omega} \equiv (\omega_{q_1}, \ldots, \omega_{q_M})$, $\boldsymbol{\phi} \equiv (\phi_{q_1}, \ldots, \phi_{q_M})$, and $\tilde{f}_{k,\boldsymbol{m}} = \mathcal{O}(\varepsilon)$ for all $k = 1, \ldots N$. Furthermore, the propagation of the amplitudes A_k in the series terms allows to interpret a variety of complex localization profiles encountered for particular initial mode excitations in the FPU problem (see the corresponding theorems in [11]).

We mentioned already that for the Lindstedt series analogous to the Birkhoff ones there exists a Birkhoff normal form yielding the same solutions as those recovered by the Lindstedt method via an indirect approach, i.e., one based on a sequence of normalizing transformations involving canonical changes of variables. It is natural to ask whether this correspondence between a direct (Lindstedt) and indirect (normal form) method extends in the case of the torus-fixing method as well. Due to the lack of a twist condition, the torus-fixing process in the isochronous case has to be dealt with using a technique based on 'counterterms' (see [27]), or a KAM algorithm 'with knobs' (see [98]). In the following sections, we present a Kolmogorov algorithm using counterterms, which is able to recover the solutions of the direct Lindstedt method in both cases of full or low-dimensional tori.

7.3 An elementary example

In order to illustrate the methods discussed above, we consider an elementary example stemming from the following one-degree of freedom Hamiltonian with a even power dependence on the canonical variables

$$\mathcal{H}(x, p) = \mathcal{H}_0 + \varepsilon \mathcal{H}_1 = \frac{\omega_0}{2}\left(p^2 + x^2\right) + \varepsilon \frac{x^4}{4}\,. \tag{7.18}$$

Using the harmonic oscillator action-angle variables $(J,\, q)$ with $x = \sqrt{2J}\sin(q)\,,\ p = \sqrt{2J}\cos(q)\,,$ we obtain

$$\mathcal{H}(q, J) = \omega_0\, J + \frac{3\,\varepsilon}{8} J^2 - \frac{\varepsilon}{2} J^2 \cos(2q) + \frac{\varepsilon}{8} J^2 \cos(4q)\,. \tag{7.19}$$

Let J_0 be the label of a given torus (periodic orbit) of the harmonic oscillator model $\mathcal{H}_0$. Consider a real neighborhood $\mathcal{D}_\varepsilon = \{J = J_0 + p \text{ with } |p| < D_\varepsilon\}$, where $D_\varepsilon = \mathcal{O}(\varepsilon)$. We illustrate four different perturbative methods to treat the dynamics in the phase-space neighborhood $\mathbb{T} \times \mathcal{D}_\varepsilon$: these are i) a Birkhoff normal form construction, with ii) its analog in terms of Lindstedt series, iii) a Lindstedt series exhibiting the torus-fixing property of the Kolmogorov method, and, finally iv) the normal form analogue of iii).

7.3.1 Birkhoff normal form

Setting $J = J_0 + p$ the Hamiltonian takes the form (apart from a constant)

$$\begin{aligned} \mathcal{H}(q, p) = \omega_0\, p + \frac{3\,\varepsilon\, J_0^2}{8} + \frac{3\, J_0\, \varepsilon}{4} p + \frac{3\,\varepsilon}{8} p^2 - \frac{\varepsilon\, J_0^2}{2} \cos(2q) - \varepsilon J_0 p \cos(2q) \\ - \frac{\varepsilon}{2} p^2 \cos(2q) + \frac{\varepsilon J_0^2}{8} \cos(4q) + \frac{\varepsilon\, J_0}{4} p \cos(4q) + \frac{\varepsilon}{8} p^2 \cos(4q)\,. \end{aligned} \tag{7.20}$$

A 'Birkhoff normal form' for the Hamiltonian (7.20) can be computed by introducing a canonical transformation eliminating the angle q. Writing the Hamiltonian (7.20) as

$$\mathcal{H}(q,p) = Z_0 + \varepsilon f_1 \,,$$

where $Z_0 = \omega_0 p$ and $f_1 = \sum_{k,l} c_{k,l}\, p^k e^{ilq}$ we will define a Lie generating function $\chi^{(1)}(q,p)$ bringing this Hamiltonian to normal form up to terms $\mathcal{O}(\varepsilon)$. In the standard procedure, it is sufficient to set $\chi^{(1)} = X^{(1)}$, where $X^{(1)}$ solves the homological equation $L_{X^{(1)}} Z_0 + \varepsilon f_1 = \varepsilon\zeta_1$, with $\zeta_1 =< f_1 >_q$ and L_X denoting the Poisson bracket operator $L_X = \{\cdot, X\}$. However, comparing the result with the one obtained by the corresponding Lindstedt method (see next subsection) requires a small modification in the definition of $\chi^{(1)}$. Consider the canonical transformation $(q,p) \to (q^{(r)}, p^{(r)})$ obtained after r normalization steps: we require that the canonical transformation be such that the initial condition $q^{(r)} = p^{(r)} = 0$ in the new variables be mapped to the initial condition $\big(q(q^{(r)}=0, p^{(r)}=0), p(q^{(r)}=0, p^{(r)}=0)\big) = (0,0) + \mathcal{O}(\varepsilon^{r+1})$ in the original variables. It is easy to see that such a requirement of control on the initial condition can be fulfilled by setting

$$\chi^{(n)}(q,p) = X^{(n)}(q,p) + K^{(n)}\, q + S^{(n)}\, p \,, \quad n = 1, \ldots, r$$

where $K^{(n)}$, $S^{(n)}$ are constants possible to compute at every step by requiring that

$$\Big(q(q^{(n)}=0, p^{(n)}=0), p(q^{(n)}=0, p^{(n)}=0)\Big) = (0,0) + \mathcal{O}(\varepsilon^{n+1}).$$

Since $\{\omega_0 p, K^{(n)}\, q\} = -\omega_0 K^{(n)}$, this procedure will only alter the normal form at the n-th step by a constant, adding, however, some trigonometric terms to the remainder at every step. As an example, we can readily verify the following formulas for the first step (and analogously for subsequent steps)

$$\chi^{(1)}(q,p) = X^{(1)}(q,p) + K^{(1)}\, q + S^{(1)}\, p \,,$$

where

$$X^{(1)}(q,p) = \sum_{\substack{l\neq 0 \\ k}} \frac{c_{k,l}}{i\, l\, \omega_0}\, p^k e^{ilq} \,, \qquad K^{(1)} = -\sum_{l\neq 0} \frac{c_{0,l}}{\omega_0} \,, \qquad S^{(1)} = -\sum_{l\neq 0} \frac{c_{1,l}}{i\, l\, \omega_0} \,.$$

Omitting details, the formulas obtained after two normalization steps as above are the following: the Hamiltonian takes the form

$$\mathcal{H}^{(2)}(q^{(2)}, p^{(2)}) = \exp L_{\varepsilon^2 \chi^{(2)}} \exp L_{\varepsilon \chi^{(1)}} \mathcal{H}\Big|_{\substack{q=q^{(2)} \\ p=p^{(2)}}} = \left(Z_0 + \varepsilon Z_1 + \varepsilon^2 Z_2 + \sum_{i\geq 3} \varepsilon^i f_i \right)\Big|_{\substack{q=q^{(2)} \\ p=p^{(2)}}} .$$

For simplicity in the notation, from now on we omit superscripts from the variables q and p unless explicitly required, adopting, instead, the convention that the symbols $(\tilde q, \tilde p)$ in any function of the form $F^{(r)}(\tilde q, \tilde p)$ imply the new canonical variables computed after r normalization steps. Then, up to order 2 in ε we obtain:

$$\mathcal{H}^{(2)}(\tilde q, \tilde p) = Z^{(2)} + R^{(2)} = \omega_0\, \tilde p + \frac{3\,\varepsilon\, J_0}{4}\, \tilde p + \frac{3\,\varepsilon\, \tilde p^2}{8} - \frac{69\,\varepsilon^2\, J_0^2}{64\,\omega_0}\, \tilde p - \frac{51\,\varepsilon^2\, J_0}{64\,\omega_0}\, \tilde p^2 - \frac{17\,\varepsilon^2}{64\,\omega_0}\, \tilde p^3 + R^{(2)}$$

where the remainder $R^{(2)}$ is $\mathcal{O}(\varepsilon^3)$. The Hamiltonian $Z^{(2)}$ can now be used to analytically compute ε^2-precise solutions to the equations of motion in the variables $(\tilde q, \tilde p)$. The equations of motion are

$$\begin{cases} \dot{\tilde q} = \dfrac{\partial \mathcal{H}^{(2)}}{\partial \tilde p} = \omega_0 + \dfrac{3\,\varepsilon\, J_0}{4} + \dfrac{3\,\varepsilon}{4}\tilde p - \dfrac{69\,\varepsilon^2\, J_0^2}{64\,\omega_0} - \dfrac{51\,\varepsilon^2\, J_0}{32\,\omega_0}\, \tilde p - \dfrac{51\,\varepsilon^2}{64\,\omega_0}\, \tilde p^2 \\ \dot{\tilde p} = -\dfrac{\partial \mathcal{H}^{(2)}}{\partial \tilde q} = 0 \end{cases} ;$$

fixing the initial condition $\tilde{p}(0) = \tilde{q}(0) = 0$ yields the solution

$$\tilde{p}(t) = 0\,, \qquad \tilde{q}(t) = \omega\, t := \varphi_B\,, \qquad \omega = \omega_0 + \frac{3\,\varepsilon\, J_0}{4} - \frac{69\,\varepsilon^2\, J_0^2}{64\,\omega_0}\,. \tag{7.21}$$

This can be back-transformed to the solution in the original variables. We have

$$q = \exp L_{\varepsilon^2\,\chi^{(2)}} \exp L_{\varepsilon\,\chi^{(1)}}\, \tilde{q}\,, \qquad p = \exp L_{\varepsilon^2\,\chi^{(2)}} \exp L_{\varepsilon\,\chi^{(1)}}\, \tilde{p}\,. \tag{7.22}$$

Substituting the solutions $(\tilde{q}(t),\, \tilde{p}(t))$ in the previous expression, we find

$$\begin{aligned}
q(t) &= \varphi_B - \frac{\varepsilon\, J_0}{2\,\omega_0}\, \sin(2\varphi_B) + \frac{31\,\varepsilon^2\, J_0^2}{32\,\omega_0^2}\, \sin(2\,\varphi_B) + \frac{\varepsilon\, J_0}{16\,\omega_0}\, \sin(4\varphi_B) \\
&\quad - \frac{\varepsilon^2\, J_0^2}{32\,\omega_0^2}\, \sin(4\,\varphi_B) - \frac{\varepsilon^2\, J_0^2}{32\,\omega_0^2}\, \sin(6\,\varphi_B) + \frac{\varepsilon^2\, J_0^2}{512\,\omega_0^2}\, \sin(8\,\varphi_B)\,, \\
p(t) &= -\frac{3\,\varepsilon\, J_0^2}{8\,\omega_0} + \frac{13\,\varepsilon^2\, J_0^3}{16\,\omega_0^2} + \frac{\varepsilon\, J_0^2}{2\,\omega_0}\, \cos(2\,\varphi_B) - \frac{33\,\varepsilon^2\, J_0^3}{32\,\omega_0^2}\, \cos(2\,\varphi_B) \\
&\quad - \frac{\varepsilon\, J_0^2}{8\omega_0}\, \cos(4\,\varphi_B) + \frac{3\,\varepsilon^2\, J_0^3}{16\,\omega_0^2}\, \cos(4\,\varphi_B) + \frac{\varepsilon^2\, J_0^3}{32\,\omega_0^2}\, \cos(6\,\varphi_B)\,, \\
J(t) &= J_0 + p(t)\,.
\end{aligned} \tag{7.23}$$

Observe that $q(0) = 0$ and $J(0) = J_0$, as was required.
Two remarks are in order:

(i) The divisors appearing in all series expressions obtained above depend on the (unique, in the case of 1DOF systems) *unperturbed* frequency of the model, i.e., the frequency ω_0 of the linear oscillator. In the case of systems with $N > 1$ degrees of freedom, the above series will produce divisors of the form $\boldsymbol{m} \cdot \boldsymbol{\omega}_0$, where $\boldsymbol{m} \in \mathbb{Z}^N$, $|\boldsymbol{m}| \neq 0$, and $\boldsymbol{\omega}_0$ is the $N-$vector of the unperturbed frequencies of the problem. This implies that the method may formally proceed only when the vector $\boldsymbol{\omega}_0$ is non-resonant. As regards the series convergence, this is guaranteed in an open domain in the 1DOF case. However, when $N > 1$ the series are in general only asymptotic (see [20] for reviews).

(ii) The value of the initial datum for the action J_0 can be chosen at the end of the process, i.e., the numerical value of J_0 need not be fixed in advance. In fact, J_0 (or, more generally, the vector $\boldsymbol{J}_0$) can be regarded as a parameter free to transfer in all iterative computations. It is, then, in terms of this parameter that we obtain an expression for the frequency(ies) ω on the torus with the initial conditions $J(0) = J_0$, $q(0) = 0$ as a function of J_0. In our example this function is given up to $\mathcal{O}(\varepsilon^2)$ in Eq (7.21).

(iii) Any choice is possible to impose on the initial phase $q(0)$, altering slightly the definition of the constants $S^{(n)}$.

7.3.2 Lindstedt solution analogous to Birkhoff

Analytical solutions in the form of formal series obtained like (7.23) above will be hereafter called 'Birkhoff solutions'. This terminology emphasizes the fact that the solutions are obtained using a Birkhoff normal form procedure. It is notworthy that Poincaré's reference to the 'Lindstedt series' (Methodes nouvelles, Ch. IX) actually consists of the construction of solutions to coupled oscillator problems obtained 'indirectly', i.e., via transformations of the variables and the engineering of the corresponding Hamiltonian function. Hence, the more general term 'Poincaré-Lindstedt' series often encountered in literature. We now give, instead, the 'direct' (i.e., without transformations) series construction of the Birkhoff solution (7.23) by implementing, instead, the original method of Lindstedt in the framework of the canonical action-angle variables of the harmonic oscillator model.

The Hamilton's equations of motion for the Hamiltonian (7.19) are

$$\begin{cases} \dot{q}(t) = \dfrac{\partial \mathcal{H}}{\partial J} = \omega_0 + \dfrac{3\,\varepsilon\,J}{4} - \varepsilon\,J\,\cos(2q) + \dfrac{\varepsilon\,J}{4}\cos(4q) & \text{(7.24a)} \\ \dot{J}(t) = -\dfrac{\partial \mathcal{H}}{\partial q} = -\varepsilon\,J^2\sin(2q) + \dfrac{\varepsilon\,J^2}{2}\sin(4q)\,. & \text{(7.24b)} \end{cases}$$

We perform the following steps:

Step 1: time re-parametrization. Set $\varphi = \omega\,t$ where ω is the (still unknown) frequency on the 1-torus (periodic orbit) corresponding to the solution with initial conditions $J(0) = J_0$, $q(0) = 0$.

Step 2: frequency expansion. This is the key element of the Lindstedt method. We expand ω as

$$\omega = \omega_0 - \varepsilon\,a_1(J_0) - \varepsilon^2\,a_2(J_0) + \dots\,. \tag{7.25}$$

Note that the corrections a_i $i = 1, 2, \dots$ are functions of the parameter J_0, i.e., of the 'amplitude' (square) of the oscillations.

Step 3: expansion of the solution. We write

$$\begin{aligned} q(\varphi) &= q_0(\varphi) + \varepsilon\,q_1(\varphi) + \varepsilon^2\,q_2(\varphi) + \dots\,, \\ J(\varphi) &= J_0(\varphi) + \varepsilon\,J_1(\varphi) + \varepsilon^2\,J_2(\varphi) + \dots\,. \end{aligned} \tag{7.26}$$

Note here a key element of the method, which is the fact that all functions q_i, J_i, $i = 0, 1, \dots$ are considered functions of the phase $\varphi = \omega\,t$ rather than of the time t itself. This is the key point in the differentiation of the method presented here with respect to the 'torus-fixing' method presented in Subsection 7.3.3. The relevant fact is that the use of the angle φ (or, more generally, of a set of angles $\boldsymbol{\varphi} \in \mathbb{T}^N$, with $\boldsymbol{\varphi} = \boldsymbol{\omega} t$ in the N-DOF case), instead of time, allows to split the equations of motion in a sequence of linear non-homogeneous equations, whose iterative solution introduces divisors depending on the unperturbed frequencies $\boldsymbol{\omega}_0$. This is made clear in the next step.

Step 4: splitting of the equations of motion in powers of ε and iterative solution. In our example, from the definition of φ we have:

$$\omega\,\frac{dq(\varphi)}{d\varphi} = \frac{dq(t)}{dt}\,, \qquad\qquad \omega\,\frac{dJ(\varphi)}{d\varphi} = \frac{dp(t)}{dt}\,.$$

Substituting (7.25) and (7.26) in the equations of motion (7.24a) and (7.24b) leads to the following expressions (up to order 2 in ε)

$$\begin{aligned} &\left(\omega_0 - \varepsilon\,a_1 - \varepsilon^2\,a_2\right)\left(\frac{dq_0(\varphi)}{d\varphi} + \varepsilon\,\frac{dq_1(\varphi)}{d\varphi} + \varepsilon^2\,\frac{dq_2(\varphi)}{d\varphi}\right) \qquad \text{(7.27a)} \\ &= \omega_0 + \frac{3\,\varepsilon\,J_0(\varphi)}{4} - \varepsilon\,J_0(\varphi)\,\cos(2\,q_0(\varphi)) + \frac{\varepsilon\,J_0(\varphi)}{4}\,\cos(4\,q_0(\varphi)) + \frac{3\,\varepsilon^2\,J_1(\varphi)}{4} - \varepsilon^2\,J_1(\varphi)\,\cos(2\,q_0(\varphi)) \\ &\quad + \frac{\varepsilon^2\,J_1(\varphi)}{4}\,\cos(4\,q_0(\varphi)) + 2\,\varepsilon^2\,J_0(\varphi)\,q_1(\varphi)\sin(2\,q_0(\varphi)) - \varepsilon^2\,J_0(\varphi)\,q_1(\varphi)\,\sin(4\,q_0(\varphi))\quad, \\ &\left(\omega_0 - \varepsilon\,a_1 - \varepsilon^2\,a_2\right)\left(\frac{dJ_0(\varphi)}{d\varphi} + \varepsilon\,\frac{dJ_1(\varphi)}{d\varphi} + \varepsilon^2\,\frac{dJ_2(\varphi)}{d\varphi}\right) \qquad \text{(7.27b)} \\ &= -\varepsilon\,J_0(\varphi)^2\,\sin(2\,q_0(\varphi)) + \frac{\varepsilon\,J_0(\varphi)^2}{2}\,\sin(4\,q_0(\varphi)) - 2\,\varepsilon^2\,J_0(\varphi)\,J_1(\varphi)\,\sin(2\,q_0(\varphi)) \\ &\quad + \varepsilon^2\,J_0(\varphi)\,J_1(\varphi)\,\sin(4\,q_0(\varphi)) - 2\,\varepsilon^2\,J_0(\varphi)^2\,q_1(\varphi)\,\cos(2\,q_0(\varphi)) + 2\,\varepsilon^2\,J_0(\varphi)^2\,q_1(\varphi)\,\cos(4\,q_0(\varphi))\,. \end{aligned}$$

Now, in order to iteratively determine the functions $q_i(\varphi), J_i(\varphi)$, we compare the two sides of the equations of motion at equal orders. At order 0 we have

$$\omega_0\,\frac{dq_0(\varphi)}{d\varphi} = \omega_0\,, \qquad \omega_0\,\frac{dJ_0(\varphi)}{d\varphi} = 0 \quad \Longrightarrow \quad q_0(\varphi) = \varphi\,, \qquad J_0(\varphi) = J_0 \quad .$$

Fixing the initial data as $q_0(0) = 0$ and $J(0) = J_0$, we then arrive at $q_0(\varphi) = \varphi$ and $J_0(\varphi) = J_0$. At order 1, we now have

$$\begin{aligned} \omega_0 \frac{dq_1(\varphi)}{d\varphi} - a_1 &= \frac{3\,J_0}{4} - J_0 \cos(2\varphi) + \frac{J_0}{4}\cos(4\varphi) \\ \omega_0 \frac{dJ_1(\varphi)}{d\varphi} &= -J_0^2 \sin(2\varphi) + \frac{J_0^2}{2}\sin(4\,\varphi)\,. \end{aligned} \tag{7.28}$$

As well known, a_1 is determined by the requirement that no secular terms be present in the series. This yields $a_1 = -3\,J_0/4$. Then, the Cauchy problem with the previous differential equations and the initial constants $q_1(0) = J_1(0) = 0$ yields the solution

$$q_1(\varphi) = -\frac{J_0}{2\,\omega_0}\,\sin(2\varphi) + \frac{J_0}{16\,\omega_0}\,\sin(4\varphi)\;, \qquad J_1(\varphi) = -\frac{3\,J_0^2}{8\,\omega_0} + \frac{J_0^2}{2\,\omega_0}\,\cos(2\varphi) - \frac{J_0^2}{8\,\omega_0}\,\cos(4\varphi)\,.$$

The process can be repeated at subsequent orders. We leave to the reader to verify the result at second order, leading eventually to

$$\begin{aligned} q(t) = \varphi &- \frac{\varepsilon\,J_0}{2\,\omega_0}\,\sin(2\varphi) + \frac{31\,\varepsilon^2\,J_0^2}{32\,\omega_0^2}\,\sin(2\,\varphi) + \frac{\varepsilon\,J_0}{16\,\omega_0}\,\sin(4\varphi) \\ &- \frac{\varepsilon^2\,J_0^2}{32\,\omega_0^2}\,\sin(4\,\varphi) - \frac{\varepsilon^2\,J_0^2}{32\,\omega_0^2}\,\sin(6\,\varphi) + \frac{\varepsilon^2\,J_0^2}{512\,\omega_0^2}\,\sin(8\,\varphi)\,, \\ J(t) = J_0 &- \frac{3\,\varepsilon\,J_0^2}{8\,\omega_0} + \frac{13\,\varepsilon^2\,J_0^3}{16\,\omega_0^2} + \frac{\varepsilon\,J_0^2}{2\,\omega_0}\,\cos(2\,\varphi) - \frac{33\,\varepsilon^2\,J_0^3}{32\,\omega_0^2}\,\cos(2\,\varphi) \\ &- \frac{\varepsilon\,J_0^2}{8\omega_0}\,\cos(4\,\varphi) + \frac{3\,\varepsilon^2\,J_0^3}{16\,\omega_0^2}\,\cos(4\,\varphi) + \frac{\varepsilon^2\,J_0^3}{32\,\omega_0^2}\,\cos(6\,\varphi)\,, \end{aligned} \tag{7.29}$$

with $\varphi = \omega\,t$ and $\omega = \omega_0 + \dfrac{3\,\varepsilon\,J_0}{4} - \dfrac{69\,\varepsilon^2\,J_0^2}{64\,\omega_0}$. Comparing the result with Eqs (7.21) and (7.23), we can see that the solutions $q(t)$, $J(t)$ of the two methods are equal. This is easy to justify by checking the structure of the l.h.s of Eq (7.27). After the expansion of the frequency, the differential equations to solve at subsequent steps all involve the operators $\omega_0 d/d\varphi$. Hence, all divisors appearing in the series terms are in terms of the unperturbed frequency ω_0.

7.3.3 Lindstedt series analogous to Kolmogorov

It was already pointed out that the Lindstedt series examined so far, as well as their 'indirect' (normal form) counterpart, produce, in general, series which are divergent and only have an asymptotic character. [1] On the other hand, Eliasson [21] and Gallavotti [28] established the existence of *convergent* Lindstedt series in nonlinear Hamiltonian systems satisfying the necessary conditions for the holding of the Kolmogorov-Arnold-Moser theorem. Gallavotti ([27]) presented a diagrammatic proof of the convergence of the Kolmogorov normal form also in the 'twistless' case, i.e., when the size of the Hessian matrix of the unperturbed Hamiltonian $\mathcal{H}_0(\mathbf{J})$ is not limited from below (it is equal to zero in the 'isochronous' case). A constructive Kolmogorov algorithm able to deal also with the twistless case is presented in [98]). The convergence of the Lindstedt series in this case is addressed, instead, in [16] (see remarks in the introduction).

As discussed in the introduction, when series constructions analogous to Kolmogorov are sought for in the isochronous case, an important point to address is the need for performing, at the final stage of the construction, a process involving *series reversal*. This reversal is necessary in order to explicitely compute the solutions $q(t)$, $J(t)$ whose initial conditions q_0, J_0 correspond to motion on

[1] The examples treated in this section are obvious exceptions, since, we deal, for simplicity, with 1DOF systems exhibiting no small divisors. Small divisors appear, instead, for $N > 1$.

a torus with given frequency vector ω. The key remark is that the value of J_0, which parametrises the solutions, cannot be fixed in advance due to the lack of a twist condition allowing to compute the mapping $\omega(J_0)$. We now discuss the application of the direct (Lindstedt) method analogous to Kolmogorov in the same example as in the previous two sections, aiming to illustrate the above points.

Fixing the frequency of the torus in the isochronous case can be implemented as described in [29]: assume that we target a particular solution of the equations of motion (7.24a) and (7.24b) represented as a trigonometric series and evolving according to a *given* pre-selected frequency ω. Inverting the expansion (7.25) we obtain

$$\omega_0 = \omega + \varepsilon\, a_1(J_0) + \varepsilon^2\, a_2(J_0) + \dots \tag{7.30}$$

Also, as before we expand the solution as

$$\begin{aligned} q(t) &= q_0(t) + \varepsilon\, q_1(t) + \varepsilon^2\, q_2(t) + \dots \\ J(t) &= J_0(t) + \varepsilon\, J_1(t) + \varepsilon^2\, J_2(t) + \dots\,. \end{aligned} \tag{7.31}$$

Note, however, that this time we perform no time-reparametrization, i.e., the solutions remain expressed as functions of the time t. Thus, replacing the above expressions in (7.24a) and (7.24b) the equations of motion lead now to the expressions (up to order 2 in ε)

$$\begin{aligned} \dot{q_0}(t) + \varepsilon\,\dot{q_1}(t) + \varepsilon^2\,\dot{q_2}(t) = \omega + \varepsilon\, a_1 &+ \frac{3\,\varepsilon\, J_0(t)}{4} - \varepsilon\, J_0(t)\,\cos(2\,q_0(t)) + \frac{\varepsilon\, J_0(t)}{4}\,\cos(4q_0(t)) \\ &+ \frac{3\,\varepsilon^2\, J_1(t)}{4} + \varepsilon^2\, a_2 - \varepsilon^2\, J_1(t)\,\cos(2\,q_0(t)) + \frac{\varepsilon^2\, J_1(t)}{4}\,\cos(4\,q_0(t)) \\ &+ 2\,\varepsilon^2\, J_0(t)\, q_1(t)\,\sin(2\,q_0(t)) - \varepsilon^2\, J_0(t)\, q_1(t)\,\sin(4\,q_0(t))\,, \end{aligned} \tag{7.32a}$$

$$\begin{aligned} \dot{J}_0(t) + \varepsilon\,\dot{J}_1(t) + \varepsilon^2\,\dot{J}_2(t) = &-\varepsilon\, J_0(t)^2\,\sin(2\,q_0(t)) + \frac{\varepsilon\, J_0(t)^2}{2}\,\sin(4q_0(t)) \\ &- 2\,\varepsilon^2\, J_0(t)\, J_1(t)\,\sin(2\,q_0(t)) + \varepsilon^2\, J_0(t)\, J_1(t)\,\sin(4q_0(t)) \\ &- 2\,\varepsilon^2\, J_0(t)^2\, q_1(t)\,\cos(2q_0(t)) + 2\,\varepsilon^2\, J_0(t)^2\, q_1(t)\,\cos(4\,q_0(t))\,. \end{aligned} \tag{7.32b}$$

Collecting now the terms of equal order we can compute iteratively all the functions $q_i(t), J_i(t)$, for $i = 0, 1, 2$, setting, at order zero:

$$q_0(t) = \omega\, t\,, \qquad J_0(t) = J_0$$

which corresponds to the choice of the initial condition $q_0(0) = 0$ and $J_0(0) = J_0$. Then, at first order we have

$$\begin{aligned} \dot{q_1}(t) &= a_1 + \frac{3\, J_0}{4} - J_0\,\cos(2\,\omega\, t) + \frac{J_0}{4}\cos(4\,\omega\, t)\,, \\ \dot{J}_1(t) &= -J_0^2\sin(2\,\omega\, t) + \frac{J_0^2}{2}\sin(4\,\omega\, t) \end{aligned} \tag{7.33}$$

implying $a_1 = -3\, J_0/4$ and

$$q_1(t) = -\frac{J_0}{2\,\omega}\,\sin(2\,\omega\, t) + \frac{J_0}{16\,\omega}\,\sin(4\,\omega\, t)\,, \qquad J_1(t) = -\frac{3\, J_0^2}{8\,\omega} + \frac{J_0^2}{2\,\omega}\,\cos(2\,\omega\, t) - \frac{J_0^2}{8\,\omega}\,\cos(4\,\omega\, t).$$

Note that the integration constants in (7.33) were set as $q_1(0) = J_1(0) = 0$, consistent with our

choice of initial condition. Repeating the procedure at second order yields

$$
\begin{aligned}
q(t) &= \omega\, t - \frac{\varepsilon\, J_0}{2\,\omega}\, \sin(2\,\omega\, t) + \frac{\varepsilon\, J_0}{16\,\omega}\, \sin(4\,\omega\, t) + \frac{19\,\varepsilon^2 J_0^2}{32\,\omega^2}\, \sin(2\,\omega\, t) + \frac{\varepsilon^2\, J_0^2}{64\,\omega^2}\, \sin(4\,\omega\, t) \\
&\quad - \frac{\varepsilon^2\, J_0^2}{32\,\omega^2}\, \sin(6\,\omega\, t) + \frac{\varepsilon^2\, J_0^2}{512\,\omega^2}\, \sin(8\,\omega\, t)\,, \\
J(t) &= J_0 - \frac{3\,\varepsilon\, J_0^2}{8\,\omega} + \frac{\varepsilon\, J_0^2}{2\,\omega}\, \cos(2\,\omega\, t) - \frac{\varepsilon\, J_0^2}{8\,\omega}\, \cos(4\,\omega\, t) + \frac{17\,\varepsilon^2\, J_0^3}{32\,\omega^2} \\
&\quad - \frac{21\,\varepsilon^2\, J_0^3}{32\,\omega^2}\, \cos(2\,\omega\, t) + \frac{3\,\varepsilon^2\, J_0^3}{32\,\omega^2}\, \cos(4\,\omega\, t) + \frac{\varepsilon^2\, J_0^3}{32\,\omega^2}\, \cos(6\,\omega\, t)\,, \\
\omega &= \omega_0 + \frac{3\,\varepsilon\, J_0}{4} - \frac{69\,\varepsilon^2\, J_0^2}{64\,\omega}\,.
\end{aligned}
\tag{7.34}
$$

It is instructive to compare the solutions (7.34) above with those (Eq (7.29)) found in the case of the original Lindstedt method. We have the following remarks:

(i) From second order and beyond the coefficients in front of the harmonics $\cos(m\omega t), \sin(m\omega t)$ for the same m are not all equal in the two solutions.

(ii) Most importantly, the structure of the divisors in the two solutions is different. In the torus fixing case (Eq (7.34)), all divisors involve the *corrected frequency*, ω, instead of the original frequency ω_0 of the linear oscillator. This is not a problem for the method to proceed, since this frequency is known in advance. In $N-$DOF systems, in general, with the 'torus fixing method' we obtain divisors of the form $\boldsymbol{m}\cdot\boldsymbol{\omega}$. Thus, the method can proceed even when the original frequencies of the N linear oscillators $\boldsymbol{\omega}_0$ are resonant, as long as we impose a non-resonant detuning in the adopted values for the final frequencies $\boldsymbol{\omega}$ on the torus.

(iii) On the other hand, the value of the initial condition J_0 leading to motion on the torus with frequency ω remains uknown up to the end of the construction. From the point of view of the symbolic implementation of the method in the computer, J_0 is a symbol whole powers have to be carried on along with the remaining powers of trigonometric monomials in all series terms and at all iterative steps.

(iv) At the end of the process, however, J_0 can be estimated by reversing the series (7.30), given that the functions $a_n(J_0)$ are monomials of degree n in J_0. In an analogous way, in the $N-$DOF case we will end up with N series equations of the form

$$
\omega_{0,j} - \omega_j = \sum_{n=1}^{\infty} \varepsilon^n a_{n,j}(J_{0,1}, \ldots, J_{0,N}) \tag{7.35}
$$

where the functions $a_{n,j}(J_{0,1}, \ldots, J_{0,N})$ have all been specified iteratively up to a maximum truncation order in n, and they are polynomial in $\boldsymbol{J}_0 \equiv (J_{0,1}, \ldots, J_{0,N})$. Thus, the series (7.35) can be formally inverted, yielding

$$
J_{0,j} = \frac{1}{\varepsilon} \sum_{n=1}^{\infty} P_{n,j}(\boldsymbol{\omega} - \boldsymbol{\omega}_0) \tag{7.36}
$$

where the functions $P_{n,j}(\boldsymbol{\omega} - \boldsymbol{\omega}_0)$ are polynomial of degree n in the differences $(\boldsymbol{\omega} - \boldsymbol{\omega}_0)$. Note that for the inverse series to converge we must require the difference $|(\boldsymbol{\omega} - \boldsymbol{\omega}_0)|$ to be smaller than ε, a fact which limits how far we can detune $\boldsymbol{\omega}$ from $\boldsymbol{\omega}_0$ in order to be able to specify the corresponding initial condition $\boldsymbol{J}_0$. An obvious choice is $|(\boldsymbol{\omega} - \boldsymbol{\omega}_0)| = \mathcal{O}(\varepsilon^2)$. At any rate, we emphasize that the convergence of the inverse series (7.35) is an open problem, crucial to the applications.

7.3.4 Kolmogorov normal form

We finally arrive at the here proposed Kolmogorov normal form algorithm yielding solutions equivalent to those discussed in the previous subsection. This is implemented by the following steps:

Step 1: substitution of the frequency series into the Hamiltonian. In our example, we substitute ω_0 in the Hamiltonian (7.20) with the series (7.30). This yields (up to second order, apart from constants)

$$\begin{aligned}\mathcal{H}(q,p) = (\omega + \varepsilon a_1 + \varepsilon^2 a_2 + \ldots)\, p + \frac{3\,\varepsilon\, J_0^2}{8} + \frac{3\, J_0\, \varepsilon}{4} p + \frac{3\,\varepsilon}{8} p^2 - \frac{\varepsilon\, J_0^2}{2}\cos(2q) - \varepsilon J_0 p \cos(2q) \\ - \frac{\varepsilon}{2} p^2 \cos(2q) + \frac{\varepsilon J_0^2}{8}\cos(4q) + \frac{\varepsilon\, J_0}{4} p \cos(4q) + \frac{\varepsilon}{8} p^2 \cos(4q) + \ldots\,.\end{aligned} \tag{7.37}$$

Step 2: normalization. To set the Hamiltonian into Kolmogorov normal form up to second order, we fix the value of the constants a_1, a_2 and we perform a sequence of Lie transformations aiming to give the Hamiltonian the form (in the transformed variables) $\mathcal{H}^{(2)}(q,p) = Z^{(2)}(q,p) + R^{(2)}(q,p)$ where the remainder $R^{(2)}$ is $\mathcal{O}(\varepsilon^3)$, while $Z^{(2)}(q,p)$ has the form $Z^{(2)}(q,p) = \omega\, p + \varepsilon\, R_1(q,p) + \varepsilon^2\, R_2(q,p)$ with both $R_i(q,p) = \mathcal{O}(||\, p\,||^2)$ $i = 1, 2$. To this end:
- First order: we fix a_1 so that the linear term $\varepsilon a_1 p$ acts as counterterm for the term $\varepsilon(3J_0/4)p$. This provides, in the twistless case, a process by which the frequency ω can be kept fixed (in the usual twist case, instead, this would have been accomplished by exploiting the Hessian matrix of $\mathcal{H}_0$). Formally, we require that

$$\left\langle h_{1,1}^{(0)} \right\rangle_q = \left\langle a_1\, p - J_0\, p\, \cos(2q) + \frac{J_0}{4}\, p \cos(4q) + \frac{3\, J_0\, p}{4} \right\rangle_q = 0 \quad , \tag{7.38}$$

leading to $a_1 = -\frac{3\, J_0}{4}$. Now, we insert this expression for a_1 in the Hamiltonian (7.37), leading to

$$\begin{aligned}\mathcal{H}(q,p) = \omega\, p + \frac{3\,\varepsilon\, J_0^2}{8} + \frac{3\,\varepsilon}{8} p^2 - \frac{\varepsilon\, J_0^2}{2}\cos(2q) - \varepsilon J_0 p \cos(2q) - \frac{\varepsilon}{2} p^2 \cos(2q) \\ + \frac{\varepsilon J_0^2}{8}\cos(4q) + \frac{\varepsilon\, J_0}{4} p \cos(4q) + \frac{\varepsilon}{8} p^2 \cos(4q) + \varepsilon^2\, a_2\, p\,.\end{aligned} \tag{7.39}$$

We can now eliminate the $O(\varepsilon)$ trigonometric terms in the Hamiltonian with the usual procedure. Namely, we define a generating function $X^{(1)}(q)$ used to eliminate terms not depending on the action p. These are

$$h_{1,0}^{(0)} = \frac{3\, J_0^2}{8} - \frac{J_0^2}{2}\cos(2q) + \frac{J_0^2}{8}\cos(4q)\,,$$

leading to $L_{X^{(1)}(q)}\,(\omega\, p) + h_{1,0}^{(0)} = \left\langle h_{1,0}^{(0)} \right\rangle_q$, that is

$$X^{(1)}(q) = \frac{J_0^2}{32\,\omega}\,\sin(4q) - \frac{J_0^2}{4\,\omega}\,\sin(2q)\,.$$

Note that, similarly as in the Birkhoff case (Subsection 2.1), here too we have to fix the initial conditions so that the relation $q(0) = p(0) = 0$ is preserved between variables before and after the canonical transformation. This is achieved by setting the generating function as $\chi_1^{(1)}(q) = X^{(1)}(q) + K^{(1)} q$, where $K^{(1)} = 3\, J_0^2/(8\,\omega)$ is a constant. The general rules for the determination of the constants $K^{(j)}$ will be discussed in Section 7.4.

Using the generating function $\chi_1^{(1)}(q)$ we obtain the intermediate Hamiltonian

$$\widehat{\mathcal{H}}^{(1)} = \exp\left(L_{\varepsilon\,\chi_1^{(1)}(q)}\right)\mathcal{H}\,,$$

given by

$$\begin{aligned}\widehat{\mathcal{H}}^{(1)} = \omega\, p + \frac{3\,\varepsilon}{8}\, p^2 - \varepsilon\, J_0\, p \cos(2q) - \frac{\varepsilon}{2}\, p^2 \cos(2q) + \frac{\varepsilon\, J_0}{4}\, p \cos(4q) + \frac{\varepsilon}{8}\, p^2 \cos(4q) \\ - \frac{17\,\varepsilon^2\, J_0^3}{64\,\omega} + \varepsilon^2\, a_2\, p - \frac{35\,\varepsilon^2\, J_0^2}{64\omega}\, p + \frac{\varepsilon^2\, J_0^3}{2\,\omega}\,\cos(2q) + \frac{7\,\varepsilon^2\, J_0^2\, p}{8\,\omega}\,\cos(2q) - \frac{11\,\varepsilon^2\, J_0^3}{32\,\omega}\,\cos(4q) \\ - \frac{7\,\varepsilon^2\, J_0^2\, p}{16\,\omega}\,\cos(4q) + \frac{\varepsilon^2\, J_0^3}{8\,\omega}\,\cos(6q) + \frac{\varepsilon^2\, J_0^2\, p}{8\,\omega}\,\cos(6q) - \frac{\varepsilon^2\, J_0^3}{64\,\omega}\,\cos(8q) - \frac{\varepsilon^2\, J_0^2\, p}{64\,\omega}\,\cos(8q)\,.\end{aligned} \tag{7.40}$$

We will now eliminate the trigonometric terms linear in the momentum in $\widehat{\mathcal{H}}^{(1)}$. These are

$$\widehat{h}^{(1)}_{1,1} = -J_0\, p \cos(2q) + \frac{1}{4}\, J_0\, p \cos(4q)$$

and can be eliminated by a generating function of the form $\chi_2^{(1)}(q,p) = \tilde{\chi}_2^{(1)}(q,p) + S^{(1)}\, p$ satisfying the homological equation $L_{\chi_2^{(1)}(q,p)}\,(\omega\, p) + \widehat{h}^{(1)}_{1,1} = 0$. As before, the value of the constant $S^{(1)}$ is fixed by the requirement that the initial phase of the solution of q be preserved to zero by the transformation. We find $S^{(1)} = 0$ (all constants $S^{(i)} = 0$ when the Hamiltonian has an even symmetry). Then

$$\tilde{\chi}_2^{(1)}(q,p) = -\frac{J_0\, p}{2\,\omega}\, \sin(2q) + \frac{J_0\, p}{16\,\omega}\, \sin(4q)\,.$$

The new Hamiltonian is

$$\mathcal{H}^{(1)} = \exp\left(L_{\varepsilon\, \chi_2^{(1)}(q,p)}\right) \widehat{\mathcal{H}}^{(1)}$$

and it is in Kolmogorov normal form up to order ε.

Repeating the same procedure at second order we arrive at the formulas

$$\begin{aligned}
a_2 &= \frac{69\, J_0^2}{64\,\omega}\,, \\
\chi_1^{(2)} &= -\frac{17\, J_0^3\, q}{64\,\omega^2} + \frac{J_0^3}{4\,\omega^2}\, \sin(2q) - \frac{11\, J_0^3}{128\,\omega^2}\, \sin(4q) + \frac{J_0^3}{48\,\omega^2}\, \sin(6q) - \frac{J_0^3}{512\,\omega^2}\, \sin(8q)\,, \\
\chi_2^{(2)} &= \frac{37\, J_0^2\, p}{64\,\omega^2}\, \sin(2q) - \frac{7\, J_0^2\, p}{64\,\omega^2}\, \sin(4q) + \frac{J_0^2\, p}{64\,\omega^2}\, \sin(6q) - \frac{J_0^2\, p}{512\,\omega^2}\, \sin(8q)\,,
\end{aligned} \tag{7.41}$$

leading to the Hamiltonian $\mathcal{H}^{(2)}(\tilde{q},\tilde{p}) = Z^{(2)}(\tilde{q},\tilde{p}) + R^{(2)}(\tilde{q},\tilde{p})$ with the Kolmogorov normal form part

$$\begin{aligned}
Z^{(2)}(\tilde{q},\tilde{p}) = \omega\,\tilde{p} + \frac{3\,\varepsilon\,\tilde{p}^2}{8} - \frac{\varepsilon\,\tilde{p}^2}{2}\, \cos(2\tilde{q}) + \frac{\varepsilon\,\tilde{p}^2}{8}\, \cos(4\tilde{q}) - \frac{51\,\varepsilon^2\, J_0\,\tilde{p}^2}{64\,\omega} + \frac{37\,\varepsilon^2\, J_0\,\tilde{p}^2}{32\,\omega}\, \cos(2\tilde{q}) \\
- \frac{7\,\varepsilon^2\, J_0\,\tilde{p}^2}{16\,\omega}\, \cos(4\tilde{q}) + \frac{3\,\varepsilon^2\, J_0\,\tilde{p}^2}{32\,\omega}\, \cos(6\tilde{q}) - \frac{\varepsilon^2\, J_0\,\tilde{p}^2}{64\,\omega}\, \cos(8\tilde{q})
\end{aligned}$$

($(\tilde{q},\tilde{p})$ denote again the new variables after new normalization steps).
Step 3: calculation of the solution on the torus. Using the compact notation

$$Z^{(2)}(\tilde{q},\tilde{p}) = \omega\,\tilde{p} + \varepsilon\, R_1(\tilde{q},\tilde{p}) + \varepsilon^2\, R_2(\tilde{q},\tilde{p})\,,$$

where $R_j(\tilde{q},\tilde{p}) = \mathcal{O}(||\,\tilde{p}\,||^2)$ $j = 1,\, 2$, the equations of motions under the Hamiltonian $Z^{(2)}$ are

$$\begin{cases}
\dot{\tilde{q}} = \dfrac{\partial Z^{(2)}}{\partial \tilde{p}} = \omega + \varepsilon\, \dfrac{\partial R_1(\tilde{q},\tilde{p})}{\partial \tilde{p}} + \varepsilon^2\, \dfrac{\partial R_2(\tilde{q},\tilde{p})}{\partial \tilde{p}} = \omega + \mathcal{O}(||\,\tilde{p}\,||) \\
\dot{\tilde{p}} = -\dfrac{\partial Z^{(2)}}{\partial \tilde{q}} = -\varepsilon\, \dfrac{\partial R_1(\tilde{q},\tilde{p})}{\partial \tilde{q}} - \varepsilon^2\, \dfrac{\partial R_2(\tilde{q},\tilde{p})}{\partial \tilde{q}} = \mathcal{O}(||\,\tilde{p}\,||^2)
\end{cases}.$$

The torus $\tilde{p}(t) = 0$, $\tilde{q}(t) = \omega\, t$ (where we chose $\tilde{q}(0) = 0$) is a solution of this system. This can be back-transformed in the original variables using

$$q = \exp L_{\varepsilon^2\, \chi_2^{(2)}} \exp L_{\varepsilon\, \chi_2^{(1)}}\, \tilde{q}\,, \qquad\qquad p = \exp L_{\varepsilon^2\, \chi_2^{(2)}} \exp L_{\varepsilon^2\, \chi_1^{(2)}} \exp L_{\varepsilon\, \chi_2^{(1)}} \exp L_{\varepsilon\, \chi_1^{(1)}}\, \tilde{p}\,. \tag{7.42}$$

Substituting the solution ($\tilde{q}(t) = \omega\, t$, $\tilde{p}(t) = 0$) in the previous expressions, we readily deduce the

solution in the original variables:

$$
\begin{aligned}
q(t) &= \omega\, t - \frac{\varepsilon\, J_0}{2\,\omega}\, \sin(2\,\omega\, t) + \frac{\varepsilon\, J_0}{16\,\omega}\, \sin(4\,\omega\, t) + \frac{19\,\varepsilon^2 J_0^2}{32\,\omega^2}\, \sin(2\,\omega\, t) + \frac{\varepsilon^2\, J_0^2}{64\,\omega^2}\, \sin(4\,\omega\, t) \\
&\quad - \frac{\varepsilon^2\, J_0^2}{32\,\omega^2}\, \sin(6\,\omega\, t) + \frac{\varepsilon^2\, J_0^2}{512\,\omega^2}\, \sin(8\,\omega\, t)\,, \\
p(t) &= -\frac{3\,\varepsilon\, J_0^2}{8\,\omega} + \frac{\varepsilon\, J_0^2}{2\,\omega}\, \cos(2\,\omega\, t) - \frac{\varepsilon\, J_0^2}{8\,\omega}\, \cos(4\,\omega\, t) + \frac{17\,\varepsilon^2\, J_0^3}{32\,\omega^2} \\
&\quad - \frac{21\,\varepsilon^2\, J_0^3}{32\,\omega^2}\, \cos(2\,\omega\, t) + \frac{3\,\varepsilon^2\, J_0^3}{32\,\omega^2}\, \cos(4\,\omega\, t) + \frac{\varepsilon^2\, J_0^3}{32\,\omega^2}\, \cos(6\,\omega\, t)\,, \\
J(t) &= J_0 + p(t)\,.
\end{aligned}
\tag{7.43}
$$

Also, using the computed expressions of a_1 and a_2 (Eqs (7.38) and (7.41)), we obtain the relation between the torus frequency and the original frequency

$$
\omega = \omega_0 + \frac{3\,\varepsilon\, J_0}{4} - \frac{69\,\varepsilon^2\, J_0^2}{64\,\omega}\,.
$$

These expressions are identical to the ones found by the Lindstedt method of Subsection 2.3 (see (7.34)).

7.3.5 Comparisons and numerical tests

In order to better visualize the differences between the methods (i) and (ii) (i.e., respectively, 'analogous to Birkhoff' and 'analogous to Kolmogorov') we report, in the Tables 7.1 and 7.2 below, the series terms corresponding to the solutions for $q(t)$ and $J(t)$ as obtained by the two methods up to order ε^2.

Method:	$\mathcal{O}(1)$	$\mathcal{O}(\varepsilon)$	$\mathcal{O}(\varepsilon^2)$
(i) 'Analogous to Birkhoff'	$\omega\, t$	$-\frac{J_0}{2\,\omega_0}\, \sin(2\,\omega\, t) + \frac{J_0}{16\,\omega_0}\, \sin(4\,\omega\, t)$	$\frac{31\,J_0^2}{32\,\omega_0^2}\, \sin(2\,\omega\, t) - \frac{J_0^2}{32\,\omega_0^2}\, \sin(4\,\omega\, t)$ $-\frac{J_0^2}{32\,\omega_0^2}\, \sin(6\,\omega\, t) + \frac{J_0^2}{512\,\omega_0^2}\, \sin(8\,\omega\, t)$
(ii) 'Analogous to Kolmogorov'	$\omega\, t$	$-\frac{J_0}{2\,\omega}\, \sin(2\,\omega\, t) + \frac{J_0}{16\,\omega}\, \sin(4\,\omega\, t)$	$\frac{19\,J_0^2}{32\,\omega^2}\, \sin(2\,\omega\, t) + \frac{J_0^2}{64\,\omega^2}\, \sin(4\,\omega\, t)$ $-\frac{J_0^2}{32\,\omega^2}\, \sin(6\,\omega\, t) + \frac{J_0^2}{512\,\omega^2}\, \sin(8\,\omega\, t)$

Table 7.1: Comparison between the series terms for the solution $q(t)$ in the Lindstedt series obtained by the methods (i) and (ii) up to order ε^2.

Method:	$\mathcal{O}(1)$	$\mathcal{O}(\varepsilon)$	$\mathcal{O}(\varepsilon^2)$
(i) 'Analogous to Birkhoff'	J_0	$-\frac{3\,J_0^2}{8\,\omega_0}+\frac{J_0^2}{2\,\omega_0}\cos(2\,\omega\,t)-\frac{J_0^2}{8\omega_0}\cos(4\,\omega\,t)$	$\frac{13\,J_0^3}{16\,\omega_0^2}-\frac{33\,J_0^3}{32\,\omega_0^2}\cos(2\,\omega\,t)$ $+\frac{3\,J_0^3}{16\,\omega_0^2}\cos(4\,\omega\,t)+\frac{J_0^3}{32\,\omega_0^2}\cos(6\,\omega\,t)$
(ii)'Analogous to Kolmogorov'	J_0	$-\frac{3\,J_0^2}{8\,\omega}+\frac{J_0^2}{2\,\omega}\cos(2\,\omega\,t)-\frac{J_0^2}{8\,\omega}\cos(4\,\omega\,t)$	$\frac{17\,J_0^3}{32\,\omega^2}-\frac{21\,J_0^3}{32\,\omega^2}\cos(2\,\omega\,t)$ $+\frac{3\,J_0^3}{32\,\omega^2}\cos(4\,\omega\,t)+\frac{J_0^3}{32\,\omega^2}\cos(6\,\omega\,t)$

Table 7.2: Comparison between the series terms for the solution $J(t)$ in the Lindstedt series obtained by the methods (i) and (ii) up to order ε^2.

From Table 7.1 above, we observe that the solutions $q(t)$ and $J(t)$ obtained by methods (i) and (ii) have the same form up to order $\mathcal{O}(\varepsilon)$, except for the fact that in method (i) all divisors depend on the frequency ω_0 rather than ω. On the other hand, the coefficients found by the two methods start differing from the order ε^2 and beyond. Moreover, the series for the frequency ω obtained by the two methods are:

$$\omega=\omega_0+\frac{3\,\varepsilon\,J_0}{4}-\frac{69\,\varepsilon^2\,J_0^2}{64\,\omega_0}\,,\qquad\qquad \omega=\omega_0+\frac{3\,\varepsilon\,J_0}{4}-\frac{69\,\varepsilon^2\,J_0^2}{64\,\omega}\,,$$

which differ again as regards their divisors.

The effect of these differences on the precision of the two methods can be seen even in the simplest case of a system with one degree of freedom in which both series are convergent (the series 'analogous to Birkhoff' are, instead, divergent when $N\geq 2$). To this end, we report below a comparison between the numerical solutions and the analytical ones, obtained by the methods (i) and (ii) in the example of the Hamiltonian (7.18). To produce the Lindstedt series (ii) in this example we work as follows: fixing the initial and final frequency ω_0 and ω, we reverse the series (7.25) according to

$$d\omega=-\sum_{i\geq 0}\varepsilon^i\,a_i(J_0):=f(J_0)\quad\Longrightarrow\quad J_0=f^{-1}(d\omega)\,,\tag{7.44}$$

where $d\omega=\omega-\omega_0$ and f^{-1} denotes the series inverse to f. Then, having specified J_0 through the inverse series (7.44), we compute all numerical coefficients in the Lindstedt series (i) and (ii) up to order ε^4. We analyze three different cases:

1) $\varepsilon=1$, $\omega_0=1$ and $\omega=1.002$;

2) $\varepsilon=1$, $\omega_0=1$ and $\omega=1.02$;

3) $\varepsilon=1$, $\omega_0=1$ and $\omega=1.2$.

Note that all results are rescalable to different choices of ε. Reversing the series (7.25) as prescribed by (7.44), we obtain, respectively, the following values for the amplitude (initial action datum): $J_0=0.0026769\,,0.0277048\,,0.383509$. Substituting these values of ε, ω, ω_0 and J_0 in the solutions $q(t)$ and $J(t)$ we obtain the solutions, as functions of t, produced by methods (i) and (ii). At the same time, it is possible to integrate the equations of motion (7.24a) and (7.24b) to produce a numerical solution, starting from the initial conditions $q(0)=0$, $J(0)=J_0$.

Figure 7.1 shows the difference (in Log_{10} scale) between the semi-analytical solutions obtained by methods (i) and (ii) as above and the numerical solution for the angle $q(t)$. Since the only systematically growing error is due to differences in the frequency estimates, all errors between the numerical and analytical solutions in the angle $q(t)$ grow linearly in time. We observe, however, that the Lindstedt method 'analogous to Kolmogorov' always produces more precise results than the one 'analogous to Birkhoff' with a difference in precision of about one order of magnitude when $d\omega$ is of order 10^{-3} and raising up to two orders of magnitude when $d\omega$ becomes of the order of unity.

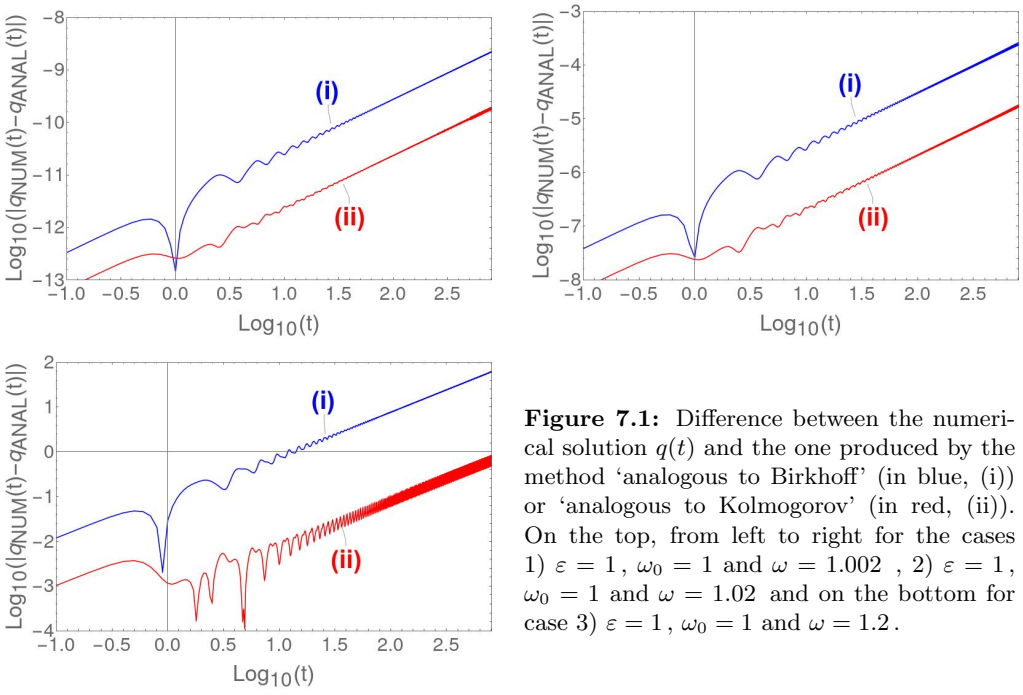

Figure 7.1: Difference between the numerical solution $q(t)$ and the one produced by the method 'analogous to Birkhoff' (in blue, (i)) or 'analogous to Kolmogorov' (in red, (ii)). On the top, from left to right for the cases 1) $\varepsilon = 1$, $\omega_0 = 1$ and $\omega = 1.002$, 2) $\varepsilon = 1$, $\omega_0 = 1$ and $\omega = 1.02$ and on the bottom for case 3) $\varepsilon = 1$, $\omega_0 = 1$ and $\omega = 1.2$.

7.3.6 Hamiltonian preparation in the case of odd nonlinear couplings

A particularity of the example treated above is the fact that the original Hamiltonian is analytic in the whole domain $J \in \mathbb{R}$. This changes, however, in more general models in which the Hamiltonian is of the form

$$\mathcal{H}(\boldsymbol{q}, \boldsymbol{J}) = \boldsymbol{\omega}_0 \cdot \boldsymbol{J} + \varepsilon h(\boldsymbol{q}, \boldsymbol{J}; \varepsilon)$$

where the development in powers of the variables $\boldsymbol{J}$ contains semi-integer powers, as is, for example, the case of polynomial nonlinear couplings containing odd terms in one or more of the oscillator variables x_j, y_j. Let us note that physical examples of such Hamiltonian systems, with oscillators non-linearly coupled through odd polynomial terms, are ubiquitous, and include the Fermi-Pasta-Ulam $\alpha-$model, the secular Hamiltonian in resonant cases of perturbed Keplerian $N-$body problems, magnetic bottle Hamiltonian models, etc. In the next section, we will present a formal algorithm applicable to a generic form for the function $\mathcal{H}_1$. The sequence of normalizations in this algorithm is arranged so that the result agrees with the corresponding one obtained with the Lindstedt series. A particular example showing this agreement is presented in Appendix F.1.

7.4 KAM algorithm for isochronous systems

We now give the Kolmogorov algorithm for generic isochronous systems with Hamiltonian

$$\mathcal{H}(\boldsymbol{q},\boldsymbol{J}) \,=\, \boldsymbol{\omega}_0\cdot\boldsymbol{J} + \sum_{i\geq 1}\sum_{s\geq 3}\varepsilon^i \tilde{h}_{i,\,s}(\boldsymbol{q},\boldsymbol{J}) \tag{7.45}$$

where $\boldsymbol{q}\in\mathbb{T}^n$, $\boldsymbol{J}\in\mathcal{B}\subseteq\mathbb{R}^n$, $\tilde{h}_{i,\,s}=\mathcal{O}(||\boldsymbol{J}||^{\frac{s}{2}})$. We assume that the Hamiltonian (7.45) has a half-integer power dependence on $\boldsymbol{J}$, i.e. admits the expansion, for $n\to\infty$, of the truncated series

$$\begin{aligned}\mathcal{H}(\boldsymbol{q},\boldsymbol{p};\boldsymbol{J}_0) \,&=\, \boldsymbol{\omega}_0\cdot\boldsymbol{J}_0 + \boldsymbol{\omega}_0\cdot\boldsymbol{p} + \sum_{i\geq 1}\sum_{s\geq 3}\varepsilon^i\tilde{h}_{i,\,s}(\boldsymbol{q},\boldsymbol{J}_0+\boldsymbol{p})\\ &=\, \boldsymbol{\omega}_0\cdot\boldsymbol{J}_0 + \boldsymbol{\omega}_0\cdot\boldsymbol{p} + \sum_{i\geq 1}\sum_{s\geq 3}\sum_{k=0}^{n}\varepsilon^i\frac{\tilde{h}^{(k)}_{i,\,s}(\boldsymbol{q},\boldsymbol{J}_0+\boldsymbol{p})|_{\boldsymbol{p}=\boldsymbol{0}}}{k!}\,\boldsymbol{p}^k\,,\end{aligned} \tag{7.46}$$

where $\tilde{h}^{(k)}$ are the $k-$th derivatives of $\tilde{h}$ with respect to $\boldsymbol{p}=\boldsymbol{J}-\boldsymbol{J}_0$.

Apart from constants, the Hamiltonian can be written in the compact notation

$$\mathcal{H}(\boldsymbol{q},\boldsymbol{p};\boldsymbol{J}_0) \,=\, \boldsymbol{\omega}_0\cdot\boldsymbol{p} + \sum_{i\geq 1}\varepsilon^i\, h_i(\boldsymbol{q},\boldsymbol{p};\boldsymbol{J}_0)\,. \tag{7.47}$$

The algorithm allows to compute quasi-periodic orbits with a frequency $\boldsymbol{\omega}$ fixed in advance, given by

$$\boldsymbol{\omega} = \boldsymbol{\omega}_0 - \sum_{i\geq 1}\varepsilon^i\,\boldsymbol{a}_i(\boldsymbol{J}_0)\,, \tag{7.48}$$

where the parameters $\boldsymbol{J}_0$, whose values are to be specified in the end of the process, give the initial conditions for $\boldsymbol{J}$ of a trajectory on the torus with frequencies $\boldsymbol{\omega}$. To this end, along with the normalizing canonical transformation, the algorith computes 'on the go' the functions $\boldsymbol{a}_i(\boldsymbol{J}_0)$ ('counter-terms').

Substituting the series (7.48) in the Hamiltonian (7.47) we arrive at:

$$\mathcal{H}(\boldsymbol{q},\boldsymbol{p};\boldsymbol{J}_0) \,=\, \boldsymbol{\omega}\cdot\boldsymbol{p} + \sum_{i\geq 1}\varepsilon^i\, h_i(\boldsymbol{q},\boldsymbol{p};\boldsymbol{J}_0) + \sum_{i\geq 1}\varepsilon^i\,\boldsymbol{a}_i(\boldsymbol{J}_0)\cdot\boldsymbol{p}\,. \tag{7.49}$$

In the following we use the notation

$$\varepsilon^i\, h^{(k)}_i(\boldsymbol{q},\boldsymbol{p};\boldsymbol{J}_0) = \varepsilon^i\left(h^{(k)}_{i,0}(\boldsymbol{q};\boldsymbol{J}_0) + h^{(k)}_{i,1}(\boldsymbol{q},\boldsymbol{p};\boldsymbol{J}_0) + \sum_{j\geq 2}h^{(k)}_{i,j}(\boldsymbol{q},\boldsymbol{p};\boldsymbol{J}_0)\right)\,, \tag{7.50}$$

where $h^{(k)}_{i,0}$ is independent from $\boldsymbol{p}$, $h^{(k)}_{i,1}$ linear in $\boldsymbol{p}$ and the remaining sum is $\mathcal{O}(||\,\boldsymbol{p}\,||^2)$. To facilitate reading, the indices (i,j,k) used in all subsequent expressions refer to

$$\begin{aligned} &i = \textit{degree of the corresponding } \varepsilon\,,\\ h^{(k)}_{i,j}\,:\;&j = \textit{degree of } \boldsymbol{p}\,,\\ &k = \textit{step of the algorithm}\,.\end{aligned} \tag{7.51}$$

We now have the following

Proposition 1. *Assume the vector $\boldsymbol{\omega}$ is non-resonant. There exist Lie generating functions $\chi_1^{(r)}$, $\chi_2^{(r)}$ such that, after r normalization steps, the Hamiltonian (7.49) is given by the formal series:*

$$\begin{aligned}\mathcal{H}^{(r)}(\boldsymbol{q}^{(r)},\boldsymbol{p}^{(r)};\boldsymbol{J}_0) &= \left(\exp(L_{\varepsilon^r\chi_2^{(r)}})\big(\exp(L_{\varepsilon^r\chi_1^{(r)}})\mathcal{H}^{(r-1)}\big)\right)\Big|_{\substack{\boldsymbol{q}^{(r-1)}=\boldsymbol{q}^{(r)}\\ \boldsymbol{p}^{(r-1)}=\boldsymbol{p}^{(r)}}}\\ &= \boldsymbol{\omega}\cdot\boldsymbol{p} + \varepsilon\, C_1 + \ldots + \varepsilon^{r-1}\, C_{r-1} + \varepsilon^r\, C_r\\ &\quad + \varepsilon\, h_1^{(r)}(\boldsymbol{q},\boldsymbol{p};\boldsymbol{J}_0) + \ldots + \varepsilon^r\, h_r^{(r)}(\boldsymbol{q},\boldsymbol{p};\boldsymbol{J}_0)\\ &\quad + \varepsilon^{r+1}\, h_{r+1}^{(r)}(\boldsymbol{q},\boldsymbol{p};\boldsymbol{J}_0) + \varepsilon^{r+1}\,\boldsymbol{a}_{r+1}(\boldsymbol{J}_0)\cdot\boldsymbol{p} + \ldots\,,\end{aligned}$$

where $h_j^{(r)} = \sum_{i\geq 0} h_{j,i}^{(r)}\ \forall\, j \geq r+1$ and $h_j^{(r)} = \sum_{i\geq 2} h_{j,i}^{(r)} \in \mathcal{O}(||\boldsymbol{p}||^2)\ \forall\, j = 1,\ldots,r$, with

$$h_{k,0}^{(r)} = C_k = \left\langle h_{k,0}^{(k-1)}\right\rangle - \boldsymbol{\omega}\cdot\boldsymbol{K}^{(k)} \qquad \forall\ 1\leq k\leq r\,,$$

$$h_{k,0}^{(r)} = h_{k,0}^{(r-1)} \qquad \forall\ r+1\leq k\leq 2r-1\,,$$

$$h_{2r,0}^{(r)} = \sum_{j=0}^{\lfloor\frac{2r-1}{r}\rfloor}\frac{1}{j!}L^j_{\chi_1^{(r)}(\boldsymbol{q})}\left(h_{2r-jr,j}^{(r-1)}\right)$$

$$\begin{aligned}h_{k,0}^{(r)} &= \sum_{j=0}^{\lfloor\frac{k-1}{r}\rfloor-2}\sum_{s=0}^{\lfloor\frac{k-jr-1}{r}\rfloor}\frac{1}{j!\,s!}L^j_{\chi_2^{(r)}(\boldsymbol{q},\boldsymbol{p})}L^s_{\chi_1^{(r)}(\boldsymbol{q})}\left(h_{k-jr-sr,s}^{(r-1)}\right)\\ &\quad + \frac{1}{\big(\lfloor\frac{k-1}{r}\rfloor-1\big)!}L^{\lfloor(k-1)/r\rfloor-1}_{\chi_2^{(r)}(\boldsymbol{q},\boldsymbol{p})}\left(h_{k-\left(\lfloor\frac{k-1}{r}\rfloor-1\right)r,0}^{(r-1)}\right) \qquad \forall\ k\geq 2r+1\,,k\neq mr\,,m\in\mathbb{N}\,,\end{aligned}$$

$$h_{k,0}^{(r)} = \sum_{j=0}^{\lfloor\frac{k-1}{r}\rfloor-1}\sum_{s=0}^{\lfloor\frac{k-jr-1}{r}\rfloor}\frac{1}{j!\,s!}L^j_{\chi_2^{(r)}(\boldsymbol{q},\boldsymbol{p})}L^s_{\chi_1^{(r)}(\boldsymbol{q})}\left(h_{k-jr-sr,s}^{(r-1)}\right) \qquad \forall\ k\geq 2r+1\,,k=mr\,,m\in\mathbb{N}\,,$$

$$h_{k,1}^{(r)} = 0 \qquad \forall\ 1\leq k\leq r\,,$$

$$h_{k,1}^{(r)} = \sum_{j=0}^{\lfloor\frac{k-1}{r}\rfloor-1}\sum_{s=0}^{\lfloor\frac{k-jr-1}{r}\rfloor}\frac{1}{j!\,s!}L^j_{\chi_2^{(r)}(\boldsymbol{q},\boldsymbol{p})}L^s_{\chi_1^{(r)}(\boldsymbol{q})}\left(h_{k-jr-sr,1+s}^{(r-1)}\right) \qquad \forall\ k\geq r+1\,,k\neq m\,r\,,\ m\in\mathbb{N}\,,$$

$$\begin{aligned}h_{k,1}^{(r)} &= \sum_{j=0}^{\lfloor\frac{k-2}{r}\rfloor}\sum_{s=0}^{\lfloor\frac{k-jr-1}{r}\rfloor}\frac{1}{j!\,s!}L^j_{\chi_2^{(r)}(\boldsymbol{q},\boldsymbol{p})}L^s_{\chi_1^{(r)}(\boldsymbol{q})}\left(h_{k-jr-sr,1+s}^{(r-1)}\right)\\ &\quad + \frac{m-1}{m!}L^{m-1}_{\chi_2^{(r)}(\boldsymbol{q},\boldsymbol{p})}\left(h_{r,1}^{(r-1)}\right) \qquad \forall\ k\geq r+1\,,k=m\,r\,,\ m\in\mathbb{N}\,,\end{aligned}$$

$$h_{k,i}^{(r)} = h_{k,i}^{(r-1)} \qquad \forall\ 1\leq k\leq r\,,\ i\geq 2\,,$$

$$h_{k,i}^{(r)} = \sum_{j=0}^{\lfloor\frac{k-1}{r}\rfloor}\sum_{s=0}^{\lfloor\frac{k-jr-1}{r}\rfloor}\frac{1}{j!\,s!}L^j_{\chi_2^{(r)}(\boldsymbol{q},\boldsymbol{p})}L^s_{\chi_1^{(r)}(\boldsymbol{q})}\left(h_{k-jr-sr,i+s}^{(r-1)}\right) \qquad \forall\ k\geq r+1\,,\ i\geq 2\,.$$

Given the Fourier series $h_{r,0}^{(r-1)}(\boldsymbol{q}) = \sum_{\boldsymbol{k}\in\mathbb{Z}^n} c_{\boldsymbol{k}}^{(r-1)} e^{i\boldsymbol{k}\cdot\boldsymbol{q}}$ and $h_{r,1}^{(r-1)}(\boldsymbol{q},\boldsymbol{p}) = \sum_{|\boldsymbol{j}|=1}\sum_{\boldsymbol{k}\in\mathbb{Z}^n} c_{\boldsymbol{j}\boldsymbol{k}}^{(r)}\boldsymbol{p}^{\boldsymbol{j}} e^{i\boldsymbol{k}\cdot\boldsymbol{q}}$, the

generating functions $\chi_1^{(r)}$, $\chi_2^{(r)}$ *are defined by*

$$\begin{aligned}
\chi_1^{(r)}(\boldsymbol{q}) &= X^{(r)}(\boldsymbol{q}) + \boldsymbol{K}^{(r)} \cdot \boldsymbol{q} = \sum_{\boldsymbol{k}\in\mathbb{Z}^n\setminus\{\boldsymbol{0}\}} \left(\frac{c_{\boldsymbol{k}}^{(r-1)}}{i\boldsymbol{k}\cdot\boldsymbol{\omega}}\, e^{i\boldsymbol{k}\cdot\boldsymbol{q}} - \frac{c_{\boldsymbol{k}}^{(r-1)}}{\boldsymbol{k}\cdot\boldsymbol{\omega}}\, \boldsymbol{k}\cdot\boldsymbol{q} \right) , \\
\chi_2^{(r)}(\boldsymbol{q},\boldsymbol{p}) &= \tilde{\chi}_2^{(r)}(\boldsymbol{q},\boldsymbol{p}) + \boldsymbol{S}^{(r)} \cdot \boldsymbol{p} \\
&= \boldsymbol{Y}^{(r)}(\boldsymbol{q}) \cdot \boldsymbol{p} + \boldsymbol{S}^{(r)} \cdot \boldsymbol{p} = \sum_{|\boldsymbol{j}|=1} \sum_{\boldsymbol{k}\in\mathbb{Z}^n\setminus\{\boldsymbol{0}\}} \left(\frac{c_{\boldsymbol{j}\boldsymbol{k}}^{(r)}}{i\boldsymbol{k}\cdot\boldsymbol{\omega}}\, e^{i\boldsymbol{k}\cdot\boldsymbol{q}} + \frac{i\, c_{\boldsymbol{j}\boldsymbol{k}}^{(r)}}{\boldsymbol{k}\cdot\boldsymbol{\omega}} \right) \boldsymbol{p}^{\boldsymbol{j}} .
\end{aligned} \tag{7.52}$$

The solution with initial data on the torus with frequency vector $\boldsymbol{\omega}$ is given by

$$\begin{aligned}
\boldsymbol{p} &= \left(\exp(L_{\varepsilon^r \chi_2^{(r)}}) \exp(L_{\varepsilon^r \chi_1^{(r)}}) \dots \exp(L_{\varepsilon \chi_2^{(1)}}) \exp(L_{\varepsilon \chi_1^{(1)}}) \boldsymbol{p}^{(r)} \right) \Big|_{\substack{\boldsymbol{p}^{(r)}=\boldsymbol{0} \\ \boldsymbol{q}^{(r)}=\boldsymbol{\omega} t}} , \\
\boldsymbol{q} &= \left(\exp(L_{\varepsilon^r \chi_2^{(r)}}) \dots \exp(L_{\varepsilon \chi_2^{(1)}}) \boldsymbol{q}^{(r)} \right) \Big|_{\substack{\boldsymbol{p}^{(r)}=\boldsymbol{0} \\ \boldsymbol{q}^{(r)}=\boldsymbol{\omega} t}} .
\end{aligned} \tag{7.53}$$

Proof of the proposition. The generic r-th iterative step of the algorithm is defined as follows: after $r-1$ steps, the hamiltonian (7.49) has the form:

$$\begin{aligned}
\mathcal{H}^{(r-1)}(\boldsymbol{q},\boldsymbol{p};\boldsymbol{J}_0) \;=& \boldsymbol{\omega}\cdot\boldsymbol{p} + \varepsilon\, C_1 + \ldots + \varepsilon^{r-1}\, C_{r-1} \\
&+ \varepsilon\, h_1^{(r-1)}(\boldsymbol{q},\boldsymbol{p};\boldsymbol{J}_0) + \ldots + \varepsilon^{r-1}\, h_{r-1}^{(r-1)}(\boldsymbol{q},\boldsymbol{p};\boldsymbol{J}_0) \\
&+ \varepsilon^r\, h_r^{(r-1)}(\boldsymbol{q},\boldsymbol{p};\boldsymbol{J}_0) + \varepsilon^r\, \boldsymbol{a}_r(\boldsymbol{J}_0)\cdot\boldsymbol{p} \\
&+ \varepsilon^{r+1}\, h_{r+1}^{(r-1)}(\boldsymbol{q},\boldsymbol{p};\boldsymbol{J}_0) + \varepsilon^{r+1}\, \boldsymbol{a}_{r+1}(\boldsymbol{J}_0)\cdot\boldsymbol{p} + \ldots ,
\end{aligned} \tag{7.54}$$

where $C_1 \ldots C_{r-1}$ are constants and $h_i^{(r-1)} \in \mathcal{O}(||\,\boldsymbol{p}\,||^2)\ \forall\, i = 1,\ldots,r-1$. Taking into account the notation (7.51), we re-define the quantity $h_i^{(k)}$ according to

$$h_{i,1}^{(k)} \leftarrow h_{i,1}^{(k)} + \boldsymbol{a}_i \cdot \boldsymbol{p} = \left(\nabla_{\boldsymbol{p}} h_{i,1}^{(k)} + \boldsymbol{a}_i \right) \cdot \boldsymbol{p} \quad \forall\, i \geq r\,. \tag{7.55}$$

The structure of the Hamiltonian $\mathcal{H}^{(r-1)}$ is visualized in Table 7.3.

								Order of the actions:
	$\vdots$	$\vdots$	$\vdots$	$\vdots$	$\vdots$	$\vdots$	$\vdots$	$\vdots$
$\mathcal{H}^{(r-1)} = \sum$	0	$\varepsilon\, h_{1,2}^{(r-1)}$	$\ldots$	$\varepsilon^{r-1}\, h_{r-1,2}^{(r-1)}$	$\varepsilon^r\, h_{r,2}^{(r-1)}$	$\varepsilon^{r+1}\, h_{r+1,2}^{(r-1)}$	$\ldots$	$\leftarrow\ \mathcal{O}(\|\|\boldsymbol{p}^2\|\|)$
	$\boldsymbol{\omega}\cdot\boldsymbol{p}$	0	$\ldots$	0	$\varepsilon^r\, h_{r,1}^{(r-1)}$	$\varepsilon^{r+1}\, h_{r+1,1}^{(r-1)}$	$\ldots$	$\leftarrow\ \mathcal{O}(\|\|\boldsymbol{p}\|\|)$
	0	$\varepsilon\, C_1$	$\ldots$	$\varepsilon^{r-1}\, C_{r-1}$	$\varepsilon^r\, h_{r,0}^{(r-1)}$	$\varepsilon^{r+1}\, h_{r+1,0}^{(r-1)}$	$\ldots$	$\leftarrow\ \mathcal{O}(\|\|\boldsymbol{p}\|\|^0)$
Order of ε:	$\uparrow$ $\mathcal{O}(\varepsilon^0)$	$\uparrow$ $\mathcal{O}(\varepsilon)$	$\ldots$	$\uparrow$ $\mathcal{O}(\varepsilon^{r-1})$	$\uparrow$ $\mathcal{O}(\varepsilon^r)$	$\uparrow$ $\mathcal{O}(\varepsilon^{r+1})$	$\ldots$	

Table 7.3: Hamiltonian $\mathcal{H}^{(r-1)}$ after $r-1$ normalization steps.

We then have:
First part of the proof: the r-th normalization step consists of two substeps, each involving a canonical transformation.

- *First half step:* we set

$$\widehat{\mathcal{H}}^{(r)} = \exp(L_{\varepsilon^r \chi_1^{(r)}(\boldsymbol{q})})\mathcal{H}^{(r-1)} = \sum_{j\geq 0} \frac{(\varepsilon^r)^j}{j!} L^j_{\chi_1^{(r)}(\boldsymbol{q})} \mathcal{H}^{(r-1)}\,, \tag{7.56}$$

where the generating function $\chi_1^{(r)}$ is defined as $\chi_1^{(r)}(\boldsymbol{q}) = X^{(r)}(\boldsymbol{q}) + \boldsymbol{K}^{(r)}\cdot\boldsymbol{q}$, with $\boldsymbol{K}^{(r)}$ an appropriate constant vector defined below, and $X^{(r)}$ is defined through the homological equation:

$$\left\{\boldsymbol{\omega}\cdot\boldsymbol{p}\,,\, X^{(r)}(\boldsymbol{q})\right\} + h^{(r-1)}_{r,0}(\boldsymbol{q}) = \left\langle h^{(r-1)}_{r,0}(\boldsymbol{q})\right\rangle\,, \tag{7.57}$$

where $\langle . \rangle$ denotes the mean over $\boldsymbol{q}$. The function $X^{(r)}(\boldsymbol{q})$ eliminates all terms of order $\mathcal{O}(\varepsilon^r)$ depending only on the angles $\boldsymbol{q}$ in the Hamiltonian $\mathcal{H}^{(r-1)}$. Writing $h^{(r-1)}_{r,0}(\boldsymbol{q})$ in the Fourier form $h^{(r-1)}_{r,0}(\boldsymbol{q}) = \sum_{\boldsymbol{k}\in\mathbb{Z}^n} c^{(r-1)}_{\boldsymbol{k}} e^{i\boldsymbol{k}\cdot\boldsymbol{q}}$ from (7.57) we find:

$$X^{(r)}(\boldsymbol{q}) = \sum_{\boldsymbol{k}\in\mathbb{Z}^n\setminus\{\boldsymbol{0}\}} \frac{c^{(r-1)}_{\boldsymbol{k}}}{i\boldsymbol{k}\cdot\boldsymbol{\omega}}\, e^{i\boldsymbol{k}\cdot\boldsymbol{q}}. \tag{7.58}$$

We then impose the condition that the terms of order $\mathcal{O}(\varepsilon^r)$ linear in $\boldsymbol{p}$ have zero

$$\left\langle h^{(r-1)}_{r,1}(\boldsymbol{q},\boldsymbol{p};\boldsymbol{J}_0)\right\rangle = 0\,. \tag{7.59}$$

This specifies $\boldsymbol{a}_r$ as a function of $\boldsymbol{J}_0$ via Eq (7.55).

Finally, we specify the constant vector $\boldsymbol{K}^{(r)}$. To this end, we impose the condition that the solution in $\boldsymbol{p}$ has the form $\sum_{\boldsymbol{k}} A_{\boldsymbol{k}}\,(\cos(\boldsymbol{k}\cdot\boldsymbol{q}) - 1)$, so that, at time $t = 0$, we have $p(0) = 0$. Writing (7.58) as

$$X^{(r)}(\boldsymbol{q}) = \sum_{\boldsymbol{k}\in\mathbb{Z}^n\setminus\{\boldsymbol{0}\}} \left[-\frac{i\,c^{(r-1)}_{\boldsymbol{k}}}{\boldsymbol{k}\cdot\boldsymbol{\omega}}\cos(\boldsymbol{k}\cdot\boldsymbol{q}) + \frac{c^{(r-1)}_{\boldsymbol{k}}}{\boldsymbol{k}\cdot\boldsymbol{\omega}}\sin(\boldsymbol{k}\cdot\boldsymbol{q})\right]\,, \tag{7.60}$$

the poisson bracket of $\chi_1^{(r)}(\boldsymbol{q})$ with the i-th component p_i $(1 \leq i \leq n)$ of the vector $\boldsymbol{p}$ yields the following expressions for the i-th components $K_i^{(r)}$ and k_i of the vectors $\boldsymbol{K}^{(r)}$ and $\boldsymbol{k}$:

$$\begin{aligned}
\{p_i\,, X^{(r)}(\boldsymbol{q})\} + \{p_i\,, \boldsymbol{K}^{(r)}\cdot\boldsymbol{q}\} &= \sum_{\boldsymbol{k}\in\mathbb{Z}^n\setminus\{\boldsymbol{0}\}} \left[-\left\{p_i\,,\, \frac{i\,c^{(r-1)}_{\boldsymbol{k}}}{\boldsymbol{k}\cdot\boldsymbol{\omega}}\cos(\boldsymbol{k}\cdot\boldsymbol{q})\right\} + \left\{p_i\,,\, \frac{c^{(r-1)}_{\boldsymbol{k}}}{\boldsymbol{k}\cdot\boldsymbol{\omega}}\sin(\boldsymbol{k}\cdot\boldsymbol{q})\right\}\right] - K_i^{(r)} \\
&= -\sum_{\boldsymbol{k}\in\mathbb{Z}^n\setminus\{\boldsymbol{0}\}} \left[\frac{i\,c^{(r-1)}_{\boldsymbol{k}}}{\boldsymbol{k}\cdot\boldsymbol{\omega}}\, k_i\,\sin(\boldsymbol{k}\cdot\boldsymbol{q}) + \frac{c^{(r-1)}_{\boldsymbol{k}}}{\boldsymbol{k}\cdot\boldsymbol{\omega}}\, k_i\,\cos(\boldsymbol{k}\cdot\boldsymbol{q})\right] - K_i^{(r)} = \\
&= -\sum_{\boldsymbol{k}\in\mathbb{Z}^n\setminus\{\boldsymbol{0}\}} \frac{i\,c^{(r-1)}_{\boldsymbol{k}}}{\boldsymbol{k}\cdot\boldsymbol{\omega}}\, k_i\,\sin(\boldsymbol{k}\cdot\boldsymbol{q}) - \sum_{\boldsymbol{k}\in\mathbb{Z}^n\setminus\{\boldsymbol{0}\}} \frac{c^{(r-1)}_{\boldsymbol{k}}}{\boldsymbol{k}\cdot\boldsymbol{\omega}}\, k_i\,(\cos(\boldsymbol{k}\cdot\boldsymbol{q}) - 1)\,.
\end{aligned} \tag{7.61}$$

Hence

$$K_i^{(r)} = -\sum_{\boldsymbol{k}\in\mathbb{Z}^n\setminus\{\boldsymbol{0}\}} \frac{c^{(r-1)}_{\boldsymbol{k}}}{\boldsymbol{k}\cdot\boldsymbol{\omega}}\, k_i\,, \tag{7.62}$$

i.e.,

$$\boldsymbol{K}^{(r)} = -\sum_{\boldsymbol{k}\in\mathbb{Z}^n\setminus\{\boldsymbol{0}\}} \frac{c^{(r-1)}_{\boldsymbol{k}}}{\boldsymbol{k}\cdot\boldsymbol{\omega}}\, \boldsymbol{k}\,. \tag{7.63}$$

Finally, we compute $\widehat{\mathcal{H}}^{(r)}$ in (7.56) (see Table 7.4) as:

$$\begin{aligned}\widehat{\mathcal{H}}^{(r)}(\boldsymbol{q},\boldsymbol{p};\boldsymbol{J}_0) \,=& \boldsymbol{\omega}\cdot\boldsymbol{p} + \varepsilon\, C_1 + \ldots + \varepsilon^{r-1}\, C_{r-1} + \varepsilon^r\, C_r \\ &+ \varepsilon\, \widehat{h}_1^{(r)}(\boldsymbol{q},\boldsymbol{p};\boldsymbol{J}_0) + \ldots + \varepsilon^{r-1}\, \widehat{h}_{r-1}^{(r)}(\boldsymbol{q},\boldsymbol{p};\boldsymbol{J}_0) \\ &+ \varepsilon^r\, \widehat{h}_r^{(r)}(\boldsymbol{q},\boldsymbol{p};\boldsymbol{J}_0) + \varepsilon^{r+1}\, \widehat{h}_{r+1}^{(r)}(\boldsymbol{q},\boldsymbol{p};\boldsymbol{J}_0) + \ldots\,,\end{aligned} \tag{7.64}$$

where $\widehat{h}_j^{(r)} = \sum_{i\geq 0} \widehat{h}_{j,i}^{(r)}\ \forall\, j \geq r$ and $\widehat{h}_j^{(r)} = \sum_{i\geq 2} \widehat{h}_{j,i}^{(r)} \in \mathcal{O}(||\,\boldsymbol{p}\,||^2)\ \ \forall\, j = 1,\ldots,r-1$, where:

$$\widehat{h}_{k,0}^{(r)} = C_k = \left\langle h_{k,0}^{(k-1)} \right\rangle - \boldsymbol{\omega}\cdot\boldsymbol{K}^{(k)} \qquad \forall\, 1 \leq k \leq r\,, \tag{7.65}$$

$$\widehat{h}_{k,0}^{(r)} = h_{k,0}^{(r-1)} \qquad \forall\, r+1 \leq k \leq 2r-1\,, \tag{7.66}$$

$$\widehat{h}_{k,0}^{(r)} = \sum_{j=0}^{\lfloor \frac{k-1}{r} \rfloor} \frac{1}{j!} L^j_{\chi_1^{(r)}(\boldsymbol{q})} \left(h_{k-jr,j}^{(r-1)} \right) \qquad \forall\, k \geq 2r \tag{7.67}$$

$$\widehat{h}_{k,1}^{(r)} = 0 \qquad \forall\, 1 \leq k \leq r-1\,, \tag{7.68}$$

$$\widehat{h}_{r,1}^{(r)} = h_{r,1}^{(r-1)}\,, \tag{7.69}$$

$$\widehat{h}_{k,i}^{(r)} = \sum_{j=0}^{\lfloor \frac{k-1}{r} \rfloor} \frac{1}{j!} L^j_{\chi_1^{(r)}(\boldsymbol{q})} \left(h_{k-jr,i+j}^{(r-1)} \right) \qquad \forall\, k \geq r+1\,,\ i \geq 1\,, \tag{7.70}$$

$$\widehat{h}_{k,i}^{(r)} = h_{k,i}^{(r-1)} \qquad \forall\, 1 \leq k \leq r\,,\ i \geq 2\,. \tag{7.71}$$

$$\widehat{\mathcal{H}}^{(r)} = \sum \begin{array}{|ccccccc|l}
 & & & & & & & \text{Order of the actions:} \\
\vdots & \vdots & \vdots & \vdots & \vdots & \vdots & \vdots & \vdots \\
0 & \varepsilon\, \widehat{h}_{1,2}^{(r)} & \ldots & \varepsilon^{r-1}\, \widehat{h}_{r-1,2}^{(r)} & \varepsilon^r\, \widehat{h}_{r,2}^{(r)} & \varepsilon^{r+1}\, \widehat{h}_{r+1,2}^{(r)} & \ldots & \leftarrow\ \mathcal{O}(||\boldsymbol{p}^2||) \\
\boldsymbol{\omega}\cdot\boldsymbol{p} & 0 & \ldots & 0 & \varepsilon^r\, \widehat{h}_{r,1}^{(r)} & \varepsilon^{r+1}\, \widehat{h}_{r+1,1}^{(r)} & \ldots & \leftarrow\ \mathcal{O}(||\boldsymbol{p}||) \\
0 & \varepsilon\, C_1 & \ldots & \varepsilon^{r-1}\, C_{r-1} & \varepsilon^r\, C_r & \varepsilon^{r+1}\, \widehat{h}_{r+1,0}^{(r)} & \ldots & \leftarrow\ \mathcal{O}(||\boldsymbol{p}||^0) \\
\hline
\uparrow & \uparrow & & \uparrow & \uparrow & \uparrow & & \\
\mathcal{O}(\varepsilon^0) & \mathcal{O}(\varepsilon) & \ldots & \mathcal{O}(\varepsilon^{r-1}) & \mathcal{O}(\varepsilon^r) & \mathcal{O}(\varepsilon^{r+1}) & \ldots & \\
\end{array}$$

Order of ε:

Table 7.4: Hamiltonian $\widehat{\mathcal{H}}^{(r)}$ after the first substep of the r-th normalization step.

- *Second half step (of r-th):* We compute

$$\mathcal{H}^{(r)} = \exp(L_{\varepsilon^r\, \chi_2^{(r)}(\boldsymbol{q},\boldsymbol{p})}) \widehat{\mathcal{H}}^{(r)} = \sum_{j\geq 0} \frac{(\varepsilon^r)^j}{j!} L^j_{\chi_2^{(r)}(\boldsymbol{q},\boldsymbol{p})} \widehat{\mathcal{H}}^{(r)}\,, \tag{7.72}$$

with a generating function $\chi_2^{(r)}(\boldsymbol{q},\boldsymbol{p})$ linear in $\boldsymbol{p}$. Setting $\chi_2^{(r)}(\boldsymbol{q},\boldsymbol{p}) = \tilde{\chi}_2^{(r)}(\boldsymbol{q},\boldsymbol{p}) + \boldsymbol{S}^{(r)}\cdot\boldsymbol{p} = \boldsymbol{Y}^{(r)}(\boldsymbol{q})\cdot\boldsymbol{p} + \boldsymbol{S}^{(r)}\cdot\boldsymbol{p}$. The function $\tilde{\chi}_2^{(r)}(\boldsymbol{q},\boldsymbol{p})$ satisfies the homological equation

$$\left\{\boldsymbol{\omega}\cdot\boldsymbol{p}\,,\, \tilde{\chi}_2^{(r)}(\boldsymbol{q},\boldsymbol{p})\right\} + \widehat{h}_{r,1}^{(r)}(\boldsymbol{q},\boldsymbol{p}) = 0\,. \tag{7.73}$$

Setting $\widehat{h}^{(r)}_{r,1}(\boldsymbol{q},\boldsymbol{p}) = \sum_{|\boldsymbol{j}|=1}\sum_{\boldsymbol{k}\in\mathbb{Z}^n} c^{(r)}_{\boldsymbol{jk}}\boldsymbol{p}^{\boldsymbol{j}} e^{i\boldsymbol{k}\cdot\boldsymbol{q}}$ the solution of (7.73) is

$$\tilde{\chi}^{(r)}_2(\boldsymbol{q},\boldsymbol{p}) = \sum_{|\boldsymbol{j}|=1}\sum_{\boldsymbol{k}\in\mathbb{Z}^n\setminus\{\boldsymbol{0}\}} \frac{c^{(r)}_{\boldsymbol{jk}}}{i\boldsymbol{k}\cdot\boldsymbol{\omega}}\boldsymbol{p}^{\boldsymbol{j}}\, e^{i\boldsymbol{k}\cdot\boldsymbol{q}}. \tag{7.74}$$

We finally compute the constant vector $\boldsymbol{S}^{(r)}$ by the condition $\boldsymbol{q}(0)=0$ at the time $t=0$. By the poisson bracket

$$\begin{aligned}
\{q_i\,,\chi^{(r)}_2\} &= \{q_i\,,\tilde{\chi}^{(r)}_2(\boldsymbol{q},\boldsymbol{p})\} + \{q_i\,,\boldsymbol{S}^{(r)}\cdot\boldsymbol{p}\} \\
&= \sum_{|\boldsymbol{j}|=1}\left(\sum_{\boldsymbol{k}\in\mathbb{Z}^n\setminus\{\boldsymbol{0}\}}\left[\Big\{q_i\,,\,\frac{c^{(r)}_{\boldsymbol{jk}}}{i\,\boldsymbol{k}\cdot\boldsymbol{\omega}}\,\boldsymbol{p}^{\boldsymbol{j}}\,\cos(\boldsymbol{k}\cdot\boldsymbol{q})\Big\} + \Big\{q_i\,,\,\frac{c^{(r)}_{\boldsymbol{jk}}}{\boldsymbol{k}\cdot\boldsymbol{\omega}}\,\boldsymbol{p}^{\boldsymbol{j}}\sin(\boldsymbol{k}\cdot\boldsymbol{q})\Big\}\right] + \Big\{q_i\,,\,S^{(r)}_{\boldsymbol{j}}\boldsymbol{p}^{\boldsymbol{j}}\Big\}\right) \\
&= \sum_{|\boldsymbol{j}|=1}\left(\sum_{\boldsymbol{k}\in\mathbb{Z}^n\setminus\{\boldsymbol{0}\}}\left[\frac{c^{(r)}_{\boldsymbol{jk}}}{i\,\boldsymbol{k}\cdot\boldsymbol{\omega}}\,j_i\,p_i^{j_i-1}\,\cos(\boldsymbol{k}\cdot\boldsymbol{q}) + \frac{c^{(r)}_{\boldsymbol{jk}}}{\boldsymbol{k}\cdot\boldsymbol{\omega}}\,j_i\,p_i^{j_i-1}\sin(\boldsymbol{k}\cdot\boldsymbol{q})\right] + S^{(r)}_{\boldsymbol{j}}\,j_i\,p_i^{j_i-1}\right) \\
&= \sum_{|\boldsymbol{j}|=1}\sum_{\boldsymbol{k}\in\mathbb{Z}^n\setminus\{\boldsymbol{0}\}}\left[\frac{c^{(r)}_{\boldsymbol{jk}}}{i\,\boldsymbol{k}\cdot\boldsymbol{\omega}}\,j_i\,p_i^{j_i-1}\,(\cos(\boldsymbol{k}\cdot\boldsymbol{q})-1) + \frac{c^{(r)}_{\boldsymbol{jk}}}{\boldsymbol{k}\cdot\boldsymbol{\omega}}\,j_i\,p_i^{j_i-1}\sin(\boldsymbol{k}\cdot\boldsymbol{q})\right]
\end{aligned} \tag{7.75}$$

we obtain

$$S^{(r)}_{\boldsymbol{j}} = \sum_{\boldsymbol{k}\in\mathbb{Z}^n\setminus\{\boldsymbol{0}\}}\frac{i\,c^{(r)}_{\boldsymbol{jk}}}{\boldsymbol{k}\cdot\boldsymbol{\omega}}\,. \tag{7.76}$$

The Hamiltonian $\mathcal{H}^{(r)}$ (Eq. (7.72)) (see Table 7.5) is:

$$\begin{aligned}
\mathcal{H}^{(r)}(\boldsymbol{q},\boldsymbol{p};\boldsymbol{J}_0) \;=& \boldsymbol{\omega}\cdot\boldsymbol{p} + \varepsilon\,C_1 + \ldots + \varepsilon^{r-1}\,C_{r-1} + \varepsilon^r\,C_r \\
&+ \varepsilon\,h^{(r)}_1(\boldsymbol{q},\boldsymbol{p};\boldsymbol{J}_0) + \ldots + \varepsilon^r\,h^{(r)}_r(\boldsymbol{q},\boldsymbol{p};\boldsymbol{J}_0) \\
&+ \varepsilon^{r+1}\,h^{(r)}_{r+1}(\boldsymbol{q},\boldsymbol{p};\boldsymbol{J}_0) + \ldots\,,
\end{aligned} \tag{7.77}$$

where $h^{(r)}_j = \sum_{i\geq 0} h^{(r)}_{j,i}\;\forall\, j \geq r+1$ and $h^{(r)}_j = \sum_{i\geq 2} h^{(r)}_{j,i} \in \mathcal{O}(||\,\boldsymbol{p}\,||^2)\,\forall\, j = 1,\ldots,r$, where:

$$h^{(r)}_{k,0} = \widehat{h}^{(r)}_{k,0} \qquad \forall\; 1\leq k\leq 2r\,, \tag{7.78}$$

$$h^{(r)}_{k,0} = \sum_{j=0}^{\lfloor\frac{k-1}{r}\rfloor}\frac{1}{j!}L^j_{\chi^{(r)}_2(\boldsymbol{q},\boldsymbol{p})}\left(\widehat{h}^{(r)}_{k-jr,0}\right) \qquad \forall\; k\geq 2r+1\,, \tag{7.79}$$

$$h^{(r)}_{k,1} = 0 \qquad \forall\; 1\leq k\leq r\,, \tag{7.80}$$

$$h^{(r)}_{k,1} = \sum_{j=0}^{\lfloor\frac{k-1}{r}\rfloor}\frac{1}{j!}L^j_{\chi^{(r)}_2(\boldsymbol{q},\boldsymbol{p})}\left(\widehat{h}^{(r)}_{k-jr,1}\right) \qquad \forall\; k\geq r+1\,, k\neq m\,r\,(m\in\mathbb{N})\,, \tag{7.81}$$

$$h^{(r)}_{k,1} = \sum_{j=0}^{\lfloor\frac{k-1}{r}\rfloor}\frac{1}{j!}L^j_{\chi^{(r)}_2(\boldsymbol{q},\boldsymbol{p})}\left(\widehat{h}^{(r)}_{k-jr,1}\right) + \frac{1}{m!}L^m_{\chi^{(r)}_2(\boldsymbol{q},\boldsymbol{p})}(\boldsymbol{\omega}\cdot\boldsymbol{p}) \qquad \forall\; k\geq r+1\,, k=m\,r\,(m\in\mathbb{N})\,. \tag{7.82}$$

$$h^{(r)}_{k,i} = \widehat{h}^{(r)}_{k,i} \qquad \forall\; 1\leq k\leq r\,,\; i\geq 2\,, \tag{7.83}$$

$$h^{(r)}_{k,i} = \sum_{j=0}^{\lfloor\frac{k-1}{r}\rfloor}\frac{1}{j!}L^j_{\chi^{(r)}_2(\boldsymbol{q},\boldsymbol{p})}\left(\widehat{h}^{(r)}_{k-jr,i}\right) \qquad \forall\; k\geq r+1\,,\; i\geq 2\,. \tag{7.84}$$

Equation (7.82), using homological equation (7.73), can be written equivalently as:

$$h^{(r)}_{k,1} = \sum_{j=0}^{m-2} \frac{1}{j!} L^j_{\chi_2^{(r)}(\boldsymbol{q},\boldsymbol{p})} \left(\widehat{h}^{(r)}_{k-jr,1}\right) + \frac{m-1}{m!} L^{m-1}_{\chi_2^{(r)}(\boldsymbol{q},\boldsymbol{p})} \left(\widehat{h}^{(r-1)}_{r,1}\right) \qquad \forall\, k \geq r+1\,, k = m\,r\,(m \in \mathbb{N}) \tag{7.85}$$

where, from (7.82) we have

$$\sum_{j=0}^{m-1} \frac{1}{j!} L^j_{\chi_2^{(r)}(\boldsymbol{q},\boldsymbol{p})} \left(\widehat{h}^{(r)}_{mr-jr,1}\right) + \frac{1}{m!} L^m_{\chi_2^{(r)}(\boldsymbol{q},\boldsymbol{p})} (\boldsymbol{\omega}\cdot\boldsymbol{p}) =$$
$$\sum_{j=0}^{m-2} \frac{1}{j!} L^j_{\chi_2^{(r)}(\boldsymbol{q},\boldsymbol{p})} \left(\widehat{h}^{(r)}_{mr-jr,1}\right) + \frac{1}{(m-1)!} L^{m-1}_{\chi_2^{(r)}(\boldsymbol{q},\boldsymbol{p})} \left(\widehat{h}^{(r)}_{r,1}\right) + \frac{1}{m!} L^m_{\chi_2^{(r)}(\boldsymbol{q},\boldsymbol{p})} (\boldsymbol{\omega}\cdot\boldsymbol{p}) =$$
$$\sum_{j=0}^{m-2} \frac{1}{j!} L^j_{\chi_2^{(r)}(\boldsymbol{q},\boldsymbol{p})} \left(\widehat{h}^{(r)}_{mr-jr,1}\right) + \frac{1}{m!} L^{m-1}_{\chi_2^{(r)}(\boldsymbol{q},\boldsymbol{p})} \left(\widehat{h}^{(r)}_{r,1} + L_{\chi_2^{(r)}(\boldsymbol{q},\boldsymbol{p})} (\boldsymbol{\omega}\cdot\boldsymbol{p})\right) + \frac{m-1}{m!} L^{m-1}_{\chi_2^{(r)}(\boldsymbol{q},\boldsymbol{p})} \left(\widehat{h}^{(r)}_{r,1}\right).$$

$$\mathcal{H}^{(r)} = \sum \begin{array}{|ccccccc|l|} \hline
\vdots & \vdots & \vdots & \vdots & \vdots & \vdots & \vdots & \text{Order of the actions:} \\
0 & \varepsilon\, h^{(r)}_{1,2} & \dots & \varepsilon^{r-1}\, h^{(r)}_{r-1,2} & \varepsilon^r\, h^{(r-1)}_{r,2} & \varepsilon^{r+1}\, h^{(r)}_{r+1,2} & \dots & \leftarrow\ \mathcal{O}(||\boldsymbol{p}^2||) \\
\boldsymbol{\omega}\cdot\boldsymbol{p} & 0 & \dots & 0 & 0 & \varepsilon^{r+1}\, h^{(r)}_{r+1,1} & \dots & \leftarrow\ \mathcal{O}(||\boldsymbol{p}||) \\
0 & \varepsilon\, C_1 & \dots & \varepsilon^{r-1}\, C_{r-1} & \varepsilon^r\, C_r & \varepsilon^{r+1}\, h^{(r-1)}_{r+1,0} & \dots & \leftarrow\ \mathcal{O}(||\boldsymbol{p}||^0) \\ \hline
\uparrow & \uparrow & \dots & \uparrow & \uparrow & \uparrow & \dots & \\
\mathcal{O}(\varepsilon^0) & \mathcal{O}(\varepsilon) & & \mathcal{O}(\varepsilon^{r-1}) & \mathcal{O}(\varepsilon^r) & \mathcal{O}(\varepsilon^{r+1}) & & \\ \hline
\end{array}$$

Order of ε:

Table 7.5: Hamiltonian $\mathcal{H}^{(r)}$ after r normalization steps.

Second part of the proof: using the formulas (7.65)–(7.71) and (7.78)–(7.84), we can express each term in the function $h^{(r)}$ in terms of the functions $h^{(r-1)}$ instead of $\widehat{h}^{(r)}$. From Eq (7.78) we have

$$h^{(r)}_{k,0} = \widehat{h}^{(r)}_{k,0} = C_k = \left\langle h^{(k-1)}_{k,0} \right\rangle - \boldsymbol{\omega}\cdot\boldsymbol{K}^{(k)} \qquad \forall\, 1 \leq k \leq r\,, \tag{7.86}$$
$$h^{(r)}_{k,0} = \widehat{h}^{(r)}_{k,0} = h^{(r-1)}_{k,0} \qquad \forall\, r+1 \leq k \leq 2r-1\,, \tag{7.87}$$
$$h^{(r)}_{2r,0} = \widehat{h}^{(r)}_{2r,0} = \sum_{j=0}^{\lfloor \frac{2r-1}{r} \rfloor} \frac{1}{j!} L^j_{\chi_1^{(r)}(\boldsymbol{q})} \left(h^{(r-1)}_{2r-jr,j}\right) = h^{(r-1)}_{2r,0} + L_{\chi_1^{(r)}(\boldsymbol{q})} \left(h^{(r-1)}_{r,1}\right), \tag{7.88}$$

where we used Eqs (7.65), (7.66) and (7.67), respectively. Using (7.71) we have

$$h^{(r)}_{k,i} = \widehat{h}^{(r)}_{k,i} = h^{(r-1)}_{k,i} \quad \forall\, 1 \leq k \leq r\,,\ i \geq 2\,. \tag{7.89}$$

Equation (7.84) can now be written in the form

$$h^{(r)}_{k,i} = \sum_{j=0}^{\lfloor \frac{k-1}{r} \rfloor - 1} \frac{1}{j!} L^j_{\chi_2^{(r)}(\boldsymbol{q},\boldsymbol{p})} \left(\widehat{h}^{(r)}_{k-jr,i}\right) + \frac{1}{\lfloor \frac{k-1}{r} \rfloor !} L^{\lfloor (k-1)/r \rfloor}_{\chi_2^{(r)}(\boldsymbol{q},\boldsymbol{p})} \left(\widehat{h}^{(r)}_{k-\lfloor \frac{k-1}{r} \rfloor r,i}\right) \tag{7.90}$$

$\forall\, k \geq r+1\,,\ i \geq 2\,.$ The indices i, j, k in the first term of the above equation satisfy the relation

$$k - jr \geq k - \lfloor \frac{k-1}{r} \rfloor r + r \geq r+1\,, \tag{7.91}$$

where we have used the inequalities $j \leq \lfloor (k-1)/r \rfloor - 1$ and $\lfloor k-1 \rfloor \leq k-1\,.$ Then Eq (7.91) ensures that the first term of (7.90) satisfies the definition (7.70). For the second term in (7.90), we have the following useful (also in the sequel) remark: we can write $k = mr + f\,,$ where $0 \leq f \leq r-1$ and $m \in \mathbb{N}\,.$ Thus

$$k - \lfloor \frac{k-1}{r} \rfloor r = mr + f - \lfloor \frac{mr+f-1}{r} \rfloor r = f - \lfloor \frac{f-1}{r} \rfloor r\,. \tag{7.92}$$

Then

$$k - \lfloor \frac{k-1}{r} \rfloor r = f - \lfloor \frac{f-1}{r} \rfloor r = r \quad \text{if } \ f = 0 \tag{7.93}$$

and

$$1 \leq k - \lfloor \frac{k-1}{r} \rfloor r = f - \lfloor \frac{f-1}{r} \rfloor r \leq r-1 \quad \text{if } \ 1 \leq f \leq r-1\,. \tag{7.94}$$

We can conclude that $1 \leq k - \lfloor (k-1)/r \rfloor r \leq r\,,$ implying that the definition (7.71) holds for the second term in (7.90). We can then write (7.90) as[2]

$$\begin{aligned} h^{(r)}_{k,i} &= \sum_{j=0}^{\lfloor \frac{k-1}{r} \rfloor - 1} \sum_{s=0}^{\lfloor \frac{k-jr-1}{r} \rfloor} \frac{1}{j!\, s!} L^{j}_{\chi^{(r)}_2(\boldsymbol{q},\boldsymbol{p})} L^{s}_{\chi^{(r)}_1(\boldsymbol{q})} \left(h^{(r-1)}_{k-jr-sr,i+s} \right) + \frac{1}{\lfloor \frac{k-1}{r} \rfloor !} L^{\lfloor (k-1)/r \rfloor}_{\chi^{(r)}_2(\boldsymbol{q},\boldsymbol{p})} \left(h^{(r-1)}_{k-\lfloor \frac{k-1}{r} \rfloor r,i} \right) \\ &= \sum_{j=0}^{\lfloor \frac{k-1}{r} \rfloor} \sum_{s=0}^{\lfloor \frac{k-jr-1}{r} \rfloor} \frac{1}{j!\, s!} L^{j}_{\chi^{(r)}_2(\boldsymbol{q},\boldsymbol{p})} L^{s}_{\chi^{(r)}_1(\boldsymbol{q})} \left(h^{(r-1)}_{k-jr-sr,i+s} \right)\,, \end{aligned} \tag{7.95}$$

$\forall\, k \geq r+1\,,\ i \geq 2\,.$

Equation (7.79) can be analyzed similarly as above, by splitting it in three different parts

$$\begin{aligned} h^{(r)}_{k,0} = &\sum_{j=0}^{\lfloor \frac{k-1}{r} \rfloor - 2} \frac{1}{j!} L^{j}_{\chi^{(r)}_2(\boldsymbol{q},\boldsymbol{p})} \left(\widehat{h}^{(r)}_{k-jr,0} \right) + \frac{1}{\left(\lfloor \frac{k-1}{r} \rfloor - 1 \right)!} L^{\lfloor (k-1)/r \rfloor - 1}_{\chi^{(r)}_2(\boldsymbol{q},\boldsymbol{p})} \left(\widehat{h}^{(r)}_{k-(\lfloor \frac{k-1}{r} \rfloor - 1)r,0} \right) \\ &+ \frac{1}{\lfloor \frac{k-1}{r} \rfloor !} L^{\lfloor (k-1)/r \rfloor}_{\chi^{(r)}_2(\boldsymbol{q},\boldsymbol{p})} \left(\widehat{h}^{(r)}_{k-\lfloor \frac{k-1}{r} \rfloor r,0} \right) \end{aligned} \tag{7.96}$$

$\forall\, k \geq 2r+1\,.$ We study separately the relations satisfied by the indices (j,k) of each of the three terms in the previous equality. Following (7.91), we have that

$$k - jr \geq k - \lfloor \frac{k-1}{r} \rfloor r + 2r \geq 2r+1\,,$$

(since $j \leq \lfloor (k-1)/r \rfloor - 2\,$). Then, the definition (7.67) holds for the first term. For the second and third terms, we have different formulas according to whether or not k is a multiple of r.

(i) First case: k is not a multiple of $r\,,$ i.e.,

$$k = mr + f \ \text{ with } \ 1 \leq f \leq r-1 \ \text{ and } \ m \in \mathbb{N}\,.$$

[2]Observe that, due to (7.93) and (7.94), we have that if $j = \lfloor (k-1)/r \rfloor\,,$ then $0 \leq \lfloor (k-jr-1)/r \rfloor = \lfloor (k - \lfloor (k-1)/r \rfloor r - 1)/r \rfloor \leq \lfloor (r-1)/r \rfloor = 0\,,$ i.e., $s = 0\,.$ This allows to join all terms in a single sum.

From (7.94) we have that $1 \leq k-\lfloor\frac{k-1}{r}\rfloor r \leq r-1$ and, consequently, $r+1 \leq k-\lfloor\frac{k-1}{r}\rfloor r+r \leq 2r-1$. Then, the definitions (7.65) and (7.66) hold, respectively, for the third and second term of (7.96). Thus, we can write equation (7.96) as

$$h^{(r)}_{k,0} = \sum_{j=0}^{\lfloor\frac{k-1}{r}\rfloor-2} \sum_{s=0}^{\lfloor\frac{k-jr-1}{r}\rfloor} \frac{1}{j!\,s!} L^j_{\chi^{(r)}_2(\boldsymbol{q},\boldsymbol{p})} L^s_{\chi^{(r)}_1(\boldsymbol{q})} \left(h^{(r-1)}_{k-jr-sr,s}\right) + \frac{1}{\left(\lfloor\frac{k-1}{r}\rfloor-1\right)!} L^{\lfloor(k-1)/r\rfloor-1}_{\chi^{(r)}_2(\boldsymbol{q},\boldsymbol{p})} \left(h^{(r-1)}_{k-(\lfloor\frac{k-1}{r}\rfloor-1)r,0}\right),$$

$\forall\, k \geq 2r+1$, $k \neq mr$, $m \in \mathbb{N}$.

(ii) Second case: k is a multiple of r, i.e.,

$$k = mr \;\text{ with }\; m \in \mathbb{N}.$$

From (7.93) we now have that $k-\lfloor\frac{k-1}{r}\rfloor r = r$ and, consequently, $k-\lfloor\frac{k-1}{r}\rfloor r + r = 2r$. Then, the definitions (7.65) and (7.67) hold, respectively, for the third and the second term of (7.96). Thus, we can write Eq (7.96) as

$$h^{(r)}_{k,0} = \sum_{j=0}^{\lfloor\frac{k-1}{r}\rfloor-1} \sum_{s=0}^{\lfloor\frac{k-jr-1}{r}\rfloor} \frac{1}{j!\,s!} L^j_{\chi^{(r)}_2(\boldsymbol{q},\boldsymbol{p})} L^s_{\chi^{(r)}_1(\boldsymbol{q})} \left(h^{(r-1)}_{k-jr-sr,s}\right), \tag{7.97}$$

$\forall\, k \geq 2r+1$, $k = mr$, $m \in \mathbb{N}$. By the same argument, we can write Eq (7.81) as:

$$h^{(r)}_{k,1} = \sum_{j=0}^{\lfloor\frac{k-1}{r}\rfloor-1} \frac{1}{j!} L^j_{\chi^{(r)}_2(\boldsymbol{q},\boldsymbol{p})} \left(\widehat{h}^{(r)}_{k-jr,1}\right) + \frac{1}{\lfloor\frac{k-1}{r}\rfloor!} L^{\lfloor(k-1)/r\rfloor}_{\chi^{(r)}_2(\boldsymbol{q},\boldsymbol{p})} \left(\widehat{h}^{(r)}_{k-\lfloor\frac{k-1}{r}\rfloor r,1}\right) \tag{7.98}$$

$\forall\, k \geq r+1$, $k \neq m\,r$ $(m \in \mathbb{N})$. In view of the inequalities (7.91) and (7.94) we then readily find that the definitions (7.70) and (7.68) hold, respectively, for the first and second part of the previous equation, i.e., (7.98) leads to

$$h^{(r)}_{k,1} = \sum_{j=0}^{\lfloor\frac{k-1}{r}\rfloor-1} \sum_{s=0}^{\lfloor\frac{k-jr-1}{r}\rfloor} \frac{1}{j!\,s!} L^j_{\chi^{(r)}_2(\boldsymbol{q},\boldsymbol{p})} L^s_{\chi^{(r)}_1(\boldsymbol{q})} \left(h^{(r-1)}_{k-jr-sr,1+s}\right), \tag{7.99}$$

$\forall\, k \geq r+1$, $k \neq m\,r$ $(m \in \mathbb{N})$. Finally, recalling again (7.91) and (7.93), we can write Eq (7.82) as[3]

$$\begin{aligned}
h^{(r)}_{k,1} &= \sum_{j=0}^{\lfloor\frac{k-1}{r}\rfloor-1} \frac{1}{j!} L^j_{\chi^{(r)}_2(\boldsymbol{q},\boldsymbol{p})} \left(\widehat{h}^{(r)}_{k-jr,1}\right) + \frac{1}{\lfloor\frac{k-1}{r}\rfloor!} L^{\lfloor(k-1)/r\rfloor}_{\chi^{(r)}_2(\boldsymbol{q},\boldsymbol{p})} \left(\widehat{h}^{(r)}_{k-\lfloor\frac{k-1}{r}\rfloor r,1}\right) + \frac{1}{m!} L^m_{\chi^{(r)}_2(\boldsymbol{q},\boldsymbol{p})} (\boldsymbol{\omega}\cdot\boldsymbol{p}) \\
&= \sum_{j=0}^{\lfloor\frac{k-1}{r}\rfloor-1} \sum_{s=0}^{\lfloor\frac{k-jr-1}{r}\rfloor} \frac{1}{j!\,s!} L^j_{\chi^{(r)}_2(\boldsymbol{q},\boldsymbol{p})} L^s_{\chi^{(r)}_1(\boldsymbol{q})} \left(h^{(r-1)}_{k-jr-sr,1+s}\right) + \frac{1}{\lfloor\frac{k-1}{r}\rfloor!} L^{\lfloor(k-1)/r\rfloor}_{\chi^{(r)}_2(\boldsymbol{q},\boldsymbol{p})} \left(h^{(r-1)}_{k-\lfloor\frac{k-1}{r}\rfloor r,1}\right) \\
&\quad + \frac{1}{m!} L^m_{\chi^{(r)}_2(\boldsymbol{q},\boldsymbol{p})} (\boldsymbol{\omega}\cdot\boldsymbol{p}) \\
&= \sum_{j=0}^{\lfloor\frac{k-1}{r}\rfloor} \sum_{s=0}^{\lfloor\frac{k-jr-1}{r}\rfloor} \frac{1}{j!\,s!} L^j_{\chi^{(r)}_2(\boldsymbol{q},\boldsymbol{p})} L^s_{\chi^{(r)}_1(\boldsymbol{q})} \left(h^{(r-1)}_{k-jr-sr,1+s}\right) + \frac{1}{m!} L^m_{\chi^{(r)}_2(\boldsymbol{q},\boldsymbol{p})} (\boldsymbol{\omega}\cdot\boldsymbol{p}),
\end{aligned} \tag{7.100}$$

[3] In the last equality, due to (7.93), we have that if $j = \lfloor(k-1)/r\rfloor$, then $\lfloor(k-jr-1)/r\rfloor = \lfloor(k-\lfloor(k-1)/r\rfloor r-1)/r\rfloor = \lfloor(r-1)/r\rfloor = 0$, i.e., $s = 0$. Thus, also here we can join the terms in a single sum.

$\forall\, k \geq r+1\,, k = m\,r$ $(m \in \mathbb{N})$ (where we used the definitions (7.70) and (7.69) for the first and second part of the sum). As before, we can then write the previous equation as

$$\sum_{j=0}^{m-1} \sum_{s=0}^{\lfloor \frac{mr-jr-1}{r} \rfloor} \frac{1}{j!\,s!} L^j_{\chi_2^{(r)}(\boldsymbol{q},\boldsymbol{p})} L^s_{\chi_1^{(r)}(\boldsymbol{q})} \left(h^{(r-1)}_{mr-jr-sr,1+s} \right) + \frac{1}{m!} L^m_{\chi_2^{(r)}(\boldsymbol{q},\boldsymbol{p})} \left(\boldsymbol{\omega} \cdot \boldsymbol{p} \right) =$$

$$\sum_{j=0}^{m-2} \sum_{s=0}^{\lfloor \frac{mr-jr-1}{r} \rfloor} \frac{1}{j!\,s!} L^j_{\chi_2^{(r)}(\boldsymbol{q},\boldsymbol{p})} L^s_{\chi_1^{(r)}(\boldsymbol{q})} \left(h^{(r-1)}_{mr-jr-sr,1+s} \right) + \frac{1}{(m-1)!} L^{m-1}_{\chi_2^{(r)}(\boldsymbol{q},\boldsymbol{p})} \left(h^{(r-1)}_{r,1} \right) + \frac{1}{m!} L^m_{\chi_2^{(r)}(\boldsymbol{q},\boldsymbol{p})} \left(\boldsymbol{\omega} \cdot \boldsymbol{p} \right) =$$

$$\sum_{j=0}^{m-2} \sum_{s=0}^{\lfloor \frac{mr-jr-1}{r} \rfloor} \frac{1}{j!\,s!} L^j_{\chi_2^{(r)}(\boldsymbol{q},\boldsymbol{p})} L^s_{\chi_1^{(r)}(\boldsymbol{q})} \left(h^{(r-1)}_{mr-jr-sr,1+s} \right) + \frac{1}{m!} L^{m-1}_{\chi_2^{(r)}(\boldsymbol{q},\boldsymbol{p})} \left(h^{(r-1)}_{r,1} + L_{\chi_2^{(r)}(\boldsymbol{q},\boldsymbol{p})} \left(\boldsymbol{\omega} \cdot \boldsymbol{p} \right) \right)$$

$$+ \frac{m-1}{m!} L^{m-1}_{\chi_2^{(r)}(\boldsymbol{q},\boldsymbol{p})} \left(h^{(r-1)}_{r,1} \right) . \tag{7.101}$$

Use of Eq (7.69) and the homological equation (7.73) then concludes the proof. □

A. Analytic calculation of Laplace coefficients

A computation of the Laplace coefficients (Eq. (1.29), subsection 1.4.5) via a multipolar expansion, is possible on the basis of the following.

Lemma 1. *The Laplace coefficients* $b^{(j)}_{s+\frac{1}{2}}$ *in the expression*

$$\frac{1}{\left(a_2^2+a_3^2-2\,a_2\,a_3\,\cos(\lambda_2-\lambda_3)\right)^{\frac{2\,s+1}{2}}}=a_3^{-(2\,s+1)}\sum_{j\geq 0} b^{(j)}_{s+\frac{1}{2}}\,(\alpha)\cos(j(\lambda_2-\lambda_3))\,,$$

can be computed as

$$\begin{aligned} b^{(0)}_{s+\frac{1}{2}}\,(\alpha) &= 1+\sum_{k=1}^{+\infty}(-1)^k\,\frac{\frac{l}{2}(\frac{l}{2}+1)\ldots(\frac{l}{2}+k-1)}{k!}\,\alpha^{2k} \\ &\quad+\sum_{h\in\mathcal{A}_2}\sum_{k=h}^{\infty}(-1)^{k-h}\frac{(s+\frac{1}{2})(s+\frac{3}{2})\ldots(s-\frac{1}{2}+k)}{\left(\frac{h}{2}\right)!\left(\frac{h}{2}\right)!(k-h)!}\alpha^{2k-h}\,, \\ b^{(j)}_{s+\frac{1}{2}}\,(\alpha) &= \sum_{h\in\mathcal{A}_j}\sum_{k=h}^{\infty}2(-1)^{k-h}\frac{(s+\frac{1}{2})(s+\frac{3}{2})\ldots(s-\frac{1}{2}+k)}{\left(\frac{h-j}{2}\right)!\left(\frac{h+j}{2}\right)!(k-h)!}\alpha^{2k-h}\,,\quad j\geq 1\,, \end{aligned} \tag{A.1}$$

where $\alpha=a_2/a_3$ *and* $\mathcal{A}_j=\left\{h\in\mathbb{N}\,:\,h=\begin{cases}2i & \text{if } j \text{ is even}\\ 2i+1 & \text{if } j \text{ is odd}\end{cases},\ i\in\mathbb{N}\,,\ i\geq\lfloor\frac{j}{2}\rfloor\right\},\ j\geq 1\,.$

Proof. We will expand

$$\frac{1}{\left(a_2^2+a_3^2-2\,a_2\,a_3\,\cos(\lambda_2-\lambda_3)\right)^{\frac{2\,s+1}{2}}}=a_3^{-(2s+1)}\frac{1}{\left(1+\alpha^2-2\alpha\cos(\lambda_2-\lambda_3)\right)^{\frac{2\,s+1}{2}}}\,, \tag{A.2}$$

in powers of $\alpha=a_2/a_3$. Defining $l=2s+1$ and $\sigma=\lambda_2-\lambda_3$ Taylor-expanding the r.h.s. in (A.2), we find

$$\frac{1}{\left(1+\alpha^2-2\alpha\cos(\sigma)\right)^{\frac{l}{2}}}=1+\sum_{k=1}^{+\infty}\frac{\frac{l}{2}(\frac{l}{2}+1)\ldots(\frac{l}{2}+k-1)}{k!}\,\left(2\alpha\cos(\sigma)-\alpha^2\right)^k\,. \tag{A.3}$$

Moreover, we can expand the quantity $\left(2\alpha\cos(\sigma)-\alpha^2\right)^k$, obtaining:

$$\begin{aligned}\frac{1}{(1+\alpha^2-2\alpha\cos(\sigma))^{\frac{l}{2}}} =&1+\sum_{k=1}^{+\infty}\frac{\frac{l}{2}(\frac{l}{2}+1)\dots(\frac{l}{2}+k-1)}{k!}\left(2\alpha\cos(\sigma)-\alpha^2\right)^k\\ =&1+\sum_{k=1}^{+\infty}\frac{\frac{l}{2}(\frac{l}{2}+1)\dots(\frac{l}{2}+k-1)}{k!}\left[\sum_{h=0}^{k}\frac{k!}{h!(k-h)!}(-1)^{k-h}\alpha^{2(k-h)}(2\alpha\cos(\sigma))^h\right]\\ =&1+\sum_{k=1}^{+\infty}\sum_{h=0}^{k}(-1)^{k-h}\,\frac{\frac{l}{2}(\frac{l}{2}+1)\dots(\frac{l}{2}+k-1)}{h!(k-h)!}\alpha^{2k-h}\,2^h\,\cos(\sigma)^h\,.\end{aligned} \tag{A.4}$$

After having explicitely written the sum corresponding to $h=0$, it is possible to reverse the order of the sums (over k and h), arriving to

$$\begin{aligned}\frac{1}{(1+\alpha^2-2\alpha\cos(\sigma))^{\frac{l}{2}}} =&\,1+\sum_{k=1}^{+\infty}(-1)^k\,\frac{\frac{l}{2}(\frac{l}{2}+1)\dots(\frac{l}{2}+k-1)}{k!}\alpha^{2k}\\ &+\sum_{h=1}^{+\infty}\sum_{k=h}^{+\infty}(-1)^{k-h}\,2^h\,\frac{\frac{l}{2}(\frac{l}{2}+1)\dots(\frac{l}{2}+k-1)}{h!(k-h)!}\alpha^{2k-h}\,\cos(\sigma)^h\\ :=&\sum_{h=0}^{+\infty}D_h\cos(\sigma)^h\,,\end{aligned} \tag{A.5}$$

where D_h (with $h\geq 0$) is defined as:

$$D_h=\begin{cases}1+\displaystyle\sum_{k=1}^{+\infty}(-1)^k\,\frac{\frac{l}{2}(\frac{l}{2}+1)\dots(\frac{l}{2}+k-1)}{k!}\,\alpha^{2k} & for\quad h=0\\ \displaystyle\sum_{k=h}^{+\infty}(-1)^{k-h}\,2^h\,\frac{\frac{l}{2}(\frac{l}{2}+1)\dots(\frac{l}{2}+k-1)}{h!(k-h)!}\,\alpha^{2k-h} & for\quad h\geq 1\end{cases}. \tag{A.6}$$

In order to compute the Laplace coefficients, we need to expand also the $\cos(\sigma)^h$ in (A.5). We set (Eq. (1.28))

$$\frac{1}{(a_2^2+a_3^2-2\,a_2\,a_3\,\cos(\sigma))^{\frac{l}{2}}}=a_3^{-l}\sum_{h\geq 0}D_h\cos(\sigma)^h=a_3^{-l}\sum_{j\geq 0}b_{\frac{l}{2}}^{(j)}(\alpha)\cos(j\sigma)\,.$$

Using again the binomial formula, we have

$$\cos(\sigma)^h=\left(\frac{e^{i\sigma}+e^{-i\sigma}}{2}\right)^h=\frac{1}{2^h}\sum_{k=0}^{h}\binom{h}{k}e^{ik\sigma}e^{-i(h-k)\sigma}=\frac{1}{2^h}\sum_{k=0}^{h}\binom{h}{k}\cos((2k-h)\sigma)\,. \tag{A.7}$$

Inserting th expression (A.7) in Eq. (A.5), we obtain

$$\begin{aligned}\frac{1}{(1+\alpha^2-2\alpha\cos(\sigma))^{\frac{l}{2}}} =&D_0+\sum_{h=1}^{+\infty}\sum_{k=0}^{h}\frac{D_h}{2^h}\frac{h!}{k!(h-k)!}\cos((h-2k)\sigma)\\ =&D_0+\sum_{h=1}^{+\infty}\sum_{j\in\mathcal{B}_h}\frac{D_h}{2^h}\frac{h!}{\left(\frac{h-j}{2}\right)!\left(\frac{h+j}{2}\right)!}\cos(j\sigma)\,,\end{aligned} \tag{A.8}$$

where we define $j=h-2k$ and the set

$$\mathcal{B}_h=\left\{j\in\mathbb{Z}\,:\,j=\begin{cases}2n & if\ h\ is\ even,\ n\in\mathbb{Z},\ -\frac{h}{2}\leq n\leq\frac{h}{2}\\ 2n+1 & if\ h\ is\ odd,\ n\in\mathbb{Z},\ \lfloor-\frac{h}{2}\rfloor\leq n\leq\lfloor\frac{h}{2}\rfloor\end{cases}\right\},\qquad h\geq 1\,.$$

On the other hand, the previous set of indexes can be thought also as

$$\mathcal{B}_h = \begin{cases} \mathcal{B}_{h_-} \cup \mathcal{B}_{h_+} \cup \{j=0\} & \textit{if } h \textit{ is even} \\ \mathcal{B}_{h_-} \cup \mathcal{B}_{h_+} & \textit{if } h \textit{ is odd} \end{cases} ,$$

where $\mathcal{B}_{h_-} = \mathcal{B}_h \cap \mathbb{Z}_{<0}$ and $\mathcal{B}_{h_+} = \mathcal{B}_h \cap \mathbb{Z}_{>0}$. With the above notation, the sum appearing in Eq. (A.8) can be decomposed as follows:

$$\sum_{h=1}^{+\infty} \sum_{j\in\mathcal{B}_h} = \sum_{\substack{h=1 \\ h\,odd}}^{+\infty} \left(\sum_{j\in\mathcal{B}_{h_-}} + \sum_{j\in\mathcal{B}_{h_+}} \right) + \sum_{\substack{h=2 \\ h\,even}}^{+\infty} \left(\sum_{j\in\mathcal{B}_{h_-}} + \sum_{j\in\mathcal{B}_{h_+}} + \sum_{j=0} \right) .$$

Thus, observing that

$$\sum_{j\in\mathcal{B}_{h_-}} \frac{D_h}{2^h} \frac{h!}{\left(\frac{h-j}{2}\right)! \left(\frac{h+j}{2}\right)!} \cos(j\sigma) = \sum_{j\in\mathcal{B}_{h_+}} \frac{D_h}{2^h} \frac{h!}{\left(\frac{h-j}{2}\right)! \left(\frac{h+j}{2}\right)!} \cos(j\sigma) ,$$

we can write Eq. (A.8) as:

$$\begin{aligned} \frac{1}{(1+\alpha^2-2\alpha\cos(\sigma))^{\frac{l}{2}}} = &\sum_{\substack{h=0 \\ h\,even}}^{+\infty} \frac{D_h}{2^h} \frac{h!}{\left(\frac{h}{2}\right)! \left(\frac{h}{2}\right)!} + \sum_{\substack{h=2 \\ h\,even}}^{+\infty} \sum_{j\in\mathcal{B}_{h_+}} \frac{D_h}{2^{h-1}} \frac{h!}{\left(\frac{h-j}{2}\right)! \left(\frac{h+j}{2}\right)!} \cos(j\sigma) \\ &+ \sum_{\substack{h=1 \\ h\,odd}}^{+\infty} \sum_{j\in\mathcal{B}_{h_+}} \frac{D_h}{2^{h-1}} \frac{h!}{\left(\frac{h-j}{2}\right)! \left(\frac{h+j}{2}\right)!} \cos(j\sigma) . \end{aligned}$$

Finally, reversing the order of the sums (over j and h), we arrive at

$$\begin{aligned} \frac{1}{(1+\alpha^2-2\alpha\cos(\sigma))^{\frac{l}{2}}} = &\sum_{\substack{h=0 \\ h\,even}}^{+\infty} \frac{D_h}{2^h} \frac{h!}{\left(\frac{h}{2}\right)! \left(\frac{h}{2}\right)!} + \sum_{\substack{j=2 \\ j\,even}}^{+\infty} \sum_{h\in\mathcal{A}_j} \frac{D_h}{2^{h-1}} \frac{h!}{\left(\frac{h-j}{2}\right)! \left(\frac{h+j}{2}\right)!} \cos(j\sigma) \\ &+ \sum_{\substack{j=1 \\ j\,odd}}^{+\infty} \sum_{h\in\mathcal{A}_j} \frac{D_h}{2^{h-1}} \frac{h!}{\left(\frac{h-j}{2}\right)! \left(\frac{h+j}{2}\right)!} \cos(j\sigma) , \\ = &\sum_{\substack{h=0 \\ h\,even}}^{+\infty} \frac{D_h}{2^h} \frac{h!}{\left(\frac{h}{2}\right)! \left(\frac{h}{2}\right)!} + \sum_{j=1}^{+\infty} \sum_{h\in\mathcal{A}_j} \frac{D_h}{2^{h-1}} \frac{h!}{\left(\frac{h-j}{2}\right)! \left(\frac{h+j}{2}\right)!} \cos(j\sigma) , \end{aligned} \tag{A.9}$$

where

$$\mathcal{A}_j = \left\{ h\in\mathbb{N} : h = \begin{cases} 2i & \textit{if } j \textit{ is even}, i\in\mathbb{N}, i\geq\frac{j}{2} \\ 2i+1 & \textit{if } j \textit{ is odd}, i\in\mathbb{N}, i\geq\lfloor\frac{j}{2}\rfloor \end{cases} \right\} , \qquad j\geq 1 .$$

Now we can finally put Eq. (A.9) in the expression (A.2) and compare the obtained quantity with (1.28), yielding

$$b^{(0)}_{s+\frac{1}{2}}(\alpha) = D_0 + \sum_{h\in\mathcal{A}_2} \frac{D_h}{2^h} \frac{h!}{\left(\frac{h}{2}\right)! \left(\frac{h}{2}\right)!} , \qquad b^{(j)}_{s+\frac{1}{2}}(\alpha) = \sum_{h\in\mathcal{A}_j} \frac{D_h}{2^{h-1}} \frac{h!}{\left(\frac{h-j}{2}\right)! \left(\frac{h+j}{2}\right)!} , \tag{A.10}$$

with $\mathcal{A}_2 = \{h\in\mathbb{N} : h = 2i\,,\, i\in\mathbb{N}\,,\, i\geq 1\}$. Finally, substituting in the previous expression (A.10) the definition of D_h (given by (A.6)) and remembering that $l = 2s+1$ and $\sigma = \lambda_2 - \lambda_3$, we obtain (A.1). This concludes the proof.

□

B. The phase space of $\mathcal{H}_{int}$ for fixed J and different values of energy $\mathcal{E}$

A similar analysis as in subsection 2.3.2.2 can be repeated fixing, as parameter, the value of the integral J instead of the level of energy $\mathcal{E}$. More precisely, it is possible to consider the sphere $\mathcal{S}_{\sigma_0}$ (Eq. (2.51)) of radius $\sigma_0 = 2J$ and the energy surfaces $\mathcal{C}_{\sigma_0,\mathcal{E}}$ (Eq. (2.52)) corresponding to a fixed value of $\sigma_0 = 2J$. In this case, we can have a physical trajectory for all values of $\mathcal{E}$ for which the surfaces $\mathcal{S}_{\sigma_0}$ and $\mathcal{C}_{\sigma_0,\mathcal{E}}$ intersect, limited by the two values $\mathcal{E} = \mathcal{E}^{(A)}$ and $\mathcal{E} = \mathcal{E}^{(B)}$ where the two surfaces become tangent (Fig. B.1).

With the help of the right panel of Fig. B.1 it is possible, now, to interpret the form of the phase portraits as in the left column of the same figure. To this end, we specify the correspondence between the various curves of the phase flow on the sphere, obtained by the intersections between the surfaces $\mathcal{S}_{\sigma_0}$ and $\mathcal{C}_{\sigma_0,\mathcal{E}}$ as $\mathcal{E}$ is altered in the interval $\mathcal{E}^{(A)} \leq \mathcal{E} \leq \mathcal{E}^{(B)}$, and the mapping of these curves to the phase space (ψ, Γ). We recall from subsection 2.3.2.2 that, since $\mathcal{H}_{int}$ does not depend on σ_2, all the curves produced by intersections of the surfaces $\mathcal{S}_{\sigma_0}$ and $\mathcal{C}_{\sigma_0,\mathcal{E}}$ contain points which lie in the meridian circle produced by the intersection of $\mathcal{S}_{\sigma_0}$ with the plane $\sigma_2 = 0$. In particular, the points of tangency A and B belong to this meridian. Besides these points, there are two critical curves which separate domains of libration of the angle ψ around the value 0 (mode A), or π (mode B), from domains where the angle ψ circulates.

By varying, now, the value of $\mathcal{E}$ in the interval $\mathcal{E}^{(A)} \leq \mathcal{E} \leq \mathcal{E}^{(B)}$ we progressively obtain curves on the sphere which pass from a librating domain around the fixed point A to a circulating domain, and then to a librating domain around the fixed point B. The first such transition occurs at a value $\mathcal{E}^{(S)}$ where the curve corresponding to the intersection between $\mathcal{S}_{\sigma_0}$ and $\mathcal{C}_{\sigma_0,\mathcal{E}^{(S)}}$ passes from the south pole S of the sphere $\mathcal{S}_{\sigma_0}$. The coordinates of the south pole are $\sigma_1^{(S)} = \sigma_2^{(S)} = 0$, $\sigma_3^{(S)} = -\sigma_0$, implying $J = -\Gamma$; due to the presence of $\sqrt{W_2}\sqrt{W_3} = \sqrt{J^2 - \Gamma^2}$ in the denominator of $\dot{\psi}$, corresponding to the south pole the angle ψ is not well defined and it jumps from $-\pi/2$ to $\pi/2$.

Passing, now, the value $\mathcal{E} = \mathcal{E}^{(S)}$, we have curves of the sphere which are projected to invariant curves still surrounding the fixed point A, but for which the ψ circulates (as, for istance, the brown curve outlined in Figure B.1). A second limit of the circulation domain occurs at a value $\mathcal{E}^{(N)}$ where the curve corresponding to the intersection between $\mathcal{S}_{\sigma_0}$ and $\mathcal{C}_{\sigma_0,\mathcal{E}^{(N)}}$ passes from the north pole N of the sphere $\mathcal{S}_{\sigma_0}$. We readily find that the curve in the sphere $\mathcal{C}_{\sigma,\mathcal{E}^{(N)}}$ yields the open black curve in the phase-space on the left of Figure B.1; corresponding to the north pole the angle ψ jumps. In fact, N has coordinates $\left(\sigma_1^{(N)} = 0,\, \sigma_2^{(N)} = 0,\, \sigma_3^{(N)} = \sigma_0\right)$, implying $W_3 = 0$, i.e. $J = \Gamma$.

Finally, for $\mathcal{E}$ in the interval $\mathcal{E}^{(N)} < \mathcal{E} \leq \mathcal{E}^{(B)}$ we find invariant curves in the sphere $\mathcal{S}_{\sigma_0}$ mapped to closed invariant curves around the tangency corresponding to the B-mode fixed point, which yield also closed curves in the phase space for which the argument ψ librates around the value

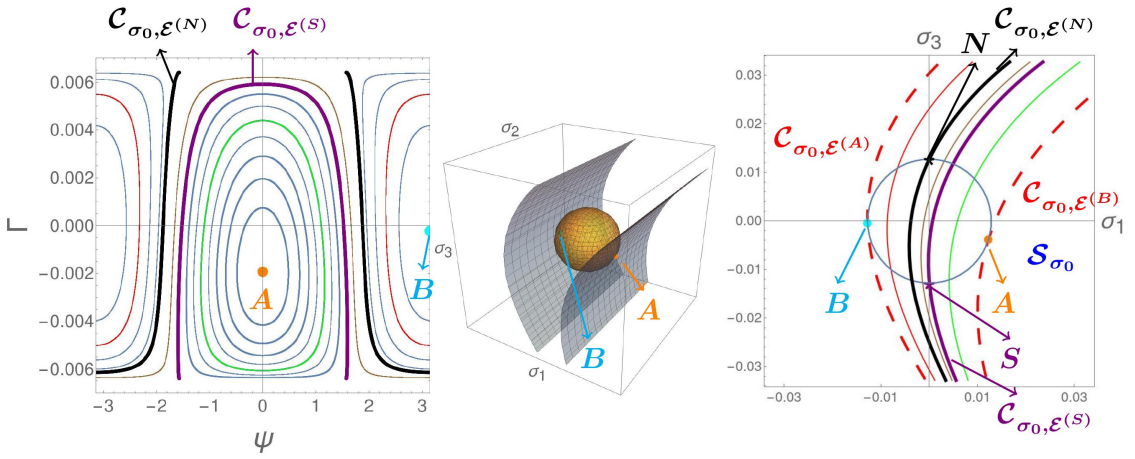

Figure B.1: Left: the phase portrait given by the numerical integration of the integrable flow ($\mathcal{H}_{int}$) for $J = 6.4 \cdot 10^{-3}$ and different values of the energy $\mathcal{E}$, projected in the variables (ψ, Γ). Centre: at the values $\sigma_0 = 2J$, the corresponding sphere $\mathcal{S}_{\sigma_0}$ become tangent to the energy surfaces $\mathcal{C}_{\sigma_0,\mathcal{E}^{(A)}}$, $\mathcal{C}_{\sigma_0,\mathcal{E}^{(B)}}$. The points of tangency yield the position of the fixed points A and B in the surface of section (see text). Right: the intersection of the spheres $\mathcal{S}_{\sigma_0}$ and of the energy surfaces $\mathcal{C}_{\sigma_0,\varepsilon}$ with the plane (σ_1, σ_3) for $\sigma_2 = 0$, for various values of $\mathcal{E}$. The intersection of the sphere with one energy surface yields a curve on the sphere which is projected to a curve in the above plane. For a particular value of $\mathcal{E} = \mathcal{E}^{(S)}$, the curve (thick purple) passes through the south pole S of the sphere $\mathcal{S}_{\sigma_0}$. This corresponds to an open trajectory (purple, thick curve of the left picture) which surrounds mode A; the angle ψ jumps from $-\pi/2$ to $\pi/2$. This curve delimits the domain of orbits whose angle $\psi = \omega_3 - \omega_2$ librates around the value $\psi = 0$. At a different value of $\mathcal{E} = \mathcal{E}^{(N)}$ the curve of constant energy (thick black in the right column) passes through the sphere's north pole N. This corresponds to an open curve in the phase space which surrounds mode B; the angle ψ jumps from $-\pi/2$ to $\pi/2$. The domain in the phase space between the thick purple and the thick black curves corresponds to orbits whose argument $\psi = \omega_3 - \omega_2$ circulates (see, for istance, the brown curve). All trajectories beyond the outer delimiting curve exhibit librations of the argument $\omega_3 - \omega_2$ around the value π, characteristic of the B-mode.

$\psi^{(B)} = \pi$, i.e., around the B-mode.

C. Secular Hamiltonian at second order in the masses

C.1 Formal algorithm

In this section we derive the secular Hamiltonian of the 3BP, at order two in the masses, without performing Jacobi's reduction of the nodes (see subsection 1.4.5.2 and [45]).
We start from the Hamiltonian of the 3BP (Eq. (4.1)), given by

$$\mathcal{H} = \sum_{j=2}^{3} \left(\frac{\boldsymbol{p}_j{}^2}{2\,\beta_j} - \frac{\mathcal{G}\,m_0\,m_j}{r_j} \right) + \frac{\boldsymbol{p}_2 \cdot \boldsymbol{p}_3}{m_0} - \frac{\mathcal{G}\,m_2\,m_3}{|\boldsymbol{r}_2 - \boldsymbol{r}_3|}\,.$$

A convenient method performing all the expansions (i.e., of the "perturbation" to the Keplerian part in powers of the eccentricities and inclinations, without performing, after, Jacobi's reduction of the nodes), is through the so called "complex dimensionless Poincaré variables" $(\Lambda_j, \lambda_j, \widetilde{\mathcal{X}}_j, i\,\overline{\widetilde{\mathcal{X}}}_j, \widetilde{\mathcal{Y}}_j, i\,\overline{\widetilde{\mathcal{Y}}}_j)$, $j = 2, 3$ (see [54]), where (Λ_j, λ_j) are the usual modified Delaunay variables $\Lambda_j = \beta_j \sqrt{\mu_j a_j}$, $\lambda_j = M_j + \varpi_j$, with $\beta_j = m_0 m_j/(m_0 + m_j)$ the reduced masses and $\mu_j = \mathcal{G}(m_0 + m_j)$, and $(\widetilde{\mathcal{X}}_j, \widetilde{\mathcal{Y}}_j)$ are defined by

$$\widetilde{\mathcal{X}}_j = \sqrt{\frac{2\Gamma_j}{\Lambda_j}} e^{-i\varpi_j} = \sqrt{2}\sqrt{1-\sqrt{1-\mathrm{e}_j^2}}\,e^{-i\varpi_j}\,, \qquad \widetilde{\mathcal{Y}}_j = \sqrt{\frac{2\Theta_j}{\Lambda_j}} e^{-i\Omega_j} = 2\sqrt[4]{1-\mathrm{e}_j^2}\,\sin\left(\frac{\mathrm{i}_j}{2}\right) e^{-i\Omega_j}\,. \tag{C.1}$$

The dimensionless quantities $\sqrt{2\Gamma_j/\Lambda_j}$ and $\sqrt{2\Theta_j/\Lambda_j}$ have the same "order of magnitude", respectively, of the eccentricity e_j and the inclination i_j, $j = 2, 3$. The expansion of the Hamiltonian (4.1), in these variables, is of the form

$$\mathcal{H} = -\sum_{j=2}^{3} \frac{\mathcal{G}m_0 m_j}{2a_j} - \frac{\mathcal{G}m_2 m_3}{a_3} \sum_{\boldsymbol{n},\,l_1,\,l_2} C_{\boldsymbol{n}}^{l_1,l_2}(\alpha)\widetilde{\mathcal{X}}_2^{n_1}\widetilde{\mathcal{X}}_3^{n_2}\overline{\widetilde{\mathcal{X}}}_2^{n_3}\overline{\widetilde{\mathcal{X}}}_3^{n_4}\widetilde{\mathcal{Y}}_2^{n_5}\widetilde{\mathcal{Y}}_3^{n_6}\overline{\widetilde{\mathcal{Y}}}_2^{n_7}\overline{\widetilde{\mathcal{Y}}}_3^{n_8} e^{i(l_1\lambda_2 + l_2\lambda_3)}\,, \tag{C.2}$$

where $\boldsymbol{n} = (n_1, n_2, n_3, n_4, n_5, n_6, n_7, n_8)$ and the coefficients $C_{\boldsymbol{n}}^{l_1,l_2}(\alpha)$ depend only on the ratio $\alpha = a_2/a_3$, with $a_2 < a_3$ and can be computed using the 'Laplace-coefficients', as explained in subsection 1.4.5.1 (see [87] and [54]). Being interested in the long-term dynamics, we need the secular formulation of the Hamiltonian; to this end, the dependence on the 'fast' angles λ_2, λ_3 has to be removed. This can be done "averaging by scissors" (as already explained subbsection 1.4.5.1,

Eq. (1.30)), that is equivalent to do a first order (in the mass ratios) averaging[1]; otherwise, in order to have a more accurate representation, this elimination can be done through a canonical transformations, corresponding to a second order (in the mass ratios) averaging.

In order to introduce the formal algorithm describing such canonical transformations, it is convenient to express the Hamiltonian (C.2) in the canonical Poincaré variables (ξ_j, η_j), (P_j, Q_j) (momenta-positions) introduced in Eq. (4.2):

$$\begin{aligned}
&\xi_j = \sqrt{2\Lambda_j}\sqrt{1-\sqrt{1-\mathrm{e}_j^2}}\cos(\varpi_j)\,, \qquad \eta_j = -\sqrt{2\Lambda_j}\sqrt{1-\sqrt{1-\mathrm{e}_j^2}}\sin(\varpi_j)\\
&P_j = 2\sqrt{\Lambda_j}\sqrt[4]{1-\mathrm{e}_j^2}\,\sin\left(\frac{\mathrm{i}_j}{2}\right)\cos(\Omega_j)\,, \quad Q_j = -2\sqrt{\Lambda_j}\sqrt[4]{1-\mathrm{e}_j^2}\,\sin\left(\frac{\mathrm{i}_j}{2}\right)\sin(\Omega_j)\,,
\end{aligned}$$

$j = 2, 3$. Moreover, we introduce a translation $L_j = \Lambda_j - \Lambda_j^*$, where Λ_j^* is defined in order to have the agreement between the semi-major axes as obtained by the Keplerian approximation of motion and by the observations; it is useful to perform an expansion of the Hamiltonian around the initial values of the semi-major axes, called a_j^* (i.e., expanding the perturbation in powers of L_2, L_3 in a neighbourhood of $(0,0)$). Thus, the Hamiltonian described by (C.2) can be written (apart from constants) as

$$\begin{aligned}
\mathcal{H} &= \mathcal{H}_{kepl}(\boldsymbol{L}) + \mu\,\mathcal{H}_{pert}(\boldsymbol{L}, \boldsymbol{\lambda}, \boldsymbol{\xi}, \boldsymbol{\eta}, \boldsymbol{P}, \boldsymbol{Q})\\
&= h_1^{(0)} + h_2^{(0)} + \ldots + h_0^{(1)} + h_1^{(1)} + h_2^{(1)} + \ldots\,,
\end{aligned} \tag{C.3}$$

where $\mu = \max\{m_2/m_0\,, m_3/m_0\}$ and we denote with $h_k^{(s)}$ the part of the Hamiltonian $\mathcal{H}$ having order s with respect to μ and degree k in the actions $\boldsymbol{L}$; therefore, the terms $h_k^{(0)}$ come from the unperturbed Keplerian part of the Hamiltonian, instead $h_k^{(1)}$ come from the perturbation. This splitting of the Hamiltonian allows to distinguish the *fast variables* $(\boldsymbol{L}, \boldsymbol{\lambda}) = (L_2, L_3, \lambda_2, \lambda_3)$ and the *secular* ones $(\boldsymbol{\xi}, \boldsymbol{\eta}, \boldsymbol{P}, \boldsymbol{Q}) = (\xi_2, \xi_3, \eta_2, \eta_3, P_2, P_3, Q_2, Q_3)$; indeed, we can observe that $\dot{\boldsymbol{\lambda}} = \mathcal{O}(1)$, while the *secular* variables are of $\mathcal{O}(\mu)$. Thus, the motion of the planet along the orbit has a different timescale with respect to the secular variables, whose variation is due to the interaction between the planets. If we are interested only in the evolution of the secular variables, a standard procedure is to average the Hamiltonian over the fast angles $\boldsymbol{\lambda}$; if we perform a simple averaging of $\mathcal{H}$, we would obtain a secular approximation with terms of order $\mathcal{O}(\mu)$, namely at order 1 in the masses. Instead, in order to have an approximation at order 2 in the masses, we can apply a 'close to the identity' canonical change of coordinates.

We first define the fundamental mean motion frequency related to the angles $\boldsymbol{\lambda}$, essential for the homological equation; more precisely, we take into account the first order correction to the frequencies. Following [73], this means redefining (with a little abuse of notation) the following quantities:

$$h_1^{(0)} \leftarrow h_1^{(0)} + \left\langle h_1^{(1)}\Big|_{\boldsymbol{\xi},\boldsymbol{\eta},\boldsymbol{P},\boldsymbol{Q}=\boldsymbol{0}} \right\rangle_{\boldsymbol{\lambda}} := \boldsymbol{n}^* \cdot \boldsymbol{L}\,, \qquad h_1^{(1)} \leftarrow h_1^{(1)} - \left\langle h_1^{(1)}\Big|_{\boldsymbol{\xi},\boldsymbol{\eta},\boldsymbol{P},\boldsymbol{Q}=\boldsymbol{0}} \right\rangle_{\boldsymbol{\lambda}}\,, \tag{C.4}$$

where $\boldsymbol{n}^*$ is the correction of the fundamental mean motion frequency related to the angles $\boldsymbol{\lambda}$. In order to remove the dependence of the Hamiltonian on $\boldsymbol{\lambda}$, we start to remove the angle-dependent terms in $h_0^{(1)}$; this can be done through a Lie series with generating function χ_1, determined by the following homological equation

$$\{\boldsymbol{n}^* \cdot \boldsymbol{L}, \chi_1\} + h_0^{(1)}(\boldsymbol{\lambda}, \boldsymbol{\xi}, \boldsymbol{\eta}, \boldsymbol{P}, \boldsymbol{Q}) = \left\langle h_0^{(1)}(\boldsymbol{\lambda}, \boldsymbol{\xi}, \boldsymbol{\eta}, \boldsymbol{P}, \boldsymbol{Q}) \right\rangle_{\boldsymbol{\lambda}}\,. \tag{C.5}$$

[1]This simply means to remove from the Hamiltonian (C.2) the terms depending upon the mean anomalies of the planets.

Thus, Fourier expanding $h_0^{(1)}$ as $h_0^{(1)} = \sum_{\boldsymbol{m},\boldsymbol{n},\boldsymbol{s},\boldsymbol{r},\boldsymbol{k}} c_{\boldsymbol{m},\boldsymbol{n},\boldsymbol{s},\boldsymbol{r},\boldsymbol{k}} \boldsymbol{\xi}^{\boldsymbol{m}} \boldsymbol{\eta}^{\boldsymbol{n}} \boldsymbol{P}^{\boldsymbol{s}} \boldsymbol{Q}^{\boldsymbol{r}} \mathrm{e}^{i\boldsymbol{k}\cdot\boldsymbol{\lambda}}$, it follows that $\chi_1 = \sum_{\substack{\boldsymbol{m},\boldsymbol{n},\boldsymbol{s},\boldsymbol{r} \\ \boldsymbol{k}\neq\boldsymbol{0}}} \frac{c_{\boldsymbol{m},\boldsymbol{n},\boldsymbol{s},\boldsymbol{r},\boldsymbol{k}}}{i\,\boldsymbol{n}^*\cdot\boldsymbol{k}} \boldsymbol{\xi}^{\boldsymbol{m}} \boldsymbol{\eta}^{\boldsymbol{n}} \boldsymbol{P}^{\boldsymbol{s}} \boldsymbol{Q}^{\boldsymbol{r}} \mathrm{e}^{i\boldsymbol{k}\cdot\boldsymbol{\lambda}}$. It is possible now to compute the transformed Hamiltonian through the application of the Lie series operator (Definition 1.1.5, section 1.1.3), that is

$$\widetilde{\mathcal{H}} = \exp L_{\chi_1} \mathcal{H} = \sum_{j=0}^{+\infty} \frac{1}{j!} L_{\chi_1}^j \mathcal{H} = \mathcal{H} + \{\mathcal{H}, \chi_1\} + \dots \,. \tag{C.6}$$

Recalling that we are interested in a Hamiltonian up to second order in the masses (i.e. of order $\mathcal{O}(\mu^2)$), and that we want to focus on the torus corresponding to $\boldsymbol{L} = \boldsymbol{0}$ (that means considering the fast variables frozen on the torus $\boldsymbol{L} = \boldsymbol{0}$, with fast frequencies $\boldsymbol{n}^*$), we can readily see that the Hamiltonian (C.6) reduces to the computation of the following terms

$$\widetilde{\mathcal{H}} = \left\langle h_0^{(1)} \right\rangle_{\boldsymbol{\lambda}} + \frac{1}{2}\{h_0^{(1)}, \chi_1\}_{(\boldsymbol{\xi},\boldsymbol{\eta},\boldsymbol{P},\boldsymbol{Q})} + \{h_1^{(1)}, \chi_1\}_{(\boldsymbol{L},\boldsymbol{\lambda})} + \frac{1}{2}\{\{h_2^{(0)}, \chi_1\}_{(\boldsymbol{L},\boldsymbol{\lambda})}, \chi_1\}_{(\boldsymbol{L},\boldsymbol{\lambda})} \,, \tag{C.7}$$

where $\{\cdot,\cdot\}_{(\boldsymbol{L},\boldsymbol{\lambda})}$ and $\{\cdot,\cdot\}_{(\boldsymbol{\xi},\boldsymbol{\eta},\boldsymbol{P},\boldsymbol{Q})}$ are the Poisson brackets involving, respectively, only the derivatives with respect to the variables $(\boldsymbol{L},\boldsymbol{\lambda})$ and $(\boldsymbol{\xi},\boldsymbol{\eta},\boldsymbol{P},\boldsymbol{Q})$.
Let us observe that, for the computation of such a kind of secular model, it is not necessary to compute the effects induced by a second generating function $\chi_2(\boldsymbol{L},\boldsymbol{\lambda})$, removing the linear terms in $\boldsymbol{L}$, since the additional terms due to the application of such a Lie series operator are neglected in the secular approximation. Indeed, we could have determined a generating function χ_2 by the following homological equation

$$\{\boldsymbol{n}^*\cdot\boldsymbol{L}, \chi_2\} + \widetilde{h}_1^{(1)}(\boldsymbol{L},\boldsymbol{\lambda},\boldsymbol{\xi},\boldsymbol{\eta},\boldsymbol{P},\boldsymbol{Q}) = \left\langle \widetilde{h}_1^{(1)}(\boldsymbol{L},\boldsymbol{\lambda},\boldsymbol{\xi},\boldsymbol{\eta},\boldsymbol{P},\boldsymbol{Q}) \right\rangle_{\boldsymbol{\lambda}} \,;$$

this χ_2 would have been necessary to remove the angular dependence in $\widetilde{h}_1^{(1)} = h_1^{(1)} + \{h_2^{(0)}, \chi_1\}_{(\boldsymbol{L},\boldsymbol{\lambda})}$ (not reported in Eq. (C.7), being 0 for $\boldsymbol{L} = \boldsymbol{0}$). However, up to order two in the masses, no terms independent of both $\boldsymbol{L}$ and $\boldsymbol{\lambda}$ are generated by $\exp L_{\chi_2} \exp L_{\chi_1} \mathcal{H}$; this means that, all terms generated by this expansion (i.e. $\exp L_{\chi_2}$) is removed when reducing the system to the secular one, i.e. considering $\boldsymbol{L} = \boldsymbol{0}$ and performing $\langle\cdot\rangle_{\boldsymbol{\lambda}}$.

In conclusion, the secular Hamiltonian up to order two in masses is given by

$$\mathcal{H}_{sec}^{(\mathcal{O}_2)}(\boldsymbol{\xi},\boldsymbol{\eta},\boldsymbol{P},\boldsymbol{Q}) = \left\langle \widetilde{\mathcal{H}} \right\rangle_{\boldsymbol{\lambda}} \,. \tag{C.8}$$

As a consequence of the D'Alembert rules, this secular Hamiltonian (C.8) is an infinite sum of even polynomials in the canonical variables $(\boldsymbol{\xi},\boldsymbol{\eta},\boldsymbol{P},\boldsymbol{Q})$. However, in practice, we can only compute a *truncated* Hamiltonian:[2]

$$\mathcal{H}_{sec}^{(\mathcal{O}_2)}(\boldsymbol{\xi},\boldsymbol{\eta},\boldsymbol{P},\boldsymbol{Q}) = \sum_{s=0}^{\mathcal{N}/2} \sum_{\substack{|\boldsymbol{i}|+|\boldsymbol{l}|+ \\ |\boldsymbol{m}|+|\boldsymbol{n}|=2s}} c_{\boldsymbol{i},\boldsymbol{l},\boldsymbol{m},\boldsymbol{n}} \prod_{j=2}^{3} \xi_j^{i_j} \eta_j^{l_j} P_j^{m_j} Q_j^{n_j} \,, \tag{C.9}$$

where $\mathcal{N}$ is the order of expansion in powers of the eccentricities and inclinations (in our application fixed equal to 8).

Finally, let us observe that, from a computational point of view, the secular Hamiltonian (C.8) can be easily obtained remembering this simple fact:

Lemma C.1.1. *Given two functions* $f := \tilde{f}(\boldsymbol{L},\boldsymbol{\xi},\boldsymbol{\eta},\boldsymbol{P},\boldsymbol{Q}) e^{i\,\boldsymbol{k}\cdot\boldsymbol{\lambda}}$ *and* $g := \tilde{g}(\boldsymbol{L},\boldsymbol{\xi},\boldsymbol{\eta},\boldsymbol{P},\boldsymbol{Q}) e^{i\,\boldsymbol{k}'\cdot\boldsymbol{\lambda}}$, *then* $\left\langle \{f,g\}_{(\boldsymbol{L},\boldsymbol{\lambda},\boldsymbol{\xi},\boldsymbol{\eta},\boldsymbol{P},\boldsymbol{Q})} \right\rangle_{\boldsymbol{\lambda}} = 0$ *if* $\boldsymbol{k} \neq -\boldsymbol{k}'$.

[2] Let us observe that, in the expression of the Hamiltonian at order two in the masses (C.9), we should have written $(\tilde{\boldsymbol{\xi}},\tilde{\boldsymbol{\eta}},\tilde{\boldsymbol{P}},\tilde{\boldsymbol{Q}})$, meaning 'new' coordinates. However, with abuse of notation, we write $(\boldsymbol{\xi},\boldsymbol{\eta},\boldsymbol{P},\boldsymbol{Q})$.

Proof. Remembering the Definition of Poisson bracket (1.1.1)[3], it is easy to compute the mean over the fast angles $\boldsymbol{\lambda}$ of the poisson bracket between f and g, that is

$$\left\langle \{f,g\}_{(\boldsymbol{L},\boldsymbol{\lambda},\boldsymbol{\xi},\boldsymbol{\eta},\boldsymbol{P},\boldsymbol{Q})} \right\rangle_{\boldsymbol{\lambda}} := \langle \{f,g\} \rangle_{\boldsymbol{\lambda}} = \left\langle \{\tilde{f}(\boldsymbol{L},\boldsymbol{\xi},\boldsymbol{\eta},\boldsymbol{P},\boldsymbol{Q}) e^{i\,\boldsymbol{k}\cdot\boldsymbol{\lambda}}, \tilde{g}(\boldsymbol{L},\boldsymbol{\xi},\boldsymbol{\eta},\boldsymbol{P},\boldsymbol{Q}) e^{i\,\boldsymbol{k}'\cdot\boldsymbol{\lambda}}\} \right\rangle_{\boldsymbol{\lambda}} =$$
$$= \left\langle \sum_{j=2}^{3} \left(i\,k_j\,\tilde{f}\,\frac{\partial \tilde{g}}{\partial L_j} - i\,k_j^{'}\,\frac{\partial \tilde{f}}{\partial L_j}\,\tilde{g} + \frac{\partial \tilde{f}}{\partial \eta_j}\frac{\partial \tilde{g}}{\partial \xi_j} - \frac{\partial \tilde{f}}{\partial \xi_j}\frac{\partial \tilde{g}}{\partial \eta_j} + \frac{\partial \tilde{f}}{\partial Q_j}\frac{\partial \tilde{g}}{\partial P_j} - \frac{\partial \tilde{f}}{\partial P_j}\frac{\partial \tilde{g}}{\partial Q_j} \right) e^{i(\boldsymbol{k}+\boldsymbol{k}')\cdot\boldsymbol{\lambda}} \right\rangle_{\boldsymbol{\lambda}} .$$

Then, if $\boldsymbol{k}+\boldsymbol{k}^{'} \neq \boldsymbol{0}$, then the previous quantity is equal to 0. This prove the Lemma. □

Thus, in order to easily compute (C.8), it is sufficient to compute in Eq. (C.7) only the poisson brackets giving a secular contribution, i.e., for the above Lemma C.1.1, the ones s.t. $\boldsymbol{k} = -\boldsymbol{k}^{'}$.

C.2 The secular quasi-periodic restricted Hamiltonian at order two in the masses (without the Jacobi's reduction of nodes)

In the following section we repeat the steps explained in Section 4.2, providing the determination of the motion of υ-And **c** and υ-And **d** through the *Frequency Analysis* method, starting, however, from the numerical integration of the secular 3BP Hamiltonian at order two in the masses (instead of the complete 3BP Hamiltonian, as in Section 4.2).

As initial orbital parameters, we fix the ones reported in Table 4.1; then, we compute their correspondent values in the Laplace reference frame and, accordingly, in the Poincaré variables $(\xi_j(0),\eta_j(0),P_j(0),Q_j(0))$ $j=2,3$, given by Eq. (4.2). However, the secular Hamiltonian at order two in the masses does not involve the 'original variables' (ξ_j,η_j,P_j,Q_j), but 'new variables' $(\tilde{\xi}_j,\tilde{\eta}_j,\tilde{P}_j,\tilde{Q}_j)$, related to the original ones through the canonical transformation leading the Hamiltonian at order two in the masses. In particular, being from (C.6)

$$\widetilde{\mathcal{H}} = \exp L_{\chi_1}\mathcal{H} = \sum_{j=0}^{+\infty} \frac{1}{j!} L_{\chi_1}^{j}\mathcal{H}\,,$$

it is necessary to compute the 'new' variables $(\tilde{\xi}_j,\tilde{\eta}_j,\tilde{P}_j,\tilde{Q}_j)$, defined through

$$\xi = \exp L_{\chi_1}\xi|_{\xi=\tilde{\xi}}, \quad \eta = \exp L_{\chi_1}\eta|_{\eta=\tilde{\eta}}, \quad P = \exp L_{\chi_1}P|_{P=\tilde{P}}, \quad Q = \exp L_{\chi_1}Q|_{Q=\tilde{Q}}\,,$$

and their correspondent initial values $(\tilde{\xi}_j(0),\tilde{\eta}_j(0),\tilde{P}_j(0),\tilde{Q}_j(0))$, $j=2,3$. Now, it is possible to numerically integrate (using a RK4 method) the Hamiltonian vector field at order two in the masses, described by

$$\begin{cases} \dot{\tilde{\xi}}_j = -\partial\mathcal{H}_{sec}^{(\mathcal{O}_2)}/\partial\tilde{\eta}_j \\ \dot{\tilde{\eta}}_j = \partial\mathcal{H}_{sec}^{(\mathcal{O}_2)}/\partial\tilde{\xi}_j \\ \dot{\tilde{P}}_j = -\partial\mathcal{H}_{sec}^{(\mathcal{O}_2)}/\partial\tilde{Q}_j \\ \dot{\tilde{Q}}_j = \partial\mathcal{H}_{sec}^{(\mathcal{O}_2)}/\partial\tilde{P}_j \end{cases}, \tag{C.10}$$

with initial contitions $(\tilde{\xi}_j(0),\tilde{\eta}_j(0),\tilde{P}_j(0),\tilde{Q}_j(0))$, $j=2,3$. Moreover, defined variables

$$\widehat{\xi}_j = \sqrt{2\Lambda_j}\sqrt{1-\sqrt{1-\mathrm{e}_j^2}}\cos(\omega_j)\,, \qquad \widehat{\eta}_j = -\sqrt{2\Lambda_j}\sqrt{1-\sqrt{1-\mathrm{e}_j^2}}\sin(\omega_j)\,, \qquad j=2,3,$$

[3]Respect to the Definition (1.1.1), in this case $\boldsymbol{\lambda}$, $\boldsymbol{\eta}$, $\boldsymbol{Q}$ play the role of the $\boldsymbol{q}$ and $\boldsymbol{\Lambda}$, $\boldsymbol{\xi}$, $\boldsymbol{P}$, their conjugate variables, play the role of the $\boldsymbol{p}$.

(already introduced in Eq. (4.9)), we report in Figure C.1 the Poincaré section with respect to the representative coordinates $(\tilde{\widehat{\xi}}_2, \tilde{\widehat{\eta}}_2) = (\widehat{\xi}_2, \widehat{\eta}_2)\big|_{\substack{e_j=\tilde{e}_j \\ \omega_j=\tilde{\omega}_j}}$, in correspondence with the hyperplane $\tilde{\widehat{\eta}}_3 = 0$, $\tilde{\widehat{\xi}}_3 > 0$ (that correspond to $\tilde{\omega}_3 = 0$, $\dot{\tilde{\omega}}_3 \geq 0$ and where we denote with the superscript $\tilde{}$ the 'new' quantities).

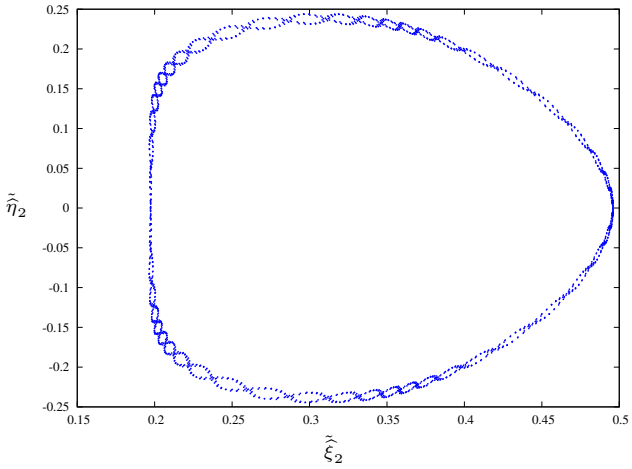

Figure C.1: Poincaré surfaces of section with respect to the representative coordinates $(\tilde{\widehat{\xi}}_2, \tilde{\widehat{\eta}}_2)$ coordinates (as defined in Eq. (4.9)), taking as Hamiltonian vector field the one at order two in the masses, given by (C.10).

Observe that a flickering behaviour is evident in Figure C.1. This is probably due to the fact that, not having done the Jacobi's reduction, the quantity $\tilde{\Omega}_2(t) - \tilde{\Omega}_3(t)$ is not perfectly conserved, but instead it fluctuates around π, as we can see from Figure C.2.

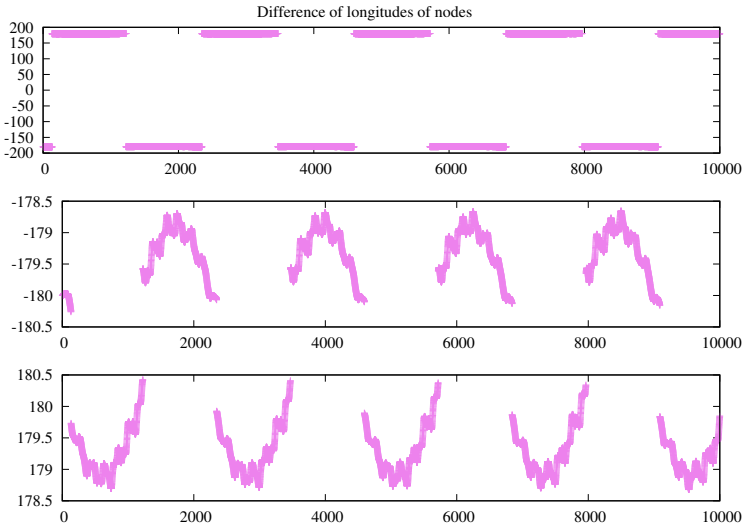

Figure C.2: Time behaviour of the difference of longitude of nodes $\tilde{\Omega}_3(t) - \tilde{\Omega}_2(t)$. In the first panel, the range of the y-axes is $[-200, 200]$; instead, in order to see the fluctuation of $\tilde{\Omega}_3 - \tilde{\Omega}_2$ around $\pm\pi$, in the second and third panel we show a zoom, being, respectively, the range of the y-axes $[-180.5, -178.5]$ and $[178.5, 180.5]$.

Having numerically integrated the Hamiltonian vector field at order two in the masses, given by Eq. (C.10), it is now possible to performe the FA of the produced discretizations of the signals $t \mapsto \tilde{\xi}_j(t) + i\tilde{\eta}_j(t)$ and $t \mapsto \tilde{P}_j(t) + i\tilde{Q}_j(t)$, as described in Subsection 4.2. Then, we use the FA to compute a quasi-periodic approximation of the secular dynamics of the giant planets υ-And **c** and υ-And **d**, i.e.

$$\tilde{\xi}_j(t) + i\tilde{\eta}_j(t) \simeq \sum_{s=1}^{\mathcal{N}_C} A_{j,s} e^{i(\boldsymbol{k}_{j,s}\cdot\boldsymbol{\theta}(t)+\vartheta_{j,s})}, \quad \tilde{P}_j(t) + i\tilde{Q}_j(t) \simeq \sum_{s=1}^{\mathcal{N}_C} \tilde{A}_{j,s} e^{i(\tilde{\boldsymbol{k}}_{j,s}\cdot\boldsymbol{\theta}(t)+\tilde{\vartheta}_{j,s})}, \quad j = 2, 3, \tag{C.11}$$

where the angular vector $\boldsymbol{\theta}(t) = \boldsymbol{\omega}\, t$ and the fundamental frequency vector $\boldsymbol{\omega} \in \mathbb{R}^3$ has components:

$$\begin{aligned} \omega_3 &= -3.90335668822162293 \cdot 10^{-2} \\ \omega_4 &= -5.50499614207990672 \cdot 10^{-3} \\ \omega_5 &= \ \ 2.80965935610450173 \cdot 10^{-3} \end{aligned} \tag{C.12}$$

Thus the motion of the outer planets $t \mapsto (\tilde{\xi}_j(t),\, \tilde{\eta}_j(t),\, \tilde{P}_j(t),\, \tilde{Q}_j(t))\,,\ j = 2, 3$, is approximated as it is written in both the r.h.s. of formula (C.11). The numerical values of the coefficients which appear in the quasi-periodic decompositions of the motions laws are reported in Tables C.1, C.2, C.3, C.4.

s	$\nu_T^{(s)}$	$k_1^{(s)}$	$k_2^{(s)}$	$k_3^{(s)}$	$\lvert\nu_T^{(s)} - \boldsymbol{k}^{(s)}\cdot\boldsymbol{\omega}\rvert$	A_s	ϑ_s
0	$-3.90335668822162293 \cdot 10^{-2}$	1	0	0	0.0000	$3.6878 \cdot 10^{-1}$	4.507
1	$-5.50499614107488947 \cdot 10^{-3}$	0	1	0	$1.0050 \cdot 10^{-12}$	$1.6514 \cdot 10^{-1}$	3.413
2	$4.46528855913945477 \cdot 10^{-2}$	-1	0	2	$3.0307 \cdot 10^{-12}$	$2.9030 \cdot 10^{-2}$	4.172
3	$-3.93035125180514130 \cdot 10^{-2}$	2	-5	4	$3.1116 \cdot 10^{-9}$	$2.1230 \cdot 10^{-2}$	6.166
4	$-3.87636203175592206 \cdot 10^{-2}$	0	5	-4	$2.1827 \cdot 10^{-9}$	$2.1007 \cdot 10^{-2}$	5.990

Table C.1: Frequency analysis of the signal $\tilde{\xi}_2 + i\,\tilde{\eta}_2$.

s	$\nu_T^{(s)}$	$k_1^{(s)}$	$k_2^{(s)}$	$k_3^{(s)}$	$\lvert\nu_T^{(s)} - \boldsymbol{k}^{(s)}\cdot\boldsymbol{\omega}\rvert$	A_s	ϑ_s
0	$-3.90335668820297604 \cdot 10^{-2}$	1	0	0	$1.8647 \cdot 10^{-13}$	$6.4038 \cdot 10^{-1}$	1.366
1	$-5.50499614207990672 \cdot 10^{-3}$	0	1	0	0.0000	$9.9884 \cdot 10^{-2}$	3.413
2	$-3.93035125141760616 \cdot 10^{-2}$	2	-5	4	$3.1154 \cdot 10^{-9}$	$3.6561 \cdot 10^{-2}$	3.024
3	$-3.87636203169931387 \cdot 10^{-2}$	0	5	-4	$2.1822 \cdot 10^{-9}$	$3.6764 \cdot 10^{-2}$	2.849
4	$-1.22720019368366143 \cdot 10^{-1}$	3	0	-2	$9.5085 \cdot 10^{-12}$	$1.4224 \cdot 10^{-2}$	1.701

Table C.2: Frequency analysis of the signal $\tilde{\xi}_3 + i\,\tilde{\eta}_3$.

s	$\nu_T^{(s)}$	$\tilde{k}_1^{(s)}$	$\tilde{k}_2^{(s)}$	$\tilde{k}_3^{(s)}$	$\lvert\nu_T^{(s)} - \tilde{\boldsymbol{k}}^{(s)}\cdot\boldsymbol{\omega}\rvert$	$\tilde{A}_s$	$\tilde{\vartheta}_s$
0	$2.80965935610450173 \cdot 10^{-3}$	0	0	1	0.0000	$5.5945 \cdot 10^{-1}$	2.769
1	$-8.08767931242924537 \cdot 10^{-2}$	2	0	-1	$3.7555 \cdot 10^{-12}$	$2.4271 \cdot 10^{-2}$	6.246
2	$2.53971335399360036 \cdot 10^{-3}$	1	-5	5	$2.7453 \cdot 10^{-9}$	$7.1529 \cdot 10^{-3}$	4.427
3	$-4.73482223766229851 \cdot 10^{-2}$	1	1	-1	$3.7777 \cdot 10^{-12}$	$7.3628 \cdot 10^{-3}$	5.151
4	$3.07960552644089263 \cdot 10^{-3}$	-1	5	-3	$2.5771 \cdot 10^{-9}$	$6.7020 \cdot 10^{-3}$	4.252

Table C.3: Frequency analysis of the signal $\tilde{P}_2 + i\,\tilde{Q}_2$.

s	$\nu_T^{(s)}$	$\tilde{k}_1^{(s)}$	$\tilde{k}_2^{(s)}$	$\tilde{k}_3^{(s)}$	$\lvert\nu_T^{(s)} - \tilde{\boldsymbol{k}}^{(s)}\cdot\boldsymbol{\omega}\rvert$	$\tilde{A}_s$	$\tilde{\vartheta}_s$
0	$2.80965935614351219 \cdot 10^{-3}$	0	0	1	$3.9010 \cdot 10^{-14}$	$5.4940 \cdot 10^{-1}$	5.910
1	$-8.08767931242797972 \cdot 10^{-2}$	2	0	-1	$3.7428 \cdot 10^{-12}$	$2.3337 \cdot 10^{-2}$	3.104
2	$2.53971335672819980 \cdot 10^{-3}$	1	-5	5	$2.7480 \cdot 10^{-9}$	$7.0611 \cdot 10^{-3}$	1.286
3	$-4.73482223787267537 \cdot 10^{-2}$	1	1	-1	$1.6739 \cdot 10^{-12}$	$7.3001 \cdot 10^{-3}$	2.010
4	$3.07960552545669770 \cdot 10^{-3}$	-1	5	-3	$2.5780 \cdot 10^{-9}$	$6.5561 \cdot 10^{-3}$	1.110

Table C.4: Frequency analysis of the signal $\tilde{P}_3 + i\,\tilde{Q}_3$.

Moreover, in order to verify that the numerical solutions are well approximated by the quasi-periodic decompositions computed above, we compare the time evolution of the variables $\tilde{\xi}_2$, $\tilde{\xi}_3$, $\tilde{\eta}_2$, $\tilde{\eta}_3$, $\tilde{P}_2$, $\tilde{P}_3$, $\tilde{Q}_2$, $\tilde{Q}_3$ as obtained by the numerical integration and by the FA. The comparison of the obtained dynamics (outlined, respectively, in blue and red) is shown in Figure (C.3).

A comparison of the Poincaré section (corresponding to $\tilde{\omega}_3 = 0\,,\ \dot{\tilde{\omega}}_3 \geq 0\,$), as obtained by the numerical integration of the Hamiltonian vector field at order two in the masses, or by the quasi-periodic approximation of the motion; the comparison is shown in Figure C.4.

C.3 Numerical integration of the secular quasi-periodic restricted model (with giant planets' motion at second order approximation)

After the steps carried out in section 4.3, the secular Hamiltonian (Eq. (4.12)) resumes the form

$$\mathcal{H}_{sec}(\boldsymbol{\xi}, \boldsymbol{\eta}, \boldsymbol{P}, \boldsymbol{Q}) = \sum_{s=0}^{\mathcal{N}/2} \sum_{\substack{|\boldsymbol{i}|+|\boldsymbol{l}|+ \\ |\boldsymbol{m}|+|\boldsymbol{n}|=2s}} c_{\boldsymbol{i},\boldsymbol{l},\boldsymbol{m},\boldsymbol{n}} \prod_{j=1}^{3} \xi_j^{i_j} \eta_j^{l_j} P_j^{m_j} Q_j^{n_j}\ ,$$

where $\mathcal{N}$ is the order of truncation in powers of eccentricity and inclination (that we fix to $\mathcal{N} = 8$). Following section 4.3, we finally introduce the following $2 + 3/2$ degrees of freedom Hamiltonian model for the secular dynamics of υ-And **b**;

$$\begin{aligned} \mathcal{H}_{sec,\,2+\frac{3}{2}}\ (\boldsymbol{p}, \boldsymbol{q}, \xi_1, \eta_1, P_1, Q_1) &= \omega_3\, p_3 + \omega_4\, p_4 + \omega_5\, p_5 \\ &+ \mathcal{H}_{sec}^{1-2}(\xi_1, \eta_1, P_1, Q_1, \xi_2(\boldsymbol{q}), \eta_2(\boldsymbol{q}), P_2(\boldsymbol{q}), Q_2(\boldsymbol{q})) \\ &+ \mathcal{H}_{sec}^{1-3}(\xi_1, \eta_1, P_1, Q_1, \xi_3(\boldsymbol{q}), \eta_3(\boldsymbol{q}), P_3(\boldsymbol{q}), Q_3(\boldsymbol{q}))\,, \end{aligned}$$

where the pairs of canonical coordinates referring to the planets υ-And **c** and υ-And **d** (that are $\xi_2\,,\ \eta_2\,,\ \ldots P_3\,,\ Q_3$) are replaced by the corresponding finite Fourier decomposition written in formula (C.11) as a function of the angles $\boldsymbol{\theta}$, renamed as $\boldsymbol{q}$ (Eq. (4.15)) and the fundamental

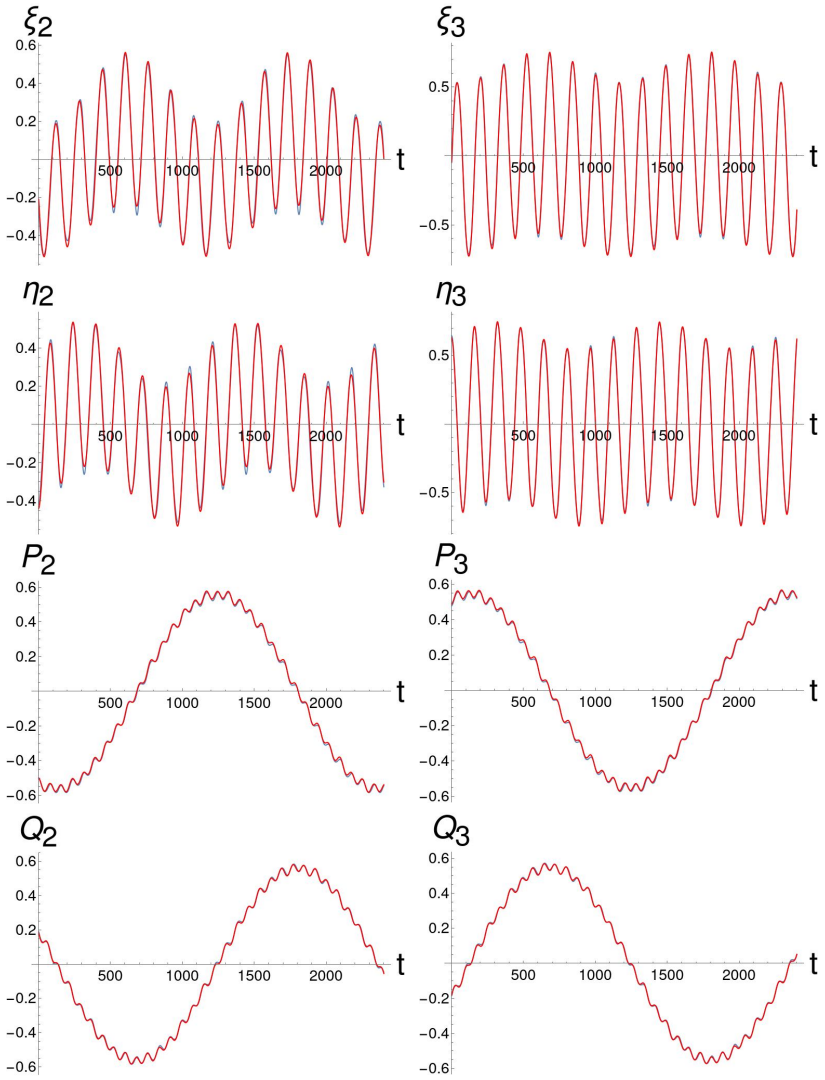

Figure C.3: Dynamical-behaviour of the variables $\tilde{\xi}_2$, $\tilde{\xi}_3$, $\tilde{\eta}_2$, $\tilde{\eta}_3$, $\tilde{P}_2$, $\tilde{P}_3$, $\tilde{Q}_2$, $\tilde{Q}_3$ as computed by numerical integration of the secular three- body problem at order two in the masses and by the quasi-periodic approximation provided by the FA; the corresponding plots are in blue and red, respectively.

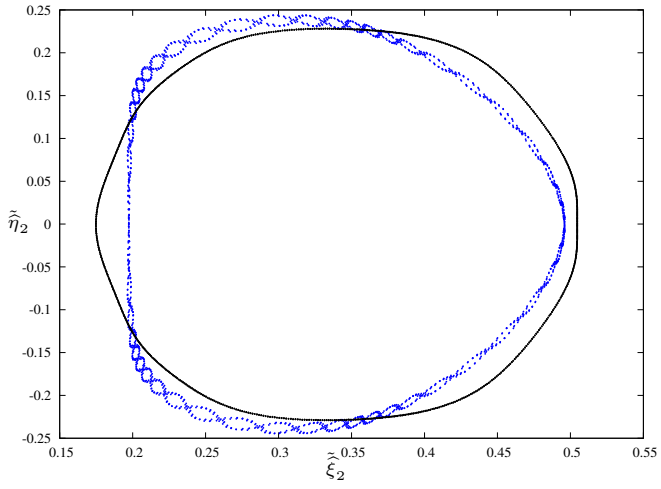

Figure C.4: Poincaré surfaces of section with respect to the representative coordinates $(\tilde{\xi}_2, \tilde{\eta}_2)$. The blue 'flickering' curve is obtained by the numerical integration of the secular Hamiltonian vector field at order two in the masses, given by Eq. (C.10). The black one is obtained considering the quasi-periodic approximation of the motion, as determined by the FA.

frequency vector has components given by Eq. (C.12). The correspondent secular quasi-periodic restricted Hamilton's equations of motion are

$$\begin{cases} \dot{q_3} = \partial \mathcal{H}_{sec,2+\frac{3}{2}}/\partial p_3 = \omega_3 \\ \dot{q_4} = \partial \mathcal{H}_{sec,2+\frac{3}{2}}/\partial p_4 = \omega_4 \\ \dot{q_5} = \partial \mathcal{H}_{sec,2+\frac{3}{2}}/\partial p_5 = \omega_5 \\ \dot{\xi}_1 = -\partial \mathcal{H}_{sec,2+\frac{3}{2}}/\partial \eta_1 \\ \dot{\eta}_1 = \partial \mathcal{H}_{sec,2+\frac{3}{2}}/\partial \xi_1 \\ \dot{P}_1 = -\partial \mathcal{H}_{sec,2+\frac{3}{2}}/\partial Q_1 \\ \dot{Q}_1 = \partial \mathcal{H}_{sec,2+\frac{3}{2}}/\partial P_1 \end{cases} . \tag{C.13}$$

However, repeating the steps explained in subsection 4.3.1.2 and performing the numerical integration of the above equation of motions, we can see that the former quasi-periodic restricted approximation is not enough accurate to represent the dynamic of the *complete* 4-body problem. In fact, taking $m_1 = 0.674$, the initial orbital parameters for υ-And **b**, a, e, M and ω as those reported in Table 4.7 and $(\mathrm{i}, \Omega) \in I_i \times I_\Omega = [6.865°, 34°] \times [0°, 360°)$, after having computed the correspondent values in the Laplace reference frame of υ-And **c** and υ-And **d**, we can numerically integrate the Hamiltonian (at order two in masses) vector field, in the secular quasi-periodic restricted approximation; the color-grid plots of the maximal value reached by the eccentricity of υ-And **b** and by the mutual inclination between υ-And **b** and υ-And **c** are shown in Figure C.5. As we can observe, they result quite different with respect to Figure 4.3, obtained by the numerical integration of the complete 4BP. Thus, we can conclude that the obtained signals (C.11) (at second order approximation), are not enough accurate to be injected in the secular restricted Hamiltonian and to correctly recover the behaviour of the complete 4 body problem.

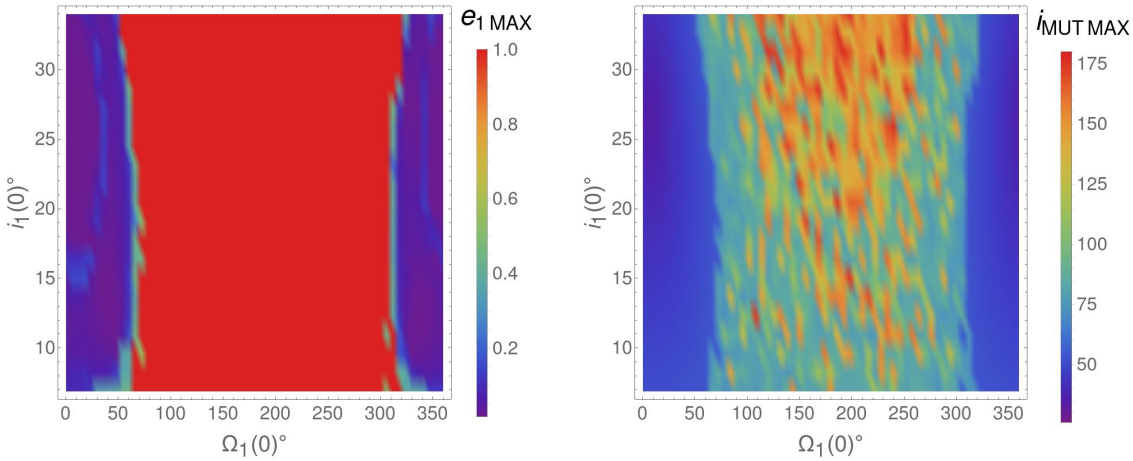

Figure C.5: Colour-grid plot of the maximal value reached by the eccentricity of υ-And **b** (on the left) and by the mutual inclination between υ-And **b** and υ-And **c** (on the right). The maxima are computed during the numerical integrations of the equations of motion (C.13), which define the SQPR model with quasi-periodic approximation of the secular giant planets' motion at order two in the masses (Eq. (C.11)).

D. Dynamics for υ-And b: comparison between the secular Hamiltonian obtained by expansion in powers of eccentricity and scissor-averaging, or multipolar expansion and closed-form averaging

In this appendix we show how the secular quasi-periodic restricted Hamiltonian, introduced in section 4.3, describing the motion of the innermost planet of the υ-Andromedæ system, can be recovered also performing a multipolar expansion jointly with a closed-form averaging (instead of performing an expansion in powers of eccentricity and inclination and a scissor-averaging, adopted in section 4.3). More precisely (following the notations already introduced in Section 4.3), called $\mathcal{H}^{\mathrm{i-j}}$ the Hamiltonian of the three-body problem for the planets i and j $(\mathrm{i} < \mathrm{j})$, i.e., (from Eq. (4.1))

$$\mathcal{H}^{\mathrm{i-j}}(\boldsymbol{r}_{\mathrm{i}}, \boldsymbol{r}_{\mathrm{j}}, \boldsymbol{p}_{\mathrm{i}}, \boldsymbol{p}_{\mathrm{j}}) = \frac{\boldsymbol{p}_{\mathrm{i}}{}^2}{2\,\beta_{\mathrm{i}}} - \frac{\mathcal{G}\,m_0\,m_{\mathrm{i}}}{r_{\mathrm{i}}} + \frac{\boldsymbol{p}_{\mathrm{j}}{}^2}{2\,\beta_{\mathrm{j}}} - \frac{\mathcal{G}\,m_0\,m_{\mathrm{j}}}{r_{\mathrm{j}}} + \frac{\boldsymbol{p}_{\mathrm{i}}\cdot\boldsymbol{p}_{\mathrm{j}}}{m_0} - \frac{\mathcal{G}\,m_{\mathrm{i}}\,m_{\mathrm{j}}}{|\boldsymbol{r}_{\mathrm{i}} - \boldsymbol{r}_{\mathrm{j}}|}\,,$$

it is possible to perform on the previous Hamiltonian 'the closed form averaging' (as already explained in Chapter 2, subsection 2.2.1) according to

$$\mathcal{H}^{\mathrm{i-j}}_{sec} = \frac{1}{4\pi^2}\int_0^{2\pi}\!\!\int_0^{2\pi} \mathcal{H}(\boldsymbol{r}_{\mathrm{i}}, \boldsymbol{r}_{\mathrm{j}}, \boldsymbol{p}_{\mathrm{i}}, \boldsymbol{p}_{\mathrm{j}})\, dM_{\mathrm{i}}\, dM_{\mathrm{j}}\,. \tag{D.1}$$

We recall, from Subsection 2.2.1, that the Keplerian part contributes only to constant terms, while the indirect term $\boldsymbol{p}_{\mathrm{i}}\cdot\boldsymbol{p}_{\mathrm{j}}$ is a zero average term. Instead, the direct part $|\boldsymbol{r}_{\mathrm{i}} - \boldsymbol{r}_{\mathrm{j}}|^{-1}$ is subjected to the multipolar expansion in powers of the small quantity $r_{\mathrm{i}}/r_{\mathrm{j}}$ (where $r_i = |\boldsymbol{r}_i|$ $i = \mathrm{i}, \mathrm{j}$); the order of approximation n of $(r_{\mathrm{i}}/r_{\mathrm{j}})^n$ gives the multipolar order of expansion. This latter averaging can be computed without expansion in the eccentricities, by the change of variables $M_{\mathrm{i}} \to E_{\mathrm{i}}$, $M_{\mathrm{j}} \to f_{\mathrm{j}}$, since

$$dM = (1 - \mathrm{e}\cos E)dE\,, \qquad dM = \frac{r^2}{a^2\sqrt{1-\mathrm{e}^2}}\,df\,, \quad \frac{1}{r} = \frac{1+\mathrm{e}\cos f}{a\,(1-\mathrm{e}^2)}\,. \tag{D.2}$$

Finally, we arrive to a Hamiltonian of the form

$$\mathcal{H}^{\mathrm{i-j}}_{sec} = -\frac{\mathcal{G}m_0m_{\mathrm{i}}}{2\,a_{\mathrm{i}}} - \frac{\mathcal{G}m_0m_{\mathrm{j}}}{2\,a_{\mathrm{j}}} - \frac{\mathcal{G}m_{\mathrm{i}}m_{\mathrm{j}}}{2\,a_{\mathrm{j}}} - \mathcal{R}_{sec}(a_{\mathrm{i}}, a_{\mathrm{j}}, \mathrm{e}_{\mathrm{i}}, \mathrm{e}_{\mathrm{j}}, \mathrm{i}_{\mathrm{i}}, \mathrm{i}_{\mathrm{j}}, \varpi_{\mathrm{i}}, \varpi_{\mathrm{j}}, \Omega_{\mathrm{i}}, \Omega_{\mathrm{j}})\,,$$

where $\mathcal{R}_{sec}$ contains, in the denominator, also powers of eccentricity, in particular of $\sqrt{1-\mathrm{e}_{\mathrm{j}}^2}$ (that comes from $dM_{\mathrm{j}}/df_{\mathrm{j}}$ described in (D.2)). Thus, avoiding Jacobi's reduction of the nodes,

it is now possible to expand the obtained secular Hamiltonian in powers of eccentricity and inclination and to pass to the Poincaré variables $(\boldsymbol{\xi}, \boldsymbol{\eta}, \boldsymbol{P}, \boldsymbol{Q})$ described in (4.2), having $\mathcal{H}^{\mathrm{i-j}}_{sec} = \mathcal{H}^{\mathrm{i-j}}_{sec}(\xi_{\mathrm{i}}, \eta_{\mathrm{i}}, P_{\mathrm{i}}, Q_{\mathrm{i}}, \xi_{\mathrm{j}}, \eta_{\mathrm{j}}, P_{\mathrm{j}}, Q_{\mathrm{j}})$. Now, following the same steps reported in section 4.3, we write the Hamiltonian describing the evolution of the innermost planet as

$$\begin{aligned}\mathcal{H}_{sec,2+\frac{3}{2}}(\boldsymbol{p}, \boldsymbol{q}, \xi_1, \eta_1, P_1, Q_1) = \omega_3\, p_3 + \omega_4\, p_4 + \omega_5\, p_5 \\ + \mathcal{H}^{1-2}_{sec}(\xi_1, \eta_1, P_1, Q_1, \xi_2(\boldsymbol{q}), \eta_2(\boldsymbol{q}), P_2(\boldsymbol{q}), Q_2(\boldsymbol{q})) \\ + \mathcal{H}^{1-3}_{sec}(\xi_1, \eta_1, P_1, Q_1, \xi_3(\boldsymbol{q}), \eta_3(\boldsymbol{q}), P_3(\boldsymbol{q}), Q_3(\boldsymbol{q}))\end{aligned}$$

where $\boldsymbol{q}$ and $\boldsymbol{\omega}$ are given, respectively, by Eq. (4.15) and (4.8).

Now, we want to focus on the part

$$\mathcal{H}_{sec}(\boldsymbol{\xi}, \boldsymbol{\eta}, \boldsymbol{P}, \boldsymbol{Q}) = \mathcal{H}^{1-2}_{sec}(\xi_1, \eta_1, P_1, Q_1, \xi_2, \eta_2, P_2, Q_2) + \mathcal{H}^{1-3}_{sec}(\xi_1, \eta_1, P_1, Q_1, \xi_3, \eta_3, P_3, Q_3)\,, \quad \text{(D.3)}$$

representing the secular Hamiltonian $\mathcal{H}_{sec}$ before substituting the variables $(\xi_j(t), \eta_j(t), P_j(t), Q_j(t))$, $j = 2, 3$ with their quasi-periodic approximation, given in Eq. (4.6). As already remarked, the secular Hamiltonian $\mathcal{H}^{\mathrm{i-j}}_{sec}$ (and, consequently, $\mathcal{H}_{sec}$ and $\mathcal{H}_{sec,2+3/2}$) can be computed performing an expansion in powers of eccentricity and inclination and a scissor-averaging[1] **or** via a multipolar expansion jointly a closed-form averaging; in order to distinguish the two procedures, we call, respectively, the obtained Hamiltonians (D.3) as $\mathcal{H}^{(L)}_{sec}$ and $\mathcal{H}^{(C)}_{sec}$. Moreover, concerning the 'closed-form averaging method', the multipolar expansion of the Hamiltonian can be computed up to a different multipolar order of truncation n; thus, we call $\mathcal{H}^{(C,n)}_{sec}$ the secular Hamiltonian obtained by a multipolar expansion up to order n and a closed-form averaging.

In this Appendix, we want to analyze the differences between the coefficients of $\mathcal{H}^{(L)}_{sec}$ and $\mathcal{H}^{(C,n)}_{sec}$, for different values of the multipolar n, and look at the dynamics of υ-And **b** as obtained by the numerical integrations of the $\mathcal{H}^{(L)}_{sec,2+3/2}$ or $\mathcal{H}^{(C,n)}_{sec,2+3/2}$ vector field.

We observe that, as we increase the multipolar order of approximation n, the accordance between the Hamiltonians $\mathcal{H}^{(L)}_{sec}$ and $\mathcal{H}^{(C,n)}_{sec}$ grows. Indeed, we have produced the Hamiltonian up to multipolar orders of expansion $n = 4, 5, 6, 7$ (called, respectively, $\mathcal{H}^{(C,4)}_{sec}$, $\mathcal{H}^{(C,5)}_{sec}$, $\mathcal{H}^{(C,6)}_{sec}$, $\mathcal{H}^{(C,7)}_{sec}$) and we have compared them with the Hamiltonian $\mathcal{H}^{(L)}_{sec}$. In Table D.1 we report **only** the quadratic part of the differences $\left(\mathcal{H}^{(C,4)}_{sec} - \mathcal{H}^{(L)}_{sec}\right)$, $\left(\mathcal{H}^{(C,5)}_{sec} - \mathcal{H}^{(L)}_{sec}\right)$, $\left(\mathcal{H}^{(C,6)}_{sec} - \mathcal{H}^{(L)}_{sec}\right)$, $\left(\mathcal{H}^{(C,7)}_{sec} - \mathcal{H}^{(L)}_{sec}\right)$, that constitute the dominant part of the dynamics; in particular, called

$$\Delta\mathcal{H}^{(n)}_s := \sum_{\substack{|\boldsymbol{i}|+|\boldsymbol{l}|+\\ |\boldsymbol{m}|+|\boldsymbol{n}|=2s}} d^{(n)}_{\boldsymbol{i},\boldsymbol{l},\boldsymbol{m},\boldsymbol{n}} \prod_{j=1,2} \xi_j^{i_j} \eta_j^{l_j} P_j^{m_j} Q_j^{n_j} + \sum_{\substack{|\boldsymbol{i}|+|\boldsymbol{l}|+\\ |\boldsymbol{m}|+|\boldsymbol{n}|=2s}} \tilde{d}^{(n)}_{\boldsymbol{i},\boldsymbol{l},\boldsymbol{m},\boldsymbol{n}} \prod_{j=1,3} \xi_j^{i_j} \eta_j^{l_j} P_j^{m_j} Q_j^{n_j}\,, \quad \text{(D.4)}$$

where

$$\begin{aligned}\left(\mathcal{H}^{(C,n)}_{sec} - \mathcal{H}^{(L)}_{sec}\right) &= \sum_{s=0}^{\mathcal{N}/2} \left(\sum_{\substack{|\boldsymbol{i}|+|\boldsymbol{l}|+\\ |\boldsymbol{m}|+|\boldsymbol{n}|=2s}} d^{(n)}_{\boldsymbol{i},\boldsymbol{l},\boldsymbol{m},\boldsymbol{n}} \prod_{j=1,2} \xi_j^{i_j} \eta_j^{l_j} P_j^{m_j} Q_j^{n_j} + \sum_{\substack{|\boldsymbol{i}|+|\boldsymbol{l}|+\\ |\boldsymbol{m}|+|\boldsymbol{n}|=2s}} \tilde{d}^{(n)}_{\boldsymbol{i},\boldsymbol{l},\boldsymbol{m},\boldsymbol{n}} \prod_{j=1,3} \xi_j^{i_j} \eta_j^{l_j} P_j^{m_j} Q_j^{n_j} \right) \\ &= \sum_{s=0}^{\mathcal{N}/2} \Delta\mathcal{H}^{(n)}_s\,,\end{aligned}$$

the expressions for $\Delta\mathcal{H}^{(4)}_1$, $\Delta\mathcal{H}^{(5)}_1$, $\Delta\mathcal{H}^{(6)}_1$, $\Delta\mathcal{H}^{(7)}_1$ are reported in Table D.1.

[1] For instance, we can start from the expanded Hamiltonian described in Eq. (C.2), pass to the Poincaré variables $(\boldsymbol{\xi}, \boldsymbol{\eta}, \boldsymbol{P}, \boldsymbol{Q})$ described in Eq. (4.2) and remove from the obtained Hamiltonian the terms depending on the fast angles.

$\Delta\mathcal{H}_1^{(4)}$	$5.79272\cdot10^{-8}\eta_1^2 - 1.37876\cdot10^{-7}\eta_1\eta_2 + 6.57671\cdot10^{-10}\eta_2^2 - 1.01152\cdot10^{-10}\eta_1\eta_3 + 1.51426\cdot10^{-13}\eta_3^2$ $-5.79272\cdot10^{-8}P_1^2 + 1.2343\cdot10^{-8}P_1P_2 - 6.57671\cdot10^{-10}P_2^2 + 2.96845\cdot10^{-12}P_1P_3 - 1.51425\cdot10^{-13}P_3^2$ $-5.79272\cdot10^{-8}Q_1^2 + 1.2343\cdot10^{-8}Q_1Q_2 - 6.57671\cdot10^{-10}Q_2^2 + 2.96845\cdot10^{-12}Q_1Q_3 - 1.51425\cdot10^{-13}Q_3^2$ $+5.79272\cdot10^{-8}\xi_1^2 - 1.37876\cdot10^{-7}\xi_1\xi_2 + 6.57671\cdot10^{-10}\xi_2^2 - 1.01152\cdot10^{-10}\xi_1\xi_3 + 1.51426\cdot10^{-13}\xi_3^2$
$\Delta\mathcal{H}_1^{(5)}$	$5.79272\cdot10^{-8}\eta_1^2 - 9.94811\cdot10^{-10}\eta_1\eta_2 + 6.57671\cdot10^{-10}\eta_2^2 - 7.84046\cdot10^{-14}\eta_1\eta_3 + 1.51426\cdot10^{-13}\eta_3^2$ $-5.79272\cdot10^{-8}P_1^2 + 1.2343\cdot10^{-8}P_1P_2 - 6.57671\cdot10^{-10}P_2^2 + 2.96845\cdot10^{-12}P_1P_3 - 1.51425\cdot10^{-13}P_3^2$ $-5.79272\cdot10^{-8}Q_1^2 + 1.2343\cdot10^{-8}Q_1Q_2 - 6.57671\cdot10^{-10}Q_2^2 + 2.96845\cdot10^{-12}Q_1Q_3 - 1.51425\cdot10^{-13}Q_3^2$ $+5.79272\cdot10^{-8}\xi_1^2 - 9.94811\cdot10^{-10}\xi_1\xi_2 + 6.57671\cdot10^{-10}\xi_2^2 - 7.84046\cdot10^{-14}\xi_1\xi_3 + 1.51426\cdot10^{-13}\xi_3^2$
$\Delta\mathcal{H}_1^{(6)}$	$3.90104\cdot10^{-10}\eta_1^2 - 9.94811\cdot10^{-10}\eta_1\eta_2 + 4.43\cdot10^{-12}\eta_2^2 - 7.84046\cdot10^{-14}\eta_1\eta_3 + 1.09707\cdot10^{-16}\eta_3^2$ $-3.90104\cdot10^{-10}P_1^2 + 8.31413\cdot10^{-11}P_1P_2 - 4.43\cdot10^{-12}P_2^2 + 2.14754\cdot10^{-15}P_1P_3 - 1.0955\cdot10^{-16}P_3^2$ $-3.90104\cdot10^{-10}Q_1^2 + 8.31413\cdot10^{-11}Q_1Q_2 - 4.43\cdot10^{-12}Q_2^2 + 2.14754\cdot10^{-15}Q_1Q_3 - 1.0955\cdot10^{-16}Q_3^2$ $+3.90104\cdot10^{-10}\xi_1^2 - 9.94811\cdot10^{-10}\xi_1\xi_2 + 4.43\cdot10^{-12}\xi_2^2 - 7.84046\cdot10^{-14}\xi_1\xi_3 + 1.09707\cdot10^{-16}\xi_3^2$
$\Delta\mathcal{H}_1^{(7)}$	$3.90104\cdot10^{-10}\eta_1^2 - 6.55238\cdot10^{-12}\eta_1\eta_2 + 4.43\cdot10^{-12}\eta_2^2 - 5.56491\cdot10^{-17}\eta_1\eta_3 + 1.09707\cdot10^{-16}\eta_3^2$ $-3.90104\cdot10^{-10}P_1^2 + 8.31413\cdot10^{-11}P_1P_2 - 4.43\cdot10^{-12}P_2^2 + 2.14754\cdot10^{-15}P_1P_3 - 1.0955\cdot10^{-16}P_3^2$ $-3.90104\cdot10^{-10}Q_1^2 + 8.31413\cdot10^{-11}Q_1Q_2 - 4.43\cdot10^{-12}Q_2^2 + 2.14754\cdot10^{-15}Q_1Q_3 - 1.0955\cdot10^{-16}Q_3^2$ $+3.90104\cdot10^{-10}\xi_1^2 - 6.55238\cdot10^{-12}\xi_1\xi_2 + 4.43\cdot10^{-12}\xi_2^2 - 5.56491\cdot10^{-17}\xi_1\xi_3 + 1.09707\cdot10^{-16}\xi_3^2$

Table D.1: Quadratic part of the difference between the Hamiltonians obtained in 'closed-form averaging' $\mathcal{H}_{sec}^{(C,n)}$ (from the first to the last row, respectively, up to multipolar order 4, 5, 6, 7) and the Hamiltonian $\mathcal{H}_{sec}^{(L)}$ expanded in powers of eccentricity and inclinations, using Laplace coefficients, and scissoring the fast angles.

In order to quantify the accordance between the two types of Hamiltonian, we are interested to compute the maximal coefficients, in absolute value, of the above described quantities $\Delta\mathcal{H}_1^{(n)}$, $n = 4, \dots, 7$; i.e. (from Eq. (D.4)), we define

$$\Delta d_s^{(n)} = \max_{\mathcal{I}}\{|d^{(n)}_{\boldsymbol{i},\boldsymbol{l},\boldsymbol{m},\boldsymbol{n}}|\,, |\tilde{d}^{(n)}_{\boldsymbol{i},\boldsymbol{l},\boldsymbol{m},\boldsymbol{n}}|\}\,,$$

where $\mathcal{I} = \{(\boldsymbol{i},\boldsymbol{l},\boldsymbol{m},\boldsymbol{n}) \in \mathbb{N} : |\boldsymbol{i}|+|\boldsymbol{l}|+|\boldsymbol{m}|+|\boldsymbol{n}| = 2s\}$ and, from Table D.1, we can compute $\Delta d_1^{(n)}$, $n = 4, \dots, 7$. However, despite the fact that $\Delta\mathcal{H}_1^{(n)}$ is the dominant part constituting the difference between the Hamiltonians, other terms are involved; in particular, we have also to compute $\Delta\mathcal{H}_s^{(n)}$, $s = 1, \dots, \mathcal{N}/2$ and, consequently, $\Delta d_s^{(n)}$, with $n = 4, \dots, 7$ and $s = 1, \dots, \mathcal{N}/2$. Having fixed the order of expansion in powers of eccentricity and inclination $\mathcal{N} = 8$, we compute (and report in Table D.2) the quantities $\Delta d_s^{(n)}$, with $n = 4, \dots, 7$ and $s = 1, \dots, 4$.

$\Delta d_1^{(4)} : 1.37876\cdot10^{-7}$	$\Delta d_1^{(5)} : 5.79272\cdot10^{-8}$	$\Delta d_1^{(6)} : 9.94811\cdot10^{-10}$	$\Delta d_1^{(7)} : 3.90104\cdot10^{-10}$
$\Delta d_2^{(4)} : 4.70006\cdot10^{-5}$	$\Delta d_2^{(5)} : 4.70006\cdot10^{-5}$	$\Delta d_2^{(6)} : 4.83136\cdot10^{-7}$	$\Delta d_2^{(7)} : 4.83136\cdot10^{-7}$
$\Delta d_3^{(4)} : 5.97175\cdot10^{-3}$	$\Delta d_3^{(5)} : 3.4579\cdot10^{-3}$	$\Delta d_3^{(6)} : 1.33901\cdot10^{-4}$	$\Delta d_3^{(7)} : 6.27007\cdot10^{-5}$
$\Delta d_4^{(4)} : 0.519394$	$\Delta d_4^{(5)} : 0.519394$	$\Delta d_4^{(6)} : 0.0182941$	$\Delta d_4^{(7)} : 0.0147369$

Table D.2: In the table are reported the maximal coefficients (in absolute value) of $\Delta\mathcal{H}_s^{(n)}$, called $\Delta d_s^{(n)}$. We consider (from left to right) different multipolar orders of truncation, and (from above to below) different power dependences of the Hamiltonians on the variables. We observe, from the first row, that the larger the order of the multipolar expansion (from left to right), the less the error on the quadratic part of the Hamiltonian. The same phenomena occurs in all other rows of the table.

In particular each column of Table D.2 corresponds to a fixed multipolar order n $(= 4, \dots, 7)$, while each row corresponds to a fixed power degree dependence of the Hamiltonian s $(= 1, \dots, 4)$.

Looking at the Table, we can see, in the first column, the maximal coefficients corresponding to multipolar order $n = 4$. The error grows going from the top to the bottom, i.e. the difference between the two Hamiltonians become as much larger as we increase the degree (on the variables $(\boldsymbol{\xi}, \boldsymbol{\eta}, \boldsymbol{P}, \boldsymbol{Q})$) of the Hamiltonian; on the other hand, fixed a row, the error become smaller passing from left to right, i.e. it became as much smaller increasing the multipolar order of truncation. Thus, we can conclude that the more we increase the multipolar order of truncation n, the better is the agreement between the two Hamiltonians.

Finally, we can repeat the same work already explained in Section 4.3, writing the $2 + 3/2$ degrees of freedom Hamiltonian:

$$\mathcal{H}^{(C,n)}_{sec,2+\frac{3}{2}}(\boldsymbol{p}, \boldsymbol{q}, \xi_1, \eta_1, P_1, Q_1) = \mathcal{H}^{(C,n)}_{sec}(\boldsymbol{p}, \boldsymbol{q}, \xi_1, \eta_1, P_1, Q_1) + \omega_3\, p_3 + \omega_4\, p_4 + \omega_5\, p_5\,, \tag{D.5}$$

where $\mathcal{H}^{(C,n)}_{sec}$ has been computed through the multipolar expansion and with the closed form averaging up to multipolar order n. More precisely, $\mathcal{H}^{(C,n)}_{sec}$ is given by Eq. (D.3), where $(\xi_2(t), \eta_2(t), P_2(t), Q_2(t))$ and $(\xi_3(t), \eta_3(t), P_3(t), Q_3(t))$ are substituted by their quasi-periodic approximation, explicitely reported in (4.6).

Fixing the order of expansion to $\mathcal{N} = 8$, we now numerically integrate the Hamiltonian vector field corresponding to (D.5), for instance, in the cases of multipolar order $n = 5$ and $n = 6$, taking, mass $m_1 = 0.674$, as initial orbital parameters for υ-And **b**, a, e, M and ω the ones reported in Table 4.7 and $(\mathrm{i}, \Omega) \in I_{\mathrm{i}} \times I_\Omega = [6.865°, 34°] \times [0°, 360°)$. The color-grid plots of the maximal value reached by the eccentricity of υ-And **b** in the cases $n = 5$, 6 are shown, respectively, in the left and right panel of Figure D.1; first of all, we can observe that a good global agreement between the two pictures. This means that arriving to order $n = 5$ or $n = 6$ produces the same global dynamics. Moreover, we can compare the two color grid plots with Figure 4.6a of Subsection 4.3.1.2 (where $\mathcal{H}^{(L)}_{sec,2+3/2}$ has been used); it is evident that, for the external region of the domain of definition of Ω_1, we have the same global behaviour. Instead, some differences arise in the internal region, that is characterized by higher values of the eccentricity.

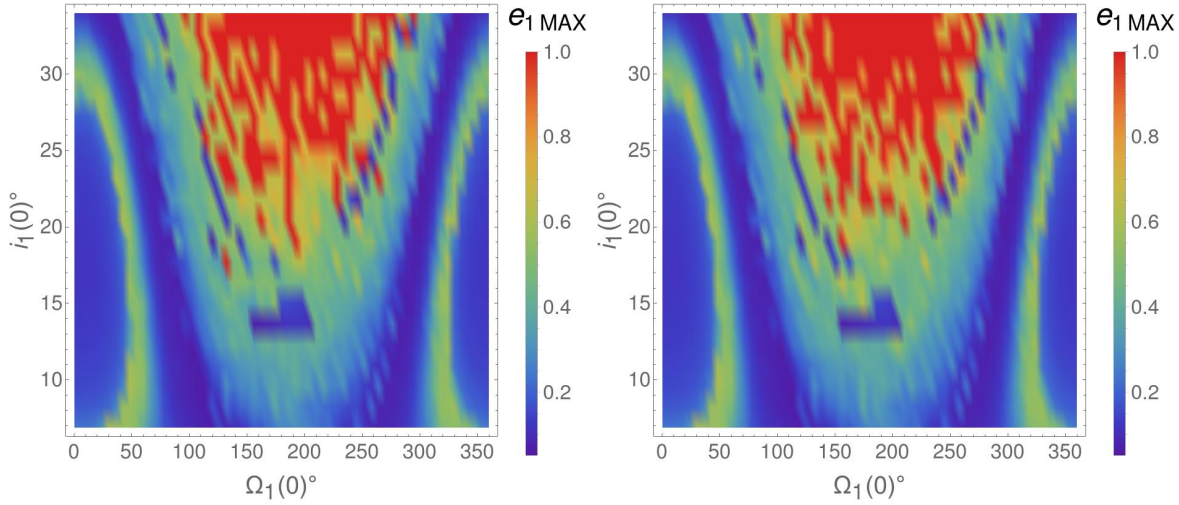

Figure D.1: Colour-grid plot of the maximal value reached by the eccentricity of υ-And **b** with an integration over 10^5 yr, taking as secular Hamiltonian the one obtained in closed form averaging up to multipolar order 5, $\mathcal{H}^{(C,5)}_{sec,2+3/2}$, on the left, and up to multipolar order 6, $\mathcal{H}^{(C,6)}_{sec,2+3/2}$, on the right.

Finally, fixing the multipolar order of expansion (e.g. at $n = 6$) it is also possible to change the order of expansion $\mathcal{N}$, passing it from 8 to 10. As before, some little differences arise only in the internal region of the pictures; the comparison is shown in Figure D.2.

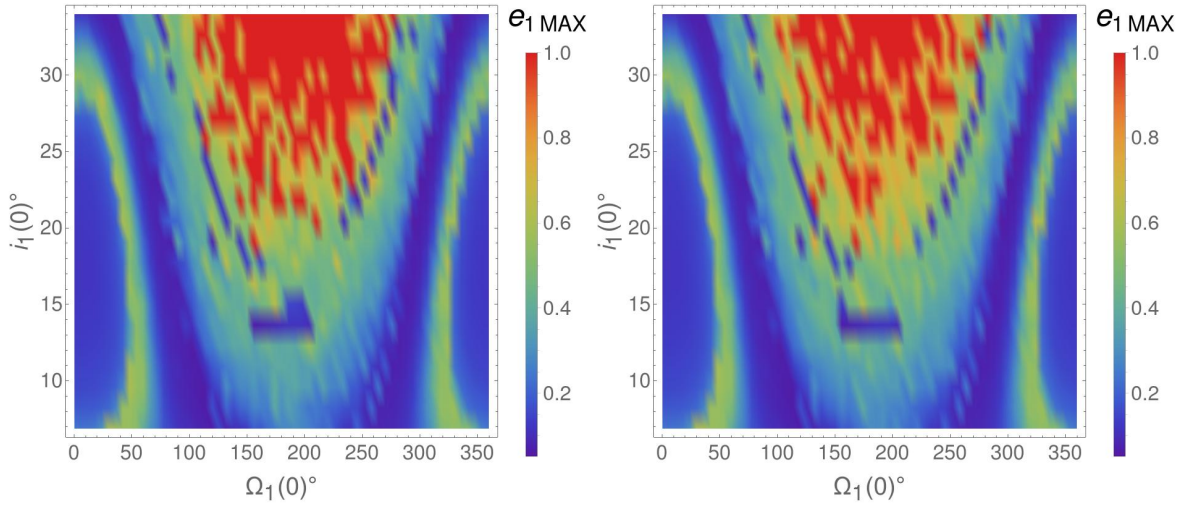

Figure D.2: Colour-grid plot of the maximal value reached by the eccentricity of υ-And **b** with an integration over 10^5 yr, taking as secular Hamiltonian the one obtained in closed form averaging up to multipolar order 6 , $\mathcal{H}^{(C,6)}_{sec,2+3/2}$, expanded up to order $\mathcal{N}$ in powers of the eccentricity and inclination, equal to $\mathcal{N} = 8$ on the left, and $\mathcal{N} = 10$, on the right.

Thus we can conclude that, considering $\mathcal{N} = 8$ is sufficient to recover the global dynamics of υ-And **b** .

E. Secular relativistic corrections

Let us start considering the Hamiltonian of a 2-body problem with GR (general relativistic) corrections, called $\mathcal{H}_{GR}$; following Richardson & Kelly [96], it is possible to rescale it for the reduced mass $\beta = m_0\, m/(m_0 + m)$, having $\widetilde{\mathcal{H}}_{GR} = \mathcal{H}_{GR}/\beta$, described by

$$\widetilde{\mathcal{H}}_{GR}(\boldsymbol{p},\boldsymbol{r}) = -\frac{1}{c^2}\left[\sigma_0\big(\boldsymbol{p}\cdot\boldsymbol{p}\big)^2 + \frac{\sigma_1}{r}\big(\boldsymbol{p}\cdot\boldsymbol{p}\big) + \frac{\sigma_2}{r^2} + \frac{\sigma_3}{r^3}\big(\boldsymbol{r}\cdot\boldsymbol{p}\big)^2\right], \tag{E.1}$$

where r $(= ||\boldsymbol{r}||)$ and $\boldsymbol{p}$ are, respectively, the astrocentric distance and momentum (normalized by β) of the planet, c the speed of the light in vacuum and with the following constants defined:

$$\sigma_0 = \frac{1-3\sigma}{8}\,, \qquad \sigma_1 = \frac{\mu\big(3+\sigma\big)}{2}\,, \qquad \sigma_2 = -\frac{\mu^2}{2}\,, \qquad \sigma_3 = \frac{\mu\sigma}{2}\,, \tag{E.2}$$

with

$$\mu = \mathcal{G}\big(m_0 + m\big)\,, \qquad\qquad \sigma = \frac{m_0\, m}{\big(m_0+m\big)^2}\,. \tag{E.3}$$

We are interested in computating of the secular general relativitic correction. To this end, let us remember, from [96], that the normalized astrocentric momentum is related to the astrocentric velocity through the following relation:

$$\boldsymbol{p} = \dot{\boldsymbol{r}} + \frac{1}{c^2}\left[4\sigma_0\big(\dot{\boldsymbol{r}}\cdot\dot{\boldsymbol{r}}\big)\dot{\boldsymbol{r}} + \frac{2\sigma_1}{r}\dot{\boldsymbol{r}} + \frac{2\sigma_3}{r^3}\big(\boldsymbol{r}\cdot\dot{\boldsymbol{r}}\big)\boldsymbol{r}\right] = \dot{\boldsymbol{r}} + \mathcal{O}\left(\frac{1}{c^2}\right). \tag{E.4}$$

Thus, by the previous expression (E.4), let us observe that it is sufficient to put $\boldsymbol{p} = \dot{\boldsymbol{r}}$ in the Hamiltonian (E.1) so to preserve it up to order $\mathcal{O}\left(1/c^4\right)$. In order to compute the secular GR contributions we need to compute the mean, over the fast angle, of (E.1), i.e.

$$\begin{aligned}\left\langle \widetilde{\mathcal{H}}_{GR}\right\rangle &:= \frac{1}{2\pi}\int_0^{2\pi} \widetilde{\mathcal{H}}_{GR}(\boldsymbol{p},\boldsymbol{r})\, dM \qquad\qquad (E.5)\\ &= -\frac{1}{2\pi\, c^2}\left[\sigma_0\int_0^{2\pi}\big(\boldsymbol{p}\cdot\boldsymbol{p}\big)^2\, dM + \sigma_1\int_0^{2\pi}\frac{\boldsymbol{p}\cdot\boldsymbol{p}}{r}\, dM + \sigma_2\int_0^{2\pi}\frac{1}{r^2}\, dM + \sigma_3\int_0^{2\pi}\frac{\big(\boldsymbol{r}\cdot\boldsymbol{p}\big)^2}{r^3}\, dM\right].\end{aligned}$$

Following Migaszewski & Goździewski [82], it is possible to compute the previous secular terms in *closed-form* by the change of variable $M \to f$, expressed by

$$dM = \frac{r^2}{a^2\sqrt{1-\mathrm{e}^2}}\, df\,, \quad \frac{1}{r} = \frac{1+\mathrm{e}\cos f}{a\,(1-\mathrm{e}^2)} \qquad \Rightarrow \qquad dM = \frac{(1-\mathrm{e}^2)^{3/2}}{(1+\mathrm{e}\cos f)^2}\, df\,. \tag{E.6}$$

Moreover, remembering the epressions for the astrocentric position $\boldsymbol{r} = (X, Y, 0)$ and velocity $\dot{\boldsymbol{r}} := \boldsymbol{v} = (v_X, v_Y, 0)$ given by[1]

$$X = r\,\cos f\,, \quad Y = r\,\sin f\,, \quad v_X = -\frac{n\,a}{\sqrt{1-\mathrm{e}^2}}\sin f\,, \quad v_Y = \frac{n\,a}{\sqrt{1-\mathrm{e}^2}}\,(\mathrm{e}+\cos f)\,,$$

(with n is the mean motion, given in Eq. (1.14), $n = dM/dt = \sqrt{\mu/a^3}$), the terms composing (E.5) can be computed as:

$$\begin{aligned}
i)\ \ &\frac{1}{2\pi}\int_0^{2\pi}\left(\boldsymbol{p}\cdot\boldsymbol{p}\right)^2 dM = \frac{1}{2\pi}\int_0^{2\pi}\left(v_X^2+v_Y^2\right)^2 dM = \frac{a^4n^4}{\sqrt{1-\mathrm{e}^2}}\left(\frac{1}{2\pi}\int_0^{2\pi}\left(\frac{1+\mathrm{e}^2+2\mathrm{e}\cos f}{1+\mathrm{e}\cos f}\right)^2 df\right)\\
&\qquad = a^4n^4\left(-3+\frac{4}{\sqrt{1-\mathrm{e}^2}}\right),\\
ii)\ \ &\frac{1}{2\pi}\int_0^{2\pi}\frac{\boldsymbol{p}\cdot\boldsymbol{p}}{r}\,dM = \frac{1}{2\pi}\int_0^{2\pi}\frac{v_X^2+v_Y^2}{r}\,dM = \frac{a\,n^2}{\sqrt{1-\mathrm{e}^2}}\left(\frac{1}{2\pi}\int_0^{2\pi}\left(\frac{1+\mathrm{e}^2+2\mathrm{e}\cos f}{1+\mathrm{e}\cos f}\right)df\right)\\
&\qquad = a\,n^2\left(-1+\frac{2}{\sqrt{1-\mathrm{e}^2}}\right),\\
iii)\ \ &\frac{1}{2\pi}\int_0^{2\pi}\frac{1}{r^2}\,dM = \frac{1}{2\pi}\int_0^{2\pi}\frac{1}{r^2}\frac{r^2}{a^2\sqrt{1-\mathrm{e}^2}}\,df = \frac{1}{a^2\sqrt{1-\mathrm{e}^2}}\,,\\
iv)\ \ &\frac{1}{2\pi}\int_0^{2\pi}\frac{(\boldsymbol{r}\cdot\boldsymbol{p})^2}{r^3}\,dM = \frac{1}{2\pi}\int_0^{2\pi}\frac{(Xv_X+Yv_Y)^2}{r^3}\,dM = \frac{a\,n^2\mathrm{e}^2}{\sqrt{1-\mathrm{e}^2}}\left(\frac{1}{2\pi}\int_0^{2\pi}\frac{(\sin f)^2}{1+\mathrm{e}\cos f}\,df\right) =\\
&\qquad = a\,n^2\left(-1+\frac{1}{\sqrt{1-\mathrm{e}^2}}\right).
\end{aligned}$$

Inserting the previous expressions $i)-iv)$ in the Hamiltonian (E.5), we arrive at

$$\left\langle\widetilde{\mathcal{H}}_{GR}\right\rangle = -\frac{3\mu^2}{a^2c^2\sqrt{1-\mathrm{e}^2}} + \frac{\mu^2(15-\sigma)}{8a^2c^2}\,, \tag{E.7}$$

that is in accordance with Eq. (28) of Migaszewski & Goździewski [82] and, passing to the canonical Delaunay variables, with Eq. (23) of Richardson & Kelly [96]. Finally, the secular general relativistic correction is given by

$$\langle\mathcal{H}_{GR}\rangle = \beta\left\langle\widetilde{\mathcal{H}}_{GR}\right\rangle = -\frac{3\mu^2\beta}{a^2c^2\sqrt{1-\mathrm{e}^2}} + \frac{\mu^2\beta(15-\sigma)}{8a^2c^2}\,; \tag{E.8}$$

in the restricted framework, it is possible to approximate the constant parameters β and μ as $\beta \sim m$ and $\mu \sim \mathcal{G}m_0$, having

$$\langle\mathcal{H}_{GR}\rangle = -\frac{3\,\mathcal{G}^2\,m_0^2\,m}{a^2c^2\sqrt{1-\mathrm{e}^2}} + \frac{15\,\mathcal{G}^2\,m_0^2\,m}{8a^2c^2} - \frac{\mathcal{G}^2\,m_0\,m^2}{8a^2c^2}\,, \tag{E.9}$$

that, apart for the last constant terms, is in accordance with Mogavero & Laskar [84]. Thus, in order to give the secular GR corrections in terms of the Poincaré variables (ξ, η, P, Q) (given by Eq. (4.2)), we need to perform an expansion of the denominator in power of the eccentricity; for example[2], it is possible to substitute $\sqrt{1-\mathrm{e}^2}$ in terms of modified Delaunay variables, i.e. $\sqrt{1-\mathrm{e}^2} = 1-\Gamma/\Lambda$

[1] The following formulæ can be found in [87]. Alternatively, we know, from Eq. (1.12), that $X = r\,\cos f$ and $Y = r\,\sin f$; thus, it is possible to compute v_X as $\dfrac{dX}{dt} = \dfrac{dX}{df}\dfrac{df}{dM}\dfrac{dM}{dt}$, using Eqs. (E.6) and (1.14). Analogously for v_Y.

[2] Another (equivalent) possibility is to expand (E.9) with respect to e and then replace it, first, in terms of the modified Delaunay variables and then of the Poincaré variables.

and (remembering that $\Gamma = \mathcal{O}(\mathrm{e}^2)$) expand with respect to $\sqrt{\Gamma}$. The Hamiltonian, up to order 8 in eccentricity, become

$$\langle \mathcal{H}_{GR} \rangle = \frac{15\,\mathcal{G}^2\,m_0^2\,m}{8a^2c^2} - \frac{\mathcal{G}^2\,m_0\,m^2}{8a^2c^2} - \frac{3\,\mathcal{G}^2\,m_0^2\,m}{a^2c^2}\left(1 + \frac{\Gamma}{\Lambda} + \frac{\Gamma^2}{\Lambda^2} + \frac{\Gamma^3}{\Lambda^3} + \frac{\Gamma^4}{\Lambda^4}\right); \tag{E.10}$$

it is now sufficients to replace $\Gamma = (\xi^2 + \eta^2)/2$ to have the secular GR correction in Poincaré variables, observing that it depends only on the variables (ξ, η).

F. Examples and technicalities concerning KAM theory for isochronous systems

F.1 Example – 1DOF Hamiltonian with an odd (cubic) degree dependence on x

Consider the following one-degree of freedom Hamiltonian, with odd power dependence on the variable x

$$\mathcal{H}(x,p) = \frac{\omega_0}{2}\left(p^2 + x^2\right) - \varepsilon\frac{x^3}{3}\,. \tag{F.1}$$

We pass to action-angle variables $(J,\, q)$ through the transformation $x = \sqrt{2J}\sin(q)\,,\, p = \sqrt{2J}\cos(q)\,,$ obtaining

$$\mathcal{H}(q,J) = \omega_0\, J - \frac{\varepsilon}{\sqrt{2}}J^{3/2}\sin(q) + \frac{\varepsilon}{3\sqrt{2}}J^{3/2}\sin(3q)\,. \tag{F.2}$$

Finally, we define the translation $J = J_0 + p$ leading to (apart from constants)

$$\mathcal{H}(q,p) = \omega_0\, p - \frac{\varepsilon}{\sqrt{2}}(J_0+p)^{3/2}\sin(q) + \frac{\varepsilon}{3\sqrt{2}}(J_0+p)^{3/2}\sin(3q)\,. \tag{F.3}$$

Since the variable $J = J_0 + p$ appears in the above Hamiltonian in half-integer powers, we expand the Hamiltonian in powers of the variable p up to the same order as the maximum normalization order in ε. This proves to be sufficient since higher powers of p only influence the process at powers (in the book keeping order) higher than the maximum normalization order. In particular, the following lemma can be easily proved:

Lemma 1. *Let $\mathcal{H}(q,J) = \omega_0\, J + \varepsilon\, h(q,J)\,,$ where $h = \mathcal{O}(J^{\frac{k}{2}})$ $k \geq 3\,.$ Then, for all $n \geq 1$ (with $n =$ number of normalization steps) $\chi_1^{(n)} = \mathcal{O}\left(J_0^{\frac{(k-2)n+2}{2}}\right)$ and $\chi_2^{(n)} = \mathcal{O}\left(J_0^{\frac{(k-2)n}{2}}\right)\,.$*

Proof. For the proof, see the appendix F.2. □

We will now illustrate the method by computing the direct (Lindstedt) and indirect (Kolmogorov) series up to order 3 in ε in the example above (the reason for reaching order 3 instead of 2 will become clear below). Starting from the Hamiltonian (F.3) we perform an expansion in p

leading to (apart from constants)

$$\mathcal{H}(q,p) = \omega_0\, p - \frac{\varepsilon\, J_0^{3/2}}{\sqrt{2}}\, \sin(q) - \frac{3\,\varepsilon\,\sqrt{J_0}}{2\,\sqrt{2}}\, p\, \sin(q) - \frac{3\,\varepsilon}{8\,\sqrt{2}\,\sqrt{J_0}}\, p^2\, \sin(q) + \frac{\varepsilon}{16\,\sqrt{2}\,J_0^{3/2}}\, p^3\, \sin(q) + \frac{\varepsilon\, J_0^{3/2}}{3\,\sqrt{2}}\, \sin(3q) + \frac{\varepsilon\,\sqrt{J_0}}{2\,\sqrt{2}}\, p\, \sin(3q) + \frac{\varepsilon}{8\,\sqrt{2}\,\sqrt{J_0}}\, p^2\, \sin(3q) - \frac{\varepsilon}{48\,\sqrt{2}\,J_0^{3/2}}\, p^3\, \sin(3q)\,. \tag{F.4}$$

F.1.1 Lindstedt series analogous to Kolmogorov

Following the same procedure as in subsection 7.3.3, we start with the equations of motion under the Hamiltonian (F.2)

$$\begin{cases} \dot{q}(t) = \dfrac{\partial \mathcal{H}}{\partial J} = \omega_0 - \dfrac{3\,\varepsilon\,\sqrt{J}}{2\,\sqrt{2}}\, \sin(q) + \dfrac{\varepsilon\,\sqrt{J}}{2\,\sqrt{2}}\, \sin(3q) & \text{(F.5a)} \\ \dot{J}(t) = -\dfrac{\partial \mathcal{H}}{\partial q} = \dfrac{\varepsilon\, J^{3/2}}{\sqrt{2}}\, \cos(q) - \dfrac{\varepsilon\, J^{3/2}}{\sqrt{2}}\, \cos(3q)\,. & \text{(F.5b)} \end{cases}$$

Replacing, as before, the expressions

$$\begin{aligned} \omega_0 &= \omega + \varepsilon\, a_1 + \varepsilon^2\, a_2 + \varepsilon^3\, a_3\,, \\ q(t) &= q_0(t) + \varepsilon\, q_1(t) + \varepsilon^2\, q_2(t) + \varepsilon^3\, q_3(t)\,, \\ J(t) &= J_0(t) + \varepsilon J_1(t) + \varepsilon^2 J_2(t) + \varepsilon^3 J_3(t)\,, \end{aligned} \tag{F.6}$$

into the equations of motion and performing an expansion up to order 3 in ε (having fixed ω) we compare terms of like orders in ε in the l.h.s and r.h.s of (F.5a) and (F.5b). At order zero we have

$$\dot{q_0}(t) = \omega\,, \qquad \dot{J}_0(t) = 0 \quad \Longrightarrow \quad q_0(t) = \omega\, t\,, \qquad J_0(t) = J_0\,,$$

where we fix the initial phase $q_0(0) = 0$ and $J_0(0) = J_0$. At order one, we find

$$\begin{aligned} \dot{q_1}(t) &= a_1 - \frac{3\,\sqrt{J_0}}{2\,\sqrt{2}}\, \sin(\omega\, t) + \frac{\sqrt{J_0}}{2\,\sqrt{2}}\, \sin(3\,\omega\, t), \\ \dot{J}_1(t) &= \frac{J_0^{3/2}}{\sqrt{2}}\, \cos(\omega\, t) - \frac{J_0^{3/2}}{\sqrt{2}}\, \cos(3\,\omega\, t)\,. \end{aligned} \tag{F.7}$$

Since no constant terms arise in $\dot{q_1}(t)$, we have that $a_1 = 0$. Then

$$q_1(t) = -\frac{2\,\sqrt{2}\,\sqrt{J_0}}{3\,\omega} + \frac{3\,\sqrt{J_0}}{2\,\sqrt{2}\,\omega}\, \cos(\omega\, t) - \frac{\sqrt{J_0}}{6\,\sqrt{2}\,\omega}\, \cos(3\,\omega\, t)\,, \quad J_1(t) = \frac{J_0^{3/2}}{\sqrt{2}\,\omega}\, \sin(\omega\, t) - \frac{J_0^{3/2}}{3\,\sqrt{2}\,\omega}\, \sin(3\,\omega\, t)$$

yielding the constants $q_1(0) = J_1(0) = 0$. At order two we now get

$$\begin{aligned} \dot{q_2}(t) &= a_2 - \frac{5\,J_0}{6\,\omega} + \frac{J_0}{\omega}\, \cos(\omega\, t) + \frac{3\,J_0}{8\,\omega}\, \cos(2\,\omega\, t) - \frac{J_0}{\omega}\, \cos(3\,\omega\, t) + \frac{J_0}{2\,\omega}\, \cos(4\,\omega\, t) - \frac{J_0}{24\,\omega}\, \cos(6\,\omega\, t), \\ \dot{J}_2(t) &= \frac{2\,J_0^2}{3\,\omega}\, \sin(\omega\, t) + \frac{4\,J_0^2}{3\,\omega}\, \sin(2\,\omega\, t) - \frac{2\,J_0^2}{\omega}\, \sin(3\,\omega\, t) + \frac{2\,J_0^2}{3\,\omega}\, \sin(4\,\omega\, t)\,; \end{aligned} \tag{F.8}$$

To compensate for the constant term in $\dot{q_2}(t)$ we now set $a_2 = 5\,J_0/(6\,\omega)$. Then,

$$\begin{aligned} q_2(t) &= \frac{J_0}{\omega^2}\, \sin(\omega\, t) + \frac{3\,J_0}{16\,\omega^2}\, \sin(2\,\omega\, t) - \frac{J_0}{3\,\omega^2}\, \sin(3\,\omega\, t) + \frac{J_0}{8\,\omega^2}\, \sin(4\,\omega\, t) - \frac{J_0}{144\,\omega^2}\, \sin(6\,\omega\, t), \\ J_2(t) &= \frac{5\,J_0^2}{6\,\omega^2} - \frac{2\,J_0^2}{3\,\omega^2}\, \cos(\omega\, t) - \frac{2\,J_0^2}{3\,\omega^2}\, \cos(2\,\omega\, t) + \frac{2\,J_0^2}{3\,\omega^2}\, \cos(3\,\omega\, t) - \frac{J_0^2}{6\,\omega^2}\, \cos(4\,\omega\, t)\,. \end{aligned} \tag{F.9}$$

In a similar way, at order 3 we find $a_3 = 0$, and the solutions

$$
\begin{aligned}
q(t) = {} & \omega\, t - \frac{2\sqrt{2}\,\varepsilon\sqrt{J_0}}{3\,\omega} + \frac{3\,\varepsilon\sqrt{J_0}}{2\sqrt{2}\,\omega}\,\cos(\omega\, t) - \frac{\varepsilon\sqrt{J_0}}{6\sqrt{2}\,\omega}\,\cos(3\,\omega\, t) + \frac{\varepsilon^2\,J_0}{\omega^2}\,\sin(\omega\, t) + \frac{3\,\varepsilon^2\,J_0}{16\,\omega^2}\,\sin(2\,\omega\, t) \\
& - \frac{\varepsilon^2\,J_0}{3\,\omega^2}\,\sin(3\,\omega\, t) + \frac{\varepsilon^2\,J_0}{8\,\omega^2}\,\sin(4\,\omega\, t) - \frac{\varepsilon^2\,J_0}{144\,\omega^2}\,\sin(6\,\omega\, t) - \frac{38\sqrt{2}\,\varepsilon^3\,J_0^{3/2}}{81\omega^3} + \frac{\varepsilon^3\,J_0^{3/2}}{\sqrt{2}\,\omega^3}\,\cos(\omega\, t) \\
& - \frac{\varepsilon^3\,J_0^{3/2}}{2\sqrt{2}\,\omega^3}\,\cos(2\,\omega\, t) + \frac{145\,\varepsilon^3\,J_0^{3/2}}{144\sqrt{2}\,\omega^3}\,\cos(3\,\omega\, t) - \frac{\sqrt{2}\,\varepsilon^3\,J_0^{3/2}}{3\,\omega^3}\,\cos(4\,\omega\, t) + \frac{\varepsilon^3\,J_0^{3/2}}{16\sqrt{2}\,\omega^3}\,\cos(5\,\omega\, t) \\
& + \frac{\varepsilon^3\,J_0^{3/2}}{18\sqrt{2}\,\omega^3}\,\cos(6\,\omega\, t) - \frac{\varepsilon^3\,J_0^{3/2}}{48\sqrt{2}\,\omega^3}\,\cos(7\,\omega\, t) + \frac{\varepsilon^3\,J_0^{3/2}}{1296\sqrt{2}\,\omega^3}\,\cos(9\,\omega\, t)\,, \\
J(t) = {} & J_0 + \frac{\varepsilon\,J_0^{3/2}}{\sqrt{2}\,\omega}\,\sin(\omega\, t) - \frac{\varepsilon\,J_0^{3/2}}{3\sqrt{2}\,\omega}\,\sin(3\,\omega\, t) + \frac{5\,\varepsilon^2\,J_0^2}{6\,\omega^2} - \frac{2\,\varepsilon^2\,J_0^2}{3\,\omega^2}\,\cos(\omega\, t) - \frac{2\,\varepsilon^2\,J_0^2}{3\,\omega^2}\,\cos(2\,\omega\, t) \\
& + \frac{2\,\varepsilon^2\,J_0^2}{3\,\omega^2}\,\cos(3\,\omega\, t) - \frac{\varepsilon^2\,J_0^2}{6\,\omega^2}\,\cos(4\,\omega\, t) + \frac{7\,\varepsilon^3\,J_0^{5/2}}{4\sqrt{2}\,\omega^3}\,\sin(\omega\, t) - \frac{8\sqrt{2}\,\varepsilon^3\,J_0^{5/2}}{9\,\omega^3}\,\sin(2\,\omega\, t) \\
& + \frac{13\,\varepsilon^3\,J_0^{5/2}}{8\sqrt{2}\,\omega^3}\,\sin(3\,\omega\, t) - \frac{4\sqrt{2}\,\varepsilon^3\,J_0^{5/2}}{9\,\omega^3}\,\sin(4\,\omega\, t) + \frac{7\,\varepsilon^3\,J_0^{5/2}}{72\sqrt{2}\,\omega^3}\,\sin(5\,\omega\, t)\,, \\
\omega = {} & \omega_0 - \frac{5\,\varepsilon^2 J_0}{6\,\omega}\,.
\end{aligned}
\tag{F.10}
$$

F.1.2 Kolmogorov normal form

Starting from the Hamiltonian (F.4), we perform canonical transformations in order to bring the Hamiltonian into Kolmogorov normal form, i.e., $\mathcal{H}(q,p) = \omega\, p + \varepsilon\, R_1(q,\,p) + \varepsilon^2\, R_2(q,\,p) + \varepsilon^3\, R_3(q,\,p)$ where $R_i(q,\,p) = \mathcal{O}(||\,p\,||^2)$ $i = 1,\,2,\,3$. Substituting, as in Section 7.3, the expression $\omega_0 = \omega + \varepsilon\, a_1 + \varepsilon^2\, a_2 + \varepsilon^3\, a_3$ in the Hamiltonian (F.4), we have

$$
\begin{aligned}
\mathcal{H}(q,p) = {} & \omega\, p + \varepsilon\, a_1\, p - \frac{\varepsilon\, J_0^{3/2}}{\sqrt{2}}\,\sin(q) - \frac{3\,\varepsilon\sqrt{J_0}}{2\sqrt{2}}\,p\,\sin(q) - \frac{3\,\varepsilon}{8\sqrt{2}\sqrt{J_0}}\,p^2\,\sin(q) \\
& + \frac{\varepsilon}{16\sqrt{2}\,J_0^{3/2}}\,p^3\,\sin(q) + \frac{\varepsilon\, J_0^{3/2}}{3\sqrt{2}}\,\sin(3q) + \frac{\varepsilon\sqrt{J_0}}{2\sqrt{2}}\,p\,\sin(3q) + \frac{\varepsilon}{8\sqrt{2}\sqrt{J_0}}\,p^2\,\sin(3q) \\
& - \frac{\varepsilon}{48\sqrt{2}\,J_0^{3/2}}\,p^3\,\sin(3q) + \varepsilon^2\, a_2\, p + \varepsilon^3\, a_3\, p\,.
\end{aligned}
\tag{F.11}
$$

At first order, we have

$$
\left\langle h_{1,1}^{(0)} \right\rangle_q = \left\langle a_1\, p - \frac{3\sqrt{J_0}}{2\sqrt{2}}\,p\,\sin(q) + \frac{\sqrt{J_0}}{2\sqrt{2}}\,p\,\sin(3\,q) \right\rangle_q = 0 \qquad \Longrightarrow \qquad a_1 = 0\,; \tag{F.12}
$$

implying that $a_1 = 0$ for the corresponding counterterm in the Hamiltonian (F.11). In order to eliminate the terms constant in the actions (depending only in the angle q) $\varepsilon\, h_{1,0}$, given by

$$
h_{1,0}^{(0)}(q) = -\frac{J_0^{3/2}}{\sqrt{2}}\,\sin(q) + \frac{J_0^{3/2}}{3\sqrt{2}}\,\sin(3\,q)\,,
$$

we define the generating function $X^{(1)}(q)$ such that $L_{X^{(1)}(q)}(\omega\, p) + h_{1,0}^{(0)} = \left\langle h_{1,0}^{(0)} \right\rangle_q$. Hence

$$
X^{(1)} = \frac{J_0^{3/2}}{\sqrt{2}\,\omega}\,\cos(q) - \frac{J_0^{3/2}}{9\sqrt{2}\,\omega}\,\cos(3\,q)\,.
$$

In order to fix the initial value of p at zero, we then set (as in Section 7.3) $\chi_1^{(1)}(q) = X^{(1)}(q) + K^{(1)}\,q$; in this case, the constant $K^{(1)} = 0$. We can now determine the intermediate Hamiltonian

$$\widehat{\mathcal{H}}^{(1)} = \exp\left(L_{\varepsilon\,\chi_1^{(1)}(q)}\right)\mathcal{H}\,.$$

Denoting by $\varepsilon\,\widehat{h}_{1,1}^{(1)}$ the terms of $\widehat{\mathcal{H}}^{(1)}$ of order one in ε and linear in p, we have

$$\widehat{h}_{1,1}^{(1)} = -\frac{3\sqrt{J_0}\,p}{2\sqrt{2}}\,\sin(q) + \frac{\sqrt{J_0}\,p}{2\sqrt{2}}\,\sin(3\,q)\,.$$

These terms are eliminated by the generating function $\chi_2^{(1)}(q,\,p) = \tilde{\chi}_2^{(1)}(q,\,p) + S^{(1)}\,p$ satisfying the homological equation $L_{\chi_2^{(1)}(q,\,p)}(\omega\,p) + \widehat{h}_{1,1}^{(1)} = 0$. In order to fix the initial value of q at zero, we readily find

$$S^{(1)} = -\frac{2\sqrt{2}\,\sqrt{J_0}}{3\,\omega}$$

and

$$\chi_2^{(1)}(q,\,p) = -\frac{2\sqrt{2}\,\sqrt{J_0}\,p}{3\,\omega} + \frac{3\sqrt{J_0}\,p}{2\sqrt{2}\,\omega}\,\cos(q) - \frac{\sqrt{J_0}\,p}{6\sqrt{2}\,\omega}\,\cos(3\,q)\,.$$

Thus, the Hamiltonian

$$\mathcal{H}^{(1)} = \exp\left(L_{\varepsilon\,\chi_2^{(1)}(q,\,p)}\right)\widehat{\mathcal{H}}^{(1)}$$

is now in Kolmogorov normal form up to first order in ε (it is easy to check that the transformed Hamiltonian contains the normal form terms $-\dfrac{3\,p^2}{8\sqrt{2}\,\sqrt{J_0}}\,\sin(q) + \dfrac{p^2}{8\sqrt{2}\,\sqrt{J_0}}\,\sin(3\,q) + \dfrac{p^3}{16\sqrt{2}\,J_0^{3/2}}\,\sin(q) - \dfrac{p^3}{48\sqrt{2}\,J_0^{3/2}}\,\sin(3\,q)$).

In a similar way we can proceed at orders 2 and 3, obtaining the formulas:

$$\begin{aligned}
a_2 &= \frac{5\,J_0}{6\,\omega}\,,\\
\chi_1^{(2)} &= -\frac{5\,J_0^2\,q}{12\,\omega^2} + \frac{5\,J_0^2}{16\,\omega^2}\,\sin(2\,q) - \frac{J_0^2}{16\,\omega^2}\,\sin(4\,q) + \frac{J_0^2}{144\,\omega^2}\,\sin(6\,q)\,,\\
\chi_2^{(2)} &= \frac{J_0\,p}{2\,\omega^2}\,\sin(q) + \frac{13\,J_0\,p}{32\,\omega^2}\,\sin(2\,q) - \frac{J_0\,p}{6\,\omega^2}\,\sin(3\,q) + \frac{J_0\,p}{288\,\omega^2}\,\sin(6\,q)
\end{aligned} \tag{F.13}$$

and

$$\begin{aligned}
a_3 &= 0\,,\\
\chi_1^{(3)} &= \frac{49\,J_0^{5/2}}{96\sqrt{2}\,\omega^3}\,\cos(q) - \frac{5\,J_0^{5/2}}{6\sqrt{2}\,\omega^3}\,\cos(2\,q) + \frac{43\,J_0^{5/2}}{432\sqrt{2}\,\omega^3}\,\cos(3\,q) + \frac{J_0^{5/2}}{3\sqrt{2}\,\omega^3}\,\cos(4\,q)\\
&\quad - \frac{29\,J_0^{5/2}}{240\sqrt{2}\,\omega^3}\,\cos(5\,q) - \frac{J_0^{5/2}}{18\sqrt{2}\,\omega^3}\,\cos(6\,q) + \frac{7\,J_0^{5/2}}{192\sqrt{2}\,\omega^3}\,\cos(7\,q) - \frac{11\,J_0^{5/2}}{5184\sqrt{2}\,\omega^3}\,\cos(9\,q)\,,\\
\chi_2^{(3)} &= -\frac{107\,J_0^{3/2}\,p}{162\sqrt{2}\,\omega^3} + \frac{295\,J_0^{3/2}\,p}{192\sqrt{2}\,\omega^3}\,\cos(q) - \frac{47\,J_0^{3/2}\,p}{36\sqrt{2}\,\omega^3}\,\cos(2\,q) + \frac{133\,J_0^{3/2}\,p}{288\sqrt{2}\,\omega^3}\,\cos(3\,q)\\
&\quad - \frac{J_0^{3/2}\,p}{18\sqrt{2}\,\omega^3}\,\cos(4\,q) + \frac{13\,J_0^{3/2}\,p}{288\sqrt{2}\,\omega^3}\,\cos(5\,q) - \frac{J_0^{3/2}\,p}{36\sqrt{2}\,\omega^3}\,\cos(6\,q) + \frac{7\,J_0^{3/2}\,p}{1152\sqrt{2}\,\omega^3}\,\cos(7\,q)\\
&\quad - \frac{J_0^{3/2}\,p}{10368\sqrt{2}\,\omega^3}\,\cos(9\,q)\,,
\end{aligned} \tag{F.14}$$

for the generating functions. The final Hamiltonian is

$$\mathcal{H}^{(3)}(\tilde{q},\tilde{p}) = \omega\,\tilde{p} + \varepsilon\,R_1(q,\,p) + \varepsilon^2\,R_2(q,\,p) + \varepsilon^3\,R_3(q,\,p)$$

where $(\tilde{q},\,\tilde{p})$ indicate the new variables, and $R_j(\tilde{q},\tilde{p}) = \mathcal{O}(||\,\tilde{p}\,||^2)$ $j = 1,2,3$. Thus, the torus $\tilde{p}(t) = 0$, $\tilde{q}(t) = \omega\,t$ is a solution for the equations of motion of this Hamiltonian. Using the Lie transformations, the solution in the original variables reads

$$\begin{aligned}
q(t) &= \omega\,t - \frac{2\sqrt{2}\,\varepsilon\sqrt{J_0}}{3\,\omega} + \frac{3\,\varepsilon\sqrt{J_0}}{2\sqrt{2}\,\omega}\,\cos(\omega\,t) - \frac{\varepsilon\sqrt{J_0}}{6\sqrt{2}\,\omega}\,\cos(3\,\omega\,t) + \frac{\varepsilon^2\,J_0}{\omega^2}\,\sin(\omega\,t) + \frac{3\,\varepsilon^2\,J_0}{16\,\omega^2}\,\sin(2\,\omega\,t) \\
&\quad - \frac{\varepsilon^2\,J_0}{3\,\omega^2}\,\sin(3\,\omega\,t) + \frac{\varepsilon^2\,J_0}{8\,\omega^2}\,\sin(4\,\omega\,t) - \frac{\varepsilon^2\,J_0}{144\,\omega^2}\,\sin(6\,\omega\,t) - \frac{38\sqrt{2}\,\varepsilon^3\,J_0^{3/2}}{81\omega^3} + \frac{\varepsilon^3\,J_0^{3/2}}{\sqrt{2}\,\omega^3}\,\cos(\omega\,t) \\
&\quad - \frac{\varepsilon^3\,J_0^{3/2}}{2\sqrt{2}\,\omega^3}\,\cos(2\,\omega\,t) + \frac{145\,\varepsilon^3\,J_0^{3/2}}{144\sqrt{2}\,\omega^3}\,\cos(3\,\omega\,t) - \frac{\sqrt{2}\,\varepsilon^3\,J_0^{3/2}}{3\,\omega^3}\,\cos(4\,\omega\,t) + \frac{\varepsilon^3\,J_0^{3/2}}{16\sqrt{2}\,\omega^3}\,\cos(5\,\omega\,t) \\
&\quad + \frac{\varepsilon^3\,J_0^{3/2}}{18\sqrt{2}\,\omega^3}\,\cos(6\,\omega\,t) - \frac{\varepsilon^3\,J_0^{3/2}}{48\sqrt{2}\,\omega^3}\,\cos(7\,\omega\,t) + \frac{\varepsilon^3\,J_0^{3/2}}{1296\sqrt{2}\,\omega^3}\,\cos(9\,\omega\,t)\,, \\
p(t) &= \frac{\varepsilon\,J_0^{3/2}}{\sqrt{2}\,\omega}\,\sin(\omega\,t) - \frac{\varepsilon\,J_0^{3/2}}{3\sqrt{2}\,\omega}\,\sin(3\,\omega\,t) + \frac{5\,\varepsilon^2\,J_0^2}{6\,\omega^2} - \frac{2\,\varepsilon^2\,J_0^2}{3\,\omega^2}\,\cos(\omega\,t) - \frac{2\,\varepsilon^2\,J_0^2}{3\,\omega^2}\,\cos(2\,\omega\,t) \\
&\quad + \frac{2\,\varepsilon^2\,J_0^2}{3\,\omega^2}\,\cos(3\,\omega\,t) - \frac{\varepsilon^2\,J_0^2}{6\,\omega^2}\,\cos(4\,\omega\,t) + \frac{7\,\varepsilon^3\,J_0^{5/2}}{4\sqrt{2}\,\omega^3}\,\sin(\omega\,t) - \frac{8\sqrt{2}\,\varepsilon^3\,J_0^{5/2}}{9\,\omega^3}\,\sin(2\,\omega\,t) \\
&\quad + \frac{13\,\varepsilon^3\,J_0^{5/2}}{8\sqrt{2}\,\omega^3}\,\sin(3\,\omega\,t) - \frac{4\sqrt{2}\,\varepsilon^3\,J_0^{5/2}}{9\,\omega^3}\,\sin(4\,\omega\,t) + \frac{7\,\varepsilon^3\,J_0^{5/2}}{72\sqrt{2}\,\omega^3}\,\sin(5\,\omega\,t)\,, \\
J(t) &= J_0 + p(t)\,.
\end{aligned} \tag{F.15}$$

Recalling also the computed values of a_1, a_2 and a_3 (Eqs (F.12)–(F.14)) we have also

$$\omega = \omega_0 - \frac{5\,\varepsilon^2 J_0}{6\,\omega}\,.$$

Thus, we obtain the same solutions as by the Lindstedt method (Eq (F.10)).

We remark that also in this case the solutions produced by the Birkhoff normal form are equal to those produced by the Lindstedt method in the version 'analogous to Birkhoff'. However, if we compare these solutions with those produced by the KAM algorithm, we also note many differences from order 3 and beyond. For completeness, we report in the following the solutions with the

Birkhoff method:

$$
\begin{aligned}
q(t) &= \omega\, t - \frac{2\sqrt{2}\,\varepsilon\sqrt{J_0}}{3\omega_0} + \frac{3\,\varepsilon\sqrt{J_0}}{2\sqrt{2}\,\omega_0}\cos(\omega\, t) - \frac{\varepsilon\sqrt{J_0}}{6\sqrt{2}\,\omega_0}\cos(3\,\omega\, t) + \frac{\varepsilon^2 J_0}{\omega_0^2}\sin(\omega\, t) + \frac{3\,\varepsilon^2 J_0}{16\,\omega_0^2}\sin(2\,\omega\, t) \\
&\quad - \frac{\varepsilon^2 J_0}{3\,\omega_0^2}\sin(3\,\omega\, t) + \frac{\varepsilon^2 J_0}{8\,\omega_0^2}\sin(4\,\omega\, t) - \frac{\varepsilon^2 J_0}{144\,\omega_0^2}\sin(6\,\omega\, t) - \frac{83\sqrt{2}\,\varepsilon^3 J_0^{3/2}}{81\,\omega_0^3} + \frac{9\,\varepsilon^3 J_0^{3/2}}{4\sqrt{2}\,\omega_0^3}\cos(\omega\, t) \\
&\quad - \frac{\varepsilon^3 J_0^{3/2}}{2\sqrt{2}\,\omega_0^3}\cos(2\,\omega\, t) + \frac{125\,\varepsilon^3 J_0^{3/2}}{144\sqrt{2}\,\omega_0^3}\cos(3\omega\, t) - \frac{\sqrt{2}\,\varepsilon^3 J_0^{3/2}}{3\,\omega_0^3}\cos(4\,\omega\, t) + \frac{\varepsilon^3 J_0^{3/2}}{16\sqrt{2}\,\omega_0^3}\cos(5\,\omega\, t) \\
&\quad + \frac{\varepsilon^3 J_0^{3/2}}{18\sqrt{2}\,\omega_0^3}\cos(6\,\omega\, t) - \frac{\varepsilon^3 J_0^{3/2}}{48\sqrt{2}\,\omega_0^3}\cos(7\,\omega\, t) + \frac{\varepsilon^3 J_0^{3/2}}{1296\sqrt{2}\,\omega_0^3}\cos(9\,\omega\, t)\,, \\
p(t) &= \frac{\varepsilon\, J_0^{3/2}}{\sqrt{2}\,\omega_0}\sin(\omega\, t) - \frac{\varepsilon\, J_0^{3/2}}{3\sqrt{2}\,\omega_0}\sin(3\,\omega\, t) + \frac{5\,\varepsilon^2 J_0^2}{6\,\omega_0^2} - \frac{2\,\varepsilon^2 J_0^2}{3\,\omega_0^2}\cos(\omega\, t) - \frac{2\,\varepsilon^2 J_0^2}{3\,\omega_0^2}\cos(2\,\omega\, t) \\
&\quad + \frac{2\,\varepsilon^2 J_0^2}{3\,\omega_0^2}\cos(3\,\omega\, t) - \frac{\varepsilon^2 J_0^2}{6\,\omega_0^2}\cos(4\,\omega\, t) + \frac{31\,\varepsilon^3 J_0^{5/2}}{12\sqrt{2}\,\omega_0^3}\sin(\omega\, t) - \frac{8\sqrt{2}\,\varepsilon^3 J_0^{5/2}}{9\,\omega_0^3}\sin(2\,\omega\, t) \\
&\quad + \frac{97\,\varepsilon^3 J_0^{5/2}}{72\sqrt{2}\,\omega_0^3}\sin(3\,\omega\, t) - \frac{4\sqrt{2}\,\varepsilon^3 J_0^{5/2}}{9\,\omega_0^3}\sin(4\,\omega\, t) + \frac{7\,\varepsilon^3 J_0^{5/2}}{72\sqrt{2}\,\omega_0^3}\sin(5\,\omega\, t)\,, \\
\omega &= \omega_0 - \frac{5\,\varepsilon^2 J_0}{6\,\omega_0}\,.
\end{aligned}
\tag{F.16}
$$

F.2 Proof of Lemma 1

Consider the Hamiltonian:

$$\mathcal{H}(q,J) = \omega_0\, J + \varepsilon\, h(q,J)\,,$$

where $h = \mathcal{O}(J^{\frac{k}{2}})$ $k \in \mathbb{N}$, $k \geq 3$. Introducing the translation $J = J_0 + p$, $h = \mathcal{O}((J_0+p)^{\frac{k}{2}})$, if k is even we obtain a finite expression in the powers of p. If k is odd, define $f(p) = \varepsilon\,(J_0+p)^{\frac{k}{2}}$ and suppose we want to compute the normalization steps by the Kolmogorov algorithm up to order ε^n $n \geq 1$. The expansion in $p = 0$ up to order n yields

$$f(p) = \varepsilon\,(J_0+p)^{\frac{k}{2}} = \varepsilon\, J_0^{\frac{k}{2}} + \varepsilon\,\frac{k}{2}\,J_0^{\frac{k}{2}-1}p + \ldots + \frac{\varepsilon}{n!}\,\frac{k}{2}\left(\frac{k}{2}-1\right)\cdots\left(\frac{k}{2}-n+1\right)J_0^{\frac{k}{2}-n}p^n\,.$$

Moreover, observe that $\chi_1^{(1)} \sim \varepsilon\, J_0^{\frac{k}{2}}$ and $\chi_2^{(1)} \sim \varepsilon\, J_0^{\frac{k}{2}-1}$. Now, we identify those terms whose Lie derivatives could modify the generating functions along the normalization process. We have $L^{n-1}_{\varepsilon\chi_1^{(1)}}\left(\varepsilon\, J_0^{\frac{k}{2}-n}p^n\right)$. Thus the term of higher degree in p in the expansion of $f(p)$, denoted by $\simeq f^{(n)}(p)$, influences $h^{(1)}_{n,1}$. In fact, since

$$
\begin{aligned}
L^{n-1}_{\varepsilon\chi_1^{(1)}}\left(\varepsilon\, J_0^{\frac{k}{2}-n}p^n\right) &= L^{n-2}_{\varepsilon\chi_1^{(1)}}\underbrace{\{\varepsilon\, J_0^{\frac{k}{2}-n}p^n, \varepsilon\chi_1^{(1)}(q)\}}_{\sim\,\varepsilon^2 J_0^{k-n}\,p^{n-1}} = L^{n-3}_{\varepsilon\chi_1^{(1)}}\underbrace{\{\{\varepsilon\, J_0^{\frac{k}{2}-n}p^n, \varepsilon\chi_1^{(1)}(q)\}, \varepsilon\chi_1^{(1)}(q)\}}_{\sim\,\varepsilon^3 J_0^{\frac{3}{2}k-n}\,p^{n-2}} \simeq \underbrace{\ldots\ldots}_{(n-3)\text{times}} \\
&\simeq \varepsilon^n J_0^{\frac{k}{2}-n}\left(J_0^{\frac{k}{2}}\right)^{n-1}p = \varepsilon^n J_0^{\frac{(k-2)n}{2}}\,p\,,
\end{aligned}
\tag{F.17}
$$

after n step a contribution stemming from the term $f^{(n)}(p)$ will appear in the generating function $\chi_2^{(n)}$. On the contrary, the term $L^{n-1}_{\varepsilon\chi_1^{(1)}}\left(\varepsilon\, f^{(n+1)}(p)\right)$ contributes to $h^{(1)}_{n,2}$ (which is quadratic in the action p), while the term $L^{n}_{\varepsilon\chi_1^{(1)}}\left(\varepsilon\, f^{(n+1)}(p)\right)$ contributes to $h^{(1)}_{n+1,1}$, which is of order ε^{n+1}.

From (F.17) it follows that $h_{n,1}^{(n)} = \mathcal{O}\left(J_0^{(k-2)n/2}\right)$. Hence, the dependence of $\chi_2^{(n)}$ on the parameter J_0 is in the power $\chi_2^{(n)} \sim J_0^{\frac{(k-2)n}{2}}$. Also

$$L^{n-1}_{\varepsilon\chi_2^{(1)}}\left(\varepsilon\, J_0^{\frac{k}{2}-1}p\right) = L^{n-2}_{\varepsilon\chi_2^{(1)}}\underbrace{\{\varepsilon\, J_0^{\frac{k}{2}-1}p, \varepsilon\chi_2^{(1)}(q,p)\}}_{\sim\,\varepsilon^2 J_0^{k-2}\,p} = \underbrace{\cdots\cdots}_{(n-2)\text{times}} \simeq \varepsilon^n J_0^{\frac{k}{2}-1}\left(J_0^{\frac{k}{2}-1}\right)^{n-1} p = \varepsilon^n J_0^{\frac{(k-2)n}{2}}\, p\,,$$

thus, again, $h_{n,1}^{(n)} = \mathcal{O}\left(J_0^{(k-2)n/2}\right)$. Finally

$$\begin{aligned} L^{n-1}_{\varepsilon\chi_1^{(1)}}\left(\varepsilon\, J_0^{\frac{k}{2}-n+1}p^{n-1}\right) &= L^{n-2}_{\varepsilon\chi_1^{(1)}}\underbrace{\{\varepsilon\, J_0^{\frac{k}{2}-n+1}p^{n-1}, \varepsilon\chi_1^{(1)}(q)\}}_{\sim\,\varepsilon^2 J_0^{k-n+1}\,p^{n-2}} = \underbrace{\cdots\cdots}_{(n-2)\text{times}} \simeq \varepsilon^n J_0^{\frac{k}{2}-n+1}\left(J_0^{\frac{k}{2}}\right)^{n-1} p \\ &= \varepsilon^n J_0^{\frac{(k-2)n+2}{2}}\, p\,, \end{aligned}$$

implying $\chi_1^{(n)} \sim J_0^{\frac{(k-2)n+2}{2}}$. This concludes the proof of the lemma. □

F.3 Example – 1DOF Hamiltonian: on the accumulation of the divisors and on the cancellation of some harmonics

Let us start from the elementary example already discussed in Section 7.3, stemming from the following one-degree of freedom Hamiltonian (Eq. 7.18) with a even power dependence on the canonical variables

$$\mathcal{H}(x,p) = \mathcal{H}_0 + \varepsilon\mathcal{H}_1 = \frac{\omega_0}{2}\left(p^2+x^2\right) + \varepsilon\frac{x^4}{4}\,.$$

As already outlined in Subsections 7.3.3 and 7.3.4, the application of the Linstedt series method analogous to Kolmogorov and of the Kolmogorov normal form, produce the same solutions for the previous Hamiltonian vector field. For instance, repeating the Linstedt series method analogous to Kolmogorov (as in Subsection 7.3.3) and the Kolmogorov normal form (as in Subsection 7.3.4) up to order 4 in ε, we arrive at the following final solutions for q and J

$$\begin{aligned} q(t) = \omega t &+ \varepsilon\left(-\frac{J_0\sin(2tw)}{2\omega} + \frac{J_0\sin(4t\omega)}{16\omega}\right) \\ &+ \varepsilon^2\left(\frac{19J_0^2\sin(2t\omega)}{32\omega^2} + \frac{J_0^2\sin(4t\omega)}{64\omega^2} - \frac{J_0^2\sin(6t\omega)}{32\omega^2} + \frac{J_0^2\sin(8t\omega)}{512\omega^2}\right) \\ &+ \varepsilon^3\Bigg(-\frac{395J_0^3\sin(2t\omega)}{512\omega^3} - \frac{497J_0^3\sin(4t\omega)}{4096\omega^3} + \frac{5J_0^3\sin(6t\omega)}{96\omega^3} + \frac{9J_0^3\sin(8t\omega)}{1024\omega^3} - \frac{J_0^3\sin(10t\omega)}{512\omega^3} \\ &+ \frac{J_0^3\sin(12t\omega)}{12288\omega^3}\Bigg) + \varepsilon^4\Bigg(\frac{7545J_0^4\sin(2t\omega)}{8192\omega^4} + \frac{5081J_0^4\sin(4t\omega)}{16384\omega^4} - \frac{253J_0^4\sin(6t\omega)}{4096\omega^4} \\ &- \frac{269J_0^4\sin(8t\omega)}{8192\omega^4} + \frac{3J_0^4\sin(10t\omega)}{2048\omega^4} + \frac{17J_0^4\sin(12t\omega)}{16384\omega^4} - \frac{J_0^4\sin(14t\omega)}{8192\omega^4} + \frac{J_0^4\sin(16t\omega)}{262144\omega^4}\Bigg), \end{aligned} \tag{F.18}$$

F.3 Example – 1DOF Hamiltonian: on the accumulation of the divisors and on the cancellation of some harmonics

$$
\begin{aligned}
J(t) = J_0 &+ \varepsilon \left(-\frac{3J_0^2}{8\omega} + \frac{J_0^2\cos(2t\omega)}{2\omega} - \frac{J_0^2\cos(4t\omega)}{8\omega} \right) \\
&+ \varepsilon^2 \left(\frac{17J_0^3}{32\omega^2} - \frac{21J_0^3\cos(2t\omega)}{32\omega^2} + \frac{3J_0^3\cos(4t\omega)}{32\omega^2} + \frac{J_0^3\cos(6t\omega)}{32\omega^2} \right) \\
&+ \varepsilon^3 \left(-\frac{765J_0^4}{1024\omega^3} + \frac{425J_0^4\cos(2t\omega)}{512\omega^3} + \frac{5J_0^4\cos(4t\omega)}{512\omega^3} - \frac{45J_0^4\cos(6t\omega)}{512\omega^3} - \frac{5J_0^4\cos(8t\omega)}{1024\omega^3} \right) \\
&+ \varepsilon^4 \left(\frac{3843J_0^5}{4096\omega^4} - \frac{3497J_0^5\cos(2t\omega)}{4096\omega^4} - \frac{37J_0^5\cos(4t\omega)}{128\omega^4} + \frac{1485J_0^5\cos(6t\omega)}{8192\omega^4} + \frac{93J_0^5\cos(8t\omega)}{4096\omega^4} \right. \\
&\left. + \frac{5J_0^5\cos(10t\omega)}{8192\omega^4} \right),
\end{aligned}
\tag{F.19}
$$

where

$$
\omega = \omega_0 + \frac{3\varepsilon J_0}{4} - \frac{69\varepsilon^2 J_0^2}{64\omega} + \frac{213\varepsilon^3 J_0^3}{128\omega^2} - \frac{40545\varepsilon^4 J_0^4}{16384\omega^3}\,, \tag{F.20}
$$

that correspond to the obtained solutions (7.34) (in Subsection 7.3.3) and (7.43) (in Subsection 7.3.4) in the case of order $\mathcal{O}(\varepsilon^2)$.
However, some differences arise between the solutions *during the normalization procedures*; more precisely, it is possible to observe that the two methods lead to a 'different accumulation of the divisors' involved in the obtained solutions. Moreover, it can be observed that in the solution $J(t)$ there occur cancellation of terms leading to the complete elimination of harmonics (allowed a priori at any normalization order). In order to analyze their structure, looking also to the 'different nature of the produced denominators', it is convenient to avoid any semplification between the numerators and the denominators of the solutions, calling (during the normalization procedure), generically, the denominators as $v[k] := k\omega$. Nevertheless, the complete 'generic' solution (i.e. with denominators indicated as $v[k]$) for $q(t)$ and $J(t)$ are composed, respectively, by 164 and 243 terms (applying the Linstedt series method analogous to Kolmogorov), and by 231 and 275 terms (applying the Kolmogorov normal form); for this reason, we do not report the explicit generic solutions, rather, we will provide explicit examples, pointing out only the main consequence.

I observation: different structure of the harmonics. As an example, we could start to analyze the solution $J(t)$; to this end, we call $J^{(L)}(t)$ and $J^{(K)}(t)$ the solution for $J(t)$ produced, respectively, by the Linsted series analogous to Kolmogorov and the Kolmogorov normal form. Thus

$$
J^{(L)} = \mathrm{J}_0 + \varepsilon\, J_1^{(L)} + \varepsilon^2\, J_2^{(L)} + \dots\,, \qquad\qquad J^{(K)} = \mathrm{J}_0 + \varepsilon\, J_1^{(K)} + \varepsilon^2\, J_2^{(K)} + \dots\,,
$$

where $J^{(L)}(t)|_{v[k]=k\omega} = J^{(K)}(t)|_{v[k]=k\omega}$, explicitely reported in Eq (F.19). Let us compare now the different terms $J_i^{(L)}$ and $J_i^{(K)}$ $(1 \le i \le 4)$ constituting the solutions: at order ε we can observe that both the solutions have the same expansion, i.e.

$$
J_1^{(L)} = J_1^{(K)} = -\frac{\mathrm{J}_0^2}{v[2]} + \frac{\mathrm{J}_0^2\,\cos(2t\omega)}{v[2]} + \frac{\mathrm{J}_0^2}{2\,v[4]} - \frac{\mathrm{J}_0^2\,\cos(4t\omega)}{2\,v[4]}\,.
$$

The differences start at order ε^2; indeed, we have that

$$
\begin{aligned}
J_2^{(L)} &= \left(\frac{7J_0^3}{2v[2]^2} - \frac{11J_0^3}{4v[2]v[4]} + \frac{J_0^3}{2v[4]^2} - \frac{J_0^3}{2v[2]v[6]} + \frac{J_0^3}{4v[4]v[6]} \right) + \left(\frac{7J_0^3}{4v[2]v[4]} - \frac{7J_0^3}{2v[2]^2} \right) \cos(2\,t\omega) \\
&\quad \left(\frac{J_0^3}{v[2]v[4]} - \frac{J_0^3}{2v[4]^2} \right) \cos(4\,t\omega) + \left(\frac{J_0^3}{2v[2]v[6]} - \frac{J_0^3}{4v[4]v[6]} \right) \cos(6\,t\omega) \\
&\equiv J_{2,0}^{(L)} + J_{2,2}^{(L)} \cos(2t\omega) + J_{2,4}^{(L)} \cos(4t\omega) + J_{2,6}^{(L)} \cos(6t\omega)\,,
\end{aligned}
\tag{F.21}
$$

and

$$\begin{aligned} J_2^{(K)} = &\left(\frac{13J_0^3}{4v[2]^2}+\frac{3J_0^3}{4v[4]^2}-\frac{7J_0^3}{2v[2]v[4]}+\frac{3J_0^3}{4v[2]v[6]}+\frac{3J_0^3}{2v[4]v[6]}-\frac{J_0^3}{2v[4]v[8]}\right)\\ &\left(-\frac{9J_0^3}{4v[2]^2}-\frac{3J_0^3}{4v[2]v[4]}\right)\cos(2\,t\omega)+\left(-\frac{J_0^3}{v[2]^2}-\frac{J_0^3}{2v[4]^2}+\frac{3J_0^3}{v[2]v[4]}\right)\cos(4\,t\omega)\\ &\left(\frac{5J_0^3}{4v[2]v[4]}-\frac{3J_0^3}{4v[2]v[6]}-\frac{3J_0^3}{2v[4]v[6]}\right)\cos(6\,t\omega)+\left(-\frac{J_0^3}{4v[4]^2})+\frac{J_0^3}{2v[4]v[8]}\right)\cos(8\,t\omega)\\ \equiv\, & J_{2,0}^{(K)}+J_{2,2}^{(K)}\cos(2t\omega)+J_{2,4}^{(K)}\cos(4t\omega)+J_{2,6}^{(K)}\cos(6t\omega)+J_{2,8}^{(K)}\cos(8t\omega)\,. \end{aligned} \tag{F.22}$$

Actually, applying opportunely the algebraic identity

$$\frac{1}{ab}=\frac{1}{b(a-b)}-\frac{1}{a(a-b)}\,, \tag{F.23}$$

it can be proved that the the harmonics of the solutions (F.21) and (F.22) are equivalent (see also [33]). Let us provide some examples, starting analyzing the simple harmonic $J_{2,8}^{(L)}$ and $J_{2,8}^{(K)}$, where

$$J_{2,8}^{(L)}=0\,,\qquad\qquad J_{2,8}^{(K)}=-\frac{\mathrm{J}_0^3}{4\,v[4]^2}+\frac{\mathrm{J}_0^3}{2\,v[4]\,v[8]}\,;$$

using the identity (F.23) on the term $\mathrm{J}_0^3/(4\,v[4]\,v[8])$ and remembering that $v[k]=k\omega$, we can write

$$\begin{aligned} J_{2,8}^{(K)} &= -\frac{\mathrm{J}_0^3}{4\,v[4]^2}+\frac{\mathrm{J}_0^3}{4\,v[4]\,v[8]}+\frac{\mathrm{J}_0^3}{4\,v[4]\,v[8]}\\ &= -\frac{\mathrm{J}_0^3}{4\,v[4]^2}+\frac{\mathrm{J}_0^3}{4\,v[4]\,(v[8]-v[4])}-\frac{\mathrm{J}_0^3}{4\,v[8]\,(v[8]-v[4])}+\frac{\mathrm{J}_0^3}{4\,v[4]\,v[8]}\\ &= -\frac{\mathrm{J}_0^3}{4\,v[4]^2}+\frac{\mathrm{J}_0^3}{4\,v[4]^2}-\frac{\mathrm{J}_0^3}{4\,v[8]\,v[4]}+\frac{\mathrm{J}_0^3}{4\,v[4]\,v[8]}=0=J_{2,8}^{(L)}\,. \end{aligned}$$

Similarly, we can continue with the harmonics $J_{2,6}^{(L)}$ and $J_{2,6}^{(K)}$, described by

$$J_{2,6}^{(L)}=\frac{\mathrm{J}_0^3}{2\,v[2]\,v[6]}-\frac{\mathrm{J}_0^3}{4\,v[4]\,v[6]}\,,\qquad\qquad J_{2,6}^{(K)}=\frac{5\,\mathrm{J}_0^3}{4\,v[2]\,v[4]}-\frac{3\,\mathrm{J}_0^3}{4\,v[2]\,v[6]}-\frac{3\,\mathrm{J}_0^3}{2\,v[4]\,v[6]}\,;$$

thanks to (F.23), we can write the following chain of equalities

$$\begin{aligned} J_{2,6}^{(K)} =& \frac{5\,\mathrm{J}_0^3}{4\,v[2]\,v[4]}-\frac{3\,\mathrm{J}_0^3}{4\,v[2]\,v[6]}-\frac{5\,\mathrm{J}_0^3}{4\,v[4]\,v[6]}-\frac{\mathrm{J}_0^3}{4\,v[4]\,v[6]}=\frac{5\,\mathrm{J}_0^3}{4\,v[2]\,v[4]}\\ &-\frac{3\,\mathrm{J}_0^3}{4\,v[2]\,v[6]}-\frac{5\,\mathrm{J}_0^3}{4\,v[4]\,(v[6]-v[4])}+\frac{5\,\mathrm{J}_0^3}{4\,v[6]\,(v[6]-v[4])}-\frac{\mathrm{J}_0^3}{4\,v[4]\,v[6]}\\ =&\frac{5\,\mathrm{J}_0^3}{4\,v[2]\,v[4]}-\frac{3\,\mathrm{J}_0^3}{4\,v[2]\,v[6]}-\frac{5\,\mathrm{J}_0^3}{4\,v[4]\,v[2]}+\frac{5\,\mathrm{J}_0^3}{4\,v[6]\,v[2]}-\frac{\mathrm{J}_0^3}{4\,v[4]\,v[6]}=J_{2,6}^{(L)}\,. \end{aligned}$$

It is possible to proceed, analogously, in order to prove the equality of the other harmonics composing $J_2^{(L)}$ and $J_2^{(K)}$ and of the entire solutions $J^{(L)}(t)$ and $J^{(K)}(t)$; the same conclusions hold also for the solution $q^{(L)}(t)$ and $q^{(K)}(t)$.

II observation: on the accumulation of the divisors. Despite the two normalizaton methods lead to the same solutions, the accumulation of divisors can be different; in order to outline this fact, we call b_i the denominators produced during the i-th normalization procedure step. Looking at the

initial Hamiltonian (7.18) (explicitely written in action-angle variables in Eq (7.19)), it is easy to observe that the denominators $v[i]\,,\ 0 \leq i \leq 4\,,$ involved in the solutions, are produced by the first normalization procedure step (being 4 the maximal trigonometric degree of the Hamiltonian); thus, the following substitution rule (for the denominators) holds

$$v[k] \rightsquigarrow \begin{cases} b_1 \text{ if } & k = 0\,,\ldots,4\,, \\ b_2 \text{ if } & k = 5\,,\ldots,8\,, \\ b_3 \text{ if } & k = 9\,,\ldots,12\,, \\ b_4 \text{ if } & k = 13\,,\ldots,16 \end{cases} . \tag{F.24}$$

Thus, with this notation, it is possible to write the solutions $q^{(L)}(t)\,,\ J^{(L)}(t)$ (produced by Lindstedt series analogous to Kolmogorov) and $q^{(K)}(t)\,,\ J^{(K)}(t)$ (produced by Kolmogorov normal form), analyzing all the possible denominators of maximal order (i.e. 4) involved; they are reported, respectively, in Tables F.1 and F.2 and in Tables F.4 and F.3.

$4b_1^4$	$8b_1^4$	$16b_1^4$	$32b_1^4$	$64b_1^4$	$192b_1^4$	$256b_1^4$	$384b_1^4$	$8b_1^3b_2$	$16b_1^3b_2$
$32b_1^3b_2$	$64b_1^3b_2$	$128b_1^3b_2$	$192b_1^3b_2$	$256b_1^3b_2$	$512b_1^3b_2$	$1536b_1^3b_2$	$16b_1^2b_2^2$	$32b_1^2b_2^2$	$64b_1^2b_2^2$
$128b_1^2b_2^2$	$256b_1^2b_2^2$	$16b_1b_2^3$	$32b_1b_2^3$	$64b_1b_2^3$	$128b_1b_2^3$	$16b_1^3b_3$	$24b_1^3b_3$	$64b_1^3b_3$	$128b_1^3b_3$
$256b_1^3b_3$	$384b_1^3b_3$	$16b_1^2b_2b_3$	$32b_1^2b_2b_3$	$64b_1^2b_2b_3$	$128b_1^2b_2b_3$	$512b_1^2b_2b_3$	$32b_1b_2^2b_3$	$64b_1b_2^2b_3$	$128b_1b_2^2b_3$
$256b_1b_2^2b_3$	$16b_1^2b_3^2$	$64b_1^2b_3^2$	$128b_1^2b_3^2$	$256b_1^2b_3^2$	$32b_1b_2b_3^2$	$64b_1b_2b_3^2$	$128b_1b_2b_3^2$	$128b_1^3b_4$	$384b_1^3b_4$
$768b_1^3b_4$	$128b_1^2b_2b_4$	$256b_1^2b_2b_4$	$128b_1^2b_3b_4$	$512b_1^2b_3b_4$	$\boxed{128b_1b_2b_3b_4}$	$\boxed{256b_1b_2b_3b_4}$			

Table F.1: All possible denominators composing the solution $q^{(L)}(t)$, using the Linstedt series (analogous to Kolmogorov) method.

b_1^4	$3b_1^4$	$32b_1^4$	$48b_1^4$	$64b_1^4$	$96b_1^4$	$128b_1^4$	$256b_1^4$	$4b_1^3b_2$	$8b_1^3b_2$
$12b_1^3b_2$	$16b_1^3b_2$	$32b_1^3b_2$	$64b_1^3b_2$	$128b_1^3b_2$	$192b_1^3b_2$	$256b_1^3b_2$	$384b_1^3b_2$	$4b_1^2b_2^2$	$8b_1^2b_2^2$
$16b_1^2b_2^2$	$32b_1^2b_2^2$	$64b_1^2b_2^2$	$128b_1^2b_2^2$	$8b_1b_2^3$	$16b_1b_2^3$	$32b_1b_2^3$	$8b_1^3b_3$	$12b_1^3b_3$	$16b_1^3b_3$
$24b_1^3b_3$	$32b_1^3b_3$	$64b_1^3b_3$	$384b_1^3b_3$	$768b_1^3b_3$	$8b_1^2b_2b_3$	$16b_1^2b_2b_3$	$32b_1^2b_2b_3$	$64b_1^2b_2b_3$	$128b_1^2b_2b_3$
$8b_1b_2^2b_3$	$16b_1b_2^2b_3$	$32b_1b_2^2b_3$	$64b_1b_2^2b_3$	$16b_1^2b_3^2$	$32b_1^2b_3^2$	$64b_1^2b_3^2$	$32b_1b_2b_3^2$	$64b_1b_2b_3^2$	$16b_1^3b_4$
$32b_1^3b_4$	$192b_1^3b_4$	$384b_1^3b_4$	$768b_1^3b_4$	$16b_1^2b_2b_4$	$32b_1^2b_2b_4$	$64b_1^2b_2b_4$	$128b_1^2b_2b_4$	$8b_1^2b_3b_4$	$16b_1^2b_3b_4$
$32b_1^2b_3b_4$	$64b_1^2b_3b_4$	$128b_1^2b_3b_4$	$\boxed{16b_1b_2b_3b_4}$	$\boxed{32b_1b_2b_3b_4}$	$\boxed{64b_1b_2b_3b_4}$				

Table F.2: All possible denominators composing the solution $J^{(L)}(t)$, using the Linstedt series (analogous to Kolmogorov) method.

As we can see, denominators of the type $b_1\,b_2\,b_3\,b_4$, i.e. produced *to every step of the normalization procedure*, do appear in the solutions produced by the Linstedt series (analogous to Kolmogorov) (see the boxed terms in Tables F.1 and F.2), but are not involved in the solutions produced by the Kolmogorov normal form; this provide a simple example on the different accumulation of the divisors involved in the two different methods and it is related to their different convergence.

III observation: on the cancellations of some harmonics. An other interesting point that we want to outline is the cancellation of some harmonics in the solution $J(t)$; more precisely, there

b_1^4	$4b_1^4$	$8b_1^4$	$16b_1^4$	$32b_1^4$	$48b_1^4$	$64b_1^4$	$96b_1^4$	$128b_1^4$	$192b_1^4$
$256b_1^4$	$512b_1^4$	$1536b_1^4$	$4b_1^3b_2$	$8b_1^3b_2$	$12b_1^3b_2$	$16b_1^3b_2$	$32b_1^3b_2$	$48b_1^3b_2$	$64b_1^3b_2$
$96b_1^3b_2$	$128b_1^3b_2$	$192b_1^3b_2$	$256b_1^3b_2$	$384b_1^3b_2$	$512b_1^3b_2$	$4b_1^2b_2^2$	$8b_1^2b_2^2$	$16b_1^2b_2^2$	$32b_1^2b_2^2$
$64b_1^2b_2^2$	$128b_1^2b_2^2$	$256b_1^2b_2^2$	$8b_1^3b_3$	$12b_1^3b_3$	$16b_1^3b_3$	$24b_1^3b_3$	$32b_1^3b_3$	$64b_1^3b_3$	$96b_1^3b_3$
$128b_1^3b_3$	$192b_1^3b_3$	$512b_1^3b_3$	$4b_1^2b_2b_3$	$8b_1^2b_2b_3$	$16b_1^2b_2b_3$	$32b_1^2b_2b_3$	$64b_1^2b_2b_3$	$128b_1^2b_2b_3$	$256b_1^2b_2b_3$
$16b_1^2b_3^2$	$32b_1^2b_3^2$	$64b_1^2b_3^2$	$128b_1^2b_3^2$	$64b_1^3b_4$	$512b_1^3b_4$	$32b_1^2b_2b_4$	$64b_1^2b_2b_4$	$256b_1^2b_2b_4$	$64b_1^2b_3b_4$
$128b_1^2b_3b_4$	$256b_1^2b_3b_4$								

Table F.3: All possible denominators composing the solution $q^{(K)}(t)$, using the Kolmogorov normal form.

b_1^4	$2b_1^4$	$4b_1^4$	$8b_1^4$	$12b_1^4$	$16b_1^4$	$32b_1^4$	$64b_1^4$	$96b_1^4$	$128b_1^4$
$384b_1^4$	$b_1^3b_2$	$2b_1^3b_2$	$3b_1^3b_2$	$4b_1^3b_2$	$6b_1^3b_2$	$8b_1^3b_2$	$12b_1^3b_2$	$16b_1^3b_2$	$32b_1^3b_2$
$64b_1^3b_2$	$128b_1^3b_2$	$192b_1^3b_2$	$b_1^2b_2^2$	$2b_1^2b_2^2$	$4b_1^2b_2^2$	$8b_1^2b_2^2$	$16b_1^2b_2^2$	$32b_1^2b_2^2$	$64b_1^2b_2^2$
$4b_1^3b_3$	$8b_1^3b_3$	$16b_1^3b_3$	$32b_1^3b_3$	$48b_1^3b_3$	$64b_1^3b_3$	$96b_1^3b_3$	$128b_1^3b_3$	$4b_1^2b_2b_3$	$8b_1^2b_2b_3$
$16b_1^2b_2b_3$	$32b_1^2b_2b_3$	$16b_1^3b_4$	$32b_1^3b_4$	$128b_1^3b_4$	$4b_1^2b_2b_4$	$16b_1^2b_2b_4$	$32b_1^2b_2b_4$	$64b_1^2b_2b_4$	

Table F.4: All possible denominators composing the solution $J^{(K)}(t)$, using the Kolmogorov normal form.

occur cancellation of terms leading to the complete elimination of harmonics (allowed a priori at any normalization order). This is due to *simplifications* and *compensations* between different terms that, coupled, lead to the complete elimination of some harmonics. This is the case (for example) of the harmonic of trigonometric degree equal to 12 (and, analogously, 14 and 16). Indeed, it is possible to write, generically, the solution $J(t)$ of the Hamiltonian vector field generated by (7.18) (up to order 4 in ε) as

$$J(t) = \sum_{i=0}^{4}\sum_{k=0}^{16} \varepsilon^i c_{k,i}\cos(k\,\omega t) = \sum_{k=0}^{16} A_k \cos(k\,\omega t)\,;$$

then, as before, we denote with the symbol $J^{(L)}(t)$ and $J^{(K)}(t)$ the solution produced, respectively, by the Lindstedt series analogous to Kolmogorov and by the Kolmogorov normal form, and with $A_k^{(L)}$ and $A_k^{(K)}$ the correspondent harmonics. Then, the produced generic 12-th harmonics are:

$$\begin{aligned} A_{12}^{(L)} &= \varepsilon^3\left(\frac{J_0^4}{32v[4]^2v[12]} - \frac{J_0^4}{16v[4]v[8]v[12]}\right) \\ &\quad \varepsilon^4\Bigg(\frac{J_0^5}{16v[4]^3v[12]} - \frac{J_0^5}{8v[2]v[4]^2v[12]} + \frac{3J_0^5}{16v[2]^2v[4]v[12]} - \frac{3J_0^5}{32v[2]v[4]v[6]v[12]} - \frac{3J_0^5}{16v[2]^2v[8]v[12]} \\ &\quad - \frac{J_0^5}{8v[4]^2v[8]v[12]} + \frac{J_0^5}{4v[2]v[4]v[8]v[12]} - \frac{3J_0^5}{16v[2]v[6]v[8]v[12]} - \frac{3J_0^5}{16v[2]v[4]v[10]v[12]} \\ &\quad + \frac{3J_0^5}{32v[4]v[6]v[10]v[12]}\Bigg) = \varepsilon^3 c_{12,3}^{(L)} + \varepsilon^4 c_{12,4}^{(L)}\,, \end{aligned} \tag{F.25}$$

F.3 Example – 1DOF Hamiltonian: on the accumulation of the divisors and on the cancellation of some harmonics

$$
\begin{aligned}
A_{12}^{(K)} = \varepsilon^3 \left(-\frac{J_0^4}{8v[4]^3} - \frac{3J_0^4}{16v[4]^2v[8]} + \frac{21J_0^4}{32v[4]^2v[12]} \right) + \\
\varepsilon^4 \Bigg(\frac{J_0^5}{4v[4]^4} + \frac{3J_0^5}{4v[2]v[4]^3} - \frac{223J_0^5}{96v[2]^2v[4]^2} - \frac{27J_0^5}{16v[4]^2v[6]^2} - \frac{27J_0^5}{32v[2]v[4]v[6]^2} + \frac{39J_0^5}{32v[2]v[4]^2v[6]} \\
- \frac{3J_0^5}{32v[2]^2v[4]v[6]} - \frac{3J_0^5}{8v[4]^2v[8]^2} - \frac{J_0^5}{16v[4]^3v[8]} - \frac{16J_0^5}{3v[2]v[4]^2v[8]} - \frac{7J_0^5}{6v[2]^2v[4]v[8]} - \frac{3J_0^5}{4v[4]^2v[6]v[8]} \\
- \frac{3J_0^5}{8v[2]v[4]v[6]v[8]} - \frac{71J_0^5}{48v[2]v[4]^2v[10]} - \frac{281J_0^5}{96v[2]^2v[4]v[10]} - \frac{3J_0^5}{32v[2]^2v[6]v[10]} - \frac{3J_0^5}{16v[2]v[4]v[6]v[10]} \\
- \frac{J_0^5}{4v[2]v[4]v[8]v[10]} - \frac{3J_0^5}{4v[4]^3v[12]} + \frac{75J_0^5}{8v[2]v[4]^2v[12]} + \frac{165J_0^5}{16v[2]^2v[4]v[12]} + \frac{27J_0^5}{8v[4]^2v[6]v[12]} \\
+ \frac{27J_0^5}{16v[2]v[4]v[6]v[12]} + \frac{3J_0^5}{4v[4]^2v[8]v[12]} + \frac{9J_0^5}{4v[2]v[4]v[8]v[12]} \Bigg) = \varepsilon^3 c_{12,3}^{(K)} + \varepsilon^4 c_{12,4}^{(K)} \,.
\end{aligned}
\tag{F.26}
$$

However, if we substituite the denominators $v[k]$ with its definition $k\omega$, it is easy to see that both the harmonics are equal to zero. Nevertheless, the same harmonic in the generating functions do exist; for istance, $\chi_1^{(4)}$ contains the following term

$$
\begin{aligned}
\varepsilon^4 \Bigg(\frac{J_0^5}{16v[4]^3v[12]} - \frac{25J_0^5}{32v[2]v[4]^2v[12]} - \frac{55J_0^5}{64v[2]^2v[4]v[12]} - \frac{9J_0^5}{32v[4]^2v[6]v[12]} - \frac{9J_0^5}{64v[2]v[4]v[6]v[12]} \\
- \frac{J_0^5}{16v[4]^2v[8]v[12]} - \frac{3J_0^5}{16v[2]v[4]v[8]v[12]} \Bigg) \sin(12q) = -\frac{59J_0^5}{8192\omega^4}\, \varepsilon^4 \sin(12q)
\end{aligned}
$$

and, analogously, $\chi_2^{(4)}$ the following one

$$
\begin{aligned}
\varepsilon^4 \Bigg(\frac{63J_0^4 p}{128v[4]^2v[12]^2} + \frac{3J_0^4 p}{64v[4]^3v[12]} - \frac{29J_0^4 p}{64v[2]v[4]^2v[12]} - \frac{7J_0^4 p}{16v[2]^2v[4]v[12]} - \frac{9J_0^4 p}{16v[4]^2v[6]v[12]} \\
- \frac{9J_0^4 p}{32v[2]v[4]v[6]v[12]} + \frac{11J_0^4 p}{32v[2]^2v[8]v[12]} - \frac{15J_0^4 p}{32v[4]^2v[8]v[12]} + \frac{41J_0^4 p}{64v[2]v[4]v[8]v[12]} + \frac{25J_0^4 p}{32v[4]^2v[10]v[12]} \\
+ \frac{25J_0^4 p}{16v[2]v[4]v[10]v[12]) } \Bigg) \sin(12q) = -\frac{23J_0^4 p}{32768\omega^4}\, \varepsilon^4 \sin(12q) \,.
\end{aligned}
$$

The conclusion is that these harmonics (as (F.25) and (F.26)) arise from different terms involved in the calculation of the Lie series and, coupled, they cancel. In particular, it is not difficult to understand which are the terms that, collected together, give contributions to a fixed harmonic and up to a fixed order of ε; thus, if we find an harmonic that cancel, it is easy to go back to the terms contributing to that cancellation. However, it is more difficult to understand, a priori, which order of harmonic will be cancelled by the compensations of different terms. Up to now and up to our knowledge, this remain an open problem.
Concerning the Lie series' terms giving contribution to the solution, it is easy to prove the following Lemma:

Lemma 1. *Consider we have $r \geq 2$ steps of the Kolmogorov algorithm. For any missing harmonic $\varepsilon^n e^{i\boldsymbol{k}\cdot\boldsymbol{q}}$, $2 \leq n \leq r$, in the solution $\boldsymbol{J}(t)$, the coefficients of the same harmonic in the following quantity*

$$
\frac{1}{i_n!} L^{i_n}_{\varepsilon^n \chi_2^{(n)}} \frac{1}{j_n!} L^{j_n}_{\varepsilon^n \chi_1^{(n)}} \cdots \frac{1}{i_1!} L^{i_1}_{\varepsilon \chi_2^{(1)}} \frac{1}{j_1!} L^{j_1}_{\varepsilon \chi_1^{(1)}} \boldsymbol{p} \,, \tag{F.27}
$$

with i_h, $j_h \in \mathbb{N}_{\geq 0}$, $h = 1, \ldots, n$ such that

$$
\sum_{h=1}^{n} h\,(i_h + j_h) = n \qquad \wedge \qquad \sum_{h=1}^{n} j_h < 2 \qquad \wedge \qquad \sum_{h=1}^{n} i_h\, h < n \tag{F.28}
$$

sum to zero.

Proof. The proof is a straightforward consequence of the definition of Lie series and of the generating function. In fact, the solution $J(t) = J_0 + p(t)$ of the Kolmogorov normal form (described by (7.53)) is obtained by

$$\boldsymbol{p}(t) = \left(\exp(L_{\varepsilon^r \chi_2^{(r)}}) \exp(L_{\varepsilon^r \chi_1^{(r)}}) \dots \exp(L_{\varepsilon \chi_2^{(1)}}) \exp(L_{\varepsilon \chi_1^{(1)}}) \boldsymbol{p}^{(r)} \right) \Big|_{\substack{\boldsymbol{p}^{(r)}=\boldsymbol{0} \\ \boldsymbol{q}^{(r)}=\boldsymbol{\omega} t}} .$$

Thus, remembering the definition of Lie series given in Subsection 1.1.3 by Eq. (1.1.5), it is easy to observe that the term involved in the solution $\boldsymbol{p}(t)$ of order ε^n is given by the sum of the terms decribed in (F.27):

$$\frac{1}{i_n!} L^{i_n}_{\varepsilon^n \chi_2^{(n)}} \frac{1}{j_n!} L^{j_n}_{\varepsilon^n \chi_1^{(n)}} \cdots \frac{1}{i_1!} L^{i_1}_{\varepsilon \chi_2^{(1)}} \frac{1}{j_1!} L^{j_1}_{\varepsilon \chi_1^{(1)}} \boldsymbol{p} ,$$

for all the possible combinations of i_h , $j_h \in \mathbb{N}_{\geq 0}$, $h = 1, \dots, n$ such that

$$n\, i_n + n\, j_n + (n-1)\, i_{n-1} + (n-1)\, j_{n-1} + \dots + i_1 + j_1 = n ,$$

i.e. $\sum_{h=1}^{n} h\,(i_h + j_h) = n$. Moreover, the expression (F.27) gives zero if $\sum_{h=1}^{n} j_h > 2$ or if $\sum_{h=1}^{n} i_h\, h = n$. In fact, if $\sum_{h=1}^{n} j_h > 2$, it means that at least two Lie derivatives, with generating function χ_1, are involved in the term (F.27); it is sufficient to recall now (from (7.52)) that $\chi_1 = \chi_1(\boldsymbol{q})$, i.e. that χ_1 depend only on the angles $\boldsymbol{q}$. Thus, in general, the term $L_{\chi_1^{(m)}(\boldsymbol{q})} L_{\chi_1^{(l)}(\boldsymbol{q})}(f(\boldsymbol{q}) \cdot \boldsymbol{p})$ (for some $1 \leq l \leq m \leq n$ and a generic function f) is equal to zero, being $L_{\chi_1^{(l)}(\boldsymbol{q})}(f(\boldsymbol{q}) \cdot \boldsymbol{p})$ dependent only on the angles $\boldsymbol{q}$. Instead, if we are in the case $\sum_{h=1}^{n} i_h\, h = n$, (remembering that $\sum_{h=1}^{n} h\,(i_h + j_h) = n$) it means that *only* the Lie derivatives with generating function $\chi_2(\boldsymbol{q}, \boldsymbol{p})$ are involved in the term (F.27); in general, $L_{\chi_2^{(l)}(\boldsymbol{q},\boldsymbol{p})}(f(\boldsymbol{q}) \cdot \boldsymbol{p})$ (for some $1 \leq l \leq n$ and a generic function f) is a linear function on the action, i.e. of the form $\tilde{f}(\boldsymbol{q}) \cdot \boldsymbol{p}$. Thus, the application of many $L_{\chi_2^{(l)}}$ to $\boldsymbol{p}$ ($1 \leq l \leq n$) will give a linear function in the action, that, evaluated in the solution $\boldsymbol{p} = \boldsymbol{0}$, will give 0. This provide that the only terms different from zero and that give contribution in the solution $\boldsymbol{p}$ (at order ε^n) are those described in (F.27) for which (F.28) is fulfilled. Obviously, if the harmonic $\varepsilon^n \mathrm{e}^{i\boldsymbol{k}\cdot\boldsymbol{q}}$ is missing in the solution, the sum of the contributions of the same harmonic gives zero. □

With this Lemma in mind, it is now easy to understand which are the terms contributing to the 12-th harmonic $A_{12}^{(K)}$ of the solution $J^{(K)}(t)$ described in (F.26).
First of all, we need to analyze the contribution of order ε^3. For Lemma F.3, we have only to consider the following contributions

$$(*) \quad \frac{\varepsilon^3}{2} L^2_{\chi_2^{(1)}} L_{\chi_1^{(1)}} p , \qquad (\star) \quad \varepsilon^3 L_{\chi_1^{(2)}} L_{\chi_2^{(1)}} p , \qquad (\diamond) \quad \varepsilon^3 L_{\chi_2^{(2)}} L_{\chi_1^{(1)}} p , \qquad (\bullet) \quad \varepsilon^3 L_{\chi_1^{(3)}} p , \tag{F.29}$$

corresponding, respectively, to $n = 3$, $(i_1, j_1, i_2, j_2, i_3, j_3) = (2,1,0,0,0,0), (1,0,0,1,0,0), (0,1,1,0,0,0)$ and $(0,0,0,0,0,1)$.[1] The coefficient of the harmonic $\cos(12\,\omega t)$ of the previous quantities are

$$(*) \quad -\frac{\varepsilon^3 J_0^4}{8v[4]^3) } , \qquad (\star) \quad -\frac{\varepsilon^3 J_0^4}{4v[4]^2 v[8]} , \qquad (\diamond) \quad \frac{\varepsilon^3 J_0^4}{16v[4]^2 v[8]} , \qquad (\bullet) \quad \frac{\varepsilon^3\, 21 J_0^4}{32v[4]^2 v[12]} ,$$

[1] The terms given by the combinations $(i_1, j_1, i_2, j_2, i_3, j_3) = (0,3,0,0,0,0)$, $(1,2,0,0,0,0)$, $(0,1,0,1,0,0)$ (s.t. $j_1 + j_2 + j_3 \geq 2$) and those given by $(i_1, j_1, i_2, j_2, i_3, j_3) = (3,0,0,0,0,0)$, $(1,0,1,0,0,0)$, $(0,0,0,0,1,0)$ (s.t. $i_1 + 2\,i_2 + 3\,i_3 = 3$) give zero.

whose sum gives exactly $\varepsilon^3\left(-\frac{J_0^4}{8v[4]^3}-\frac{3J_0^4}{16v[4]^2v[8]}+\frac{21J_0^4}{32v[4]^2v[12]}\right)$, described in (F.26), and that, with the substitution $v[k]=k\omega$, is equal to zero.
Finally, we need to analyze the contribution of order ε^4. For Lemma F.3, we have only to consider the following contributions

$$(*)\quad \frac{\varepsilon^4}{6}L^3_{\chi_2^{(1)}}L_{\chi_1^{(1)}}p\,,\qquad (\star)\quad \frac{\varepsilon^4}{2}L_{\chi_1^{(2)}}L^2_{\chi_2^{(1)}}p\,,\qquad (\diamond)\quad \varepsilon^4 L_{\chi_2^{(2)}}L_{\chi_2^{(1)}}L_{\chi_1^{(1)}}p\,,\qquad (\bullet)\quad \varepsilon^4 L_{\chi_2^{(2)}}L_{\chi_1^{(2)}}p\,,$$
$$(\triangle)\quad \varepsilon^4 L_{\chi_1^{(3)}}L_{\chi_2^{(1)}}p\,,\qquad (\circ)\quad \varepsilon^4 L_{\chi_2^{(3)}}L_{\chi_1^{(1)}}p\,,\qquad (\square)\quad \frac{\varepsilon^4}{24}L_{\chi_1^{(4)}}p\,, \tag{F.30}$$

corresponding, respectively, to $n=4$, $(i_1,j_1,i_2,j_2,i_3,j_3,i_4,j_4)=(3,1,0,0,0,0,0,0)$, $(2,0,0,1,0,0,0,0)$, $(1,1,1,0,0,0,0,0)$, $(0,0,1,1,0,0,0,0)$, $(1,0,0,0,0,1,0,0)$, $(0,1,0,0,1,0,0,0)$ and $(0,0,0,0,0,0,0,1)$.
The coefficient of the harmonic $\cos(12\,\omega t)$ of the previous quantities are

$$(*)\ -\varepsilon^4\,\frac{223J_0^5}{96v[2]^2v[4]^2}\,,$$
$$(\star)\quad \varepsilon^4\left(-\frac{3J_0^5}{16v[2]v[4]^2v[6]}-\frac{3J_0^5}{32v[2]^2v[4]v[6]}\right),$$
$$(\diamond)\quad \varepsilon^4\left(\frac{J_0^5}{4v[4]^4}+\frac{3J_0^5}{4v[2]v[4]^3}+\frac{45J_0^5}{32v[2]v[4]^2v[6]}+\frac{J_0^5}{8v[2]^2v[4]v[8]}\right),$$
$$(\bullet)\quad \varepsilon^4\left(-\frac{27J_0^5}{16v[4]^2v[6]^2}-\frac{27J_0^5}{32v[2]v[4]v[6]^2}-\frac{7J_0^5}{16v[4]^3v[8]}-\frac{15J_0^5}{8v[2]v[4]^2v[8]}\right),$$
$$(\triangle)\quad \varepsilon^4\left(\frac{5J_0^5}{16v[4]^3v[8]}-\frac{15J_0^5}{4v[2]v[4]^2v[8]}-\frac{11J_0^5}{8v[2]^2v[4]v[8]}-\frac{25J_0^5}{16v[2]v[4]^2v[10]}-\frac{25J_0^5}{8v[2]^2v[4]v[10]}\right),$$
$$\begin{aligned}(\circ)\quad \varepsilon^4\Bigg(&-\frac{3J_0^5}{8v[4]^2v[8]^2}+\frac{J_0^5}{16v[4]^3v[8]}+\frac{7J_0^5}{24v[2]v[4]^2v[8]}+\frac{J_0^5}{12v[2]^2v[4]v[8]}-\frac{3J_0^5}{4v[4]^2v[6]v[8]}-\frac{3J_0^5}{8v[2]v[4]v[6]v[8]}\\&+\frac{J_0^5}{12v[2]v[4]^2v[10]}+\frac{19J_0^5}{96v[2]^2v[4]v[10]}-\frac{3J_0^5}{32v[2]^2v[6]v[10]}-\frac{3J_0^5}{16v[2]v[4]v[6]v[10]}-\frac{J_0^5}{4v[2]v[4]v[8]v[10]}\Bigg)\end{aligned}$$
$$\begin{aligned}(\square)\quad \varepsilon^4\Bigg(&-\frac{3J_0^5}{4v[4]^3v[12]}+\frac{75J_0^5}{8v[2]v[4]^2v[12]}+\frac{165J_0^5}{16v[2]^2v[4]v[12]}+\frac{27J_0^5}{8v[4]^2v[6]v[12]}\\&+\frac{27J_0^5}{16v[2]v[4]v[6]v[12]}+\frac{3J_0^5}{4v[4]^2v[8]v[12]}+\frac{9J_0^5}{4v[2]v[4]v[8]v[12]}\Bigg),\end{aligned}$$

whose sum gives the term of order ε^4 described in (F.26). The same conclusions arise for the harmonics $\cos(14\,\omega t)$ and $\cos(16\,\omega t)$.
Obviously, this type of cancellation (leading to the complete elimination of some harmonics) does not occur in the solution $\boldsymbol{q}(t)$, being described by (7.53).

F.4 Example – 2DOF Hamiltonian: on the cancellations of the harmonics

Consider the following two-degrees of freedom Hamiltonian:

$$\mathcal{H}(x,y,p_x,p_y)=\mathcal{H}_0+\varepsilon\mathcal{H}_1=\frac{p_x^2\omega_{0,1}}{2}+\frac{p_y^2\omega_{0,2}}{2}+\frac{\omega_{0,1}x^2}{2}+\frac{\omega_{0,2}y^2}{2}+\varepsilon x^4-\varepsilon x^2y^2\,. \tag{F.31}$$

Using the harmonic oscillator action-angle variables $(\boldsymbol{J},\boldsymbol{q}) = (J_1, J_2, q_1, q_2)$ with $x = \sqrt{2J_1}\sin(q_1)$, $y = \sqrt{2J_2}\sin(q_2)$, $p_x = \sqrt{2J_1}\cos(q_1)$, $p_y = \sqrt{2J_2}\cos(q_2)$ we obtain

$$\begin{aligned}\mathcal{H}(\boldsymbol{q},\boldsymbol{J}) = \boldsymbol{\omega}_0\cdot\boldsymbol{J} + \varepsilon\,\frac{3J_1^2}{2} - \varepsilon\,J_1J_2 - 2\,\varepsilon\,J_1^2\,\cos(2q_1) + \varepsilon\,J_1J_2\cos(2q_1) + \varepsilon\,\frac{J_1^2}{2}\cos(4q_1)\\ - \varepsilon\,\frac{J_1J_2}{2}\cos(2q_1-2q_2) + \varepsilon\,J_1J_2\cos(2q_2) - \varepsilon\,\frac{J_1J_2}{2}\cos(2q_1+2q_2)\,,\end{aligned} \tag{F.32}$$

where $\boldsymbol{\omega}_0 = (\omega_{0,1},\omega_{0,2})$. Analogously to the one-degree of freedom model, let $\boldsymbol{J}_0 = (J_{0,1}, J_{0,2})$ be the label of a given torus (periodic orbit) of the model $\mathcal{H}_0$ and we introduce the traslated actions $\boldsymbol{p} = \boldsymbol{J} - \boldsymbol{J}_0$. Thus, we proceed as explained in Section 7.4, substituting the 'initial' frequency vector $\boldsymbol{\omega}_0$ with the 'final' one $\boldsymbol{\omega}$, through Eq. (7.48), explicitely written as follows:

$$\boldsymbol{\omega} = \boldsymbol{\omega}_0 - \sum_{i\geq 1}\varepsilon^i\,\boldsymbol{a}_i(\boldsymbol{J}_0)\,,$$

where $\boldsymbol{a}_i = (a_{i,1}, a_{i,2})$. This yields (apart from constants)

$$\begin{aligned}\mathcal{H}(\boldsymbol{q},\boldsymbol{p}) = \big(\boldsymbol{\omega} + \varepsilon\,\boldsymbol{a}_1 + \varepsilon^2\,\boldsymbol{a}_2 + \ldots\big)\cdot\boldsymbol{p} + \varepsilon\,\frac{3J_{0,1}^2}{2} - \varepsilon\,J_{0,1}J_{0,2} + \varepsilon\,3J_{0,1}p_1 - \varepsilon\,J_{0,2}p_1 + \varepsilon\,\frac{3p_1^2}{2} - \varepsilon\,J_{0,1}^2\cos(2q_1)\\ - \varepsilon\,J_{0,1}p_2 - \varepsilon\,p_1p_2 + \varepsilon\,\frac{1}{2}J_{0,1}^2\cos(4q_1) + \varepsilon\,J_{0,1}J_{0,2}\cos(2q_1) - \varepsilon\,4J_{0,1}p_1\cos(2q_1)\\ + \varepsilon\,J_{0,1}p_2\cos(2q_1) + \varepsilon\,J_{0,2}p_1\cos(2q_1) - \varepsilon\,2p_1^2\cos(2q_1) + \varepsilon\,p_1p_2\cos(2q_1) + \varepsilon\,J_{0,1}p_1\cos(4q_1)\\ + \varepsilon\,\frac{1}{2}p_1^2\cos(4q_1) - \varepsilon\,\frac{1}{2}J_{0,1}J_{0,2}\cos(2q_1-2q_2) + \varepsilon\,J_{0,1}J_{0,2}\cos(2q_2) - \varepsilon\,\frac{1}{2}J_{0,1}p_2\cos(2q_1-2q_2)\\ - \varepsilon\,\frac{1}{2}J_{0,2}p_1\cos(2q_1-2q_2) - \varepsilon\,\frac{1}{2}p_1p_2\cos(2q_1-2q_2) + \varepsilon\,J_{0,1}p_2\cos(2q_2) + \varepsilon J_{0,2}p_1\cos(2q_2)\\ - \varepsilon\,\frac{1}{2}J_{0,1}J_{0,2}\cos(2q_1+2q_2) - \varepsilon\,\frac{1}{2}J_{0,1}p_2\cos(2q_1+2q_2) - \varepsilon\,\frac{1}{2}J_{0,2}p_1\cos(2q_1+2q_2)\\ - \varepsilon\,\frac{1}{2}p_1p_2\cos(2q_1+2q_2) + \varepsilon\,p_1p_2\cos(2q_2)\,.\end{aligned}$$

It is possible now to apply the Kolmogorov algorithm explained in Section 7.4 and already applied to the one-degree of freedom Hamiltonian (7.18) in the Subsection 7.3.4; despite the choice of a 'small' order in ε, the two-degrees of freedom dependence (rather than one) make the formula and the solutions longer with respect to the ones reported in Subsection 7.3.4. For this reason, we do not report explicitely the form of the solutions[2]. However, we want to point out that in the solution $\boldsymbol{J}(t)$ there occur cancellation of terms leading to the complete elimination of harmonics (allowed a priori at any normalization order): we want to provide some examples.

i) Order 2 in ε. Let us write, generically, the solution $\boldsymbol{J}(t)$ (up to order 2 in ε) as

$$\boldsymbol{J}(t) = \sum_{i=0}^{2}\sum_{\substack{\boldsymbol{k}\in\mathbb{Z}^2\\ |\boldsymbol{k}|=8}}\varepsilon^i\boldsymbol{c}_{\boldsymbol{k},i}\cos(\boldsymbol{k}\cdot\boldsymbol{\omega}t) = \sum_{\substack{\boldsymbol{k}\in\mathbb{Z}^2\\ |\boldsymbol{k}|=8}}\boldsymbol{A}_{\boldsymbol{k}}\cos(\boldsymbol{k}\cdot\boldsymbol{\omega}t)\,;$$

whit $\boldsymbol{A}_{\boldsymbol{k}} = (A_{1_{\boldsymbol{k}}}, A_{2_{\boldsymbol{k}}})$ the coefficient of the $\boldsymbol{k}$-th harmonic, and $|\boldsymbol{k}| = |k_1| + |k_2|$. We can observe that $\boldsymbol{A}_{\boldsymbol{k}}$ is equal to zero (thus the $\boldsymbol{k}$-th harmonic is missing in the final solution $\boldsymbol{J}(t)$) in the cases $(k_1,k_2) = (4,4)$, $(4,-4)$, $(6,2)$, $(6,-2)$, $(8,0)$, also if the same harmonics are allowed in the

[2]Let us observe that, taking 2 as order of ε, the solutions for $J_1(t)$, $J_2(t)$, $q_1(t)$, $q_2(t)$ are composed (apart possible rimanipolations), respectively, by 130, 119, 93, 82 terms.

normalization procedure and are different from zero in the generating functions[3]. More precisely,

$$A_{1_{(4,4)}} = \varepsilon^2 \left(-\frac{J_{0,1}^2 J_{0,2}}{2(2\omega_1+2\omega_2)^2} + \frac{J_{0,1}^2 J_{0,2}}{(2\omega_1+2\omega_2)(4\omega_1+4\omega_2)} - \frac{J_{0,1} J_{0,2}^2}{2(2\omega_1+2\omega_2)^2} + \frac{J_{0,1} J_{0,2}^2}{(2\omega_1+2\omega_2)(4\omega_1+4\omega_2)} \right)$$

and $A_{2_{(4,4)}} = A_{1_{(4,4)}}$. Then, it is easy to see that $\boldsymbol{A}_{(4,4)} = \boldsymbol{0}$. Nevertheless, the same harmonic in the generating functions do exist; for istance, $\chi_1^{(2)}$ and $\chi_2^{(2)}$ contain, respectively, the following harmonic:

$$-\varepsilon \frac{J_{0,1} J_{0,2}(J_{0,1}+J_{0,2})}{32(\omega_1+\omega_2)^2} \sin(4q_1+4q_2)\,, \qquad -\varepsilon \frac{J_{0,1} J_{0,2}(p_1+p_2)}{32(\omega_1+\omega_2)^2} \sin(4q_1+4q_2)\,.$$

For Lemma F.3, the terms giving contributions to the harmonics at order 2 in ε are

$$(*) \quad \varepsilon^2 L_{\chi_2^{(1)}} L_{\chi_1^{(1)}} \boldsymbol{p}\,, \qquad\qquad (\star) \quad \varepsilon^2 L_{\chi_1^{(2)}} \boldsymbol{p}\,, \tag{F.33}$$

corresponding, respectively, to $n=2$, $(i_1,j_1,i_2,j_2)=(1,1,0,0)$ and $(0,0,0,1)$.[4] The coefficient of the harmonic $\cos(4q_1+4q_2)$ of the previous quantities are

$$\begin{aligned}
&(*) \quad \varepsilon^2 \left(-\frac{J_{0,1}^2 J_{0,2}}{2(2\omega_1+2\omega_2)^2} - \frac{J_{0,1} J_{0,2}^2}{2(2\omega_1+2\omega_2)^2}, -\frac{J_{0,1}^2 J_{0,2}}{2(2\omega_1+2\omega_2)^2} - \frac{J_{0,1} J_{0,2}^2}{2(2\omega_1+2\omega_2)^2} \right), \\
&(\star) \quad \varepsilon^2 \Bigg(\frac{J_{0,1}^2 J_{0,2}}{(2\omega_1+2\omega_2)(4\omega_1+4\omega_2)} + \frac{J_{0,1} J_{0,2}^2}{(2\omega_1+2\omega_2)(4\omega_1+4\omega_2)}, \\
&\qquad \frac{J_{0,1}^2 J_{0,2}}{(2\omega_1+2\omega_2)(4\omega_1+4\omega_2)} + \frac{J_{0,1} J_{0,2}^2}{(2\omega_1+2\omega_2)(4\omega_1+4\omega_2)} \Bigg),
\end{aligned}$$

whose sum (component with component), giving $\boldsymbol{A}_{(4,4)}$, leads to the complete elimination of the correspondent harmonic. Similarly

$$\begin{aligned}
A_{1_{(4,-4)}} &= \varepsilon^2 \left(-\frac{J_{0,1}^2 J_{0,2}}{(4\omega_1-4\omega_2)(2\omega_1-2\omega_2)} + \frac{J_{0,1}^2 J_{0,2}}{2(2\omega_1-2\omega_2)^2} + \frac{J_{0,1} J_{0,2}^2}{(4\omega_1-4\omega_2)(2\omega_1-2\omega_2)} - \frac{J_{0,1} J_{0,2}^2}{2(2\omega_1-2\omega_2)^2} \right), \\
A_{1_{(6,2)}} &= \left(\frac{3J_{0,1}^2 J_{0,2}}{4\omega_1(2\omega_1+2\omega_2)} - \frac{3J_{0,1}^2 J_{0,2}}{4\omega_1(6\omega_1+2\omega_2)} - \frac{3J_{0,1}^2 J_{0,2}}{(2\omega_1+2\omega_2)(6\omega_1+2\omega_2)} \right), \\
A_{1_{(6,-2)}} &= \left(\frac{3J_{0,1}^2 J_{0,2}}{4\omega_1(2\omega_1-2\omega_2)} - \frac{3J_{0,1}^2 J_{0,2}}{4\omega_1(6\omega_1-2\omega_2)} - \frac{3J_{0,1}^2 J_{0,2}}{(2\omega_1-2\omega_2)(6\omega_1-2\omega_2)} \right),
\end{aligned} \tag{F.34}$$

and $A_{2_{(4,-4)}} = -A_{1_{(4,-4)}}$, $A_{2_{(6,2)}} = A_{1_{(6,2)}}/3$, $A_{2_{(6,2)}} = -A_{1_{(6,2)}}/3$. Summing, respectively, the coefficient of the quantities (F.33) of the harmonic $\cos(4q_1-4q_2)$, given by

$$\begin{aligned}
&(*) \quad \varepsilon^2 \left(\frac{J_{0,1}^2 J_{0,2}}{2(2\omega_1-2\omega_2)^2} - \frac{J_{0,1} J_{0,2}^2}{2(2\omega_1-2\omega_2)^2}, -\frac{J_{0,1}^2 J_{0,2}}{2(2\omega_1-2\omega_2)^2} + \frac{J_{0,1} J_{0,2}^2}{2(2\omega_1-2\omega_2)^2} \right), \\
&(\star) \quad \varepsilon^2 \Bigg(\frac{J_{0,1} J_{0,2}^2}{(4\omega_1-4\omega_2)(2\omega_1-2\omega_2)} - \frac{J_{0,1}^2 J_{0,2}}{(4\omega_1-4\omega_2)(2\omega_1-2\omega_2)}, \\
&\qquad - \frac{J_{0,1} J_{0,2}^2}{(4\omega_1-4\omega_2)(2\omega_1-2\omega_2)} + \frac{J_{0,1}^2 J_{0,2}}{(4\omega_1-4\omega_2)(2\omega_1-2\omega_2)} \Bigg),
\end{aligned}$$

[3] Concerning the solution $J_2(t)$, also in the case $(k_1,k_2)=(4,2)$ there occur cancellations, leading to the elimination of the correspondend harmonic.

[4] The terms given by the combinations $(i_1,j_1,i_2,j_2)=(0,2,0,0)$ (s.t. $j_1+j_2 \geq 2$) and those given by $(i_1,j_1,i_2,j_2)=(2,0,0,0)$, $(0,0,1,0)$ (s.t. $i_1+2\,i_2=2$) give zero.

of the harmonic $\cos(6q_1 + 2q_2)$, described by

$$
\begin{aligned}
(*) \quad & \varepsilon^2 \left(\frac{3J_{0,1}^2 J_{0,2}}{4\omega_1(2\omega_1 + 2\omega_2)}, \frac{J_{0,1}^2 J_{0,2}}{4\omega_1(2\omega_1 + 2\omega_2)} \right), \\
(\star) \quad & \varepsilon^2 \Bigg(- \frac{3J_{0,1}^2 J_{0,2}}{4\omega_1(6\omega_1 + 2\omega_2)} - \frac{3J_{0,1}^2 J_{0,2}}{(2\omega_1 + 2\omega_2)(6\omega_1 + 2\omega_2)}, \\
& \qquad - \frac{J_{0,1}^2 J_{0,2}}{4\omega_1(6\omega_1 + 2\omega_2)} - \frac{J_{0,1}^2 J_{0,2}}{(2\omega_1 + 2\omega_2)(6\omega_1 + 2\omega_2)} \Bigg),
\end{aligned}
$$

and of the harmonic $\cos(6q_1 - 2q_2)$, that is

$$
\begin{aligned}
(*) \quad & \varepsilon^2 \left(\frac{3J_{0,1}^2 J_{0,2}}{4\omega_1(2\omega_1 - 2\omega_2)}, -\frac{J_{0,1}^2 J_{0,2}}{4\omega_1(2\omega_1 - 2\omega_2)} \right), \\
(\star) \quad & \varepsilon^2 \Bigg(- \frac{3J_{0,1}^2 J_{0,2}}{4\omega_1(6\omega_1 - 2\omega_2)} - \frac{3J_{0,1}^2 J_{0,2}}{(2\omega_1 - 2\omega_2)(6\omega_1 - 2\omega_2)}, \\
& \qquad \frac{J_{0,1}^2 J_{0,2}}{4\omega_1(6\omega_1 - 2\omega_2)} + \frac{J_{0,1}^2 J_{0,2}}{(2\omega_1 - 2\omega_2)(6\omega_1 - 2\omega_2)} \Bigg),
\end{aligned}
$$

we recover the harmonics $\boldsymbol{A}_{(4,-4)}$, $\boldsymbol{A}_{(6,2)}$ and $\boldsymbol{A}_{(6,-2)}$, that are completely cancelled in the final solution. Finally, we observe that the harmonic $\boldsymbol{A}_{(8,0)} = (0,0)$, also if the generating functions $\chi_1^{(2)}$ and $\chi_2^{(2)}$ contain, respectively, the following terms:

$$
- \varepsilon^2 \frac{J_{0,1}^3}{32\omega_1^2} \sin(8q_1), \qquad\qquad -\varepsilon^2 \frac{J_{0,1}^2 p_1}{32\omega_1^2} \sin(8q_1) .
$$

In this last case, the coefficient of the harmonic $\cos(8q_1)$ of the contributions described in (F.33) are

$$
(*) \quad \varepsilon^2 \left(-\frac{J_{0,1}^3}{4\omega_1^2}, 0 \right), \qquad\qquad (\star) \quad \varepsilon^2 \left(\frac{J_{0,1}^3}{4\omega_1^2}, 0 \right),
$$

whose sum gives 0.

ii) Order 3 in ε. In this case, we can write, generically, the solution $\boldsymbol{J}(t)$ (up to order 3 in ε) as

$$
\boldsymbol{J}(t) = \sum_{i=0}^{3} \sum_{\substack{\boldsymbol{k} \in \mathbb{Z}^2 \\ |\boldsymbol{k}|=12}} \varepsilon^i \boldsymbol{c}_{\boldsymbol{k},i} \cos(\boldsymbol{k} \cdot \boldsymbol{\omega} t) = \sum_{\substack{\boldsymbol{k} \in \mathbb{Z}^2 \\ |\boldsymbol{k}|=12}} \boldsymbol{A}_{\boldsymbol{k}} \cos(\boldsymbol{k} \cdot \boldsymbol{\omega} t) .
$$

The obtained solutions are quite longer[5] than the ones produced in the case of order 2 in ε and much more harmonics are missing in the final solution $\boldsymbol{J}(t)$; for istance, in the cases $(k_1, k_2) = (4, \pm 6)$, $(6, \pm 4)$, $(6, \pm 6)$, $(8, \pm 2)$, $(8, \pm 4)$ and $(10, \pm 2)$, also if the same harmonics are allowed in the normalization procedure and are different from zero in the generating functions. As an example,

[5] Taking 3 as order of ε, the solutions for $J_1(t)$, $J_2(t)$, $q_1(t)$, $q_2(t)$ are composed (apart possible rimanipolations), respectively, by 1494, 1366, 1302, 1126 terms.

we can analyze one harmonic, as $\boldsymbol{A}_{(8,4)}$, that is

$$
\begin{aligned}
A_{1_{(8,4)}} = \varepsilon^3 \Bigg(& -\frac{5J_{0,1}^3 J_{0,2}}{16\omega_1(2\omega_1+2\omega_2)^2} - \frac{J_{0,1}^3 J_{0,2}}{16\omega_1(2\omega_1+2\omega_2)(6\omega_1+2\omega_2)} - \frac{J_{0,1}^3 J_{0,2}}{4(2\omega_1+2\omega_2)^2(6\omega_1+2\omega_2)} \\
& - \frac{J_{0,1}^3 J_{0,2}}{4\omega_1(2\omega_1+2\omega_2)(4\omega_1+4\omega_2)} + \frac{J_{0,1}^3 J_{0,2}}{\omega_1(2\omega_1+2\omega_2)(8\omega_1+4\omega_2)} + \frac{2J_{0,1}^3 J_{0,2}}{(2\omega_1+2\omega_2)^2(8\omega_1+4\omega_2)} \\
& - \frac{11J_{0,1}^2 J_{0,2}^2}{16\omega_1(2\omega_1+2\omega_2)^2} - \frac{5J_{0,1}^2 J_{0,2}^2}{16\omega_1(2\omega_1+2\omega_2)(6\omega_1+2\omega_2)} - \frac{5J_{0,1}^2 J_{0,2}^2}{4(2\omega_1+2\omega_2)^2(6\omega_1+2\omega_2)} \\
& - \frac{J_{0,1}^2 J_{0,2}^2}{2\omega_1(2\omega_1+2\omega_2)(4\omega_1+4\omega_2)} + \frac{5J_{0,1}^2 J_{0,2}^2}{2\omega_1(2\omega_1+2\omega_2)(8\omega_1+4\omega_2)} + \frac{5J_{0,1}^2 J_{0,2}^2}{(2\omega_1+2\omega_2)^2(8\omega_1+4\omega_2)} \,, \Bigg)
\end{aligned}
$$

$$
\begin{aligned}
A_{2_{(8,4)}} = \varepsilon^3 \Bigg(& -\frac{3J_{0,1}^3 J_{0,2}}{16\omega_1(2\omega_1+2\omega_2)^2} - \frac{J_{0,1}^3 J_{0,2}}{16\omega_1(2\omega_1+2\omega_2)(6\omega_1+2\omega_2)} - \frac{J_{0,1}^3 J_{0,2}}{4(2\omega_1+2\omega_2)^2(6\omega_1+2\omega_2)} \\
& + \frac{J_{0,1}^3 J_{0,2}}{2\omega_1(2\omega_1+2\omega_2)(8\omega_1+4\omega_2)} + \frac{J_{0,1}^3 J_{0,2}}{(2\omega_1+2\omega_2)^2(8\omega_1+4\omega_2)} - \frac{5J_{0,1}^2 J_{0,2}^2}{16\omega_1(2\omega_1+2\omega_2)^2} \\
& - \frac{5J_{0,1}^2 J_{0,2}^2}{16\omega_1(2\omega_1+2\omega_2)(6\omega_1+2\omega_2)} - \frac{5J_{0,1}^2 J_{0,2}^2}{4(2\omega_1+2\omega_2)^2(6\omega_1+2\omega_2)} + \frac{5J_{0,1}^2 J_{0,2}^2}{4\omega_1(2\omega_1+2\omega_2)(8\omega_1+4\omega_2)} \\
& + \frac{5J_{0,1}^2 J_{0,2}^2}{2(2\omega_1+2\omega_2)^2(8\omega_1+4\omega_2)} \Bigg) ;
\end{aligned}
$$

it is easy to verify that this harmonic is actually zero. However, the same harmonic do exist in the generating functions, $\chi_1^{(3)}$ containing (after an appropriate semplification) the term

$$
-\varepsilon^3 \frac{J_{0,1}^2 J_{0,2}(2J_{0,1}+5J_{0,2})}{128\omega_1(\omega_1+\omega_2)^2} \sin(8q_1+4q_2)
$$

and $\chi_2^{(3)}$ the following one

$$
\varepsilon^3 \frac{J_{0,1} J_{0,2}(2J_{0,1}p_1 - J_{0,1}p_2 - J_{0,2}p_1)}{192\omega_1(\omega_1+\omega_2)^2} \sin(8q_1+4q_2) \,.
$$

Finally, it is easy to analyze the coefficients of the harmonic $\cos(8q_1+4q_2)$ of the terms giving contributions at order ε^3 , that, for Lemma F.3, are described by (F.29):

$$
(*) \quad \frac{\varepsilon^3}{2} L^2_{\chi_2^{(1)}} L_{\chi_1^{(1)}} \boldsymbol{p} \,, \qquad (\star) \quad \varepsilon^3 L_{\chi_1^{(2)}} L_{\chi_2^{(1)}} \boldsymbol{p} \,, \qquad (\diamond) \quad \varepsilon^3 L_{\chi_2^{(2)}} L_{\chi_1^{(1)}} \boldsymbol{p} \,, \qquad (\bullet) \quad \varepsilon^3 L_{\chi_1^{(3)}} \boldsymbol{p} \,.
$$

These are described by the following expressions:

$$
(*) \quad \varepsilon^3 \left(-\frac{5J_{0,1}^3 J_{0,2}}{16\omega_1(2\omega_1+2\omega_2)^2} - \frac{11J_{0,1}^2 J_{0,2}^2}{16\omega_1(2\omega_1+2\omega_2)^2}, -\frac{3J_{0,1}^3 J_{0,2}}{16\omega_1(2\omega_1+2\omega_2)^2} - \frac{5J_{0,1}^2 J_{0,2}^2}{16\omega_1(2\omega_1+2\omega_2)^2} \right) ,
$$

$$
\begin{aligned}
(\star) \quad \varepsilon^3 \Bigg(& -\frac{J_{0,1}^3 J_{0,2}}{8\omega_1(2\omega_1+2\omega_2)(6\omega_1+2\omega_2)} - \frac{J_{0,1}^3 J_{0,2}}{2(2\omega_1+2\omega_2)^2(6\omega_1+2\omega_2)} - \frac{J_{0,1}^3 J_{0,2}}{2\omega_1(2\omega_1+2\omega_2)(4\omega_1+4\omega_2)} \\
& - \frac{3J_{0,1}^2 J_{0,2}^2}{8\omega_1(2\omega_1+2\omega_2)(6\omega_1+2\omega_2)} - \frac{3J_{0,1}^2 J_{0,2}^2}{2(2\omega_1+2\omega_2)^2(6\omega_1+2\omega_2)} - \frac{J_{0,1}^2 J_{0,2}^2}{2\omega_1(2\omega_1+2\omega_2)(4\omega_1+4\omega_2)} \,, \\
& - \frac{J_{0,1}^3 J_{0,2}}{8\omega_1(2\omega_1+2\omega_2)(6\omega_1+2\omega_2)} - \frac{J_{0,1}^3 J_{0,2}}{2(2\omega_1+2\omega_2)^2(6\omega_1+2\omega_2)} - \frac{3J_{0,1}^2 J_{0,2}^2}{8\omega_1(2\omega_1+2\omega_2)(6\omega_1+2\omega_2)} \\
& - \frac{3J_{0,1}^2 J_{0,2}^2}{2(2\omega_1+2\omega_2)^2(6\omega_1+2\omega_2)} \Bigg) ,
\end{aligned}
$$

$$
\begin{aligned}
(\diamond)\quad \varepsilon^3\Bigg(& \frac{J_{0,1}^3 J_{0,2}}{16\omega_1(2\omega_1+2\omega_2)(6\omega_1+2\omega_2)} + \frac{J_{0,1}^3 J_{0,2}}{4(2\omega_1+2\omega_2)^2(6\omega_1+2\omega_2)} + \frac{J_{0,1}^3 J_{0,2}}{4\omega_1(2\omega_1+2\omega_2)(4\omega_1+4\omega_2)} \\
& + \frac{J_{0,1}^2 J_{0,2}^2}{16\omega_1(2\omega_1+2\omega_2)(6\omega_1+2\omega_2)} + \frac{J_{0,1}^2 J_{0,2}^2}{4(2\omega_1+2\omega_2)^2(6\omega_1+2\omega_2)}\,,\ \frac{J_{0,1}^3 J_{0,2}}{16\omega_1(2\omega_1+2\omega_2)(6\omega_1+2\omega_2)} \\
& + \frac{J_{0,1}^3 J_{0,2}}{4(2\omega_1+2\omega_2)^2(6\omega_1+2\omega_2)} + \frac{J_{0,1}^2 J_{0,2}^2}{16\omega_1(2\omega_1+2\omega_2)(6\omega_1+2\omega_2)} + \frac{J_{0,1}^2 J_{0,2}^2}{4(2\omega_1+2\omega_2)^2(6\omega_1+2\omega_2)}\Bigg)\,, \\
(\circ)\quad \varepsilon^3\Bigg(& \frac{J_{0,1}^3 J_{0,2}}{\omega_1(2\omega_1+2\omega_2)(8\omega_1+4\omega_2)} + \frac{2J_{0,1}^3 J_{0,2}}{(2\omega_1+2\omega_2)^2(8\omega_1+4\omega_2)} + \frac{5J_{0,1}^2 J_{0,2}^2}{2\omega_1(2\omega_1+2\omega_2)(8\omega_1+4\omega_2)} \\
& + \frac{5J_{0,1}^2 J_{0,2}^2}{(2\omega_1+2\omega_2)^2(8\omega_1+4\omega_2)}\,,\ \frac{J_{0,1}^3 J_{0,2}}{2\omega_1(2\omega_1+2\omega_2)(8\omega_1+4\omega_2)} + \frac{J_{0,1}^3 J_{0,2}}{(2\omega_1+2\omega_2)^2(8\omega_1+4\omega_2)} \\
& + \frac{5J_{0,1}^2 J_{0,2}^2}{4\omega_1(2\omega_1+2\omega_2)(8\omega_1+4\omega_2)} + \frac{5J_{0,1}^2 J_{0,2}^2}{2(2\omega_1+2\omega_2)^2(8\omega_1+4\omega_2)}\Bigg)\,.
\end{aligned}
$$

The sum of the previous coefficients constitute the harmonic $\boldsymbol{A}_{(8,4)}$, leading to its complete elimination in the final solution.

Bibliography

[1] M. Bartuccelli and G. Gentile. Lindstedt series for perturbations of isochronous systems: a review of the general theory. *Rev. Math. Phys.*, 14(2):121–171, 2002.

[2] C. Beaugé, S. Ferraz-Mello, and T. Michtchenko. Extrasolar planets in mean-motion resonance: apses alignment and asymmetric stationary solutions. *The Astrophysical Journal*, 593(2):1124–1133, 2003.

[3] C. Beaugé, S. Ferraz-Mello, and T. A. Michtchenko. Multi-planet extrasolar systems-detection and dynamics. *Research in Astronomy and Astrophysics*, 12(8):1044, 2012.

[4] G. Benettin. Appunti per il corso di meccanica analitica. `https://www.math.unipd.it/~benettin/links-MA/ma-17_10_25.pdf`, 2014.

[5] D. Brouwer. Solution of the problem of artificial satellite theory without drag. *The Astronomical Journal*, 64:378–397, 1959.

[6] C. Caracciolo. On the stability in the neighborhood of invariant elliptic tori. *PhD Thesis, Univ. of Rome 'Tor Vergata'*, 2021.

[7] C. Caracciolo. Normal form for lower dimensional elliptic tori in Hamiltonian systems. *Mathematics in Engineering*, 4(6):1–40, 2022.

[8] C. Caracciolo and U. Locatelli. Computer-assisted estimates for Birkhoff normal forms. *Journal of Computational Dynamics*, 7(2):425–460, 2020.

[9] I. Cavallari and C. Efthymiopoulos. Closed-form perturbation theory in the restricted three-body problem without relegation. *Celestial Mechanics and Dynamical Astronomy*, 134, 2022.

[10] A. Celletti, A. Giorgilli, and U. Locatelli. Improved estimates on the existence of invariant tori for Hamiltonian systems. *Nonlinearity*, 13(2):397, 2000.

[11] H. Christodoulidi and C. Efthymiopoulos. Low-dimensional q-tori in FPU lattices: Dynamics and localization properties. *Physica D: Nonlinear Phenomena*, 261:92–113, 2013.

[12] H. Christodoulidi, C. Efthymiopoulos, and T. Bountis. Energy localization on q-tori, long-term stability, and the interpretation of Fermi-Pasta-Ulam recurrences. *Phys. Rev. E*, 81:016210, Jan 2010.

[13] G. Contopoulos. A third integral of motion in a galaxy. *Zeitschrift fur Astrophysik*, 49:273–291, 1960.

[14] G. Contopoulos. Resonance cases and small divisors in a third integral of motion. I. *Astron. J.*, 68:763–779, 1963.

[15] G. Contopoulos and M. Moutsoulas. Resonance cases and small divisors in a third integral of motion. *Astron. J.*, 70:817–835, Dec. 1965.

[16] L. Corsi, G. Gentile, and M. Procesi. KAM theory in configuration space and cancellations in the lindstedt series. *Communications in mathematical physics*, 302(2):359–402, 2011.

[17] R. H. Cushman and L. M. Bates. *Global aspects of classical integrable systems*. Birkhauser, 1997.

[18] R. Deitrick, R. Barnes, B. McArthur, T. R. Quinn, R. Luger, A. Antonsen, and G. F. Benedict. The three-dimensional architecture of the υ Andromedae planetary system. *The Astrophysical Journal*, 798(1):46, 2015.

[19] C. Efthymiopoulos. Canonical perturbation theory; stability and diffusion in Hamiltonian systems: applications in dynamical astronomy. In *Workshop series of the asociacion argentina de astronomia*, volume 3, pages 3–146, 2012.

[20] C. Efthymiopoulos, A. Giorgilli, and G. Contopoulos. Nonconvergence of formal integrals: II. improved estimates for the optimal order of truncation. *Journal of Physics A: Mathematical and General*, 37(45):10831–10858, oct 2004.

[21] L. H. Eliasson. Absolutely convergent series expansions for quasi periodic motions. 1996.

[22] F. Farago and J. Laskar. High-inclination orbits in the secular quadrupolar three-body problem. *Monthly Notices of the Royal Astronomical Society*, 401(2):1189–1198, 2010.

[23] S. Ferraz-Mello. *Canonical perturbation theories: degenerate systems and resonance*, volume 345. Springer Science & Business Media, 2007.

[24] S. Flach, M. V. Ivanchenko, and O. I. Kanakov. q-breathers and the Fermi-Pasta-Ulam problem. *Phys. Rev. Lett.*, 95:064102, Aug 2005.

[25] S. Flach, M. V. Ivanchenko, and O. I. Kanakov. q-breathers in Fermi-Pasta-Ulam chains: Existence, localization, and stability. *Phys. Rev. E*, 73:036618, Mar 2006.

[26] E. B. Ford, B. Kozinsky, and F. A. Rasio. Secular evolution of hierarchical triple star systems. *The Astrophysical Journal*, 535(1):385–401, 2000.

[27] G. Gallavotti. Twistless KAM tori. *Communications in Mathematical Physics*, 164(1):145–156, 1994.

[28] G. Gallavotti. Twistless KAM tori, quasi flat homoclinic intersections, and other cancellations in the perturbation series of certain completely integrable Hamiltonian systems: a review. *Reviews in Mathematical Physics*, 6(03):343–411, 1994.

[29] A. Giorgilli. Small denominators and exponential stability: From Poincaré to the present time. *Rendiconti del Seminario Matematico e Fisico di Milano*, 68(1):19–57, 1998.

[30] A. Giorgilli. Notes on exponential stability of Hamiltonian systems. Pubblicazioni della Classe di Scienze, Scuola Normale Superiore, Pisa. Centro di Ricerca Matematica "Ennio De Giorgi", 2003.

[31] A. Giorgilli. *Notes on Hamiltonian Dynamical Systems*, volume 102. Cambridge University Press, 2022.

[32] A. Giorgilli, A. Delshams, E. Fontich, L. Galgani, and C. Simó. Effective stability for a Hamiltonian system near an elliptic equilibrium point, with an application to the restricted three–body problem. *J. Differential Equations*, 77:167–198, 1989.

[33] A. Giorgilli and U. Locatelli. On classical series expansions for quasi-periodic motions. *Mathematical Physics Electronic Journal*, 3:1–25, 1997.

[34] A. Giorgilli, U. Locatelli, and M. Sansottera. On the convergence of an algorithm constructing the normal form for lower dimensional elliptic tori in planetary systems. *Celestial Mechanics and Dynamical Astronomy*, 119:397–424, 2014.

[35] A. Giorgilli, U. Locatelli, and M. Sansottera. Secular dynamics of a planar model of the Sun-Jupiter-Saturn-Uranus system; effective stability in the light of Kolmogorov and Nekhoroshev theories. *Regular and Chaotic Dynamics*, 22:54–77, 2017.

[36] W. Gröbner. *Die Lie-reihen und ihre Anwendungen*, volume 3. Deutscher Verlag der Wissenschaften, 1967.

[37] G. F. Gronchi and A. Milani. Averaging on Earth-Crossing Orbits. *Celestial Mechanics and Dynamical Astronomy*, 71(2):109–136, 1998.

[38] J. D. Hadjidemetriou. The continuation of periodic orbits from the restricted to the general three-body problem. *Celestial mechanics*, 12(2):155–174, 1975.

[39] J. D. Hadjidemetriou. Symmetric and asymmetric librations in extrasolar planetary systems: a global view. *Celestial Mechanics and Dynamical Astronomy*, 95(1):225–244, 2006.

[40] B. M. Hansen and S. Naoz. The stationary points of the hierarchical three-body problem. *Monthly Notices of the Royal Astronomical Society*, 499(2):1682–1700, 2020.

[41] M. Hénon and C. Heiles. The applicability of the third integral of motion: some numerical experiments. *The astronomical journal*, 69:73, 1964.

[42] J. Henrard and A.-S. Libert. The secular planetary three body problem revisited. *Proceedings of the International Astronomical Union*, 2004(IAUC197):49–54, 2004.

[43] N. H. Hoang, F. Mogavero, and J. Laskar. Long-term instability of the inner Solar System: numerical experiments. *Monthly Notices of the Royal Astronomical Society*, 514(1):1342–1350, 2022.

[44] T. Ito and K. Ohtsuka. The Lidov-Kozai Oscillation and Hugo von Zeipel. *Monographs on Environment, Earth and Planets*, 7:1–113, 11 2019.

[45] C. G. J. Jacobi. Sur l'élimination des noeuds dans le problème des trois corps. Par M. Jacobi. *Astronomische Nachrichten*, 20:81–102, 1842.

[46] À. Jorba and J. Masdemont. Dynamics in the center manifold of the collinear points of the restricted three body problem. *Physica D: Nonlinear Phenomena*, 132(1):189–213, 1999.

[47] A. Kolmogorov. Preservation of conditionally periodic movements with small change in the hamilton function. 93:51–56, 1979.

[48] Y. Kozai. Secular perturbations of asteroids with high inclination and eccentricity. *The Astronomical Journal*, 67(9):591–598, 1962.

[49] J. Laskar. Introduction to frequency map analysis. *Hamiltonian systems with three or more degrees of freedom*, pages 134–150, 1999.

[50] J. Laskar. On the spacing of planetary systems. *Physical Review Letters*, 84(15):3240–3243, 2000.

[51] J. Laskar. Frequency map analysis and quasiperiodic decompositions. In E. Lega, D. Benest, and C. Froeschlé, editors, *Hamiltonian systems and Fourier analysis: new prospects for gravitational dynamics*. Cambridge Scientific Pub Ltd, 2005.

[52] J. Laskar and M. Gastineau. Existence of collisional trajectories of Mercury, Mars and Venus with the Earth. *Nature*, 459(7248):817–819, 2009.

[53] J. Laskar and A. Petit. AMD-stability and the classification of planetary systems. *Astronomy & Astrophysics*, 605:A72, 2017.

[54] J. Laskar and P. Robutel. Stability of the planetary three-body problem. *Celestial Mechanics and Dynamical Astronomy*, 62(3):193–217, 1995.

[55] J. Laskar and P. Robutel. High order symplectic integrators for perturbed hamiltonian systems. *Celestial Mechanics and Dynamical Astronomy*, 80(1):39–62, 2001.

[56] G. Laughlin, J. Chambers, and D. Fischer. A dynamical analysis of the 47 Ursae Majoris planetary system. *The Astrophysical Journal*, 579(1):455–467, 2002.

[57] M. H. Lee and S. Peale. Secular evolution of hierarchical planetary systems. *The Astrophysical Journal*, 592(2):1201–1216, 2003.

[58] A.-S. Libert and N. Delsate. Interesting dynamics at high mutual inclination in the framework of the Kozai problem with an eccentric perturber. *Monthly Notices of the Royal Astronomical Society*, 422(3):2725–2736, 2012.

[59] A.-S. Libert and J. Henrard. Exoplanetary systems: The role of an equilibrium at high mutual inclination in shaping the global behavior of the 3-D secular planetary three-body problem. *Icarus*, 191(2):469–485, 2007.

[60] A.-S. Libert, C. Hubaux, and T. Carletti. The global symplectic integrator: an efficient tool for stability studies of dynamical systems. Application to the Kozai resonance in the restricted three-body problem. *Monthly Notices of the Royal Astronomical Society*, 414(1):659–667, 2011.

[61] A.-S. Libert and K. Tsiganis. Kozai resonance in extrasolar systems. *Astronomy & Astrophysics*, 493(2):677–686, 2009.

[62] M. Lidov. The evolution of orbits of artificial satellites of planets under the action of gravitational perturbations of external bodies. *Planetary and Space Science*, 9(10):719–759, 1962.

[63] M. L. Lidov and S. Ziglin. Non-restricted double-averaged three body problem in Hill's case. *Celestial Mechanics*, 13(4):471–489, 1976.

[64] A. Lindstedt. Ueber die allgemeine form der integrale des dreikörperproblems. *Astronomische Nachrichten*, 105(7):97–112, 1883.

[65] A. Lindstedt. Ueber die integration einer gewissen differentialgleichung. *Astronomische Nachrichten*, 104(10):145–150, 1883.

[66] A. Lindstedt. Sur les séries trigonométriques dans le problème des trois corps. *Bulletin astronomique, Observatoire de Paris*, 3(1):217–221, 1886.

[67] Y. Lithwick and S. Naoz. The eccentric Kozai mechanism for a test particle. *The Astrophysical Journal*, 742(2):94, 2011.

[68] U. Locatelli. Metodi numerici di studio dei sistemi dinamici hamiltoniani. `http://www.mat.uniroma2.it/~locatell/MCSH/testi.html`.

[69] U. Locatelli. CAP4KAM2D: Computer-assisted proofs for demonstrating the existence of 2-dimensional KAM tori. `https://doi.org/10.17632/jdx22ysh2s.1`, 2021.

[70] U. Locatelli. CAP4KAM_nDOF: Computer-assisted proofs of existence of KAM tori in hamiltonian systems with n (>= 2) degrees of freedom. `https://doi.org/10.17632/tsffjx7pyr.1`, 2022.

[71] U. Locatelli, C. Caracciolo, M. Sansottera, and M. Volpi. Invariant KAM tori: from theory to applications to exoplanetary systems. *I-Celmech training school, Springer PROMS*, 2022.

[72] U. Locatelli, C. Caracciolo, M. Sansottera, and M. Volpi. A numerical criterion evaluating the robustness of planetary architectures; applications to the υ andromedæ system. *Proceedings of the International Astronomical Union*, 15(S364):65–84, 2022.

[73] U. Locatelli and A. Giorgilli. Invariant tori in the secular motions of the three-body planetary systems. *Celestial Mechanics and Dynamical Astronomy*, 78(1):47–74, 2000.

[74] P. J. Lowrance, J. D. Kirkpatrick, and C. A. Beichman. A distant stellar companion in the υ andromedae system. *The Astrophysical Journal*, 572(1):L79, 2002.

[75] R. Mastroianni and C. Efthymiopoulos. The phase-space architecture in extrasolar systems with two planets in orbits of high mutual inclination. *arXiv preprint arXiv:2212.10569*, 2022.

[76] R. Mastroianni and C. Efthymiopoulos. Kolmogorov algorithm for isochronous Hamiltonian systems. *Mathematics in Engineering*, 5(2):1–35, 2023.

[77] R. Mastroianni and U. Locatelli. Secular orbital dynamics of the innermost exoplanet of the υ-Andromedæ system. *(submitted)*, 2023.

[78] B. E. McArthur, G. F. Benedict, R. Barnes, E. Martioli, S. Korzennik, E. Nelan, and R. P. Butler. New observational constraints on the υ Andromedae system with data from the Hubble Space Telescope and Hobby-Eberly Telescope. *The Astrophysical Journal*, 715(2):1203–1220, 2010.

[79] T. Michtchenko, S. Ferraz-Mello, and C. Beaugé. Modeling the 3-D secular planetary three-body problem: Discussion on the outer υ Andromedae planetary system. *Icarus*, 181(2):555–571, 2006.

[80] T. A. Michtchenko and R. Malhotra. Secular dynamics of the three-body problem: application to the υ Andromedae planetary system. *Icarus*, 168(2):237–248, 2004.

[81] C. Migaszewski and K. Goździewski. A secular theory of coplanar, non-resonant planetary system. *Monthly Notices of the Royal Astronomical Society*, 388(2):789–802, 2008.

[82] C. Migaszewski and K. Goździewski. Secular dynamics of a coplanar, non-resonant planetary system under the general relativity and quadrupole moment perturbations. *Monthly Notices of the Royal Astronomical Society*, 392(1):2–18, 2009.

[83] C. Migaszewski and K. Goździewski. The non-resonant, relativistic dynamics of circumbinary planets. *Monthly Notices of the Royal Astronomical Society*, 411(1):565–583, 2011.

[84] F. Mogavero and J. Laskar. Long-term dynamics of the inner planets in the solar system. *Astronomy & Astrophysics*, 655:A1, 2021.

[85] F. Mogavero and J. Laskar. The origin of chaos in the Solar System through computer algebra. *Astronomy & Astrophysics*, 662:L3, 2022.

[86] A. Morbidelli. *Modern celestial mechanics: aspects of solar system dynamics*. 2002.

[87] C. D. Murray and S. F. Dermott. *Solar system dynamics*. Cambridge university press, 1999.

[88] S. Naoz. The eccentric Kozai-Lidov effect and its applications. *Annual Review of Astronomy and Astrophysics*, 54:441–489, 2016.

[89] S. Naoz, W. M. Farr, Y. Lithwick, F. A. Rasio, and J. Teyssandier. Secular dynamics in hierarchical three-body systems. *Monthly Notices of the Royal Astronomical Society*, 431(3):2155–2171, 2013.

[90] J. F. Palacián, P. Yanguas, S. Fernández, and M. A. Nicotra. Searching for periodic orbits of the spatial elliptic restricted three-body problem by double averaging. *Physica D: Nonlinear Phenomena*, 213(1):15–24, 2006.

[91] T. Pauwels. Secular orbit-orbit resonance between two satellites with non-zero masses. *Celestial mechanics*, 30(3):229–247, 1983.

[92] A. C. Petit, J. Laskar, and G. Boué. Hill stability in the AMD framework. *Astronomy & Astrophysics*, 617:A93, 2018.

[93] D. Piskorz, B. Benneke, N. R. Crockett, A. C. Lockwood, G. A. Blake, T. S. Barman, C. F. Bender, J. S. Carr, and J. A. Johnson. Detection of water vapor in the thermal spectrum of the non-transiting hot Jupiter Upsilon Andromedae b. *The Astronomical Journal*, 154(2):78, 2017.

[94] H. Poincaré. *Les méthodes nouvelles de la mécanique céleste: Méthodes de MM. Newcomb, Gyldén, Linstadt et Bohlin*, volume 2. Gauthier-Villars et fils, imprimeurs-libraires, 1893.

[95] J. Pöschel. Nekhoroshev estimates for quasi-convex hamiltonian systems. *Math. Z*, 213(2):187–216, 1993.

[96] D. L. Richardson and T. J. Kelly. Two-body motion in the post-Newtonian approximation. *Celestial Mechanics*, 43:193–210, 1988.

[97] P. Robutel. Stability of the planetary three-body problem: II. Kam theory and existence of quasiperiodic motions. *Celestial Mechanics and Dynamical Astronomy*, 62:219–261, 1995.

[98] M. Sansottera and V. Danesi. Kolmogorov variation: KAM with knobs (à la Kolmogorov). *arXiv preprint arXiv:2109.06345*, 2021.

[99] A. Szeto and K. Lambeck. On eccentricity functions for eccentric orbits. *Celestial mechanics*, 27(4):325–337, 1982.

[100] F. Thomas and A. Morbidelli. The Kozai resonance in the outer solar system and the dynamics of long-period comets. *Celestial Mechanics and Dynamical Astronomy*, 64(3):209–229, 1996.

[101] H. von Zeipel. Sur l'application des séries de M. Lindstedt à l'étude du mouvement des comètes périodiques. *Astronomische Nachrichten*, 183:345, 1910.

[102] E. T. Whittaker. *A treatise on the analytical dynamics of particles and rigid bodies : with an introduction to the problem of three bodies*. Cambridge University press, Cambridge, 2th edition, 1917.

Acknowledgements

As my supervisor says, the PhD is made not only by research, but also by psychology. So, I would like to express my gratitude to all the people who accompanied me throughout this path.

First, I want to thank the University of Padua, that gave me the opportunity to work in the research field. In particular, my gratitude goes to the PhD course, to Prof. Bardi and Prof. Colombo for investing their time for our training. Many thanks go also to the administration, to Loretta and Marinella, for their (friendly) help in every situation.

I would like to express my gratitude also to the group of Mathematical Physics of the University of Padua. I really appreciate their effort to train young people and to transmit them all their experience and their devotion to this beautiful field. For the same reason, I thank also other groups of Celestial Mechanics, as the one in Tor Vergata and in Pisa, for their work and the beautiful conferences organized during these years. A particular mention to Prof. Alessandra Celletti, because her master course of Celestial Mechanics made me realize that this field was my path. Finally, I really want to thank Prof. Francesco Fassò, because his courses allowed me to look at my field from a different perspective.

My gratitude goes also to the referee of this thesis, Prof. Antonio Giorgilli and Prof. Philippe Robutel, for their constructive comments and suggestions.

I would like to thank also other wonderful people I had the pleasure to meet during this journey (and before), for the scientific (and not) discussions, support and patience: Chiara Caracciolo, Mara Volpi, Veronica Danesi and my PhD colleagues. In particular, Mattia Rossi, who shared with me lots of discussions, talks, conferences and who helped me many times. And I have to mention also Daniele Troletti, for his technical support!

Finally, the most important. All my gratitude goes to my supervisors. Christos, who constantly encorauged me, trying to bring out the best in me and to fight my (big) anxiety. By sharing all his expertise with me, he allowed me to grow significantly in every scientific aspect. Ugo, because without his teachings and patience during the master thesis (but, also, during the PhD) I wouldn't be here today. I had the great pleasure to work with him also during the PhD and he continuously supported me, limiting my weaknesses and enhancing my (mathematical and non-mathematical) strengths and knowledge.

I would like to include also some more personal acknowledgements, but, for these ones, I'll pass to Italian.

Il primo ringraziamento va ai miei genitori, perchè senza il loro lavoro, la loro dedizione e i loro impegni non avrei avuto alcuna possibilità di fare tutto questo percorso.

Un grazie va anche a Fabiola e Giancarlo, che mi hanno sempre incoraggiata e che mi hanno accolta in casa come una figlia.

Concludo come sono partita: Piero. Il mio grazie di cuore va a lui, che da ben più di 3 anni condivide con me il suo cammino. Ha condiviso con me i dubbi, le debolezze, le cadute e le gioie e non ha mai smesso di credere in me e di supportarmi. Comunque andrà, accanto a lui ho un posto nel mondo.